Physics
Falon

THE JOURNAL
OF
CHEMICAL PHYSICS

VOLUME 23, NUMBER 1 JANUARY, 1955

Some Theorems Concerning the Mutual Polarizabilities of Atoms and Bonds in Conjugated Molecules

H. H. JAFFÉ*
Venereal Disease Experimental Laboratory, U. S. Public Health Service, School of Public Health, University of North Carolina, Chapel Hill, North Carolina

(Received July 28, 1954)

Atom bond polarizabilities $\pi_{r,st}$ in alternant hydrocarbons (AH's) vanish identically. The calculation of $\pi_{r,st}$ in ions derived from AH's by addition or removal of one or more electrons (AHI's) is discussed, and the conditions under which they vanish are examined. Mutual atom polarizabilities $\pi_{r,s}$ and mutual bond polarizabilities $\pi_{rs,tu}$ in AHI's are related to the corresponding quantities in the parent AH's. The dependence of all the polarizabilities on Coulomb and resonance integrals is examined.

THE perturbation theory developed by Coulson and Longuet-Higgins[1] has recently been used extensively in molecular orbital (MO) calculations of physical properties and chemical reactivity of conjugated organic compounds. Application of this theory to the calculation of electron densities and bond orders requires the evaluation of certain polarizabilities, the mutual polarizabilities of atoms ($\pi_{r,s}$) and of bonds ($\pi_{rs,tu}$), and the atom bond polarizabilities ($\pi_{r,st}=2\pi_{st,r}$). In connection with some calculations now being carried out in this laboratory, a knowledge of some general properties of these polarizabilities was desired. The present paper reports several theorems relating to these polarizabilities, and their dependence on the Coulomb and resonance integrals. These theorems are proven by first-order perturbation theory, and accordingly are valid only as long as first order perturbation theory is valid. This limitation is of no consequence since the polarizabilities themselves are useful primarily, if not exclusively, in calculations by first order perturbation theory.

ATOM BOND POLARIZABILITIES

All atom bond polarizabilities in alternant hydrocarbons (AH's) vanish identically.[1b] For other compounds these quantities are given by[1a,2]

$$\pi_{r,st}=2\pi_{st,r}=4\sum_{j}^{\text{occ.}}\sum_{k}^{\text{unocc.}}c_{rj}c_{rk}(c_{sj}c_{tk}+c_{tj}c_{sk})/(\epsilon_j-\epsilon_k). \tag{1}$$

The numerical evaluation of Eq. (1) for any real compound involves some quite tedious computation, and hence it is not surprising that little use of atom bond polarizabilities has been made in numerical calculations. However, in the realm of perturbation theory real compounds are treated as derived from certain reference structures by perturbation of the relevant Coulomb and resonance integrals. These reference structures are usually either AH's, or ions derived from AH's by addition or removal of one or more electrons. We propose to call such ions *alternant hydrocarbon ions* (AHI's); if they bear a single (positive or negative) charge they will be called monovalent, if they bear multiple charges, polyvalent. Equation (1) can be greatly simplified for AHI's.

For the anion derived from an odd AH[3,4] (free radical) by the addition of a single electron, Eq. (1)

* Present address: Department of Chemistry, University of Cincinnati, Cincinnati, Ohio.

[1] C. A. Coulson and H. C. Longuet-Higgins, Proc. Roy. Soc. (London) (a) **A191**, 39 (1947); (b) **A192**, 16 (1947).

[2] Singly occupied MO's are not included in either summation of Eq. (1).

[3] Odd AH's are AH's with an odd number of atoms in the conjugated system, and an odd number of π electrons. Such AH's always have at least one MO (ψ_0) of zero energy ($\epsilon_0=0$).

[4] H. C. Longuet-Higgins, J. Chem. Phys. **18**, 265 (1950).

may be split into two terms[5]:

$$\pi_{r,st}=4\sum_{j<0}\sum_{k>0}c_{rj}c_{rk}(c_{sj}c_{tk}+c_{tj}c_{sk})/(\epsilon_j-\epsilon_k)$$
$$+4\sum_{k>0}c_{r0}c_{rk}(c_{s0}c_{tk}+c_{sk}c_{t0})/(-\epsilon_k). \quad (2)$$

The first term on the right-hand side of Eq. (2) vanishes since it is $\pi_{r,st}$ for the odd AH (parent AH), from which the AHI is derived by addition of one electron. In an AH, and equally in an AHI, all atoms can be divided into two sets, a starred and an unstarred set,[4,6] and we shall assign the symbols s and t to atoms so that atom s is always starred, and hence atom t always unstarred; then c_{t0} always vanishes.[4] In any AH the energy levels occur in pairs, with energies of equal absolute magnitude but opposite sign. Hence, for each ϵ_j of Eq. (2) there is an $\epsilon_k=-\epsilon_j$, and vice versa; for these pairs $c_{rk}=\pm c_{rj}$, where the sign depends only on the set (starred or unstarred) in which atom r is found. Using these facts, we can reduce Eq. (2) to[7]

$$\pi_{r,st}=-4\sum_{j<0}c_{r0}c_{rj}c_{s0}c_{tj}/\epsilon_j. \quad (3)$$

Equation (3) can also be derived for cationic AHI's, except in such ions the right-hand side carries a positive sign. Equation (3) contains much useful information, which is summarized in the following theorems.

Theorem 1

The bond orders p_{st} of the bond between atoms s and t in a compound derived by perturbation from a monovalent AHI is independent of the Coulomb integrals α_r of all atoms r if the coefficient c_{s0} of atom s in the zero energy MO ψ_0 vanishes; p_{st} is also independent of the Coulomb integrals α_r of all those atoms r for which c_{r0} vanishes.

Theorem 2

The electron density q_r at atom r in a compound derived by perturbation from a monovalent AHI is independent of the resonance integrals β_{st} of all bonds if c_{r0} vanishes; q_r is also independent of the resonance integrals β_{st} of those bonds for which c_{s0} vanishes.

However, the c_{r0} vanish for all unstarred atoms.[4] Hence, we have the following theorem.

Theorem 3

The electron densities at all unstarred atoms of a molecule derived by perturbation from an AHI are independent of the resonance integrals of all bonds,[8] and the bond orders of all bonds are independent of the Coulomb integrals of all unstarred atoms. Theorem 3 is implied in theorems 1 and 2, but is more restrictive than they are, particularly since in many compounds the c_{r0} of some of the starred atoms vanish.

As a corollary of theorems 1 and 2, $\pi_{r,st}$ and $\pi_{st,r}$ cannot be neglected unless the stated conditions are fulfilled.

The above arguments must now be extended to polyvalent AHI's. Two cases must here be distinguished.

(1) The parent AH has as many zero energy MO's as the AHI has charges.[9] Then, Eq. (2) becomes, after simplification,

$$\pi_{r,st}=-4\sum_{k}\sum_{j<0}c_{rk}c_{rj}(c_{sk}c_{tj}-c_{tk}c_{sj})/\epsilon_j, \quad \text{all } \epsilon_k=0, \quad (4)$$

where s and t are assigned so that r and s are in the same set, and the summation over k extends over all k for which $\epsilon_k=0$ (zero energy MO's). If the number of atoms in the starred set exceeds the number in the unstarred set by the number of zero energy MO's (compounds in which this condition holds will be designated as compounds of class IA), all c_{rk} for the unstarred set vanish, and theorem 3 holds. For these compounds Eq. (4) takes the form

$$\pi_{r,st}=-4\sum_{k}\sum_{j<0}c_{rk}c_{rj}c_{sk}c_{tj}/\epsilon_j, \quad \text{all } \epsilon_k=0, \quad (5)$$

and theorems 1 and 2 are replaced by the following theorem.

Theorem 4

In polyvalent AHI's in which the number of zero energy MO's equals the number of charges, $\pi_{r,st}$ and $\pi_{st,r}$ (with r and s in the same set) vanish whenever, for each zero energy MO ψ_k, either c_{rk} or c_{sk} vanishes.

If the number of starred atoms does not exceed the number of unstarred atoms by the number of zero energy MO's (such compounds will be designated as class IB), there is no set for which all c_{sk} vanish. Hence, theorem 3 is not applicable to compounds of class IB, but theorem 4 applies to these compounds as well.

(2) If the parent AH has fewer zero energy MO's than the AHI has charges (such compounds will be denoted as class II), Eq. (4) takes the form

$$\pi_{r,st}=-4\sum_{k}\sum_{j}c_{rk}c_{rj}(c_{sk}c_{tj}-c_{sj}c_{tk})/(\epsilon_j+\epsilon_k), \quad (6)$$

where the summation over j extends over all occupied MO's of energy ϵ_j such that MO's of energy $-\epsilon_j$ are unoccupied, and where the summation over k extends

[5] In Eq. (2) and subsequent equations, summation over $j<0$ means summation over those j for which $\epsilon_j<0$, over $k>0$ over those k for which $\epsilon_k>0$.

[6] We shall define the set with the larger number of atoms as the starred set throughout this paper, whenever the number of atoms in the two sets is unequal.

[7] The right-hand side of Eq. (3) should be written with a $\pm$ sign, the plus being applicable when r and t are in the same set. However, since t is unstarred by definition, the right-hand side of Eq. (3) vanishes when r and t are in the same set, since c_{r0} vanishes, and hence the minus sign alone is sufficient.

[8] The first part of this theorem is implied in the work of Longuet-Higgins, reference 4.

[9] The number of zero energy MO's can be derived in the manner outlined in reference 4.

over all the remaining occupied MO's. In compounds of class II there is no set for which all the c_{rk} vanish; further, the c_{rk} for MO's with nonzero energy do not commonly vanish for many atoms. Then, generally, none of the $\pi_{r,st}$ and $\pi_{st,r}$ vanish for compounds of class II, although, for each k included in the summation of Eq. (6), either $c_{rk}=0$, or $c_{sk}=c_{tk}=0$ is a sufficient condition for the vanishing of $\pi_{r,st}$ and $\pi_{st,r}$.

MUTUAL ATOM POLARIZABILITIES

The mutual polarizability $\pi_{r,s}$ of two atoms r and s does not vanish in AH's; this quantity has been evaluated for a number of compounds, and such values are tabulated in various places in the literature.[1b,10] It is of interest to note that the $\pi_{r,s}$ of AHI's can readily be related to the $\pi_{r,s}$ for parent AH's by much the same reasoning used above, giving[11]:

$$\pi_{r,s}(\mathrm{AHI})=\pi_{r,s}(\mathrm{AH})+4\sum_{k}\sum_{j<0}c_{rk}c_{rj}c_{sk}c_{sj}/\epsilon_j \qquad \text{all } \epsilon_k=0. \quad (7)$$

Equation (7) applies to monovalent AHI's and to polyvalent AHI's of classes IA and IB, but not of class II. Equation (7) leads to the following theorems.

Theorem 5

Mutual atom polarizabilities in monovalent AHI's and in polyvalent AHI's of class IA are equal to the corresponding $\pi_{r,s}$ in the parent AH if either r or s is in the unstarred set.

Theorem 6

Mutual atom polarizabilities in polyvalent AHI's of classes IA and IB are equal to the corresponding $\pi_{r,s}$ in the parent AH if, for each zero energy MO, either c_{rk} or c_{sk} vanishes.

MUTUAL BOND POLARIZABILITIES

The mutual polarizability, $\pi_{rs,tu}$ of bonds rs and tu, for monovalent AHI's and the polyvalent AHI's of classes IA and IB can be related to the corresponding polarizabilities for the parent AH. Choosing r and t in the same set, and choosing this set so that c_{r0} and c_{t0} do not both vanish, unless both c_{s0} and c_{u0} also vanish,[12] this relation becomes

$$\pi_{rs,tu}(\mathrm{AHI})=\pi_{rs,tu}(\mathrm{AH})+2\sum_{k}\sum_{j<0}c_{rk}c_{sj}c_{tk}c_{uj}/\epsilon_j, \qquad \text{all } \epsilon_k=0. \quad (8)$$

Equation (8) implies the following theorem.

[10] (a) H. C. Longuet-Higgins and C. A. Coulson, J. Chem. Soc. 971 (1949); H. H. Jaffé, J. Am. Chem. Soc. **76**, 3527 (1954); (b) H. H. Jaffé, J. Am. Chem. Soc. (to be published).

[11] The second term in Eq. (7) should have a negative sign when r and s are in different sets, but in that case either c_{rk} or c_{sk} vanishes, and hence the whole term vanishes.

[12] It should be noted that in AHI's of class IB, different zero energy MO's require different assignments of the symbols r and s, and t, and u to the two atoms of any given bond.

Theorem 7

The $\pi_{rs,tu}$ of a monovalent AHI, or of a polyvalent AHI of classes IA or IB do not differ from the $\pi_{rs,tu}$ of the parent AH whenever, for each zero energy MO, either c_{rk} or c_{tk} vanishes.

A simplification in the calculation of $\pi_{rs,tu}(\mathrm{AH})$ arises out of the fact that for $\epsilon_j=-\epsilon_k$ the terms $c_{rj}c_{sk}+c_{rk}c_{sj}$ and $c_{tj}c_{uk}+c_{tk}c_{uj}$ of Eq. (67) of reference 1a vanish, and hence all terms in the double sum for which $\epsilon_j=-\epsilon_k$ may be omitted. The terms for which $\epsilon_j\neq-\epsilon_k$ occur in pairs with equal $\epsilon_j-\epsilon_k$. Such terms can be readily combined, giving after simplification

$$\pi_{rs,tu}=4\sum_{j<k<0}\sum c_{rj}c_{sk}(c_{tj}c_{uk}-c_{tk}c_{uj})/(\epsilon_j+\epsilon_k). \quad (9)$$

DEPENDENCE OF POLARIZABILITIES ON COULOMB AND RESONANCE INTEGRALS

So far we have dealt only with the calculation of polarizabilities in AH's and AHI's. These quantities are needed for the calculation, by perturbation theory, of charge densities and bond orders in actual molecules derived from the AH's and AHI's by perturbation of certain Coulomb and resonance integrals. However, in some instances the polarizabilities in the perturbed molecules also are of interest. Thus, if all q_r are equal, as is the case in AH's,[1b] it may be assumed that the reactivity at position r depends on the self-polarizability $\pi_{r,r}$ at this position.[13] Also, occasionally one wishes to compare the effect of a perturbation, not on an AH or AHI, but on a compound derived from it by a perturbation. A knowledge of the dependence of the polarizabilities on the various perturbation parameters is desirable for such calculations. To the first approximation, this dependence can be expressed as

$$\delta\pi=\sum_{r}\frac{\partial\pi}{\partial\alpha_r}\delta\alpha_r+\sum_{r<s}\sum\frac{\partial\pi}{\partial\beta_{rs}}\delta\beta_{rs},$$

where π may be any of the polarizabilities $\pi_{r,s}$, $\pi_{r,st}\pi_{rs,t}$, or $\pi_{rs,tu}$. Hence, we must investigate the various partial derivatives $\partial\pi/\partial\alpha_r$ and $\partial\pi/\partial\beta_{rs}$.

According to Coulson and Longuet-Higgins,[1a] and using their notation, the polarizabilities can be expressed in terms of certain contour integrals:

$$\pi_{r,s}=\frac{\partial q_r}{\partial\alpha_s}=-\frac{1}{\pi}\int\left(\frac{\Delta_{r,s}}{\Delta}\right)^2dy$$

$$\pi_{r,st}=\frac{\partial q_r}{\partial\beta_{st}}=2\pi_{st,r}=2\frac{\partial p_{st}}{\partial\alpha_r}=(-1)^{r+s}\frac{2}{\pi}\int\frac{\Delta_{r,t}\Delta_{s,t}}{\Delta^2}dy,$$

and

$$\pi_{rs,tu}=\frac{\partial p_{rs}}{\partial\beta_{tu}}=(-1)^{r+s+t+u}\frac{1}{\pi}\int\frac{\Delta_{r,u}\Delta_{s,t}+\Delta_{r,t}\Delta_{s,u}}{\Delta^2}dy.$$

[13] R. D. Brown, Quart. Rev. **6**, 63 (1952).

Upon differentiation, and using Jacobi's formula, we find in a manner analogous to that used by Coulson and Longuet-Higgins for the derivation of the polarizabilities[1a]

$$\frac{\partial \pi_{r,s}}{\partial \alpha_t} = \frac{2}{\pi}\int \frac{\Delta_{r,s}\Delta_{r,t}\Delta_{s,t}}{\Delta^3}dy \tag{10}$$

$$\frac{\partial \pi_{r,st}}{\partial \alpha_u} = \frac{\partial^2 q_r}{\partial \alpha_u \partial \beta_{st}} = \frac{\partial \pi_{r,u}}{\partial \beta_{st}} = (-1)^{s+t+1}\frac{2}{\pi}\int \frac{\Delta_{r,u}}{\Delta^3}(\Delta_{r,t}\Delta_{s,u}+\Delta_{r,s}\Delta_{t,u})dy \tag{11}$$

$$\frac{\partial \pi_{rs,tu}}{\partial \alpha_v} = \frac{\partial^2 p_{rs}}{\partial \alpha_v \partial \beta_{tu}} = \frac{\partial \pi_{rs,v}}{\partial \beta_{tu}} = (-1)^{r+s+t+u+1}\frac{1}{\pi}\int \frac{\Delta_{r,v}(\Delta_{s,t}\Delta_{u,v}+\Delta_{s,u}\Delta_{t,v})+\Delta_{s,v}(\Delta_{r,t}\Delta_{u,v}+\Delta_{r,u}\Delta_{t,v})}{\Delta^3}dy \tag{12}$$

$$\frac{\partial \pi_{rs,tu}}{\partial \beta_{vw}} = (-1)^{r+s+t+u+v+w+1}\frac{1}{\pi}\int [\Delta_{s,u}(\Delta_{r,w}\Delta_{t,v}+\Delta_{r,v}\Delta_{t,w})+\Delta_{r,t}(\Delta_{s,w}\Delta_{u,v}+\Delta_{s,v}\Delta_{u,w})$$
$$+\Delta_{s,t}(\Delta_{r,w}\Delta_{u,v}+\Delta_{r,v}\Delta_{u,w})+\Delta_{r,u}(\Delta_{s,w}\Delta_{t,v}+\Delta_{s,v}\Delta_{t,w})]dy/\Delta^3. \tag{13}$$

Consideration of the parity[14] of the minors $\Delta_{k,l}$ shows that the integrands in Eqs. (10) and (12) are always odd, those in Eqs. (11) and (13) are always even. Hence, we have the following theorem.

Theorem 8

In compounds derived by perturbation from AH's, mutual atom and mutual bond polarizabilities are independent of the Coulomb integrals of all atoms, and atom bond polarizabilities are independent of the resonance integrals of all bonds.

Evaluation of the $\partial\pi/\partial\alpha_r$ and $\partial\pi/\partial\beta_{rs}$ in terms of the c_{rj} is straightforward by the method used by Coulson and Longuet-Higgins for the polarizabilities.[1a] However, the process is laborious and it is doubtful, given the equations, that the numerical computation of the quantities would be practical. We have derived such a formula only for $\partial\pi_{r,s}/\partial\alpha_t$, which we will simplify for use with AHI's. In the general case it can readily be shown that

$$\frac{\partial \pi_{rs}}{\partial \alpha_t} = 4\sum_{j=1}^{m}\sum_{k=m+1}^{n}\sum_{i=1}^{m}\frac{c_{rj}c_{sj}c_{tk}c_{ti}(c_{rk}c_{si}+c_{ri}c_{sk})}{(\epsilon_j-\epsilon_k)(\epsilon_k-\epsilon_i)}+4\sum_{j=1}^{m}\sum_{k=m+1}^{n}\sum_{i=m+1}^{n}\frac{c_{rk}c_{sk}c_{tj}c_{ti}(c_{rj}c_{si}+c_{ri}c_{sj})}{(\epsilon_j-\epsilon_k)(\epsilon_j-\epsilon_i)}. \tag{14}$$

The evaluation of Eq. (14) for monovalent AHI's is simple. Since $\partial\pi_{r,s}/\partial\alpha_t$ vanishes for AH's, the summation over j can be replaced by consideration of the zero energy MO only. Hence, the first term in Eq. (14) vanishes when either r or s is in the unstarred set, and the second term vanishes when either t, or both r and s are in the unstarred set. These facts lead to the following theorem.

Theorem 9

The mutual polarizabilities $\pi_{r,s}$ in a compound derived by perturbation from a monovalent AHI are independent of the Coulomb integrals α_t of atom t whenever at least two of the three atoms r, s, and t belong to the unstarred set.

The facts which led to this theorem can also be used to greatly simplify the computations when at least two of the atoms r, s, and t are in the starred set, and hence Eq. (19) does not vanish.

Of special interest in the treatment of chemical reactivity is the dependence of the self-polarizability $\pi_{r,r}$ of an atom on the Coulomb integral of various atoms in the molecule. For monovalent AHI's this quantity vanishes when r is unstarred (theorem 9), and otherwise takes the form

$$\frac{\partial \pi_{r,r}}{\partial \alpha_t} = 8\sum_{k>0}\sum_{i<0}\frac{c_{r0}^2 c_{rk}c_{ri}c_{tk}c_{ti}}{(\epsilon_i-\epsilon_k)\epsilon_k}+8\sum_{k>0}\sum_{i>0}\frac{c_{rk}^2 c_{t0}c_{ti}c_{r0}c_{ri}}{\epsilon_k\epsilon_i}.$$

No detailed discussion of the theorems here derived will be given. Many of these theorems are being used in actual calculations,[10b] and their implications will be apparent in connection with such calculations.

[14] See Table I of reference 1b.

Thermoelectric Behavior of Nickel Oxide

G. PARRAVANO*
The Franklin Institute Laboratories for Research and Development, Philadelphia, Pennsylvania
(Received June 7, 1954)

Measurements have been made on the thermoelectric power of several nickel oxide samples containing foreign ions. Using an energy model recently proposed for nickel oxide, the effect of the nature and concentration of additions on the Fermi level, hole concentration, and mobility is derived and discussed. For most of the samples hole concentration can be related to chemical composition. A case of change in valence of the addition induced upon introduction into the matrix is found. The use of the thermoelectric effect to determine impurity in nickel oxide is discussed. The energy scheme of nickel oxide which emerges from this work and that of Morin is emphasized as a drastic departure from the classical model of an electrical semiconductor.

INTRODUCTION

A FUNDAMENTAL problem arising in connection with oxide semiconductors is concerned with the extent to which present concepts of the band theory of solids can be successfully applied to the elucidation of the electronic structure of metal oxides. In the case of nickel oxide a discrepancy between theory and experiment has been repeatedly pointed out in the literature. Although a *d* hole conductor, nickel oxide has an electrical conductivity of the same order of magnitude as cuprous oxide, which does not have unfilled *d* orbitals. Different qualitative explanations had been advanced to circumvent this theoretical difficulty. Recently the problem has received new impetus from the proposal by Morin[1] of a new energy pattern, which has quantitatively explained the experimental data.

It is well known that the thermoelectric power of electrical conductors is a truly thermodynamic quantity, part of which is thermostatic and part kinetic. Theoretical considerations and experimental investigations have shown that in some instances the kinetic contribution to the total effect is negligible.[2] In these cases the thermoelectric power can be considered, to a very good approximation, a thermostatic quantity. Such a fortunate situation occurs with nickel oxide.[1] Therefore thermoelectric investigations on nickel oxide afford a simple, yet interesting, method of deducing thermostatic characteristics of the oxide. Furthermore, it has already been pointed out that measurements of thermoelectric power of semiconductors are not likely to be affected by the state of aggregation of the material.[3] This is a considerable practical advantage when substances not in single crystal form are used.

With these considerations in mind, the present work was undertaken in order to gain more knowledge about the effect of the introduction of foreign ions into the nickel oxide lattice. This communication refers to data on the thermoelectric power of different nickel oxide samples, from room temperature up to 900°C in air. It will be shown that the interpretation of the experimental results in terms of the energy diagram proposed by Morin leads to a quantitative fit of the data, and allows a number of conclusions as to changes of the electronic electrochemical potential and hole mobility as a function of temperature and nature and concentration of additions.

EXPERIMENTAL

Nickel oxide samples were prepared from standardized solutions of cp nitrates, mixed in appropriate amounts, dried at 110°C, and decomposed at 400°C for four hours. The resulting oxides were thoroughly ground and fired at 900°C in air for four additional hours. A pure nickel oxide sample was prepared in a similar way; it was a gray-green material, which had a B.E.T. surface area of 2.2 sq m/g. The chemical determination of the excess oxygen[4] of this sample gave a value of 7×10^{-4} g0/gNiO.

The main source of error in measurements of thermoelectric power lies in the determination of the temperature difference ΔT between the two ends of the sample. In order to reduce this error, the thermal contact between the thermocouple and semiconductor should be good and the thermocouple itself should not appreciably change the temperature distribution in its surroundings. To meet the first requirement a large metal surface, in the form of a platinum foil, was used to contact the sample. The foil was used also as one member of a thermocouple. In this way optimum thermal contact between sample and thermocouple was assured. Furthermore, in order to minimize heat conduction between thermocouple junction and leads, the latter were made out of wires of as small cross section as was compatible with low electrical resistance and chemical homogeneity.

The apparatus finally adopted is shown in Fig. 1. The powdered sample was placed inside a short length of Vycor tubing (7 mm i.d.), between two flat platinum electrodes, which were cemented on lavite supports. Each electrode had a small opening in its center (not

* Present address: Forrestal Research Center, Princeton University, Princeton, New Jersey.

[1] F. J. Morin, Phys. Rev. **93**, 1199 (1954).

[2] C. Herring and M. H. Nichols, Revs. Modern Phys. **21**, 185 (1949); F. J. Morin, Phys. Rev. **83**, 1005 (1951); **93**, 1195, 1199, (1954); C. A. Domenicali, Revs. Modern Phys. **26**, 237 (1954).

[3] H. K. Henisch, Z. physik. Chem. **198**, 41 (1951).

[4] W. Krauss, Z. Elektrochem. **53**, 320 (1949).

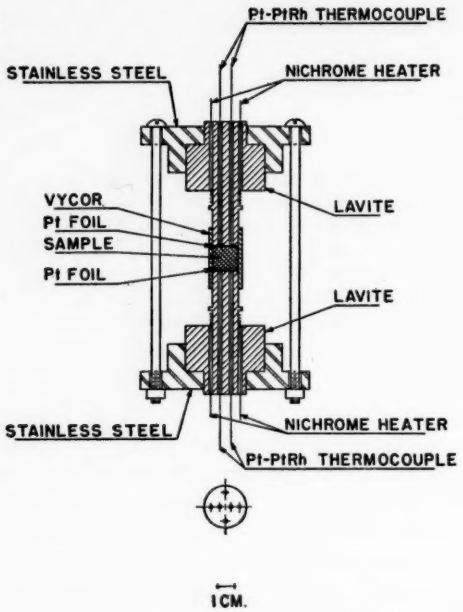

FIG. 1. Thermoelectric cell.

shown in Fig. 1), through which a Pt—PtRh thermocouple was placed. The tip of each of these two thermocouples was electrically insulated from the sample. A second thermocouple was welded onto each electrode on the lavite side of the platinum foil. The eight ends of the thermocouples were soldered to copper leads from the switchboard, and each junction was set in a small paraffin cup immersed in an ice water bath. The two lavite supports were kept aligned and the electrode assemblies were tightly pressed against the sample by means of two stainless steel rings, which were clamped together with two stainless steel bolts. In order to reduce thermal convection currents, the apparatus was mounted horizontally in the furnace. The temperature of the furnace was controlled by an electronic thermoregulator. Supplementary heating was provided by means of two separate coils of nichrome wire, wound around each lavite support.

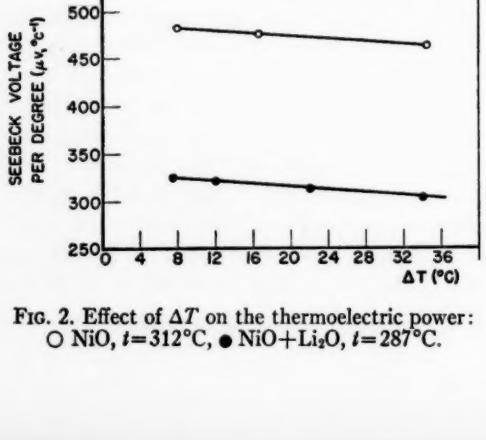

FIG. 2. Effect of ΔT on the thermoelectric power: ○ NiO, $t=312°C$, ● NiO+Li_2O, $t=287°C$.

The temperature of each electrode, T_1 and T_2, could be separately measured by means of the welded thermocouples. The difference in temperature, $\Delta T=T_1-T_2$, between the two electrodes, could be best obtained by direct measurement. For this purpose it was found that the welded thermocouples were unsuitable, because, as the resistance of the sample decreased, an appreciable amount of current would flow through the sample, thus introducing a serious error in the determination of ΔT. This latter therefore was measured with the aid of the central thermocouples, which were electrically insulated from the sample by means of high temperarure cement. The insulation was continually checked

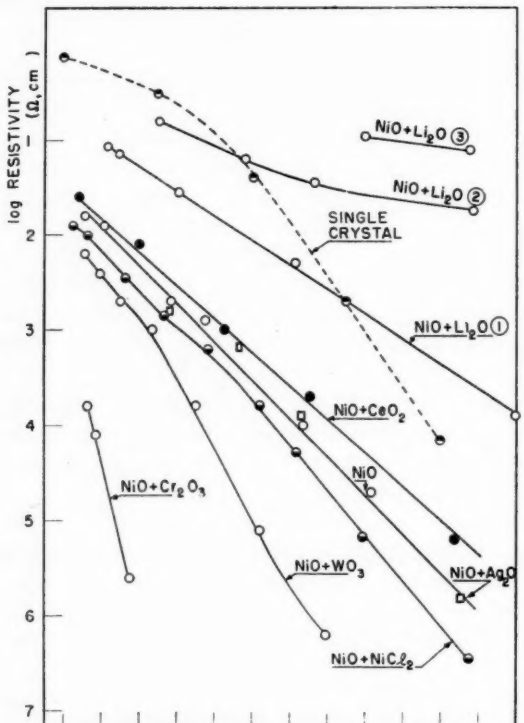

FIG. 3. Direct current resistivity curves for nickel oxide contining foreign ions.

during an experiment. The thermoelectric voltage, developed by each sample, was measured between the two platinum wires of the welded thermocouples, with the aid of a Leeds and Northrup type K-2 potentiometer. A high resistance mirror galvanometer was used as a null instrument. A second K-2 potentiometer was used to measure ΔT and the temperature of one of the two ends of the sample. In high resistance samples ΔT measurements were also checked by separate measurements of T_1 and T_2. The ambient temperature was taken as the average of the temperatures of the two ends of the sample. With these precautions the dependence of the thermoelectric power on temperature gradient was small (Fig. 2). All measurements were carried out with $\Delta T=15-20°C$. For all samples the

cold end of the specimen was found positive (hole conduction). Resistance measurements were taken with a test meter, using a calibrated rheostat. Due to the limited use of resistivity data in this work, the approximations involved in the determination of this parameter by means of the above apparatus, would not invalidate the general conclusions reached in this work. The reproducibility of the measurements was tested by repeated experiments under similar conditions. Data agreed within ±2.5 percent.

EXPERIMENTAL RESULTS

For all samples conductivity data could be fitted to a Boltzmann expression with more than one term (Fig. 3). However, if the degeneracy temperature is calculated with the well known formula:

$$T_g=(h^2/8km^*)(3/\pi)^{\frac{2}{3}}p^{\frac{2}{3}}, \quad (1)$$

where h is the Planck constant, k the Boltzmann constant, p the hole concentration, and m^*, the effective

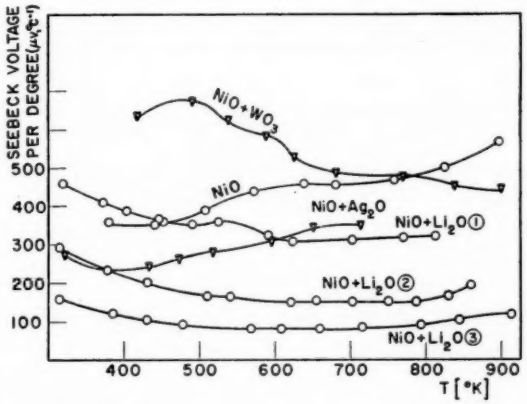

FIG. 4. Seebeck voltage per degree as a function of temperature.

electron mass (equal to the free electron mass), it should be expected that some samples would show degenerate behavior. The expected degenerate behavior was not found experimentally, however. Its absence can be explained by assuming that Eq. (1) is not applicable to nickel oxide and/or that the effective electron mass is much larger than the free electron mass.

The behavior of the conductivity and its temperature dependence as a function of the nature of the added ions is consistent with previous observations.[5] At high temperatures the conductivity of all samples tends to a common value, probably because of the approaching range of intrinsic behavior. No appreciable difference in conductivity from that of the pure oxide was found in samples containing Mg, Th, Al. It is interesting to note that additions of Cl, which conceivably enter the lattice substitutionally, produce effects similar to the introduction of cations of charge greater than two.

[5] Verwey, Haamyman, and Romeijn, Chem. Weekblad. 44, 705 (1948).

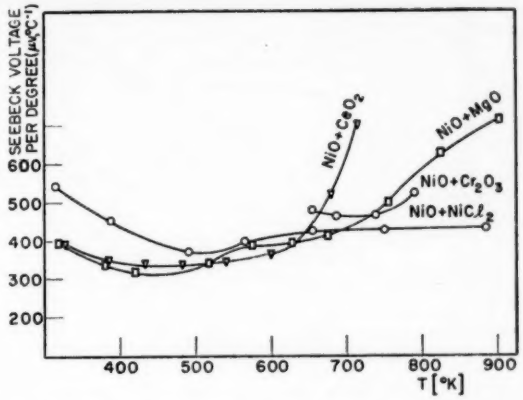

FIG. 5. Seebeck voltage per degree as a function of temperature.

Data on the Seebeck voltage per degree for different samples are shown in Figs. 4 and 5. The results for samples containing alumina and thoria were found to be similar to those for pure nickel oxide.

DISCUSSION

It is assumed, in accordance with the energy pattern proposed by Morin,[1] that nickel ions form localized levels in the energy gap between the filled and empty sp oxygen bands (Fig. 6). This assumption leads, as shown by Morin, to the conclusion that the kinetic energy term of the expression for thermoelectric power is negligible. Thus for a d hole conductor one has

$$QT=E_F, \quad (2)$$

in which Q is the thermoelectric power in volts per degree and E_F is the distance between the Fermi and the filled d levels from nickel ions (Fig. 6). Essentially this energy scheme can be considered a quantitative interpretation of an earlier suggestion by Verwey[6] on the conduction mechanism in nickel oxide. The possibility that electronic conduction in group VIII oxides involves ion pairs, like $Ni^{+2}-Ni^{+3}$, has, of course, been widely accepted in the case of magnetite. Values of E_F, calculated according to Eq. (2) from Seebeck voltage data, are presented in Figs. 7 and 8. These plots indicate the position of the Fermi level at different temperatures and with different impurities and impurity concentrations. For all samples E_F moves upward as the tempera-

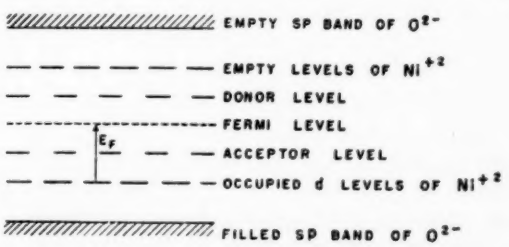

FIG. 6. Energy diagram of nickel oxide (1).

[6] J. H. de Boer and E. J. W. Verwey, Proc. Phys. Soc. (London), 49, (extra part) (1937).

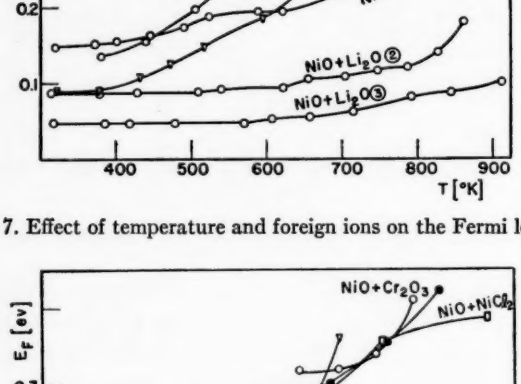

FIG. 7. Effect of temperature and foreign ions on the Fermi level.

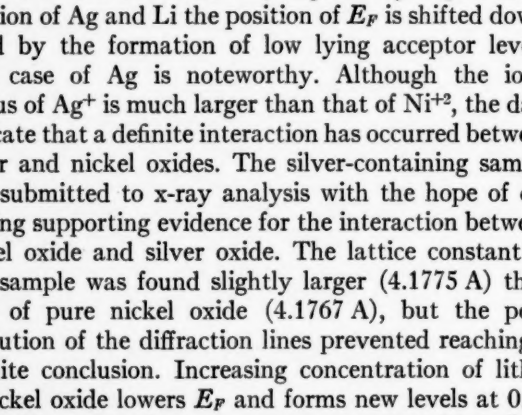

FIG. 8. Effect of temperature and foreign ions on the Fermi level.

ture increases. From the temperature dependency of E_F it is possible to deduce that in pure nickel oxide levels at about 0.13 and 0.30 ev are present, which become ionized at 100°C and 300°C, respectively. Upon introduction of Ag and Li the position of E_F is shifted downward by the formation of low lying acceptor levels. The case of Ag is noteworthy. Although the ionic radius of Ag^+ is much larger than that of Ni^{+2}, the data indicate that a definite interaction has occurred between silver and nickel oxides. The silver-containing sample was submitted to x-ray analysis with the hope of obtaining supporting evidence for the interaction between nickel oxide and silver oxide. The lattice constant of this sample was found slightly larger (4.1775 A) than that of pure nickel oxide (4.1767 A), but the poor resolution of the diffraction lines prevented reaching a definite conclusion. Increasing concentration of lithia in nickel oxide lowers E_F and forms new levels at 0.09 and 0.05 ev. The behavior of sample NiO+Li_2O ① is anomalous at temperatures below 150°C. Additions of tungsten trioxide raise the position of E_F, producing an impurity level at 0.34 ev. Thus these results parallel those obtained from measurements of electrical conductivity, but are free from all the complicating features affecting conductivity data. At temperatures below 230°C, E_F is raised by additions of nickel chloride, while chromia produces a high lying level at 0.32 ev.

For all samples investigated E_F was found to continue to rise with increasing temperature at high temperatures, which confirm the conclusion that the samples have not yet entered the intrinsic region ($E_{F\,(\text{intrinsic})} = 0.96(1)$).

Hole concentration, p, can be estimated from total level density:

$$p = N \cdot \exp(-E_F/kT) \tag{3}$$

where $N = 5.6 \times 10^{22}$ nickel atoms per cc of crystal. Figures 9 and 10 have been computed using Eq. (3). From these plots the effect of the nature and concentration of additions on hole concentration and hole ionization energy can be evaluated. It is found that the concentration of holes is increased and their ionization energy correspondingly decreased by adding monocharged cations to nickel oxide, while the opposite effect occurs upon addition of cations having charges higher than two. The behavior of sample NiO+Li_2O ① is again found to be anomalous. In this sample $[Ni^{+3}] = 9.7 \times 10^{20}$ ions per cc, while $[Li^+] = 6.7 \times 10^{19}$ ions per cc. It seems therefore that when $[Li^+] < [Ni^{+3}]$, the addition of lithia to nickel oxide decreases the hole concentration and raises the position of E_F with respect to the pure oxide. This behavior is consistent with

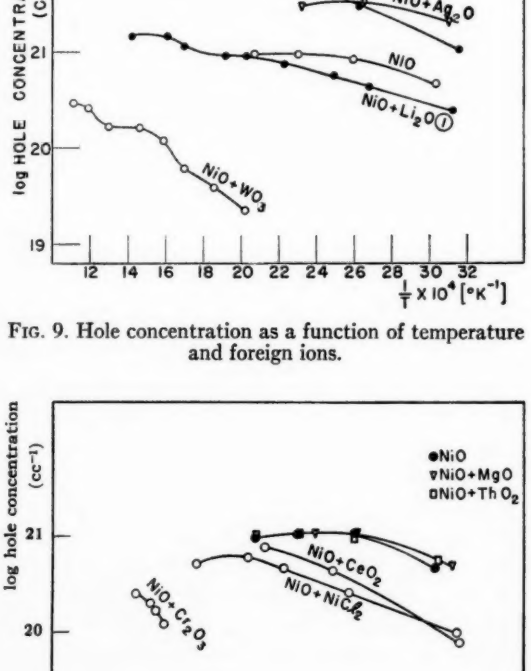

FIG. 9. Hole concentration as a function of temperature and foreign ions.

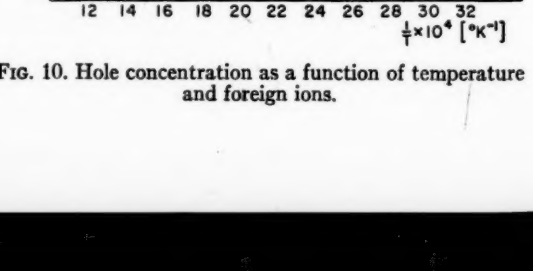

FIG. 10. Hole concentration as a function of temperature and foreign ions.

TABLE I. Additions of foreign ions to nickel oxide.

Sample	Addition concentration (chemical) atoms per cc	Hole concentration (electrical) holes per cc	Holes found (referred to pure NiO) holes per cc	Holes destroyed (referred to pure NiO) holes per cc	Ratio (chemical/electrical)
NiO		9.8×10^{20}			
NiO+Li_2O ①	1.07×10^{20}	8.6×10^{20}		1.2×10^{20}	0.89
NiO+Li_2O ②	5.6×10^{20}	6.3×10^{21}	5.3×10^{21}		0.10
NiO+Li_2O ③	1.02×10^{21}	1.6×10^{22}	1.51×10^{22}		0.068
NiO+Ag_2O	1.59×10^{21}	2.5×10^{21}	1.52×10^{21}		1.04
NiO+Cr_3O_2	6.0×10^{20}	4.0×10^{20}		5.8×10^{20}	1.03
NiO+WO_3	8.0×10^{20}	1.6×10^{20}		8.2×10^{20}	0.98
NiO+CeO_2	1.05×10^{21}	4.3×10^{20}		5.5×10^{20}	1.82
NiO+$NiCl_2$	5.25×10^{20}	4.2×10^{20}		8.2×10^{20}	1.06

data on the lattice constant of solid solutions of NiO +Li_2O.[7] Upon additions of lithia, the lattice constant of nickel oxide increases until $[Li^+]=[Ni^{+3}]$. This is caused by the formation of one Ni^{+2} for every Li^+ introduced, by the filling up of cationic vacancies. Increased amounts of lithia beyond the above value were found to decrease the lattice constant, because of the formation of one Ni^{+3} for every Li^+ introduced.

From Figs. 9 and 10 the concentration of holes can be estimated and compared with the chemical composition of the samples. The results are presented in the following Table I.

The nickel oxide used was not spectroscopically pure. Its main impurity, sodium, was probably responsible for an impurity level at about 0.15 ev with a hole concentration of 9.8×10^{20} holes per cc. The anomalous behavior of sample NiO+Li_2O ① has already been discussed, and, with that data from Table I, the anomalous behavior can almost quantitatively be accounted for. In samples NiO+Li_2O ② and ③, the hole concentration is much larger than the amount of lithium added. No explanation can be offered at present for this discrepancy. However, it must be recalled that the treatment of the thermoelectric data followed in this work requires that $QT\gg kT$, but in samples highly doped with acceptors this is not true. In samples NiO+Li_2O ② and ③ $QT\cong kT$.

For all other samples the ratio of the concentration of addition to the concentration of holes formed or destroyed in the pure oxide by the addition has been computed and is reported in the last column of Table I. This ratio is found to be almost unity, except in the case of the sample containing ceria, but this can be explained by assuming that the solubility limit of ceria in nickel oxide is less than 2.3 percent by weight. The agreement between the concentration of addition and the concentration of holes, formed or destroyed in the pure oxide by the addition, enlarges the heuristic value of the energy model, proposed for nickel oxide inasmuch as this treatment can be used to analyze nickel oxide electrically, with regard to deviations from stoichiometric composition and with regard to impurity content. One more interesting fact emerges from inspection of Table I. In the sample containing tungsten, this impurity was added as tungsten trioxide. However, the data show that, to a very good approximation, for every tungsten atom added one positive hole was destroyed. Therefore the hexavalent tungsten ion has been changed, upon introduction into the nickel oxide lattice, to some sort of trivalent ion. It seems, therefore, that thermoelectric data on "nickel oxide" can be used to reveal the valence acquired by the foreign ion upon introduction into the nickel oxide lattice.

The process responsible for the ionization of acceptors can be visualized as follows:

$$Ni^{+3}\rightleftharpoons Ni^{+2}+p. \tag{4}$$

The oxygen equilibrium, *viz*:

$$4Ni^{+2}+O_2\rightleftharpoons 4Ni^{+3}+2cv+2O^{-2}\ (cv=\text{cationic vacancy}),$$

does not appreciably affect the bulk properties of the oxide up to temperatures of the order of $0.5T_m$(1115°K).[8] At lower temperatures the number of Ni^{+3}, ionized or not, can be considered constant and equal to the excess oxygen. The equilibrium constant of reaction (4) is $K=[Ni^{+3}]/[Ni^{+2}][p]$. Since $[Ni^{+2}]$ is practically constant, from the concentration of holes and the excess oxygen it is possible to calculate a value for K. For pure nickel oxide, at 380° and 450°C, it is found that $K=7.05$ and 63, respectively. From these values, $\Delta F_{653}=-1.5$, $\Delta F_{723}=-3.5$ kcal/mole, $\Delta H=-14.5$ kcal/mole, $\Delta S_{653}\cong\Delta S_{723}=41.4$ eu. These values are highly speculative, but they seem reasonable.

Hole mobility, calculated from conductivity and hole concentration, was found dependent on the type and concentration of impurity added, and the temperature. This agrees with the findings of Morin.[1] Cations with a charge higher than two decrease the mobility and increase its activation energy, while the opposite effects occur with monocharged cations. This result shows that great care should be exercised in deducing changes in charge carrier concentration from conductivity data in metal oxides of the type under discussion. This, unfortunately, has not been widely done in the past, as it has been customary to assume a constant mobility value over large variations of impurity content, tem-

[7] L. D. Brownlee and E. W. J. Mitchell, Proc. Phys. Soc. **B65**, 710 (1952).

[8] Bevan, Shelton, and Anderson, J. Chem. Soc. **1948**, 1729.

perature, and nature of the impurities. It is clear that in the interpretation of future results for this type of oxides, it will be necessary to take into account changes of electron or hole mobility with temperature and impurity content.

CONCLUSION

The picture of nickel oxide which emerges from the work of Morin and the work presented in this paper is a drastic departure from the classical one of a semiconductor (germanium, silicon, zinc, or cuprous oxide). Oxides containing electronic defects derived from *d* electrons do not seem to have a typical conduction band. Rather the conduction electrons migrate along localized levels. The formation of ion pairs for such a process depends on the energetic possibility of the lattice to deviate from the stoichiometric composition. The exchange of electrons within ion pairs is probably constrained by the presence of the large oxygen anion. This constraint is reflected in the low electronic mobility of these oxides, and in the fact that it is necessary to furnish energy to "activate" the electrons, even though they have already been "separated" from the ionic cores by an ionization mechanism. Clearly, under these conditions, electrons are far from free, and such a solid should be considered to be more a semi-insulator than a semiconductor.

ACKNOWLEDGMENTS

I wish to thank Dr. F. J. Morin, of the Bell Telephone Laboratories, for graciously providing me with his data before publication, and Dr. C. A. Domenicali, of this Laboratory, for critical discussions and much helpful advice in the experimental part. Many fruitful discussions on this subject with Dr. D. P. Detwiler are gratefully acknowledged. Finally I would like to thank Dr. F. C. Nix for his interest in this work.

THE JOURNAL OF CHEMICAL PHYSICS VOLUME 23, NUMBER 1 JANUARY, 1955

A Phenomenological Theory of the Soret Diffusion

JAMES A. BIERLEIN
Aeronautical Research Laboratory, Wright Air Development Center, Wright-Patterson Air Force Base, Ohio

(Received February 22, 1954)

The classical Soret diffusion problem is solved analytically for the case of unrestricted composition in a binary liquid system, taking account of the temperature-variation of the density of the mixture. Previous treatments have neglected the phenomenon of thermal dilatation entirely and have not developed a unique general solution which applies both to dilute and to nondilute mixtures.

The rigorous solution derived in the present work is similar in form to de Groot's well-known equation for dilute mixtures, but contains additional parameters characterizing the initial composition of the system and its coefficient of thermal expansion. These parameters disappear in the asymptotic approximation for a vanishing temperature gradient, but this approximation differs from that proposed by de Groot, even for dilute solutions. The asymptotic expression has practical importance for estimating the Soret coefficient and the ordinary diffusion coefficient of a system from experimental data taken during the thermodiffusional unmixing period; some examples of its application in this connection are discussed.

WHEN a temperature gradient is applied to a convection-free binary liquid confined between horizontal plates, the pure Soret effect is observed; a composition gradient develops with time and asymptotically approaches an equilibrium state characterized by the equality of the rates of the opposing effects of ordinary diffusion and thermal diffusion. A mathematical analysis of the transient behavior in this process was first given by de Groot,[1] but his treatment contains two implicit assumptions which render it highly specialized. These assumptions are that the mole fraction of one component of the mixture is essentially unity and that the density of the system is uniform throughout. The first of these conditions restricts the theory to dilute solutions, and the second (implying a vanishing thermal expansion coefficient over a finite temperature range) is logically unsatisfying because it does not correspond to the behavior of any known liquid. Thomaes[2] has reproduced de Groot's result in a slightly different form, and has also indicated the use of a chordal approximation[3] to extend it to the case of systems that are not dilute; he also neglects the phenomenon of thermal expansion.

Inasmuch as the theory of the Soret effect has application in the interpretation of thermodiffusion experiments,[4,5] it is of interest to re-examine the problem with a view to developing a single solution which is ap-

[1] S. R. de Groot, Physica **9**, 699 (1942).

[2] G. Thomaes, Physica **17**, 885 (1951).

[3] R. C. Jones and W. L. Furry, Revs. Modern Phys. **18**, 151 (1946).

[4] S. R. de Groot, J. phys. radium **8**, 129 (1947).

[5] C. C. Tanner, Trans. Faraday Soc. **49**, 611 (1953).

propriate to all regimes of composition and which incorporates a more realistic assumption about the effect of temperature on the density.

THE PROBLEM

Following de Groot, we take as a physical model the ordinary sandwich-type Soret cell consisting of two thermostated plates of infinite lateral extent, with the cooler plate situated below to eliminate convection. At the initial time, a homogeneous binary liquid of known composition is introduced between the plates. It is assumed that the liquid instantly attains the thermal steady-state dictated by the plate temperatures and by its own conductivity; this idealization is justified by the fact, demonstrable both theoretically and experimentally,[5] that the approach to temperature equilibrium is virtually complete in advance of any appreciable unmixing. The problem is to find the composition as a function of time and location in the ensuing one-dimensional diffusion.

The general phenomenological expression[6] applying to this case may be written

$$\Gamma = -\rho D\frac{\partial n}{\partial x} - \rho D' n(1-n)\frac{\partial T}{\partial x} = -\rho D\left[\frac{\partial n}{\partial x} + \sigma n(1-n)\frac{\tau}{a}\right], \quad (1)$$

where

x = distance measured up from bottom (cold) plate, cm
Γ = flux density in x-direction for the component which diffuses down the temperature gradient, mols/cm^2 sec
n = mol fraction of this component
T = temperature, deg
ρ = local mass density of mixture, mol/cm^3
D = ordinary diffusion coefficient, cm^2/sec
D' = thermal diffusion coefficient, cm^2/sec deg
$\sigma = D'/D$ = Soret coefficient, deg^{-1}
τ = temperature difference between the plates, deg
a = separation of plates, cm.

The associated initial condition is

$$\lim_{t\to 0} n = n_0, \quad (0<x<a), \quad (2)$$

(n_0 being the original composition), and the boundary conditions are given by

$$\lim_{x\to 0}\Gamma = 0 = \lim_{x\to 0}\left[\frac{\partial n}{\partial x} + \sigma n(1-n)\frac{\tau}{a}\right], \quad (t>0), \quad (3)$$

and

$$\lim_{x\to a}\Gamma = 0 = \lim_{x\to a}\left[\frac{\partial n}{\partial x} + \sigma n(1-n)\frac{\tau}{a}\right], \quad (t>0), \quad (4)$$

which state that there is no diffusion through the plates. The conventional assumption $\partial T/\partial x = \tau/a = \text{constant}$, used in (1)–(4), presumes a constant value for the thermal conductivity of the liquid. We shall also consider the coefficients D, D', and σ to be constants. Actually, all of these transport properties are functions of both temperature and composition, but the dependence is weak and the assumption of constancy is valid if T and n do not vary by more than a few percent across the cell. This requirement is adequately fulfilled in the typical experimental arrangement, where $\tau \leq 20°$ and the consequent Δn at equilibrium is rarely as great as 0.03 mol fraction.

It is necessary to eliminate the flux Γ as an explicit variable in (1); this may be done through the equation of continuity

$$\frac{\partial \Gamma}{\partial x} = -\rho\frac{\partial n}{\partial t} - n\frac{\partial \rho}{\partial t} = -\left(\rho + n\frac{\partial \rho}{\partial n}\right)\frac{\partial n}{\partial t} - n\frac{\partial \rho}{\partial T}\frac{\partial T}{\partial t}. \quad (5)$$

According to our previous arguments, $\partial T/\partial t$ vanishes. A further simplification results if we neglect $n\partial\rho/\partial n$ in comparison with ρ at the same temperature (i.e., the same x).[7] Then we have

$$\frac{\partial \Gamma}{\partial x} = -\rho\frac{\partial n}{\partial t}. \quad (6)$$

Comparing (1) and (6) gives

$$\frac{\partial n}{\partial t} = D\left[\frac{\partial^2 n}{\partial x^2} + \frac{\sigma\tau}{a}(1-2n)\frac{\partial n}{\partial x} + \frac{\partial n}{\partial x}\frac{\partial}{\partial x}\ln\rho + \frac{\sigma\tau}{a}n(1-n)\frac{\partial}{\partial x}\ln\rho\right]. \quad (7)$$

We write

$$\frac{\partial}{\partial x}\ln\rho = \frac{\partial}{\partial T}\ln\rho\cdot\frac{\partial T}{\partial x} = \frac{R\tau}{a}, \quad (8)$$

in which we recognize that $R = \partial \ln\rho/\partial T = -\partial \ln v/\partial T$

[5] K. E. Grew and T. L. Ibbs, *Thermal Diffusion in Gases* (Cambridge University Press, New York, 1952), pp. 108 ff.

[7] Unfortunately, there is no general rule, relating the density of a mixture to its temperature and composition, which would allow $\partial\rho/\partial n$ to be expressed analytically; and even if such a relation were available, the subsequent mathematical difficulties might be formidable, if not insuperable. The simplification introduced here is incorporated implicitly in some form in all previous treatments of the problem. It requires that the partial molal volumes, $\bar{v}_1$ and $\bar{v}_2$, of the individual components be nearly equal for all temperatures and compositions encountered within the cell, since $\rho = [n\bar{v}_1 + (1-n)\bar{v}_2]^{-1}$ and $\partial\rho/\partial n = (\bar{v}_1 - \bar{v}_2)\rho^2$. This requirement is nearly fulfilled in any system in which the density approximates to a linear function of composition and in which the densities of the pure components do not differ much; mixtures of nonpolar organic liquids afford abundant examples of this class of system. Further, the requirement of nearly-equal partial molal volumes *may* often be fulfilled over certain composition ranges in systems that deviate strongly from the "ideal" behavior just cited: *viz.*, in the neighborhood of maxima or minima in the density-composition diagram. In any case, it is important to recognize the limitations of this simplification and to examine its validity when applying the end results of the present analysis. I am indebted to the referee for calling attention to this point.

is the negative of the local thermal expansion coefficient. Since we deal only with small ranges of temperature and composition, R may be taken to be constant—an excellent approximation for any liquid which is not near its critical point. For convenience, we also define the following dimensionless parameters:

$$\xi=x/a, \quad \tau=Dt/a^2, \quad A=R\tau, \quad p=\sigma\tau. \tag{9}$$

Then (7) becomes

$$\frac{\partial n}{\partial \tau}=\frac{\partial^2 n}{\partial \xi^2}+[A+p(1-2n)]\frac{\partial n}{\partial \xi}+Apn(1-n), \tag{10}$$

and the auxiliary conditions (2)–(4) are

$$\lim_{\tau\to 0} n=n_0, \quad (0<\xi<1), \tag{11}$$

$$\lim_{\xi\to 0}\left[\frac{\partial n}{\partial \xi}+pn(1-n)\right]=0, \quad (\tau>0), \tag{12}$$

$$\lim_{\xi\to 1}\left[\frac{\partial n}{\partial \xi}+pn(1-n)\right]=0, \quad (\tau>0). \tag{13}$$

The last four equations comprise the most general statement of the Soret diffusion problem which is consistent with our knowledge of the process and with the properties of real liquids. In particular, this formulation holds for all ranges of composition and takes account (in the finite constant A) of thermal expansion. The equations used by de Groot as his starting point may be obtained as a special case of the foregoing relations by setting $1-n=1$ and $A=0$.

THE TANGENTIAL APPROXIMATION

We wish to produce a single general solution of Eq. (10), subject only to the conditions (11)–(13). This is not feasible, however, unless some approximate treatment is used. The fact that $n(1-n)$ is quadratic in n is the difficulty that complicates the solution; but this difficulty is easily overcome without compromising the generality of the analysis.

Since the composition at any point in the diffusion cell never changes much from its original value n_0, the quadratic function may be approximated very closely by the linear expression

$$n(1-n)=f(n)\cong n_0(1-n_0)+N(n-n_0), \tag{14}$$

where N stands for $f'(n_0)=1-2n_0\equiv f'(n)=1-2n$. This amounts to replacing the curve $f(n)$, for a short interval in the vicinity of n_0, by its tangent at n_0. The tangential approximation is to be preferred to Thomaes' chordal formulation, not only for its greater simplicity, but also because it eliminates the ambiguity attending the arbitrary choice of the end points of the chord spanning n_0.

Applying the general tangential approximation to (10)–(13) transforms them to

$$\frac{\partial n}{\partial \tau}=\frac{\partial^2 n}{\partial \xi^2}+(A+pN)\frac{\partial n}{\partial \xi}+ApNn+Apn_0^2, \tag{15}$$

$$\lim_{\tau\to 0} n=n_0, \quad (0<\xi<1), \tag{16}$$

$$\lim_{\xi\to 0}\left[\frac{\partial n}{\partial \xi}+pNn+pn_0^2\right]=0, \quad (\tau>0), \tag{17}$$

$$\lim_{\xi\to 1}\left[\frac{\partial n}{\partial \xi}+pnN+pn_0^2\right]=0, \quad (\tau>0). \tag{18}$$

The solution of these equations in a Fourier series is facilitated by rewriting them as functions of a new variable,

$$\phi=\left[n+\frac{n_0^2}{N}\right]\exp[\tfrac{1}{2}(A+pN)\xi]. \tag{19}$$

The subsequent mathematical manipulation is identical with that described by de Groot.[1] The final result is

$$n=n^*-2\pi pn_0(1-n_0)\times\sum_{k=1}^{\infty}\frac{kV_kW_k\exp[-(B^2+k^2\pi^2)\tau-P\xi]}{(B^2+k^2\pi^2)(P^2+k^2\pi^2)}, \tag{20}$$

where n^* is the steady-state term, given either by

$$n^*=\tfrac{1}{2}n_0\left[\frac{p(1+N)\exp(-pN\xi)}{1-\exp(-pN)}+\frac{N-1}{N}\right], \quad (N\neq 0), \tag{21a}$$

or by

$$n^*=\tfrac{1}{2}[1+\tfrac{1}{2}p(\tfrac{1}{2}-\xi)], \quad (N=0), \tag{21b}$$

and the terms in the summation are

$$B=\tfrac{1}{2}(A-pN), \tag{22}$$

$$P=\tfrac{1}{2}(A+pN), \tag{23}$$

$$V_k=1-(-1)^k\exp P, \tag{24}$$

$$W_k=B\sin k\pi\xi+k\pi\cos k\pi\xi. \tag{25}$$

According to Eq. (20), the thermal dilatation of the system affects the transient behavior of the diffusion, but not the equilibrium state; the initial-composition parameter N enters into all the terms. The steady-state term is obviously a generalized form of the expression originally derived by Hiby and Wirtz[8] for dilute solutions and becomes identical with the latter if N is set equal to unity.[9]

[8] J. W. Hiby and K. Wirtz, Physik. Z. 41, 77 (1940).

[9] A very simple test can be made to check the accuracy of the steady-state solutions (21a) and (21b). If Eq. (1) is solved for the case of zero flux, the result is

$$[n^*/1-n^*]_{\xi=\xi}=[n^*/1-n^*]_{\xi=0}\exp(-p\xi),$$

which is an exact solution for the steady-state composition profile,

SOME WORKING EQUATIONS

Although illuminating from the theoretical standpoint, the exact series solution is cumbersome to use. However, certain convenient approximate relations can be derived from it.

If we consider the usual ranges of the physical and operating parameters that determine B and P (*viz.*, $-0.002<R<0$, $0.01>\sigma>0$, $20>\tau>0$, $1>N>-1$), it is clear that B and P will typically lie inside the limits ± 0.1. Therefore, the squares of these constants are negligible compared with $k^2\pi^2$, and it is apparent that the infinite series in Eq. (20) converges so rapidly that all terms after the first may be discarded. Then we have

$$n=n^*-\frac{2pn_0}{\pi^3}[1-n_0][1+\exp P]\times[B\sin\pi\xi+\pi\cos\pi\xi][\exp(-P\xi)]\times[\exp(-t/\theta)], \quad (26)$$

where θ is identical with de Groot's relaxation time and is given by

$$\theta=a^2/\pi^2D. \quad (27)$$

The discrepancy between (20) and (26) is not more than a few parts in a thousand, even for the extreme values of B and P.

If we impose a slightly more stringent limitation on the permissible size of B and P, we may write $V_1\cong 2$, $W_1\cong\pi\cos\pi\xi$, and $\exp(-P\xi)\cong 1$. We may also represent n^* by the expression

$$n^*=n_0[1+p(1-n_0)(\tfrac{1}{2}-\xi)], \quad (28)$$

which is the limiting law of (21a) as p decreases and which holds with negligible error for the customary small values of p. Then (26) becomes

$$n=n_0\left[1+p(1-n_0)(\tfrac{1}{2}-\xi)-\frac{4p}{\pi^2}(1-n_0)(\cos\pi\xi)\exp(-t/\theta)\right]. \quad (29)$$

The last equation is obviously the asymptotic form of the more general solution Eq. (26) for the case of vanishing τ. Note that the parameter describing thermal expansion does not appear in the asymptotic approximation; this result could not have been predicted with certainty in advance of a rigorous solution of the problem. A useful expression for the composition gradient at any time and place in the cell is

$$\frac{\partial n}{\partial\xi}=-pn_0(1-n_0)\left[1-\frac{4}{\pi}(\sin\pi\xi)\exp(-t/\theta)\right], \quad (30)$$

obtained directly by differentiation of (29).

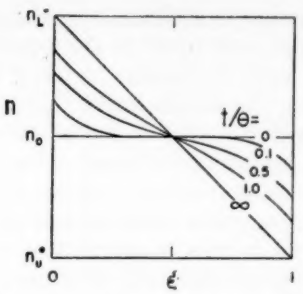

FIG. 1. Soret diffusion under a small temperature difference.

$$n_L^*=n_0\left[1+\frac{p}{2}(1-n_0)\right],\quad n_U^*=n_0\left[1-\frac{p}{2}(1-n_0)\right].$$

Figure 1 shows composition profiles in a typical Soret diffusion at small τ, calculated for various times after the start according to Eq. (29). The graph affords ready visualization of the essential features of the process. The behavior at low values of t/θ, in which the unmixing is confined principally to the vicinity of the plates, is in harmony with the "border effect" found experimentally by Tanner.[10]

APPLICATIONS

The phenomenological Soret theory finds its principal value in providing rational equations to which experimental data may be fitted for the purpose of determining both p and θ (hence, σ and D) from a series of measurements describing the approach to equilibrium. This type of analysis has been attempted by de Groot[4] and by Tanner.[5] However, they use de Groot's theory indiscriminately for solutions that are not dilute. Furthermore, even in the case of dilute solutions, their treatments are subject to the objection that they are based on the oversimplified relaxation approximation proposed by de Groot as a working version of his theory. According to this approximation, the fraction of the equilibrium change accomplished at any place within a specified elapsed time is independent of position and is a function of time only; the transient composition profiles then have the same shape (almost linear) as the steady-state distribution. As shown by Fig. 1, this relation is a poor representation of the facts—especially in the earlier stages of the diffusion—and is too crude to yield accurate quantitative results. The present theory affords an improved basis for interpreting data in all composition ranges.

although the constant coefficient of the exponential is undetermined. If the values of n^* predicted by (21a), or by (21b) for the special case $n_0=\frac{1}{2}$, are inserted in this equation, agreement of the two members is obtained to at least five significant figures, for all values of ξ and for any value of p lying in the physical range of interest, i.e., $0<p\lesssim 0.2$. Since the approximate solutions also satisfy the necessary condition $\int_0^1 n d\xi=n_0$, this excellent fit is direct proof that negligible error is introduced into the steady-state part of the solution by the approximations made in the differential equations; and by indirection, it gives confidence in the transient part also, since the tangential approximation is exact for the initial time and has its maximum error for the steady-state, when maximum unmixing has occurred.

[10] C. C. Tanner, Trans. Faraday Soc. **23**, 75 (1927).

It is instructive to indicate how the present theory could be applied with profit to the experiments treated by de Groot and by Tanner. In using the theory for data reduction, the simple forms Eq. (29) or Eq. (30) are preferable to Eq. (26) or its derivative, in order to minimize the mathematical labor of curve fitting. This consideration points up the practical importance of using an experimental temperature difference sufficiently small to supress B and P to a negligible level, so that Eq. (29) is valid; this precaution has the additional advantage of obviating the need for independent information about the magnitude of the thermal expansion coefficient. In what follows, we shall assume the condition of small τ to be fulfilled.

In the problem analyzed by de Groot, the difference in composition at the plates is given for known times. Use of de Groot's relaxation theory in this situation leads to the expression

$$\Delta n = -pn_0[1-\exp(-t/\theta)], \tag{31}$$

in which $\Delta n = n_U - n_L$, the observed composition difference between the cell contents at the upper and lower plates. The subsequent mathematical manipulations amount to fitting the equation to two or more data points to determine the best statistical values of p and θ. Applying Eq. (29) to the same problem gives

$$\Delta n = -pn_0(1-n_0)\left[1-\frac{8}{\pi^2}\exp(-t/\theta)\right]. \tag{32}$$

Even for the case of dilution solutions, where $1-n_0$ may be set equal to unity, the two formulations are seen to differ by the presence of the coefficient $8/\pi^2$ which multiplies the exponential in the more accurate expression.

Tanner uses a schlieren method in which the composition gradients in the system are inferred from the angular deviation of a thin collimated beam of light, allowed to enter the cell normal to one of its side-walls. The total gradient in refractive index which causes the bending of the light is composed of two parts: one due to the temperature gradient and sensibly constant since the composition change is small, the other due to the composition gradient at constant temperature and variable in time as the unmixing proceeds. Mathematically, this is written

$$d\mu/d\xi = (\partial\mu/\partial n)(dn/d\xi) + \tau(\partial\mu/\partial T), \tag{33}$$

where μ stands for the refractive index; both of the partial differential coefficients are constants of the mixture determined in advance of the diffusion experiment. Using Fermat's principle for the case of small deviations and linear refractive index gradients, Tanner attributes that part of the total angular deviation which is not accounted for by the temperature gradient to a constant composition gradient. The subsequent analysis is based substantially on Eq. (31), in which Δn is taken equal to the experimental $dn/d\xi$.

The difficulty in Tanner's analysis is that the instantaneous composition profiles are not linear during the unmixing period. The residual bending of the light ray cannot be identified with any single composition gradient, but is instead the over-all contribution of all the gradients encountered by the ray in its curved path between the entry plane ξ_1 and the exit plane ξ_2. Tanner tacitly recognizes this difficulty and tries to take care of it by adding to each observed deviation an arbitrary constant, selected to give the best fit of Eq. (31) to the data. This procedure has no basis in theory and moreover is not adequate in practice, since Tanner gets different results for a given system upon changing the dimensions of his cell. Obviously a beam-path integration technique is needed here, and this may be developed through the use of Eq. (30). Referring to Eq. (33), we substitute into it the theoretical value of $dn/d\xi$ and obtain

$$d\mu/d\xi = -pK_1\left[1-\frac{4}{\pi}(\sin\pi\xi)\exp(-t/\theta)\right]+K_2, \tag{34}$$

where $K_1 = n_0(1-n_0)(\partial\mu/\partial n)$ and $K_2 = \tau\partial\mu/\partial T$. The total refractive index gradient is also given by the Fermat small-angle relation

$$d\mu/d\xi = a^2 d^2\xi/dz^2 \tag{35}$$

in which z is the length of the cell in the direction of travel of the light ray. If both sides of Eq. (35) are multiplied by $d\xi/dz$, the resulting expression is

$$\frac{d\mu}{d\xi}\frac{d\xi}{dz} = a^2\left(\frac{d^2\xi}{dz^2}\right)\frac{d\xi}{dz} = \frac{1}{2}a^2\frac{d}{dz}\left(\frac{d\xi}{dz}\right)^2 \cong \frac{1}{2}\frac{d}{dz}(\alpha)^2, \tag{36}$$

α being the local angular deviation of the beam, which for small angles is identical with the slope of the beam path, $ad\xi/dz$. Comparing Eq. (34) and Eq. (36) leads to the equation

$$\tfrac{1}{2}\alpha_2^2 - K_2(\xi_2-\xi_1) = -pK_1 \times\left[(\xi_2-\xi_1)+\frac{4}{\pi^2}(\cos\pi\xi_2-\cos\pi\xi_1)\exp(-t/\theta)\right], \tag{37}$$

where α_2 is the total deviation suffered by the emergent beam. Since the entrance and exit points ξ_1 and ξ_2 can be observed experimentally, the equation contains only p and θ as unknowns. The formal similarity of Eq. (37) to Eq. (32) is evident, and the statistical fitting process is relatively simple.

I am grateful to several colleagues, especially Dr. L. A. Wood and Mr. K. Scheller, for helpful discussion and criticism.

Photoconductivity and Crystal Imperfections in Cadmium Sulfide Crystals. Part I. Effect of Impurities

RICHARD H. BUBE AND S. MILTON THOMSEN
Radio Corporation of America, RCA Laboratories Division, Princeton, New Jersey
(Received March 29, 1954)

The conductivity and photosensitivity of cadmium sulfide crystals can be controlled by the incorporation of suitable impurities. The conductivity and photosensitivity are increased by the incorporation of a halide or a trivalent cation, and decreased by the incorporation of copper or silver. A possible mechanism by which such impurities may produce the observed effects on the photoconductivity is presented.

INTRODUCTION

RESEARCH in the field of luminescence of zinc sulfide phosphors has shown that major luminescence effects are associated with the incorporation of copper or silver as activators.[1–3] The effective operation of these activators usually requires, however, that a halide[4–7] or a trivalent cation be incorporated also, presumably to act as co-activator in enabling the activator to be incorporated in the proper manner in the crystal. This paper reports the results of incorporating these same types of impurities in cadmium sulfide crystals, where major effects are observed on the conductivity and photosensitivity.

Veith[8] and Goercke[9] have reported on the effect of copper and silver impurities on the photoconductivity of cadmium sulfide. The results described in the present paper indicate the same type of effects as those reported by Veith and Goercke, but show that the effects may be obtained over a much wider range of conductivity, and that there is an intimate connection between the presence of halide and the effects due to copper or silver.

The conductivity of cadmium sulfide crystals is increased by the incorporation of a halide or a trivalent cation. Simultaneously, the photosensitivity (measured in terms of the number of charges passed through the crystal per photon absorbed) is increased. The incorporation of copper or silver in a halide-containing crystal decreases to some extent both the conductivity and the photosensitivity.[9a]

[1] R. H. Bube, Phys. Rev. **80**, 655 (1950).
[2] F. A. Kroeger and J. Dikhoff, Physica **16**, 297 (1950).
[3] R. H. Bube, Phys. Rev. **90**, 70 (1953).
[4] F. A. Kroeger and J. E. Hellingman, J. Electrochem. Soc. **93**, 156 (1948); **95**, 68 (1949).
[5] Kroeger, Hellingman, and Smit, Physica **15**, 990 (1949).
[6] R. H. Bube, J. Chem. Phys. **19**, 985 (1951).
[7] R. H. Bube, J. Chem. Phys. **20**, 708 (1952).
[8] W. Veith, Compt. rend. **230**, 947 (1950).
[9] P. Goercke, Ann. d. Telecommunications **6**, 325 (1951).
[9a] Since this paper was submitted for publication, a paper by Kroeger, Vink, and van den Boomgaard has appeared in Z. physik. Chem. **203**, 1 (1954), describing the control of conductivity in CdS crystals with Ga, In, Sb, Cl, and Ag impurity.

PREPARATION OF MATERIALS

Crystal Growth

Crystals of CdS were grown from the vapor phase reaction between cadmium vapor and hydrogen sulfide in a modification of the general method of Frerichs.[10] Figure 1 is a schematic drawing of the crystal-growing furnace. Cadmium, vaporized in the first zone of a three-zone furnace, is carried by a carrier gas (hydrogen, nitrogen, helium, etc.) into the second warmer zone of the furnace, where the reaction with hydrogen sulfide occurs. The crystals are deposited in the second zone and between the second and third zone, the third zone being slightly cooler than the second.

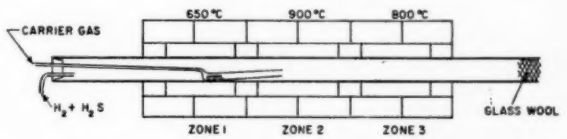

FIG. 1. Schematic drawing of the furnace and experimental arrangement for the preparation of cadmium sulfide crystals.

X-ray analysis[11] of the crystals shows that most of the crystals are single, with the hexagonal structure.

Incorporation of Halide

Halide may be conveniently introduced into the crystals during their growth by passing the carrier gas for the cadmium vapor through a source of halide, such as a solution of hydrochloric acid, bromine water, or a container of iodine. The control of the proportion of halide incorporated by varying the concentration of the halide source is difficult, and generally the crystals formed will have a wide range of halide proportions, regardless of the concentration of the halide source. In the work described in this paper, a plentiful supply of halide was provided in all cases, so that the crystals incorporated as much halide as they would tolerate under the preparation conditions.

[10] R. Frerichs, Phys. Rev. **72**, 594 (1947).
[11] X-ray analysis by J. A. Amick.

Incorporation of Copper or Silver

After the cadmium sulfide crystals were grown in the presence of halide, copper or silver was incorporated in a subsequent treatment. The crystals were immersed in a solution of copper or silver salt to permit reaction with the cadmium sulfide. After a suitable time in the solution, the crystals were washed, dried, and then heated to 700°C in an inert atmosphere to diffuse in the copper or silver. Experiments performed on crystals treated with copper in this way, involving the measurement of photoconductivity properties as increasing proportions of the crystal were dissolved away, indicated fairly uniform penetration of the impurities into the cadmium sulfide crystals.

Incorporation of Trivalent Cations

Trivalent cations, such as aluminum, gallium, and indium, were incorporated[12] in cadmium sulfide crystals by the same diffusion methods described above, after the desired proportion of metal had been evaporated on the surface of the crystals.

RESULTS

Crystals prepared without any impurity have a low conductivity and a low photosensitivity. Table I gives the data showing the effects on the resistivity caused by incorporating (1) chloride; (2) aluminum, gallium, or indium; and (3) copper, in crystals containing chloride.

TABLE I. Dependence of resistivity on impurity.

Impurity added	Dark resistivity, ohm cm	Light resistivity, ohm cm[a]
None	10^{12}	10^{8}
Chloride[b]	4×10^{-1}	$4\times10^{-1}-$
Chloride plus following ppm Cu[c]		
1	20	17
2	70	50
4	10^{7}	3×10^{3}
10	10^{8}	5×10^{3}
Following ppm Al[d]		
10	10^{12}	10^{8}
20	10^{11}	2×10^{5}
40	10^{9}	5×10^{3}
50	10^{8}	2×10^{3}
60	10^{6}	10^{3}
100	10^{3}	2×10^{2}
500	10^{2}	$10^{2}-$
Following ppm Ga[d]		
1	10^{10}	3×10^{4}
2	10^{9}	2×10^{4}
4	10^{5}	5×10^{3}
10	10^{4}	10^{3}
20	10^{2}	$10^{2}-$
Following ppm In[d]		
1	10^{9}	2×10^{4}
3	10^{6}	2×10^{3}
4	10^{5}	10^{3}
10	10^{2}	$10^{2}-$

[a] For 9 foot-candle incandescent illumination.
[b] Proportion of chloride incorporated under conditions where crystals may incorporate all the chloride possible during their growth; about 5 ppm.
[c] Total weight of copper in the solution with which the crystals were treated; not necessarily the proportion of copper incorporated. There is no change in resistivity in dark or light for proportions of copper greater than 10 ppm for this type of treatment.
[d] Total weight of metal evaporated on the surface of the crystal; not necessarily the proportion of metal incorporated.

[12] These preparations were made by C. J. Busanovich.

Detailed measurements on the photoconductivity characteristics of the "pure" crystals and of the crystals containing chloride are presented in Part II of the present paper.[13]

The decay time for the photocurrent is also very dependent on the presence of impurity. The decay time for the "pure" cadmium sulfide crystals may be as small as a fraction of a millisecond, whereas the decay time for conducting crystals containing halide may be as large as a hundred milliseconds.

DISCUSSION

The observation of an increasing photosensitivity and decay time with increasing proportions of incorporated halide requires that the formation of centers with small capture cross section for electrons be, in some way, associated with the incorporation of halide. A formal model is presented here, which at least demonstrates one mechanism by which this association may be achieved. Evidence for the existence of centers of such small capture cross section in several photoconducting materials has been summarized by Rose.[14]

In a "pure" crystal, there is a low conductivity, a low photosensitivity, and a small decay time. The low conductivity is found because there are few centers to provide electrons for the dark current. Excitation of an electron produces an electron in the conduction band and a hole which may be trapped at a defect or other crystal imperfection where recombination with a free electron is highly probable. The result is a small decay time and a consequently low photosensitivity. Such a process is shown schematically in Fig. 2a. In the absence of light, the Fermi level is located at some position in the forbidden band determined by the type and concentration of levels in the crystal itself. Let it be assumed that these levels are of such a nature that those below the Fermi level (at room temperature, and under these conditions) are neutral when an electron has been captured, and that those above the Fermi level are neutral when empty. Upon excitation, the hole formed is captured by a center which becomes positive when the hole has been captured. This charged center would have a large capture cross section for the free electron.

As the proportion of halide incorporated is increased, the conductivity increases, the photosensitivity increases, and the decay time increases. The incorporation of a halide ion in place of a sulfide ion results in the formation of a center consisting of the halide ion and an electron bound to the center:

$$S^{-2}=Cl^{-1}+e. \qquad (1)$$

[13] R. H. Bube, following article, J. Chem. Phys. **23**, 18 (1955).
[14] A. Rose, RCA Rev. **12**, 362 (1951).

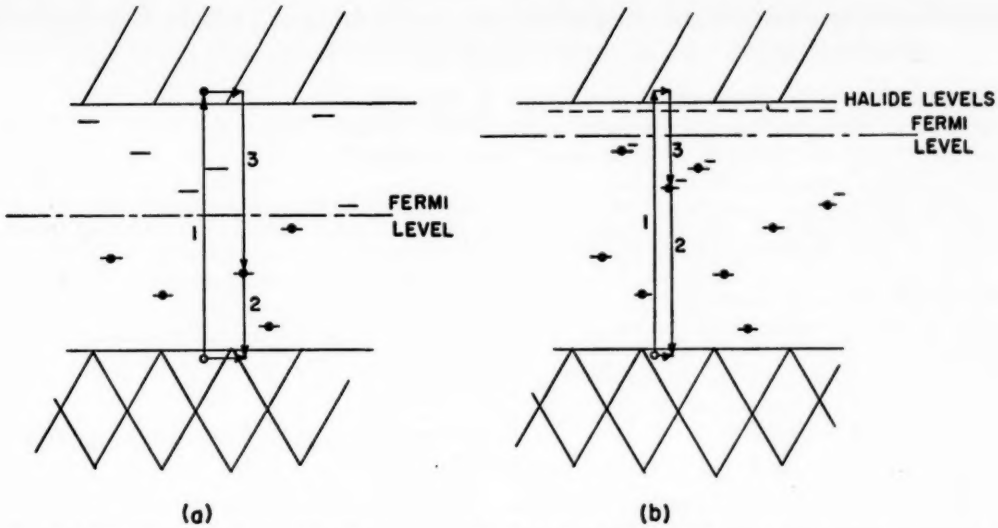

FIG. 2. (a) Excitation and recombination processes for "pure" cadmium sulfide crystals at room temperature. (b) Excitation and recombination processes for cadmium sulfide crystals with halide impurity.

As will be shown in Part II of this paper,[13] the binding energy of this electron is sufficiently small so that practically all of the halide centers are ionized at room temperature. The electrons contributed in this manner increase the conductivity. A portion of these electrons, however, will fill up levels in the forbidden gap, raising the Fermi level to agree with the new concentration of charge carriers in the conduction band. The centers which capture these electrons become negatively charged. As indicated in Fig. 2b, excitation produces holes which may now be trapped in centers, which before capture of a hole are negatively charged and after capture of a hole are neutral. Hence the capture cross section of these centers is likely to be high for holes, because of the attractive Coulomb field, and low for electrons, because of the absence of a Coulomb field. The capture cross section of these centers, therefore, is much smaller for free electrons than the capture cross section of the positively-charged centers found in the "pure" crystals. The result is an increased decay time and hence an increased photoconductivity. Exactly the same type of mechanism may be proposed for the incorporation of a trivalent cation, where a trivalent cation substituted for a cadmium ion forms a center consisting of the trivalent cation with an electron loosely bound in an orbit about the center:

$$Cd^{+2}=Al^{+3}+e. \tag{2}$$

As the proportion of copper or silver incorporated in a conducting crystal is increased, the conductivity decreases, the photosensitivity decreases, and the decay time decreases. The incorporation of copper or silver increases the concentration of levels in the forbidden gap which are able to accept electrons from the halide centers. An increase in red sensitivity accompanies the incorporation of copper, indicating that the copper level lies about 1.5–2 ev below the conduction band. The ionized halide (or trivalent cation) center and the monovalent copper or silver center form a stable neutral pair in the crystal:

$$Cd^{+2}+S^{-2}=Cu^{+1}+Cl^{-1}, \tag{3}$$

$$2Cd^{+2}=Cu^{+1}+Al^{+3}. \tag{4}$$

If a hole is captured by such a copper or silver center, a positively charged center would be formed with a relatively large capture cross section for free electrons. The net result of the incorporation of copper or silver would be a decrease in conductivity because of a decrease in the number of halide centers with electrons to contribute to the dark current. Such a decrease in conductivity would again lower the Fermi level so that the number of centers with small capture cross section would be decreased, with a corresponding decrease in photosensitivity and decay time.

If such a specialized model as has been discussed in the previous paragraphs were to have any physical reality, it would be expected that the room-temperature location of the Fermi level in the "pure" crystals would correspond with a minimum photosensitivity, and the photosensitivity would be expected to increase for either decreasing or increasing temperature. The measurements given in Part II of this paper[13] show that such a variation of photosensitivity with temperature is experimentally observed.

The authors wish to express their appreciation to Dr. A. Rose for helpful discussions.

Photoconductivity and Crystal Imperfections in Cadmium Sulfide Crystals. Part II. Determination of Characteristic Photoconductivity Quantities

RICHARD H. BUBE
Radio Corporation of America, RCA Laboratories Division, Princeton, New Jersey
(Received March 29, 1954)

From measurements of photoconductivity on low conductivity "pure" cadmium sulfide single crystals, and on high conductivity cadmium sulfide crystals with chloride impurity, values for the following characteristic photoconductivity quantities have been obtained: (1) concentration of levels in the forbidden gap, (2) energy distribution of such levels, (3) attempt-to-escape frequency for electrons in traps, (4) capture cross section of traps, (5) capture cross section of recombination centers, (6) mobility for electron charge carriers, and (7) binding energy for the electron held in an orbit around the chloride ion in conducting crystals.

INTRODUCTION

THE control of the conductivity and photosensitivity of cadmium sulfide crystals by the incorporation of suitable impurities has been discussed in Part I of the present paper.[1] Part II, presented here, discusses various measurements of photoconductivity properties: (1) spectral response, (2) thermally stimulated current, (3) conductivity as a function of temperature, (4) photocurrent as a function of light intensity at various temperatures, (5) photocurrent decay time as a function of light intensity at various temperatures. From these measurements are deduced the values of a number of characteristic photoconductivity quantities for cadmium sulfide crystals, without added impurity, and with a high proportion of chloride impurity.

A summary of previous photoconductivity measurements of such values, as well as the development of the type of mathematical formulation used in this paper, has been presented by Rose.[2]

THEORY

Photoconductivity

The fundamental equation expressing the gain of a photoconductor is:

$$\text{Gain}=\frac{\text{Number of charges passed through crystal}}{\text{Number of photons absorbed}}. \quad (1)$$

Excitation produces a free electron and a hole which is rapidly trapped. The free electron moves through the crystal, under the influence of the field, to the positive electrode, and hence out of the crystal. At the time that an electron moves out of the crystal at the positive electrode, another electron enters the crystal from the negative electrode. Charge continues to flow through the crystal until recombination occurs between the trapped hole and a free electron. Gains much larger than unity may be obtained by this mechanism; values of the gain as high as 10^4 have been observed in cadmium sulfide.

The gain may be expressed in terms of the lifetime of a free electron, τ, and the transit time of an electron between electrodes, t:

$$\text{Gain}=\tau/t. \quad (2)$$

If t is expressed in terms of the mobility, μ, the applied voltage, V, and the distance between electrodes, L, Eq. (2) for the gain, G, may be converted to:

$$G=(\tau\mu V)/L^2. \quad (3)$$

The true lifetime used in Eqs. (2) and (3) will be equal to the experimentally measured decay time only at high conductivities, such that the concentration of free electrons is greater than the concentration of trapped electrons. Under these conditions the effect of trapping on the measured decay time is effectively eliminated. A measurement of decay time for such high conductivity conditions provides data for the calculation of the mobility[3] from Eq. (3), and also for the calculation of the capture cross section of recombination centers according to the following equation:

$$\tau=1/(vsn_c), \quad (4)$$

where v is the thermal velocity of the electrons, s is the capture cross section of a recombination center for electrons, and n_c is the concentration of electrons in the conduction band (for these conditions, n_c is equal to the concentration of available recombination centers).

For any center, the capture cross section is related directly to the attempt-to-escape "frequency," f,[2,4] which is actually the product of the true frequency with which an escape is possible and the transition probability of such an escape occurring:

$$f/s=10^{26}(T/300)^2. \quad (5)$$

[This equation may be derived from Eqs. (9) and (18) following.] This attempt-to-escape "frequency" enters the expression for the probability, P, of an electron escaping from a center in the following manner, ac-

[1] R. H. Bube and S. M. Thomsen, preceding article, J. Chem. Phys. **23**, 15 (1955).
[2] A. Rose, RCA Rev. **12**, 362 (1951).
[3] R. W. Smith, RCA Rev. **12**, 350 (1951).
[4] N. F. Mott and R. W. Gurney, *Electronic Processes in Ionic Crystals* (Oxford University Press, London, 1940), p. 108.

cording to Randall and Wilkins[5]:

$$P=f\exp(-E^*/kT), \tag{6}$$

where E^* is the thermal activation energy for escape from the center, and T is the absolute temperature.

Fermi-Level Analysis

The location of the Fermi-level may be determined at a given temperature for a semiconductor simply from the conductivity. The conductivity, σ, may be used to determine the concentration of charge carriers:

$$\sigma=n_c e\mu; \tag{7}$$

then E_F, the energy difference between the lower edge of the conduction band and the location of the Fermi-level, can be calculated as follows:

$$n_c/N_c=\exp(-E_F/kT). \tag{8}$$

In this equation, N_c is the concentration of levels present in the lowest kT-wide part of the conduction band; it is relatively simple to show[2] that:

$$N_c=f/sv. \tag{9}$$

The ratio n_c/N_c represents the probability of the levels in the lowest kT-wide part of the conduction band being filled. This probability is also given by the Fermi-function, which appears on the right side of Eq. (8) in the approximation which obtains when $\exp(E_F/kT)$ is very much larger than unity.

Knowledge of the location of the Fermi-level from conductivity data permits the correlation of conductivity effects, under variations of external conditions, with the levels present in the forbidden gap in the immediate neighborhood of the Fermi-level.

If Eq. (8) is substituted in Eq. (7), including the fact that $N_c=10^{19}(T/300)^{\frac{3}{2}}$ and that $\mu=\mu_0(T/300)^{-\frac{3}{2}}$, where μ_0 is the value of mobility at room temperature (assuming variation of mobility with temperature to be caused only by lattice scattering),

$$\sigma=10^{19}e\mu_0\exp(-E_F/kT). \tag{10}$$

The slope of a plot of $\ln\sigma$ *vs* $1/T$, calculated from Eq. (10) is:

$$\text{slope}=T/k(dE_F/dT)-E_F/k. \tag{11}$$

This slope will be constant for either of two conditions: (a) E_F is not a function of temperature; the slope then equals $-E_F/k$; (b) $E_F=aT+b$; the slope then equals $-b/k$. Straight portions of $\ln\sigma$ *vs* $1/T$ plots must therefore be subjected to further analysis to separate out cases where the constant slope is due to a constant fermi-level from cases where the constant slope is due to a linear dependence of Fermi-level on temperature.

[5] J. T. Randall and M. H. F. Wilkins, Proc. Roy. Soc. (London) **A184**, 366, 390 (1945).

Correlation of Fermi-Level with Donor (Acceptor) Activation Energy

If it is assumed that there is a concentration of N_D donors of one type of impurity in an otherwise perfect crystal, and if E is the energy difference between the lower edge of the conduction band and the location of the donor levels, the equilibrium value of n_c will be determined by the equation:

$$(N_D-n_c)f\exp(-E/kT)=svn_c^2. \tag{12}$$

Eliminating n_c by means of Eq. (8), it is possible to solve for E_F in terms of E. In the case of only partial ionization of the donors, the solution is:

$$E_F=E/2+\frac{kT}{2}\ln(N_c/N_D). \tag{13}$$

For this case, therefore, the values of E_F calculated from a plot of $\ln\sigma$ *vs* $1/T$ will be a linear function of T, with intercept equal to the slope of the $\ln\sigma$ *vs* $1/T$ plot, which is equal also to one-half the donor activation energy. The calculated Fermi-level is independent of temperature only for the special case of $N_D=N_c$.

In most real crystals, however, it is reasonable to assume that there are levels in the forbidden gap near the filled land, which are able to accept electrons. If it is assumed that the concentration of such levels is N_A, and that such levels are completely filled, the equilibrium value of n_c may be expressed:

$$(N_D-N_A-n_c)f\exp(-E/kT)=svn_c(n_c+N_A). \tag{14}$$

Again using Eq. (8) to eliminate n_c, E_F is given as a function of E by the following equation for the approximation where $n_c\ll N_A$:

$$E_F=E+kT\ln[N_A/(N_D-N_A)], \tag{15}$$

and by the following equation for the approximation where $n_c\gg N_A$:

$$E_F=E/2+kT/2\ln[N_c/(N_D-N_A)]. \tag{16}$$

In either case, the calculated Fermi-level will be a function of temperature except for a particular relationship between donors and acceptors: $N_D=2N_A$ for the case of Eq. (15), and $N_D-N_A=N_c$ for the case of Eq. (16).

In the case of an *intrinsic* semiconductor, the Fermi-level will be given in terms of the energy of the forbidden gap, E_G, by the equation:

$$E_F=E_G/2+3kT/4\ln(m_e/m_h), \tag{17}$$

where m_e is the effective electron mass, and m_h is the effective hole mass. Equation (17) follows directly from the fact that we must substitute for N_D in Eq. (13) the quantity N_v, the number of levels in the uppermost kT-wide part of the valence band, and that both N_c

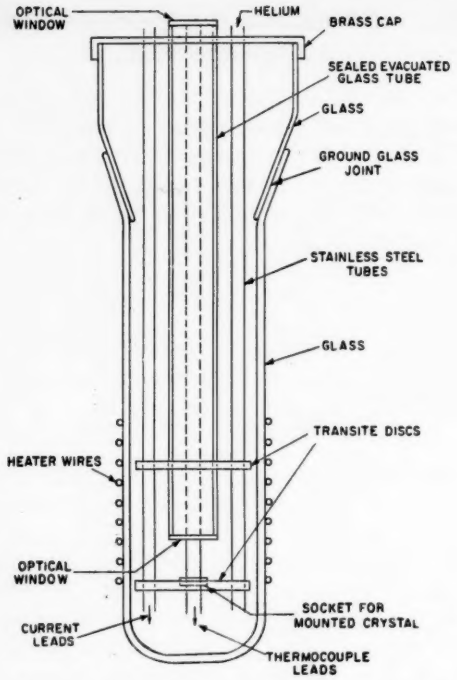

FIG. 1. Schematic diagram of experimental apparatus for measuring photoconductivity as a function of temperature.

and N_v may be expressed in terms of fundamental constants[4]:

$$N_c = (2\pi m_e kT)^{\frac{3}{2}} h^{-3}, \tag{18}$$

$$N_v = (2\pi m_h kT)^{\frac{3}{2}} h^{-3}. \tag{19}$$

Although all of the above mathematical development has been carried out for the case of a donor impurity, i.e., for n-type conductivity, the same relations may be applied to p-type conductivity by a simple transformation.

EXPERIMENTAL

The crystals measured in this paper were of two types: "pure" CdS single crystals prepared without added impurity, and CdS single crystals prepared in an atmosphere containing a plentiful supply of chloride. The actual preparation details are given in Part I.[1]

Electrical contact to the crystals was made with indium electrodes melted on the crystals at a temperature of about 300°C. These electrodes provide an ohmic photocurrent[6] over the whole range of voltages, currents, and temperatures involved in the measurements to be discussed.

TABLE I.

Crystal	Crystal dimensions, mm Length[a]	Width	Thickness
1*I*	2.3	2.6	0.052
2*I*	4.2	1.8	0.027
1*C*	1.6	1.7	0.075
2*C*	0.8	1.2	0.025

[a] The length given is the distance between electrodes.

[6] R. W. Smith and A. Rose, Phys. Rev. **92**, 857 (1953).

A schematic drawing of the measuring apparatus is given in Fig. 1. Measurements were carried out in an atmosphere of helium between temperatures of −196°C, obtained by enclosing the glass tube with a Dewar of liquid nitrogen, and about 100°C, obtained by passing current through the heater windings around the tube. The currents to be measured were recorded with a Leeds and Northrup *X-Y* recorder, either directly, or through a Leeds and Northrup micromicroammeter.

All measurements except the determination of spectral response were made with incandescent excitation from a GE 1493 bulb. The spectral response was measured with a 500-mm Bausch and Lomb grating monochromator. Variations of excitation intensity with white-light excitation were obtained by using neutral filters.

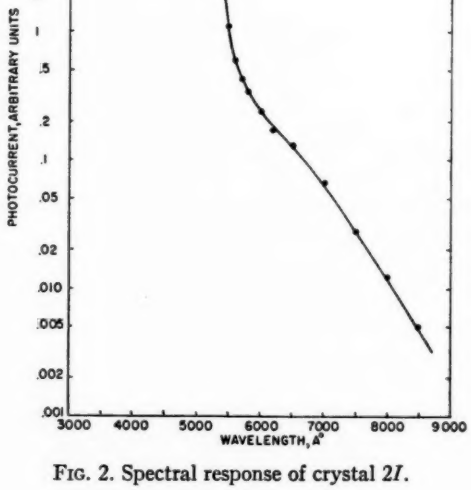

FIG. 2. Spectral response of crystal 2*I*.

Measurements of dark conductivity as a function of temperature were made by M. L. Schultz, using a Collins cryostat.

RESULTS

General Characteristics

The data presented in this paper are taken from measurements on four typical crystals: two "pure" insulating crystals, designated as 1*I* and 2*I*; and two conducting crystals with chloride impurity, designated as 1*C* and 2*C*. The dimensions of these crystals are given in Table I.

The conductivity in the dark at room temperature

for the insulating "pure" crystals is about 10^{-10} mho/cm; for the conducting crystals it is about 1 mho/cm. These conductivities correspond to locations of the Fermi-level of about 0.7 and about 0.09 ev, respectively, below the lower edge of the conduction band.

Measurements of the spectral response of photoconductivity show that the excitation is almost totally a process involving absorption by the cadmium sulfide crystal, with the raising of an electron from the filled band to the conduction band. Figure 2 gives the spectral response for crystal 2*I*. The maximum of response at 5150 A (2.4 ev) corresponds closely to the absorption edge of CdS, showing that the principal excitation transition is from filled to conduction band. The spectral response for the conducting crystals is very similar to

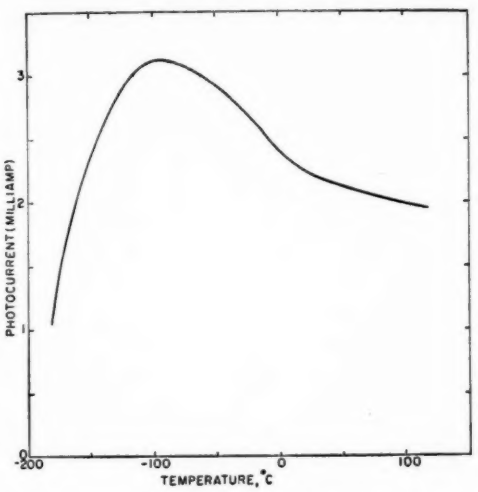

FIG. 3. Photocurrent of crystal 2*C* as a function of temperature; 2 volts applied, 900 ft-c illumination.

that of the insulating crystals, although in general showing slightly less blue, and slightly more red sensitivity.

Photoconductivity as a Function of Temperature

The variation of photocurrent with temperature is markedly different between the insulating crystals and the conducting crystals. Figure 3 show the variation of photocurrent with temperature for crystal 2*C*, and Fig. 4 gives the similar curve for crystal 1*I*. The conducting crystals all show only a very slight dependence of photosensitivity on temperature, with a maximum near −100°C (in the temperature range just below that at which the dark conductivity saturates with increasing temperature because of ionization of all donors). The insulating crystals show a much greater variation of photosensitivity with temperature, with a minimum photosensitivity near room temperature, and with large increases in sensitivity below and above room temperature.

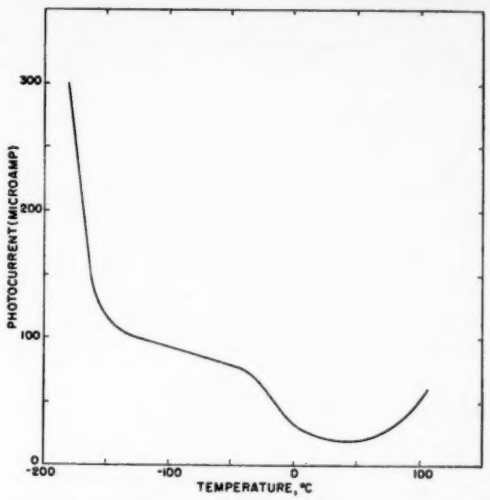

FIG. 4. Photocurrent of crystal 1*I* as a function of temperature; 6 volts applied, 900 ft-c illumination.

Thermally Stimulated Current

Measurements of thermally stimulated current were made in the following manner, completely analogous to luminescence glow-curve measurements: The crystal is cooled to liquid nitrogen temperature, and exposed to illumination for a fixed time; the illumination is removed and the crystal is heated in the dark at a linear rate. As the crystal is heated, the current is measured; the difference between the current measured in this way and the normal dark current at the corresponding temperature is the thermally stimulated current. The thermally stimulated current is thus associated with the motion of electrons freed from traps by thermal energy.

Figure 5 gives the curve of thermally stimulated current for crystal 2*C*, for a linear heating rate of 0.77°/sec. Figure 6 gives the curves for crystal 1*I* at two heating rates of 0.11°/sec and 0.77°/sec. Figure 7 gives the curve for crystal 2*I*, for a heating rate of 0.77°/sec.

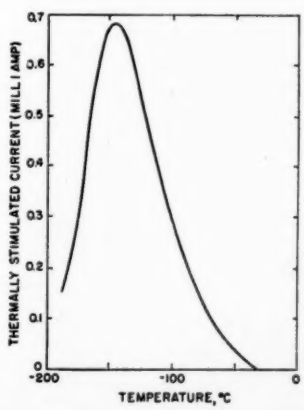

FIG. 5. Thermally stimulated current of crystal 2*C* as a function of temperature; 2 volts applied, heating rate of 0.77°/sec.

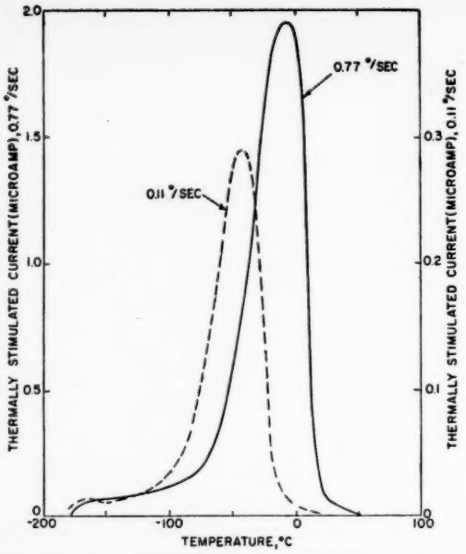

FIG. 6. Thermally stimulated current of crystal 1*I* as a function of temperature; 100 volts applied, heating rates of 0.11°/sec and 0.77°/sec.

The conducting crystals have a single peak of thermally stimulated current at about −147°C. Insulating crystals show a much smaller thermally stimulated current, with peaks at about −160°, −10°, and 60°C; the −10°C peak is most prominent in crystal 1*I*, whereas the −160°C peak is most prominent in crystal 2*I*. All of the peak temperatures mentioned in this paragraph are for the 0.77°/sec heating rate.

Dark Conductivity as a Function of Temperature

The variation of the dark conductivity of crystal 1*C* as a function of temperature is given in Fig. 8. At room temperature the conductivity is decreasing with increasing temperature because of the decreasing mobility; all of the donor centers themselves are ionized. Below room temperature, however, a plot of log conductivity against $1/T$ gives a curve with two linear portions, the slopes of which correspond to energies of 0.038 and 0.0015 ev. The 0.038 ev slope obtains between about 125° and 50°K, and the 0.0015-ev slope obtains from 20° down to at least 4°K.

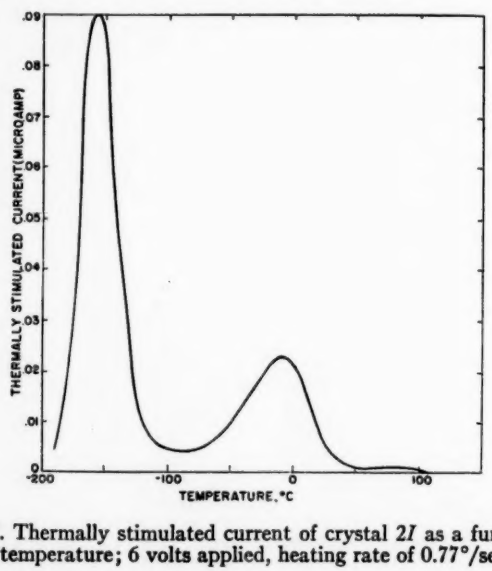

FIG. 7. Thermally stimulated current of crystal 2*I* as a function of temperature; 6 volts applied, heating rate of 0.77°/sec.

Photocurrent as a Function of Light Intensity

Detailed measurements of photocurrent as a function of light intensity have been made thus far only with insulating crystals. In general, at low light intensities, the concentration of available recombination centers is very much larger than the concentration of free electrons, most of the excited electrons having been trapped. Under these conditions, the photocurrent varies linearly with light intensity. When the light intensity is increased past some critical value, the photocurrent varies with the square-root of the light intensity. The transition from linear to square-root variation marks the condition for which the concentration of electrons in the conduction band is equal to the concentration of electrons in traps.

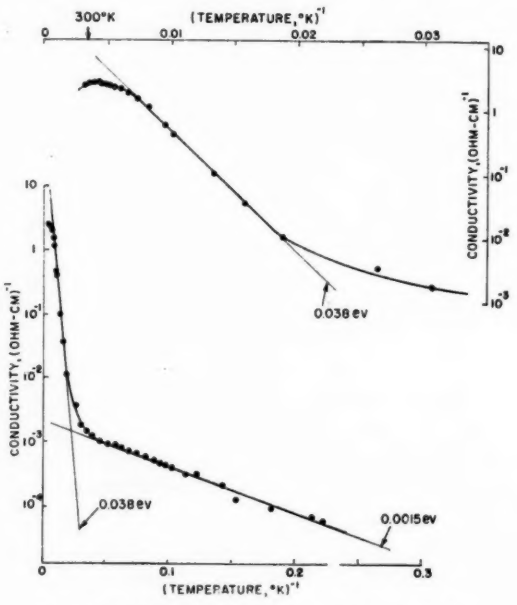

FIG. 8. Conductivity of crystal 1*C* as a function of temperature in the dark.

Experimentally it is found that a change in the variation of photocurrent with light intensity from linear to square-root does occur at the conductivity expected from the above considerations, for crystal 2*I* at all temperatures, and for crystal 1*I* at low temperatures. At room temperature and above, however, the transition point for crystal 1*I* appears to be associated not with the equality between the concentration of free and trapped electrons, but rather with the conductivity for which the Fermi level is located in the neighborhood of the major trap concentration. This effect merits further experimentation.

Decay Time as a Function of Light Intensity

The decay time of the photocurrent as a function of light intensity was measured for crystal 2*I* at 17° and 95°C; the results are given in Table II. Measurements of decay time at very high light intensities were made also for crystal 2*C* and other conducting crystals, at room temperature, with results which will be presented in the following discussion.

DISCUSSION

Trap Concentrations

A summary of the values obtained for the concentration of traps is given in Table III. The reasoning involved in obtaining these values is the following.

(1) Thermally stimulated current curves. If the total area under a curve of thermally stimulated current is measured, it is possible to calculate the concentration of electrons which contributed to the current during the measurement (i.e., time-integral of current gives total charge). In order to make the correlation between the number of electrons/cm³ contributing to the current, and the concentration of traps, however, a gain factor must be applied which takes into account the fact that for each electron freed from a trap, a much larger number of electrons may contribute to the current [Eq. (1)]. The determination of this gain factor is somewhat difficult, but the values given in Table III were obtained by using gain factors determined from photoconductivity measurements of each crystal at the same current and temperature as obtained in the measurement of thermally stimulated current, averaged over the temperature range of the thermally stimulated current curve.

TABLE II. Photocurrent and decay time as a function of light intensity for crystal 2*I*[a] (100 volts applied).

Light, foot-candles	17°C Photocurrent, microamp	17°C Decay time, millisec	95°C Photocurrent, microamp	95°C Decay time, millisec
900	640	15	780	13
330	440	17	590	17
130	290	23	400	24
20	87	34	150	42
3.0	23	110	51	68
0.47	5.5	1200	13	85

[a] All of the values given in this table (except for 0.47 ft-c at 95°C) occur under conditions where the photocurrent is varying as the square root of the light intensity.

(2) Photocurrent *vs* light intensity. When the transition occurs from a linear variation of photocurrent as a function of light intensity to a square-root variation, the concentration of free electrons is equal to the concentration of traps located between the corresponding Fermi-level and the dark conductivity Fermi-level.

(3) Decay time *vs* light intensity. When the decay time increases very rapidly with decreasing light intensity (as between 20 and 0.47 foot-candle illumination at 17°C in Table II for crystal 2*I*), the concentration of free electrons is equal to the concentration of traps in the neighborhood of the corresponding Fermi-level.

TABLE III. Summary of the values obtained for the concentration of traps.

Measurement	Crystal	Number of traps/cm³
Thermally stimulated current, 0.77°/sec	2*I*	5×10^{14}
Photocurrent *vs* light intensity	2*I*	3×10^{13}
Decay time *vs* light intensity	2*I*	2×10^{13}
Thermally stimulated current, 0.77°/sec	1*I*	7×10^{15}
0.11°/sec		3×10^{16}
Photocurrent *vs* light intensity	1*I*	2×10^{13}
Thermally stimulated current, 0.77°/sec	2*C*	3×10^{19}

The results tabulated in Table III show that the concentration of trapping levels in "pure" insulating cadmium sulfide crystals[7] is between 10^{13} and 10^{16} per cm³. In conducting crystals the concentration of trapping levels is about 10^4 times larger, or between 10^{17} and 10^{20} per cm³.

Distribution of Trapping Levels

According to the treatment of trap emptying given by Randall and Wilkins,[5] the trap depth, E^*, may be calculated from the temperature of maximum intensity, T_m, in a luminescence glow curve measurement from the equation:

$$E^* = (\ln f) k T_m (1+a), \tag{20}$$

where f is the attempt-to-escape "frequency," and a is a correction factor of the order of 0.1, involving all the other variables and the linear heating rate. In order to calculate E^* from a single luminescence glow curve measurement, a value for f must be assumed.

On the other hand, if measurements of thermally stimulated current are made, the calculation of the location of the Fermi-level at the temperature for maximum current will give the trap depth independently (excepting special distributions of trapping levels, for

TABLE IV. Summary of results of analysis of curves of thermally stimulated current.

Crystal	Heating rate, °/sec	T_m, °C	E^*, ev	f, sec^{-1}	s, cm²
1*I*	0.77	−8	0.36	3×10^5	4×10^{-21}
1*I*	0.11	−43	0.35	3×10^5	5×10^{-21}
1*I*	0.11	−165	0.19	10^7	10^{-18}
1*I*	0.11	62	0.63	2×10^7	2×10^{-19}
2*I*	0.77	−11	0.36	5×10^5	7×10^{-21}
2*I*	0.77	−158	0.15	3×10^5	2×10^{-20}
2*I*	0.77	87	0.59	7×10^6	4×10^{-20}
2*C*	0.77	−147	0.06	10	10^{-24}

[7] Measurements of trap concentration by the method of space-charge-limited current [see: A. Rose and R. W. Smith, Phys. Rev. **92**, 857 (1953)] on other "pure" crystals give a value of 10^{14}/cm³ for the trap concentration.

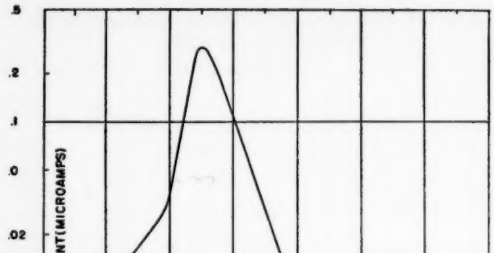

FIG. 9. Thermally stimulated current of crystal 1*I* as a function of calculated Fermi-level, varying withv arying temperature; 100 volts applied, heating rate of 0.11°/sec.

which the Fermi-level would not be located in the neighborhood of the traps associated with the maximum thermally stimulated current). Then this trap depth may be substituted in Eq. (20) to determine f.

A summary of the analysis of the curves of Figs. 5 through 7 is given in Table IV. Principal trap depths in the insulating crystals are about 0.17, 0.35, and 0.61 ev. In the conducting crystals there is but one major trap depth of 0.06 ev. The method of analysis is internally justified by the agreement of values of E^* and f obtained in Fig. 6 for two different heating rates, differing by a factor of seven. Figure 9 is a replot of the dotted curve of Fig. 6, measured at the slower heating rate, where the thermally stimulated current has been plotted directly against the calculated location of the Fermi-level. It must be remembered that the exact shape of the curve cannot be considered significant, since correction for variation of gain and mobility with temperature must be introduced.

Attempt-to-Escape Frequency for Traps

The values of attempt-to-escape "frequency," as determined by analysis of curves of thermally stimulated current, are given in Table IV. The values for the insulating crystals lie mainly between 10^5 and 10^6 sec^{-1}, with a few values slightly higher. For the conducting crystal, a very low value of about 10 sec^{-1} is obtained from the calculated trap depth. It is possible in this case that the location of the calculated Fermi-level may differ to a small extent from the actual trap depth; for such a shallow trap, a small energy difference would result in a relatively large difference in the calculated attempt-to-escape "frequency." Since the frequency of crystal vibrations is about 10^{13} sec^{-1}, the low values obtained for the attempt-to-escape "frequency" indicate either that the trapping centers are not coupled tightly to their surround, or that the transition probability from trap to conduction band is very small.[8]

Capture Cross Section of Traps

From the values of the attempt-to-escape frequency given in Table IV, calculated from the analysis of curves of thermally stimulated current, the capture cross section may be calculated from Eq. (5). These results are also given in Table IV; the values for the capture cross section of traps in insulating crystals is about 10^{-20} cm^2; for traps in the conducting crystals, the calculated capture cross section is 10^{-24} cm^2.

Capture Cross Section of Recombination Centers

The capture cross section of recombination centers may be calculated from the measurement of decay time for high light intensities, according to Eq. (4). The results of this calculation, using the data of Table II, are given in Table V for insulating crystal 2*I*. The value of the capture cross section of recombination centers is found to be equal to the capture cross section of trapping centers in insulating crystals. This result suggests that the same type of centers may act as both trapping centers and recombination centers.

The capture cross section of recombination centers in conducting crystals is given from data obtained with crystal 2*C*. At room temperature and 900 ft-c illumination, a photocurrent of 2.2 milliamp and a decay time of 76 milliseconds are obtained for an applied voltage of 2 volts. The calculated capture cross section is 10^{-23} cm^2. Similar measurements on other conducting crystals indicate a cross section for recombination centers at room temperature which is one thousand times smaller in conducting crystals than in insulating crystals. The factor of one thousand difference in capture cross section of recombination centers agrees well with the observed difference by a factor of about one thousand in room-temperature sensitivity between conducting and insu-

TABLE V. Capture cross section of recombination centers for crystal 2*I* (95°C).

Light, foot-candles	s, cm^2
900	2×10^{-20}
330	2×10^{-20}
130	2×10^{-20}
20	3×10^{-20}
3	5×10^{-20}

[8] That the method used in this paper to determine values of trap depth, attempt-to-escape "frequency," and capture cross sections of traps, is not in itself responsible for the low values of f and s found for cadmium sulfide, is shown by similar measurements on cadmium selenide crystals, for which much larger values of f and s are found.

lating crystals. As in insulating crystals, the capture cross section of traps and of recombination centers is of the same order of magnitude also in conducting crystals.

Mobility

The mobility is determined from the photocurrent and decay time at high light intensities according to Eq. (3). Values of mobility calculated from the data of Table II for crystal 2*I* are given in Table VI.

The transition from a linear to a square-root variation of photocurrent with light intensity occurs between 0.47 and 3 ft-c illumination. According to the simple theoretical picture, the mobility should be constant above this transition point. Actually, the maximum value of mobility is obtained somewhat below the transition point, and the mobility decreases above the transition point. Since the maximum value of mobility calculated is most likely to be nearest to the actual value, a mobility of about 20 cm²/volt sec is indicated. This value, although substantiated by measurements on several other crystals at high light intensities, both insulating and conducting, is considerably less than the value of about 100 cm²/volt sec previously reported for sensitive cadmium sulfide crystals.[3]

Chloride Centers in Conducting Crystals

The proportion of chloride incorporated in the conducting cadmium sulfide crystals is not accurately known. Chemical analysis[9] indicates nephelometrically that there is less than 20 ppm of chloride incorporated. Assuming that each chloride center has contributed one electron to the conductivity at room temperature gives an estimate of about 5 ppm of incorporated chloride. Such a value seems reasonable in view of the fact that the incorporation of copper in a conducting crystal has its major effect when between 2 and 4 ppm of copper are incorporated.[1]

TABLE VI. Mobility calculated from data of Table II for crystal 2*I*, 95°C.

Light, foot-candles	Mobility, cm²/volt sec
900	3.0
330	4.6
130	5.5
20	7.9
3	11.1
0.47	14.2
0.09	18.6
0.014	9.8

[9] Analysis by M. C. Gardels.

TABLE VII. Calculated fermi-levels for data of Fig. 8.

Temperature, °K	Fermi-level, ev
120	0.035
98	0.037
74	0.037
62	0.037
53	0.036
20	0.022
10	0.0097
6.7	0.0070
5	0.0056
4	0.0048

For the lower set of temperatures, the Fermi-level in ev is given by the equation: $E_F = 0.0008T + 0.0016$.

The data of Fig. 8, showing the variation of conductivity in the dark with temperature, should provide information concerning the binding energy with which the excess electron is held to the chloride center[1] in cadmium sulfide crystals. The data of Fig. 8 were subjected to Fermi-level analysis using Eq. (10) with an assumed mobility of 20 cm²/volt sec at room temperature. The results are given in Table VII.

Between 53° and 125°K, the calculated Fermi-level is independent of temperature and approximately equal to the slope calculated from the plot of Fig. 8: 0.038 ev. A consideration of Eqs. (13), (15), (16), and (17) in the light of other data already presented, indicates that Eq. (15) is the one which is applicable to this result. Since N_D is of the order of 10^{16}/cm³, and N_c is of the order of 10^{19}/cm³, N_D is neither equal to N_c, nor equal to N_c plus N_A; thus Eqs. (13) and (16) are eliminated. It is clear that this is not a case of intrinsic semiconduction; thus Eq. (17) is eliminated. The fact that the Fermi-level is independent of temperature indicates, according to Eq. (15), that there are a number of acceptors per unit volume equal to one-half the number of donors, and that the calculated Fermi-level, which equals the calculated slope, is equal to the energy difference between the donor levels and the conduction band.

Between 4° and 20°K, the calculated Fermi-level is not constant, but varies linearly with temperature. The interpretation of this linear low-temperature portion of the curve is probably not a simple one; a consistent correlation between this portion of the curve and the higher temperature portion cannot be made using the equations derived in this paper.

The author wishes to express his appreciation to Dr. R. E. Shrader for assistance with the experimental apparatus, and to Dr. A. Rose, and Dr. E. E. Hahn for helpful discussions.

Properties of the Hydrogen Bond. The Role of Lone Pair Electrons*

W. G. SCHNEIDER†
Department of Theoretical Chemistry, Cambridge, England
(Received June 7, 1954)

The properties of the hydrogen bond are discussed in relation to the equivalent orbital representation of lone pair electrons. The dependence of the energy of the hydrogen bond on the nature of the hybridized lone pair orbital is pointed out. On the basis of point charge models for the water and hydrogen fluoride molecules, and on the basis of a consideration of known hydrogen-bonded structures, evidence is presented to show that the directional properties of the hydrogen bond are determined largely by the directional properties of the lone pair orbital, and that the strongest bonds result when the hydrogen bond direction is collinear with the lone pair orbital direction.

1. INTRODUCTION

IN a recent series of papers the theory of equivalent orbitals has been developed and applied to a variety of molecules by Lennard-Jones and co-workers.[1–3] One of the major successes of the theory, resulting from the representation of lone pair electrons in terms of equivalent orbitals, was a new interpretation of the role played by lone pairs in determining the equilibrium configuration of molecules. It was shown[4] that besides having an important influence on the directional properties of bonding orbitals centered on the same atom, the lone pair orbitals also make a substantial contribution to the dipole moment of the molecule. Since the direction of the lone pair orbital in a number of molecules is well defined, such molecules will have strongly directed external force fields and may be expected to take part in a variety of molecular association phenomena.[5] The present paper is an extension of these ideas to the hydrogen bond.

The hydrogen bond may be regarded as a special case of donor-acceptor interaction. In order to form a stable hydrogen bond, which we may write as X−H···Y, the only essential requirement of the acceptor is that the charge distribution of the X−H bond orbital be such as to leave the proton sufficiently unscreened. The conditions to be met by the donor lone pair are less readily defined, and it is of interest to inquire why these conditions are met only by lone pairs of first row elements and, moreover, only when the latter elements occur in certain chemical combinations.

Of particular interest is the important question of the directional properties of the hydrogen bond relative to the molecule *Y*. To examine this question, point charge models were employed for the H_2O and HF molecules, and the interaction energy for various probable orientations was determined. The models were chosen so as to represent as nearly as possible the charge distributions of the entire molecule.

2. DIRECTIONAL PROPERTIES OF LONE PAIR ORBITALS

The directional properties of lone pair orbitals, like those of bonding orbitals in the first row elements, are due primarily to the directional characteristics of the atomic *p* orbitals. In the earlier LCAO approximation for molecular orbitals the lone pair electrons centered on any one atom in the molecule were considered to have the same electron configuration as in the corresponding free atom in the ground state. On this basis the lone pair electrons were described by either *s* or *p* atomic orbitals, uninfluenced by the process of molecule formation. An improved representation has been given recently by Lennard-Jones and Pople,[3] and it was shown that the directional properties of bonding orbitals and lone pair orbitals centered on the same atom are closely interdependent. Accordingly, hybridization of atomic orbitals, which nearly always occurs to some degree in bonding orbitals, will also cause hybridization of the lone pair atomic orbitals. An important consequence of hybridization which has been pointed out by Coulson[6] is that the charge distribution of the orbital relative to the nucleus is thereby made unsymmetrical, giving rise to an effective orbital dipole.‡ The magnitude of the lone pair orbital dipole can be obtained by determining the centroid of charge of the hybridized lone pair orbital. If $\psi=[1+\lambda^2]^{-\frac{1}{2}}(s+\lambda p_x)$ is the wave function for the hybrid orbital, where λ is a hybridization parameter and *s* and p_x are the usual one electron atomic functions, then as shown by Coulson,[6] the centroid of charge is expressed by the relation:

$$\bar{x}=\frac{2\lambda}{1+\lambda^2}\int sxp_x d\tau=\frac{2\lambda}{1+\lambda^2}\cdot\frac{5}{\sqrt{3}Z},$$

* National Research Council No. 3434.
† On leave from the National Research Laboratories, Ottawa, Canada.
[1] J. E. Lennard-Jones, Proc. Roy. Soc. (London) **A198**, 1, 14 (1949).
[2] G. G. Hall and J. E. Lennard-Jones, Proc. Roy. Soc. (London) **A202**, 155 (1950).
[3] J. E. Lennard-Jones and J. A. Pople, Proc. Roy. Soc. (London) **A202**, 166 (1950).
[4] J. A. Pople, Proc. Roy. Soc. (London) **A202**, 323 (1950).
[5] J. E. Lennard-Jones and J. A. Pople, Proc. Roy. Soc. (London) **A205**, 155 (1951).
[6] C. A. Coulson, Trans. Faraday Soc. **38**, 433 (1942); Proc. Roy. Soc. (London) **A207**, 63 (1951).
‡ The term "atomic dipole" used by Coulson in this connection is somewhat misleading since it cannot occur in the free atom but only when the atom forms part of a molecule.

TABLE I.

Element	$\bar{x}$ (Angstroms) Digonal	Trigonal	Tetrahedral
C	0.468		
N	0.390	0.369	0.339
O		0.316	0.290
F			0.254

where x is measured relative to the nucleus in the direction of the orbital. In Table I some values of $\bar{x}$ for C, N, O, and F are given for digonal, trigonal, and tetrahedral hybrid orbitals. Slater's[7] values for the effective nuclear charge Z were used. The actual values of the dipoles corresponding to the individual lone pair hybrid orbitals are obtained by multiplying by the total charge $-2e$.

If the hydrogen bond is regarded as resulting from an H−X group of a second molecule directed at a lone pair orbital, then the dominant term in the interaction energy could be considered to be the interaction of the proton with the lone pair dipole. This interpretation is, however, extremely rough, and may even be misleading in certain cases, as ordinarily the charge distribution of the rest of the molecule must be taken into account. Nevertheless, on this very naive picture, the figures in Table I can be regarded as a rough measure of the relative "donor" properties of lone pair orbitals centered on the four elements shown. Thus, for example, considering the central hydride molecules NH_3, H_2O, and HF, the lone pairs of which can be represented approximately by tetrahedral hybrid orbitals we would conclude that, relative to a common H−X group, the NH_3 lone pair would form stronger hydrogen bonds than the HF lone pair, with the water lone pair intermediate. Similarly, trigonally hybridized lone pair orbitals, as presumably occur on the O atom of the carbonyl group, should form stronger hydrogen bonds than the corresponding tetrahedral hybrid lone pair orbital on the O atom in the water molecule, or in alcohol and ether molecules. Extending this to the N lone pair, and assuming that the hybridization in the azo-compounds is approximately trigonal, and in the nitriles approximately digonal, then we should expect, relative to a common H−X, the hydrogen bond energy to be in the order: nitriles>azo-compounds>NH_3 or amines. The lone pair on the C atom in carbon monoxide can be represented very approximately by a digonal hybrid orbital; Moffit,[8] however, ascribes to it a slightly greater s character. A similar configuration can presumably also be assigned to the C lone pair in the iso-nitriles. On the basis of the foregoing arguments we would anticipate that the strongest hydrogen bonds would occur when a strong acid such as HF is hydrogen bonded to the nitriles or iso-nitriles.

Finally, it is apparent from the above formula for the centroid of charge $\bar{x}$ that when the lone pair orbital is of predominantly s character, i.e., small λ, $\bar{x}$ will be very small. The molecule accordingly has poor "donor" properties and will not form stable hydrogen bonds. An illustration of these conditions is found, for example, in the nitrogen molecule, which has been discussed previously.[5,9]

3. POINT CHARGE MODEL REPRESENTATIONS OF THE HYDROGEN BOND

Since the hydrogen bond is known to be primarily electrostatic in nature, attempts have been made to represent the energy of interaction in terms of either dipole interaction or in terms of the interaction of point charge models. A point charge model for the water molecule has been used with some success by Bauer and Magat,[10] though on the basis of more recent knowledge of the structure of the water molecule, the model used is unsatisfactory. A representation of the HF polymer based on dipole interaction has been given by Briegleb.[11] He finds for the configuration of lowest energy the structure

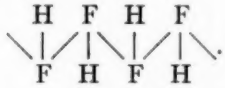

While this structure is capable of providing an explanation of the observed zig-zag nature of the F−F−F configuration of the polymer, it is not in agreement with the fact that the polarization of the vapor, below 60°C, increases with pressure and it must accordingly be ruled out. Generally speaking, a dipole approximation to the hydrogen bond interaction is unsatisfactory. In the first place, because of the rather large separation of charges within the molecule relative to the distance of approach of the second molecule, a dipole approximation is, under these circumstances, a poor one; secondly, it is not possible to take satisfactory account of the charge distribution of the whole molecule, particularly a nonlinear molecule, in terms of a single dipole. Any model representation of the hydrogen bond must not only give the correct order of magnitude of the energy of interaction, but it must also demonstrate the important directional properties of the hydrogen bond.

A complete calculation of the association energy of two molecules must include the electrostatic interaction of the nuclei and of the charge distributions of both bonding and nonbonding orbitals of the two molecules. Since such a calculation cannot readily be carried out we shall make use of point charge models chosen so as to approximate the charge distributions of the entire molecule. Such a model is readily constructed on the basis of the equivalent orbital representation of the molecule; we assume the total electronic charge of each

[7] J. C. Slater, Phys. Rev. **36**, 57 (1930).
[8] W. E. Moffit, Proc. Roy. Soc. (London) **A196**, 524 (1949).
[9] G. G. Hall and J. E. Lennard-Jones, Proc. Roy. Soc. (London) **A205**, 357 (1951).
[10] E. Bauer and M. Magat, J. phys. radium **9**, 319 (1938).
[11] G. Briegleb, Z. physik. Chem. **B51**, 9 (1941).

FIG. 1. Tetrahedral point charge models for (a) water molecule and (b) hydrogen fluoride molecule. The molecular axis is indicated by a dotted line. Indicated dimensions are in angstrom units.

localized orbital (either a bonding or lone pair orbital) to be concentrated at a point at the centroid of the orbital. Equivalent orbital representations of the H_2O and HF molecules have been reported by Pople[4] and by Duncan and Pople.[12] To simplify the present calculations we assume further that these two molecules are represented exactly by tetrahedral structures. The centroids of the lone pair orbitals on O and F are listed in Table I. To fix the centroid of the bonding orbitals, the observed dipole moment of the molecule was used. In this way the point charge models shown in Fig. 1 were obtained for the H_2O and HF molecules. The electrostatic interaction energy of two such models was then calculated for the following orientations:

(i) The H−X group of one molecule directed in line with the direction of a lone pair orbital of the second molecule.

(ii) The H−X group of one molecule directed along the molecular axis of the second, about which the lone pair orbital directions are symmetrical. For HF, orientation (ii) is that in which the H atom of one molecule is directed into the center of the "funnel" formed by the three lone pair orbitals of the second molecule, while for the H_2O configuration the O−H of one molecule is directed along the bisector of the angle formed by the two lone pair directions of the second molecule. Alternately, orientation (ii) may be regarded as an end to end alignment of the molecular dipoles. The results, listed in Table II, show that for both the H_2O dimer and the HF dimer, orientation (i) in which the H−X and the lone pair orbital directions are collinear, is more favorable by approximately one kcal/mole. In the present calculations the overlap energy as well as the dispersion and polarization energy have been neglected. Since, however, these will partially compensate each other, and since the electrostatic energy makes by far the largest contribution, the present models apparently yield the correct order of magnitude for the energy of the hydrogen bond.

TABLE II. Interaction energy of H_2O and of HF molecules on the basis of point charge models.

Orientation	or d_{F-F} (A)	E kcal/mole
Water		
(i) O−H directed along lone pair orbital direction	2.76	−6.83
(ii) O−H directed along molecular axis	2.76	−5.76
(iii) "Side by side" interaction (see text)	2.76	−3.63
Hydrogen fluoride		
(i) F−H directed along lone pair orbital direction	2.55	−7.50
(i) Same	2.62	−6.43
(ii) F−H directed along molecular axis	2.62	−5.56

For the H_2O dimer, an O−O separation of 2.76 A has been used throughout. The corresponding F−F distance in the HF dimer is not as well established. From electron diffraction measurements of the polymer in the vapor state Bauer, Beach, and Simons[13] obtain 2.55 A for the F−F distance, while from x-ray diffraction measurements of crystalline HF, which might be expected to yield a smaller distance, Gunther, Holm, and Strunz[14] obtain 2.7 A. A mean of 2.62 A was used for the present calculations, and as shown in Table II, when this distance is taken as 2.55 A, the interaction energy is increased by approximately one kcal/mole. A more accurate determination of the crystal structure of HF would be highly desirable. On the basis of the present model the F−F−F angle in the HF polymer would be predicted to be in the neighborhood of the tetrahedral angle; the present experimental values are approximately 134° from the crystal measurements and 140° from electron diffraction data.

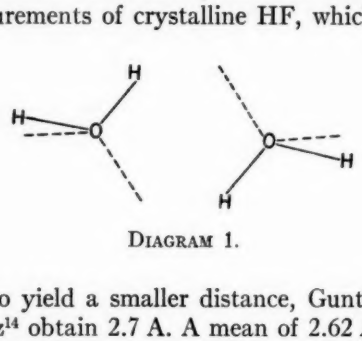

DIAGRAM 1.

An additional orientation (iii) was considered for the H_2O dimer (see Table II) involving both a lone pair and an OH on each of the two interacting molecules; the OH group of each molecule subtends a lone pair orbital in the second molecule, as shown in Diagram 1, but now the O−H- - -O configuration is not a linear one. This "side by side" arrangement, though not important in the crystal structure of water, may possibly have some significance for binary interaction in the liquid or vapor states. At an equivalent separation it is evidently less favorable than the other two orientations

[12] A. B. F. Duncan and J. A. Pople, Trans. Faraday Soc. 49, 217 (1953).

[13] Bauer, Beach, and Simons, J. Am. Chem. Soc. 61, 19 (1939).

[14] Gunther, Holm, and Strunz, Z. physik. Chem. 43, 229 (1939).

considered. Whether this arrangement, or the corresponding three-point arrangement in which a lone pair and two OH groups of one molecule are oriented toward an OH group and two lone pair orbitals of the second molecule such that each OH subtends a lone pair, could lead to a closer approach (in keeping with the higher density in liquid water), and accordingly become relatively more favorable, cannot be answered without a detailed knowledge of the overlap energy and dispersion energy.

The above results based on tetrahedral point charge models indicate that in the absence of steric influences the direction of the hydrogen bond is determined not by the direction of the dipole moment of the molecule but rather by the direction of the lone pair orbital. While the numerical results of the calculations would be slightly altered if the actual bond angles and lone pair angles for the respective molecules[12] were used rather than tetrahedral angles, the present conclusions would not be altered. It must be emphasized, however, that at best a point charge model is a rather crude and highly simplified representation of the actual charge distribution of the molecule. In particular, since the total charge defined by an orbital is regarded as concentrated at a point instead of being distributed over a region of space, the directional characteristics of such a model will be somewhat exaggerated. It is possible therefore that the differences in energy between the two orientations considered, (i) and (ii), are in fact not as large as the above calculations would indicate.

4. DIRECTIONAL PROPERTIES OF THE HYDROGEN BOND

Further evidence to support the conclusion that the hydrogen bond direction relative to the molecule *Y* is coincident with the direction of the lone pair orbital centered on *Y* can be found in a number of hydrogen-bonded structures which have been established experimentally. The hydrogen-bonded tetrahedral structure of the ice crystal is well known. On the basis of the tetrahedral structure of the water molecule described by Pople,[4] the ice structure is readily accounted for if each lone pair orbital on the oxygen atom is directed in the H—O direction of a neighboring molecule.

An important class of compounds which form strong hydrogen bonds are compounds containing the carbonyl group. The lone pair orbitals of the carbonyl oxygen

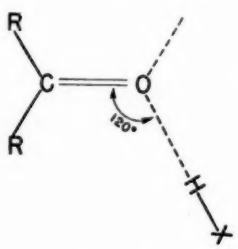

DIAGRAM 2.

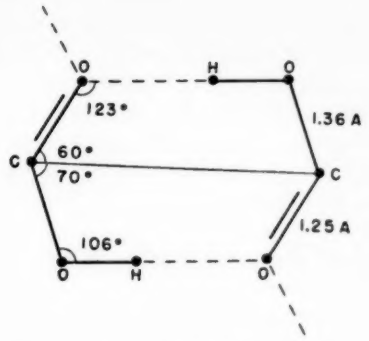

FIG. 2. Schematic diagram of the dimer of acetic acid showing hydrogen bond angles.

atom are known to have strong "donor" properties and, as mentioned above, the configuration of these orbitals can be represented approximately as trigonal *sp* hybrid orbitals. On this basis we may expect the bonding H—X group to be directed at an angle of 120° relative to the C=O direction of the carbonyl group shown in Diagram 2. This configuration is supported, for example, by the carboxylic acid dimers. From the parameters determined by Karle and Brockway[15] for the C and O positions in the acetic acid dimer in the vapor state, the configuration shown in Fig. 2 was constructed. Assuming a linear configuration for the O···H—O bonds gives the reasonable value of 106° for the COH angle and a value of 123° for the direction of the lone pair orbital relative to the C=O direction, in good agreement with the postulated value of 120°.

In the carboxylic acid dimer the second lone pair on the carbonyl oxygen, indicated by dotted lines in Fig. 1, is not engaged in hydrogen bonding due to the fact that there is but one H per molecule which can form hydrogen bonds. In the acid amides the ratio of H atoms to lone pairs is more favorable; in the crystal structure of acetamide[16] two hydrogens from two separate molecules are bonded to each carbonyl O atom. The H···O···H angle is in the neighborhood of 120°. A similar configuration is even more clearly demonstrated in the crystal of succinamide[17] which forms a planar hydrogen-bonded structure.

One of the most striking examples of a directed hydrogen bond is found in the hydrogen fluoride polymer. If the hydrogen bond direction in the HF polymer is coincident with the lone pair direction, then, as previously pointed out by Duncan and Pople[13] and supported by the results of the previous section, the zig-zag nature of the polymer is readily accounted for. In hydrogen fluoride the number of lone pairs to bondable H atoms is 3:1, and in the crystal only one lone pair is engaged in hydrogen bonding. In the vapor at moderate pressures, however, due to the small size of the HF molecules, there is a definite possibility that

[15] J. Karle and L. O. Brockway, J. Am. Chem. Soc. **66**, 574 (1944).
[16] F. Senti and D. Harker, J. Am. Chem. Soc. **62**, 2008 (1940).
[17] R. A. Pasternak, Acta Cryst. **6**, 808 (1953).

more than one lone pair may be engaged and branching of the zig-zag polymer chains could occur. Such branching would provide a possible explanation for the experimentally observed falling-off of association energy with increasing pressure, since it may be expected that when a second lone pair is simultaneously engaged in hydrogen bonding, the energy of the bond will be somewhat less.

A very strong hydrogen bond in which the hydrogen of hydrogen fluoride is bonded to a lone pair of the fluoride ion occurs in the crystal of KHF_2. The greater strength of this hydrogen bond compared to that in pure hydrogen fluoride is due to the additional electrostatic interaction energy provided by the negative fluoride ion. The fluoride ion presumably has four tetrahedrally directed lone pair orbitals. If more than one of these can be simultaneously engaged in hydrogen bonding, the compounds KF·HF, KF·2HF, KF·3HF, and KF·4HF may be expected to occur. Compounds of these compositions have been reported by Cady.[18] The structures suggested here would appear to be possible because of the small size of the HF molecule, and moreover they may be expected to be more stable than the alternative structures in which the multiple HF molecules attached to each fluoride ion form a zig-zag chain (as in the pure hydrogen fluoride crystal) by reason of the added ionic interaction contributing to each hydrogen bond. Thus, in the compound KF·4HF, the cation is the complex ion ($\bar{F}$·4HF), in which the fluoride ion is tetrahedrally surrounded by four HF molecules.

In the nitriles the lone pair can be represented by a digonal sp hybrid orbital directed along the CN axis. Association of the linear molecule HCN would therefore be expected to yield a linear polymer, in agreement with observation.

The author is greatly indebted to Professor John Lennard-Jones for his interest and encouragement during the course of the present work, and to Dr. J. A. Pople and Dr. G. G. Hall for helpful discussion.

[18] G. H. Cady, J. Am. Chem. Soc. **56**, 1431 (1934).

THE JOURNAL OF CHEMICAL PHYSICS VOLUME 23, NUMBER 1 JANUARY, 1955

An Explicit Derivation for the s Vectors in the Normal Coordinate Treatment of Molecular Vibrations

ROBERT J. MALHIOT* AND SALVADOR M. FERIGLE
Spectroscopy Laboratory,† Illinois Institute of Technology, Chicago 16, Illinois
(Received March 30, 1954)

The equations $\Sigma_n \mathbf{s}_n{}^i=0$ and $\Sigma_n \mathbf{r}_n{}^0\times\mathbf{s}_n{}^i=0$, together with the gradient properties are used to derive the **s** vectors for the four principal types of internal motion of a polyatomic molecule.

IN a previous paper,[1] the consistency of Wilson's[2] treatment of molecular vibrations with the Eckart conditions[3] was discussed. It was shown there that the **s** vectors must satisfy the following two equations:

$$\sum_n \mathbf{s}_n{}^i=0 \tag{1}$$

and

$$\sum_n \mathbf{r}_n{}^0\times\mathbf{s}_n{}^i=0, \tag{2}$$

where $\mathbf{s}_n{}^i$ is the **s** vector corresponding to the nth atom and the ith internal coordinate, and $\mathbf{r}_n{}^0$ is the position vector of the equilibrium position of the nth atom with respect to the center of mass of the molecule.

It was also shown that the **s** vectors, can be expressed as gradients of appropriately chosen scalar functions of the position vectors of the N atoms forming the polyatomic molecule.

In this paper the above conditions (1) and (2) together with the geometry of the appropriate system will be used to derive the **s** vectors for the four main types of internal coordinates, namely: bond stretching, interbond bending, bond torsion, and out of plane bending, all of which have been described in detail by Decius.[4]

Let us define the equilibrium position of the nth atom by a vector $\mathbf{r}_n$ such that

$$\mathbf{r}_n{}^0=\mathbf{R}+\mathbf{r}_n, \tag{3}$$

where **R** is the position vector of a new arbitrary origin with respect to the center of mass. We have then from Eq. (2)

$$\mathbf{R}\times\sum_n \mathbf{s}_n{}^i+\sum_n \mathbf{r}_n\times\mathbf{s}_n{}^i=0.$$

But the first term is zero by virtue of Eq. (1), hence we now have a more general form for Eq. (2), i.e.,

$$\sum_n \mathbf{r}_n\times\mathbf{s}_n{}^i=0. \tag{4}$$

* One of the investigations carried out in partial fulfillment of the requirements for the Master of Science Degree.
† Publication No. 101.
[1] R. J. Malhiot and S. M. Ferigle, J. Chem. Phys. **22**, 717 (1954).
[2] E. B. Wilson, Jr., J. Chem. Phys. **7**, 1047 (1939); **9**, 76 (1941).
[3] C. Eckart, Phys. Rev. **47**, 552 (1935).
[4] J. C. Decius, J. Chem. Phys. **17**, 1315 (1949).

The following nomenclature will be used:

Q_{ij}: The reciprocal of the equilibrium distance between the ith and jth atoms.

q_{ij}: The change in the bond distance, between the ith and the jth atoms, from the equilibrium position.

$\phi_{jk}{}^{i}$: The equilibrium value of the angle with the ith atom at the apex and the jth and kth atoms at the end.

$\alpha_{jk}{}^{i}$: The change in the $j-i-k$ interbond angle from the equilibrium value.

$T_{jk}{}^{il}$: The equilibrium value of the dihedral angle between the $i-j-k$ plane and the $j-k-l$ plane.

$\tau_{jk}{}^{il}$: The change in the dihedral angle, between the $i-j-k$ plane and the $j-k-l$ plane, from equilibrium position.

$\Gamma_{ijk}{}^{l}$: The equilibrium value of the angle between the $k-l$ bond and the $i-j-k$ plane.

$\gamma_{ijk}{}^{l}$: The change in the angle, between the $k-l$ bond and the $i-j-k$ plane from equilibrium position.

$\mathbf{e}_{ij}$: A unit vector along the equilibrium $i-j$ bond directed from the ith toward the jth atom.

$\mathbf{f}_{jk}{}^{i}$: A unit vector in the $i-j-k$ plane, perpendicular to the equilibrium $i-j$ bond and directed toward the kth atom.

$\mathbf{h}_{ijk}{}^{l}$: A unit vector perpendicular to the equilibrium $i-j-k$ plane, and directed toward the lth atom.

BOND STRETCHING

The scalar function corresponding to a change in the bond length between the ith and jth atoms is simply

$$f=|\mathbf{r}_i-\mathbf{r}_j|$$

From Eq. (26) of reference 1,

$$\mathbf{s}(q_{ij};i)=\frac{\partial}{\partial \mathbf{r}_i{}^0}|\mathbf{r}_i{}^0-\mathbf{r}_j{}^0|=(\mathbf{r}_i{}^0-\mathbf{r}_j{}^0)/|\mathbf{r}_i{}^0-\mathbf{r}_j{}^0|=-\mathbf{e}_{ij}. \quad (5)$$

By Eq. (1)

$$\mathbf{s}(q_{ij};j)=-\mathbf{s}(q_{ij};i)=\mathbf{e}_{ij}. \quad (6)$$

Equations (5) and (6) are the **s** vectors for a stretching coordinate, as given by Wilson.[2]

INTERBOND BENDING

Using the gradient properties of the **s** vector, we note that the direction of maximum change of the interbond angle for an arbitrary displacement $\mathbf{d}_j$ of the jth atom is simply $-\mathbf{f}_{jk}{}^{i}$ (see Fig. 1). The magnitude of $\mathbf{d}_j$ in this direction is $-\mathbf{d}_j\cdot\mathbf{f}_{jk}{}^{i}$; hence the magnitude of the change in the interbond angle due to $\mathbf{d}_j$ is $-\mathbf{d}_j\cdot\mathbf{f}_{jk}{}^{i}Q_{ij}$. The **s** vector is then

$$\mathbf{s}(\alpha_{jk}{}^{i};j)=-Q_{ij}\mathbf{f}_{jk}{}^{i}. \quad (7)$$

Similarly

$$\mathbf{s}(\alpha_{jk}{}^{i};k)=-Q_{ik}\mathbf{f}_{kj}{}^{i}. \quad (8)$$

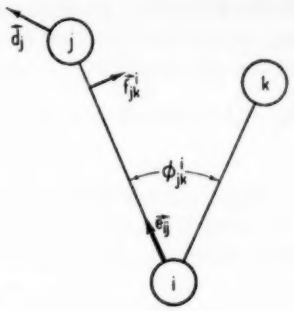

FIG. 1. The equilibrium configuration for the interbond bending coordinate.

From Eq. (1)

$$\mathbf{s}(\alpha_{jk}{}^{i};i)=Q_{ij}\mathbf{f}_{jk}{}^{i}+Q_{ik}\mathbf{f}_{kj}{}^{i}. \quad (9)$$

When the atoms i, j, and k are not collinear, one obtains

$$\mathbf{f}_{jk}{}^{i}=\operatorname{cosec}\phi_{jk}{}^{i}(\mathbf{e}_{ik}-\mathbf{e}_{ij}\cos\phi_{jk}{}^{i}),$$

and a similar expression for $\mathbf{f}_{kj}{}^{i}$ by interchanging indices; which equations are given also by Eliashevich.[5]

By substitution of these expressions of the **f** vectors in Eqs. (7)–(9) we can obtain the **s** vectors corresponding to bending coordinates as given by Wilson.[2] For the case of linear molecules the above given expression for **f** does not hold; this case has been discussed elsewhere.[6]

BOND TORSION

In a manner analogous with that used to obtain Eq. (7) we see from Fig. 2 that

$$\mathbf{s}(\tau_{jk}{}^{il};i)=-\mathbf{h}_{ijk}{}^{l}Q_{ij}\operatorname{cosec}\phi_{ik}{}^{j} \quad (10)$$

and

$$\mathbf{s}(\tau_{jk}{}^{il};l)=-\mathbf{h}_{ljk}{}^{i}Q_{kl}\operatorname{cosec}\phi_{jl}{}^{k}. \quad (11)$$

We now use Eq. (4), with the origin at the kth atom, together with Eqs. (10) and (11) giving

$$\mathbf{e}_{kj}\times\mathbf{s}_\tau{}^{j}/Q_{kj}-\mathbf{e}_{kl}\times\mathbf{h}_{lkj}{}^{i}\operatorname{cosec}\phi_{jl}{}^{k}$$
$$-Q_{ij}\operatorname{cosec}\phi_{ik}{}^{j}(\mathbf{e}_{kj}/Q_{kj}+\mathbf{e}_{ji}/Q_{ji})\times\mathbf{h}_{ijk}{}^{l}=0.$$

Transposing the last three terms to the right side of the equation and "crossing" $\mathbf{e}_{kj}$ into each side we obtain

$$(\mathbf{e}_{kj}\cdot\mathbf{s}_\tau{}^{j})\mathbf{e}_{kj}-\mathbf{s}_\tau{}^{j}=Q_{kj}\operatorname{cosec}\phi_{jl}{}^{k}(\mathbf{e}_{kj}\times\mathbf{f}_{lj}{}^{k})$$
$$+Q_{ji}\operatorname{cosec}\phi_{ik}{}^{j}(\mathbf{e}_{kj}\times\mathbf{f}_{ki}{}^{j})+Q_{kj}\operatorname{cosec}\phi_{ik}{}^{j}(\mathbf{e}_{kj}\times\mathbf{f}_{ik}{}^{j}).$$

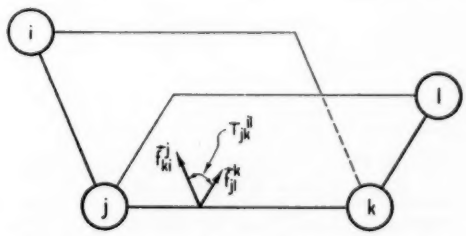

FIG. 2. The equilibrium configuration for the bond torsion coordinate.

[5] M. Eliashevich, Compt. rend. acad. sci. U.R.S.S. **28**, 604 (1940).

[6] S. M. Ferigle and A. G. Meister, J. Chem. Phys. **19**, 982 (1951).

Since $\mathbf{s}_\tau{}^j$ is the gradient of T, it must be normal to $\mathbf{e}_{kj}$ ($\mathbf{e}_{kj}$ is the direction of zero τ for a displacement $\mathbf{d}_j$ of the jth atom) and therefore

$$\mathbf{s}_\tau{}^j = Q_{kj}\cot\phi_{jl}{}^k\mathbf{h}_{lkj}{}^i + Q_{ij}\operatorname{cosec}\phi_{ik}{}^j\mathbf{h}_{ijk}{}^l - Q_{kj}\cot\phi_{ik}{}^j\mathbf{h}_{ijk}{}^l.$$

Although this last equation is a perfectly good representation for $\mathbf{s}$ we can use the following vector equation and obtain a more recognizable form for this $\mathbf{s}$ vector:

$$\mathbf{h}_{lkj}{}^i = -\cos T_{jk}{}^{il}\mathbf{h}_{ijk}{}^l + \sin T_{jk}{}^{il}\mathbf{f}_{ki}{}^j$$

then

$$\mathbf{s}(\tau_{jk}{}^{il};\, j) = \mathbf{h}_{ijk}{}^l(Q_{ij}\operatorname{cosec}\phi_{ik}{}^j - Q_{kj}\cot\phi_{ik}{}^j - Q_{kj}\cot\phi_{jl}{}^k\cos T_{jk}{}^{il}) + Q_{kj}\mathbf{f}_{ki}{}^j\cot\phi_{jl}{}^k\sin T_{jk}{}^{il}. \quad (12)$$

Since

$$\mathbf{h}_{ijk}{}^l = \operatorname{cosec}\phi_{ik}{}^j\mathbf{e}_{ij}\times\mathbf{e}_{jk}, \quad (13)$$

and

$$\mathbf{f}_{ki}{}^j = -\mathbf{e}_{jk}\times(\mathbf{e}_{ij}\times\mathbf{e}_{jk})\operatorname{cosec}\phi_{ik}{}^j, \quad (14)$$

Eqs. (10) and (11) are equivalent to the form given by Decius.[7] Similarly

$$\mathbf{s}(\tau_{jk}{}^{il};\, k) = \mathbf{h}_{jkl}{}^i(Q_{kl}\operatorname{cosec}\phi_{jl}{}^k - Q_{kj}\cot\phi_{jl}{}^k - Q_{kj}\cot\phi_{ik}{}^j\cos T_{jk}{}^{il}) + Q_{kj}\mathbf{f}_{jl}{}^k\cot\phi_{ik}{}^j\sin T_{jk}{}^{il}. \quad (15)$$

OUT OF PLANE BENDING

It is convenient to proceed by letting

$$\mathbf{s}(\gamma_{ijk}{}^l;\, l) = Q_{kl}\mathbf{u},$$

where $\mathbf{u}$ is a unit vector perpendicular to the $k-l$ bond and in the direction of $\mathbf{s}_\gamma{}^l$. See Fig. 3. Since γ is zero for a displacement of the lth atom which lies in a cone about the line normal to the $i-j-k$ plane, and through the kth atom, grad Γ is normal to this cone, or

$$\mathbf{u} = a\mathbf{h}_{ijk}{}^l + b\mathbf{e}_{kl}.$$

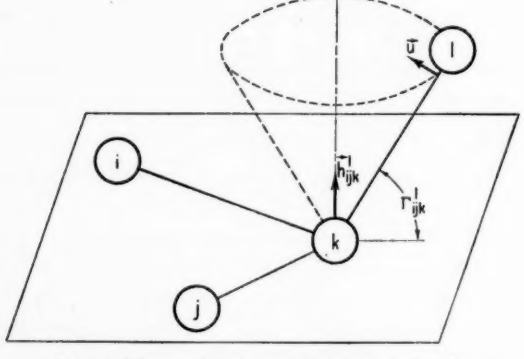

FIG. 3. The equilibrium configuration for the out-of-plane bending coordinate.

[7] J. C. Decius, J. Chem. Phys. 16, 1025 (1948).

By "dotting" $\mathbf{h}_{ijk}{}^l$ and $\mathbf{e}_{kl}$ into both sides of this equation we can solve for a and b giving

$$\mathbf{s}(\gamma_{ijk}{}^l;\, l) = Q_{kl}\sec\Gamma_{ijk}{}^l(\mathbf{h}_{ijk}{}^l - \sin\Gamma_{ijk}{}^l\mathbf{e}_{kl}). \quad (16)$$

Using Eq. (4) and letting our origin be at the kth atom we obtain

$$\mathbf{e}_{ki}\times\mathbf{s}_\gamma{}^i/Q_{ki} + \mathbf{e}_{kj}\times\mathbf{s}_\gamma{}^j/Q_{kj} + \mathbf{e}_{kl}\times\mathbf{s}_\gamma{}^l/Q_{kl} = 0.$$

"Dotting" $\mathbf{e}_{kj}$ into this equation the second term drops out; substituting from Eq. (16), and rearranging, we obtain

$$\mathbf{s}_\gamma{}^i\cdot(\mathbf{e}_{kj}\times\mathbf{e}_{ki})/Q_{ki} + \mathbf{h}_{ijk}{}^l\cdot(\mathbf{e}_{kj}\times\mathbf{e}_{kl})\sec\Gamma_{ijk}{}^l = 0.$$

Using

$$\mathbf{h}_{ijk}{}^l = -\operatorname{cosec}\phi_{ij}{}^k\mathbf{e}_{kj}\times\mathbf{e}_{kl}$$

we have

$$\mathbf{s}_\gamma{}^i\cdot\mathbf{h}_{ijk}{}^l = Q_{ki}\operatorname{cosec}^2\phi_{ij}{}^k\sec\Gamma_{ijk}{}^l(\mathbf{e}_{kj}\times\mathbf{e}_{kl})\cdot(\mathbf{e}_{kj}\times\mathbf{e}_{ki}).$$

Using a vector identity this becomes

$$\mathbf{s}_\gamma{}^i\cdot\mathbf{h}_{ijk}{}^l = -Q_{ki}\operatorname{cosec}^2\phi_{ij}{}^k\sec\Gamma_{ijk}{}^l \times[\mathbf{e}_{kl}\cdot\mathbf{e}_{ki} - (\mathbf{e}_{kj}\cdot\mathbf{e}_{ki})(\mathbf{e}_{kl}\cdot\mathbf{e}_{kj})] = -Q_{ki}\psi_{ijl}{}^k\operatorname{cosec}^2\phi_{ij}{}^k\sec\Gamma_{ijk}{}^l,$$

where

$$\psi_{ijl}{}^k = \mathbf{e}_{kl}\cdot\mathbf{e}_{ki} - (\mathbf{e}_{kj}\cdot\mathbf{e}_{ki})(\mathbf{e}_{kl}\cdot\mathbf{e}_{kj}) = \cos\phi_{il}{}^k - \cos\phi_{ij}{}^k\cos\phi_{jl}{}^k.$$

Since the direction of $\mathbf{s}_\gamma{}^i$ is $\mathbf{h}_{ijk}{}^l$ we have finally

$$\mathbf{s}(\gamma_{ijk}{}^l;\, i) = -Q_{ki}\psi_{ijl}{}^k\operatorname{cosec}^2\phi_{ij}{}^k\sec\Gamma_{ijk}{}^l\mathbf{h}_{ijk}{}^l. \quad (17)$$

By analogy

$$\mathbf{s}(\gamma_{ijk}{}^l;\, j) = -Q_{kj}\psi_{jil}{}^k\operatorname{cosec}^2\phi_{ij}{}^k\sec\Gamma_{ijk}{}^l\mathbf{h}_{ijk}{}^l. \quad (18)$$

Using Eq. (1) we obtain

$$\mathbf{s}(\gamma_{ijk}{}^l;\, k) = \sec\Gamma_{ijk}{}^l \times[Q_{kl}\sin\Gamma_{ijk}{}^l\mathbf{e}_{kl} - (Q_{kl}\sin^2\phi_{ij}{}^k - Q_{ik}\psi_{ijl}{}^k - Q_{jk}\psi_{jil}{}^k)\mathbf{h}_{ijk}{}^l\operatorname{cosec}^2\phi_{ij}{}^k]. \quad (19)$$

Equations (16)–(19) are equivalent to those given by Lohman[8] for out-of-plane bending coordinates.

ACKNOWLEDGMENT

This work was part of a research program aided by a contract with the Office of Ordnance Research, U. S. Army, and by grants from the Research Corporation, the Socony-Vacuum Laboratories, and the American Academy of Arts and Sciences.

[8] J. B. Lohman, Office of Naval Research, Tech. Report 17 (1951).

Molecular Calculations. III. A Modification of the Naive Semiempirical MO Method*

LIONEL GOODMAN† AND HARRISON SHULL
Institute for Atomic Research and Department of Chemistry, Iowa State College, Ames, Iowa
(Received April 5, 1954)

It is shown in this paper how the conventional naive semiempirical molecular orbital approach for conjugated hydrocarbons may be complemented by means of theoretically computed electron repulsion integrals in a manner suggested by the more rigorously founded SCF procedure. This is shown to give satisfying results in three examples with a considerable reduction in labor as compared to the complete ASMO method. The method is carried over in a natural and simple manner to substituted hydrocarbons, providing unambiguous methods of evaluating empirical resonance and inductive parameters. The concept of "weak" and "strong" substituent is developed and it is shown how these provide simple intuitive approaches to the estimation of interaction parameters in the theory. The inductive and resonance effects upon the energy levels are shown to be far from additive, and indeed are dependent upon each other. The dependence is analyzed and it is indicated which ones are important (and determinable) from various experimental situations.

I. BASIC APPROACH

IN this paper we formulate a general approach to substitution of conjugated hydrocarbons. The framework is that of the familiar π-electron approximation, in which explicit account is taken only of those electrons occupying molecular orbitals (MO's) which are antisymmetric to the molecular plane, the σ electrons being considered only by their influence upon the effective field in which the π electrons move. In a later paper, this framework is extended to the nonbonding (n) electrons which are σ in symmetry type but are rather sharply differentiated from the remaining bonding σ electrons.

II. SEMIEMPIRICAL TREATMENT OF MONOSUBSTITUTION

We consider first a conjugated hydrocarbon of N conjugated carbon atoms, each of which is regarded as being in a state of sp^2 hybridization and having an identical effect on its π electron. In addition, we assume that the π MO's and orbital energies are known for the hydrocarbon. These may be obtained, say by detailed self-consistent-field (SCF) or semiempirical treatment, although the final results will depend to some extent on this choice. In either case, the MO's are taken as a linear combination of atomic orbitals (LCAO) and are given by

$$\Phi_j=\sum_{u=1}^{N} c_{ju}\phi_u \quad (j=1\cdots N), \tag{1}$$

where the ϕ_u are $2p\pi$ carbon atomic orbitals (AO' s). Φ_j must transform according to the irreducible representation of the molecular point group; the role of symmetry in the formulation will be discussed further on.

We begin by utilizing Dewar's[1] formulation of molecular orbital theory in terms of linear combinations of molecular orbitals (LCMO), but inquire somewhat more critically into several steps of this process. One uses the set of orbitals Φ_j of the reference hydrocarbon [Eq. (1)] as the basis for a perturbation treatment (Dewar) in which the perturbing function is that of the π orbital on the substituent, Φ_x. We should notice that in general, Φ_x is not orthogonal to Φ_j, $j=1, \cdots N$, although the latter set is orthonormal.

In the simplified MO approach which we are using, it is assumed implicitly that the Hamiltonian can be divided into a linear combination of one-electron effective Hamiltonians, and furthermore, that a simple product wave function, not antisymmetrized, is a satisfactory representation of the correct wave function. With these assumptions, minimization of the total energy is equivalent to minimization of the energy of the individual MO's, with the restriction that they remain mutually orthogonal. From the energy minimization or from the perturbation treatment, one obtains a secular equation of degree $(N+1)$ which can be solved to obtain the orbital energies and the orbital wave functions, ψ_i. Each of the latter is a linear combination of the Φ_j and Φ_x:

$$\psi_i=\sum_{j=1}^{N+1} a_{ij}\Phi_j \quad (i=1\cdots N+1), \tag{2}$$

in which Φ_{N+1} is taken as Φ_x.

In the event that the substituted molecule has no symmetry (above that of a plane of reflection in the molecular plane) no reduction in size of the secular equation is possible. The form of the determinant is then identical with Eq. (3) below, but is $(N+1)$-dimensional. Should the monosubstituted hydrocarbon possess some other twofold symmetry element, either a twofold axis, a vertical plane of symmetry, or both, then reduction in size of the secular equation is possible. In particular, for the case of C_{2v} symmetry, which is the highest symmetry a monosubstituted hydrocarbon may possess, K of the $N+1$ orbitals, including Φ_x, will belong to the B_2 irreducible representation (antisymmetric to C_2 and symmetric to σ_v), while $L=N+1-K$ will belong to A_2 (symmetric to C_2 and antisymmetric to σ_v). As a result, the secular

* Contribution No. 340 from the Institute for Atomic Research and Department of Chemistry, Iowa State College, Ames, Iowa. Work was supported in part by the Ames Laboratory of the Atomic Energy Commission.
† Present address: Department of Chemistry, Florida State University, Tallahassee, Florida.
[1] M. J. Dewar, Proc. Cambridge Phil. Soc. 45, 638 (1949).

equation is factorable into two parts, one Kth-order equation [Eq. (3)], and one Lth-order equation [Eq. (4)].

$$\begin{vmatrix} H_{11}-E & \cdots & H_{1j} & \cdots & H_{1x}-S_{1x}E \\ \cdot & \cdots & \cdot & \cdots & \cdot \\ H_{j1} & \cdots & H_{jj}-E & \cdots & H_{jx}-S_{jx}E \\ \cdot & \cdots & \cdot & \cdots & \cdot \\ H_{x1}-S_{x1}E & \cdots & H_{xj}-S_{xj}E & & H_{xx}-E \end{vmatrix} = 0, \quad (3)$$

$$\begin{vmatrix} H_{ii}-E & \cdots & H_{ik} \\ \cdot & \cdots & \cdot \\ H_{ki} & \cdots & H_{kk}-E \end{vmatrix} = 0. \quad (4)$$

Equations (3) and (4) take explicit account of the fact that Φ_x is orthogonal to the A_2 orbitals by symmetry, but not orthogonal to those of the set having B_2 symmetry. H_{ij} is here defined as $\int \Phi_i H \Phi_j dv$, in which H is the total Hamiltonian of the substituted hydrocarbon. S_{ij} is the corresponding overlap integral.

The total Hamiltonian is now divided into a linear combination of two parts: a term H^0, which has as eigenfunctions the Φ_j of Eq. (1), and a perturbation term H', due to the substituent. This of course glosses over the question of electron interaction, but the procedure will be partially justified later. The matrix elements may now be written:

$$H_{ij} = \int \Phi_i H \Phi_j dv = H_{ij}{}^0 \delta_{ij} + H_{ij}' \quad \text{for} \quad i, j \neq x$$
$$H_{ix} = H_{xi} = H_{ix}{}^0 + H_{ix}'. \quad (5)$$

We now expand the off-diagonal elements not involving Φ_x ($i \neq j \neq x$) by using Eq. (1).

$$H_{ij}' = \sum_{u=1}^{N} \sum_{w=1}^{N} C_{ju} C_{iw} \int \phi_u H' \phi_w dv$$
$$= \sum_{u=1}^{N} C_{ju} C_{iu} \int \phi_u H' \phi_u dv$$
$$+ \sum_{u=1}^{N} \sum_{w=1}^{N} C_{ju} C_{iw} \int \phi_u H' \phi_w dv. \quad u \neq w. \quad (6)$$

The integral $\int \phi_u H' \phi_u dv$ is the increment in the Coulomb integral of the uth carbon atom in the hydrocarbon arising from the presence of the substituent. Similarly, $\int \phi_u H' \phi_w dv$ is the increment in the exchange integral between carbon atoms u and w. It is clear that these are just the quantities that have been attributed to the inductive effect by Coulson and Longuet-Higgins in the LCAO method.[2] Solution of an LCMO equation for this effect is considerably simpler than the equivalent LCAO formulation, but we will defer further details on this point to part V.

[2] C. A. Coulson and H. C. Longuet-Higgins, Proc. Roy. Soc. (London) **A191**, 39 (1947).

The matrix elements involving i or $j=x$ may be written

$$H_{jx} = \sum_{u=1}^{N} C_{ju} \left[\int \phi_u H^0 \Phi_x dv + \int \phi_u H' \Phi_x dv \right],$$
$$H_{xx} = \int \Phi_x H^0 \Phi_x dv + \int \Phi_x H' \Phi_x dv. \quad (7)$$

At this point especial caution is needed in the interpretation of H_{xx}'. The arbitrary separation of the Hamiltonian into two parts H^0+H' was made on the basis of choosing H^0 so that Φ_i of Eq. (1) were its eigenfunctions. As a result, H' must contain not only terms arising from the substituent alone, but also electron repulsion terms arising from the perturbation of the electron arrangement of the parent hydrocarbon resulting from the presence of the substituent. Examination of the magnitude to be expected from the latter terms shows them to be very significant, and in addition, very sensitive to the perturbed charge distribution. It is therefore quite incorrect to assume that Φ_x can be taken as an eigenfunction of H', i.e., $H'\Phi_x = E_x\Phi_x$ corresponding to an eigenvalue of the free substituent radical. Such an assumption does indeed permit a theoretical calculation of H_{jx} and H_{xx} as Sklar and Herzfeld have done[3,4] (with additional assumptions as well), but their procedure must be regarded as fundamentally in error as a result. Evaluation of the matrix elements H_{ix}' and H_{xx}' must be carried out through an empirical process, and the values thus obtained have, in general, no relation to those obtained by the Sklar-Herzfeld procedure. Alternatively, H could have been broken up in the following manner: $H = H^{0\prime} + H''$. Here, H'' represents the SCF Hamiltonian for the free substituent, so that $H''\Phi_x = E_x\Phi_x$ rigorously. In this case, however, $H^{0\prime}$ contains electron interaction terms in addition to those in H^0, and determines by an empirical procedure a new set of Coulomb and exchange integrals for the hydrocarbon atoms, not equal to those for the parent hydrocarbon.

We now turn to the consideration of the determinantal Eqs. (3) and (4). The solution of (4) is straightforward. The roots are dependent only upon the inductive effect, and in general are not equal to the corresponding hydrocarbon orbital energies. The exact solutions of (3) yield an expression which can be solved for any energy level by an iterative procedure. In the advent of a small perturbation which leaves E near one H_{ii}, but not close to any other H_{ii}, one can reduce the secular equation (which is equivalent to generalized perturbation theory) to the equations of ordinary second order perturbation theory, by neglecting all the off-diagonal elements except those in the ith row or column.

[3] A. L. Sklar, J. Chem. Phys. **7**, 984 (1939).
[4] K. F. Herzfeld, Chem. Rev. **41**, 233 (1947).

One obtains for any orbital energy:

$$E_j=H_{jj}+\sum_{i=1}^{N+1}{}'\frac{(H_{ji}-S_{ji}H_{jj})^2}{H_{jj}-H_{ii}}, \tag{8}$$

in which the prime indicates omission of the term $i=j$. This expression may be rewritten with application of Eq. (5) to give:

$$E_j=H_{jj}+\sum_{i=1}^{N}{}'\frac{(H_{ji})^2}{H_{jj}-H_{ii}}-\frac{(H_{jx}-S_{jx}H_{jj})^2}{H_{xx}-H_{jj}}, \quad j\neq x$$
$$E_x=H_{xx}+\sum_{i=1}^{N}\frac{(H_{xi}-S_{xi}H_{xx})^2}{H_{xx}-H_{ii}}. \tag{9}$$

Equation (9) admits simple physical interpretation: if the integrals in Eq. (6) defining the inductive effect are zero, then the first equation of (9) becomes:

$$E_j=H_{jj}^0+\frac{(H_{jx}-S_{jx}H_{jj}^0)^2}{H_{jj}^0-H_{xx}}. \tag{10}$$

The second equation of (9) remains unchanged. The latter, together with (10), is the generalization of Matsen's formulas for the resonance effect in substituted benzenes.[5] If there is no resonance interaction between the substituent and hydrocarbon,

$$E_j=H_{jj}+\sum_{i=1}^{N}{}'\frac{(H_{ji}')^2}{H_{jj}-H_{ii}}, \tag{11}$$
$$E_x=H_{xx}.$$

Equations (11) are formally identical to the formulas of Coulson and Longuet-Higgins for the influence of the inductive effect on orbital energies.[2]

The total energy (the sum over the energies of the occupied MO's) of the ground state assuming a closed shell configuration,[6] $\psi_1^2\cdots\psi_{N/2}^2\psi_x^2$, is

$$E_g=2\sum_{j=1}^{N/2}H_{jj}+2H_{xx}+2\sum_{j=1}^{N/2}\sum_{i=1}^{N}{}'\frac{(H_{ji}')^2}{H_{jj}-H_{ii}}$$
$$+2\sum_{j=1}^{N/2}\frac{(H_{jx}-S_{jx}H_{jj})^2}{H_{jj}-H_{xx}}+2\sum_{i=1}^{N}\frac{(H_{xi}-S_{xi}H_{xx})^2}{H_{xx}-H_{ii}}. \tag{12}$$

A similar expression for the total energy of an excited state is obtained by transferring an electron from a filled orbital a to an orbital b vacant in the ground state. If one assumes that the excitation process leaves the remaining orbitals unchanged, one finds for the excitation energy:

$$E_e-E_g=H_{bb}-H_{aa}+\sum_{i=1}^{N}\left[\frac{(H_{bi}')^2}{H_{bb}-H_{ii}}-\frac{(H_{ai}')^2}{H_{aa}-H_{ii}}\right]$$
$$+\frac{(H_{bx}-S_{bx}H_{bb})^2}{H_{bb}-H_{xx}}-\frac{(H_{ax}-S_{ax}H_{aa})^2}{H_{aa}-H_{xx}}. \tag{13}$$

This may be compared with the energy of the corresponding transition in the hydrocarbon itself:

$$E_e^0-E_g^0=H_{bb}^0-H_{aa}^0. \tag{14}$$

Since our approach is empirical, we shall try to have as many "errors" cancel out as is possible. Consequently, we shall in general consider the difference between the transition energy of the substituted compound and that of the corresponding transition in the hydrocarbon itself. This has the disadvantage of requiring identification of "corresponding" transitions, but attendant therewith is the advantage of not infrequently being able to use the theory to identify the transition. The difference between Eqs. (14) and (13) yields:

$$(E_e-E_g)-(E_e^0-E_g^0)=\Delta^2E=(H_{bb}-H_{bb}^0)$$
$$-(H_{aa}-H_{aa}^0)+\sum_{i=1}^{N}{}'\left[\frac{(H_{bi}')^2}{H_{bb}-H_{ii}}-\frac{(H_{ai}')^2}{H_{aa}-H_{ii}}\right]$$
$$+\frac{(H_{bx}-S_{bx}H_{bb})^2}{H_{bb}-H_{xx}}-\frac{(H_{ax}-S_{ab}H_{aa})^2}{H_{aa}-H_{xx}}. \tag{15}$$

III. SELF-CONSISTENT-FIELD FOUNDATION OF EMPIRICAL METHOD

It is worthwhile at this point to consider the empirical MO method from the following viewpoint. One examines what the best MO treatment possible is, involving a single configuration for the ground state. For the LCAO procedure, this best method, the self-consistent-field (SCF) method, has been developed in detail by Roothaan,[7] and indeed has been applied to several hydrocarbons.[8-10] Now it is possible to examine the types of integrals involved in this "best" treatment, and separate them into groups which can be associated with corresponding terms in the semiempirical treatment. In the following, we assume with Roothaan that the "excited" orbitals arising from the minimization of the ground state energy are sufficiently good approximations to the orbitals which would have been obtained had the energy of the excited state configuration been minimized directly. SCF theory yields the result that the ionization potential from the highest filled orbital a, is just the negative of the SCF orbital energy, ϵ_a:

$$I_a^0=-\epsilon_a^0=-\bar{H}_a^0-\sum_j^0(2J_{aj}-K_{aj}), \tag{16}$$

[5] F. A. Matsen, J. Am. Chem. Soc. **72**, 5243 (1950).

[6] This necessarily restricts the treatment to derivatives of parent hydrocarbons with even numbers of π electrons.

[7] C. C. J. Roothaan, Revs. Modern Phys. **23**, 69 (1951).

[8] R. G. Parr and B. L. Crawford, J. Chem. Phys. **16**, 526 (1948).

[9] C. C. J. Roothaan and R. G. Parr, J. Chem. Phys. **17**, 1001 (1949).

[10] R. G. Parr and R. S. Mulliken, J. Chem. Phys. **18**, 1338 (1950).

in which j runs over the occupied ground-state orbitals. $\bar{H}_a{}^0$ refers to the nuclear field energy of orbital a, the J's and K's to Coulomb and exchange integrals. In essence the semiempirical method utilizes an "effective" Hamiltonian, which, if ionization energies and other ground-state information are used to fix the empirical parameters, may be regarded as a SCF (Fock) Hamiltonian corresponding to the ground-state configuration. The orbital energies obtained from the semiempirical procedure may then be regarded as approximate eigenvalues[11] of this ground-state Fock Hamiltonian, which has the form:

$$F=\bar{H}+\sum_j{}^0(2J_j-K_j), \tag{17}$$

$\bar{H}$ being the nuclear field part and J_j and K_j the electron repulsion part of the potential field operating on an electron in each MO. Similarly the semiempirical wave functions may be regarded as approximate eigenfunctions of (17).

IV. MODIFICATION OF SEMIEMPIRICAL METHOD

We now turn to a comparison of the simple MO procedure, with the corresponding SCF LCAO treatment of transition energies. From Roothaan's equation 67[7] for the excitation energy to the lowest excited singlet state (excitation of an electron from a filled nondegenerate orbital a to a vacant nondegenerate orbital b), one obtains:

$$E_e{}^0-E_g{}^0=\bar{H}_b{}^0-\bar{H}_a{}^0+\sum_j{}^0(2J_{jb}-K_{jb}) -\sum_j{}^0(2J_{aj}-K_{aj})-(J_{ab}-2K_{ab}). \tag{18}$$

Now as long as the empirical parameters in the corresponding semiempirical Eq. (14) have been determined from ionization potentials, Eq. (14) is equivalent to just the difference in SCF orbital energies:

$$\epsilon_b{}^0-\epsilon_a{}^0.$$

But if the appropriate SCF orbital energies defined by Eq. (16) are substituted in Eq. (18) (with generalization to the triplets), one has:

$$^{1,3}\Delta E=\epsilon_b{}^0-\epsilon_a{}^0-(J_{ab}-K_{ab})\pm K_{ab}, \tag{19}$$

which of course is not equivalent to the corresponding empirical expression (14), with parameters determined from the ground state. It would seem logical, however, to use Eq. (19) to relate ionization potential data with spectral absorption data. Thus, one can obtain empirical parameters from data on ionization potentials, compute from these the orbital energy differences, and correct the latter by the electron repulsion integrals[12] of Eq. (19), in order to obtain a transition energy which may be compared with experiment. In addition, the process may be applied in exactly the opposite direction to predict orbital energies and thus ionization potentials, using empirical parameters determined from the much more easily experimentally observable transition frequencies. Insofar as the electron repulsion integrals do not cancel out, it is generally impossible to proceed directly from ΔE to ΔI, or vice versa, without explicitly including these terms.

A corollary of this procedure is to use orbital energies determined from the frequency of some particular transition and the appropriate electron repulsion integrals, and then predict the frequencies of other transitions. In this manner, for example, singlet-triplet transition energies may be predicted from a knowledge of the corresponding singlet-singlet excitation energy. The advantage over the usual empirical MO theory, which makes no distinction between states of different multiplicity, is obvious (see following).

For a hydrocarbon with equivalent carbon atoms, the semiempirical orbital energies are given by $\epsilon_j=n_j\beta$, where ϵ_j is referred to the carbon Coulomb integral as zero. β is the conventional carbon-carbon exchange integral of semiempirical theory, defined by $\int\phi_u H\phi_{u\pm1}d\tau$. Substitution of the appropriate semiempirical hydrocarbon orbital energies in Eq. (19) with inversion allows an "effective" carbon-carbon nearest neighbor exchange integral, β^*, to be evaluated from the observed center of gravity, $\langle\Delta E\rangle$, of the energy of the lowest excitations, or from the lowest excited singlet energy, $^1\Delta E$, using semiempirical orbital energy differences plus SCF electron interaction terms:

$$\langle\beta^*\rangle=\frac{\langle\Delta E\rangle+J_{ab}-K_{ab}}{n_b-n_a}=\beta^s+\frac{J_{ab}-K_{ab}}{n_b-n_a},$$

and

$$^1\beta^*=\frac{^1\Delta E+J_{ab}-2K_{ab}}{n_b-n_a}. \tag{20}$$

β^s is the spectroscopic β of conventional semiempirical theory. From the effective exchange integral an effective Coulomb integral may be obtained, using ionization potential data as in the naive MO procedure. The energy levels of the hydrocarbon may now be found from Eq. (20) using orbital energies calculated from β^*.

It is worth while now to examine this approach from another viewpoint. The ground state energy in naive theory is expressed by the sum of the energies of the occupied orbitals, as in Eq. (12). This, however, is not equivalent to the corresponding SCF expression, which for a closed shell ground state is (7)

$$E_g=2\sum_j{}^0\epsilon_j-\sum_{i,j}(2J_{ij}-K_{ij}),$$

[11] Neglected in conventional semiempirical theory are non-nearest-neighbor exchange integrals and higher order inductive effects. If these could all be evaluated empirically, the orbital energies would be exact eigenvalues of the SCF Hamiltonian.

[12] The integrals J_{ab} and K_{ab} are then determined from the semiempirical eigenfunctions. In cases where the MO's involved in the transitions under consideration (Φ_a and Φ_b) are completely determined by symmetry and orthogonality conditions, these MO's are exact eigenfunctions of (17), rather than approximate ones, and the electron interaction terms J_{ab} and K_{ab} are identical when computed by semiempirical theory or exact SCF theory.

not equal to a simple sum of SCF orbital energies. As shown by Mulliken[20] and Parr,[37] expression of the total ground-state energy by a simple sum of orbital energies requires the effective Hamiltonian of empirical theory, H^0 to be not equal to the SCF Hamiltonian, but

$$H^0=\tfrac{1}{2}(\bar{H}+F).$$

In terms of this Hamiltonian, the excitation energy expression is equivalent to neither (14) nor (19); instead,

$$^{1,3}\Delta E=\epsilon_b-\epsilon_a-\tfrac{1}{2}(J_{ab}-K_{ab})\pm\tfrac{1}{2}K_{ab}, \qquad (19')$$

where the ϵ's now are eigenvalues of H^0. Inversion of Eq. (19′) allows one to obtain empirical α and β values from transition energies, which in principle should be correlated with those obtained from resonance energies, but not with theoretical quantities defined in terms of F. Equation (14), however, corresponds to an effective Hamiltonian equal to neither F nor H^0 (and implies that the excited state Hamiltonian is $F+J_b-K_b$), hence spectroscopic parameters of naive theory may be correlated with neither resonance nor theoretical SCF quantities. Since Eqs. (16) and (19) are derived from the SCF Hamiltonian, F, the empirical parameters defined by Eq. (20), in principle, should be correlatable with the theoretical quantities calculated from F: $\beta=\int\phi_u F\phi_{u\pm1}d\tau$, $\alpha=\int\phi_u{}^2Fd\tau$. This is affirmed in Table I. This does not mean, of course, that one can interpret the empirically determined quantities of Eq. (20) as yielding values of theoretically defined integrals. It merely suggests that success of this semiempirical procedure lies in its introduction, empirically, of the right kinds of parameters as judged from the SCF procedure.

TABLE I. Exchange and Coulomb integrals[a] for ethylene,[b] benzene,[c] and *trans*-butadiene[d] (ev).

Molecule	β	β^N	$\langle\beta^*\rangle$	$^1\beta^*$	α^s	α^N	$^1\alpha^*$
Ethylene	−3.0	−3.5	−6.7	−5.8	−8.25	−5.1	−5.86
Butadiene	−3.8	−6.8	−8.2	−6.75	−7.0	−5.7	−5.41
Benzene	−2.56	−5.0	−5.63	−5.54	−7.2	−6.6	−4.72

[a] β^N and α^N are theoretical LCAO exchange and Coulomb integrals defined in reference 20. They are taken from references 10 and 20. β^s and α^s are spectroscopic integrals, determined from the first ionization potential and the center of gravity of the lowest excitation, by the naive MO method. $\langle\beta^*\rangle$ and $^1\beta^*$ are effective exchange integrals determined from the center of gravity and lowest singlet excitation, respectively, by our modified MO procedure.
[b] For ethylene, the necessary electron repulsion integrals are from reference 8.
[c] Since the lowest excitation in benzene takes place between degenerate orbitals, Eqs. (22) and (23) do not apply; additional excited state interaction integrals are needed. These will be discussed in a forthcoming publication.
[d] The necessary electron interaction integrals for butadiene were calculated using wave functions obtained from the naive MO procedure, overlap included.

TABLE II. Electronic energy levels of ethylene and benzene.

Molecule	State[a]	Theoretical[b] LCAO energy	Modified[c] empirical energy		Observed[d] energy
Ethylene	$^1A_{1g}$	0.0	0.0	(0.0)	0.0
	$^3B_{1u}$	1.8	0.9	−0.8	3.1–5.6
	$^1B_{1u}$	10.2	9.3	(7.6)	7.6
Benzene	$^1A_{1g}$	0.0	0.0	(0.0)	0.0
	$^1B_{2u}$	5.7	5.2	(4.9)	4.9
	$^1B_{1u}$	6.9	6.4	6.1	6.2
	$^1E_{1u}$	9.5	9.0	8.7	7.0
	$^3B_{2u}$	5.4	4.9	4.6	···
	$^3B_{1u}$	2.8	2.3	2.0	3.8
	$^3E_{1u}$	4.1	3.6	3.3	···

[a] For notation, see references 8, 9, and 10.
[b] From references 8, 9, and 10, with configuration interaction neglected.
[c] Values in the first column are calculated by the modified theory outlined in this paper, using $\langle\beta^*\rangle$; the second column, using $^1\beta^*$.
[d] The assignments of all these bands are not certain. See references 13 and 14.

TABLE III. Electron repulsion integrals in *trans*-butadiene (ev).

Integral[a]	Exact SCF method	Modified empirical method
J_{12}	9.31	8.66
J_{13}	9.22	8.39
J_{24}	9.43	9.32
J_{14}	9.96	10.81
K_{12}	2.55	3.02
K_{13}	2.09	1.68
K_{24}	2.17	1.91
K_{14}	1.83	2.13

[a] These values are for Slater $2p\pi$ AO's with effective charge $Z=3.18$. The SCF values are taken from reference 10. The empirical method integrals are computed from LCAO wave functions obtained by conventional semiempirical MO theory, overlap included, and all carbons considered identical. The necessary AO integrals are from reference 10.

TABLE IV. Electronic energy levels in *trans*-butadiene.[a]

State[b]	Theoretical LCAO energy[c]	Modified empirical energy[d]	Naive MO energy[e]	Observed energy[f]
^1A_g	0.0	0.0	0.0	0.0
^1B_u	8.2	6.0	4.9	6.0
^1A_g	10.3	7.7	7.2	7.2
^1A_g	11.0	16.5	12.6	···
^1B_u	12.6	19.6	14.8	···
^3B_u	3.2	−0.1	4.9	···
^3A_g	6.1	4.3	7.2	···
^3A_g	6.6	12.6	12.6	···
^3B_u	8.9	15.3	14.8	···

[a] We are very much indebted to Mr. Stanley Hagstrom for carrying out the computations on butadiene.
[b] For notation, see reference 10.
[c] Taken from reference 10.
[d] Computed with $\beta^*=-6.75$ ev, and electron repulsion integrals given in Table III.
[e] Computed with $\beta^s=3.8$ ev, and inclusion of nearest neighbor overlaps, all carbons considered identical.
[f] Assignment of the 7.2-ev band is not certain. See reference 13.

In order to test the validity of our approach, we introduce here some computations of the energy levels of hydrocarbons, based on the modified theory. Recently, Parr, and Pariser[13] have given a semiempirical theory of electronic levels of unsaturated molecules, which, for application to hydrocarbons, is similar to ours in philosophy and scope. The assumptions and mathematical details inherent in the two theories are different in a number of places, but both make use of empirical core integrals, though in different ways. Both are formulated in the language of the purely theoretical methods of antisymmetrized molecular orbitals, theirs in terms

[37] R. G. Parr, J. Chem. Phys. 19, 799 (1951).

[13] R. Pariser and R. G. Parr, J. Chem. Phys. 21, 466, 767 (1953).

TABLE V. Singlet-triplet splitting of energy levels in ethylene, benzene and butadiene (ev).

Molecule	State[a]	$E_{\text{singlet}}-E_{\text{triplet}}$ modified empirical method[b]	$E_{\text{singlet}}-E_{\text{triplet}}$ theoretical LCAO method
Ethylene		identical for all states	
Butadiene	B_u	6.0	5.1
	A_g	3.4	4.2
	A_g	3.8	4.3
	B_u	4.2	3.7
Benzene		identical for all states	

[a] For butadiene, the order is that given in Table IV.
[b] For molecules in which the orbitals are determined by symmetry, the singlet-triplet splitting must be identical by both the completely theoretical and the modified empirical theories, as then K_{ij} is identical for both procedures. Hence, both methods give identical singlet-triplet splitting for ethylene and benzene.

of a Goeppert-Mayer-Sklar type procedure[14] plus configuration interaction, ours in terms of Hartree-Fock SCF theory. What combination of assumptions will be the most satisfactory in the long run remains an open question at this point. Tables I–V give the results of such calculations applied to ethylene, benzene, and butadiene, as well as the results from the purely theoretical method. The agreement is quite reasonable for the low lying transitions and for the singlet-triplet splitting. It is not so good for higher excitation processes, but these are just the ones which configuration interaction will affect most in either method. Further refinements could be made, such as adjusting the singlet-triplet splitting, empirically, or including configuration interaction as Parr and Pariser have done.[13,15] However, the spirit of the computations presented here is not to obtain the best possible energy levels, but to test the reasonableness of the procedure.

It is important at this point to notice that MO calculations of energy levels of molecules using LCAO wave functions are rarely successful from the viewpoint of the spectroscopist. This is true whether the calculations are by purely theoretical or by semiempirical MO procedures, for the approximate nature of LCAO wave functions impose such uncertainties in the integrals entering these various formulations, that calculations accurate enough to be useful for spectroscopic purposes (accuracy of 1000 cm^{-1} or less) are virtually impossible without inclusion of extensive configuration interaction. If, however, *shifts* in energy levels are considered in going to a substituted molecule from a reference molecule, one is required to know only *changes* in integrals rather than the integrals themselves. Much of the error incurred in using the admittedly approximate LCAO wave functions for calculation of eigenvalues will be lost when used for calculation of *perturbations*. We now extend the framework of this section to monosubstituted hydrocarbons. However, it is understood that the methods described are general and can easily be applied to the problem of adding ethylenic links or multiple substitution. Thus, for the reference hydrocarbon itself, Eq. (16) gives the ionization potential. An analogous equation can be written for the monosubstituted hydrocarbon, using primed quantities throughout. The primes indicate, first, that the Hamiltonian now has a perturbation added to it, and second, that the SCF orbital wave functions occurring in the electron repulsion integrals are, of course, somewhat changed from the corresponding unperturbed hydrocarbon wave functions.

Let us now consider the shift in ionization potential in going from the hydrocarbon to the substituted hydrocarbon. For this we take the difference between the surtituent analog of Eq. (16) and Eq. (16) itself. This yields:

$$\Delta I = I_a' - I_a^0 = -\bar{H}_a' + \bar{H}_a^0 - \sum_j^0 (2J_{aj}' - 2J_{aj} - K_{aj}' + K_{aj}) - (2J_{ax}' - K_{ax}'). \quad (21)$$

The additional terms involving x appear, of course, since there is one additional occupied ground-state orbital, ψ_x, in the substituted hydrocarbon. Equation (21) may be associated with the corresponding equation from the semiempirical approach:

$$\Delta I = I_a' - I_a = (-H_{aa}' + H_{aa}^0) - \sum_{i=1}^{N} \frac{(H_{ai}')^2}{H_{aa} - H_{ii}} - \frac{(H_{ax} - S_{ax}H_{aa})^2}{H_{aa} - H_{xx}}, \quad (22)$$

as long as one evaluates empirically the quantities involved, for then the simple MO orbital energies take on the aspects of the theoretically better founded SCF orbital energies, especially with respect to inclusion of the electron repulsion integrals. If we now consider the shift in transition energy for a substituted hydrocarbon from that of the hydrocarbon itself,

$$^{1,3}\Delta^2 E = (E_e' - E_g') - (E_e^0 - E_g^0) = (\epsilon_b' - \epsilon_b^0) - (\epsilon_a' - \epsilon_a^0) - (J_{ab}' - J_{ab}) + (K_{ab}' - K_{ab}) \pm (K_{ab}' - K_{ab}), \quad (23)$$

with the shift in SCF orbital energies given by Eq. (15), as long as the empirical parameters in the corresponding semiempirical equation (15) have been determined from ionization potentials. [If transition energies are used, an obvious analog of Eq. (20) will be needed.] It should be remarked that this procedure avoids the difficulty of the too large singlet-triplet separations found in purely theoretical calculations, inasmuch as one makes no attempt to use a theoretically computed singlet-triplet splitting. One uses the theoretically computed values of the electron repulsion integrals together with the parameters determined from the shift of the singlet-singlet spectrum to predict the shift in the singlet-triplet spectrum from the observed singlet-triplet energy in the parent hydrocarbon.

We now turn to a consideration of the electron repulsion integrals. The change in the wave function can be attributed to two essentially independent points. First is the contribution from the non-orthogonality of Φ_x to the parent hydrocarbon MO's, $\Phi_1, \cdots, \Phi_N$, mentioned previously. The use of the SCF development,[7] however, requires orthogonalized wave functions. We can classify

[14] M. Goeppert-Mayer and A. L. Sklar, J. Chem. Phys. **6**, 645 (1938).
[15] R. Pariser, J. Chem. Phys. **21**, 568 (1953).

this minimum necessary orthogonalization, following Mulliken,[16] as "forced hybridization." It was found instructive to form the Löwdin many-center orbital wave functions[17] from the hydrocarbon MO's and the substituent AO for two cases: aniline and aminobutadiene. These are listed in detail in Appendix A. The interesting point concerning these orbitals orthogonalized by Löwdin's recipe is the small amount of mixing introduced by the orthogonalization condition. It can be concluded safely that forced hybridization does not, of itself, cause a very large change in the orbital wave functions. The second factor influencing the form of the wave function is the actual perturbation of the wave functions by the presence of the substituent. It is apparent that, depending upon the amount of interaction between the substituent and the parent hydrocarbon, the hydrocarbon wave functions may be changed only to a very slight extent or in considerable degree. This aspect of the problem is considered in detail in succeeding papers of this series. Suffice it to point out here that in practice, substituents exist which influence the unperturbed wave functions to a moderate extent only, and for which it is reasonable to assume that the corresponding electron repulsion integrals in the hydrocarbon and the substituted hydrocarbon, respectively, are equal. Substituents falling into this category will be labeled here "weak" substituents, whereas those for which considerable changes in the wave functions occur will be designated as "strong" substituents. Mathematically speaking, weak substituents are those for which $|H_{jj}-H_{xx}|$ or H_{ij}' are large. The opposite statement holds for strong substituents.

For weak substituents, the shifts in transition energy and ionization potential may be obtained from Eqs. (23) and (21), by canceling out the corresponding electron interaction integrals:

$$\begin{aligned}\Delta^2E&=(H_b'-H_b^0)-(H_a'-H_a^0)\\&\quad+(2J_{xb}'-K_{xb}')-(2J_{ax}'-K_{ax}')\\&=(\epsilon_b'-\epsilon_b^0)-(\epsilon_a'-\epsilon_a^0)=\Delta^2\epsilon,\end{aligned}\tag{24}$$

and

$$\Delta I=-(H_a-H_a^0)-(2J_{ax}-K_{ax}).\tag{25}$$

The terms involving $j=x$ remain, of course, because of the additional occupied ground state orbital in the substituted hydrocarbon. Equation (25), for the shift in ionization potential, now involves exactly those terms concerning orbital a which appear in Eq. (24) for Δ^2E. It can be concluded therefore, that for sufficiently weak substituents, transition energy shifts can be predicted directly by Eq. (15) using empirical parameters from shifts in ionization potentials and vice versa. A little reflection shows that the difference between the shifts in singlet and triplet energies of the excited states in the SCF procedure involves only electron repulsion integrals which, for weak substituents, cancel out. This cancellation holds, whether any particular configuration or the center of gravity of all the excited configurations is under consideration, irrespective of any possible degeneracy of orbitals a or b. This is tantamount to the statement that, for weak substituents, the energy shift of the center of gravity is the same as that of any one of the individual configurations. Since Eq. (15) applies to the center of gravity of the transitions, it is apparent that one is justified, for sufficiently weak substituents, in comparing observed energy shifts of any of the transitions with the semiempirically calculated shifts of the center of gravity involving the same orbitals.[18]

V. EVALUATION OF EMPIRICAL PARAMETERS

It is assumed at the outset that the matrix elements H_{ii}^0, $i\neq x$, of Eq. (5) have been determined empirically from spectral data on the parent conjugated hydrocarbon, yielding a coulomb integral, α, and a carbon-carbon exchange integral, β. In order to evaluate empirically the unknown matrix element H_{xx} in Eq. (3), we follow Wheland and Pauling[19] and Matsen[5] in establishing H_{xx} as $\alpha+\delta\beta$. Here, α and β are the integrals determined from the parent hydrocarbon, whereas δ now assumes the position of an empirical parameter which is a function of the substituent. As Mulliken[20] has pointed out, α and β will vary from hydrocarbon to hydrocarbon, since they depend on non-nearest neighbor effects. Such variation will shift the δ values for a substituent as a function of the parent hydrocarbon under consideration, but this need not concern us, as the effect is merely a shift in origin, and relative δ values for different substituents will remain significant.

The matrix elements remaining to be evaluated empirically are those related to the inductive effect: H_{ij}' $(i,j\neq x)$. In Eq. (7), these were expressed in terms of the AO integrals: $\int\phi_\mu H'\phi_\mu dv$ and $\int\phi_\mu H'\phi_\nu dv$. The first of these is denoted empirically by $\delta_\mu\beta$, after Wheland and Pauling.[19] It is clear that the largest of these integrals is the one involving AO's on the carbon atom to which the substituent is attached. In succeeding notation, we will designate this carbon atom by the subscript s, and refer to it as "the substituted carbon." Various arbitrary relationships between this integral and those involving carbon atoms adjacent to the substituted carbon have been used.[19,21] ranging from $\delta_{(s\pm1)}=\delta_s/10$ to $\delta_s/3$. These recipes may be regarded as too arbitrary to be satisactory. It is possible to determine uniquely all the δ_μ's if one uses the spectra and ionization potentials of the disubstituted hydrocarbons. For the present, it will be assumed for simplicity that

[16] R. S. Mulliken, J. Chem. Phys. **19**, 912 (1951).
[17] P. O. Löwdin, J. Chem. Phys. **18**, 365 (1950).
[18] The semiempirical center of gravity is, of course, not quite the same as the SCF center of gravity. However, as they differ by just $(J_{ab}-K_{ab})$, the shifts in both centers of gravity are identical for sufficiently weak substituents.
[19] G. Wheland and L. Pauling, J. Am. Chem. Soc. **57**, 2086 (1936).
[20] R. S. Mulliken, J. chim. phys. **46**, 695 (1949).
[21] H. H. Jaffé, J. Chem. Phys. **20**, 279 (1952).

$\delta_{\mu\pm s}=0$, and in addition, that the exchange integral perturbations, $\int\phi_\mu H'\phi_r dv$, are negligible.

The exchange integral H_{jx} is approximated by $C_{js}\int\phi_s H\Phi_x dv$. While this may be poor for substituents whose π electrons have principal quantum numbers much higher than two, it is not inconsistent with the neglect of higher order inductive effects. Our state of knowledge about this integral is such that about all we can do is regard it equal to the carbon-carbon value β, or adopt Wheland's assumption, and assume it to be proportional to the overlap integral $\int\Phi_x\phi_s dv$.[22] If the C−X bond is strongly polar, neither of these assumptions appears *a priori* valid, and one must view them with caution. Since the empirical parameters must compensate, at least in part, for the inadequacy of these assumptions, they can be expected to differ in numerical magnitude but not in qualitative order for different parent hydrocarbons. With these assumptions, the secular equation, (3) and (4), if symmetry is present, take on a form particularly amenable to simple solution. In the case of symmetry splitting the secular equation, Eq. (4) reduces to diagonal form such that its roots are just the orbital energies of the parent hydrocarbon. Inasmuch as there is evidence[23] that these orbital energies may be considerably perturbed from the values for the parent hydrocarbon, the need for an adequate method of determining higher order δ_μ's is pointed up.

The orbital energies may now be obtained from Eq. (3) as a function of the known parameters α, β, and the overlap integrals, $\int\phi_\mu\Phi_x dv$, and of the unknown parameters, δ and δ_s. The latter may be determined from any two independent experimental data which can be expressed in terms of them. The most convenient data are the shifts in the vertical ionization potentials (given theoretically by the shift in energy of the highest occupied orbital) and the shifts in the vertical transition energies [given by the shift of the difference between appropriate orbital energies supplemented by electron interaction integrals as in Eq. (23)[24]]. One could use as well data on two different electronic transitions. In special cases, additional simplifying assumptions can be made. Thus, for example, the case of the anilinium ion should be an example of a virtually pure inductive effect, in which case H_{jx} and S_{jx} may be regarded as zero. The other extreme of a substituent introducing purely a resonance effect, strictly speaking does not exist, since H' is never zero. For certain substituents, however, δ_s is small and may in practice be found negligible.

It is obvious that empirical values of the parameters δ and δ_s will depend strongly on the degree of approximation in which the secular equation is solved. With respect to overlap integrals, for example, this includes solution of the secular equations (3) and (4) including or omitting overlap integrals between the AO's in the parent hydrocarbon, and likewise including or omitting the off-diagonal S_{jx} terms. Neglect of the first of these affects the unperturbed energies (but not the unperturbed wave functions). The S_{jx} terms may, on the other hand, be largely compensated for by the semi-empirical procedure as far as the energy levels are concerned,[25] but can be expected to influence considerably the wave functions. This influence is felt particularly strongly through the electron repulsion integrals of Eq. (21). In Appendix B we develop a computationally simple approach by which it is possible to take into account the inclusion of overlap, given the solutions obtained omitting overlap.

Longuet-Higgins and Coulson have in many papers presented the important properties of the special class of molecules termed by them "alternant hydrocarbons." We digress to show how these molecules can be treated by the scheme we are following in this paper. We begin conceptually with an alternant hydrocarbon substituted with a hypothetical radical which exerts only a resonance effect. We wish to inquire as to the nature of the inductive effect, i.e., how the orbital energies depend upon the Coulomb integral of the carbon to which the substituent is attached. We follow the Taylor series expansion used by Coulson and Longuet-Higgins[2] when they were examining the inductive effect alone:

$$\Delta E=\Delta E'+\left(\frac{\partial\Delta E'}{\partial\alpha_s}\right)_{\Delta=0}\delta\alpha_s+\cdots+, \qquad (26)$$

where $\Delta E'$ is the transition energy for the substituted hydrocarbon with the Coulomb integral of carbon s equal to α_s. The coefficient of $\delta\alpha_s$ is found using (10):

$$\left(\frac{\partial\Delta E'}{\partial\alpha_s}\right)_{\Delta=0}=\left[1-\frac{(H_{bx}-S_{bx}H_{bb}{}^0)^2}{(H_{bb}{}^0-H_{xx})^2}-2S_{bx}\frac{(H_{bx}-S_{bx}H_{bb}{}^0)}{H_{bb}{}^0-H_{xx}}\right]\left(\frac{\partial H_{bb}{}^0}{\partial\alpha_s}\right)_{\Delta=0}-\left[1-\frac{(H_{ax}-S_{ax}H_{aa}{}^0)^2}{(H_{aa}{}^0-H_{xx})^2}-2S_{ax}\frac{(H_{ax}-S_{ax}H_{aa}{}^0)}{(H_{aa}{}^0-H_{xx})}\right]\left(\frac{\partial H_{aa}{}^0}{\partial\alpha_s}\right)_{\Delta=0}. \qquad (27)$$

[22] G. Wheland, J. Am. Chem. Soc. **64**, 900 (1942).

[23] L. Goodman and H. Shull, unpublished work.

[24] Ionization potentials determined from electron impact data presumably yield values corresponding to vertical ionization, but, unfortunately, the data available have not been found sufficiently accurate for use for this purpose. Hence, adiabatic ionization potentials determined from spectroscopic observations on Rydberg series have been used. For a closely related series of molecules, the shifts in the adiabatic ionization potentials are not expected to deviate too greatly from the shifts of vertical ionization potentials. Vertical transition energies correspondingly require the use of the frequency of the smoothed maximum of the absorption band. For lack of sufficient accuracy in this experimental datum, we have used the 0−0 band frequencies for determining shifts. These are primary reasons (in addition to theoretical reasons mentioned earlier) why we consider shifts in experimental data rather than the absolute data.

[25] R. S. Mulliken and C. A. Rieke, J. Am. Chem. Soc. **63**, 1770 (1941).

One needs the well-known relation

$$\left(\frac{\partial H_{jj}^0}{\partial \alpha_s}\right)_{\Delta=0} = C_{js}^2, \tag{28}$$

noticing also that $|C_{bs}| = |C_{as}|$, if one is interested in a transition between corresponding alternant levels and if carbon-carbon overlap integrals are neglected.[26] These relationships result in the dropping out of all but two terms, which may be combined to yield:

$$\left(\frac{\partial \Delta E'}{\partial \alpha_s}\right)_{\Delta=0} = C_{bs}^4 \frac{(H_{bb}^0 - H_{xx})^2(h_{sx} - SH_{aa}^0)^2 - (H_{aa}^0 - H_{xx})^2(h_{sx} - SH_{bb}^0)^2}{(H_{bb}^0 - H_{xx})^2(H_{aa}^0 - H_{xx})^2}. \tag{29}$$

In this equation, h_{sx} refers to $\int \phi_s H \Phi_x dv$, and S to the corresponding overlap integral. For the case of little or no resonance interaction, every $|H_{jj} - H_{xx}|$ is large, and $(\partial \Delta E'/\partial \alpha_s)_{\Delta=0}$ is small or zero, as found by Coulson,[27] who considered just this case. On the other hand, if there is a strong resonance interaction between the substituent and the ring, then at least one $|H_{jj}^0 - H_{xx}|$ will be small, and in nearly all cases $|H_{aa}^0 - H_{xx}|$ will be smaller than $|H_{bb}^0 - H_{xx}|$. The greater the resonance interaction, the more pronounced this inequality will be. For this case, Eq. (29) reduces to:

$$\left(\frac{\partial \Delta E'}{\partial \alpha_s}\right)_{\Delta=0} = C_{bs}^4 \frac{(h_{sx} - SH_{aa}^0)^2}{(H_{aa}^0 - H_{xx})^2}. \tag{30}$$

If one substitutes this in Eq. (26) and adds in the shift in transition energy produced by the resonance effect alone, $(\Delta^2 E')$, one obtains for the total shift in transition energy[28]:

$$\Delta^2 E = C_{bs}^4 \frac{(h_{sx} - SH_{aa}^0)^2}{(H_{aa}^0 - H_{xx})^2} \delta_s \beta + \Delta^2 E'. \tag{31}$$

For a sufficiently large inductive effect, the first term of Eq. (31) may become a considerable portion of the total transition energy shift.[29]

The important conclusion to be drawn here is that for strong resonance interaction between substituent and hydrocarbon, one is not justified in neglecting the influence of the inductive effect upon the frequencies, as some authors have done (e.g., Sklar,[3] Herzfeld,[4] and Robertson and Matsen[30]). If one goes to the other extreme of a weak resonance effect, one can show rather easily that the inductive first term of Eq. (31) goes to zero faster than the resonance shift.[31] As a result, the transition shifts are essentially independent of the inductive parameter δ_s for small resonance interaction.[32] In this special case, a one-parameter theory (resonance parameter) may provide a good approximation for calculation of excitation energies. Conversely, where little or no resonance interaction exists (e.g., if the substituent is $-NH_3^+$) excitation energy data are unsatisfactory for the evaluation of inductive parameters.

An analysis similar to that on the transition energies may be carried out on the ionization energy, leading to

$$\left(\frac{\partial I}{\partial \alpha_s}\right)_{\Delta=0} = -\left[1 - \frac{(h_{sx} - SH_{aa}^0)^2}{(H_{aa}^0 - H_{xx})^2} - 2S\frac{(H_{ax} - SH_{aa}^0)}{(H_{aa}^0 - H_{xx})}\right] C_{as}^4. \tag{32}$$

For little or no resonance interaction, a large inductive effect provides large shifts in the orbital energies, and under these conditions, the ionization energy shift may be considered a function of δ_s alone. Thus the inductive parameter may be determined from this information directly. If the resonance interaction is large, however, this simplification is not valid. Equation (32) shows that $(\partial I/\partial \alpha_s)_{\Delta=0}$ has a maximum value of $-C_{as}^4$ when there is no resonance interaction. For large resonance interaction this term may become quite small,[33] and the ionization energy shift will not depend very strongly on the inductive parameter. The conclusions on ionization potentials are of course independent of whether the hydrocarbon is alternant or not. Another important result is that the empirical parameter in heterocyclics

[26] If these overlaps are included, $C_{bs} = C_{as}(1 - n_b S_c)/(1 - n_a S_c)$, which makes $|C_{bs}|$ approximately, rather than exactly, equal to $|C_{as}|$.

[27] C. A. Coulson, Proc. Phys. Soc. (London) **A65**, 933 (1952).

[28] H. C. Longuet-Higgins and R. G. Snowden, J. Chem. Soc. **1952**, 1404, have derived a similar relation for methylated alternant hydrocarbons. Their derivation, however, starts with the parent hydrocarbon orbitals and assume that the resonance and inductive effects upon the transition energy shift are independent and additive. Our derivation concludes that interaction terms are far from negligible.

[29] This is true even within the validity of Eq. (31), which was developed with the assumption of a small inductive effect. It can be shown that more nearly exact treatments including higher derivatives or direct solution of the secular equation reinforce this general viewpoint. The results are changed only slightly by inclusion of carbon-carbon overlap. For no resonance interaction, $(\partial \Delta E/\partial \alpha_s)_{\Delta=0}$ does not quite go to zero, as Coulson has shown. For large resonance interaction, the qualitative results of this section are still valid.

[30] W. W. Robertson and F. A. Matsen, J. Am. Chem. Soc. **72**, 5252 (1950).

[31] From Eq. (10), for the resonance shift, $\Delta^2 E'$ depends only on the square of the coefficient of carbon s, and inversely on the first power of $(H_{aa}^0 - H_{xx})$. $|C_{bs}|$ is always less than unity. As $(H_{aa}^0 - H_{xx})$ becomes large (resonance effect becoming smaller) the resonance term, $\Delta^2 E'$, rapidly becomes dominating.

[32] This is not precisely true, since the inductive effect does have a strong influence on the orbital energies themselves in this limiting case, whereas the differences between orbital energies cancel. As a result, there is a change in the orbital wave functions, which is felt through the electron repulsion integrals of Eq. (23). For the cases we have considered (benzene, butadiene, ethylene), the effect is not large, but not negligible either. For very large parent hydrocarbons where the orbital levels are close together, the effect may become considerable.

[33] The general result is true even though Eq. (32) breaks down when $|H_{aa}^0 - H_{xx}|$ is small.

derived from alternant hydrocarbons should not be determined from transitions between the alternant levels, but from the ionization potential or other transitions.

VI. CALCULATION OF INTEGRALS

The electron repulsion integrals entering the modified semiempirical theory can be expanded by Eq. (2) to

$$M_{ijkl}'=\sum_{t}\sum_{t'}^{N+1}\sum_{s}\sum_{s'}a_{it}a_{jt'}a_{ks}a_{ls'}M_{ss'tt'}, \qquad (33)$$

where

$$M_{ss'tt'}=\int\Phi_s(\mu)\Phi_{s'}(\mu)\frac{1}{r^{\mu\nu}}\Phi_t(\nu)\Phi_{t'}(\nu)dv_\mu dv_\nu$$

and

$$M_{ijkl}'=\int\psi_i(\mu)\psi_j(\mu)\frac{1}{r^{\mu\nu}}\psi_k(\nu)\psi_l(\nu)dv_\mu dv_\nu.$$

From Eq. (33), it would seem that a great number of integrals of the type $M_{ss'tt'}$ would be needed to calculate a single Coulomb or exchange integral for the substituted hydrocarbon. Since the integrals are obtained over all possible charge distributions, the number that need independent evaluation is reduced to a specially great extent through use of symmetry properties of these MO's, by the methods of group theory. It is plain that the degree of simplification is more highly dependent upon the symmetry of the parent hydrocarbon than upon that of the substitution product. In addition, two other practicable simplifications have been found very helpful. It is shown in Appendix C that

$$|M_{ijkl}|\leqq(M_{ijij}+M_{klkl})/2=(K_{ij}+K_{kl})/2$$
$$\leqq(M_{iijj}+M_{kkll})/2=(J_{ij}+J_{kl})/2. \qquad (34)$$

In practice, a number of cases are found in which the exchange integrals are so small as to be negligible, or almost so. For each such case, a number of the integrals M_{ijkl} may be discarded as well.

Secondly, we are considering a perturbation of the hydrocarbon by the substituent orbital, If the substituent orbital energy is far from the energy of any particular parent hydrocarbon orbital, then that orbital will be essentially unperturbed [in which case, only the a_{ii} term of Eq. (2) need be retained], or at the very worst, mixing will be important only with orbitals of nearly the same energy, and the remainder may be eliminated. It has been found by actual computation that orbitals with energies more than 2β removed from Φ_i of Eq. (2) need not be considered in the expansion.

For the special case of a substituted hydrocarbon possessing C_{2v} symmetry, the combination of symmetry with small coefficients and with Eq. (34) make it unnecessary to calculate any integrals over the substituent orbital, Φ_x, for many interesting transitions. In these cases, the electron interaction integrals are determined solely by the change in electron repulsion due to the perturbed charge distribution in the hydrocarbon part of the molecule. Molecules which fall under this situation and whose parent hydrocarbons have been subjected to an SCF procedure may need no calculation of new integrals, and even if the SCF procedure has not been carried out, all necessary integrals can be determined frequently from published tables. As an indication of the simplification possible, one might mention that in the case of monosubstituted benzenes, of approximately 2400 integrals potentially required, only about 20 need specific evaluation, and for two sets of transitions, no integrals over substituent AO's need be calculated.

The calculation of energy shifts provides a further reduction in the number of integrals that need be computed, which would not be possible if absolute energy values were calculated. This hinges upon the assumption of neglect of all δ_μ, $\mu\neq s$. For then, orbitals which do not mix with Φ_x on symmetry grounds remain unchanged with respect to those in the parent hydrocarbon, and the difference $(M_{ijkl}'-M_{ijkl})$ vanishes, provided i, j, k, and l refer to such orbitals.

APPENDIX A. ORTHOGONALIZED ORBITALS FOR ANILINE AND *TRANS*-1-AMINOBUTADIENE

The matrix form of the orthogonalized orbitals, calculated by Löwdin's procedure[17] is given below. Note that all overlap integrals have been included, both between carbon AO's and between the substituent and all the various hydrocarbon AO's. For aniline, the overlap integrals are from Fischer[34]; for aminobutadiene, they have been calculated from formulas given by Mulliken, Rieke, Orloff, and Orloff,[35] assuming the same $C-N$ bond distance and Z value as in aniline:

Aniline

$$\begin{bmatrix}\Phi_1^0\\ \Phi_2^0\\ \Phi_3^0\\ \Phi_6^0\\ \Phi_{NH_2}^0\end{bmatrix}=\begin{bmatrix}1.0026 & 0.0037 & 0.0038 & 0.0062 & -0.0433\\ 0.0037 & 1.0045 & 0.0055 & 0.0091 & -0.0631\\ 0.0038 & 0.0055 & 1.0056 & 0.0092 & -0.0640\\ 0.0062 & 0.0091 & 0.0092 & 1.0151 & -0.1053\\ -0.0433 & -0.0631 & -0.0639 & -0.1053 & 1.0350\end{bmatrix}\begin{bmatrix}\Phi_1\\ \Phi_2\\ \Phi_3\\ \Phi_6\\ \Phi_{NH_2}\end{bmatrix}$$

Trans-1-aminobutadiene

$$\begin{bmatrix}\Phi_1^0\\ \Phi_2^0\\ \Phi_3^0\\ \Phi_4^0\\ \Phi_{NH_2}^0\end{bmatrix}=\begin{bmatrix}1.0030 & 0.0036 & 0.0029 & 0.0037 & -0.0424\\ 0.0036 & 1.0050 & 0.0040 & 0.0050 & -0.0580\\ 0.0029 & 0.0040 & 1.0032 & 0.0040 & -0.0466\\ 0.0037 & 0.0050 & 0.0040 & 1.0050 & -0.0583\\ -0.0424 & -0.0580 & -0.0466 & -0.0583 & 1.0161\end{bmatrix}\begin{bmatrix}\Phi_1\\ \Phi_2\\ \Phi_3\\ \Phi_4\\ \Phi_{NH_2}\end{bmatrix}$$

APPENDIX B. MATHEMATICAL FORM OF SOLUTIONS OF THE SECULAR EQUATION

We consider in this appendix the problem of computing the energy and wave functions from the complete secular equation (3), including the overlap integrals S_{jx}. The matrix method developed by Chirgwin and Coulson[36] and Löwdin[17] breaks down for heteromolecules since the matrix H does not commute with the matrix S (as is readily ascertained by direct computation). Löwdin[17] has developed another method involving the calculation of a matrix H', $H'=(1+S)^{-\frac{1}{2}}H(1+S)^{-\frac{1}{2}}$, by means of which the solutions of (3) with overlap integrals included may be obtained from the much more easily obtained solutions, neglecting the overlap integrals. We have found this method unwieldy for the molecules considered here, and have developed an alternative computationally simple procedure for accomplishing this end.

We first solve (3) in the approximation that:

$$S_{jx}=0;\quad H_{jx}=C_{js}\beta;\quad H_{jj}=\alpha+n_j\beta+C_{js}^2\delta_s\beta;\quad j\neq x$$
$$H_{ij}=\delta_s C_{is}C_{js}\beta,\ i\neq j\neq x;\quad H_{xx}=\alpha+\delta\beta. \qquad (35)$$

[34] I. Fischer, Arkiv Fysik **5**, 377 (1952).
[35] Mulliken, Rieke, Orloff, and Orloff, J. Chem. Phys. **17**, 1248 (1949).
[36] B. H. Chirgwin and C. A. Coulson, Proc. Roy. Soc. (London) **A201**, 196 (1950).

In Eq. (35), the c's are as defined by (1) and the subscript s refers to the carbon atom to which the substituent is attached. If we introduce the notation that $A_j=(\alpha-E_j)/\beta$ where E_j is a root of (3) under the conditions (35), then the general solution of the determinantal equation may be written in the form:

$$\delta=F_j-A_j, \tag{36}$$

where

$$F_j=\frac{\sum_{k=1}^{N} C_{ks}^2 \prod_{i\neq k=1}^{N}{}' (A_j+n_i)}{\prod_{i=1}^{N} (A_j+n_i)+\delta_s \sum_{k=1}^{N} C_{ks}^2 \prod_{i\neq k=1}^{N}{}' (A_j+n_i)}. \tag{37}$$

From (36) and (37) one may conveniently construct a graph plotting A_j as a function of δ for given values of n_i and δ_s. The wave functions corresponding to these orbital energies are given by Eq. (2), for which the individual a_{ji} may be explicitly determined from the normalization condition and from the ratio of the coefficients of Φ_i and Φ_x in ψ_j of (2) determined from the equation

$$\frac{a_{ji}}{a_{jx}}=\frac{C_{is} \prod_{k\neq i=1}^{N}{}' (A_j+n_k)}{\prod_{k=1}^{N} (A_j+n_k)+\delta_s \sum_{k=1}^{N} C_{ks}^2 \prod_{l\neq k=1}^{N}{}' (A_j+n_l)}. \tag{38}$$

Equations (35) to (38) may be utilized whether the carbon-carbon overlap integrals in the parent hydrocarbon have been included or not. Chirgwin and Coulson[36] and Wheland[22] have shown how to obtain the hydrocarbon MO's and wave functions including overlap from those obtained omitting it. In particular, if n_j and C_{js} as used in (35) are obtained from results omitting this overlap, then it can readily be shown that Eqs. (35) to (38) hold exactly for the case with overlap if n_j and C_{js} are replaced by

$$n_j'=\frac{n_j}{1+s_c n_j}\frac{\gamma}{\beta} \quad \text{and} \quad C_{js}'=\frac{C_{js}}{(1+s_c n_j)^{\frac{1}{2}}}. \tag{39}$$

Here s_c is the nearest neighbor carbon-carbon overlap integral. In the case with overlap, the empirically determined parameter, β, must be now replaced by Mulliken and Rieke's $\gamma=\beta-s_c\alpha$ (26) in H_{jj} and H_{xx} but not in H_{ij} or H_{jx}.

We now consider the introduction of the substituent-hydrocarbon MO overlap integral, S_{jx} [Eq. (3)] and possible additional assumptions concerning the nature of the element H_{jx}. We have obtained the general solutions of (3) under the following revised approximations:

$$\begin{aligned} &S_{jx}=C_{js}, \quad s=\int \phi_x\phi_s dv; \quad H_{jx}=C_{js}R\beta; \\ &H_{jj}=\alpha+n_j\beta+C_{js}^2\delta_s\beta; \quad j\neq x \\ &H_{xx}=\alpha+\delta'\beta; \quad H_{ij}=\delta_s C_{is}C_{js} \quad i\neq j,\ i,\ j\neq x. \end{aligned} \tag{40}$$

In this case, instead of Eq. (36), we find the related relationship:

$$\delta'=(f_j-1+R)^2F_j-A_j, \tag{41}$$

in which F_j is given by Eq. (37), and

$$f_j=1-s\left(\frac{\alpha}{\beta}-A_j\right). \tag{42}$$

The wave function coefficients with the revised assumptions can be obtained from those of Eq. (38) by

$$\frac{a_{ji}'}{a_{jx}'}=\frac{a_{ji}}{a_{jx}}(f_j-1+R), \quad i\neq x, \tag{43}$$

followed by the usual normalization procedure. In this manner one can obtain the energy values and wave functions for the complete range of δ in at most a few hours' time.

Finally it should be noted that inclusion of the factor R covers the two approximations most commonly used: that of Matsen and Pauling, for which $R=1$, and that of Wheland, for which $R=s/s_c$.

APPENDIX C. INEQUALITY RELATIONS AMONG ELECTRON REPULSION INTEGRALS

The proof of the left-hand inequality in Eq. (34) can be obtained in the same manner that Roothaan[7] has given for the other inequalities. The energy of a continuous charge distribution $\rho(x, y, z)$ is

$$\int \frac{\rho^\mu \rho^\nu}{r^{\mu\nu}} dv^{\mu\nu}=\frac{1}{8\pi}\int E^2 dv \geqq 0,$$

where $\rho^\mu=\rho(x^\mu, y^\mu, z^\mu)$, $E=\text{Div}\ \rho$; the equal sign holding if and only if $\rho\equiv 0$. Following Roothaan, let $\rho=e^2(\Phi_i^*\Phi_j-\Phi_k^*\Phi_l)$; then

$$\begin{aligned} 0 &\leqq e^4\int \frac{(\Phi_i^*\Phi_j-\Phi_k^*\Phi_l)(\Phi_i^*\Phi_j-\Phi_k^*\Phi_l e)dv^{\mu\nu}}{r^{\mu\nu}} \\ &=K_{ij}+K_{kl}-2M_{ijkl}. \end{aligned} \tag{44}$$

Hence

$$M_{ijkl}\leqq (K_{ij}+K_{kl})/2,$$

the equal sign holding if and only if

$$\Phi_l^*\Phi_j=\Phi_k^*\Phi_l.$$

Next let

$$\rho=e^2(\Phi_i^*\Phi_j+\Phi_k^*\Phi_l),$$

then

$$-M_{ijkl}\leqq (K_{ij}+K_{kl})/2, \tag{45}$$

and since K_{ij} and K_{kl} are $\geqq 0$, we have established the inequality

$$|M_{ijkl}|\leqq (K_{ij}+K_{kl})/2. \tag{46}$$

Raman and Infrared Spectral Data and Tentative Assignments for *cis*- and *trans*-Diiodoethylene

SIDNEY I. MILLER, *Department of Chemistry, Illinois Institute of Technology, Chicago 16, Illinois*
AND
ALFONS WEBER AND FORREST F. CLEVELAND, *Spectroscopy Laboratory,* Department of Physics, Illinois Institute of Technology, Chicago 16, Illinois*

(Received April 8, 1954)

Raman displacements, relative intensities, and depolarization factors, as well as wave numbers and estimated relative intensities for the infrared absorption bands in the region 400–4000 K (K=kayser=cm^{-1}), have been obtained. Tentative assignments are given for the observed wave numbers and the applicability of the sum and product rules of Mizushima and Bernstein is discussed.

SEVERAL articles[1–5] have appeared recently on the spectra of ethylene and its halogen and deuterium derivatives. However, except for a single investigation[6] of the infrared spectrum in the region 525–1450 K,[7] no quantitative spectral data for *cis* and *trans* IHC=CHI could be found. The present article gives Raman and infrared spectral data and tentative assignments for these molecules.

EXPERIMENTAL

The preparation of the compounds has been described previously.[8] Since pure *cis* IHC=CHI was not available, measurements were made on the eutectic liquid which contains about 20 percent of the solid *trans* isomer dissolved in the liquid *cis* isomer. The data for pure *trans* IHC=CHI were obtained from solutions in CCl_4 and CS_2. No spectral data could be obtained for the gaseous state because of the low vapor pressures at room temperature.

The Raman spectral data were obtained from spectrograms made with a Hilger E612 Raman spectrograph using the $f/1.5$ camera whose inverse dispersion is 66 A/mm at 4358 A. Both the *cis* and *trans* samples decomposed rapidly, with formation of I_2, upon exposure to Hg 4358 A. The resultant discoloration of the samples, as well as continuous background on the plates, made exposures longer than 1 hr unrewarding.

The depolarization factors (single-exposure method[9]) were obtained by use of both a Gaertner microdensitometer and a Leeds and Northrup microphotometer. Although the polarization state of a given band is rarely in doubt, most of the depolarization factors are only approximate.

Wave numbers and estimated relative intensities for the infrared absorption spectra were obtained with a Beckman IR-2 spectrophotometer with KBr optics and a 0.11 mm cell from 400 to 1000 K, and with a Perkin-Elmer Model 21 double-beam spectrometer with NaCl optics and matched cells of *ca* 0.1 and 0.025 mm from 600 to 4000 K.

Once the spectrum of *trans* IHC=CHI was known, it was possible to eliminate the obvious *trans* wave numbers from the spectrum of the eutectic solution and thus to obtain the wave numbers of *cis* IHC=CHI. Fortunately, overlapping of the two spectra appeared not to be too serious.

DISCUSSION OF RESULTS

The observed wave numbers, relative intensities, depolarization factors, and tentative assignments, together with Emschwiller and Lecomte's[6] earlier data for the *cis* and *trans* compounds, are given in Tables I and II. Because the wave numbers obtained from CCl_4 and CS_2 solutions of *trans* IHC=CHI differed consistently, data for both solutions are reported. Figures 1–4 show the transmission curves for the *trans* and *cis* compounds from 600 to 4000 K.

trans IHC=CHI

Of the six fundamentals allowed in the Raman spectrum for the *trans* compound, the 3026, 1537, 1225, 663, and 154 K bands can be assigned to the a_g type vibrations.[10] The weak 592 K band was assigned to the b_g mode, consistent with its appearance in summation tones and its depolarization factor. Of the six fundamentals allowed in the infrared, the 907 K band was assigned as one of the a_u modes and the 3069, 1128, and 588 K bands were assigned to the b_u vibration type.

* Publication No. 99. Presented at the 125th American Chemical Society Meeting, March, 1954.

[1] R. L. Arnett and B. L. Crawford, Jr., J. Chem. Phys. **18**, 118 (1950).

[2] H. J. Bernstein and D. A. Ramsay, J. Chem. Phys. **17**, 556 (1949).

[3] H. J. Bernstein, J. Chem. Phys. **17**, 256 (1949).

[4] J. Charette and C. Manneback, Ann. Soc. Sci. Bruxelles **66**, 178 (1952).

[5] P. Torkington, J. Chem. Phys. **17**, 1279 (1949); Proc. Roy. Soc. (London) **A206**, 17 (1951).

[6] G. Emschwiller and J. Lecomte, J. phys. radium **8**, 130 (1937).

[7] In accord with the recommendation of the Joint Commission for Spectroscopy, σ is used as the symbol for wave number and K (kayser) is used for the wave number unit. See J. Opt. Soc. Am. **43**, 410 (1953).

[8] S. I. Miller and R. M. Noyes, J. Am. Chem. Soc. **73**, 2376 (1951); **74**, 629 (1950).

[9] F. F. Cleveland, J. Chem. Phys. **13**, 101 (1945).

[10] The normal modes, symmetry types, selection rules, and the numbering of the fundamentals are similar to those given for *cis* and *trans* ClHC=CHCl; see G. Herzberg, *Infrared and Raman Spectra of Polyatomic Molecules* (D. Van Nostrand Company, Inc., New York, 1945), p. 330.

TABLE I. Raman and infrared spectral data and tentative assignments for *trans* IHC=CHI.[a]

Raman (CCl_4, CS_2 solutions)				Infrared							
				EL	*PR*(CCl_4)		*PR*(CS_2)			Theoretical tentative assignment	Type
$\Delta\sigma$	*I*	ρ	*PS*	σ	σ	I_e	σ	I_e	σ_c		
...	...	...	...	...	...	...	...	...	73[b]	σ_7	a_u
154	1000	0.32	*P*	...	...	...	...	...	...	σ_5	a_g
...	...	...	...	...	...	...	...	...	214[b]	σ_{12}	b_u
...	...	...	...	...	(500	vvw)	...	...	501	$\sigma_7+2\sigma_{12}$	a_u
553	(1)	...	...	...	...	...	...	...	562	$\sigma_3-\sigma_4$	a_g
...	...	...	...	...	(567	vw)	...	...	560	$\sigma_3-(\sigma_7+\sigma_8)$	b_u
...	...	...	...	588	589	s	586	s	...	σ_{11}	b_u
592	(2)	0.79	*D*	...	...	...	...	...	...	σ_8	b_g
663	150	0.47	*P*	...	...	...	...	...	...	σ_4	a_g
...	...	...	...	664	666	vw	666	vw	665	$\sigma_7+\sigma_8$	b_u
...	...	...	...	704	(701	vvw)	700	vvw	700	$\sigma_{10}-2\sigma_{12}$	b_u
...	...	...	...	730	...	...	740	w	736, 742	$\sigma_4+\sigma_7$ or $\sigma_5+\sigma_{11}$	a_u or b_u
...	...	...	...	...	866	vw	866	w	877	$\sigma_4+\sigma_{12}$	b_u
...	...	...	...	895	908	vs	906	vs	...	σ_6	a_u
...	...	...	...	...	1011	vw	...	...	1011	$\sigma_3-\sigma_{12}$	b_u
...	...	...	...	1051	1057	w	1054	w	1061	$\sigma_5+\sigma_6$	a_u
...	...	...	...	1120	1130	vs	1126	vs	...	σ_{10}	b_u
1178	3	...	...	...	...	...	...	...	1178, 1184	$2\sigma_{11}$ or $2\sigma_8$	a_g
1225	97	0.44	*P*	...	...	...	...	...	...	σ_3	a_g
...	...	...	...	...	1228	m	1225	m	1229	$(\sigma_3+\sigma_8)-\sigma_{11}$	a_u
1321	(3)	(0.79	*P*)	...	...	...	...	...	1326	$2\sigma_4$	a_g
1537	11	0.68	*P*	...	...	...	...	...	...	σ_2	a_g
...	...	...	...	...	1609	s	1604	s	1610	$\sigma_2+\sigma_7$	a_u
...	...	...	...	...	1799	w	1793	w	1791	$\sigma_4+\sigma_{10}$	b_u
...	...	...	...	...	1817	w	1813	w	1813	$\sigma_3+\sigma_{13}$	b_u
...	...	...	...	...	2666	w	2656	w	2665	$\sigma_2+\sigma_{10}$	b_u
3026	11	(0.82	*P*)	...	...	...	...	...	...	σ_1	a_g
...	...	...	...	...	3075	vs	3062	vs	...	σ_9	b_u
3080	12	0.63	*P*	...	...	...	...	...	3074	$2\sigma_2$	a_g
...	...	...	...	...	3745	w	3731	w	3732	$\sigma_4+\sigma_9$	b_u

[a] $\Delta\sigma$ = Raman displacement in K; *I* = relative intensity; ρ = depolarization factor; *PS* = polarization state (*P*, polarized; *D*, depolarized); σ = wave number in K; I_e = estimated relative intensity (s = strong, m = medium, w = weak, v = very); *EL* = Emschwiller and Lecomte, reference 6; *PR* = present results for the indicated solvents; σ_c = calculated wave number in K; and parentheses enclose uncertain or approximate quantities.
[b] Deduced from combinations.

The two remaining infrared fundamentals had to be deduced from combination tones since they were outside the range of the available instruments; the values obtained are $\sigma_7(a_u)=73$ K and $\sigma_{12}(b_u)=214$ K. The majority of the remaining bands were assigned as binary combinations or first overtones, but the 567, 700, and 1228 K bands had to be assigned as ternary combinations. Since no vapor phase spectra could be obtained, it was not possible to use band contours as an aid in making the assignments.

cis IHC=CHI

The assignments for the five a_1 fundamentals for the *cis* compound offered no difficulty. The 3023, 1219, 672, and 400 K bands were assigned to the b_1 modes. The Raman bands for the b_1 fundamentals σ_9 and σ_{10} may have been overlapped by bands of the *trans* compound. The 645 band was assigned as the b_2 fundamental. It is probably weak in the Raman and may have been overlapped by the 663 K *trans* band. The majority of the remaining bands could be assigned as binary combinations. Of these the 3082 K band was probably overlapped by the *trans* 3080 K band. Two weak bands —237 (anti-Stokes) and 440 (Stokes)—were omitted from Table II since they were considered to be the 176 and 496 K bands excited by 4358 A. (Presumably the strong 156 K band should also have appeared by secondary excitation at 211 K, anti-Stokes, but it was not found.)

Since we had some difficulty in assigning the two a_2 bands, it seems desirable to discuss this problem in some detail. Data and assignments for ClHC=CHCl were available in the literature and these were known also for BrHC=CHBr.† If a regular sequence or trend were the criterion for making the a_2 assignments in the *cis* series ClHC=CHCl, BrHC=CHBr, IHC=CHI, one might have for $\sigma_7(a_2)$ the values 406, 370, and 337 K, respectively; and for $\sigma_6(a_2)$ one might extrapolate from 876 and 868 K to the hypothetical 860 K band for *cis* IHC=CHI. However, no such regularity has been observed or justified, nor has it been observed for the $\sigma_6(a_u)$ bands in the corresponding *trans* series 895, 748, and 907 K.

Originally, the depolarized Raman bands 176 and 337 K were assigned as $\sigma_7(a_2)$ and $\sigma_6(a_2)$. However, on the basis of his work on the ClHC=CHCl and ClDC=CDCl compounds, H. J. Bernstein has suggested that the *cis* σ_6 and σ_7 vibrations are appreciably hydrogenic, and that at least one of these assignments—probably

† H. J. Bernstein, private communication, June 14, 1954.

TABLE II. Raman and infrared spectral data and tentative assignments for liquid *cis* IHC=CHI (containing *ca* 20 percent *trans*).[a]

Raman				Infrared					
				EL	*PR*			Theoretical tentative	
$\Delta\sigma$	*I*	ρ	*PS*	σ	σ	I_e	σ_c	assignment	Type
85	vs	0.58	*P*	...	...	...	...	σ_5	a_1
156	(240)	0.30	*P*	...	...	...	...	Probably *trans*	...
176	190	0.94	*D*	...	...	...	...	σ_7	a_2
337	37	>1.0	*D*	...	...	...	352	$2\sigma_7$	a_1
400	270	0.77	*D*	...	...	...	...	σ_{11}	b_1
...	...	...	...	...	484	vw	485	$\sigma_5+\sigma_{11}$	b_1
496	1000	0.07	*P*	...	494	s	...	σ_4	a_1
...	...	...	...	586	584	vs	...	Probably *trans*	...
...	...	...	...	653	645[b]	s	...	σ_{12}	b_2
664	330	0.48	*P*	...	...	...	...	Probably *trans*	...
...	...	...	...	...	672	vs	...	σ_{10}	b_1
...	...	...	...	730	733	m	...	Probably *trans*	...
...	...	...	...	...	785	w	788	$\sigma_2-(\sigma_5+\sigma_{10})$	b_1
...	...	...	...	...	874	w	873	$\sigma_2-\sigma_{10}$	b_1
...	...	...	...	905	908	s	...	Probably *trans*	...
...	...	...	...	...	1006	w	...	Probably *trans*	...
...	...	...	...	...	1050	w	...	Probably *trans*	...
1121	175	(0.87	*D*)	1094	1118	vs	...	σ_3	a_1
...	...	...	...	1163	...	...	...	...	...
...	...	...	...	...	1219	vs	...	σ_9	b_1
1226	140	0.37	*P*	...	...	...	...	Probably *trans*	...
...	...	...	...	...	1307	m	1304	$\sigma_5+\sigma_9$	b_1
...	...	...	...	...	1337	m	1344	$2\sigma_{10}$	a_1
...	...	...	...	1448	(1457	vw)	1460	$\sigma_2-\sigma_5$	a_1
...	...	...	...	...	1512	s	1520	$\sigma_3+\sigma_{11}$	b_1
1543	29	0.55	*P*	...	1547	vs	...	σ_2	a_1
...	...	...	...	...	1604	m	...	Probably *trans*	...
...	...	...	...	...	1791	w	1792	$\sigma_3+\sigma_{10}$	b_1
...	...	...	...	...	1812	w	...	Probably *trans*	...
...	...	...	...	...	1893	m	1891	$\sigma_9+\sigma_{10}$	a_1
...	...	...	...	...	1944	vw	1945	$\sigma_2+\sigma_{11}$	b_1
...	...	...	...	...	1997	vw	1989	$2\sigma_{10}+\sigma_{12}$	b_2
...	...	...	...	...	2040	vw	2040	$\sigma_2+\sigma_4$	a_1
...	...	...	...	...	2237	w	2240	$2\sigma_3$	a_1
...	...	...	...	...	2323	vw	2337	$\sigma_3+\sigma_9$	b_1
...	...	...	...	...	2428	w	2438	$2\sigma_9$	a_1
...	...	...	...	...	2655	w	2665	$\sigma_2+\sigma_3$	a_1
...	...	...	...	...	2750	m	2764	$\sigma_2+\sigma_9$	b_1
...	...	...	...	...	3023	vs	...	σ_8	b_1
3030	130	0.46	*P*	...	...	...	...	σ_1	a_1
...	...	...	...	...	(3056)	s	...	Probably *trans*	...
3082	22	0.15	*P*	...	...	...	3090	$2\sigma_2$	a_1
...	...	...	...	...	3419	w	3423	$\sigma_8+\sigma_{11}$	a_1
...	...	...	...	...	3513	w	3518	$\sigma_4+\sigma_8$	b_1
...	...	...	...	...	3675	vw	3675	$\sigma_1+\sigma_{12}$	b_2
...	...	...	...	...	3711	m	3702	$\sigma_1+\sigma_{10}$	b_1
...	...	...	...	...	3878	w	3878	$\sigma_1+\sigma_7+\sigma_8$	b_2
...	...	...	...	...	(4901	m)[c]	4914	$\sigma_8+\sigma_9+\sigma_{10}$	b_1

[a] From eutectic solution containing *ca* 20 percent *trans* IHC=CHI. Symbols have same meaning as in Table I.
[b] From solutions in CCl_4 or cyclohexane.
[c] Observed with the Beckman IR-2 instrument. Actual value is quite uncertain.

337, $\sigma_6(a_2)$—was incorrect. It is conceivable that σ_6, which is expected to be a weak depolarized band allowed only in the Raman spectrum, may not have appeared on our plates, or may have been overlapped by the strong 664 K band. With some reservations, we finally assigned 176 K as $\sigma_7(a_2)$, 664 K (unobserved) as $\sigma_6(a_2)$, and 337 K as the first overtone of 176 K. (As the first overtone of 176 K, the 337 K band is somewhat low and would not be expected to be depolarized.)

It should be emphasized that the assignments proposed here are only tentative pending a further check by means of a normal cooordinate analysis. The probable values of the fundamentals are listed in Table III.

THE SUM AND PRODUCT RULES FOR *CIS-TRANS* ISOMERS

As an additional aid in making the assignments for *cis* IHC=CHI, the sum and product rules for geometrical isomers were used. In applying the sum rule of Mizushima *et al.*,[11] it was found that $\sum_{i=1}^{12} \sigma_i^2$ was $25.79\cdot10^6$ for the *trans* and $25.20\cdot10^6$ for the *cis*, a difference of 2.3 percent. Similarly, the sum rule of

[11] Mizushima, Shimanouchi, Nakagawa, and Miyake, J. Chem. Phys. **21**, 215 (1953).

Bernstein and Pullin,[12] in which $\sum_{i=1}^{12} \sigma_i$ was evaluated, gave 13 176 for the *trans* and 13 074 for the *cis*, a difference of 0.8 percent. This is relatively good agreement, but one must remember that these sum rules are least sensitive in the low wave number region where the difficulties in making the present assignments were greatest.

The Bernstein product rule[3] for the totally symmetric vibrations may be written as

$$\Pi a_g/\Pi a_1=(4I_z^t/Md^2)^{\frac{1}{2}}, \quad (1)$$

where Πa_g is the product of the five a_g fundamentals (wave numbers) for the *trans*, Πa_1 is the product of the five a_1 fundamentals for the *cis*, I_z^t is the moment of inertia of the *trans* isomer about its twofold symmetry axis in awu A^2, M is the molecular weight in awu, and d is the C=C bond distance in A. Application of this rule yielded 2.63 for the ratio of the wave number products (left-hand side) and 3.48 for the right-hand side, a difference of 24 percent.[13]

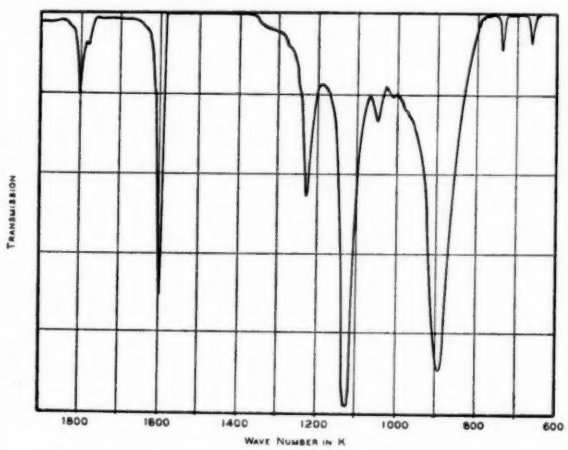

FIG. 1. Infrared absorption bands for *trans* IHC=CHI in the region 600–1900 K (CS_2 solvent).

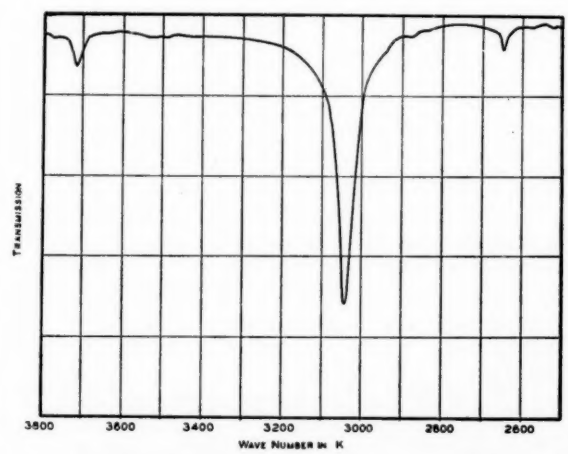

FIG. 2. Infrared absorption bands for *trans* IHC=CHI in the region 2500–3800 K (CS_2 solvent).

[12] H. J. Bernstein and A. D. E. Pullin, J. Chem. Phys. **21**, 2188 (1953).

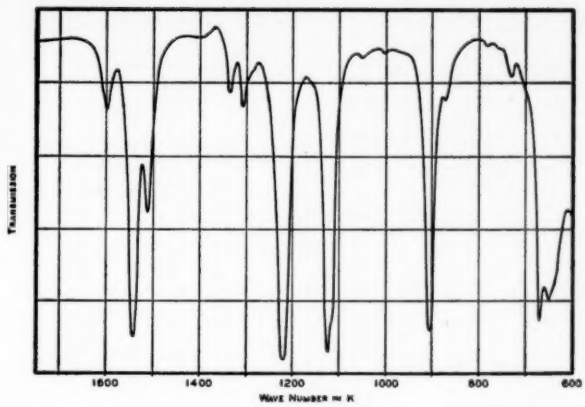

FIG. 3. Infrared absorption bands for *cis* IHC=CHI in the region 600–1700 K.

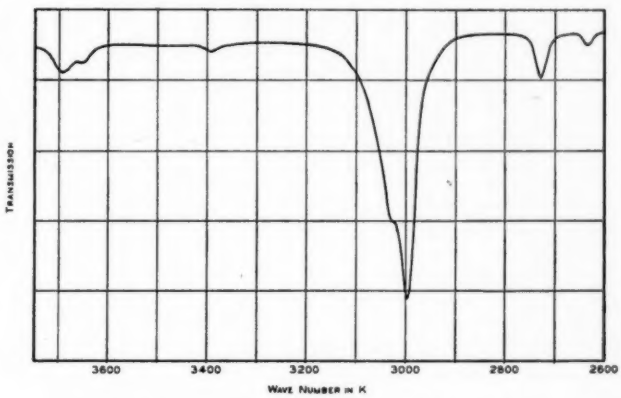

FIG. 4. Infrared absorption bands for *cis* IHC=CHI in the region 2600–3700 K.

For the planar bending vibrations, the product rule[3] may be written as

$$\Pi b_u/\Pi b_1=(Md^2/4I_z^c)^{\frac{1}{2}}, \quad (2)$$

where Πb_u is the product of the four b_u fundamentals, Πb_1 is the product of the four b_1 fundamentals, I_z^c is the moment of inertia of the *cis* isomer about its twofold symmetry axis, and other symbols have the same meaning as in Eq. (1). This yielded 0.440 for the ratio of the wave number products (left-hand side) and 0.383 for the right-hand side, a difference of 13 percent.[14] Since the a_g and a_1 assignments appear to be unambiguous,

[13] The following values were used in computing the principal moments of inertia: $m_H=1.008$, $m_C=12.01$, $m_I=126.9$ awu; C−I=2.03, C−H=1.071, C=C=d=1.353 A; C=C−H=120° and C=C−I (*trans*)=122° (see reference 5 and P. W. Allen and L. E. Sutton, Acta Cryst. **3**, 46 (1950)). The results were: $I_x^t=1547$, $I_y^t=1537$, and $I_z^t=9.972$ awu A^2. The value of M was 279.9 awu. The values used for the fundamentals were those given in Table III.

[14] The values used for the fundamentals were those given in Table III. The constants are the same as those given for the *trans* (reference 13), except that C=C−I (*cis*)=125°. The calculated moments of inertia were: $I_x^c=874.1$, $I_y^c=72.67$, and $I_z^c=946.8$ awu A^2.

the large difference in that case suggests a weakness in the product rule. It must be kept in mind, however, that the product rule is not expected to hold unless most of the corresponding potential constants of the two isomers are nearly equal. This may not be the case at all for *cis* and *trans* IHC=CHI. Even for BrHC=CHBr, the difference for the corresponding isomers is already 10 percent.[3]

Although the product rule for geometrical isomers seems to have definite limitations in this type of problem, it may, nevertheless, aid in making assignments, especially in the low wave number region where it is most sensitive to relatively small changes in the fundamentals.

ENERGY DIFFERENCE OF THE *CIS* AND *TRANS* ISOMERS

Given the equilibrium,

$$trans\ \text{IHC=CHI} \rightleftharpoons cis\ \text{IHC=CHI}, \tag{3}$$

and assuming the rigid rotator and harmonic oscillator approximations, one may write[2,15]

$$\tfrac{1}{2}\log_e\frac{(I_x{}^cI_y{}^cI_z{}^c)}{(I_x{}^tI_y{}^tI_z{}^t)}-\frac{\Delta E_0{}^0}{RT}=\log_e K-\log_e\prod_{i=1}^{12}\frac{[1-\exp(-hc\sigma_i{}^t/kT)]}{[1-\exp(-hc\sigma_i{}^c/kT)]}, \tag{4}$$

where $\Delta E_0{}^0$ is the energy difference between the *cis* and *trans* forms at 0°K, R is the gas constant, T is the temperature in degrees Kelvin, K is the equilibrium constant for (3), h is Planck's constant, c is the velocity of light, k is Boltzmann's constant, and $\sigma_i{}^t$ and $\sigma_i{}^c$ are the wave numbers for the ith fundamental for the *trans* and *cis* isomers, respectively.

If the results of Noyes *et al.*[16] for the equilibrium (3) in decalin solvent are recalculated on the basis that their *cis* isomer contained 20.5 percent *trans*,[8] one finds that K is 0.475, 0.514, and 0.542 at 129.8°, 144.1°, and 159.2°C, respectively, and that $\Delta H°$ is 1550 cal mole^{-1}. Assuming that these equilibrium constants and the present σ_i values apply in the gas phase, and plotting the right-hand side[17] of Eq. (4) against T^{-1}, it is found that $\Delta E_0{}^0$ is 1700 cal mole^{-1}. Also, one finds that $I_x{}^cI_y{}^cI_z{}^c/I_x{}^tI_y{}^tI_z{}^t$ is 41, a figure about 16 times 2.54, the value obtained from electron diffraction data. Nevertheless, these values easily "agree" within the 1000 cal uncertainty given for the equilibrium data.

TABLE III. Tentative values of the fundamentals (wave numbers in K) for *cis* and *trans* IHC=CHI.

Designation[a]	*cis*[b] σ	*cis*[b] Type	*trans*[c] σ	*trans*[c] Type
σ_1	3030	a_1	3026	a_g
σ_2	1545	a_1	1537	a_g
σ_3	1120	a_1	1225	a_g
σ_4	495	a_1	663	a_g
σ_5	85	a_1	154	a_g
σ_6	664[d]	a_2	907	a_u
σ_7	176	a_2	73[d]	a_u
σ_8	3023	b_1	592	b_g
σ_9	1219	b_1	3069	b_u
σ_{10}	672	b_1	1128	b_u
σ_{11}	400	b_1	588	b_u
σ_{12}	645	b_2	214[d]	b_u

[a] All of the fundamentals are nondegenerate (degeneracy = 1).
[b] Values for the liquid.
[c] Values for CCl_4 and CS_2 solutions.
[d] Not observed directly.

ACKNOWLEDGMENTS

This work was part of a research program for which the Spectroscopy Laboratory was aided by a contract with the Office of Ordnance Research, U. S. Army, and by grants from the Research Corporation, the Socony-Vacuum Laboratories, and the American Academy of Arts and Sciences. The infrared transmission curves were drawn by Mr. Fred L. Voelz. Dr. H. J. Bernstein aided the work by kindly making available some unpublished data on the BrHC=CHBr compounds and by helpful discussions. The authors are grateful for all this assistance.

[15] See reference 10, page 526.
[16] Noyes, Dickinson, and Schomaker, J. Am. Chem. Soc. **67**, 1319 (1945).
[17] The last term in Eq. (4) was evaluated from Johnston, Savedoff, and Belzer, *Contributions to the Thermodynamic Functions by a Planck-Einstein Oscillator in One Degree of Freedom*, NAVEXOS P-646 (Superintendent of Documents, U. S. Government Printing Office, Washington 25, D. C., 1949).

THE JOURNAL OF CHEMICAL PHYSICS VOLUME 23, NUMBER 1 JANUARY, 1955

Forces between Unlike Molecules and the Properties of Gaseous Mixtures

EDWARD A. MASON
Department of Chemistry, Pennsylvania State University, State College, Pennsylvania
(Received April 19, 1954)

The intermolecular potentials for a number of pairs of unlike molecules have been calculated from the known potentials for pairs of like molecules, by means of semi-empirical combination rules. The intermolecular potential used was of the exp-six form, $\varphi(r)=\epsilon/(1-6/\alpha)[(6/\alpha)e^{\alpha(1-r/r_m)}-(r_m/r)^6]$. The validity of the combination rules were tested by calculating a number of properties of binary gas mixtures for comparison with experimental values. The resulting agreement was quite reasonable, and it was concluded that the combination rules can be used with some confidence.

THE intermolecular potentials between like molecules for some simple nonpolar molecules have recently been determined from experimental gas and crystal properties.[1a,b] The potential used was of the exp-six form,

$$\varphi(r)=\epsilon/(1-6/\alpha)[(6/\alpha)e^{\alpha(1-r/r_m)}-(r_m/r)^6], \quad (1)$$

where $\varphi(r)$ is the potential energy of two molecules at a separation distance r, ϵ is the depth of the potential energy minimum, r_m is the position of the minimum, and α is a parameter which is a measure of the steepness of the repulsion energy. In principle, the intermolecular potentials between unlike molecules could also be determined from experimental gas properties, but not enough experimental measurements on gaseous mixtures of sufficient accuracy and over a large enough temperature range are available for the purpose. The difficulty lies partly in the fact that the properties of a gaseous mixture depend to some extent on the interaction potentials between the like molecules in the mixture as well as on the potentials between the unlike molecules. Thus measurements of extreme accuracy are required since the dependence of a property on the potential between the unlike molecules is partly masked by the dependence on the potentials between the like molecules in the mixture. In view of the lack of sufficient experimental data suitable for the direct determination of the interactions between unlike molecules, it would be useful to be able to predict such interactions from the known interactions for the like molecules. Thus properties of gaseous mixtures could be calculated from data on the pure components. Semiempirical combination rules for the exp-six potential have been suggested for this purpose, but have been tested only for helium-hydrogen mixtures.[1a] It is the purpose of the present paper to make a more extensive test of proposed combination rules by calculating properties of some binary gas mixtures for comparison with available experimental data.

[1] (a) E. A. Mason and W. E. Rice, J. Chem. Phys. **22**, 522 (1954); (b) J. Chem. Phys. **22**, 843 (1954).

DETERMINATION OF POTENTIAL PARAMETERS

If Eq. (1) is written in the form

$$\varphi(r)=Ae^{-br}-C/r^6=e^{a-br}-C/r^6,$$

a combination rule for the potential parameters is suggested from the quantum-mechanical theory of intermolecular forces. Zener[2] has shown that the parameter b for an unlike interaction may be obtained from the relation

$$b_{12}=\tfrac{1}{2}(b_{11}+b_{22}),$$

where b_{12} refers to the unlike interaction, and b_{11} and b_{22} refer to the like interactions. The theory of the dispersion energy suggests the following combination rule[3] for the parameter C:

$$C_{12}=(C_{11}C_{22})^{\frac{1}{2}}.$$

Theory does not give a combination rule for the third parameter, so an empirical relation has been used, based on the fact that the parameters A and C occur in the expression for $\varphi(r)$ in a similar way, as do the parameters a and b. These analogies lead to the two relations

$$A_{12}=(A_{11}A_{22})^{\frac{1}{2}}$$

and

$$a_{12}=\tfrac{1}{2}(a_{11}+a_{22}),$$

which are entirely equivalent.

The above combination rules become more complicated in terms of the parameters ϵ, r_m, and α of Eq. (1). The parameter $(r_m)_{12}$ for the unlike interaction is found by numerical solution of the equation

$$(GH)(r_m)_{12}^7=\exp[(G)(r_m)_{12}], \quad (2)$$

where

$$G=\frac{1}{2}\left[\frac{\alpha_{11}}{(r_m)_{11}}+\frac{\alpha_{22}}{(r_m)_{22}}\right],$$

$$H=(\alpha_{11}\alpha_{22})^{-\frac{1}{2}}[(r_m)_{11}(r_m)_{22}]^{-3}\exp[(\alpha_{11}+\alpha_{22})/2].$$

The parameters α_{12} and ϵ_{12} are then found from the

[2] C. Zener, Phys. Rev. **37**, 556 (1931).
[3] J. A. Beattie and W. H. Stockmayer, *States of Matter*, H. S. Taylor and S. Glasstone, Editors (D. van Nostrand Company, Inc., New York, 1951), pp. 350–352; J. D. Hirschfelder and W. E. Roseveare, J. Phys. Chem. **43**, 15 (1939).

relations

$$\alpha_{12}=(G)(r_m)_{12}, \tag{3}$$

$$\epsilon_{12}=(\epsilon_{11}\epsilon_{22})^{\frac{1}{2}}\left[\frac{(\alpha_{12}-6)^2}{(\alpha_{11}-6)(\alpha_{22}-6)}\right]^{\frac{1}{2}}\exp\left(\frac{\alpha_{11}+\alpha_{22}-2\alpha_{12}}{2}\right)$$

$$=(\epsilon_{11}\epsilon_{22})^{\frac{1}{2}}\left[\frac{(r_m)_{11}(r_m)_{22}}{(r_m)_{12}^2}\right]^3\left[\frac{(1-6/\alpha_{12})^2}{(1-6/\alpha_{11})(1-6/\alpha_{22})}\right]^{\frac{1}{2}}. \tag{4}$$

Substitution of the exp-six potential parameters previously found[1a,b] into Eqs. (2)–(4) leads to the values of ϵ_{12}, $(r_m)_{12}$, and α_{12} summarized in Table I. For comparison, the parameters for the like interactions are also included in the table, as well as the parameters for the system H_2-He, which has been discussed previously.[1a] These parameters may be used to calculate properties of mixtures, and the extent of the agreement of such calculations with experimental measurements serves as a test of the suitability of the combination rules. Experimentally measured properties available for comparison are the second virial coefficient, the coefficients of viscosity, thermal conductivity, and ordinary diffusion, the thermal diffusion factor, and the scattering cross section.

It is possible to formulate other combination rules which are simpler than Eqs. (2)–(4), although their basis is somewhat more empirical. One such simple alternative combination rule is discussed in the last section of this article. Although this simpler rule leads to results which are very little different from those obtained with Eqs. (2)–(4), we have confined our attention to the latter rule.

COMPARISON WITH EXPERIMENT

A. Second Virial Coefficient

The second virial coefficient of a binary gas mixture, $\mathbf{B}_m$, is given by

$$\mathbf{B}_m=x_1^2\mathbf{B}_{11}+2x_1x_2\mathbf{B}_{12}+x_2^2\mathbf{B}_{22}, \tag{5}$$

where x_1 and x_2 are the mole fractions of the two components, $\mathbf{B}_{11}$ and $\mathbf{B}_{22}$ are the virial coefficients of the pure components, and $\mathbf{B}_{12}$ is the virial coefficient of a hypothetical pure gas whose molecules interact according to the potential law for (1,2) interactions. The quantities $\mathbf{B}_m$, $\mathbf{B}_{11}$, and $\mathbf{B}_{22}$ for three of the mixtures of Table I have been measured,[4] so that experimental values of $\mathbf{B}_{12}$ may be calculated from Eq. (5). These experimental values are compared in Table II with the values calculated for the exp-six potential from the equation

$$\mathbf{B}_{12}=(2\pi N_0/3)(r_m)_{12}^3[\mathbf{B}^*+(\Lambda_{12}^2/T_{12}^*)\mathbf{B}_I^*+\cdots], \tag{6}$$

where

$$T_{12}^*=kT/\epsilon_{12},$$

$$\Lambda_{12}=h/[(r_m)_{12}(m_{12}\epsilon_{12})^{\frac{1}{2}}],$$

$$m_{12}=2m_1m_2/(m_1+m_2),$$

and N_0 is Avogadro's number, k is Boltzmann's constant, T is the absolute temperature; h is Planck's constant, and m_1 and m_2 are the masses of molecules of types 1 and 2, respectively. The dimensionless function $\mathbf{B}^*$ depends on α_{12} and T_{12}^*, and has been tabulated[5]; the dimensionless function $\mathbf{B}_I^*$ also depends on α_{12} and T_{12}^*, and represents a small quantum correction. The value of $\mathbf{B}_I^*$ was estimated from the tabulations for the Buckingham-Corner potential,[6] which is similar to the exp-six potential.

The agreement between calculated and observed values of $\mathbf{B}_{12}$ is very good for the systems H_2-A and $He-Ne$; the average absolute deviations are only 0.63 and 0.59 cc/mole, respectively. The agreement for $He-A$ is rather worse; here the average absolute deviation amounts to 3.13 cc/mole. Since the experimental uncertainty in $\mathbf{B}_{12}$ is undoubtedly rather large, this agreement is probably not to be considered unsatisfactory.

B. Viscosity

Since the viscosities of a number of the binary mixtures in Table I have been measured, a more extensive test of the potential combination rule can be obtained from a comparison of calculated and experimental viscosity values than from second virial coefficients. The viscosity of a binary mixture, η_m, is given by

$$\eta_m=(1+Z_\eta)/(X_\eta+Y_\eta), \tag{7}$$

TABLE I. Exp-six potential parameters for interactions between unlike molecules.

Parameter	Gas	H_2	He	Ne	A	Kr	Xe	CH_4
ϵ/k, °K	H_2	37.3	18.27	38.0	69.7	87.1	110.1	81.0
	He		9.16	18.71	33.4	42.2	52.3	38.3
	Ne			38.0	73.7	95.3	121.8	87.3
	A				123.2	143.0	178.5	138.5
	Kr					158.3	191.0	154.3
	Xe						231.2	191.1
	CH_4							152.8
r_m, Å	H_2	3.337	3.244	3.235	3.574	3.601	3.739	3.700
	He		3.135	3.143	3.488	3.500	3.650	3.619
	Ne			3.147	3.443	3.449	3.574	3.552
	A				3.866	3.947	4.108	4.026
	Kr					4.056	4.251	4.140
	Xe						4.450	4.315
	CH_4							4.206
α	H_2	14.0	13.22	14.24	13.97	13.01	13.31	13.92
	He		12.4	13.46	13.21	12.23	12.55	13.18
	Ne			14.5	14.17	13.17	13.45	14.10
	A				14.0	13.13	13.44	13.99
	Kr					12.3	12.65	13.17
	Xe						13.0	13.48
	CH_4							14.0

[4] L. Holborn and J. Otto, Z. Physik **23**, 77 (1924) (He–Ne); C. C. Tanner and I. Masson, Proc. Roy. Soc. (London) **A126**, 268 (1930) (H_2-A, He–A).

[5] W. E. Rice and J. O. Hirschfelder, J. Chem. Phys. **22**, 187 (1954).

[6] R. A. Buckingham and J. Corner, Proc. Roy. Soc. (London) **A189**, 118 (1947). Here is tabulated the function $F_1(\alpha,x)=(2\pi/3)\mathbf{B}_I^*(\alpha,T^*)$, where $x=1/T^*$.

where

$$X_\eta=(x_1^2/\eta_1)+(2x_1x_2/\eta_{12})+(x_2^2/\eta_2),$$

$$Y_\eta=\tfrac{3}{5}A_{12}^*\left\{\frac{x_1^2}{\eta_1}\left(\frac{M_1}{M_2}\right)+\frac{2x_1x_2}{\eta_{12}}\left[\frac{(M_1+M_2)^2}{4M_1M_2}\right]\times\left(\frac{\eta_{12}^2}{\eta_1\eta_2}\right)+\frac{x_2^2}{\eta_2}\left(\frac{M_2}{M_1}\right)\right\},$$

$$Z_\eta=\tfrac{3}{5}A_{12}^*\left\{x_1^2\left(\frac{M_1}{M_2}\right)+2x_1x_2\left[\frac{(M_1+M_2)^2}{4M_1M_2}\times\left(\frac{\eta_{12}}{\eta_1}+\frac{\eta_{12}}{\eta_2}\right)-1\right]+x_2^2\left(\frac{M_2}{M_1}\right)\right\},$$

and η_1 and η_2 are the viscosities of the pure components, and M_1 and M_2 are their molecular weights. The quantity η_{12} is the viscosity of a hypothetical pure gas whose molecules interact according to the potential law for (1,2) interactions, and whose molecular weight is $[2M_1M_2/(M_1+M_2)]$. The dimensionless quantity A_{12}^* is a function of α_{12} and T_{12}^*, and has been tabulated.[7] The pure gas viscosities, η_1, η_2, and η_{12}, may be written as

$$10^7\eta=\frac{266.93(MT)^{\frac{1}{2}}}{r_m^2}\frac{f_\eta^{(3)}}{\Omega^{(2,2)*}}, \tag{8}$$

where η is in g-cm^{-1}-sec^{-1}, M is the molecular weight, r_m is in angstroms, and $f_\eta^{(3)}$ and $\Omega^{(2,2)*}$ are dimensionless functions of α and T^* which have been tabulated.[7] In the calculation of values of η_m from Eq. (7) for comparison with measured values, experimental values of η_1 and η_2 were used, and only η_{12} was calculated from Eq. (8). Thus any discrepancies between calculated and measured values of η_m can probably be attributed directly to the parameters in Table I for unlike interactions.

Viscosities of nine of the mixtures of Table I have been measured[8] at a number of temperatures. All the experimental values were corrected to a uniform relative basis in which the viscosity of air at 23°C was taken as 1833.0×10^{-7} g-cm^{-1}-sec^{-1}. The calculations are too lengthy to be published in detail, but the results may be summarized as follows: except for mixtures containing krypton or xenon the agreement between calculated and observed viscosity values is good; the average absolute deviation is less than one percent except for a few cases in which the experimental results are not that accurate, but in these cases the agreement is at least as good as the consistency of the data. Some typical results are shown in Fig. 1. Part A shows η_m as a function of composition at 293.2°K for some gas pairs which exhibit a number of different curve shapes; part B shows two more mixtures, and includes results at several temperatures. Thus both the composition dependence and the temperature dependence of η_m are shown. For mixtures containing krypton or xenon the agreement is poor: the average absolute deviation amounts to 2 to 5 percent. However, these deviations do not seem to be due to the inadequacy of the combination rule for krypton and xenon, as indicated by the fact that the deviations for mixtures containing these gases are less than the deviations of calculated viscosities for pure krypton and xenon. The discrepancies are basically due to the fact that with the exp-six potential model, the experimental viscosities of krypton and xenon are not consistent with experimental crystal and equation of state data. It remains to be seen whether this is the result of large experimental errors or of the failure of the exp-six model for krypton and xenon.

TABLE II. Comparison of observed values of the second virial coefficient interaction term, $\mathbf{B}_{12}$, for mixtures with those calculated from the combination rule for the exp-six potential.

Mixture	T, °K	$\mathbf{B}_{12}$, cc/mole Calc.	Obs.	Dev., cc/mole
H_2-A	298.2	7.79	7.93	+0.14
	322.2	9.46	9.30	+0.16
	348.2	10.85	10.98	+0.13
	373.2	11.85	12.53	+0.68
	398.2	12.87	13.78	+0.91
	423.2	13.82	14.88	+1.06
	447.2	14.46	15.82	+1.36
He−Ne	273.2	12.74	13.49	+0.75
	373.2	13.40	13.94	+0.54
	473.2	13.28	13.18	−0.10
	573.2	13.15	12.79	−0.36
	673.2	12.93	11.72	−1.21
He−A	298.2	15.28	18.38	+3.10
	323.2	15.78	18.78	+3.00
	348.2	16.24	19.28	+3.04
	373.2	16.65	19.68	+3.03
	398.2	17.01	20.22	+3.21
	423.2	17.32	20.60	+3.28
	447.2	17.58	20.86	+3.28

C. Thermal Conductivity

In using experimental values of the thermal conductivity of mixtures to test the combination rule, we are restricted completely to monatomic gases, since no adequate theory exists for the thermal conductivity of gases whose molecules can transport energy in internal degrees of freedom. The thermal conductivity of a binary mixture of monatomic gases, λ_m, is given by

$$\lambda_m=(1+Z_\lambda)/(X_\lambda+Y_\lambda), \tag{9}$$

[7] E. A. Mason, J. Chem. Phys. **22**, 169 (1954).

[8] A. G. Nasini and C. Rossi, Gazz. Chim. Ital. **58**, 898 (1928) (He−Ne, He−Kr); M. Trautz and K. F. Kipphan, Ann. Physik **2**, 743 (1929) (He−Ne, He−A, Ne−A); M. Trautz and W. Ludewigs, *ibid.*, **3**, 409 (1929) (H_2−A); M. Trautz and H. E. Binkele, *ibid.*, **5**, 561 (1930) (H_2−Ne, H_2−A, He−Ne, He−A, Ne−A); M. Trautz and K. G. Sorg, *ibid.*, **10**, 81 (1931) (H_2-CH_4); M. Trautz and R. Heberling, *ibid.*, **20**, 118 (1934) (H_2−Xe, He−Xe); van Itterbeek, van Paemel, and van Lierde, Physica **13**, 88 (1947) (H_2−Ne); de Troyer, van Itterbeek, and van den Berg, *ibid.*, **16**, 669 (1950) (H_2−Ne, He−Ne); J. W. Buddenberg and C. R. Wilke, J. Phys. & Colloid Chem. **55**, 1491 (1951) (H_2−Ne); Rietveld, van Itterbeek, and van den Berg, Physica **19**, 517 (1953) (He−A).

where

$$X_\lambda=(x_1^2/\lambda_1)+(2x_1x_2/\lambda_{12})+(x_2^2/\lambda_2),$$
$$Y_\lambda=(x_1^2/\lambda_1)U^{(1)}+(2x_1x_2/\lambda_{12})U^{(Y)}+(x_2^2/\lambda_2)U^{(2)},$$
$$Z_\lambda=x_1^2U^{(1)}+2x_1x_2U^{(Z)}+x_2^2U^{(2)},$$

and

$$U^{(1)}=\frac{4}{15}A_{12}^*-\frac{1}{12}\left(\frac{12}{5}B_{12}^*+1\right)\left(\frac{M_1}{M_2}\right)+\frac{(M_1-M_2)^2}{2M_1M_2},$$

$$U^{(2)}=\frac{4}{15}A_{12}^*-\frac{1}{12}\left(\frac{12}{5}B_{12}^*+1\right)\left(\frac{M_2}{M_1}\right)+\frac{(M_2-M_1)^2}{2M_1M_2},$$

$$U^{(Y)}=\frac{4}{15}A_{12}^*\left[\frac{(M_1+M_2)^2}{4M_1M_2}\right]\frac{\lambda_{12}^2}{\lambda_1\lambda_2}-\frac{1}{12}\left(\frac{12}{5}B_{12}^*+1\right)$$
$$-\frac{5}{32A_{12}^*}\left(\frac{12}{5}B_{12}^*-5\right)\left[\frac{(M_1-M_2)^2}{M_1M_2}\right],$$

$$U^{(Z)}=\frac{4}{15}A_{12}^*\left[\frac{(M_1+M_2)^2}{4M_1M_2}\left(\frac{\lambda_{12}}{\lambda_1}+\frac{\lambda_{12}}{\lambda_2}\right)-1\right]$$
$$-\frac{1}{12}\left(\frac{12}{5}B_{12}^*+1\right),$$

TABLE III. Comparison of observed values of the diffusion coefficient with those calculated from the combination rule for the exp-six potential.

Mixture	T, °K	Calc. D_{12}, cm²/sec $x_1=0$	$x_2=0$	Obs. D_{12}, cm²/sec	Exptl. range for x_1	Ref.
H_2-A	287.9	0.754	0.773	0.828	0–1	f
	293.2	0.778	0.797	0.772	0–1	d
	354.2	1.081	1.111	1.111	0–1	f
	418.0	1.437	1.481	1.714	0–1	f
H_2-CH_4	288.2	0.704	0.717	0.694	0–1	a
	298.2	0.748	0.762	0.726	0–1	e
He−A	287.9	0.693	0.713	0.697	0–1	f
	288.2	0.694	0.714	0.696	0–1	b
				0.706	0–1	b
				0.678	0–0.55	e
				0.731	0.53–1	e
	354.2	0.986	1.015	0.979	0–1	f
	418.0	1.308	1.346	1.398	0–1	f
A−Xe	194.7	...	0.0501	0.0518	1	g
	273.2	...	0.0973	0.0975	1	g
	329.9	...	0.140	0.138	1	g
		0.139	...	0.139	0	g
	378.0	...	0.180	0.178	1	g

All data at one atmosphere pressure.
x_1 is the mole fraction of the heavy gas.
[a] A. von Obermayer, Sitzber. Akad. Wiss. Wien **87**, 188 (1883).
[b] R. Schmidt, Ann. Physik **14**, 801 (1904).
[c] A. Lonius, Ann. Physik **29**, 664 (1909).
[d] L. Waldmann, Naturwiss. **32**, 223 (1944); Z. Naturforsch. **1**, 59 (1946); Z. Physik **124**, 2 (1947).
[e] Boyd, Stein, Steingrimsson, and Rumpel, J. Chem. Phys. **19**, 548 (1951).
[f] R. A. Strehlow, J. Chem. Phys. **21**, 2101 (1953).
[g] T. F. Schatzki, thesis, Mass. Inst. of Tech. (1954). These values, which are preliminary in nature, were obtained from measurements made with radioactive tracers.

and λ_1 and λ_2 are the thermal conductivities of the pure components, λ_{12} is the thermal conductivity of the hypothetical pure (1,2) gas, B_{12}^* is a tabulated[7] dimensionless function of α_{12} and T_{12}^*, and the other quantities are as previously defined. The pure gas thermal conductivities, λ_1, λ_2, and λ_{12}, may be written as

$$10^7\lambda=\frac{1989.1T^{\frac{1}{2}}}{M^{\frac{1}{2}}r_m^2}\frac{f_\lambda{}^{3)}}{\Omega^{(2,2)^*}}, \tag{10}$$

where λ is in cal-cm^{-1}-sec^{-1}-deg^{-1}, $f_\lambda^{(3)}$ is a dimensionless function tabulated in reference 7, and the other quantities are as defined in connection with Eq. (8).

The only rare gas mixture examined experimentally is He−A.[9] Figure 2 shows the calculated and experimental values of λ_m for this system. As in the case of viscosity, experimental values of λ_1 and λ_2 were used in Eq. (9), and only λ_{12} was calculated from Eq. (10). The average absolute deviation of the λ_m values is 2.1 percent, which is probably satisfactory since it is intermediate between the deviations between the experimental values of λ_1 and λ_2 and those calculated from Eq. (10).

D. Diffusion Coefficient

The mixture properties considered thus far, $\mathbf{B}_m$, η_m, and λ_m, all depend not only on the unlike (1,2) molecular interactions, but also depend strongly on the like molecular interactions, (1,1) and (2,2). They are thus less suitable as a test of a potential combination rule than the coefficient of ordinary diffusion, D_{12}, which to a first approximation depends only on (1,2) interactions. Unfortunately, diffusion coefficients are difficult to measure accurately, and few measurements are available over an appreciable temperature range. Indeed, data are available for only four of the mixtures listed in Table I. Furthermore, the diffusion coefficient may vary with composition by as much as several percent, so that in a diffusion experiment D_{12} will have slightly different values in various parts of the diffusion apparatus because of the different gas compositions in these parts, and will vary with time as the local composition varies. It has not been possible to allow for this effect, and in analyzing experimental diffusion results D_{12} is always assumed to be constant. Thus, with the exception of experiments involving radioactive tracers, experimental values of D_{12} represent some sort of average value, which may depend weakly on the particular geometry of the apparatus used and on the length of time for which diffusion was allowed to proceed.

The coefficient of diffusion of a binary mixture of gases of types 1 and 2 may be written as

$$D_{12}=\frac{2.6280\times10^{-3}T^{\frac{1}{2}}}{pM_{12}{}^{\frac{1}{2}}(r_m)_{12}{}^2}\frac{f_D}{\Omega_{12}{}^{(1,1)^*}}, \tag{11}$$

[9] J. Wachsmuth, Physik. Z. **9**, 235 (1908).

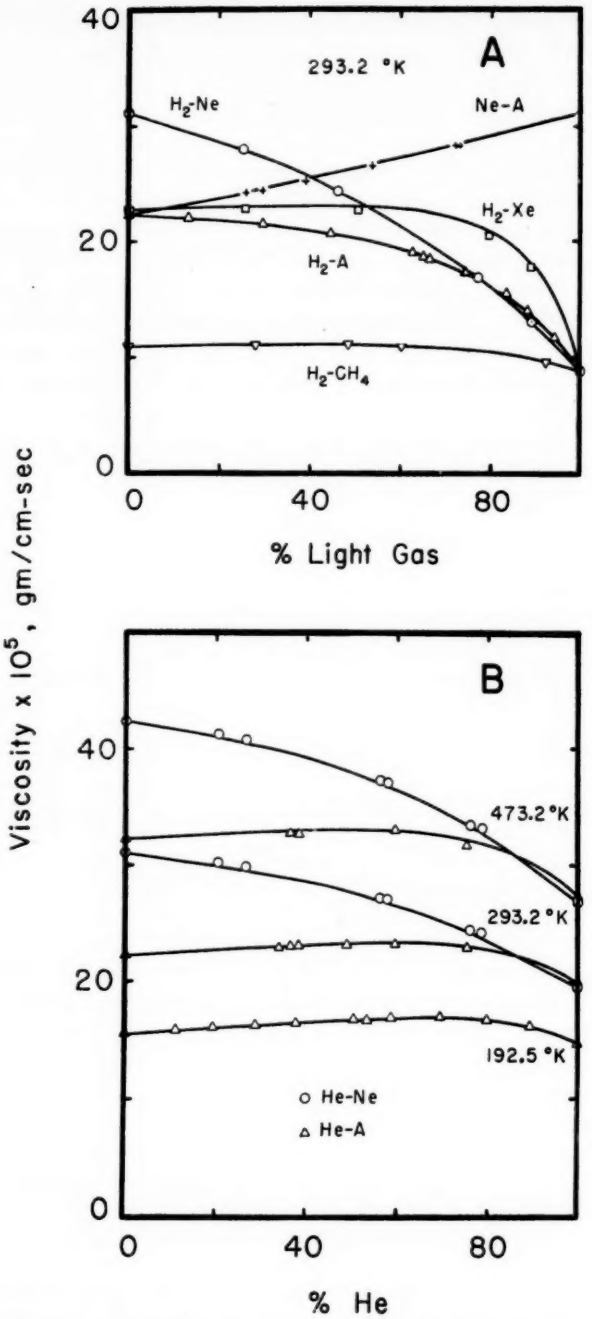

FIG. 1. Comparison of observed values of the viscosity of some binary mixtures with those calculated from the combination rule for the exp-six potential.

where D_{12} is in cm²/sec, p is the pressure in atmospheres, M_{12} is the molecular weight ratio $[2M_1M_2/(M_1+M_2)]$, $(r_m)_{12}$ is in angstroms, and $\Omega_{12}^{(1,1)*}$ is a dimensionless function of α_{12} and T_{12}^* which may be obtained from the tabulations in reference 7. The dimensionless quantity f_D is close to unity, and represents a series of higher approximations to D_{12}. The dependence of D_{12} on the composition of the diffusing mixture is entirely contained in this term, as well as the weak dependence of D_{12} on (1,1) and (2,2) molecular interactions. The very complicated third approximation to f_D, as calculated by the method of Chapman and Cowling,[10] has been given in reference 7. For the four mixtures considered here, however, it is interesting that a much simpler expression for f_D, calculated by a method due to Kihara[11] gives values of D_{12} which differ by less than 0.2 percent from those calculated from Chapman and Cowling's complicated third approximation. Kihara's second approximation to f_D, designated as $f_D^{(2)}$ and valid for vanishing concentration of component 1 of the binary mixture, is

$$f_D^{(2)}=1+\frac{M_2^2(6C_{12}^*-5)^2}{16M_1M_2A_{12}^*+10(3M_1^2+M_2^2)}, \quad (12)$$

where C_{12}^* is a dimensionless function of α_{12} and T_{12}^* tabulated in reference 7, and the other quantities are as previously defined. The expression for $f_D^{(2)}$ which is valid for vanishing concentration of component 2 is obtained from the above expression by interchanging M_1 and M_2.

In Table III are compared the experimental values of D_{12} and the values calculated from Eq. (12) for the systems H_2-A, H_2-CH_4, He−A, and A−Xe. Two values of the calculated D_{12} are given, corresponding to the two extreme compositions possible. Also indicated is the concentration range involved in the experimental measurements. Except for the highest temperature for the system H_2-A, the agreement appears to be within the probable experimental error, indicating that the potential combination rule holds for these systems.

E. Thermal Diffusion Factor

Another property which depends primarily on the interactions between unlike molecules in a mixture is

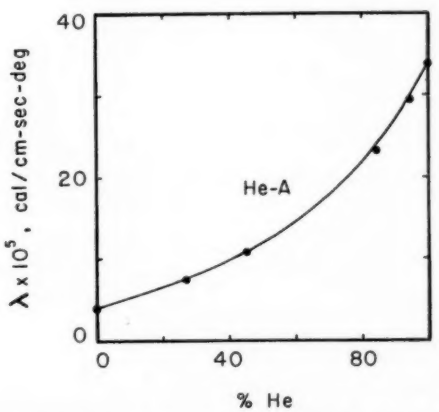

FIG. 2. Comparison of observed values of the thermal conductivity of helium-argon mixtures at 273.2°K with those calculated from the combination rule for the exp-six potential.

[10] S. Chapman and T. G. Cowling, *The Mathematical Theory of Non-Uniform Gases* (Cambridge University Press, London, 1952), second edition, Chap. 9.

[11] T. Kihara, *Imperfect Gases*, originally published in Japanese (Asakusa Bookstore, Tokyo, 1949) and translated into English by the U. S. Office of Air Research, Wright-Patterson Air Force Base, Chapter 6. See also Revs. Modern Phys. 25, 831 (1953).

the thermal diffusion factor, designated as α_T. This quantity can be measured experimentally either by observation of the extent of separation of a gas mixture under the influence of a temperature gradient (thermal diffusion), or by observation of the temperature gradients arising from the interdiffusion of different gases (diffusion thermoeffect).[12] The thermal diffusion factor depends on the composition, so that experimental values usually represent an average value over a composition range of a few percent, a situation similar to that encountered in measurements of the ordinary diffusion coefficient. In addition, measurement of α_T by the thermal separation method yields a value of α_T which represents an average over the temperature range involved, unless enough measurements are taken so that slopes of a separation *vs* temperature ratio curve may be determined.[13] However, to a good approximation, such an average value of α_T over a temperature range from T to T' corresponds to the actual value of α_T at an intermediate temperature, $\bar{T}$, given by the expression[14]

$$\bar{T}=\frac{TT'}{T'-T}\ln(T'/T). \tag{13}$$

The available theoretical approximations for the thermal diffusion factor may differ from the limiting theoretical value by much larger amounts than was the case for any of the other transport properties. Three different theoretical expressions for α_T are available, depending on the approximation procedures used: the first and second approximations of Chapman and Cowling,[1,7,10] and the first approximation of Kihara.[1,7,11] The most accurate of these is probably Chapman and Cowling's second approximation, but this is rather complicated, and the numerical computations involved are quite tedious. A few sample calculations indicated that Kihara's expression is more accurate than Chapman and Cowling's first approximation (see references 1a and 7 for examples), and usually differs from their second approximation by less than the scatter in different experimental determinations of α_T. It therefore seemed satisfactory for the present purpose to use Kihara's approximation, although as more accurate experimental measurements become available, it will probably become advantageous to use more accurate theoretical expressions for α_T. Kihara's approximation may be written in the form

$$\alpha_T=(6C_{12}^*-5)\frac{x_1S_1-x_2S_2}{x_1^2Q_1+x_2^2Q_2+x_1x_2Q_{12}}, \tag{14}$$

where[15]

$$S_1=\frac{M_1}{M_2}\left(\frac{2M_2}{M_1+M_2}\right)^{\frac{1}{2}}\left[\frac{\Omega_{11}^{(2,2)*}}{\Omega_{12}^{(1,1)*}}\right]\left[\frac{(r_m)_{11}}{(r_m)_{12}}\right]^2 -\left[\frac{4M_1M_2}{(M_1+M_2)^2}\right]A_{12}^*-\frac{15M_2(M_2-M_1)}{2(M_1+M_2)^2},$$

$$Q_1=\frac{2}{M_2(M_1+M_2)}\left(\frac{2M_2}{M_1+M_2}\right)^{\frac{1}{2}}\left[\frac{\Omega_{11}^{(2,2)*}}{\Omega_{12}^{(1,1)*}}\right] \times\left[\frac{(r_m)_{11}}{(r_m)_{12}}\right]^2\left(M_1^2+3M_2^2+\frac{8}{5}M_1M_2A_{12}^*\right),$$

$$Q_{12}=\frac{15(M_1-M_2)^2}{(M_1+M_2)^2}+\left[\frac{32M_1M_2}{(M_1+M_2)^2}\right]A_{12}^* +\frac{8}{5}\frac{(M_1+M_2)}{(M_1M_2)^{\frac{1}{2}}}\left[\frac{\Omega_{11}^{(2,2)*}}{\Omega_{12}^{(1,1)*}}\right]\left[\frac{\Omega_{22}^{(2,2)*}}{\Omega_{12}^{(1,1)*}}\right]\left[\frac{(r_m)_{11}(r_m)_{22}}{(r_m)_{12}^2}\right]^2.$$

The relations for S_2 and Q_2 are obtained from those for S_1 and Q_1 by an interchange of subscripts. The subscripts on the $\Omega^{(l,n)*}$ and the r_m refer to the three different binary molecular interactions which may occur in a binary gas mixture. By convention, the subscript 1 refers to the heavier gas. The principal contribution to the temperature dependence of α_T comes from the factor $(6C_{12}^*-5)$, which involves only the unlike (1,2) molecular interactions. The term involving the quantities S and Q determines the composition dependence of α_T, and depends only slightly on the temperature; this term involves all three possible binary molecular interactions.

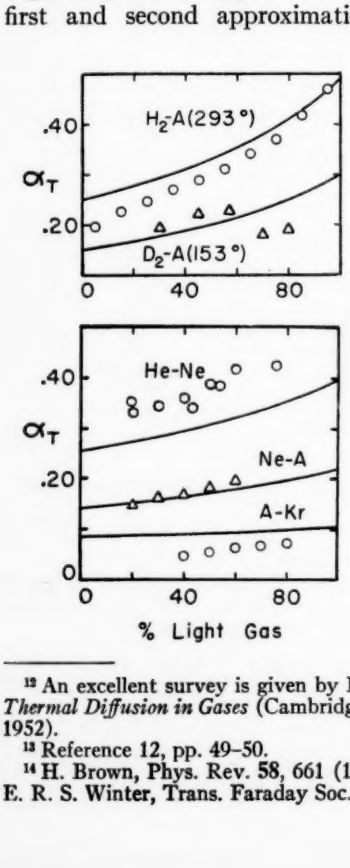

FIG. 3. Comparison of the observed and calculated composition dependence of the thermal diffusion factor, α_T, for some binary mixtures. Unless otherwise noted, $\bar{T}$ is equal to 327°K.

[12] An excellent survey is given by K. E. Grew and T. L. Ibbs, *Thermal Diffusion in Gases* (Cambridge University Press, London, 1952).

[13] Reference 12, pp. 49–50.

[14] H. Brown, Phys. Rev. **58**, 661 (1940); A. N. Davenport and E. R. S. Winter, Trans. Faraday Soc. **47**, 1160 (1951).

[15] In Eq. (16) of reference 1a, the factor 2 in the denominator of the third term of S_1 was inadvertently omitted.

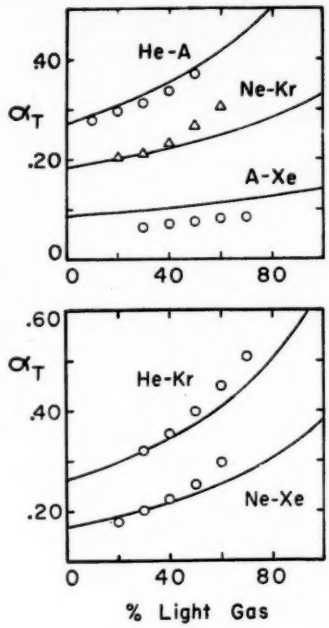

FIG. 4. Comparison of the observed and calculated composition dependence of the thermal diffusion factor, α_T, for some binary mixtures. The mean temperature, $\bar{T}$, is equal to 327°K.

Experimental values of α_T have been determined[16] for thirteen of the mixtures of Table I at a number of temperatures and compositions. Since α_T depends rather strongly on both composition and temperature, it is convenient to consider these variables separately in comparing observed and calculated values of α_T. The composition dependence of α_T is illustrated in Figs. 3 and 4, which show results for most of the mixtures examined experimentally. The calculated composition dependence is seen to be in the same direction as is observed, but is smaller in magnitude. Part of this disagreement is caused by the use of a first approximation to the theoretical expression for α_T. Use of a higher approximation, such as the second approximation of Chapman and Cowling, would tend to reduce the disagreement, but some of the discrepancy may well be due to inadequacy of the exp-six potential model and the combination rule.

A more direct test of the combination rule comes from the temperature dependence of the thermal diffusion factor, which depends principally on the interactions of unlike molecules through the factor $(6C_{12}^*-5)$ in Eq. (14). Figure 5 shows a comparison between calculated and observed values of α_T as a function of temperature for most of the mixtures of Table I for which experimental results are available. These results all refer to mixtures of approximately 50–50 mole percent of the components. In most cases the agreement is quite good, but in some the deviation between theory and observation is large, although the calculated curve is of the correct shape. This result seems to be mainly due not to the failure of the combination rules, but more likely due to the failure of the theoretical approximation to give the correct composition dependence, as for example in the case of neon-krypton mixtures. For this system the temperature dependence of α_T has been measured at a composition of 53 percent neon, and at such a composition the discrepancy between theory and experiment is already considerable, as was shown in Fig. 4. Presumably the agreement for neon-krypton shown in Fig. 5 would have been much better if the measurements had been carried out on a mixture containing about 20–30 percent neon.

The agreement between calculation and experiment for the thermal diffusion factor thus seems on the whole

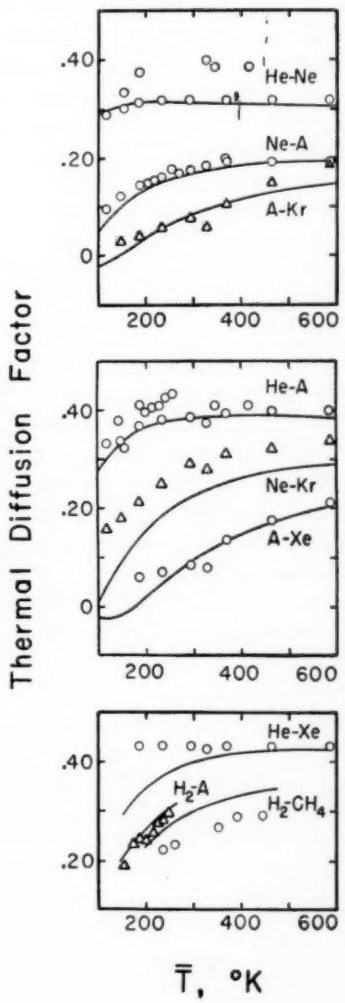

FIG. 5. Comparison of the observed and calculated temperature dependence of the thermal diffusion factor, α_T, for the systems He–Ne (53.8 percent He), Ne–A (51.5 percent Ne), A–Kr (53.5 percent A), He–A (51.2 percent He), Ne–Kr (53 percent Ne), A–Xe (56.4 percent A), He–Xe (53.6 percent He), H_2–A (47 percent H_2), and H_2–CH_4 (50 percent H_2).

[16] T. L. Ibbs, Proc. Roy. Soc. (London) **A107**, 470 (1925) (H_2–A); Ibbs, Grew, and Hirst, Proc. Phys. Soc. (London) **41**, 456 (1929) (H_2–A); T. L. Ibbs and K. E. Grew, Proc. Phys. Soc. (London) **43**, 142 (1931) (H_2–Ne, He–Ne, He–A, Ne–A); M. Puschner, Z. Physik **106**, 597 (1937) (He–Ne, He–A); Atkins, Bastick, and Ibbs, Proc. Roy. Soc. (London) **A172**, 142 (1939) (He–Ne, He–A, He–Kr, He–Xe, Ne–A, Ne–Kr, Ne–Xe, A–Kr, A–Xe, Kr–Xe); L. Waldmann, Z. Physik **124**, 2 (1947) (H_2–A by the diffusion thermoeffect); K. E. Grew, Proc. Roy. Soc. (London) **A189**, 402 (1947) (He–Ne, He–A, He–Kr, He–Xe, Ne–A, Ne–Kr, Ne–Xe, A–Kr, A–Xe); van Itterbeek, van Paemel, and van Lierde, Physica **13**, 231 (1947) (H_2–Ne, He–Ne); Drickamer, Downey, and Pierce, J. Chem. Phys. **17**, 408 (1949) (H_2–CH_4); H. G. Drickamer and J. R. Hofto, J. Chem. Phys. **17**, 1165 (1949) (Ne–A); A. van Itterbeek and A. de Troyer, Physica **16**, 329 (1950) (H_2–Ne, H_2–A, D_2–A, He–Ne, He–A); de Troyer, van Itterbeek, and van den Berg, Physica **16**, 669 (1950) (H_2–Ne, D_2–Ne, He–Ne).

TABLE IV. Some typical exp-six potential parameters for interactions between unlike molecules, as calculated from Eqs. (15)–(17). Percent deviations from the values in Table I are shown in parentheses.

Parameter	Gas	Ne	Xe
ϵ/k, °K	He	18.66 (0.3)	46.0 (12.0)
	Ne		93.7 (23.1)
r_m, A	He	3.141 (0.1)	3.792 (3.9)
	Ne		3.798 (6.3)
α	He	13.45 (0.1)	12.70 (1.2)
	Ne		13.75 (2.2)

to be reasonable, and most of the discrepancies observed may be explained as at least partially due to the use of an approximate theoretical expression.

F. Scattering Cross Section

One final check on the combination rules is of interest. The interaction potential at close distances of approach between a helium atom and an argon atom has recently been obtained directly from measurements of the scattering of high velocity helium atoms in room temperature argon, and of high velocity argon atoms in room temperature helium.[17] Although the potential derived from these measurements is correct for separation distances smaller than those for which the exp-six potential for helium-argon may be considered valid, so that the regions of validity of the two potentials do not overlap, nevertheless the regions are close enough together to ascertain that the potentials are in reasonably good concordance.[17] This furnishes a very direct check on the usefulness of the potential combination rules.

DISCUSSION

On the whole, the combination rules given in Eqs. (2)–(4) lead to quite reasonable agreement between observed and calculated properties of gaseous mixtures. It would thus seem that estimates of interactions between unlike molecules can be made with some confidence from the known interactions between like molecules. When more measurements of good accuracy become available for the diffusion coefficient and the thermal diffusion factor, it should be possible to evaluate the unlike interactions directly from experimental results rather than from semiempirical combination rules.[18]

The use of Eqs. (2)–(4) involves some trial and error numerical calculations, which are sometimes inconvenient. It should be pointed out that other combination rules, having a somewhat more empirical basis, may also be formulated. For instance, reasonable combination rules for r_m and ϵ are

$$(r_m)_{12}=\tfrac{1}{2}[(r_m)_{11}+(r_m)_{22}], \tag{15}$$

$$\epsilon_{12}=(\epsilon_{11}\epsilon_{22})^{\frac{1}{2}}. \tag{16}$$

Equation (15) is exact for rigid elastic spheres of diameter r_m, and Eq. (16) is based on the quantum theory of the dispersion energy.[3] Equations (15) and (16) have been widely used in connection with the two parameter Lennard-Jones (12–6) potential,

$$\varphi(r)=\epsilon\left[\left(\frac{r_m}{r}\right)^{12}-2\left(\frac{r_m}{r}\right)^{6}\right],$$

for calculation of gas properties,[19] and have also been applied to simple nonpolar liquid solutions.[20,21] For the exp-six potential, a further combination rule involving α is needed. Since α only varies from 12.3 to 14.5 for the molecules considered here, the simple arithmetic mean is probably satisfactory:

$$\alpha_{12}=\tfrac{1}{2}(\alpha_{11}+\alpha_{22}). \tag{17}$$

Equations (15)–(17) lead to values of ϵ_{12}, $(r_m)_{12}$, and α_{12} which do not deviate greatly from the values calculated from Eqs. (2)–(4) and tabulated in Table I. In Table IV are shown some typical results obtained from Eqs. (15)–(17); these include the systems with the smallest and the largest deviations from the corresponding values in Table I. Furthermore, the deviations in the parameters are in such a direction and of such relative magnitude as to compensate each other almost completely in the calculation of gas mixture properties at ordinary temperatures. Thus use of Eqs. (15)–(17) leads to calculated values of the properties of mixtures which at ordinary temperatures differ by only a few percent from the values calculated from Eqs. (2)–(4). However, Eqs. (2)–(4) have been used throughout the present article.

[17] Amdur, Mason, and Harkness, J. Chem. Phys. **22**, 1071 (1954).

[18] B. N. Srivastava and M. P. Madan, Proc. Phys. Soc. (London) **A66**, 277 (1953), have recently made approximate calculations of this type for the two parameter Lennard-Jones (12–6) potential. They found that the accuracy of the experimental data was such as to justify neglect of the temperature dependence of the factor containing the quantities S and Q in the theoretical expression for α_T, for practical purposes. However, some error was probably introduced into their values of the potential parameters because of their use of Chapman and Cowling's first approximation for α_T.

[19] Hirschfelder, Curtiss, and Bird, *Molecular Theory of Gases and Liquids* (John Wiley and Sons, Inc., New York, 1954), Chapters 3 and 8.

[20] J. H. Hildebrand and R. L. Scott, *The Solubility of Nonelectrolytes* (Reinhold Publishing Corporation, New York, 1950), pp. 121–132.

[21] G. Scatchard, Ann. Rev. Phys. Chem. **3**, 261–262 (1952).

Near Infrared Spectrum of Nitric Oxide*

NATHAN L. NICHOLS,† C. D. HAUSE, AND R. H. NOBLE‡
Michigan State College, East Lansing, Michigan
(Received June 18, 1954)

The 2−0 and 3−0 vibration-rotation bands of NO at 2.69 μ and 1.8 μ have been obtained and measured. The envelope of the 4−0 band at 1.36 μ was obtained. Careful reduction of the data yields the following rotational constants:

$B_0=1.6965$ cm^{-1} $\quad \alpha_e=0.0180$ cm^{-1}
$B_2=1.6631$ cm^{-1} $\quad I_e=16.404\times10^{-40}$ g cm^2
$B_3=1.6408$ cm^{-1} $\quad r_e=1.1503\times10^{-8}$ cm
$B_e=1.7060$ cm^{-1}

INTRODUCTION

NITRIC oxide, one of the few diatomic molecules which is chemically stable, has been the subject of a number of spectroscopic investigations in the ultraviolet, the infrared and recently the microwave regions.[1–10] Molecular constants for the ground state and excited electronic states were originally obtained from detailed analyses of electronic band systems. Inconsistencies in these constants obtained from analyses of the β and γ electronic band systems led Gillette and Eyster[1] to investigate the fundamental rotation-vibration band in the near infrared. As a further check on the rotational and vibrational constants the authors have examined the first (2−0) and second (3−0) overtones in the near infrared region and have re-examined the electronic data involving the ground state.

Infrared Spectrum of NO

The nitric oxide molecule is the only stable diatomic molecule to have an odd number of electrons (15), and therefore is the only stable diatomic molecule to exhibit a Q branch in the infrared. The form of the infrared bands is easily understood by a consideration of Fig. 1 which shows a typical band. Since the ground state is a $^2\Pi$ state with the $^2\Pi_{\frac{1}{2}}$ and $^2\Pi_{\frac{3}{2}}$ substates separated by 121 cm^{-1}, the band consists of two almost superimposed subbands each having P, Q, and R branches. The stronger P and R branches arise from transitions between the $^2\Pi_{\frac{3}{2}}$ substates, and the weaker P and R branches from transitions between the $^2\Pi_{\frac{1}{2}}$ substates. The weak and unresolved Q branches can be seen at the center of the band.

The infrared spectrum of NO was first observed by Warburg and Leithauser[2] in 1908. They obtained the envelope of the fundamental and located its center at 5.3 μ. In 1929 Snow, Rawlins, and Rideal[3] were able to resolve 42 lines in both P and R branches of the fundamental, but apparently used only six lines in each branch in determining the rotational constants. Their work on the first overtone[4] confirmed the existence of P, Q, and R branches, but gave no measurable quantities. In 1939 two papers dealing with the fundamental appeared, one by Nielsen and Gordy,[5] the second by Gillette and Eyster.[1] The rotational constants quoted by Herzberg[11] are taken from the work of Gillette and Eyster, which seems to be the most thorough infrared work done on NO.

EXPERIMENTAL

The nitric oxide gas, obtained from the Matheson Gas Company, had a stated purity of about 99 percent, and was used without further purification. The multiple path absorption cell was of the J. U. White type[12] having aluminum coated mirrors of five inch diameter and 35 cm radius of curvature. The recording vacuum spectrograph, built by one of the authors,[13] employed paraboloidal mirrors having apertures of $f/5$ as beam collimators and had a rock salt foreprism monochromator. It was equipped with two plane gratings having 7200 and 1800 lines per in. and had, as its detector, a lead sulfide cell.

The anharmonic constants of NO are such that overtones can be obtained with reasonable absorbing paths. The 3−0 band was obtained with an absorbing path of about 4½ meter-atmospheres (40 traversals, one-third atmos NO pressure). Figure 1 shows a typical 3−0 spectrogram in which the two P branches are resolved, the branch arising from the $2\Pi_{\frac{1}{2}}$ substates showing

* A portion of a thesis submitted by the first-named author to the School of Graduate Studies of Michigan State College in partial fulfillment of the requirements for the Ph.D. degree.
† Now at Alma College, Alma, Michigan.
‡ Now at Leeds and Northrup Company, Philadelphia, Pennsylvania.
[1] R. H. Gillette and E. H. Eyster, Phys. Rev. **56**, 113 (1939).
[2] E. Warburg and G. Leithauser, Ber. deut. chem. Ges. **1**, 145 (1908).
[3] Snow, Rawlins, and Rideal, Proc. Roy. Soc. (London) **124**, 453 (1929).
[4] C. P. Snow and E. K. Rideal, Proc. Roy. Soc. (London) **126**, 355 (1929).
[5] A. H. Nielsen and W. Gordy, Phys. Rev. **56**, 781 (1939).
[6] Jenkins, Barton, and Mulliken, Phys. Rev. **30**, 150 (1927).
[7] L. Gero and R. Schmid, Proc. Phys. Soc. (London) **60**, 533 (1948).
[8] Gero, Schmid, and von Szily, Physica **11**, 144 (1944).
[9] Schmid, Konig, and Farkas, Z. Physik **64**, 84 (1930).
[10] C. A. Burrus and Walter Gordy, Phys. Rev. **92**, 1437 (1953).
[11] G. Herzberg, *Spectra of Diatomic Molecules* (D. Van Nostrand Company, Inc., New York, 1950), p. 558.
[12] J. U. White, J. Opt. Soc. Am. **32**, 285 (1942).
[13] R. H. Noble, J. Opt. Soc. Am. **43**, 330 (1953).

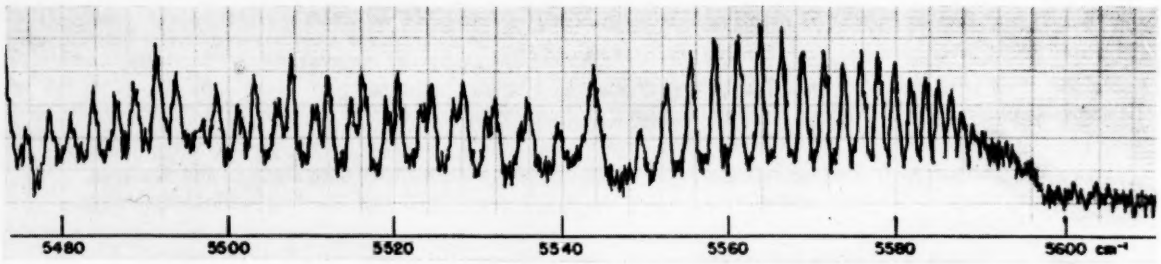

FIG. 1. Spectrogram of 3−0 band of NO at 1.80 μ taken with an absorbing path of 4½ meter-atmospheres. The P lines show the doublet splitting.

relatively greater intensity. In the spectrograms actually measured, taken at slower grating speeds and with an effective slit width of 0.4 cm^{-1}, the two P branches were completely resolved; the two R branches were resolved for $J>13/2$. The two Q branches and the individual Q lines were unresolved. The 2−0 band at 2.69 μ was obtained with an absorbing path of about 2½ meter-atmospheres (40 traversals, one-fifth atmos NO pressure).

An attempt was made to obtain the 4−0 band at 1.36 μ by increasing the absorbing path to 60 meter-atmospheres (100 traversals, two atmos NO pressure). Since the available combination of source, grating, and detector was not favorable to this region, it was necessary to use a slit of effective width 15 cm^{-1} to get recognizable absorption. Only the envelope of this band was obtained, but it showed the existence of the P, Q, and R branches with the center of the Q branch at 7337 cm^{-1}.

The frequencies of the band lines were obtained by superimposing known mercury, argon, and neon emission lines on the spectrograms as comparison standards. It is believed that the maximum error in locating the relative positions of the lines in the bands does not exceed 0.2 cm^{-1}.

MOLECULAR CONSTANTS

The energy levels for the ground state of NO may be represented by an equation due to Hill and Van Vleck which applies to doublet states having coupling intermediate between Hund's cases (a) and (b).[14] Since NO approaches pure case (a) coupling ($A/B\approx 73$), a simple expansion of the Hill and Van Vleck equation gives approximate expressions for the energies of the substates. Neglecting the small term $F(K, J-K)$ and assuming the same centrifugal force term as in pure case (a), one obtains:

$$\begin{aligned} T_1 &= T_e - A/2 + G_{1v} + B_{v1}/4 + B_{v1}J(J+1) \\ &\qquad - D_{v1}J^2(J+1)^2\cdots, \\ T_2 &= T_e + A/2 + G_{2v} - 7B_{v2}/4 + B_{v2}J(J+1) \\ &\qquad - D_{v2}J^2(J+1)^2\cdots. \end{aligned} \tag{1}$$

The first equation applies to the $^2\Pi_{\frac{1}{2}}$ substate and the second to the $^2\Pi_{\frac{3}{2}}$ substate. The B and D in the above equation are to be interpreted as effective values, the

TABLE I. Frequencies of the first and second overtones of NO.

	3−0 Band				2−0 Band				
$J+\frac{1}{2}$	$R_1(J)$	$P_1(J)$	$R_2(J)$	$P_2(J)$	$J+\frac{1}{2}$	$R_1(J)$	$P_1(J)$	$R_2(J)$	$P_2(J)$
1	5548.81	...	...	...	1	3729.10	...	...	...
2	(5551.81)[a]	5538.95	(5551.81)[a]	...	2	(3732.09)[a]	3719.28	(3732.09)[a]	...
3	(5554.79)	5535.69	(5554.79)	5534.80	3	(3735.14)	(3715.71)[a]	(3735.14)	(3715.71)[a]
4	(5557.81)	5532.19	(5557.81)	5531.11	4	(3738.18)	3712.63	(3738.18)	3711.85
5	(5560.63)	5528.40	(5560.63)	5527.30	5	(3741.10)	3708.93	(3741.10)	3707.87
6	(5563.41)	5524.64	(5563.41)	5523.44	6	(3744.26)	3704.88	(3744.26)	3703.67
7	(5565.97)	5520.80	(5565.97)	5519.39	7	(3746.96)	3700.97	(3746.96)	3699.77
8	5568.26	5516.80	5568.51	5515.28	8	(3749.66)	3697.26	(3749.66)	3696.08
9	5570.64	5512.53	5570.92	5510.78	9	(3752.37)	3693.29	(3752.39)	3692.01
10	5572.71	5508.22	...	5506.50	10	(3755.11)	3689.37	(3755.11)	3687.92
11	5574.88	5503.88	...	5502.03	11	(3757.56)	3685.18	(3757.56)	3683.75
12	5576.89	5499.46	5577.43	5497.49	12	(3760.01)	3681.07	(3760.01)	3679.29
13	5578.92	5494.92	...	5492.85	13	(3762.39)	3676.95	(3762.39)	3675.13
14	5580.71	5490.13	5581.18	5488.03	14	3764.83	3672.87	3765.63	3670.93
15	5582.43	5485.57	5582.90	5483.13	15	3767.02	3668.59	3767.74	3666.60
16	5584.01	5480.48	5584.52	5478.03	16	3769.25	3664.09	3770.07	3661.98
17	5585.41	5475.41	5585.80	5472.90	17	3771.23	3659.86	3771.83	3657.54
18	5586.79	5470.50	5587.30	5467.51					
19	5588.04	5465.30	5588.51	5462.32					

[a] Two components unresolved. Maximum of unresolved Q_1 and Q_2 branches at 5543.0 and 3724.0 cm^{-1}.

[14] R. S. Mulliken, Revs. Modern Phys. 2. 60 (1930).

true B_v and D_v being simply the mean of B_{v1} and B_{v2}, and D_{v1} and D_{v2}, respectively. Due to Λ-type doubling each of the above levels should be double, resulting in six branches in each sub-band. However, this doubling is much too small[6] to be observed in the infrared with the available dispersion and resolution.

Equations (1) show the simple J dependence of a pure case (a) molecule, and with the application of the appropriate selection rules lead directly to the observed band structure.

ROTATIONAL CONSTANTS

The wave numbers of the lines in the P and R branches for both the $^2\Pi_{\frac{1}{2}}$ and $^2\Pi_{\frac{3}{2}}$ sub-bands are given in Table I for the first and second overtones. Table II gives the combination differences:

$$\Delta_2F''(J)=R(J-1)-P(J+1)$$
and
$$\Delta_2F'(J)=R(J)-P(J). \quad (2)$$

TABLE II. Combination differences for NO.

$J+\frac{1}{2}$	$\Delta_2F_1''(J)$ (3−0, 2−0)	$\Delta_2F_2''(J)$ (3−0, 2−0)	$\Delta_2F_1'(J)$ (3−0)	$\Delta_2F_2'(J)$ (3−0)	$\Delta_2F_1'(J)$ (2−0)	$\Delta_2F_2'(J)$ (2−0)
2	13.21	...	12.86	...	12.81	...
3	19.57	20.55	19.10	19.99	19.43	19.43
4	26.33	27.42	25.62	26.70	25.55	26.33
5	33.21	34.42	32.23	33.33	32.17	33.23
6	39.93	41.27	38.77	39.97	39.38	40.59
7	46.74	48.15	45.15	46.58	45.99	47.19
8	53.52	55.11	51.46	53.23	52.40	53.58
9	60.12	61.92	58.11	60.14	59.08	60.36
10	66.90	68.80	64.49	...	65.74	67.19
11	73.51	75.82	71.00	...	72.38	73.81
12	80.18	82.43	77.43	79.94	78.94	80.72
13	86.89	89.35	84.00	...	85.44	87.26
14	93.50	95.79	90.58	93.15	91.96	94.70
15	100.40	103.32	96.86	99.77	98.43	101.14
16	107.07	110.07	103.53	106.49	105.16	108.09
17	113.51	117.01	110.00	112.90	111.37	114.29
18	120.11	123.48	116.29	119.79		
19			122.74	126.19		

The values for the lower state ($v=0$) are the averages of the values obtained from the 3−0 and 2−0 bands. In computing this average, values from the 3−0 band were given double weight, as the accuracy of the data warranted.

These combination differences were used in the graphical manner suggested by Herzberg[15] to determine the rotational constants:

$$\Delta_2F(J)-4\tilde{B}_v(J+\tfrac{1}{2})+8D_v(J+\tfrac{1}{2})^3=4\Delta B_v(J+\tfrac{1}{2}), \quad (3)$$

where $4\tilde{B}_v$ is an approximate value of $4B_v$. The subtraction of $4\tilde{B}_v(J+\frac{1}{2})$ from each combination difference allows plotting to a much larger scale. The infrared data do not extend to sufficiently high J values to allow calculation of centrifugal force constants. Accordingly, values were computed from electronic band systems and then included in Eq. (3) wherever the correction was of

[15] G. Herzberg, reference 11, p. 181.

TABLE III. Rotational constants for NO.

	Infrared 3−0, 2−0[a] cm^{-1}	Infrared 1−0[b] cm^{-1}	Electronic cm^{-1}	Electronic cm^{-1}
B_{01}	1.6706	1.6696	1.6703[c]	1.6706[d]
B_{02}	1.7224	1.7200	1.7182[c]	1.7239[d]
B_0	1.6965	1.6948	1.6943[c]	1.6973[d]
B_{21}	1.6406		1.6390[e]	1.6342[f]
B_{22}	1.6855		1.6808[e]	1.6869[f]
B_2	1.6631		1.6599[e]	1.6606[f]
B_{31}	1.6150		1.6199[g]	1.6193[h]
B_{32}	1.6665		1.6629[g]	1.6651[h]
B_3	1.6408		1.6414[g]	1.6422[h]

[a] Nichols, Hause, and Noble.
[b] Gillette and Eyster (see reference 1).
[c] Gero and Schmid, γ 1−0, 2−0 (see reference 7).
[d] Schmid, Konig, and Farkas, γ 0−0, 1−0 (see reference 9).
[e] Gero, Schmid, and von Szily, ϵ 0−2 (see reference 8).
[f] Schmid, Konig, and Farkas, β 2−2, 4−2; γ 0−2, 2−2 (see reference 9).
[g] Gero, Schmid, and von Szily, ϵ 0−3 (see reference 8).
[h] Schmid, Konig, and Farkas, β 2−3, 3−3, 4−3; γ 0−3, 1−3, 2−3 (see reference 9).

significance. Using the data of Gero and Schmid[7] on the 1−0 and 2−0 bands of the γ system, it was found that D_{01} was negligible for values of J up to about 59/2, and that D_{02} was 6.63×10^{-6} cm^{-1}. The data of Gero, Schmid, and von Szily[8] on the 0−2 and 0−3 bands of the ϵ system indicated that D_{21} and D_{31} were negligible for low J values, and D_{22} and D_{32} were 6.88×10^{-6} and 6.85×10^{-6}, respectively. The three D_{v2} values are somewhat smaller than that calculated by Gillette and Eyster, and the scatter is such that values for D_e and β_e in the equation $D_v=D_e+\beta_e(v+\frac{1}{2})$ would have little meaning.

All graphical determinations of B_{v1} were checked by least squares calculations. These values are listed in Table III along with the true B values obtained by taking the mean of these effective values for the two

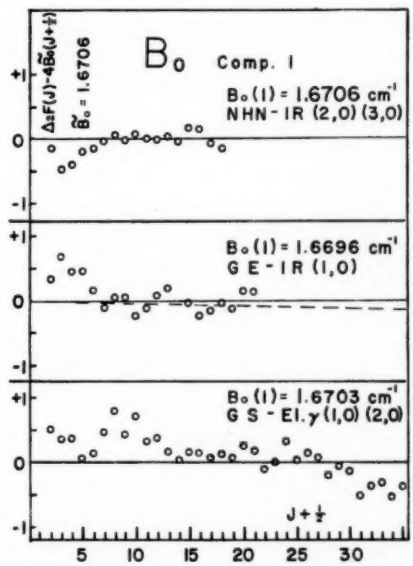

FIG. 2. Graphical determination of B_0 for the $^2\Pi_{\frac{1}{2}}$ component. Data from Nichols, Hause, and Noble infrared 2−0 and 3−0; Gillette and Eyster infrared 1−0; and Gero and Schmid electronic γ 1−0 and 2−0.

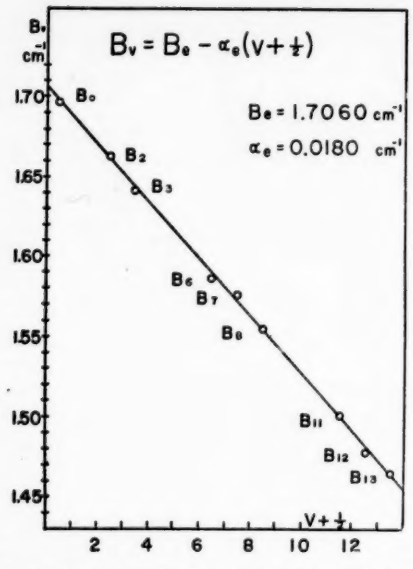

FIG. 3. Graphical determination of B_e and α_e. Values for B_0, B_2, and B_3, from Nichols, Hause, and Noble; B_6 through B_{13} from electronic β bands of Jenkins, Barton, and Mulliken.

components. For comparison, the constants derived from the infrared fundamental and from the various electronic investigations are included. The microwave value for B_{01} is 1.67198 cm^{-1}.[10] Figure 2 shows a comparison of the author's graphical determination of B_{01} with that by Gillette and Eyster[1] and Gero and Schmid.[7] The authors' final value of B_{01} was taken as the approximate value B_{01}, making the slope of the curve, and therefore B_{01} in Eq. (3), equal to zero.

In Fig. 3 is shown a plot of the relation:

$$B_v = B_e - \alpha_e(v+\tfrac{1}{2}). \qquad (4)$$

The points B_0, B_2, and B_3 are from the authors' data, and are used with points for B_6 through B_{13}, as taken from the electronic β system of Jenkins, Barton, and Mulliken.[6] Values of B_e and α_e obtained from these data by a least squares calculation and the computed values of I_e and r_e are given in Table IV. The values obtained by Gillette and Eyster from the fundamental, and the values obtained from the β system are included for comparison. The close agreement of these values attests the accuracy of the infrared work in quite different spectral regions.

Shortly after completion of this work Burrus and Gordy[10] and Gallagher, Bedard, and Johnson[16] reported microwave measurements of the $J=\frac{1}{2}\rightarrow J=\frac{3}{2}(v=0)$ rotational transition of the $^2\Pi_{\frac{1}{2}}$ state of NO. Results from the two laboratories show remarkable agreement, and the computed constants B_e, I_e, and r_e are not only in essential agreement with the final values given by Gillette and Eyster, but are given with much greater precision. This agreement is however only apparent. The microwave data give $B_{01}(B_{0\text{eff}})$, and B_0 is computed from the relation $B_{0\text{eff}}=B_0(1-B_0/A)$. Burrus and Gordy obtain 1.67198 cm^{-1} for B_{01} and Gallagher, Bedard, and Johnson report 1.67196 cm^{-1}. These values are to be compared with 1.6706 in the present work. The microwave values are appreciably higher in each case. B_0 is obtained from the infrared data by taking the mean value of B_{01} and B_{02}. If B_0 is computed from B_{01} and B_{02} using the above relation, each substate gives a different value of B_0. This seems to indicate the relation

TABLE IV. B_e, α_e, I_e, and r_e values.

	Infrared 3−0, 2−0	Infrared 1−0 (plus electronic β)
B_e	1.7060	1.7046 cm^{-1}
α_e	0.0180	0.0178 cm^{-1}
I_e	16.404×10^{-40}	16.423×10^{-40} g cm^2
r_e	1.1503	1.1508 A

[16] Gallagher, Bedard, and Johnson, Phys. Rev. **93**, 729 (1954).

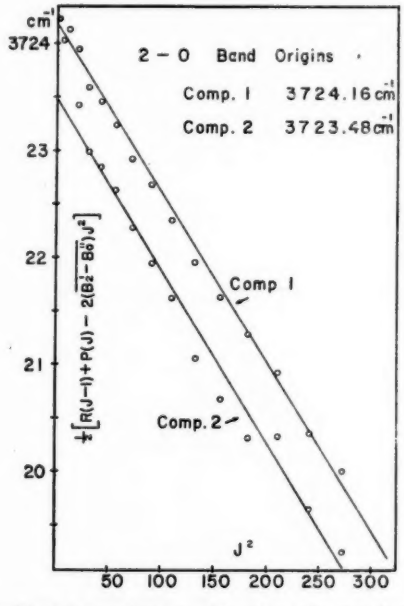

FIG. 4. Graphical determination of band origins for the $^2\Pi_{\frac{1}{2}}$ and $^2\Pi_{\frac{3}{2}}$ components of the 2−0 band of NO at 2.69 μ.

$B_{0\text{eff}}=B_0(1-B_0/A)$ is not quite adequate for the determination of B_0 and thus B_e, I_e, and r_e in the case of NO.

BAND ORIGINS

Combination sums $R(J-1)P(J)$ were used to determine graphically the band origins as suggested by Herzberg.[17] The actual relation used was:

$$\tfrac{1}{2}[R(J-1)+P(J)-2(\langle B_{v'}-B_{v''}\rangle_{Av})J^2 = \nu_0+\Delta(B_{v'}-B_{v''})J^2, \qquad (5)$$

in which the subtraction of the approximate value $2(\langle B_{v'}-B_{v''}\rangle_{Av})$ from each sum allowed plotting to a much larger scale. All results were checked by least squares calculations. Figure 4 shows the graphs for the

[17] G. Herzberg, reference 11, p. 186.

TABLE V. Band origins.

Bands	Nichols, Hause, Noble	Gillette, Eyster; Eq. (6)
3−0 (1)	5544.28	5544.21
3−0 (2)	5543.69	5543.35
2−0 (1)	3724.16	3724.22
2−0 (2)	3723.48	3723.51

two 2−0 components, the Y intercepts giving the band origins.

Table V shows the origins for the 3−0 and 2−0 bands and also the values computed from the relations given as Eq. (6) in the article by Gillette and Eyster[1]:

$$G_1(v)=1904.03(v+\tfrac{1}{2})-13.97(v+\tfrac{1}{2})^2-0.00120(v+\tfrac{1}{2})^3$$
$$G_2(v)=1903.68(v+\tfrac{1}{2})-13.97(v+\tfrac{1}{2})^2-0.00120(v+\tfrac{1}{2})^3 \quad (6)$$

in which the constants are ω_e, $\omega_e x_e$, and $\omega_e y_e$. The experimental 2−0 and 3−0 band origins do not deviate appreciably from the values given by these equations.

CONCLUSION

The molecular constants for the ground state are summarized below. For the completeness the vibrational constants as obtained by Gillette and Eyster are included.

$\omega_{e1}=1904.03\ \text{cm}^{-1}$ $\quad B_e=1.7060\ \text{cm}^{-1}$

$\omega_{e2}=1903.68\ \text{cm}^{-1}$ $\quad \alpha_e=0.0180\ \text{cm}^{-1}$

$\omega_e x_e=13.97\ \text{cm}^{-1}$ $\quad I_e=16.404\times10^{-40}\ \text{g cm}^2$

$\omega_e y_e=0.00120\ \text{cm}^{-1}$ $\quad r_e=1.1503\times10^{-8}\ \text{cm}$

$D_{v2}=6.8\times10^{-6}\ \text{cm}^{-1}$

The authors wish to acknowledge their indebtedness to E. F. Barker and the University of Michigan for the loan of the 7200 lines per inch grating which was used in most of the work.

THE JOURNAL OF CHEMICAL PHYSICS VOLUME 23, NUMBER 1 JANUARY, 1955

Electrochemical Polarization in Isopropyl Ether*

JOHN A. RIDER
Louisiana State University, Baton Rouge, Louisiana†
(Received April 30, 1954)

Measurements have been made of the polarization effects in electrical conduction through isopropyl ether. This liquid was chosen because its conductivity is intermediate between that of dielectric liquids and water. Correlation of experimental results in this range with the Jaffé theory had not heretofore been checked. The present results provide a bridge across the gap which formerly existed in polarization measurements between conductivities of 10^{-6} ohm^{-1} cm^{-1} and 10^{-18} ohm^{-1} cm^{-1}.

Observations were made of the time dependence of current following the application of various voltages to the electrodes of a cell containing the liquid.

Measurements in the present range broaden the pattern of agreement of the Jaffé theory with experiment. Such agreement now extends from semiconductors and aqueous solutions to dielectric liquids. In all cases good quantitative agreement is obtained provided part of the conductance is attributed to carriers of considerably lower mobility than the ordinary conductivity carriers.

I. INTRODUCTION

CORRELATION of the polarization effects observed in all phases of electrical conduction came within the realm of possibility in 1933 when Jaffé published his *Theory of Conductivity of Polarizable Media*.[1] This theory was originally applied to correlate the effects of polarization in crystals but it has been extended and applied to semiconductors,[2] electrolytic solutions,[3,4] and to dielectric liquids.[5]

In the range of conductivity intermediate between that of dielectric liquids and electrolytic solutions very little research of value in polarization studies has been done. Even investigations of specific conductivity alone are not very numerous and the results of different investigations vary widely. It was therefore deemed important to collect and analyze data in this range.

The present investigation is part of a systematic survey of polarization effects in electrical conduction. The theory and experimental work in other conductivity ranges may be found in references 1–5.

II. CURRENT AMPLIFICATION

The current conducted through the liquid was continuously observed for some time after the application of a dc potential to the electrodes of the cell. These currents were of the order of 10^{-10} amperes and were measured with the dc amplifier of a Leeds and North-

* Supported in part by the U. S. Office of Naval Research.
† Present address: University of Houston, Houston, Texas.
[1] G. Jaffé, Ann. Physik **5**, 217 (1933).
[2] G. Jaffé, Phys. Rev. **85**, 354 (1952).
[3] H. C. Chang and G. Jaffé, J. Chem. Phys. **20**, 1071 (1952).
[4] G. Jaffé, and J. A. Rider, J. Chem. Phys. **20**, 1077 (1952).
[5] G. Jaffé and C. LeMay, J. Chem. Phys. **21**, 920 (1953).

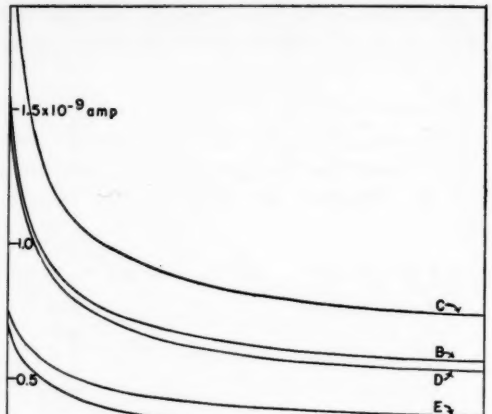

FIG. 1. Isopropyl ether—current *vs* time for five series representing three applied voltages taken in the following order: A, 90 volt; B, 180 volt; C, 270 volt; D, 180 volt; E, 90 volt. Electrode separation constant at 0.10 cm.

rup, Knorr-Albers, microphotometer Model 6700-Al.[6] The output of the amplifier was fed to a Leeds and Northrup Speedomax recorder Model 6700-P2. The currents were continuously recorded on strip chart paper driven at a standard chart speed of 4 in. per hour. Thus, a continuous record of current *versus* time was obtained.

The only modification that was made on the amplifier was the installation of a coaxial cable connector and a switch to enable one to connect the apparatus for measurement of current through the conductance cell. With this arrangement the microphotometer could be returned to normal use with no inconvenience.

In addition, another current measuring system was used for some currents below 10^{-10} amp.[7] This system consisted of a Lindemann electrometer used as described by Jaffé and LeMay.[5]

III. CONDUCTANCE CELL

Design criteria for a conductance cell to be used with liquids in this range were much more stringent than for a cell to be used with electrolytic solutions. The smaller currents being measured required the use of much better insulation which at the same time had to be inert to the liquid. Nevertheless, it was possible to use a cell which was structurally very similar to the one previously used with electrolytic solutions.[8] Basically, the cell was a plane-parallel plate condenser with a guard ring about one electrode and with the other electrode so mounted as to provide micrometer adjustment of electrode separation. A few of the distinguishing features are as follows:

(*a*) *Shielding.*—The cover plate and container were made of brass and were maintained at ground potential. Besides the guard ring, supplementary shielding was inserted behind the central electrode and surrounding its lead. All shielding and the guard ring were connected to each other by silver solder.

(*b*) *Insulation.*—The central electrode was held in place by a fused quartz support tube to which it was attached by "Cerroseal" solder. The quartz support tube in turn was made fast in an adjustable bushing screwed to the cover plate. Electrical connection to the electrode was by means of a wire which passed inside of the quartz tube.

(c) *High voltage electrode.*—As in the electrolytic cell the opposite electrode was so mounted as to provide micrometer adjustment of electrode separation. However, the use of a solid brass grounded cover plate made it necessary to use good insulation between the micrometer assembly (which supported the opposite or high voltage electrode) and the cover plate. This was done by inserting a $\frac{3}{8}$ in. plate of polystyrene between the cover plate and the micrometer mount.

(*d*) *Electrode material and surfacing.*—To minimize asymmetry in the cell, both electrodes were machined from the same piece of brass. After machining, their surfaces were first ground on a flat surface with No. 400 carborundum grit and then fine ground and polished with optical grinding equipment. They were then cleaned by alternate washings in distilled water and ether. The final cleaning after assembly of the cell was by repeated soaking and washing with successive batches of increasingly pure isopropyl ether.

The important dimensions of the electrodes were as follows:

radius of central electrode	1.024 cm,
inner radius of guard ring	1.078 cm,
effective area of central electrode	3.45 cm².

IV. MEASUREMENTS

A series of measurements consisted of the observation of current conducted through the liquid following the application of a voltage to the electrodes. The observations for each such application were continued for about an hour whereupon the voltage was removed and both electrodes grounded for ten minutes. Next, the same amount of voltage but of opposite polarity was applied and the observations continued as with the initial polarity. The currents for the two polarities often differed by as much as 30 percent and therefore were averaged to eliminate effects of asymmetry.

Each series was repeated several times so that a

[6] H. V. Knorr and V. M. Albers, Rev. Sci. Instr. 8, 183 (1937).

[7] Most measurements in the 10^{-10} to 10^{-15} amp range were done on hexane as a continuation of the work of Jaffé and LeMay (see reference 5). Of particular interest was a group of measurements studying the effects of varying electrode separation on the polarization in hexane. The theoretical prediction was confirmed that polarization effects are independent of electrode separation as long as the separation is large compared to the polarization layer thickness.

[8] See reference 4, page 1079, where the electrolytic cell is discussed and diagrammed.

comparison could be made between the results of duplicate series with opposite sequences of polarity, series taken at different times after the liquid was put into the cell, and series taken after prolonged application of electric fields.

Groups of series were made on each sample of liquid with several values of applied voltage and with several values of electrode separation. The results of the measurements are given in the following section.

V. RESULTS OF THE MEASUREMENTS

Figure 1 gives the results obtained in one group of measurements. The curves show average current *vs* time for five series representing three applied voltages with an electrode separation constant at 0.1 cm. Many such groups of measurements were made but the results are all qualitatively so uniform that only one need be represented here. An analysis of a similar set of measurements based on the Jaffé theory is given in Sec. VI.

Some idea of the dependence of current on applied voltage is given in the curves of Fig. 2. These curves are of average current *vs* applied voltage at various times after the application of voltage. As can readily be noted, the dependence is not in general linear but approaches linearity for those measurements taken at least twenty minutes after the application of voltage.

There was no observable dependence of the polarization effects on distance of electrode separation. Families of curves taken with different distances, but with the same applied field, were found to fit the same theoretical curve very closely.

By way of comparison of these results with those obtained on hexane by Jaffé and LeMay, two factors should be stated. First, there were no observable discharge currents (see reference 5, page 924). Extreme care was exercised in attempting to observe these small back currents upon removal of voltage but none were observed.[9] Second, current decay was observable over a longer period with isopropyl ether than with hexane and other dielectric liquids. Currents did not reach a stationary value even after an hour of continuous application of dc voltage.

No absolute value of specific conductivity may be given as this quantity changes during the course of measurements. Apart from polarization effects, the conductance increases with continued application of electric fields and also by merely remaining in the cell. For all of the measurements of the present investigation, the specific conductivity was $(1.0\pm0.3)\times10^{-13}$ ohm^{-1} cm^{-1}.

Values in this range were reached after about an hour from the initial application of voltage and could be reproduced for as long as a week after the liquid had been placed in the cell.

[9] Details of all these measurements along with others on hexane and on electrolytic solutions may be found in the author's doctoral thesis: *Studies on Electrochemical Polarization in Liquids*, Louisiana State University, 1953.

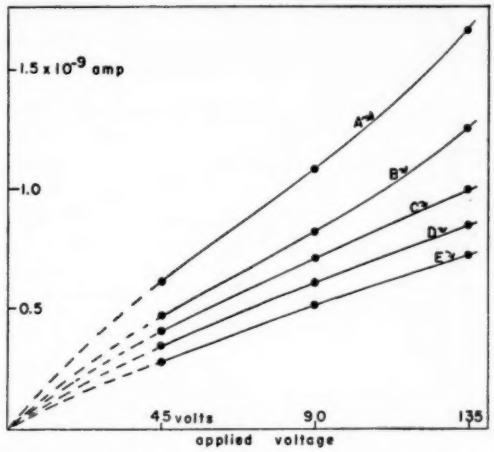

FIG. 2. Isopropyl ether—current *vs* applied voltage at various times after the application of voltage. The curves were graphically drawn through the experimental points and extrapolated to the origin. Curves A, B, C, D, and E are for data taken one minute, five minutes, ten minutes, twenty minutes, and fifty minutes, respectively after the application of voltage. Electrode separation constant at 0.10 cm.

VI. COMPARISON OF RESULTS WITH THEORY

Analysis of the results was done in the manner of Jaffé and LeMay.[5] Here again, it was found necessary to account for a slow current-decay process. This was done by the assumption of the existence of a species of slow ions, the effect of which could be approximated by a single exponentially decreasing term.

Agreement might have been obtained by including some alternate assumption rather than that of the slow ions. For example, recent analysis by Chang[10] indicates that good agreement can be obtained for the electrolytic case using only one species of carriers but assuming the existence of an insulating layer between the electrode and the polarization layer.

No explanation is offered as to the nature of these ions of low mobility. It is only claimed that the assumption of their presence affords a satisfactory model for interpretation of the experimental results. In the absence of a better model, the slow ion assumption has been used successfully.

The methods of analysis will not be repeated here as they may be found in the references. After plotting the logarithmic current ratios and determining the theoretical parameters to fit the data, the theoretical curve was constructed and compared to the experimental results. Figure 3 shows an example of the extent to which agreement is obtained. The solid curve is theoretical while the points indicate experimental results. Only three representative series are shown although many more were taken on this one sample of liquid. All experimental curves fell within the limits indicated by the points on this plot. The theoretical curve could have been made to yield a good fit to any

[10] Chang, H. C., *Electric Conduction at an Interface*, Doctoral dissertation, Louisiana State University, June, 1953.

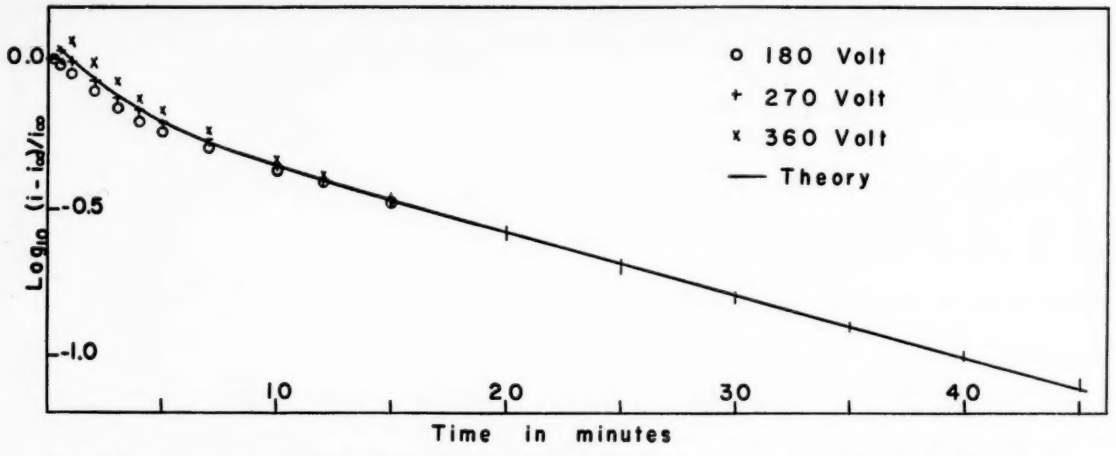

FIG. 3. Isopropyl ether—comparison of the results of three series with theory. Electrode separation constant at 0.20 cm. Constants used in the construction of the theoretical curve are found in Table I.

one of the experimental curves by a slightly different choice of the parameters.

The constants used for the construction of the theoretical curve of Fig. 3 are listed in Table I along with the ionic data determined from them. The coefficients C_1 and C_2 are proportional to the concentrations of the fast and the slow ions, respectively.[11] The value of T/t is determined by matching curves for the current component due to the fast ions. Its significance is given by theory as

$$T/t = D_1/l^2, \tag{1}$$

where D_1 is the diffusivity of the fast ions, and l is the thickness of the polarization layer. The constant, λ_1, is the exponent of decay for the component of current due to the slow ions. Together with λ_1' from the Jaffé theory, λ_1 serves to determine the ratio D_2/l^2, where D_2 is the diffusivity of the slow ions. We have

$$\lambda_1/\lambda_1' = D_2/l^2. \tag{2}$$

The values $\rho=1$ and $v=8$ were determined by trial and error as the ones which gave the best fit to all of the data.

In addition to equations (1) and (2) the Townsend relation,

$$b/D = \epsilon/kT, \tag{3}$$

is used to determine the ionic data.

The mobility of the normal ions, b_1, is taken as $\delta\times10^{-4}$ cm²/volt sec. The constant, δ, should be approximately of unit value if the ions in this case are of the same nature as those studied in dielectric liquids by Jaffé.[12]

By way of summary, polarization effects in isopropyl ether lend themselves to straightforward quantitative analysis by the Jaffé theory. The agreement is good and fits the general pattern of agreement over all ranges of conductance in polarizable media. In this case, as in all the others, the presence of groups of ions of widely different mobilities was assumed. The ionic constants determined here are of the same order of magnitude as those determined by Jaffé and LeMay.

TABLE I. Theoretical parameters and ionic constants determined from the data for Fig. 3.

C_1	(concentration coefficient, fast ions)	0.73
C_2	(concentration coefficient, slow ions)	0.73
T/l	(time scale)	1.75×10^{-2} min^{-1}
i_∞	(asymptotic equilibrium current)	
	360 volt series	7.8×10^{-10} amp
	270 volt series	6.2×10^{-10} amp
	180 volt series	5.0×10^{-10} amp
λ_1	(exponent of decay, slow ions)	0.050 min^{-1}
b_1	(mobility of slow ions-assumed)	$\delta\times10^{-4}$ cm²/volt sec
b_1/b_2	(mobility ratio)	9.55
l	(thickness of polarization layer)	$\delta^{\frac{1}{2}}\times9.4\times10^{-2}$ cm
d	(electrode separation)	0.20 cm

[11] The symbols used are the same as those of reference 5, Equations 22–27 and 36. It should be mentioned that there is an error in Equation 36; the left side should be divided by i_∞.

[12] G. Jaffé, Ann. Physik **32**, 148 (1910); **36**, 25 (1911).

Low-Temperature Absorption Spectra of Selected Olefins in the Farther Ultraviolet Region*†

W. J. Potts, Jr.‡§
Laboratory of Molecular Structure and Spectra, Department of Physics, The University of Chicago, Chicago, Illinois
(Received May, 17, 1954)

A "red shoulder" on the $N \rightarrow V$ absorption curve of olefins, observed at room temperature, but not at low temperature, results from the fact that the potential curves for twist about the double bond in the ground and excited states have slopes of opposite sign. The weaker absorption in the region 40–48 000 cm^{-1} is assigned to the $N \rightarrow T$ absorption on the basis of its analogy to the $N \rightarrow V$ transition in position, extinction coefficient, and oscillator strength.

INTRODUCTION

THERE has long been a great interest in the far ultraviolet absorption spectra of ethylenes, for these molecules are the simplest of all π-electronic systems. The ultraviolet absorption work of E. Carr, L. Pickett, and co-workers[1–4] on several olefins in solution and vapor phases, and the work of Price and Tutte[5] in the vapor phase has given much information about the double bond. From work in *n*-heptane solution, Platt, Klevens, and Price[6] give extinction coefficients in the farther ultraviolet region of a few olefins. A rather complete bibliography of the literature on ethylenes is given by Platt and Klevens.[7]

The above authors, (especially those in references 3 and 5), have shown that the magnitude of the red shift with increasing alkyl substitution of the $N \rightarrow V$ transition (the strong, allowed transition near 18 000 A) depends primarily on the *number* of alkyl substituents, and only to a lesser extent upon the size and position of substituents.

Extensive theoretical investigations by Mulliken[8–10] have to a great measure correlated and explained the existing data. Mulliken and Roothaan[10] have made MO calculations which predict semi-quantitatively the potential energy (*vs* twist about the double bond) curves of ethylene in its ground and excited electronic states.

The present research was undertaken to compare the ultraviolet absorption spectra of four alkyl-substituted ethylenes, (i.e., tetramethylethylene, trimethylethylene, cyclohexene, and hexene-1), in solution at room temperature (298°K) and in a rigid hydrocarbon glass at liquid-nitrogen temperature (77°K), and to see what effect, if any, low temperature might have on the spectra, which are presumably sensitive to twist about the double bond. It was also hoped that the well-known effect of producing sharper spectra at low temperature would be achieved, and thereby locate the $N \rightarrow T$ (absorption to the triplet state) transition.

EXPERIMENTAL

Materials

The four olefins studied were National Bureau of Standards samples, with the following maximum impurities: tetramethylethylene (540–5S), 0.10±0.05 mole percent; trimethylethylene (286–5S), 0.06±0.04 mole percent; cyclohexene (522–5S), 0.023±0.02 mole percent; and hexene-1 (519–5S), 0.14±0.08 mole percent. These compounds were used without further purification. All measurements on any compound were run the same day the sealed tube was opened, the solutions being made up and measurements taken as rapidly as physically possible. This was done because the rate at which the solutions of these compounds become impure when exposed to the air (presumably due to peroxide formation) is excessive, particularly in the case of hexene-1.

Methods

The room-temperature data above 2200 A were obtained in 3-methyl pentane solution with a Beckman model DU quartz spectrophotometer, using 1-cm quartz cells. The data below 2200 A were obtained with a Cario-Schmitt-Ott vacuum fluorite spectrograph, using techniques similar to those of Jacobs and Platt.[11] A 1-cm cell was used, except in the farthest ultraviolet region (below 1850 A), where a 0.13-mm cell was em-

* This work was assisted in part by the Office of Ordnance Research under Project TB2-0001(505) of Contract DA-11-022-ORD-1002 with The University of Chicago.

† This paper is essentially an extract version of Part II of a doctoral dissertation ("Low-Temperature Spectroscopy in the Farther Ultraviolet Region," Chicago, March, 1953) submitted to the Faculty of the Division of the Physical Sciences, The University of Chicago.

‡ U. S. Atomic Energy Commission Predoctoral Fellow, 1950–52.

§ Present address: Spectroscopy Department, The Dow Chemical Company, Midland, Michigan.

[1] E. Carr and M. Walker, J. Chem. Phys. **4**, 751 (1936).
[2] E. Carr and G. Walter, J. Chem. Phys. **4**, 756 (1936).
[3] E. Carr and H. Stücklen, J. Chem. Phys. **4**, 760 (1936).
[4] Pickett, Muntz, and McPherson, J. Am. Chem. Soc. **73**, 4862 (1951).
[5] W. C. Price and W. T. Tutte, Proc. Roy. Soc. (London) **A174**, 207 (1940).
[6] Platt, Klevens, and Price, J. Chem. Phys. **17**, 466 (1949).
[7] J. R. Platt and H. B. Klevens, Revs. Modern Phys. **16**, 182 (1944).
[8] R. S. Mulliken, Phys. Rev. **41**, 751 (1932); **43**, 297 (1933); J. Chem. Phys. **3**, 522 (1933); **7**, 29 (1939).
[9] R. S. Mulliken, Revs. Modern Phys. **14**, 265 (1942).
[10] R. S. Mulliken and C. C. J. Roothaan, Chem. Revs. **41**, 219 (1947).
[11] L. E. Jacobs and J. R. Platt, J. Chem. Phys. **16**, 1137 (1948).

ployed. The solvent was a mixture of 3-methylpentane and isopentane.

All the low-temperature data were obtained in a rigid hydrocarbon glass (the mixture of six parts isopentane and one part 3-methylpentane as discussed by Potts).[12] The apparatus and techniques used are those described elsewhere by Potts.[12]

Errors

As has been discussed by Potts,[12] errors of reciprocity failure of emulsions, spectrophotometer errors, inaccuracies of sample preparation, etc., are small compared to the error of variance of the optical density of the solvents and glasses in this farther ultraviolet region. An index of error is provided by the closeness of agreement with Beer's law as solutions of different concentration were used. (All solutions were in steps of factors of five in concentration.) The maximum error of extinction coefficient is somewhat more than 15 percent at the far ultraviolet end, becoming progressively better toward the nearer ultraviolet, being about 10 percent at 2000 A and 5 percent at 2500 A. In the regions of the spectra where data from the Beckman spectrophotometer overlap with data from the vacuum fluorite spectrograph, the agreement is generally quite good.

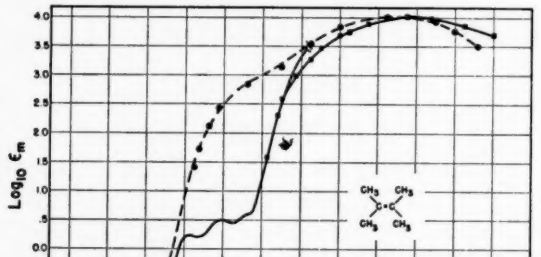

FIG. 1. Absorption spectrum of tetramethylethylene (solid curve, low temperature; dashed curve, room temperature).

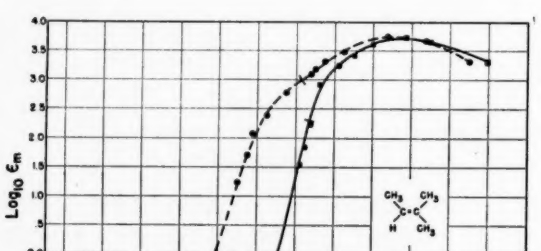

FIG. 2. Absorption spectrum of trimethylethylene.

[12] W. J. Potts, Jr., J. Chem. Phys. **20**, 809 (1952); **21**, 191 (1953).

Agreement of Room-Temperature Data with Previous Work

For solution data above 2200 A the agreement is generally good. Tetramethylethylene and trimethylethylene data are in essential agreement with those of Carr.[1,2] Disagreement of their data on hexene-1 with the present data is perhaps due to the fact that the very pure NBS standard samples were not available at the time of their work. The solution data on tetramethylethylene and hexene-1 obtained by Stevenson,[13] using NBS standard samples, agree very closely with the present work.

The data, below 2200 A, of vapor-phase investigations of Carr and Stücklen[3] and of Price and Tutte[5] are qualitative. The sharper bands superimposed upon the $N \rightarrow V$ transition are not found in the present (solution) work, a fact which is explained below. Otherwise, the data seem in approximate agreement.

The data of Pickett *et al.*[4] on cyclohexene in the vapor phase, using an NBS sample, show general agreement with the present solution data, although a shoulder on the red side of the $N \rightarrow V$ transition seems better resolved in their work. This is due, perhaps, to the expected difference in resolution between vapor and solution spectra. The cyclohexene solution data of

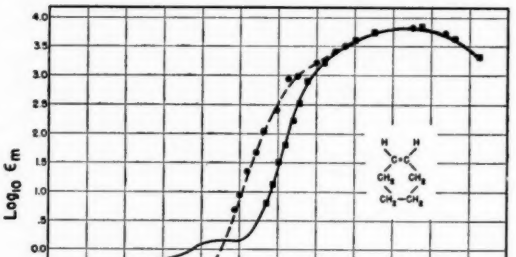

FIG. 3. Absorption spectrum of cyclohexene.

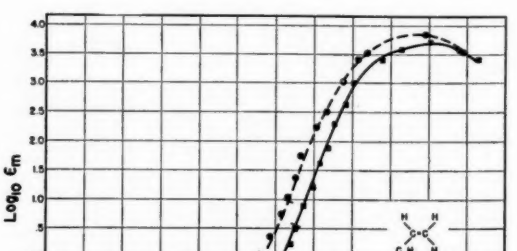

FIG. 4. Absorption spectrum of hexene-1.

[13] D. P. Stevenson, Shell Development Company (private communication).

TABLE I. Positions of the $N \rightarrow V$ transitions in olefins.

Structural formula	Tetramethylethylene 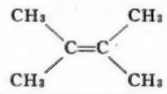		Trimethylethylene 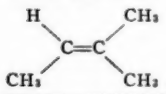		Cyclohexene 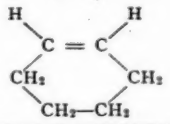		Hexene-1 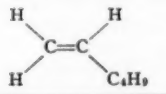	
Temperature	298°K	77°K	298°K	77°K	298°K	77°K	298°K	77°K
ν_{max} of $N \rightarrow V$ transition ± 500 cm^{-1}	52 250	53 750	53 000	54 000	54 750	55 500	56 000	56 500
ϵ_{max}	10 000±700	10 500±900	5800±700	5600±900	6800±700	6800±900	6300±700	5400±900
Red shift from ν_{max} of ethylene (61 400 cm^{-1})[a]	9150		8400		6700		5400	
Low-temperature blue shift, cm^{-1}		1500		1000		750		500
f-number	0.45±0.10		0.34±0.09		0.38±0.09		0.29±0.08	

[a] (See references 5 and 15).

Platt *et al.*[6] are in general agreement with the present work, but show a much higher absorption at the low-frequency end of the $N \rightarrow V$ absorption than the present work. This again may be due to the fact that NBS standard samples were not used in their work, for the present author has had much difficulty in keeping this compound "spectroscopically" pure.

The ultraviolet solution data of Platt *et al.*,[6] on octene-1, agree rather poorly with the present work on hexene-1, whose spectra presumably should be quite similar. Their extinction coefficient of the $N \rightarrow V$ transition is considerably higher (50 percent or so) than the present work. Furthermore they indicate a much sharper peak to the band than the present work. This disagreement is difficult to explain, as the techniques used in obtaining these data were identical. Critical examination of both sets of data seems to indicate that the present ϵ_{max} is probably too low, while that of Platt *et al.* is perhaps somewhat high.

RESULTS

Absorption Data

Figures 1–4 give the room-temperature (dashed curve) and low-temperature (solid curve) absorption spectra from 2500 A to 1700 A of tetramethylethylene, trimethylethylene, cyclohexene, and hexene-1, respectively. $\text{Log}_{10}\epsilon_m$ (molar extinction coefficient), obtained from measured optical density, cell length, and known concentration by the usual relation $\epsilon lc = -\log_{10}(I/I_0) = \text{o.d.}$ (l in cm, c in moles/liter), is plotted against the frequency in wave numbers. When the rigid glass is employed, it is necessary to correct the concentration values for the 22 percent contraction of the glass in cooling.

Table I gives the frequency of the absorption maximum, corresponding peak molar extinction coefficient, and estimated oscillator strength (room temperature only) of the rather broad, allowed $N \rightarrow V$ transition for the various olefins studied here. There is an uncertainty of about 500 cm^{-1} in the position of the absorption peaks because of the broadness of these peaks. The shift toward the red is seen to depend primarily on the *number* of alkyl substituents at both temperatures.

Normally, in going from solution to a rigid glass medium a *red* shift of the absorption peak is observed, because of the greatly increased refractive index of the medium. The observance of *blue* shift of the absorption peak in olefins is accounted for below.

It was thought inadvisable to calculate the oscillator strengths[14] of the $N \rightarrow V$ transitions at low temperature, because the limit of the experimental technique was 1700 A, and it seems probable that the broad $N \rightarrow V$ transition extends to yet shorter wavelengths.[3,5] There are not sufficient data in the present work to calculate accurately the oscillator strengths at room temperature, but these values were estimated by extrapolating the present data to higher frequencies, using the qualitative results of Price and Tutte[5] as a guide. Their data on propene are used to extrapolate hexene-1, for presumably these compounds should have very similar absorption spectra.[3,9]

There are some weak bands appearing in the region 40 000–48 000 cm^{-1} [15] which are masked at room temperature by the strong shoulder in the red side of the $N \rightarrow V$ absorption, but which are seen at low temperatures. That their existence is due to a ground-state-to-triplet ($N \rightarrow T$) transition (and not to trace impurities!)

[14] f number, or oscillator strength, is defined as:

$$f = 10^3(\log_{10}e)\frac{mc^2}{\pi e^2 N}\int \epsilon_\nu d\nu = 4.3\times 10^{-9}\int \epsilon_\nu d\nu,$$

where ν is in cm^{-1}, ϵ is molar extinction coefficient.

[15] P. G. Wilkinson and H. L. Johnston, J. Chem. Phys. **18**, 190 (1950).

TABLE II. Positions of the $N \rightarrow T$ (?) transitions in olefins.

	Tetramethyl-ethylene	Trimethyl-ethylene	Cyclohexene	Hexene-1
"Center" of the $N \rightarrow T$ transition	43 800 cm^{-1}	44 200 cm^{-1}	44 000 cm^{-1}	46 400 cm^{-1}
Average ϵ	2.5±0.5	0.6±0.1	1.0±0.2	0.2±0.1
f number	$4.2\pm1.0\times10^{-5}$	$1.0\pm0.5\times10^{-5}$	$2.7\pm0.8\times10^{-5}$	$0.26\pm0.1\times10^{-5}$
Vibrational segaration	1400±100 cm^{-1}	1400±100 cm^{-1}		

is a possible explanation[16] and is discussed below. The "centers" of the transitions, average molar extinction coefficient, and oscillator strengths of these transitions are given in Table II. The vibrational separation (?) is tabulated where it is sufficiently resolved.

Most curious is the low-temperature spectrum of cyclohexene in the region 40 000–45 000 cm^{-1}. The low-temperature absorption is decidedly greater than the absorption at room temperature. By showing that the room-temperature absorption is reproduced within experimental error upon the warming of the identical solutions used for the low-temperature determinations, indicates that this surprising effect is probably real.

Three molecules are obvious by their omission from this study, namely, the three dimethylethylenes: *cis*- and *trans*-butene-2, and 2-methylpropene. Their absorption-spectra curves would be expected to be about midway between trimethylethylene and hexene-1.[2,3] (Hexene-1 should have essentially the same ultraviolet spectrum as propene[3]; it was chosen only for convenience of physical properties.)

Ethylene should also be included in this study, however, new experimental techniques are necessary before a gas can be studied by the low-temperature methods used in this work.

In Fig. 5 the low-temperature absorption curves of all four compounds are plotted together for comparison.

Search for Phosphorescence

Observation of olefin phosphorescence ($T \rightarrow N$ long-lived emission) would lend strong support to the singlet-triplet[17] ($N \rightarrow T$) assignment given the weaker bands in the 40–48 000 cm^{-1} region. Hence a search for phosphorescence was made, using the methods described elsewhere by Potts.[12] In this setup, the slit of the Cario-Schmitt-Ott fluorite spectrograph was made very wide (1 mm), and the very fast Eastman SWR plates were used in order to detect the weakest radiations. With this arrangement it was possible to record the notably weak phosphorescence of benzene[18] with an exposure time of only 15 minutes.

Tetramethylethylene was chosen for this study because of its higher absorption less far in the ultraviolet. No phosphorescence was observed.

The phosphorescences of chloro-ethylenes reported by Kasha[18,19] must probably be regarded as erroneous because their reported lifetimes are much too long. Phosphorescence of these compounds (if it exists at all! —see following discussion) would be very short-lived, for the only selection rule forbidding the transition in chloro-ethylenes is the singlet triplet intercombination rule, and chloro-substitution tends to break down this very rule.[20]

DISCUSSION

As noted above, the larger the number of alkyl substituents about the double bond, the lower is the energy (longer the wavelength) of the $N \rightarrow V$ transition peak. This effect, due to increasing hyperconjugation[9,21] and/or increased inductive transfer of charge towards the double bond from the more electro-positive alkyl groups with increasing alkyl substitution,[5] has been dealt with at length by other authors[3,5,9] and hence will not be discussed further here.

In the vapor absorption spectra of Carr and Stücklen[3] and of Price and Tutte[5] several sharp bands appear superimposed on the broad $N \rightarrow V$ absorption. These bands have been interpreted as belonging to a Rydberg-type transition[5,9,22] called $N \rightarrow R$ in the notation of Mulliken.[9] No such bands were observed in the present work.

The explanation of their nonappearance (if they are truly Rydberg-type transitions) lies in the fact that one would not expect such spectral states to be observed in a condensed medium (solution or low-temperature glass) because the large-sized Rydberg orbitals would probably be strongly perturbed by closely neighboring solvent molecules. When these bands have been observed by other authors it has always been in the vapor phase at low pressures.

[16] First suggested by Snow and Alsopp, Trans. Faraday Soc. **30**, 93 (1934). Also see E. P. Carr and H. Stücklen, J. Chem. Phys. **4**, 760 (1936), who review all the experimental data then available. Using these and other data on the alkyl-substituted ethylenes, Mulliken (see reference 9, footnote e of Table I) obtained a value of about 2.2 ev as the potential curves of the T and V states for these molecules; unfortunately the details (see footnote 10 of reference 9) were never published.

[17] It has been quite firmly established that phosphorescence in electronic systems is due to the lowest-triplet-to-ground-singlet emission. (See reference 18.)

[18] G. N. Lewis and M. Kasha, J. Am. Chem. Soc. **66**, 2100 (1944).

[19] M. Kasha, Chem. Revs. **41**, 401 (1947).

[20] D. S. McClure, J. Chem. Phys. **17**, 905 (1949).

[21] Mulliken, Rieke, and Brown, J. Am. Chem. Soc. **63**, 41 (1941).

[22] E. Carr and H. Strücklen, J. Chem. Phys. **7**, 631 (1939).

Shape of the $N \rightarrow V$ Absorption Curve at Low Temperature

It is noticed that in each compound there is a shoulder in the absorption curve of greater or smaller size on the red side of the $N \rightarrow V$ transition. The width of this shoulder decreases as one goes from tetramethylethylene, the most substituted ethylene, to hexene-1, the least substituted. For an explanation of these phenomena, we refer to Mulliken and Roothaan's picture[10] of the potential energy of the various electronic states of ethylene as a function of twist about the double bond. An adaptation of their figure is shown in Fig. 6.[23]

The curves represent the potential energy as a function of angle of twist, θ, about the double bond of ethylene for the normal (ground singlet) state, the excited state, V, and its corresponding triplet state, T. They are drawn to the qualitative scale indicated by the LCAO MO calculations of Mulliken and Roothaan,[10] as corrected by the present author to correspond with the corrected assignment of the twisting frequency of Arnett and Crawford.[24]

From Fig. 6, it is seen that the ground state has its minimum energy in the planar form, while the planar form gives maximum energy for the excited states. That is, the slopes of the ground-state and excited-state curves are of opposite sign. Thus, in an $N \rightarrow V$ spectral transition, the more the molecule is twisted, the less the energy required for the transition, and hence the longer the wavelength of the absorption. The fact that absorption sets in at longer wavelength at room temperature than at low temperature [$(N \rightarrow V)_{HT}$ and $(N \rightarrow V)_{LT}$ in Fig. 6] must indicate that the low-temperature conditions restrict the amount of twist either in the upper (V) state or in the ground (N) state, or both.

From the corrected assignment of the twisting frequency in the ground (N) electronic state of ethylene[24] one calculates $k_\gamma = 2.71 \times 10^4$ wave numbers/radian for the force constant, which allows 11.1° twist in the ground level and 19.3° twist in the first vibrational level (1027 cm^{-1}), using $V = \frac{1}{2} k_\gamma \theta^2$, where V is potential energy in cm^{-1}. From Fig. 6 it is seen that a vertical (Franck-Condon allowed) transition from the most twisted configuration of the first excited vibrational level in the ground electronic state [labeled $(N \rightarrow V)_{HT}$ in the figure] is of lower energy by some 3–4000 cm^{-1} than a corresponding transition from the lowest vibrational level [$(N \rightarrow V)_{LT}$], most of this energy being due to the steepness of the upper (V) state potential curve. Statistics allow only 0.7 percent of the molecules in the first excited vibrational level at room temperature, hence a low-temperature medium would not be expected to have much effect upon the absorption-spectrum of ethylene compared to the spectrum at room temperature.

The values of the twisting frequencies of alkyl-substituted ethylenes are still in doubt,[25] and only estimates of their values may be made. In the case of tetramethylethylene, which has the same symmetry properties as ethylene, if the force constant of twist (k_γ) is the same as in ethylene, the energy of the first vibrational level of twist is calculated to be 264 cm^{-1}.

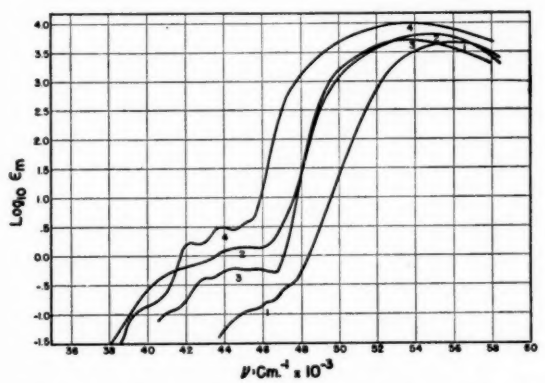

FIG. 5. Low-temperature spectra compared. 1 Hexene-1. 2 Cyclohexene. 3 Trimethylethylene. 4 Tetramethylethylene.

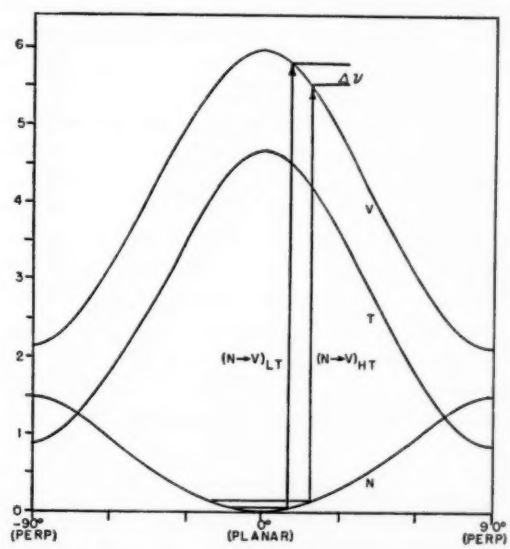

FIG. 6. The potential energy of the electronic states of ethylene as a function of twist about the double bond. (See reference 23.) Energy is in 10 000's of wave numbers. The vertical arrows represent the $N \rightarrow V$ transitions.

[23] It should be noted, however, that the heights of all the curves should almost certainly be increasingly revised upward as they go from 0° to ±90°. This was indicated already by the calculations of Mulliken and Roothaan (reference 10, see caption of their Fig. 1), and is confirmed by recent experimental work of Rabinowitch, Douglas, and Looney, **20**, 1807 (1952), who find, for the height of state N at ±90°, 2.66±0.05 ev, instead of 1.5 ev as in the present Fig. 6. Also, the height of the T state at ±90° may be only *slightly* below that of the N state, according to a private communication from P. O. Löwdin, based on theoretical calculations. Fortunately, these changes at ±90° do not at all seriously affect the following discussion.

[24] R. L. Arnett and B. L. Crawford, J. Chem. Phys. **18**, 118 (1950).

[25] N. Sheppard and G. B. B. M. Sutherland, Proc. Roy. Soc. (London) **A196**, 195 (1949).

The corresponding maximum twist angles are 9.8° for the first excited level of twist, 5.7° for the ground level. The application of statistics shows that 28 percent of the molecules will be in the first excited vibrational level of twist at room temperature.

The assumption that the force constant of tetramethylethylene will be the same as ethylene is, of course, a poor one. Examination of a Fischer-Hirschfelder atom model of tetramethylethylene indicates that the van der Waals radii of the H-atoms on the methyl groups would actually overlap considerably in the planar configuration if free rotation of methyl groups could take place. This must be regarded as a rather strong repulsion by the methyl groups, which would tend to force the molecule into a more twisted configuration. This in turn would tend to decrease the force constant of twist about the double bond, and thus make the ground-state potential curve (N) somewhat flatter than pictured in Fig. 6. On the other hand, the repulsion of methyl groups in tetramethylethylene will tend to *steepen* the potential curve for the upper (V) electronic state, particularly in the region of planarity.

An additional effect of the low-temperature rigid glass may result from the increased viscosity of the surroundings at low temperature. This increased viscosity would make the energy of rotation about the double bond somewhat greater, which would slightly steepen the ground-state (N) potential curve, slightly flatten the excited-state (V) curve at low temperature (compared to the curves of the same molecule at room temperature). This effect should be small, however, in view of the high value of the twisting force constant for the ground state and the probably yet higher (negative), force constant for the excited state (perhaps at least a factor of 3 greater, probably more in the more highly substituted ethylenes).

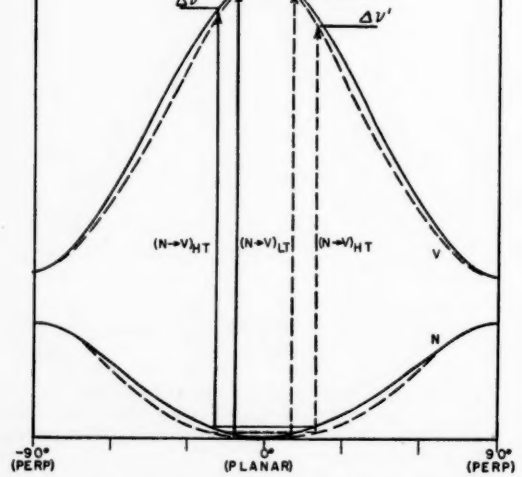

FIG. 7. Potential curves of ethylene (solid) and probable curves of tetramethylethylene (dashed) compared. (See reference 23.)

Less highly substituted ethylenes (mono-, di-, tri-) should have values somewhere between ethylene and tetramethylethylene for the above effects, i.e., force constant of twist, twist vibrational energy separation, percent population of the first vibrational level, viscosity-dependent resistance to twist. These effects all operate in the same direction: the more alkyl substituents, the greater the "twisted population" at room temperature compared to low temperature.

Thus, from these considerations, it seems reasonable to suppose that the larger the number of alkyl substituents, the more likely will be the $N \rightarrow V$ transition between the *twisted* states of the substituted ethylene at room temperature, as compared to low temperature. That is, with increased alkyl substitution, one observes a *lower* frequency (energy) for the onset of appreciable absorption at room temperature compared to the onset of absorption at low temperature. This seems to account in a satisfactory manner for the increasing width of the "red shoulder" on the $N \rightarrow V$ absorption curve with increasing alkyl substitution, which disappears at low temperature. (This "red shoulder" effect is, of course, a separate effect from the red shift of the absorption *peak* with increased alkyl substitution.)

Plotted together, in Fig. 7 for purposes of comparison, are potential curves for the ground (N) and excited singlet (V) states of ethylene (solid), and the probable curves for tetramethylethylene (dashed).[23] Also shown are the $N \rightarrow V$ transitions from the zeroth and first levels of twist vibration. In comparing them, one must bear in mind that at room temperature the first vibrational level of ethylene will be very sparingly (0.7 percent) populated, while in tetramethylethylene the first vibrational level will be strongly (at least 28 percent) populated. [The absolute heights of the upper (V) state curves are drawn as if the peaks of the $N \rightarrow V$ transitions of these molecules coincided, but of course they do not; however, this is immaterial to the present discussion.]

Cyclohexene is a somewhat different case from the other olefins considered here in that it is a ring structure. Comparison of the $N \rightarrow V$ absorption curves at room and low temperatures indicate that, insofar as the "red shoulder" on the $N \rightarrow V$ transition is concerned, it behaves essentially like a dialkyl ethylene. Apparently the shape of the *complete* $N \rightarrow V$ absorption curve (including data below 1700 A) is quite different from that of a *cis*-olefin,[3,4] a difference which Platt *et al.*[6] consider to be due to a permanent twist of the double bond. But references cited by them and the more recent work of Beckett, Freeman, and Pitzer[26] indicate that there is no such permanent twist of the double bond in cyclohexene. The effect of the structure of cyclohexene on its ultraviolet absorption spectra will be considered below in more detail in the discussion of the triplet state.

[26] Beckett, Freeman, and Pitzer, J. Am. Chem. Soc. **70**, 4227 (1948).

The Triplet State of Olefins

When the red shoulder of the $N \rightarrow V$ transition is "removed" at low temperature, a weaker band is revealed in the region 40–48 000 cm^{-1}. Similar bands, but at longer wavelengths, are seen in the room temperature spectra (see Figs. 1–4) and were assigned by Snow and Alsopp[16] to ground-to-triplet ($N \rightarrow T$) transitions. The following reasons justify the same assignment for the low-temperature bands.

If we neglect cyclohexene for the moment, reference to Fig. 5 shows a certain regularity to these transitions. This regular trend closely parallels that of the position of the singlet ($N \rightarrow V$) peaks, suggesting that the two transitions may be related. The singlet-triplet separation of the excited states is approximately constant throughout the compounds, and is about the same as for the room temperature bands.[16] Reference to Tables I and II shows that the trend of both ϵ and oscillator strength is qualitatively the same for both the $N \rightarrow V$ and $N \rightarrow T$ transitions. The values and oscillator strengths of the $N \rightarrow T$ transitions are within the range of what could be expected for a singlet-triplet transition between π-electronic states corresponding to an allowed singlet-singlet transition in olefins.[20]

There is the possibility that the bands observed in the 40–48 000 cm^{-1} region are due to impurities. Olefins are difficult to keep "spectroscopically" pure; however, it is felt that the source of materials and experimental precautions used in obtaining these data were sufficiently good to render impurities unlikely.

Upon exposure to air these compounds begin to show increased absorption in just this "triplet" region, but this is exactly the region wherein one expects formation of impurities to be most noticeable. At higher frequencies any impurity would be masked by the already great absorption of the pure compound itself, while at lower frequencies the expected impurities (oxygen containing compounds) would have small absorption themselves.[7,27]

In the molecules where they are resolved, vibration peak separations of 14 000 cm^{-1} appear in the $N \rightarrow T$ transition. This is approximately the ground-state C=C stretch frequency. That these should be observed in the $N \rightarrow T$ transition, whereas in the $N \rightarrow V$ transition intervals of about 800 cm^{-1} are observed,[9] is unexplained.

If these bands in the region 40–48 000 cm^{-1} are then truly the $N \rightarrow T$ transitions, there is one point a bit more difficult to explain. Their ϵ values and oscillator strengths (see Table II) increase by a factor of 20 in going from the least substituted ethylene (hexene-1) to the most substituted (tetramethylethylene), while the corresponding values of the $N \rightarrow T$ transition increase by only a factor of two. A plausible explanation of these erratic f values is the following. It may be that the f value for tetramethylethylene is more or less correct, but that the lower values for the other substituted ethylenes are due to a masking of the most intense part of the $N \rightarrow T$ absorption by the much stronger $N \rightarrow V$ absorption; this looks especially plausible (see Fig. 4) for hexene-1, where the $N \rightarrow T$ f value given in Table II is especially low. At room temperature, the masking is apparently much greater than at low temperatures because of the presence of the "red shoulder" on the $N \rightarrow V$ transitions The f values which would be computed for the $N \rightarrow T$ transitions on the basis of the room temperature data would actually be much lower (see Figs. 1–4) than those given in Table II.

On the other hand, the difference between the $N \rightarrow T$ curves at room and low temperatures appears itself to involve a "red shoulder" effect like that for the $N \rightarrow V$ transitions. The potential curve of the excited triplet state (T) is predicted to be of the same general shape as for the excited singlet (V) state (Figure 6). Hence, the same arguments about a red shoulder at higher temperatures that obtain for the $N \rightarrow V$ transition apply for the $N \rightarrow T$ transition. This shoulder can be seen at room temperature in Figs. 1, 2, and 4.

In connection with the $N \rightarrow T$ transition, attention may be called to a long series of bands observed by Reid in absorption in the range 30–37 000 cm^{-1} in long columns of liquid ethylene.[28] They may represent an extension of the $N \rightarrow T$ transition.

Phosphorescence and the Triplet State

Observation of a comparatively long-lived light emission (phosphorescence), which is now well established as triplet-singlet emission[17–19,29] ($T \rightarrow N$ in the present discussion), might confirm the present $N \rightarrow T$ assignment. As mentioned above, no such phosphorescence was observed in tetramethylethylene. If a low-temperature glass does not appreciably affect the potential curves (N, V, or T), the nonappearance of phosphorescence is easily explained. For as the molecules get into the triplet state, they could rapidly lose vibrational energy to the surroundings as they cascaded down through vibrational levels of the triplet state, eventually reaching the excited triplet (T) and ground singlet (N) crossover point, at $\theta \approx 60°$ (see Fig. 6). Here they become singlet states, and cascade through the ground-state vibrational levels back to zero energy. This radiationless process would be far more rapid than a triplet-singlet ($T \rightarrow N$) emission.[19] Thus, no longer-lived (phosphorescent) emission would be observed.

Cyclohexene

Cyclohexene is a somewhat different case from the other olefins already discussed. Superimposed upon the double-bond twisting potential will be certain strain potentials resulting from the fact that it is a six membered ring structure. As the infrared frequency assign-

[27] H. Sponer and E. Teller, Revs. Modern Phys. 13, 76 (1941).

[28] C. Reid, J. Chem. Phys. 18, 1299 (1950).

[29] M. Kasha, Discussions Faraday Soc. 9, 14 (1950).

ments are still in doubt, no attempt will be made to go into the finer details of cyclohexene structure. Certain general statements may be made which, it is hoped, will be sufficient to explain the absorption spectrum to some extent.

It is expected that steric forces of the ring will have little effect upon the energy of C=C twist in its region of planarity. This is expected from the high energy of C=C twist, about 1.3 kcal/deg (as estimated from Arnett and Crawford's value in ethylene),[24] and the comparatively small strain energy of the entire ring, about 1.6 kcal.[26] The 1.6 kcal of strain will be taken up by distortions other than this high-energy twist distortion. The only change in the region of double-bond planarity might be a small tendency toward flattening the ground-state (N) curve near planarity. Of course, for the region of large angle of twist ($\theta > 45°$, say) the potential curve would be greatly altered, because it would require braking a C−C bond. Presumably, this more highly twisted region is not of importance in the present discussion.

At low temperature, negligible change (compared to room temperature) in the V and T state potential curves is expected in the region of planarity, as in the case of noncyclic olefins, and for the same reason—namely, that energy of C=C twist is too great. Nor is much change anticipated in the ground-state (N) twist-potential curve in going to low temperature, except some small steepening of the curve which is due to contraction of the surroundings.

From this reasoning the behavior of the $N \rightarrow V$ transition should in principle be just like the other olefins at room and low temperatures, and this is what is observed: a red shoulder on the $N \rightarrow V$ absorption, disappearing at low temperature.

In cyclohexene the behavior of the weaker transition at 43 000 cm^{-1} (presumably the $N \rightarrow T$ absorption) is quite different from that of the other olefins in that the longer wavelength part of its absorption is greatly increased at low temperature. Although it may be coincidental, it is interesting to note that the oscillator strength of this transition, compared to the other olefins, follows the same trend as the oscillator strength of the $N \rightarrow V$ transition. This gives additional support to its assignment as the $N \rightarrow T$ transition.

A further experiment suggests itself (regrettably at too late a date to pursue): a search should be made for a phosphorescence in cyclohexene. If the molecule could be excited to the triplet state by the use of the techniques mentioned above in the case of tetramethylethylene, a phosphorescence should be observed. With cyclohexene a radiationless transition to the ground state cannot take place without rupture of a C−C bond. Thus, upon excitation, if a relatively long-lived ($\sim 10^{-2}$ sec)[19] phosphorescence were observed at ~36–40 000 cm^{-1}, then such a phosphorescence would presumably be the reverse process of the absorption at 43 000 cm^{-1}, and this absorption is correctly interpreted as $N \rightarrow T$.

ACKNOWLEDGMENTS

The author expresses his thanks and appreciation to Professors J. R. Platt and C. C. J. Roothaan for many helpful suggestions and discussions. The author is especially indebted to Professor R. S. Mulliken for his valuable corrections and additions to the manuscript.

Low-Temperature Absorption Spectra of Benzene, Toluene, and Para-Xylene in the Farther Ultraviolet Region*†

W. J. Potts, Jr.‡§
Laboratory of Molecular Structure and Spectra, Department of Physics, The University of Chicago, Chicago 37, Illinois
(Received May 17, 1954)

The absorption spectra of the 2100 A and 1850 A transitions of benzene, toluene, and para-xylene show sharp structure at low temperature. The sharp structure of the 1850 A transition shows that it is a $\pi-\pi$ type transition, and not a dissociation band. Its correct assignment is $^1A_{1g}\rightarrow{}^1E_{1u}$, with analogous assignments in toluene and para-xylene. The 2100 A transitions of these molecules can be assigned to $^1A_{1g}\rightarrow{}^1B_{1u}$ and its analogs, while the 2600 A transitions are assigned to $^1A_{1g}\rightarrow{}^1B_{2u}$. Evidence presented indicates that there is no $^1A_{1g}\rightarrow{}^1E_{2g}$ transition in this region of the spectrum.

INTRODUCTION

PERHAPS no polyatomic molecule has been investigated spectroscopically as extensively as has benzene. In spite of the vast amount of literature on this subject, comparatively few investigations have been made of the shorter wavelength transitions (below 2200 A) of benzene, and of these only a very few have given absolute extinction coefficients.

The nearer ultraviolet absorption bands of benzene (at 2600 A, assigned to the $^1A_{1g}\rightarrow{}^1B_{2u}$ transition by most authors) have such extensive literature that only a few selected references will be cited here. The nearer ultraviolet absorption spectra of benzene and several alkyl benzenes have been systematically investigated in hydrocarbon solution,[1] in the vapor state,[2] in the crystalline state at low temperature,[3] and in rigid-glassy media at low temperature.[4] While the low-temperature spectra of the 2600 A transitions of benzene and alkyl benzenes are very much sharper than the room-temperature solution spectra, the low-temperature method still cannot compete with vapor spectra in resolution of these bands. Hence, vapor spectra have been used for the complete analysis of the 2600 A transitions of benzene[5] and the analogous transitions of substituted benzenes.[6]

In the farther ultraviolet region, the spectral data on benzene and substituted benzenes become far scarcer. The far ultraviolet *vapor* spectrum of benzene has been obtained qualitatively by Carr and Stücklen,[7] and, along with that of toluene and the xylenes, by Price and others.[8,9] The vapor spectrum of benzene has been obtained quantitatively by Pickett and co-workers,[10] and by Romand and Vodar.[11]

The absorption spectra of benzene, toluene, and the xylenes have been obtained quantitatively in *n*-heptane solution by Platt and Klevens in the region 2200–1700 A.[12] Their work shows nearly as much resolution of structure as most of the aforementioned vapor work. In their work, as in the vapor absorption spectra, the strong transitions of benzene and the alkyl benzenes at about 1850 A are quite diffuse.

Romand and Vodar[11] have obtained the far ultraviolet spectrum of benzene in the crystalline state at liquid-nitrogen temperature, but their work shows decidedly less sharpening of the spectrum than either their own vapor spectrum or the room-temperature solution spectra of Platt and Klevens.[12]

The present research was undertaken to see if use of rigid glasses at low temperature would give increased resolution in the diffuse transitions in the farther ultraviolet region of benzene and alkyl benzene absorption spectra. The results are most encouraging and show that these far ultraviolet transitions in aromatics do indeed have sharp structure. The absolute extinction coefficients and positions of several vibrational bands have been obtained for the farther ultraviolet (2200–1700 A region) spectral transitions of benzene, toluene, and para-xylene both at room temperature and at low temperature. Generally, much more vibrational structure is seen at low temperature.

EXPERIMENTAL

Materials

Benzene and toluene used in this research were Merck Reagent Grade chemicals; para-xylene was Eastman "White-Label" grade, m.p. 13°C. Each was purified by

* This work was assisted in part by the Office of Ordnance Research under Project TB2-0001(505) of Contract DA-11-022-ORD-1002 with The University of Chicago.

† This paper is essentially an extract version of Part III of a doctoral dissertation ("Low-temperature spectroscopy in the farther ultraviolet region," Chicago, March, 1953) submitted to the Faculty of the Division of the Physical Sciences, The University of Chicago.

‡ U. S. Atomic Energy Commission Predoctoral Fellow, 1950–1952.

§ Present address: Spectroscopy Department, The Dow Chemical Company, Midland, Michigan.

[1] Catalog of Ultraviolet Spectrograms, American Petroleum Institute, Project 44 (1945–1950).

[2] H. Sponer, J. Chem. Phys. **8**, 705 (1940).

[3] A. Kronenberger, Z. Physik **63**, 494 (1930).

[4] E. Clar, Spectrochim. Acta **4**, 116 (1950).

[5] Sponer, Nordheim, Sklar, and Teller, J. Chem. Phys. **7**, 207 (1939).

[6] H. Sponer, Revs. Modern Phys. **14**, 224 (1942).

[7] E. Carr and H. Stücklen, J. Chem. Phys. **6**, 645 (1938).

[8] W. C. Price and W. D. Walsh, Proc. Roy. Soc. (London) **A191**, 22 (1947).

[9] Hammond, Price, Teegan, and Walsh, Discussions Faraday Soc. **9**, 53 (1950).

[10] Pickett, Muntz, and McPherson, J. Am. Chem. Soc. **73**, 4862 (1951).

[11] J. Romand and B. Vodar, Compt. rend. **223**, 930 (1951).

[12] J. R. Platt and H. B. Klevens, Chem. Revs. **41**, 301 (1947).

several recrystallizations from itself, then distilled from sodium wire to remove any possible condensed water from the crystallization process. Although this method gives a product of extremely high purity,[13] the problem of impurities in this research is small, for only regions of intense absorption ($\epsilon > 5000$) were being investigated. The only trouble that might arise in this respect would be small amounts of ortho- and meta-xylenes in the para-xylene. The original melting point of the source of para-xylene and its method of purification however ensure against this.

Method

The spectra at room temperature were obtained in a mixture of isopentane and 3-methylpentane by the same methods used by Platt and Klevens[12] and described elsewhere.[14] The liquid-nitrogen temperature spectra were obtained by the methods described elsewhere by Potts.[15] For both series of spectra the Cario-Schmitt-Ott vacuum fluorite spectrograph was employed, and Ilford Ql-plates were used.

Errors

The errors in these methods have been discussed elsewhere by Potts[15,16] and are believed to be about 8 percent in molar extinction coefficient at 2200 A, increasing to somewhat greater than 15 percent at 1700 A, the limit of the present techniques. Samples of different concentrations gave results consistent within these errors. However, the error may well be higher than estimated in the region at the "blue" end of the first absorption (2100 A transition), which is being overlapped by the beginning of a region of stronger absorption (1850 A transition), where it is difficult to pick a solution of favorable concentration. Also, the errors in the room-temperature data at the extreme end of the region investigated (1730 A) are probably quite high, as the solvents are rapidly cutting off here at room temperature.

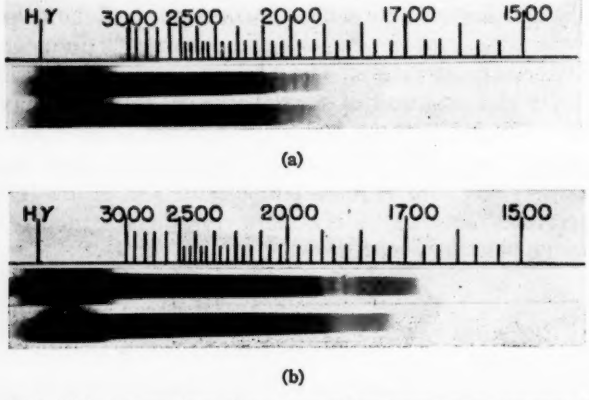

FIG. 1(a). Comparison of room- and low-temperature spectra of benzene 2100 A transition (low-temperature spectrum above). (b). Comparison of room- and low-temperature spectra of benzene 1850 A transition (low-temperature spectrum above).

Agreement with Other Authors

The room-temperature data presented here are essentially a repetition of the work of Platt and Klevens[12] and generally agree fairly well with their results. Other workers in this laboratory have independently verified many of these values of extinction coefficient.[17] However, the present data differ materially from those of Platt and Klevens in one instance: the present work shows no weak transition at 1730 A in toluene, which Platt and Klevens observed and have interpreted, in a later paper,[18] as being analogous to a $^1A_{1g} \rightarrow {}^1E_{2g}$ transition in benzene. This discrepancy will be discussed in detail below.

The present work shows none of the very sharp Rydberg bands superimposed upon the strong 1850 A transition in any of these compounds which have been observed in the vapor spectra of Carr and Stücklen,[7] Price *et al.*,[8,9] and Pickett *et al.*[10] This is presumably to be expected when spectra are obtained in condensed phases, however, because of the large size of the Rydberg orbitals, which would become strongly perturbed by closely neighboring molecules.

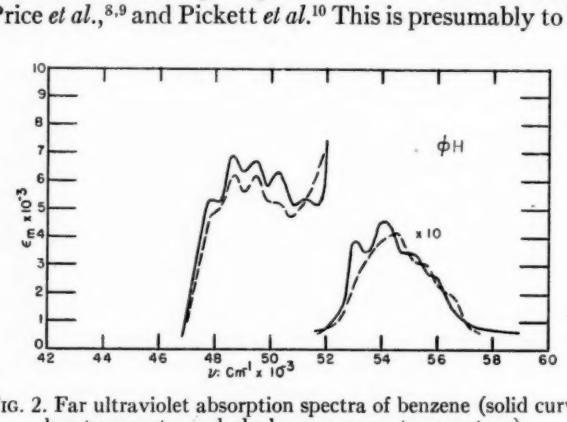

FIG. 2. Far ultraviolet absorption spectra of benzene (solid curve, low temperature; dashed curve, room temperature).

The value of peak extinction coefficient of the benzene 1850 A transition at room temperature obtained here, and agreeing with Platt and Klevens[12] and with Cohn and Ham[17] (all of whose data were obtained under similar conditions in hydrocarbon solutions), disagrees with the vapor phase value of both Pickett *et al.*[10] and Romand and Vodar[11] (whose results approximately agree). That our solution values of ϵ for the strong transition of benzene ($\epsilon = 45\,000$) should be a little more than one-half the vapor phase value obtained by others ($\epsilon = 80\,000$) is difficult to explain, as it has been shown that spectra in solution and in vapor have about the same molar extinction coefficient.[14]

[13] G. N. Lewis and M. Kasha, J. Am. Chem. Soc. **66**, 2100 (1944).
[14] L. E. Jacobs and J. R. Platt, J. Chem. Phys. **16**, 1137 (1948).
[15] W. J. Potts, Jr., J. Chem. Phys. **20**, 809 (1952); **21**, 191 (1953).
[16] W. J. Potts, Jr., preceding paper, J. Chem. Phys. **23**, 65 (1955).
[17] Unpublished data of J. S. Ham and of C. E. Cohn.
[18] J. R. Platt, J. Chem. Phys. **19**, 1418 (1951).

RESULTS

As a vivid example of the increased sharpening of benzene spectra one can obtain with a rigid glass at low temperature, some of the benzene plates have been reproduced in Fig. 1. Figure 1(a) shows absorption of the 2100 A transition; the lower exposure is at room temperature, the upper exposure is the identical solution frozen to a glass at liquid-nitrogen temperature. Figure 1(b) gives a similar picture for the 1850 A transition of benzene. That low temperatures are of value in this farther ultraviolet region is clearly shown by the effect on the 1850 A transition; not even vapor spectra have produced such sharpening of this transition.

In Figs. 2, 3, and 4 are plotted the molar extinction

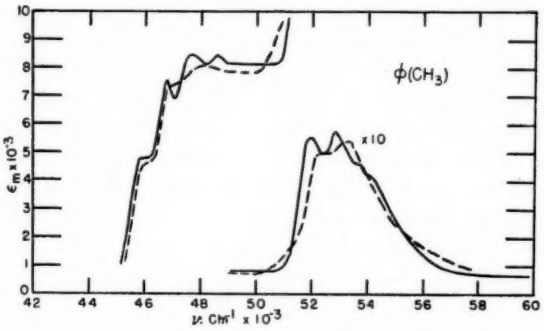

FIG. 3. Far ultraviolet absorption spectra of toluene.

coefficients of benzene, toluene, and para-xylene, respectively, against the frequency in wave numbers. The solid curve represents the data at low temperature, the dashed curve the data at room temperature. Figures 5, 6, and 7 give the same data on a $\log_{10}$ plot.

Because the molecular symmetries of benzene, toluene, and para-xylene differ, analogous spectral transitions in these molecules properly get different symmetry labels. Thus, to avoid confusion, for the present we shall designate the transition near 2100 A (47 500 cm^{-1}) in all three molecules as the "2100 A transition," the much stronger transition near 1850 A (54 000 cm^{-1}) as the "1850 A transition."

In Table I are tabulated the "electronic" features of the various transitions, data being given for both temperatures. The "centers" of the transitions are chosen as the points which divide in half the integrated absorption intensity, or oscillator strength,[19] of each transition. These values are uncertain to about 250 cm^{-1}. In a separate column are tabulated the (estimated) analogs of these positions in the vapor, using the data of Price *et al.*[8,9]

The molar extinction coefficients are for the strongest vibration peak in all cases. The error is roughly 15 percent or less.

The oscillator strengths,[19] of f numbers, given are

[19] f number, or oscillator strength, is defined as: $f=10^3(\log_{10}e)\cdot(mc^2/\pi e^2N)\int\epsilon_\nu d\nu=4.32\times10^{-9}\int\epsilon_\nu d\nu$, where ν is in cm^{-1}, ϵ_ν is molar extinction coefficient.

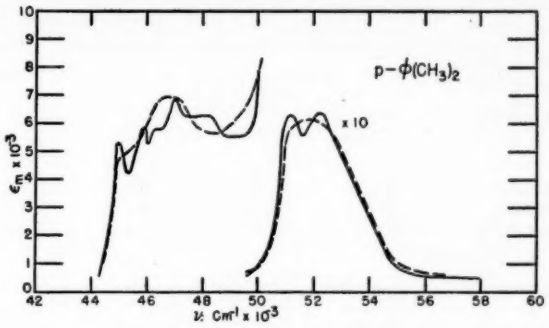

FIG. 4. Far ultraviolet absorption spectra of para-xylene.

subject to some uncertainty not only from error of extinction coefficient, but also from the selection of cut-off points on either side of the transition. This latter error may be particularly bad for the 2100 A transitions, in that they lie so close to the much stronger 1850 A transitions. The choice for the junction between the 2100 A and 1850 A transitions was the point where the slope of the log plot (see Figs. 5, 6, and 7) was zero just before the steep rise of the 1850 A transition. In toluene, because this zero slope extends some 1500 cm^{-1}, its midpoint, namely 49 550 cm^{-1}, was chosen as the junction between the 1850 A and 2100 A transitions. Hence the larger uncertainty tabulated for the f number of the 2100 A transition of toluene. (Percentagewise, this position uncertainty has little effect on the f number of the 1850 A transition.)

The oscillator strengths for room and low temperature agree within experimental error, as theory demands. The room-temperature values tend to be somewhat lower than those reported by Platt and Klevens,[12] but within probable experimental error of both sets of data.

Table II gives the vibrational-structure features of the 2100 A and 1850 A transitions of the three molecules. Values are given for both room-temperature and low-temperature conditions. The positions of the vibration peaks have been obtained not from the absorption curves, but by two independent measurements of the plates themselves. They are believed to be accurate to ±100 cm^{-1}. Those vibration peaks at room temperature

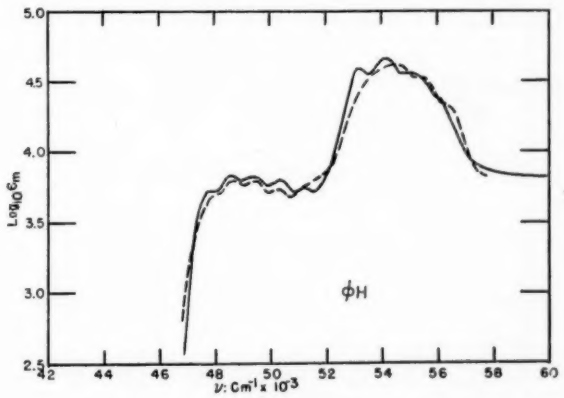

FIG. 5. Spectra of benzene on a log plot.

TABLE I. Electronic features of aromatic spectra.

Compound	Transition center ±250 cm⁻¹ 298°K	77°K	Vapor[a]	Shift from benzene (cm⁻¹) 298°K	77°K	ϵ_{max} 298°K	77°K	f number 298°K	77°K
				2100 A transition					
Benzene	49 750	49 500	50 600			6200	6800	0.10±0.01	0.11±0.01
Toluene	48 400	48 300	49 000	1350	1200	8100	8500	0.13±0.03	0.13±0.03
Para-xylene	47 000	47 000	47 500	2750	2500	6900	6900	0.12±0.02	0.12±0.02
				1850 A transition					
Benzene	54 600	54 250	55 900			42 000	46 000	0.60±0.07	0.63±0.07
Toluene	53 000	52 850	54 100	1600	1400	55 000	57 000	0.80±0.08	0.82±0.08
Para-xylene	52 100	52 000	52 600	2500	2250	61 000	63 000	0.89±0.08	0.89±0.08

[a] See text.

followed by (?) are rather doubtful, and would not have been reported had they not had definite analogs at low temperature.

As is well known, spectra shift to the red as the refractive index of the medium increases[14]; thus the low-temperature vibration peaks are all shifted to the red of the values obtained at room temperature, which in turn are shifted to the red of what would be observed in the vapor phase. In a third column appear the *low-temperature* frequency values "corrected" to the vapor state. These "corrections" are made by comparison with selected values of vapor spectra of other authors,[7–9] assuming that in one given transition all peaks shift the same amount. That this assumption is reasonable is shown by the rather close agreement in positions between the calculated "vapor" peaks and those which are sufficiently resolved from actual observations in the vapor.[7,9] For the 1850 A transitions a certain amount of personal judgment has been used to "correct" the vibration peaks, as they are not resolved in the vapor state. The vibrational separations of Table II are from these "vapor" listings.

DISCUSSION

Vibrational Structure

The low-temperature rigid-glass method produces decidedly increased sharpening of vibration structure,

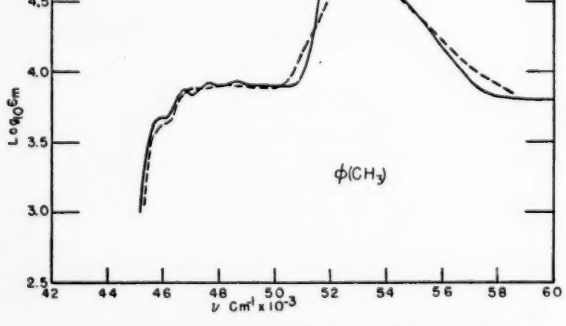

FIG. 6. Spectra of toluene on a log plot.

particularly in the 1850 A transitions. The results given here are not sufficiently accurate to warrant a vibrational analysis of states, but there is good indication that sufficiently accurate spectra may be obtained if one uses an instrument of higher dispersion and resolution than the small instrument used for this research.

In Table I the frequencies of the electronic transitions were taken as the approximate centers of integrated absorption in each transition. It is also desirable to know the frequencies of these transitions with respect to the equilibrium configurations of their nuclei; that is, the 0—0 band of the transition.[20]

The 2100 A transition is forbidden in benzene, but allowed in toluene and para-xylene (see below). In an allowed transition the 0—0 band is seen, but in a forbidden transition it is not; for it is vibrational inter-

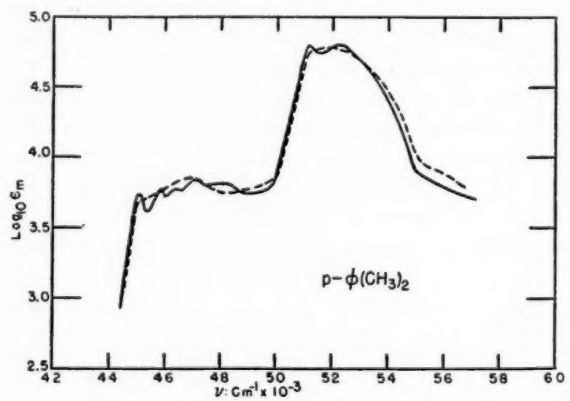

FIG. 7. Spectra of para-xylene on a log plot.

action which makes the transition appear at all,[21] and the 0—0 band of course contains no vibrational interaction. Thus the first band appearing in the 2100 A transition in toluene and para-xylene is probably the 0—0 band, but in benzene the 0—0 band is not seen.

Further, if one expects the 0—0 band of the 2100 A transition to shift to the red at about the same rate as the "center" of the transition shifts as methyl groups are added to benzene, then the first observed vibrational

[20] Nordheim, Sponer, and Teller, J. Chem. Phys. 8, 455 (1940).
[21] H. Sponer and E. Teller, Revs. Modern Phys. 13, 76 (1941).

band in the 2100 A transition of benzene bears no correlation to the first band observed in toluene and para-xylene. However, if one subtracts about 650 cm^{-1} from the positions of the benzene vibration peaks, then the first two vibration peaks correlate well in all these compounds, both at room and low temperature and in the calculated vapor state. This 650 cm^{-1} is the value of the ϵ_{2g} vibration which makes the transition allowed[20-22] (also see below) and is also the interval observed between the faint 0−0 band and first strong peak in the 2600 A transition of benzene.[5,21] Thus, for the 2100 A transition, it is probably safe to assert that the first vibrational peaks in toluene and para-xylene are the 0−0 bands (allowed transitions), the first observed peak in benzene is the 0−0 band. *plus* the 650 cm^{-1} ϵ_{2g} vibration which makes the transition allowed. (Correlation of higher vibrational bands is not possible, because there apparently is more than one vibrational level being excited in the 2100 A transition of para-xylene, judging from the separations.)

The first two vibrational peaks in the 1850 A transition of the three molecules seem to correlate fairly well with the shift of the transition "centers." As this transition is strongly allowed[20,22] (also see below) in all three molecules, the first vibrational peak should be the 0−0 band.

In Table III are given the positions of the electronic transitions, using the 0−0 band as a "point of reference." The 0−0 band of benzene (2100 A transition) is obtained by subtracting 650 cm^{-1} from the first observed band, assuming that the ϵ_{2g} vibration in the 2100 A transition has about the same frequency as in the 2600 A transition.[20,22]

TABLE II. Vibrational features of aromatic spectra.

Compound	Vibration peaks, ±100 cm^{-1} 298°K	77°K	"Vapor" (see text)	Separation, ±150 cm^{-1}
	2100 A transition			
Benzene	47 960	47 720	48 970	810
	48 660	48 430	49 680	950
	49 630	49 380	50 630	1000
	50 630	50 380	51 630	770
	51 410(?)	51 150	52 400	
Toluene	46 080	45 980	46 700	970
	47 060	46 950	47 670	900
		47 850	48 570	810(?)
		48 660(?)	49 380(?)	
Para-xylene	45 050	45 050	45 650	820
	46 080(?)	45 870	46 470	430
		46 300	46 900	760
	47 050(?)	47 060	47 660	1020
		48 080 (diffuse)	48 680	
	1850 A transition			
Benzene		53 050	54 700	860
	54 350(?)	53 910	55 560	1040
	55 250(?)	54 950	56 600	1070
		56 020	57 670	
Toluene	52 080(?)	51 810	53 060	1100
	53 190(?)	52 910	54 160	1000
		53 910	55 160	1040(?)
		54 950(?)	56 200(?)	
Para-xylene	(not resolved)	51 020	51 620	1200
		52 220	52 820	

TABLE III. 0−0 bands of the aromatic transitions.

Compound	0−0 band position ±100 cm^{-1} 298°K	77°K	"vapor"	Shift from benzene ±300 cm^{-1} 298°K	77°K
	2100 A transition				
Benzene	*ca* 47 310[a]	*ca* 47 070[a]	*ca* 48 320[a]		
Toluene	46 080	45 980	46 700	1220	1020
Para-xylene	45 050	45 050	45 650	2250	1950
	1850 A transition				
Benzene		53 050	54 700		
Toluene	52 080(?)	51 810	53 060		1240
Para-xylene		51 020	51 620		2030

[a] Calculated. See text.

Group Theory Notation

In discussing the more theoretical aspects of these spectral states it will be necessary to list the symmetries, group theory notations, and selection rules of the three molecules. These are tabulated in Table IV. The reductions of symmetry from D_{6h} (benzene) to C_{2v} (toluene) and V_h (para-xylene) are made by rotating the (substituted) benzene molecule about the x symmetry axis (so that $x \to x$, $y \to z$, $z \to y$). This is necessary to obtain C_{2v} symmetry for toluene, desirable to obtain V_h symmetry so that the symmetry axes of toluene and para-xylene have the same notation. (There are, of course, several alternative choices for axis assignment in reducing D_{6h} to V_h; and, although each gives some different assignments for states, the same selection rules are obtained.) The corresponding spectral transitions have been placed in the same row. If the transition is

TABLE IV. Symmetry properties of benzene, toluene, and para-xylene.[a]

	Benzene	Toluene	Para-xylene
Symmetry	D_{6h}	C_{2v}	V_h
Method of reduction	C_2^x C_2^y C_2^z σ_h	C_2^z σ_v^y	C_2^y C_2^z C_2^x σ_v^y
Transitions and selection rules	$^1A_{1g} \to {}^1B_{1u}$(forb) $^1A_{1g} \to {}^1B_{2u}$(forb)	$^1A_1 \to {}^1A_1(T_z)$ $^1A_1 \to {}^1B_1(T_z)$	$^1A_g \to {}^1B_{1u}(T_z)$ $^1A_g \to {}^1B_{2u}(T_z)$
	$^1A_{1g} \to {}^1E_{1u}(T_y, T_z)$	$^1A_1 \to \{{}^1A_1(T_z), {}^1B_1(T_z)\}$	$^1A_g \to \{{}^1B_{1u}(T_z), {}^1B_{2u}(T_z)\}$
	$^1A_{1g} \to {}^1E_{2g}$(forb)	$^1A_1 \to \{{}^1A_1(T_z), {}^1B_1(T_z)\}$	$^1A_g \to \{{}^1A_g$(forb), $^1B_{1g}$(forb)$\}$

[a] For a general treatment of group theory as applied to electronic spectra, see Sponer and Teller (reference 22).

[22] C. C. J. Roothaan and R. S. Mulliken, J. Chem. Phys. **16**, 118 (1948).

symmetry forbidden, it is followed by "forb"; if allowed, it is followed by the moment in which direction it takes place in order to be allowed.[21]

The notations in Table IV will be frequently referred to in the following discussion.

In benzene there are only two group-theoretically allowed types of (singlet) transition: $^1A_{1g}\rightarrow{}^1E_{1u}$ and $^1A_{1g}\rightarrow{}^1A_{2u}$. The latter is unlikely as an electronic transition because its transition moment lies along the axis perpendicular to the plane of the benzene ring. Two other transitions, $^1A_{1g}\rightarrow{}^1B_{1u}$ and $^1A_{1g}\rightarrow{}^1B_{2u}$, are forbidden in benzene but may be made allowed by interaction of an ϵ_{2g} type of vibration[23]: $\epsilon_{2g}\times\left\{\begin{matrix}B_{1u}\\B_{2u}\end{matrix}\right\}={}^1E_{1u}$.[20] Molecular orbital treatment of benzene[24] shows that the only one-electron (singlet) transitions likely in benzene are $^1A_{1g}\rightarrow{}^1B_{1u}$, $\rightarrow{}^1B_{2u}$, $\rightarrow{}^1E_{1u}$, which all arise from an upper ϵ_{1g} electron going to an unfilled ϵ_{2u} orbital. All of these transitions become allowed in toluene and para-xylene.

Another possible transition for benzene is the $^1A_{1g}\rightarrow{}^1E_{2g}$ transition predicted by Sklar[25] from the Heitler-London approximation. It is forbidden in benzene, but could be made allowed by an ϵ_{1u} vibration. Because of its even, or "g" character, the analogous transition is allowed in toluene, but forbidden in para-xylene. Further, if such a transition exists, according to MO theory[24] it must either be a two-electron transition (two ϵ_{1g} electrons going to an ϵ_{2u} orbital) or a one-electron transition from the lower α_{2u} orbital to an ϵ_{2u} orbital. In either case this requires more energy than the other one-electron transitions mentioned above, and thus would be found only in the very far ultraviolet if at all.

The 1850 A Transitions

These transitions may now be assigned with certainty to the $^1A_{1g}\rightarrow{}^1E_{1u}$ transition for benzene, the $^1A_1\rightarrow\left\{\begin{matrix}A_1\\B_1\end{matrix}\right\}$ for toluene, and the $^1A_g\rightarrow\left\{\begin{matrix}B_{1u}\\B_{3u}\end{matrix}\right\}$ transition for *para*-xylene. This one-electron transition is group-theoretically allowed and should be strong; it is the only allowed non-Rydberg one-electron transition in benzene which has its transition moment in the plane of the molecule. It is noted from the character tables of benzene[21] that the $^1A_{1g}\rightarrow{}^1E_{1u}$ transition is doubly degenerate, and methyl substitution breaks down this degeneracy in toluene and para-xylene.

The assignment of $^1A_{1g}\rightarrow{}^1E_{1u}$ for the 1850 A transition in benzene has been advocated before.[22] The present work helps confirm this assignment because the low-temperature methods, while obliterating the sharp Rydberg bands superimposed on this transition, have sharpened the transition to the point where vibrational structure is seen beyond question. Hence the 1850 A transition is *not* a dissociation or predissociation band,[20] but a definite $\pi-\pi$ type electronic transition.

The 2100 A Bands

These transitions are group-theoretically allowed in toluene and para-xylene, but forbidden in benzene, whether one assigns $^1A_{1g}\rightarrow{}^1B_{1u}$ or $^1A_{1g}\rightarrow{}^1B_{2u}$ (and their analogs in toluene and para-xylene) to the transition. That they are allowed in the substituted benzenes but not in benzene itself is experimentally shown from the respective appearance and nonappearance of what have been tentatively assigned as the 0—0 bands.

If these 0—0 band assignments are correct, then the transition may *not* be assigned to $^1A_{1g}\rightarrow{}^1E_{2g}$ and its analogs as has been proposed by Sklar,[25] for these assignments predict the transition to be allowed in toluene, but not in benzene or para-xylene. Furthermore, as noted above, the energy of the $^1A_{1g}\rightarrow{}^1E_{2g}$ transition must be at least *more* than the energy of the $^1A_{1g}\rightarrow{}^1E_{1u}$, or 1850 A transition, thus ruling it out as an assignment for the 2100 A transition.

The transition at 2100 A must therefore be assigned to either $^1A_{1g}\rightarrow{}^1B_{1u}$ or $^1A_{1g}\rightarrow{}^1B_{2u}$ in benzene, to their analogs in toluene and para-xylene. Most authors have assigned it to $^1A_{1g}\rightarrow{}^1B_{1u}$ and assigned the near ultraviolet transition (2600 A bands) to $^1A_{1g}\rightarrow{}^1B_{2u}$. This matter will not be further discussed at present, but the results presented may be reconciled with the above assignment.

ACKNOWLEDGMENTS

The author expresses his thanks and appreciation to Professor J. R. Platt and Professor C. C. J. Roothaan for many helpful suggestions and discussions. Greatest appreciation is also due Professor C. Reid for much of the work in editing and refining this paper for publication.

[23] Small Greek letters are used for vibrations or orbitals; capital Roman letters for electronic states.

[24] Much of the MO theory in this paper has been borrowed from C. C. J. Roothaan, "New Developments in Molecular Orbital Theory, with Applications to Benzene," Technical Report, Laboratory of Molecular Structure and Spectra, University of Chicago, 1949–1950, Part Two.

[25] A. L. Sklar, J. Chem. Phys. **5**, 669 (1937).

Modified Valence-Bond Treatment of Unsaturated and Aromatic Compounds

G. W. WHELAND
Department of Chemistry, University of Chicago, Chicago 37, Illinois
(Received May 20, 1954)

The conventional valence-bond treatment, by being put upon a more frankly empirical basis, can be modified in such a way that the difficulties arising from the nonorthogonality of the atomic orbitals centered about different atoms are largely bypassed. Although the extension of the new treatment to molecules more complex than that of benzene is rendered impracticable by the increased mathematical difficulties, the results obtained for 1,3-butadiene, cyclobutadiene, and benzene suggest that many of the essential features of the older calculations can be given a better theoretical justification than hitherto seemed possible. On the other hand, the importance of the relatively unstable structures with formal bonds appears to have been overrated.

IN the extremely approximate applications of the valence-bond method to the calculation of such quantities as the resonance energies of unsaturated and aromatic compounds,[1] one ordinarily makes the two following assumptions: (1) orbital degeneracy can be ignored so that, for any given molecule, only those wave functions derived from a single predetermined electronic configuration need be considered; and (2) all exchange integrals of unity and all multiple-exchange integrals of the energy are equal to zero. Neither of these simplifying assumptions, however, can be theoretically justified. The first makes it impossible to treat resonance among structures with different distributions of formal charges, and hence requires that all bonds be considered as either purely covalent or purely ionic; the second implies that the individual atomic orbitals are mutually orthogonal, and hence is inconsistent with the results of direct integration,[2] and also with the experimental observation that the ground states of molecules ordinarily have the lowest possible multiplicities.[3]

In spite of the foregoing difficulties, however, the simple valence-bond calculations have in a great many instances led to quantitatively satisfactory results.[1] Moreover, even the purely descriptive resonance treatments have often been found[4] to permit qualitatively correct conclusions. And finally, of course, the classical structural theory of organic chemistry, upon which these relatively recent quantum-mechanical developments are based, has been amazingly successful in providing valid descriptions of organic molecules. For these reasons, therefore, there appears to be some justification for the belief that the valence-bond approach must, after all, have a real theoretical significance.

Several authors have attempted to remove the limitations and inconsistencies of the usual valence-bond treatments, and hence to put the calculations upon a sounder basis. As early as 1936, Van Vleck advanced reasons for supposing that the errors resulting from the neglect of the multiple-exchange integrals of the energy might be approximately canceled by the simultaneous neglect of all the exchange integrals of unity.[5] It is by no means certain, however, that this cancellation would be either sufficiently general or sufficiently complete to explain the success of the simplified calculations. More recently, Mueller and Eyring[6] have pointed out that bonds which are intermediate between the covalent and ionic extremes can be accommodated within the formalism of the valence-bond treatment if the atomic orbitals, which are centered about single nuclei, are replaced by "semilocalized" orbitals, which are spread over several adjacent nuclei. Although this procedure has the additional advantage of making possible the treatment of bonds in which the two bonding electrons are unequally shared by the atoms concerned, it has the serious disadvantage of accentuating the difficulties arising from nonorthogonality. Indeed, if the atomic orbitals were mutually orthogonal, the semilocalized ones would not be; and, quite generally, the overlap integrals are greater for semilocalized than for atomic orbitals. In this paper, we shall present still a further approach in which, since the problem of orthogonality is largely bypassed, the use of semilocalized orbitals does not introduce serious trouble.

OUTLINE OF THE MODIFIED METHOD

The principles underlying the present method can be most easily explained by means of a detailed discussion of a single example, which we shall take as 1,3-butadiene. For this substance, we shall need to consider the three structures I, II, and III, in which all bonds, both the

[1] See, for example, L. Pauling and G. W. Wheland, J. Chem. Phys. **1**, 362 (1933); Eyring, Walter, and Kimball, *Quantum Chemistry* (John Wiley and Sons, New York, 1944), Chap. XIII; B. Pullman and A. Pullman, *Les Théories Electroniques de la Chimie Organique* (Masson et Cie., Paris, 1952), p. 121 ff.

[2] See, for example, Mulliken, Rieke, Orloff, and Orloff, J. Chem. Phys. **17**, 1248 (1949).

[3] This conclusion is based on the fact that single-exchange integrals of the energy between orthogonal orbitals are necessarily positive. See K. S. Pitzer, *Quantum Chemistry* (Prentice-Hall, Inc., New York, 1953), pp. 419 and 79.

[4] See, for example, G. W. Wheland, *The Theory of Resonance* (John Wiley and Sons, Inc., New York, 1944).

[5] J. H. Van Vleck, Phys. Rev. **49**, 232 (1936).

[6] See C. R. Mueller, J. Chem. Phys. **21**, 1013 (1953) and earlier papers cited there.

effective ones between adjacent atoms

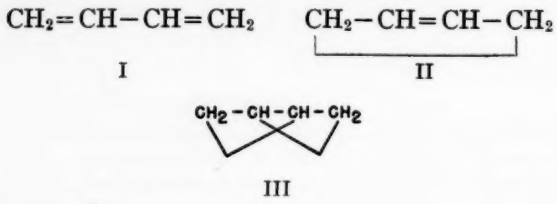

and the formal ones between nonadjacent atoms, are for the sake of convenience represented by full lines. Although structure III contains crossing bonds, and so is noncanonical, it cannot here be ignored, as it can in the conventional treatments. For the structures I, II, and III, we now set up the respective wave functions ψ_1, ψ_2, and ψ_3 in the usual way.[1] With each of these functions, the constant numerical factor is taken as equal to $(2^p N!)^{-\frac{1}{2}}$, where p, the number of pi bonds, is equal to 2 and N, the number of pi electrons, is equal to 4. If the atomic (or semilocalized) orbitals were mutually orthogonal, the functions ψ_1, ψ_2, and ψ_3 would be correctly normalized; since, however, the orbitals cannot be considered orthogonal, the molecular wave functions are, in general, not normalized.

For ease of reference, let us use the letters a, b, c, and d to designate the (atomic or semilocalized) pi orbitals associated with the four carbon atoms, and let us specify that the orbitals come in alphabetical order from the left to the right sides of structures I, II, and III. The energy calculated for the structure I is then

$$W_1=\frac{H_{11}}{\Delta_{11}}=\frac{Q+J_{ab}-\frac{1}{2}J_{bc}+J_{cd}+\text{other terms}}{1+S_{ab}{}^2-\frac{1}{2}C_{bc}{}^2+S_{cd}{}^2+\text{other terms}}, \quad (1)$$

where $H_{11}=\int\psi_1\mathbf{H}\psi_1 d\tau$ and $\Delta_{11}=\int\psi_1{}^2 d\tau$. Moreover, Q is the Coulomb integral, J_{ab} is the single-exchange integral of the energy between the orbitals a and b; S_{ab} is the overlap integral for orbitals a and b, so that $S_{ab}{}^2$ is the corresponding single-exchange integral of unity; and so on for the remaining J's and S's. The "other terms" in the numerator of the fraction include all the single-exchange integrals of the energy for nonadjacent pi orbitals, all the multiple-exchange integrals of the energy for the pi orbitals, and all the exchange integrals of the energy, of all types, which involve one or more sigma orbitals; the "other terms" in the denominator of the fraction include all the corresponding single- and multiple-exchange integrals of unity.

In the usual applications of the valence-bond method, the above expression for the energy W_1 is simplified by the neglect of all the "other terms" in both the numerator and denominator, and also the terms in S^2 in the denominator. (More precisely, some of these "other terms" in the numerator are not actually neglected but are instead absorbed in the parameter Q.) Equation (1) then becomes

$$W_1=Q+J_{ab}-\tfrac{1}{2}J_{bc}+J_{cd}. \quad (2)$$

Similarly, and to the same approximation,

$$W_2=Q-\tfrac{1}{2}J_{ab}+J_{bc}-\tfrac{1}{2}J_{cd}, \quad (3)$$

and

$$W_3=Q-\tfrac{1}{2}J_{ab}-\tfrac{1}{2}J_{bc}-\tfrac{1}{2}J_{cd}. \quad (4)$$

For the reasons that have already been outlined, there is no legitimate theoretical justification for supposing that Eqs. (2)–(4) are even approximately correct; they are, however, of entirely reasonable *form*, as can be most easily seen when they are rewritten in the completely equivalent ways

$$W_1=(Q-\tfrac{1}{2}J_{ab}-\tfrac{1}{2}J_{bc}-\tfrac{1}{2}J_{cd})+\tfrac{3}{2}J_{ab}+\tfrac{3}{2}J_{cd}, \quad (2')$$

$$W_2=(Q-\tfrac{1}{2}J_{ab}-\tfrac{1}{2}J_{bc}-\tfrac{1}{2}J_{cd})+\tfrac{3}{2}J_{bc}, \quad (3')$$

and

$$W_3=(Q-\tfrac{1}{2}J_{ab}-\tfrac{1}{2}J_{bc}-\tfrac{1}{2}J_{cd}). \quad (4')$$

The term $(Q-\frac{1}{2}J_{ab}-\frac{1}{2}J_{bc}-\frac{1}{2}J_{cd})$, which is common to all three equations, can now be identified with the total energy resulting from the electrostatic interactions other than the ones responsible for the pi bonds; and the remaining terms, $\frac{3}{2}J_{ab}$, $\frac{3}{2}J_{bc}$, and $\frac{3}{2}J_{cd}$, which differ from structure to structure, can be identified with the energies of the pi bonds between the specified pairs of adjacent atoms. Let us therefore assume that Eqs. (2)–(4), or (2')–(4'), are correct, but with the qualification that the quantities Q, J_{ab}, J_{bc}, and J_{cd} are purely empirical parameters that need have no close relation to the Coulomb and single-exchange integrals with which they were originally identified. Moreover, since it has been found that the total energies of molecules can be fairly accurately predicted on the assumption of constant bond energies, we are presumably justified in supposing that J_{ab}, J_{bc}, and J_{cd} are at least approximately equal to each other and also to the corresponding parameters that appear in the analogous calculations for all other molecules with pi bonds between carbon atoms. (In a more careful treatment, the J's would have to be considered functions of the internuclear distances; we shall here, however, ignore this refinement.) The common value of all these parameters can therefore be represented as simply J, so that the foregoing equations become

$$W_1=Q+\tfrac{3}{2}J, \quad (2'')$$

$$W_2=Q, \quad (3'')$$

and

$$W_3=Q-\tfrac{3}{2}J. \quad (4'')$$

With the parameters Q and J defined in the way just described, Eqs. (2'')–(4'') are probably fairly accurate. Moreover,

$$H_{11}=W_1\Delta_{11}=(Q+\tfrac{3}{2}J)\Delta_{11},$$

$$H_{22}=W_2\Delta_{22}=Q\Delta_{22},$$

and

$$H_{33}=W_3\Delta_{33}=(Q-\tfrac{3}{2}J)\Delta_{33}.$$

Since the functions ψ_1, ψ_2, and ψ_3 are not necessarily

normalized, we cannot set $\Delta_{11}=\Delta_{22}=\Delta_{33}=1$; we can, however, obtain the values of these matrix elements by direct integration. If, for the sake of simplicity, we assume that all carbon-carbon distances are equal to about 1.40 A, and that the orbitals a, b, c, and d are atomic rather than semilocalized (however, see below), then S_{ab}, S_{bc}, and S_{cd} are equal[2] to about $\frac{1}{4}$; and all other overlap integrals, such as S_{ac}, S_{ad}, etc., are negligibly small. Since the largest of the multiple-exchange integrals of unity are then the ones involving double exchanges of adjacent orbitals, and since these are equal to $(1/4)^4$, or $1/256$, we may assume that only the single-exchange integrals need be considered. Thus, we find that, under these conditions,

$$\begin{aligned}\Delta_{11}&=1+S_{ab}{}^2-\tfrac{1}{2}S_{bc}{}^2+S_{cd}{}^2\\&=1+\tfrac{3}{2}S^2=35/32,\end{aligned}\tag{5}$$

where S, the common value of S_{ab}, S_{bc}, and S_{cd}, has been set equal to $\frac{1}{4}$. Similarly,

$$\Delta_{22}=1,\tag{6}$$

and

$$\Delta_{33}=1-\tfrac{3}{2}S^2=29/32.\tag{7}$$

If we treat 1,3-butadiene as a hybrid of structures I and II, we are led to the secular equation

$$\begin{vmatrix}H_{11}-\Delta_{11}W & H_{12}-\Delta_{12}W\\ H_{21}-\Delta_{21}W & H_{22}-\Delta_{22}W\end{vmatrix}=0.$$

We have already obtained expressions for all the terms which here appear along the main diagonal of the determinant; the nondiagonal elements H_{12} (which is identical with H_{21}) and Δ_{12} (which is identical with Δ_{21}), however, remain to be evaluated. In order to obtain these quantities, we now make use of the identity[7]

$$\psi_3\equiv-\psi_1+\psi_2,$$

from which we derive the relation[8]

$$H_{33}=H_{11}+H_{22}-2H_{12}.$$

Hence

$$\begin{aligned}H_{12}&=\tfrac{1}{2}(H_{11}+H_{22}-H_{33})\\&=\tfrac{1}{2}[(Q+\tfrac{3}{2}J)(1+\tfrac{3}{2}S^2)+Q-(Q-\tfrac{3}{2}J)(1-\tfrac{3}{2}S^2)]\\&=\tfrac{1}{2}[Q(1+3S^2)+3J].\end{aligned}$$

Similarly,

$$\begin{aligned}\Delta_{12}&=\tfrac{1}{2}(\Delta_{11}+\Delta_{22}-\Delta_{33})\\&=\tfrac{1}{2}[(1+\tfrac{3}{2}S^2)+1-(1-\tfrac{3}{2}S^2)\\&=\tfrac{1}{2}(1+3S^2).\end{aligned}$$

The secular equation therefore becomes

$$\begin{vmatrix}(1+\frac{3}{2}S^2)(Q-W+\frac{3}{2}J) & \frac{1}{2}(1+3S^2)(Q-W)+\frac{3}{2}J\\ \frac{1}{2}(1+3S^2)(Q-W)+\frac{3}{2}J & Q-W\end{vmatrix}=0,$$

or

$$\begin{vmatrix}(1+\frac{3}{2}S^2)(x+\frac{3}{2}) & \frac{1}{2}(1+3S^2)x+\frac{3}{2}\\ \frac{1}{2}(1+3S^2)x+\frac{3}{2} & x\end{vmatrix}=0,$$

where the new parameter x is defined by either of the equivalent equations

$$x=(Q-W)/J$$

or

$$W=Q-xJ.$$

If we now, for the moment, assume that $S=0$, so that $\Delta_{11}=\Delta_{22}=\Delta_{33}=1$, the secular equation takes the form

$$\begin{vmatrix}x+\frac{3}{2} & \frac{1}{2}x+\frac{3}{2}\\ \frac{1}{2}x+\frac{3}{2} & x\end{vmatrix}=0.$$

The roots are therefore

$$x=\pm(3)^{\frac{1}{2}}$$

so that

$$W=Q\mp(3)^{\frac{1}{2}}J.$$

Since J is certainly negative, the energy of the ground state is $Q+(3)^{\frac{1}{2}}J$; and, since the energy associated with the more stable structure, I, is $Q+\frac{3}{2}J$, the resonance energy is $Q+1.50J-(Q+1.73J)=-0.23J$. The wave function for the ground state is then $N_0(\psi_1+0.36\psi_2)$ where N_0 is a normalization constant. All these results are, of course, identical with those obtained by the older treatment, in which S is similarly assumed to be equal to zero.

Let us now consider the modifications required when S is assigned the more realistic value of $\frac{1}{4}$. Since Δ_{11}, Δ_{22}, and Δ_{33} now have the values given in Eqs. (5), (6), and (7), the secular equation becomes

$$\begin{vmatrix}\frac{35}{32}\left(x+\frac{3}{2}\right) & \frac{19}{32}x+\frac{3}{2}\\ \frac{19}{32}x+\frac{3}{2} & x\end{vmatrix}=0,$$

so that $x=-1.65$, $+1.84$ and $W=Q+1.65J$, $Q-1.84J$. Since the energy associated with the structure I is again $Q+\frac{3}{2}J$, the resonance energy is $Q+1.50J-(Q+1.65J)=-0.15J$. The wave function for the ground state is $N_1(\psi_1+0.32\psi_2)$.

If the orbitals a, b, c, and d are considered to be semilocalized, so that the carbon-carbon bonds are given partial ionic characters, the overlap integral S must be greater than $\frac{1}{4}$. In order to have a definite figure, let us suppose that $S=\frac{2}{5}$. Moreover, although this simplification is more questionable than before, let us again assume that, in calculating the integrals Δ_{11}, Δ_{22}, and Δ_{33}, we can ignore all exchange integrals of unity except those related to single exchanges of adjacent orbitals. In this way, we find that $\Delta_{11}=31/25$, $\Delta_{22}=1$, and $\Delta_{33}=19/25$. The energies of the ground and excited

[7] G. Rumer, Nachr. Ges. Wiss. Göttingen, Math.-physik. Kl. 1932, 337.

[8] Compare J. C. Slater, Phys. Rev. **38**, 1109 (1931).

TABLE I. Results of calculations.

Compound	S	Energy of ground state	Energy of least stable state	Resonance energy in ground state	Ratio of coefficients[a]
1,3-Butadiene	0	$Q+1.73J$	$Q-1.73J$	$-0.23J$	0.36
	$\frac{1}{4}$	$Q+1.65J$	$Q-1.84J$	$-0.15J$	0.32
	$\frac{2}{5}$	$Q+1.56J$	$Q-2.08J$	$-0.06J$	0.22
Cyclobutadiene	0	$Q+2.00J$	$Q-2.00J$	$-1.00J$	···
	$\frac{1}{4}$	$Q+1.78J$	$Q-2.00J$	$-0.78J$	···
	$\frac{2}{5}$	$Q+1.52J$	$Q-2.00J$	$-0.52J$	···
Benzene[b]	0	$Q+2.40J$	Q	$-0.90J$	···
	$\frac{1}{4}$	$Q+2.28J$	Q	$-0.78J$	···
	$\frac{2}{5}$	$Q+2.15J$	Q	$-0.65J$	···
Benzene[c]	0	$Q+2.61J$	$Q-3.61J$	$-1.11J$	0.43
	$\frac{1}{4}$	$Q+2.34J$	$Q-5.05J$	$-0.84J$	0.25
	$\frac{2}{5}$	$Q+2.18J$	$Q-7.65J$	$-0.68J$	0.16

[a] In the wave function for the ground state. Since equivalent structures necessarily have equal coefficients, it is sufficient here to list only the ratios of the coefficients for the less stable structure (or structures), if any, to those for the more stable structure (or structures).
[b] Only the resonance between the Kekulé structures is considered.
[c] Resonance among all Kekulé and Dewar structures is considered. For each value of S, there is also obtained a state which, in all respects, is identical with the less stable one resulting from resonance between only the two Kekulé structures.

states are then, respectively, $Q+1.56J$ and $Q-2.08J$; the resonance energy is $-0.06J$; and the wave function for the ground state is $N_2(\varphi_1+0.22\psi_2)$.

DISCUSSION AND CONCLUSIONS

The same treatment that is here applied to 1,3-butadiene can be extended to other unsaturated and aromatic hydrocarbons. The results thus obtained for cyclobutadiene and for benzene are summarized in Table I in which, for the sake of completeness, the figures previously derived for 1,3-butadiene are also listed.

Only a moderate further complication of the calculations would be required if variations in the carbon-carbon distances, and hence also in the values of S and of J, were allowed. On the other hand, an extension of the treatment to molecules more complex than that of benzene would be extremely difficult (see also the Appendix). With 1,3-butadiene, for example, the non-diagonal matrix elements of the energy and of unity were expressed in terms of the corresponding diagonal elements for all three of the structures I–III, even though only the first two of these structures are canonical. Similarly, in the treatment of benzene, we had to take explicitly into account not only the two Kekulé and three Dewar structures, of types IV and V, respectively, but also all ten noncanonical structures of types VI–VIII. Even when we treated only the resonance

IV V VI VII VIII

between the Kekulé structures, we had to consider the complete set of fifteen structures. And, with naphthalene, for which there are 42 canonical and 903 noncanonical structures, the calculation would clearly be extremely tedious.

Since it therefore seems impracticable to consider any additional, more complex molecule, let us see what conclusions can be drawn from the rather meager data contained in the above Table. In the first place, it may be noted that, just as in the conventional valence-bond treatments,[1] the parameter Q cancels out of the calculations, so that the resonance energies are obtained as multiples of the single parameter J. Moreover, the cancellation of Q has the further fortunate effect of again making possible the deriving of definite expressions for the wave functions of the resonance hybrids. These convenient simplifications of the treatment are not restricted to the few hydrocarbons here considered, but can be shown to be generally valid.

The further conclusions that can be drawn are considerably more tentative than are the ones just discussed. The most interesting of these is doubtless that, as the value of the overlap integral S is increased, the relative importance of the unstable structures with formal bonds decreases. This generalization follows most clearly from a comparison of the values given in the last column of Table I. With benzene, for example, the ratio of the coefficient of each function representing a Dewar structure V to that of each function representing a Kekulé structure IV is 0.43 when $S=0$, 0.25 when $S=\frac{1}{4}$, and 0.16 when $S=\frac{2}{5}$. A similar, but less pronounced, trend is observed also with 1,3-butadiene. Further evidence leading to this same conclusion is provided by the fact that, with benzene, the fraction of the total calculated resonance energy which is due to the Dewar structures is 0.19 when $S=0$, 0.07 when $S=\frac{1}{4}$, and 0.04 when $S=\frac{2}{5}$. And finally, the ratio of the calculated resonance energies of 1,3-butadiene and of benzene decreases from 0.22 when $S=0$ to 0.18 when $S=\frac{1}{4}$, and further to 0.09 when $S=\frac{2}{5}$. If, as seems quite likely, these trends are encountered also with other hydrocarbons, it follows that, in all previous work in which S is set equal to zero, the importance of the structures with formal bonds has been overrated, as has also the magnitude of the stabilization resulting from the resonance with such structures. In particular, there is now reason to question the significance of the conclusion[9] that, with anthracene, structure IX has a larger weight in the resonance than does the more stable structure X; and, more generally, the common practice

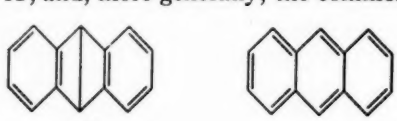

IX X

of ignoring the structures with formal bonds is seen to have a better theoretical justification than it has often been assumed to have.

[9] M. B. Oakley and G. E. Kimball, J. Chem. Phys. **17**, 706 (1949).

It would be gratifying if the present method of calculation provided a satisfactory explanation for the puzzling properties of cyclobutadiene. This hope is, however, not borne out by the data listed in the Table. Although the calculated resonance energy of this hydrocarbon, relative to that of benzene, does indeed decrease somewhat as S is increased from 0 to $\frac{2}{5}$, the effect is much too small to account for the apparent instability of the four membered ring. Moreover, since the procedure has not been extended to the treatment of triplet states, no additional evidence regarding the identity of the ground state can be obtained.

ACKNOWLEDGMENT

The author wishes to thank Professors J. R. Arnold and J. R. Platt for helpful discussions.

APPENDIX

This concluding section is devoted to a discussion of two further matters which did not require mention in the foregoing outline of the modified calculations. In the first place, we may note that, although the secular equation can in general be written down only with reference to all canonical and noncanonical structures, there is an alternative and much simpler approach which provides some, but unfortunately not all, of the required matrix elements. In the usual valence-bond treatment, in which the overlap integral S is set equal to zero, the elements of the secular determinant are expressed in the form

$$H_{ij}^0-\Delta_{ij}^0W^0=(Q-W^0)\Delta_{ij}^0+R_{ij}^0J \tag{8}$$

and simple rules for the evaluation of the numerical coefficients Δ_{ij}^0 and R_{ij}^0 have been devised.[10] In the present modification of the treatment, the corresponding elements are instead given by the equation

$$H_{ij}-\Delta_{ij}W=\Sigma_k\, p_{ij,k}(H_{kk}-\Delta_{kk}W),$$

where the constants $p_{ij,k}$ are obtainable in the manner outlined previously. Hence,

$$\begin{aligned}H_{ij}-\Delta_{ij}W&=\Sigma_k\, p_{ij,k}(W_k-W)\Delta_{kk}\\&=\Sigma_k\, p_{ij,k}[(Q+R_{kk}^0J)-W](1+R_{kk}^0S^2)\\&=(Q-W)\Sigma_k\, p_{ij,k}+[J+(Q-W)S^2]\Sigma_k\, p_{ij,k}R_{kk}^0\\&\quad+JS^2\Sigma_k\, p_{ij,k}(R_{kk}^0)^2\\&=(Q-W)\Delta_{ij}+R_{ij}J\end{aligned} \tag{9}$$

with

$$\Delta_{ij}=\Sigma_k\, p_{ij,k}(1+S^2R_{kk}^0)$$

and

$$R_{ij}=\Sigma_k\, p_{ij,k}[R_{kk}^0+S^2(R_{kk}^0)^2].$$

Since Eq. (9) must reduce to 8 when $S=0$, it follows that

$$\Delta_{ij}^0=\Sigma_k\, p_{ij,k}$$

and

$$R_{ij}^0=\Sigma_k\, p_{ij,k}R_{kk}^0.$$

Consequently,

$$\Delta_{ij}=\Delta_{ij}^0+S^2R_{ij}^0$$

and

$$R_{ij}=R_{ij}^0+S^2\,\Sigma_k\, p_{ij,k}(R_{kk}^0)^2.$$

Aside from the remaining summation in the final equation, therefore, the elements H_{ij} and Δ_{ij} can be easily written down with the aid of the more readily obtainable quantities R_{ij}^0 and Δ_{ij}^0. This fact provides a useful check upon the correctness of the values found for the numerous coefficients $p_{ij,k}$. Since, however, the evaluation of the foregoing summation requires explicit knowledge of these coefficients, the complete secular determinant can still be obtained only by the complicated procedure originally described.

One further mathematical detail must be discussed before the present modification of the valence bond method can be considered theoretically significant. In order that the treatment be self-consistent, it is essential that the total resonance energy calculated for two (or more) independent systems be equal to the sum of the resonance energies calculated separately for the component systems. For example, the resonance energy of n isolated benzene molecules must be just n times that of one benzene molecule; or, more simply, if resonance with all structures that have formal bonds is ignored, the resonance energies of cyclobutadiene XI, vinylcyclobutadiene XII, and allylcyclobutadiene XIII must all

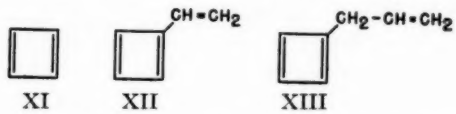

XI XII XIII

be identical. For the last three hydrocarbons, however, the calculated resonance energies are found to be, respectively, $-(1-2S^2)J/(1+2S^2)$, $-(2-3S^2)J/(2+5S^2)$, and $-(1-S^2)J/(1+3S^2)$. Although these values are clearly different (when $S\neq0$), the explanation for the discrepancy is simple. In evaluating the matrix elements of unity Δ_{ij}, we have assumed that the overlap integral S is so small that its powers higher than the square can be neglected. Consequently, the results that are obtained can be reliable only up to and including the terms in S^2. If the three foregoing expressions for the resonance energy are expanded in powers of S, each becomes equal to $-(1-4S^2)J+$terms in S^4, S^6, $\cdots$. Within the limitations imposed by the approximations employed, the treatment is therefore self-consistent. Although this conclusion is not restricted to the simple example considered, but is instead generally valid, the proof need not be given here.

[10] H. Eyring and G. E. Kimball, J. Chem. Phys. **1**, 239, 626 (1933); L. Pauling, *ibid.* 280.

Appearance Potential Studies. II. Nitromethane*

RICHARD J. KANDEL
University of California, Los Alamos Scientific Laboratory, Los Alamos, New Mexico
(Received May 24, 1954)

Appearance potentials and excess kinetic energies have been determined for the ions produced by the ionization and dissociation of nitromethane by electron impact in a mass spectrometer. Bond dissociation energies and mechanisms of fragmentation have been deduced where possible. $D(CH_3-NO_2)$ has been found to be 2.56 volts, a value in agreement with thermochemical data. The dissociation and ionization process yielding NO^+, the most abundant ion in the nitromethane mass spectrum, is believed to yield, at the same time, a CH_3O radical. A new value for the ionization potential of NO_2, 9.91 volts, is reported.

INTRODUCTION

IN a previous paper[1] a method was described for determining excess kinetic energies associated with ions produced during appearance potential measurements. This removes many of the uncertainties involved in the interpretation of appearance potential data in terms of bond dissociation energies. The present work on nitromethane is the first in a series of investigations of organic nitro compounds and related species. The mass spectrum of nitromethane has been studied and appearance potentials have been determined for all ions present in sufficient abundance. Excess kinetic energies have been determined in the vicinity of the appearance potentials. Where auxiliary data were available from other sources, bond dissociation energies and ionization potentials were deduced. In other cases, where such deductions could not be made, it was still possible to draw some conclusions about the mechanism of fragmentation.

The following symbols will be used throughout the remainder of this discussion: $A(X^+)$—appearance potential of X^+; $E(X^+)$—total excess kinetic energy of both X^+ and the other fragment or fragments formed along with it; $I(X)$—ionization potential of X; $EA(Y)$—electron affinity of Y; $D(X-Y)$—bond dissociation energy of the $X-Y$ bond; $\Delta H_f^0(XY)$—the standard heat of formation of XY at 25°C.

EXPERIMENTAL

Instrument

The instrument used in this work was a Consolidated Engineering Corporation Model 21–103 mass spectrometer. A magnetic scan circuit was incorporated into the instrument and was used in all appearance potential and excess kinetic energy determinations. The metastable suppressor and repeller circuits were modified as previously described.[1]

Chemicals

The nitromethane was a specially purified sample furnished by Commercial Solvents Corporation. Its purity was 99.8 percent by weight. The argon and krypton used as calibrating gases were taken from cylinders and used without further purification. The purity of each gas was determined, mass spectrometrically, to be better than 99 percent.

Procedures

Appearance potentials were determined by the method of initial breaks. Excess kinetic energies were measured by using the metastable ion suppressor as a retarding potential device. Both procedures have been previously described.[1] The mass spectrum of nitromethane was obtained in the conventional manner.

RESULTS

Mass Spectrum

The relative intensities of the ions formed by ionization and dissociation in nitromethane are given in Table I. These values were obtained at an ionizing voltage of 70 volts, an ionizing current of 15 μa, and with a conventional voltage scan. There was no variation in these relative intensities as either the ionizing current or pressure was changed, indicating that none of the ions was formed by multiple electron collisions or by collisions between ions and molecules. No metastable ions were found in the spectrum.

At an ionizing voltage of 50 volts the ions CH_3^+, NO^+, and NO_2^+ exhibited a marked increase in intensity (relative to the total number of ions formed). The ions C^+, CH^+, CH_2^+, O^+, CN^+, and CHN^+, products of more extensive dissociation processes than the above ions, showed decreases in intensity at 50 volts. The relative abundances of the other ions remained essentially constant.

Appearance Potentials

The appearance potentials listed in Table I are divided into groups and discussed below. In obtaining these appearance potentials argon $[A(A^+)=15.77$ volts$]$ and krypton $[A(Kr^+)=14.02$ volts$]$ were used as standards.

$CH_xNO_2^+$ Peaks

m/e = 61.—$CH_3NO_2 \rightarrow CH_3NO_2^+$.

$$A(CH_3NO_2^+)=I(CH_3NO_2)=11.34 \text{ volts.} \quad (1)$$

* This work was performed under the auspices of the U. S. Atomic Energy Commission.
[1] R. J. Kandel, J. Chem. Phys. **22**, 1496 (1954).

There is no value for $I(CH_3NO_2)$ reported in the literature with which to compare this one.

m/e=60.—$CH_3NO_2 \rightarrow CH_2NO_2^+ + H$.

$$A(CH_2NO_2^+) = D(H-CH_2NO_2) + I(CH_2NO_2) = 11.97 \text{ volts.} \quad (2)$$

If $D(H-CH_2NO_2)$ is about the same as $D(H-CH_3)$, then $I(CH_2NO_2)$ is approximately 7.6 volts. If, on the other hand, the nitro group had a tendency to weaken the carbon-hydrogen bond, then $I(CH_2NO_2)$ would be higher.

CH_xNO^+ and O^+ Peaks

m/e=45.—$CH_3NO_2 \rightarrow CH_3NO^+ + O$.

$$A(CH_3NO^+) = D(CH_3NO-O) + I(CH_3NO) = 11.31 \text{ volts.} \quad (3)$$

The nitrogen-oxygen bond dissociation energy in NO_2 is 3.12 volts.[2] If the same value applied here, $I(CH_3NO)$ would be 8.2 volts. If the reaction resulting in the formation of CH_3NO^+ is the simple fragmentation listed above, it is surprising that $A(CH_3NO^+)$ should equal $A(CH_3NO_2^+)$ since that would imply that the reaction $CH_3NO_2^+ \rightarrow CH_3NO^+ + O$ takes place without the absorption of energy. This is not in accord with the observation that the intensity of the $CH_3NO_2^+$ peak is 8.5 times that of the CH_3NO^+ peak nor with the absence of a metastable peak resulting from the decomposition of $CH_3NO_2^+$ ions beyond the ion source. It seems possible, therefore, that some exothermal rearrangement takes place during this fragmentation. This postulate is in agreement with the observations on the O^+ ion (see below).

m/e=16.—$CH_3NO_2 \rightarrow O^+ + CH_3NO$.

$$A(O^+) = D(CH_3NO-O) + I(O) + E(O^+) = 14.50 \text{ volts.} \quad (4)$$

Since $E(O^+)$ is 0.3 volt and $I(O)$ is 13.6 volts,[3] a value of 0.6 volt is obtained for $D(CH_3NO-O)$. This is much too low in view of the known stability of nitromethane. Again, it appears that a rearrangement has taken place along with the fragmentation. Although there are no quantitative data to support the postulate, it seems likely that a rearrangement of the nitrosomethane ion to form a formaldoxime ion takes place since the rearrangement of the molecular species is known to occur,[4] and the reverse reaction never occurs.[5]

m/e=42–44.—$CH_3NO_2 \rightarrow CHNOH^+$, $CNOH^+$, and CNO^+. Here, without knowledge of the energy involved in the rearrangement, little can be said about the other products formed. The hydrogen and oxygen atoms eliminated may combine to form OH or H_2. The negative ions OH^- and O^- may also be formed.

TABLE I. Relative intensities, appearance potentials, and excess kinetic energies of ions from nitromethane.

m/e	Ion[a]	Relative intensities at 70 volts	Appearance potentials (volts)	Excess kinetic energies (volts)
2	H_2^+	0.57		
12	C^+	1.94	22.83±0.05	2.6±0.3
13	CH^+	3.48	20.50±0.08	0
14	CH_2^+	8.30	17.92±0.08	0
15	CH_3^+	51.62	13.58±0.06	1.1±0.2
16	O^+	5.65	14.50±0.16	0.3±0.1
26	CN^+	1.61	19.15±0.09	0
			33.6 ±1.0	?
27	CHN^+	6.95	13.94±0.08	0
			17.1 ±0.5	?
			22.7 ±1.0	?
28	CH_2N^+	6.35	13.69±0.06	0
29	CH_3N^+	8.09	12.21±0.04	0
30	NO^+	100.00	12.01±0.06	0
31	*i*,[b] CH_3O^+	1.43		
32	*i*	0.53		
42	CNO^+	1.50	13.51±0.05	?
43	$CHNO^+$	3.11	12.52±0.13	0
44	CH_2NO^+	4.73	13.25±0.04	0
45	CH_3NO^+	6.26	11.31±0.10	0
46	NO_2^+	35.53	12.47±0.02	0
47	*i*	0.17		
48	*i*	0.15		
59	$CHNO_2^+$	0.06		
60	$CH_2NO_2^+$	4.00	11.97±0.02	0
61	$CH_3NO_2^+$	53.49	11.34±0.09	0
62	*i*	1.00		
63	*i*	0.22		

[a] Formulas listed are molecular rather than structural.
[b] Ions designated by "*i*" are isotopic peaks.

CH_xN^+ Peaks

m/e=29.—$CH_3NO_2 \rightarrow CH_3N^+ + ?$. Since the ionization potential of CH_3N is not known, it is difficult to decide on the fate of the oxygen atoms. The appearance potential is sufficiently low that it seems possible that they split off as an oxygen molecule. The appearance potentials of the CH_2N^+, CHN^+, and CN^+ peaks, involving the elimination of two oxygen and from one to three hydrogen atoms, cannot yield unambiguous information at present. The mere fact that three appearance potentials are observed for the CHN^+ peak and two for the CN^+ peak indicates that several processes are taking place. Even though the ionization potentials of HCN and CN are known, it is impossible to tell whether the hydrogen and oxygen atoms are present in the forms O, H, O_2, H_2, OH, H_2O, O^-, OH^-, or others.

CH_x^+, NO_2^+, and NO^+ Peaks

m/e=15.—$CH_3NO_2 \rightarrow CH_3^+ + NO_2$.

$$A(CH_3^+) = D(CH_3-NO_2) + I(CH_3) + E(CH_3^+) = 13.58 \text{ volts.} \quad (5)$$

[2] F. Rossini *et al.*, *Selected Values of Chemical Thermodynamic Properties* (U. S. National Bureau of Standards, Washington, 1949).
[3] R. F. Bacher and S. Goudsmit, *Atomic Energy States* (McGraw-Hill Book Company, Inc., New York, 1932).
[4] C. S. Coe and T. F. Doumani, J. Am. Chem. Soc. **70**, 1516 (1948).
[5] G. W. Wheland, *Advanced Organic Chemistry* (John Wiley and Sons, Inc., New York, 1949), p. 624.

$I(CH_3)$ is 10.08 volts[6] and $E(CH_3^+)$ is 1.1 volts. Therefore, $D(CH_3-NO_2)$ is approximately 2.4 volts. The uncertainty in the determination of the excess kinetic energy renders this bond energy inaccurate.

m/e=14.—$CH_3NO_2 \rightarrow CH_2^+ + H + NO_2$.

$$A(CH_2^+) = D(CH_3-NO_2) + D(CH_2-H) + I(CH_2) = 17.92 \text{ volts.} \quad (6)$$

It is extremely unlikely that N^+ contributes to m/e 14 in the vicinity of the appearance potential in view of the energy necessary to form it. The above fragmentation process is, indeed, the only one consistent with the required energy. Since $D(CH_2-H)=3.45$ volts[7] and $I(CH_2)=11.9$ volts,[8] $D(CH_3-NO_2)$ is found to be 2.57 volts.

m/e=13.—$CH_3NO_2 \rightarrow CH^+ + 2H + NO_2$.

$$A(CH^+) = D(CH_3-NO_2) + D(CH_2-H) + D(CH-H) + I(CH) = 20.50 \text{ volts.} \quad (7)$$

$D(CH-H)$ is 3.40 volts[7] and $I(CH)$ is 11.1 volts.[9] Consequently, $D(CH_3-NO_2)$ is 2.55 volts. Again, the above process is the only one consistent with the energy requirements.

m/e=12.—$CH_3NO_2 \rightarrow C^+ + H_2 + H + NO_2$.

$$A(C^+) = D(CH_3-NO_2) + D(CH_2-H) + D(CH-H) + D(C-H) + I(C) - D(H_2) + E(C^+) = 22.83 \text{ volts.} \quad (8)$$

A fragmentation yielding three hydrogen atoms would require over 27 volts. The aforementioned process, therefore, is the only plausible one. The total excess kinetic energy cannot be determined accurately since neither the exact mechanism of fragmentation nor the distribution of energy among the fragments is known. The value of 2.6±0.3 volts listed is a minimum value and the carbon-nitrogen bond energy deduced therefrom is a maximum value. $D(C-H)$ is 3.47 volts,[10] $I(C)$ is 11.27 volts,[3] and $D(H_2)$ is 4.48 volts.[2] $D(CH_3-NO_2)$, therefore, is less than or equal to 3.1 volts. If a mechanism is assumed whereby the C^+ fragment has an amount of excess kinetic energy inversely proportional to its mass as compared with the undissociated nitromethane molecule, then the over-all excess kinetic energy would be 61/49 of the measured amount or 3.2 volts. $D(CH_3-NO_2)$ would then be 2.5 volts. Since there is no plausible fragmentation mechanism which could account for such an energy distribution, the agreement of this value with the other deduced values for $D(CH_3-NO_2)$ is most likely coincidental. It can only be stated with surety on the basis of the analysis of the m/e=12 peak that $D(CH_3-NO_2)$ is less than or equal to 3.1 volts.

Since the presence of excess kinetic energy renders the carbon-nitrogen bond energies deduced from the m/e 12 and 15 peaks rather uncertain, the value to be used in the remainder of this discussion will be the average of those obtained from the m/e 13 and 14 peaks, namely 2.56 volts.

m/e=46.—$CH_3NO_2 \rightarrow CH_3 + NO_2^+$.

$$A(NO_2^+) = D(CH_3-NO_2) + I(NO_2) = 12.47 \text{ volts.} \quad (9)$$

Stevenson[11] has pointed out that, in general, when the alternative dissociations $AB \rightarrow A^+ + B$ and $AB \rightarrow A + B^+$ can take place, there will be no excess kinetic energy associated with the formation of that fragment which has the lower ionization potential. If that criterion is applied to the CH_3^+ and NO_2^+ peaks, the presence of excess kinetic energy in CH_3^+ and its absence in NO_2^+ would indicate that NO_2 has an ionization potential lower than 10.08 volts. This is lower than the values reported in the literature which range from 11 to 12.5 volts.[12,13] If the value of 2.56 volts for $D(CH_3-NO_2)$ is substituted into (9), $I(NO_2)$ is found to be 9.91 volts.

It is possible that the 12.5 volt value reported by Price and Simpson on the basis of spectroscopic data may be due to oxygen in the sample. The ionization potential of oxygen is close to this value, and they state that the electron removed in the ionization process is a nonbonding oxygen electron rather than the "odd" electron in the nitrogen-oxygen bond.

m/e=30.—$CH_3NO_2 \rightarrow NO^+ + ?$. If the other fragments formed during this dissociation are (a) CH_3 and O, then

$$A(NO^+) = D(CH_3-NO_2) + D(NO-O) + I(NO). \quad (10a)$$

Since $D(CH_3-NO_2)$ is 2.56 volts, $D(NO-O)$ 3.12 volts,[2] and $I(NO)$ 9.23 volts,[14] the appearance potential of NO^+ would be expected to be 14.9 volts. This is considerably higher than the observed value of 12.01 volts. Consequently, it must be postulated that the other fragments are either (b) CH_3+O^- or (c) CH_3O. If reaction (b) prevails,

$$A(NO^+) = D(CH_3-NO_2) + D(NO-O) + I(NO) - EA(O), \quad (10b)$$

and, since $EA(O)$ is 2.2 volts,[15,16] $A(NO^+)$ would be 12.7 volts. This is still outside the range of experimental error. Finally, if (c) obtains,

$$A(NO^+) = D(CH_3-NO_2) + D(NO-O) + I(NO) - D(CH_3-O). \quad (10c)$$

[6] J. A. Hipple and D. P. Stevenson, Phys. Rev. **63**, 121 (1943).
[7] C. A. McDowell and J. W. Warren, Discussions Faraday Soc. **10**, 53 (1951).
[8] A. Langer and J. A. Hipple, Phys. Rev. **69**, 691 (1946).
[9] A. E. Douglas and G. Herzberg, Can. J. Research **20A**, 71 (1942).
[10] G. Herzberg, *Spectra of Diatomic Molecules* (D. Van Nostrand Company, Inc., New York, 1950).
[11] D. P. Stevenson, Discussions Faraday Soc. **10**, 35 (1951).
[12] H. D. Smyth and E. C. G. Steuckelberg, Phys. Rev. **36**, 478 (1930).
[13] W. C. Price and D. M. Simpson, Trans. Faraday Soc. **37**, 106 (1941).
[14] Watanabe, Marmo, and Inn, Phys. Rev. **91**, 1155 (1953).
[15] H. D. Hagstrum, Revs. Modern Phys. **23**, 185 (1950).
[16] M. Metlay and G. E. Kimball, J. Chem. Phys. **16**, 774 (1948).

Pauling[17] gives a value of 3.0 volts for the carbon-oxygen bond energy in ethers. If that value is substituted into (10c), then $A(NO^+)$ is found to be 11.9 volts in good agreement with the observed 12.0 volts.

If the nitromethane molecule rearranges during ionization and dissociation into NO and CH_3O, the abundance of the species NO^+ and CH_3O^+ should largely depend on the relative values of the ionization potentials of the radicals. That species with the lower ionization potential would be expected to be present to a greater extent. Only if there is a large discrepancy between the two ionization potentials might one of the ionic species be expected to be absent completely. Unfortunately, such a discrepancy might be expected to be found here. No value has been reported for $I(CH_3O)$, but, in view of the known high electronegativity of the methoxy radical, a high ionization potential might be expected.

An attempt was made to find some CH_3O^+ in the nitromethane mass spectrum. It should appear at m/e 31. The isotopic species $N^{15}O^+$ and NO^{17+} should also appear at m/e 31. Their contribution was calculated to be 0.38 percent of the m/e 30 peak. The m/e 31 peak is actually 1.43 percent of the m/e 30 peak. In order to demonstrate that this excess is not caused by some isotopic fractionation during dissociation, the abundance of the isotopic species $N^{15}O_2^+$ and $NO^{16}O^{17+}$ at m/e 47 was calculated to be 0.46 percent of the m/e 46 peak and compared with the observed value of 0.48 percent.

In addition, the m/e 31 appearance potential curve, while it could not be subjected to a detailed quantitative analysis, was found to have a decidedly different shape than the m/e 30 curve. There appeared to be a break in it above the appearance potential of NO^+.

[17] L. Pauling, *Nature of the Chemical Bond* (Cornell University Press, Ithaca, 1946), p. 53.

Comparison with Thermochemical Data

Consider the reaction $CH_3NO_2 \rightarrow CH_3 + NO_2$.

$$\Delta H_f^0(CH_3) + \Delta H_f^0(NO_2) - \Delta H_f^0(CH_3NO_2) = D(CH_3-NO_2). \quad (11)$$

$\Delta H_f^0(CH_3)$ is 1.39 volts[2] and $\Delta H_f^0(NO_2)$ is 0.35 volt.[2] The most reliable value for the heat of formation of liquid nitromethane is −1.17 volts.[18] The heat of vaporization of nitromethane is 0.39 volt.[19] $D(CH_3-NO_2)$, as deduced from these data, is 2.52 volts. This confirms the value obtained in this study.

Cottrell and Reid[20] have reported an activation energy of 52.7 kcal (2.28 volts) for the thermal decomposition of nitromethane. Hillenbrand and Kilpatrick[21] have reported a value of 50.6 kcal (2.19 volts). Both sets of workers regard the primary process as the breaking of the carbon-nitrogen bond. This work supports that contention. The discrepancies between the activation energies and the carbon-nitrogen bond energy may be due to the presence of chains during the decomposition.

ACKNOWLEDGMENTS

The author would like to express his thanks to Mr. Candelario Esquibel for his help in running the spectrometer and to Dr. Louis C. Smith for his many suggestions during the course of this work. He would also like to thank James Neerman of Commercial Solvents Corporation, not only for supplying the nitromethane sample, but also for furnishing considerable data on the purity and mass spectrum of the compound.

[18] U. S. National Bureau of Standards, private communication.
[19] D. E. Holcomb and C. L. Dorsey, Ind. Eng. Chem. **41**, 2788 (1949).
[20] T. L. Cottrell and T. J. Reid, J. Chem. Phys. **18**, 1306 (1950).
[21] L. J. Hillenbrand and M. L. Kilpatrick, J. Chem. Phys. **21**, 525 (1953).

Measurement of the Molecular Weights of Vapors at High Temperature. II. The Vapor Pressure of Germanium and the Molecular Weight of Germanium Vapor*†

ALAN W. SEARCY‡ AND ROBERT D. FREEMAN§
Department of Chemistry, Purdue University, West Lafayette, Indiana

(Received June 11, 1954)

The vapor pressure of germanium and the molecular weight of germanium vapor have been determined by use of an apparatus for the simultaneous measurement of the weight of vapor effusing through two small orifices and of the force exerted by the effusing vapor. The molecular weight of germanium vapor at 1750°K was found to be 58±16 compared to the atomic weight of 72.60. The heat of sublimation of germanium at 298°K is 91.5±3.0 kcal.

HONIG[1] has recently reported mass spectrometric evidence for the presence of a number of polyatomic species in germanium vapor. The fraction of polyatomic species cannot be calculated with certainty from the mass spectrometric data, because neither the collision cross sections nor the fragmentation probabilities for the various molecular species are known. Honig has estimated that enough polyatomic molecules are present to cause a 10 percent error in a vapor pressure determination[2] by the Knudsen method, in which the vapor was assumed to be monatomic. Because high energy electrons (45 v) were used in Honig's investigation, fragmentation could have been very important, and the actual concentration of polyatomic species could have been considerably higher than Honig's estimate. Accordingly, an investigation of the degree of polymerization of germanium vapor is highly desirable.

This paper reports an investigation of germanium vapor with an apparatus for the simultaneous measurement of vapor pressures and of molecular weights of vapors. The apparatus has been previously applied to a study of tin vapor; that study has confirmed Honig's estimate[1] that the percentage of polyatomic species in tin vapor is small.[3]

EXPERIMENTAL

Equations

The effective molecular weight M^* of vapor effusing through holes in a Torsion cell is obtained from simultaneous determinations of the pressure in the cell by the Knudsen and the Torsion methods.[3] The Knudsen value for the pressure P_K is related to the weight w of vapor effusing in unit time through holes of area a_1 and a_2 from a cell at temperature T°K by

$$P_K = w(2\pi RT/M)^{\frac{1}{2}}/k(a_1+a_2), \quad (1)$$

in which k is the Clausing factor[4] for a tubular hole, R is the gas constant, and M is the molecular weight of the vapor. A second value for the pressure, P_T, is calculated from the angle φ through which the cell is rotated by the effusion of vapor through the holes of area a_1 and a_2 at distances q_1 and q_2 from the axis about which the cell rotates on a fine wire of torsion constant D,

$$P_T = 2D\varphi/(q_1a_1+q_2a_2)f. \quad (2)$$

The factor f is the ratio of the force resulting from the effusion of vapor through a tubular hole to the force expected if the hole has negligible length.[5] The torsion constant D is calculated from the period of oscillation t of the suspension alone, and the period t_w with a weight of known moment of inertia I added,

$$D = 4\pi^2 I/(t_w^2 - t^2).$$

If some arbitrary value for the molecular weight M is assumed for calculation of P_K by Eq. (1), the average effective molecular weight M^* is then given by

$$M^* = M(P_K/P_T)^2. \quad (3)$$

A description of the apparatus and a more detailed discussion of the method have been published.[3]

Measurements on Germanium

Germanium was heated in a graphite torsion cell in which the holes a_1 and a_2 had areas of 0.04543 and 0.04626 cm². These holes were at distances $q_1 = 0.990$ cm and $q_2 = 1.008$ cm from the axis of rotation of the cell. The average length to radius ratio of the holes was 0.621.

Spectrographic analysis of the germanium showed no significant impurity. Any undetected impurities sufficiently volatile to affect the vapor pressure measurements were vaporized during preliminary heatings. It has been previously demonstrated[2] that germanium shows no evidence of carbon contamination after being heated to 2125°K in a graphite cell, and that the effusing vapor consists of germanium only.

* Work supported by the Office of Naval Research through Purdue Research Foundation.

† Based on a thesis submitted by R. D. Freeman in partial fulfillment of the requirements for the Ph.D. degree at Purdue University.

‡ Present address: Division of Mineral Technology, University of California, Berkeley, California.

§ Present address: Goodyear Atomic Corporation, P. O. Box 628, Portsmouth, Ohio.

[1] R. E. Honig, J. Chem. Phys. **21**, 573 (1953).

[2] A. W. Searcy, J. Am. Chem. Soc. **74**, 4789 (1952).

[3] A. W. Searcy and R. D. Freeman, J. Am. Chem. Soc. (to be published).

[4] P. Clausing, Ann. Physik [5] **12**, 961 (1932).

[5] R. D. Freeman and A. W. Searcy, J. Chem. Phys. **22**, 762 (1954).

The experimental results are summarized in Table I. In calculating P_K, germanium vapor was assumed to be monatomic.

DISCUSSION

Molecular Weight of Germanium Vapor

The logarithms of the pressures calculated in Table I are plotted in Fig. 1 as functions of $1/T$ for comparison with a previous determination.[2] It seems probable that the earlier work gave apparent pressures that were slightly higher than the true pressures because of vaporization of material from the elaborate shielding system onto the collector plate. Recent measurements of the vapor pressure of germanium made with a conventional Knudsen cell[6] are in very close agreement with results reported here.

To obtain M^*, least squares solutions for equations of $\log P$ *vs* $1/T$ were found for the Knudsen and the Torsion data. These equations are: $\log P_K = 6.116 - (18\,570/T)$ and $\log P_T = 5.361 - (17\,160/T)$. Solution of these two equations for (P_K/P_T) and subsequent substitution of the results into Eq. (3) gives

$$M^* = 58 \pm 16$$

compared to the atomic weight 72.60. The uncertainty quoted is based on an estimated maximum error in Torsion pressure determinations of 15 percent.

This result, of course, indicates that germanium vapor is predominantly monatomic. Fragmentation of polyatomic germanium species by 45 volt electrons in a mass spectrometer is apparently a negligible source of error in estimating concentrations from ion intensities. The experimental uncertainty in the molecular weight obtained in this research is too great to justify definitely rejecting or accepting Honig's estimate that a 10 percent error in vapor pressure arises from the assumption that the vapor is exclusively monatomic. But, the concentration of polyatomic species is probably less than his estimate.

TABLE I. The vapor pressure of germanium.

Temp. (°K)	Weight of vapor effused (g.)	Duration of experiment (sec)	Angle of rotation φ (rad.)	Pressure, (atmos $\times 10^5$) P_K[c]	P_T
1608[a]	0.0155	6762	0.034	0.345	0.34
1645[a]	0.0116	3003	0.094	0.588	0.94
1651[a]	0.0145	3131	0.107	0.707	1.07
1713[b]	0.0217	1527	0.294	2.20	2.98
1713[b]	0.0192	1456	0.242	2.06	2.45
1718[b]	0.0255	1860	0.206	2.14	2.09
1726[b]	0.0128	954	0.262	2.10	2.66
1780[a]	0.0378	1216	0.492	4.93	4.93
1782[a]	0.0305	1058	0.484	4.57	4.85
1885[b]	0.0823	762	1.650	17.7	16.7

[a] The torsion constant $D = 3.815$ dynes/radian.
[b] The torsion constant $D = 3.860$ dynes/radian.
[c] Vapor assumed to be monatomic.

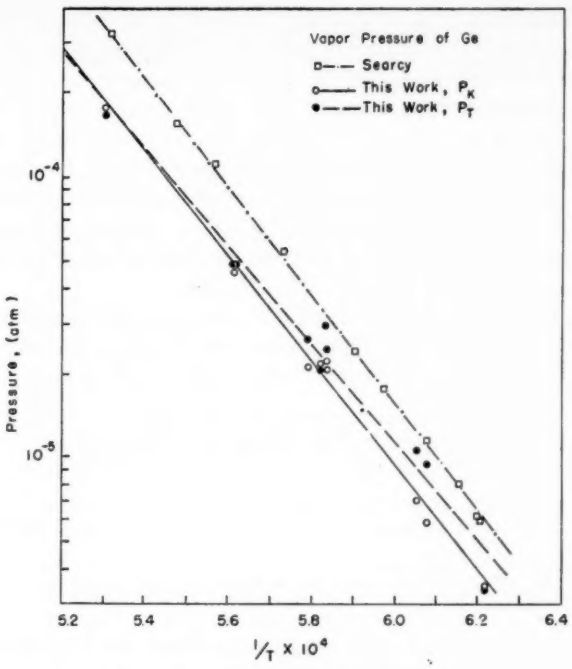

FIG. 1. The vapor pressure of germanium.

Heat of Sublimation of Germanium

Data of a previous paper[2] on the heat of sublimation of germanium have been recalculated with use of recent low temperature heat capacity data for germanium yielding the value 89.2±4.0 kcal for the heat of sublimation of germanium at 291°K.[7] Lehovec, Rosen, MacDonald, and Broder determined the heat of vaporization of liquid germanium by a novel method.[8] Combining their heat value with heat content data for germanium yields 88.5 kcal for the heat of sublimation at 298°K. Calculations of the heat of sublimation at 298°K from our data are summarized in Table II. For calculation of the $(\Delta F^\circ - \Delta H^\circ_{298})/T$ values, heat capacity data of Estermann and Weertman[9] were integrated graphically from 0 to 200°K to obtain for solid

TABLE II. Calculation of ΔH°_{298} for sublimation of germanium.

Temp. (°K)	$-(\Delta F^\circ - \Delta H^\circ_{298})/T$ (cal mole^{-1} deg^{-1})	$\Delta F^\circ/T$ Knudsen	(cal mole^{-1} deg^{-1}) Torsion	ΔH°_{298} Knudsen	(kcal mole^{-1}) Torsion
1608	32.20	24.99	25.01	91.96	91.99
1645	32.09	23.94	22.99	92.17	90.61
1651	32.08	23.56	22.74	91.86	90.51
1713	31.90	21.29	20.71	91.11	90.12
1713	31.90	21.44	21.10	91.37	90.79
1718	31.89	21.36	21.41	91.48	91.57
1726	31.87	21.40	20.93	91.94	91.13
1780	31.72	19.70	19.70	91.53	91.53
1782	31.71	19.86	19.74	91.90	91.68
1885	31.47	17.17	17.28	91.69	91.89

[6] A. W. Searcy and J. M. Criscione (unpublished data).

[7] E. C. Baughan, Quart. Revs. (London) **7**, 103 (1953).
[8] K. Lehovec, Rosen, MacDonald, and Broder, J. Appl. Phys. **24**, 513 (1953).
[9] I. Estermann and J. R. Weertman, J. Chem. Phys. **20**, 972 (1952).

germanium $S°_{200}=5.32$ Cal. The heat capacity equation $C_P=4.62+2.27\times10^{-3}T$ given by Baughan[7] was used between 200 and 1232°K; the heat capacity of liquid germanium was assumed to be constant and equal to 7.5 cal mole^{-1} deg^{-1}. The heat of fusion was taken as 7.13 kcal from the work of Wittig.[10] In light of the molecular weight found for germanium vapor, it was assumed to be essentially monatomic, and entropy and heat capacity data for gaseous germanium atoms were taken from the compilation of Brewer.[11]

The average values for $\Delta H°_{298}$ are, from the Knudsen data, 91.7±0.3 kcal and, from the Torsion data, 91.2 ±0.5 kcal. The average for all data is 91.5±0.4 kcal. All errors quoted are average deviations. The value for the heat of sublimation of germanium quoted by Baughan[7] is considered to be somewhat less reliable than those obtained in the present research because of the temperature dependent error noted by Searcy in the work[2] on which Baughan's calculations were based. Because of the inherent errors in calculating heats of sublimation from log$P$ *vs* $1/T$ plots[12] the value for $\Delta H°_{298}$ calculated from the work of Lehovec and co-workers[8] is also believed to be somewhat less reliable than the values obtained in the present research. Considering the uncertainties in entropy and heat capacity data we quote a value of 91.5±3.0 kcal for the heat of sublimation of germanium at 298°K.

[10] F. E. Wittig, Z. Metallkunde **43**, 158 (1952).
[11] L. Brewer, Natl. Nuclear Energy Ser. (McGraw-Hill Book Company, Inc., New York, N. Y., 1950), Vol. 19B, paper 3.
[12] L. Brewer and A. W. Searcy, J. Chem. Educ. **26**, 548 (1949).

THE JOURNAL OF CHEMICAL PHYSICS VOLUME 23, NUMBER 1 JANUARY, 1955

Single Ion Free Energies and Entropies of Aqueous Ions

WENDELL M. LATIMER
University of California, Berkeley, California
(Received May 24, 1954)

Single ion free energies of hydration were assigned by Latimer, Pitzer, and Slansky by choosing a set of ion radii which made both negative and positive ions fall on the theoretical Born curve in a plot of ΔF against $1/r'$. The r' values were the crystal ion radii plus 0.1 A for negative ions and plus 0.85 A for positive ions. It is now shown that this assignment of single ion free energies is consistent with the single ion entropies of hydration if $\bar{S}_{H^+}$ is -2.1 (the Eastman value). The ΔS values are proportional to Z/r' and the tentative suggestion is made that it is the temperature coefficient of r' which leads to the Z/r' function. It is proposed that the ΔF values be used to calculate a consistent set of radii of aqueous ions which will take into account coordination numbers and polarization.

THE free energies of hydration are now known with considerable accuracy for combinations of all the common positive and negative ions in aqueous solutions, as for example, $Na^+ + Cl^-$, $Ca^{++} - Mg^{++}$, or $I^- - Br^-$. The assignment of values to the individual ions is still highly questionable. The theoretical Born equation for the reaction, ion (gas) = ion (aqueous), $\Delta F=-Z^2/2r(1-1/K)$ has the limitation that the effective dielectric constant K and the ion radius (or ion cavity) r are not known. Latimer, Pitzer, and Slansky[1] proposed values for the effective "Born radii" which would make the free energies of both the positive and negative ions fall on the theoretical curve (ΔF against Z/r). The effective radii chosen were the crystal ion radii plus 0.1 A for negative ions and 0.85 A for positive ions. These "single ion" values not only gave agreement with the Born curve but also gave the correct values for the sums of the positive and negative ions and for the differences in ions of like charge. Table I indicates the type of agreement which is obtained between the experimental values (with $Cl^- = -85$ kcal) and those calculated from the Born equation. The experimental values are for the ion (gas) = ion (aq) (0.041 M), that is with no change in volume. It should also be noted that the Born equation applies only to the electrical energy while the experimental values also include a change in thermal energy which is around 2 kcal positive. The agreement also implies that the dielectric constant, K, is large with respect to 1.

There has been no substantiation of the Latimer-Pitzer-Slansky assignment of single ion free energies, but we now have sufficient data to show that this assignment is consistent with the absolute entropies of the single ions. Since the entropy of hydration is the temperature coefficient of the free energies of hydration, the choice of ion radii which gives the correct assignment of single ion free energies should also give the correct division of the entropies. The absolute entropy of H^+, as given by Eastman and his students,[2] is $\bar{S}_{H^+}=-2.1$ eu at 25°C. It seems probable that this value is not in error by more than one or two units.

In Table II the data for the monocharged ions have been summarized. ΔS has been calculated for three

[1] Latimer, Pitzer, and Slansky, J. Chem. Phys. **7**, 108 (1939).
[2] E. D. Eastman as reported by Goodrich, Goyan, Morse, Preston, and Young, J. Am. Chem. Soc. **72**, 4411 (1950).

values of $\bar{S}_{H^+}$, -2.1, -4.1 and 0. It may be observed that ΔF, ΔS, and r' have the same ordered arrangement if the value of $\bar{S}_{H^+}$ is taken as -2.1 (the Eastman value) but this is not true for the higher and lower values of $\bar{S}_{H^+}$. In other words, if $\bar{S}_{H^+}$ is taken as -2.1 eu then the single ion values for both the free energies and entropies of hydration have the same dependence upon our r' values. The agreement is very sensitive to the absolute entropy of H^+ and appears to fix that value within one entropy unit.

In Table II ΔH^0 of hydration was calculated from the Bureau of Standards data[3] for the ΔH^0 of formation of the ion (gas) and ion (aqueous). The ΔS values were calculated from the Sackur equation for the gas ions and the values of Latimer[4] for the aqueous ions corrected to 0.041 M (1 over molal volume at 25°C). ΔF was calculated from the ΔH^0 and ΔS.

Summaries of the data for doubly and triply charged ions are given in Tables III and IV. The ordered agreement of ΔF, ΔS and r' is again perfect with the exception of Pb^{++}, S^{--}, and Al^{+++}. The latter two are within the experimental uncertainties. The divergence of Pb^{++} is unresolved. In calculating the ΔF for the positive ions as for example Al^{+++}, the ΔF for $AlCl_3$ was first found and then the value for 3 Cl^- was subtracted to obtain Al^{+++}. Hence any error in Cl^- is multiplied by 3 in the Al^{+++} value. The same is also true for an error in $\bar{S}_{H^+}$. In the case of ΔS for S^{--} if the $\bar{S}_{H^+}$ was taken as -4.1 eu the ΔS for S^{--} would be 30 and that for Ba^{++} 37, that is, a change of 4 in the relative values. Thus the general agreement for the doubly and triply charged ions adds considerable weight to the contention that the correct r' values have been assigned.

A plot of $-\Delta S$ against Z/r' is given in Fig. 1. A fairly good linear dependence may be noted, with however a definite break between the singly and doubly charged ions. Part of this may be due to the fact that all of the experimental ΔS does not arise from the interaction of the charge with water dipoles. The restricted vibration of the ion in the ion cavity and an unknown term for the reduced mass of the ion-water system certainly makes some contribution. For the singly charged ions with their small ΔS values this will be a much greater relative correction that for the higher charged ions with their much larger ΔS values. However the dependence upon Z is definitely to the first power and not the square as one would expect from the Born equation.

If the temperature coefficient of the dielectric constant for the bound water is small for long wavelengths, as it is in ice, then the temperature coefficient of the free energy may depend largely upon the change of the radius of the ion cavity with temperature. By differentiation of the Born equation one obtains

$$\Delta S = -\frac{d\Delta F}{dT} = \frac{Z^2}{(r')^2}\frac{dr'}{dT}(1-1/K). \qquad (1)$$

TABLE I. Comparison of experimental and Born values for the free energies of hydration with values in kcal.

	r'	$-\Delta F$ Exp.	$-\Delta F$ Born
F^-	1.43	115	117
Li^+	1.53	113	107
Na^+	1.83	91.5	89
Cl^-	1.91	(85)	88
Br^-	2.06	78	82
K^+	2.18	76	77
Br^-	2.29	70	73
Be^{++}	1.15	565	560
Mg^{++}	1.50	434	447
S^{--}	2.00	320	335
Ba^{++}	2.14	297	313
Fe^{+++}	1.40	1019	1030
Al^{+++}	1.35	1090	1110

TABLE II. The dependence of ΔS of hydration upon the choice of $\bar{S}_{H^+}$ ΔH and ΔF in kcal, ΔS in cal/deg.

	$-\Delta H^0$	$-\Delta F$	$-\Delta S$ $H^+=-2.1$	$H^+=-4.1$	$H^+=0$	r'
F^-	123	115	28.2	26.1	30.3	1.43
Li^+	120.3	113	24.1	26.1	22.2	1.53
Ag^+.	112.7	106	17.9	19.9	15.8	
Na^+	96.5	91.5	16.6	18.6	14.5	1.83
Cl^-	89	85	14.9	12.9	17.0	1.91
Br^-	81	78	11.2	9.2	13.4	2.06
Tl^+	78	75	9.1	11.9	7.0	
K^+	76.5	74.1	8.1	10.1	6.0	2.18
I^-	72	70	5.8	3.8	7.9	2.29
Rb^+	69	67	5.2	7.2	3.1	2.33
Cs^+	62	61	4.3	6.3	2.2	2.52

TABLE III. Comparison of ΔF and ΔS of hydration of doubly charged ions with ΔS calculated for $\bar{S}_{H^+}=-2.1$ eu.

	$-\Delta H^0$	$-\Delta S$	$-\Delta F$	r'
Be^{++}	591	87	565	1.15
Cu^{++}	499	63	480	
Zn^{++}	485	62	466	
Mg^{++}	456	61	434	1.50
Mn^{++}	438	56	421	
Cd^{++}	428	52	413	
Ca^{++}	377	48	363	1.79
Pb^{++}	350	37	339	
Sr^{++}	348	46	334	1.95
S^{--}	330	32	320	2.00
Ba^{++}	308	35	297	2.14

TABLE IV. Comparison of ΔF and ΔS of hydration for triply charged ions if ΔS calculated for $\bar{S}_{H^+}=-2.1$ eu.

	$-\Delta H^0$	$-\Delta S$	$-\Delta F$	r'
Al^{+++}	1120	110	1690	1.35
Fe^{+++}	1052	110	1019	1.45
In^{+++}	996	95	965	1,70
Tl^{+++}	988	86	962	1.80
Pu^{+++}		81		1.85

[3] National Bureau of Standards Selected Values of Chemical Thermodynamic Constants, Washington, D. C.

[4] W. M. Latimer, *The Oxidation States of the Elements and Their Potentials in Aqueous Solutions* (Prentice-Hall, New York, 1952), second edition.

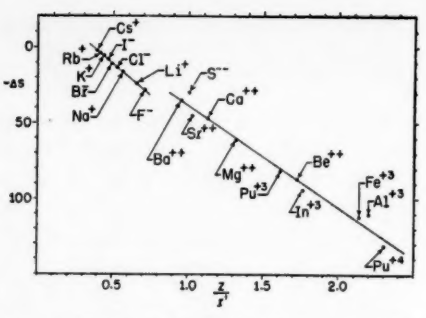

FIG. 1. Plot of ΔS against charge over radius.

We do not have values for dr'/dT, but from the values for crystals, Table V, we may conclude that it is roughly proportional to r'/Z and hence substituting for dr'/dT above, ΔS becomes proportional to Z/r' and not Z^2/r'. The value of dr'/dT for sodium ion to give the correct entropy of hydration is 3×10^{-4}. Such a value seems reasonable in comparison to the values of the coefficient for crystals in view of the higher forces between the ions. This picture is offered as an explanation of the puzzling dependence of ΔS upon the first power of Z but certainly cannot be considered more than a tentative proposal.

It will be noted that values for r' have been omitted for a number of ions in the various tables. This has been done because a reasonable value does not exist. Thus the crystal radius of Ag^+ depends upon the coordination number in the ion lattice and upon the polarization of the negative ion; it varies considerably between AgCl and Ag_2O. For an aqueous solution of Ag^+ we do not know either the coordination number or the polarization of the oxygen of the water. This suggests that the experimental values for the ΔF of hydration may be used to calculate a consistent set of radii for aqueous ions. The ΔF's are known with considerable accuracy for most simple ions and the "radius" calculated from them would give a parameter which is adjusted for or by the coordination number and the polarization.

Table VI is given as a sample of such calculation.

TABLE V. Coefficients of linear expansion.

NaCl	4×10^{-5}
KI	4.3×10^{-5}
CaF_2	1.9×10^{-5}

By the substitution of ΔF in the Born equation, r' is the value calculated for the ion "cavity." L is my value calculated for the radius by subtracting 0.1 A for negative ions and 0.85 A for positive ions from r'. The columns P, Z, and G are the values given by Pauling,[5] Zachariasen,[6] and Goldschmidt.[7]

For ions which are not highly polarized themselves, or which do not polarize the water, the agreement of L, P, Z, and G is very good. For an ion such as Zn^{++} my value of 0.59 A is considerably below the Pauling value of 0.74 A. His radius is calculated for a coordination number of 6. One finds experimentally the value 0.58 A for zincite in which the zinc has four oxygen bonds. The zinc ion in water is doubtless $Zn(H_2O)_4^{++}$ and the 0.59 A value appears to be in agreement with this formula. Similar comments might be made about Cd^{++}, Mn^{++} and In^{+++}. From this tabulation it does appear that radii calculated from the ΔF of hydration values for the single ions probably give our most reliable and self-consistent values for the aqueous ions.

TABLE VI. The use of ΔF of hydration to calculate a consistent set of radii for aqueous ions.

	ΔF kcal	r' cavity	Ion radius L	P	Z	G
F^-	115	1.45	1.35	1.33	1.36	1.33
Li^+	113	1.48	0.65	0.60	0.68	0.78
Be^{++}	565	1.18	0.33	0.31	0.30	0.34
Zn^{++}	466	1.44	0.59	0.74	···	(0.58)[a]
Mg^{++}	434	1.54	0.69	0.65	0.65	0.78
Mn^{++}	421	1.59	0.74	0.80	···	0.91
Cd^{++}	413	1.62	0.77	0.97	···	1.03
Ca^{++}	363	1.84	0.99	0.99	0.94	1.06
Sr^{++}	334	2.00	1.15	1.13	1.10	1.27
S^{--}	320	2.09	1.99	1.84	1.90	···
Ba^{++}	304	2.25	1.40	1.35	1.29	1.43
Al^{+++}	1087	1.38	0.53	0.50	0.49	0.39
Fe^{+++}	1019	1.43	0.58	0.60	···	0.67
In^{+++}	965	1.56	0.71	0.81		0.92
Zr^{+4}	1770	1.57	0.72	0.80		

[a] From zincite.

[5] L. Pauling, *The Nature of the Chemical Bond* (Cornell Press, Ithaca, New York, 1940), second edition.

[6] W. H. Zachariasen, Abstracts of the American Crystallographic Association Meeting, April, 1950.

[7] V. M. Goldschmidt, Skrifter Norske Videnskaps-Akad. Oslo. I. Matemat.-Naturv. Kl. **1926**, No. 8, 69.

The System Pyridine-Pyrrole and the Association of Pyrrole

SERGE N. VINOGRADOV* AND ROBERT H. LINNELL†
Department of Chemistry, American University of Beirut, Beirut, Lebanon
(Received May 26, 1954)

Pyridine and pyrrole react together to form a 1:1 complex as shown by infrared, heat of reaction, viscosity, refractive index, and density data. The heat of formation of this complex is 3.8 kcal/mole. Pyrrole itself is associated, but, like the simple alcohols, cannot be represented by a simple equilibrium. The heat of dilution of pyrrole in CCl_4 is 1.4 kcal/mole at infinite dilution.

A PRELIMINARY note on an infrared study of mixtures of pyridine-pyrrole has previously been published.[1] This paper reports the complete infrared work, calorimetric measurements, viscosity, refractive index, and density measurements. Since association of pyrrole molecules would markedly influence our calorimetric results on pyrrole-pyridine, we have also measured the heat of dilution of pyrrole in carbon tetrachloride.

Deželić[2a] and Deželić and Belia[2b] studied the viscosity of pyridine-pyrrole mixtures and interpreted a maximum in the curve at mole fraction 0.7 pyrrole as due to a complex between two pyrrole molecules and one pyridine. The inductive capacity measurements of Laurent[3] indicate a one-to-one mole complex. Rodebush[4] and coworkers ran the infrared spectrum of a one-to-one mole ratio mixture of pyridine and pyrrole and attributed the band at 3.11 μ to a strong hydrogen bond between the pyrrole N—H and the pyridine N. Recently Zezyulinskii[5] studied the molecular interaction between pyrrole and several other compounds by near infrared solution spectra in the regions 0.75 to 1.2 μ and 1.3 to 1.6 μ. He found for pyridine-pyrrole mixtures the 1st overtone of the N—H band shifted 7.8 percent to longer wavelength and the second overtone disappeared completely. This was attributed to a strong hydrogen bond between pyrrole and pyridine.

Fuson[6] and co-workers studied the N—H fundamental of pyrrole in the gas phase, pure liquid, and at various concentrations in CCl_4 solution. This band appears at 2.83 μ in the vapor (7 mm, room temperature) and at 2.95 μ in the pure liquid, while in CCl_4 solution two bands may appear—the band near 2.86 μ ("unassociated band") is intensified as the concentration of pyrrole decreases while the band near 2.92 μ ("associated band") decreases in intensity with decreasing concentration. Below about 0.3 molar concentration the 2.92-μ band is negligible. The exact nature of pyrrole association is not known and Tuomikoski[7] has suggested that the infrared results of Fuson are due to changing dielectric constant of the solvent. However Josien and Fuson[8] have now studied the 3-μ region of pyrrole in a wide variety of solvents and plotted the Kirkwood-Bauer relationship, $\delta\nu/\nu = C(D-1)/(2D+1)$ where C is a constant and D is the solvent dielectric constant. While pyrrole in C_6H_{14}, C_6H_{12}, CCl_4, CS_2, dichloroethane, and nitrobenzene obeys the Kirkwood-Bauer relationship, the pure pyrrole and pyrrole-pyridine systems do not, thus showing that a purely dielectric effect is not sufficient to explain the behavior of these cases.

EXPERIMENTAL

The infrared spectra were run on a Perkin-Elmer Model 21 instrument equipped with NaCl optics and cells. Refractive indices were determined with an Abbe refractometer thermostated to ± 0.1°C. Densities were determined with an Ostwald-Sprengel pycnometer following the method given in Weissberger.[9] Viscosity measurements were made on a simple Ostwald type viscometer held in a water bath by a heavy brass clamp. The capillary of the viscometer was adjusted to a vertical position by screws on the base of the water bath using a cathetometer in two positions at right angle to each other. The calorimeter was designed after that of Zellhoefer and Copley.[10] The calorimeter is shown in Fig. 1 and the circuit diagram in Fig. 2.

Pyridine and pyrrole were distilled in an all Pyrex glass column (Fenske rings, 22 theoretical plates at total reflux with benzene-CCl_4 test mixture). The pyridine was stored over NaOH pellets. For the pyridine $n_D^{30} = 1.5033$ and $d_4^{30} = 0.9730$. On standing the distilled pyrrole (water clear) always turned brown even when distilled and stored under nitrogen so that it was always used after freshly distilling. The physical constants of the pyrrole were $n_D^{30} = 1.5046$ and $d_4^{30} = 0.9613$. Merck

* Present address: Chemistry Department, Illinois Institute of Technology, Chicago, Illinois.
† Present address: Research Department, R. J. Reynolds Tobacco Company, Winston-Salem, North Carolina.

[1] R. Linnell, J. Chem. Phys. **21**, 179 (1953).
[2] (a) M. Deželić, Trans. Faraday Soc. **33**, 713 (1937); (b) M. Deželić and B. Belia, Ann. Chem. Justus Liebigs **535**, 291 (1938); M. Deželić and B. Belia, Bull. Soc. Roy. Yougoslav **9**, 151 (1938).
[3] P. Laurent, Ann. Chim. **10**, 397 (1938).
[4] Buswell, Downing, and Rodebush, J. Am. Chem. Soc. **61**, 3252 (1939).
[5] V. Zezyulinskii, Zhur. Fiz. Chim. **24**, 1442 (1950).
[6] N. Fuson and M. L. Josien, J. Chem. Phys. **20**, 1043 (1952); Fuson, Josien, Powell, and Utterback, J. Chem. Phys. **20**, 145 (1952).
[7] P. Tuomikoski, J. Chem. Phys. **20**, 1054 (1952).
[8] M. L. Josien and N. Fuson, J. Chem. Phys. **22**, 1169 (1954). We wish to thank Dr. Fuson for his kindness in sending us a manuscript of this work.
[9] A. Weissberger, ed. *Physical Methods of Organic Chemistry* (Interscience Publishers, Inc., 1949), Vol. 1, part 1, pp. 272–276.
[10] G. Zellhoefer and M. Copley, J. Am. Chem. Soc. **60**, 1343 (1938).

TABLE I. The pyridine-pyrrole system.

Moles[a] C_4H_4NH	Moles[a] C_5H_5N	Ratio C_4H_4NH/C_5H_5N	nD^{30}	d_4^{30}	η_{30} millipoise	q exp.[b] calories		K'	K''
0	pure	...	1.5033	0.9730	8.42	...	...	...	...
0.057	0.197	0.29	1.5066	0.9717	9.61	109	108	9.3	9.0
0.072	0.123	0.59	1.5064	0.9700	10.35	123	127	8.8	9.5
0.144	0.185	0.778	...	...	...	217	...	7.2	7.8
0.129	0.136	0.949	...	...	...	184	183	6.3	8.8
0.144	0.123	1.17	1.5070	0.9676	11.10	169	166	4.0	6.8
0.215	0.123	1.75	1.5069	0.9658	11.26	194	...	3.5	6.8
0.144	0.062	2.32	1.5062	0.9647	11.35	108	105	4.2	6.6
0.230	0.049	4.69	1.5059	0.9632	11.32	82	82	3.6	5.0
pure	0	...	1.5046	0.9613	11.29	...	...	...	...

[a] Moles calculated from d_4^{30} of present work.
[b] Data in columns 7 and 8 are from different experiments under the same conditions. These values, when calculated on a mole basis, extrapolate to 2.4±0.1 kcal per mole of complex; see text under results. The calorimeter Dewar flask was immersed in a water bath at 30±0.1°C with the room temperature 30±2°C.

pharmaceutical grade carbon tetrachloride was used without purification.

RESULTS

Table I gives the experimental results for a number of mixtures of pyridine and pyrrole. The refractive index data show a maximum at about mole fraction 0.5. The density data gives a broad inflection in the region of 0.5 mole fraction. The viscosity values are very similar to those of previous workers[2] and show a slight maximum at 0.7 mole fraction pyrrole. The high viscosity of pyrrole (compared to pyridine), which is no doubt due to the association of pyrrole, gives it a viscosity near that of the complex with pyridine and thus makes viscosity data of very little value. The calorimetric data has been treated in the following way: the experimental q is divided by the number of moles of the deficient component (defined by assumption of one-to-one complex) and plotted against mole ratio pyrrole to pyridine giving a sharp minimum at mole ratio 1.0 (Fig. 3). This is strong evidence in favor of one-to-one complex. From the graph of $\log\Delta H$ kcal/mole of pyrrole *versus* mole ratio pyrrole/pyridine the extrapolated value of ΔH at zero mole ratio is 2.4±0.1 kcal/mole of complex.

The heat of dilution of pyrrole in CCl_4 was measured in the same calorimeter. The experimental values are given in Table II together with the extrapolated heat of solution at infinite dilution.

If we assume that the following equilibrium exists in pyridine-pyrrole solutions

$$C_5H_5N+HNC_4H_4 \rightleftharpoons C_5H_5N\cdots HNC_4H_4, \qquad (1)$$

then we can calculate the equilibrium constant from the calorimetric data. Several possible assumptions can be used as a basis for these calculations; of these the following two procedures appear to be the most reasonable:

I. (a)—In forming the complex with pyridine the pyrrole must completely dissociate; each mole of complex formed thus requires +1400 calories to dissociate the pyrrole. (This is the heat of dilution at infinite dilution in CCl_4 obtained by extrapolation of data from Table II.)

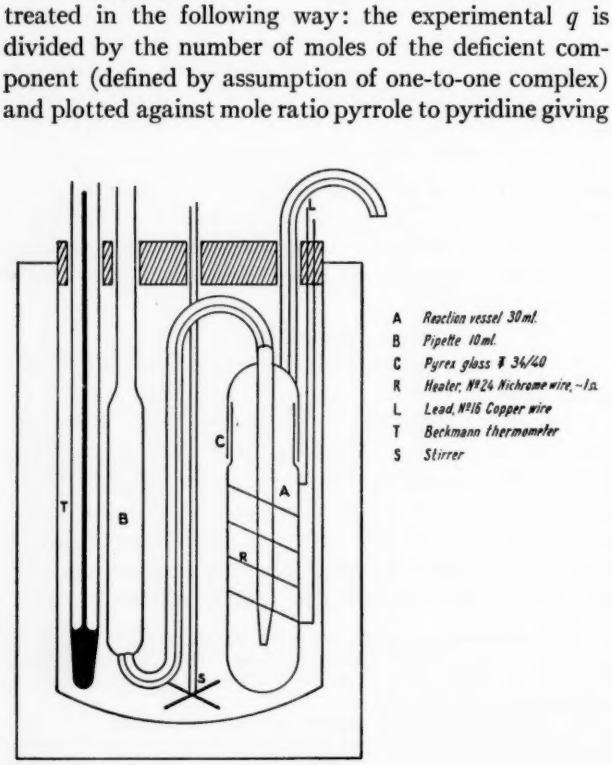

FIG. 1. Calorimeter.

TABLE II. Heat of dilution of pyrrole.

Moles CCl_4[a]	Moles C_4H_4NH[b]	Ratio C_4H_4NH/CCl_4	q experimental calories[c]		ΔH kcal/mole of pyrrole
0.052	0.145	2.79	19.8		0.14
0.103	0.145	1.41	28.3		0.19
0.103	0.072	0.07	38.6	39.4	0.54
0.155	0.072	0.46	48.2		0.67
0.206	0.072	0.35	53.8	55.5	0.75
0.309	0.072	0.23	67.3		0.94
0.309	0.044	0.14	48.0	50.7	1.14
0.309	0.029	0.094	45.6		1.58

Extrapolated heat of dilution = 1.4 ± 0.1 kcal/mole of pyrrole

[a] Calculated using value for d_4^{20} CCl_4 as 1.5940, J. Timmermans, *Physico Chemical Constants of Pure Organic Compounds* (Elsevier Publishers, New York, 1950), p. 226.
[b] d_4^{20} of pyrrole taken as 0.9684 from d_4^{25} 0.9651, Tuomikoski, Airola and Huuskonen, Trans. Faraday Soc. **49**, 786 (1952) and d_4^{30} (present work.)
[c] Data in columns 4 and 5 from different runs under identical conditions. The calorimeter Dewar flask was immersed in a water bath at 30±0.1°C with the room temperature 20±2°C.

TABLE III. Infrared absorption of pyridine-pyrrole in CCl_4.[a]

Moles pyrrole n_1'	Moles pyridine n_2'	C_4H_4NH/C_5H_5N n_1'/n_2'	Moles CCl_4	O.D. 2.84 μ	O.D. 3.11 μ	Moles free[c] pyrrole n_1	Moles free pyridine $n_2=n_2'-n_{12}$	Moles complex n_{12}	K[b]
0.0140	0.0124	1.13	0.237	0.260	0.357	0.0087	0.0071	0.0053	1.8
0.0140	0.00622	2.25	0.243	0.310	0.210	0.0111	0.0033	0.0029	1.4
0.00698	0.00869	0.803	0.246	0.170	0.077	0.0049	0.0066	0.0021	0.9
0.00698	0.00746	0.936	0.247	0.162	0.159	0.0046	0.0051	0.0024	1.2
0.00698	0.00746	0.936	0.247	0.162	0.150	0.0046	0.0051	0.0024	1.2
0.00698	0.00186	3.75	0.251	0.189	0.062	0.0056	0.0004	0.0014	4.6
0.00698	0.00497	1.40	0.249	0.184	0.199	0.0055	0.0035	0.0015	0.8
0.00698	0.00994	0.702	0.244	0.162	0.214	0.0046	0.0075	0.0024	1.0
0.00698	0.00248	2.81	0.251	0.204	0.064	0.0061	0.0016	0.0009	0.8
0.00698	0.00348	2.01	0.250	0.193	0.085	0.0057	0.0022	0.0013	1.0
0.00698	0.00746	0.936	0.247	0.169	0.160	0.0049	0.0054	0.0021	1.0
0.00698	0.01240	0.563	0.243	0.133	0.240	0.0037	0.0091	0.0033	1.6

Average value $K=1.2\pm0.2$
(95% confidence level, reject value of 4.6)

[a] All measurements made in 0.145 mm NaCl cell.
[b] Calculated in terms of mole fractions *without* including the solvent.
[c] From calibration curve using data of Table IV.

(b) The pyrrole which has not formed the complex dissolves in the excess pyridine requiring the same number of calories as in CCl_4 solvent.

Values of K' calculated by this method are listed in Table I.

II. Assumption (a) of I is still used.—(b) The excess pyrrole dissolves in the excess pyridine + complex requiring the same number of calories as in CCl_4. (That is, the complex is considered a solvent similar to CCl_4.)

Values of the equilibrium constant are again calculated by successive approximation as before. These values are listed in Table I as K''.

In both these methods it is assumed there is no heat of dilution of pyridine, as this has been shown to be small.[11]

Let n_1' = original No. of moles of pyrrole
n_2' = original No. of moles of pyridine
n_1 = No. moles pyrrole at equilibrium
n_2 = No. moles pyridine at equilibrium
n_{12} = No. of moles complex formed at equilibrium
q' = corrected experimental heat of reaction
$\Delta H=-3800$ calories‡ extrapolated experimental heat of formation per mole of complex.

A sample calculation for the ratio $C_4H_4NH/C_5H_5N=0.29$ using assumption I is the following:

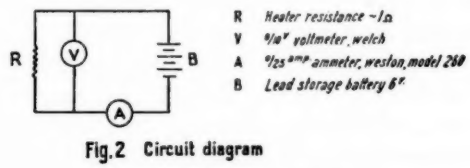

Fig.2 Circuit diagram

FIG. 2. Circuit diagram.

$n_{12}=(109+48\S)/3800=0.0413$
$n_2=0.196-0.041=0.155$
$n_1=0.0570-0.0413=0.0157$
$q'=(0.0413\times1400)+18.4\|+109=186.5$ calories
$n_{12}=186.5/3800=0.0491$
$n_2=0.196-0.049=0.147$
$n_1=0.0570-0.0491=0.0079$
$q'=(0.0491\times1400)+10.6\dagger+109=188.3$ calories
$n_{12}=188.3/3800=0.0496$
$n_2=0.196-0.050=0.146$
$n_1=0.0570-0.0496=0.0074$.

For the infrared study a series of solutions of pyrrole in CCl_4 were made up and the optical density at 2.84 μ was measured. All solutions were sufficiently dilute (0.3 molar or less) so that there was no band at 2.92 μ (the "associated band"). A series of mixtures of pyrrole and

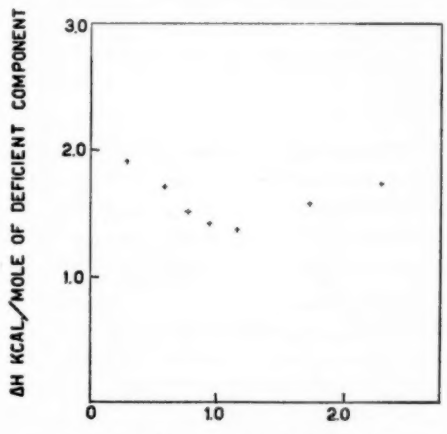

FIG. 3. Mole ratio C_4H_4NH/C_5H_5N.

[11] C. Staverman-Pekelder and A. Staverman, Rec. trav. chim. 59, 1081 (1940).

‡ Actually the sum of the heat of reaction obtained from extrapolation of data Table I *vs* mole ratio C_4H_4NH/C_5H_5N and the heat of dilution of pyrrole in CCl_4.

§ Obtained graphically from Table II assuming all the pyrrole dissolves in the pyridine with the same heat of solution as pyrrole in CCl_4.

‖ These values are graphically obtained for heat of dilution of free pyrrole in free pyridine using solution heat data of Table II.

TABLE IV. Infrared absorption of pyrrole in CCl_4.[a]

Moles pyrrole	Moles CCl_4	O.D. 2.84 μ
0.02792	0.238	0.675
0.02094	0.243	0.530
0.01396	0.248	0.375
0.00698	0.253	0.210
0.00349	0.256	0.130

[a] All measurements made in 0.145-mm NaCl cell.

pyridine were also made up and the optical density measured for the 2.84-μ band and the 3.11-μ band. The values are given in Table III.

The first six columns in Table III are experimental data; the seventh column is determined from the corresponding 2.84-μ o.d. values by means of a calibration curve of the pyrrole-CCl_4 solution concentrations *vs* 2.84-μ o.d. values tabulated in Table IV; column nine is the difference between columns one and seven; column eight is the difference between columns two and nine; column ten is calculated from data in the preceding columns according to the relationship:

$$K=\frac{(C_5H_5N\cdots HNC_4H_4)}{(C_5H_5N)(C_4H_4NH)}=\frac{n_{12}\cdot N}{n_2\cdot n_1}=\frac{(n_1'-n_1)\cdot N}{(n_1'-n_{12})\cdot n_1},$$

where N = total number of moles at equilibrium $=n_1'+n_2'-n_{12}$, n_1 = number of moles free pyrrole as determined from the infrared band at 2.84 μ (determined from calibration curve of pyrrole-CCl_4 solutions). Values of K are listed in the last column of Table III and are seen to be in reasonably good agreement with the assumed equilibria. A further independent check on the validity of the assumed equilibria is afforded by plotting the *calculated* concentration of complex (i.e., $n_1'-n_1$) *vs* the experimental o.d. at 3.11 μ (which is due to H-bonded pyrrole) where a straight line should result. The values given in Table III do yield a straight line with some scatter which can be attributed to experimental factors.

TABLE V. Boiling points of pyrroles and related compounds.[a]

Pyrrole	130°C	*N*-methyl pyrrole	114.5°C
Furan	32°C	*N*-ethyl pyrrole	130°C
Thiophen	84°C	2-methyl pyrrole	148°C
Cyclopentane	49.5°C	3-methyl pyrrole	143°C

Comparison of pyrrole and *N*-methyl pyrrole.[b]

	T_{fus} °A	H_{vap} kcal/mole	H_{fus} kcal/mole
Pyrrole	238.8°	11.134	15.017
N-methyl pyrrole	231.2°	10.058	3.990

[a] Mme. Martinet and J. Martinet, Bull. Soc. Chim., France 71, (1948).
[b] G. Milazzo, Bull. Sci. Fac. Chim. ind., Bologna, No. 6, 94 (1941).

DISCUSSION

The experimental results presented here definitely indicate that pyridine and pyrrole react together forming a one-to-one complex. Whether this reaction is called hydrogen-bonding or a Lewis acid-base interaction is probably immaterial. Other molecules capable of being electron donors can act similarily and we are now studying systems of pyrrole and substituted pyridines, piperidine and acetone.[8] The extent of reaction with pyrrole appears to be directly related to the strength of the Lewis base as would be expected.

The high viscosity of pyrrole compared to pyridine (Table I) indicates association in pyrrole and the small maximum in the viscosity plot for pyridine-pyrrole mixtures points to a predominance of dimerization. Table V lists boiling points of several pyrroles and related compounds which further emphasizes the pyrrole association. If we assume a simple monomer-dimer equilibrium in liquid pyrrole a value for the equilibrium constant can be calculated from infrared data[6] by using the 2.84-μ band as monomer pyrrole and the 2.92-μ band as dimerized pyrrole molecules. Such a treatment does not yield a consistent K value. The heat of solution values also are not consistent with a simple monomer-dimer equilibrium. The situation may be similar to that in simple alcohols. The treatment of Kempter and Mecke[12] assumes a series of equilibria, monomer, dimer, trimer, etc. all with equal equilibrium constants K. This treatment also failed when applied to the infrared data for pyrrole. The method of Coggeshall and Saier[13] using one equilibrium constant for the monomer-dimer and a second equilibrium constant for the dimer-timer, trimer-tetramer, etc., may yield better results. Further work on this problem will be reported later.

It is not possible to directly compare the absolute values of K as determined by infrared and by calorimetric methods. Since the situation in the calorimetric work involved the pure liquid pyrrole and pyridine, the solutions will be far from ideal. It is not surprising that both K' and K'' show trends with mole ratio of C_4H_4NH/C_5H_5N as the molecular environment must be quite different with excess pyridine than with excess pyrrole. Both K' and K'' tend to be lower when the C_5H_5NH is in excess but values of K'' appear to be more nearly constant. Method II for calculation of K'' would seem to be favored on theoretical grounds since the pyrrole unreacted with pyridine must dissolve in the whole mixture which includes the "molecules" of complex. Pyrrole itself probably exists as a monomer, dimer, trimer, etc., equilibrium. When pyrrole is the deficient component, a significant fraction of the total pyrrole is complexed with pyridine so that use of 1.4 kcal as the heat of dissociation of pyrrole is justified. As the pyrrole

[12] H. Kempter and R. Mecke, Z. Physik. Chem. 46, 229 (1941).
[13] N. Coggeshall and E. Saier, J. Am. Chem. Soc. 73, 5414 (1951).

becomes the excess component, only a small fraction of the total pyrrole is complexed with pyridine and the value 1.4 kcal as the heat of dissociation for the pyrrole complexing with pyridine is not justified and a smaller value should be used. This correction will increase the value of n_{12} which increases K' or K''. Thus the decreasing heat of dissociation of pyrrole as the ratio C_4H_4NH/C_5H_5N increases will account for our results. By this argument the most correct value of K' or K'' should be about 9. A recent study of equilibrium constants for the association of organic acids[14] by infrared gave values differing by factors greater than 10 in some cases from these same constants as determined by other methods. It would be desirable to carry out calorimetric work using dilute CCl_4 solutions comparable to those used in the infrared work but this requires more sensitive equipment than ours.

The authors wish to thank the Research Corporation for helping to make this work possible.

[14] J. Harris and M. Hobbs, J. Am. Chem. Soc. **76**, 1419 (1954).

THE JOURNAL OF CHEMICAL PHYSICS VOLUME 23, NUMBER 1 JANUARY, 1955

The Normal Coordinates of *N*-Dimethylaminodiborane

R. G. Breene, Jr.
Geophysics Research Directorate, Air Force Cambridge Research Center, Air Research and Development Command
(Received June 17, 1954)

The multiple origin method has been utilized for the selection of initial coordinates for the description of the normal vibrations of *N*-dimethylaminodiborane. Symmetry considerations were then used in order to obtain symmetry coordinates from these MOM coordinates, and, under the assumption of a diagonal potential function, these coordinates were assigned to vibrational frequencies which have been recently reported by Mann. The valence force constants for the methyl-*N*-methyl framework vibrations were then calculated and the results compared with similar constants obtained from the dimethylamine molecule.

I. INTRODUCTION

THE *N*-dimethylaminodiborane molecule whose experimental vibrational spectrum has been recently reported by Mann[1] would appear to offer an interesting application of Deeds' multiple origin method[2] (MOM) for the selection of vibrational coordinates and the resultant simplification of the vibrational secular determinant.

Deeds' method is essentially predicated on the additivity of the kinetic energy since we will surely obtain the over-all vibrational energy of the molecule by adding the vibrational energies of certain selected subgroups of the molecule to the vibrational energy which results from the vibrational motion of these subgroups with respect to each other. In referring to the vibrations of the subgroups, we tacitly infer certain infinitesimal hindered rotations of these groups about their equilibrium principal axes. The MOM is possessed of the distinct advantages of (a) assuring a diagonal kinetic energy matrix and (b) giving a reasonable approximation of the normal vibrations when a diagonal quadratic potential energy matrix is utilized. The maximum realization of advantage (b) is, of course dependent on the care with which we select our initial coordinates. There is no equation for the selection of these coordinates, but rather an intuitive type approach based on the over-all symmetry of the molecule must be utilized. In this paper we shall select the proper coordinates, set up the kinetic and potential energy expressions, and assume a diagonal potential energy expression in the resulting vibrational secular determinant.

II. SELECTION OF THE INITIAL VIBRATIONAL COORDINATES

Figure 1 yields the arrangement of the 16 nuclear mass points which has been obtained by Hedberg and Stosick[3] from electron diffraction, and we shall assume that this arrangement goes to make up the *N*-dimethylaminodiborane molecule. We shall also take the internuclear distances and the angles between the vectors defining these distances from the data of these authors.

We first establish a coordinate system whose origin lies at the molecular center-of-mass and subsequently rotate it by diagonalizing our rotary inertia tensor to obtain the principal axis system indicated in Fig. 1. Later, we shall refer our framework coordinates to this coordinate system. Inspection of the molecular framework next tells us that this atomic arrangement belongs to the symmetry point group C_{2v}. The twofold axis corresponds to the Z axis.

We now turn to the selection of the atomic subgroups. For the molecule under consideration, our choice is virtually made for us by the "natural groups" which present themselves in the structure. Not only are the two CH_3 and the two BH_2 groups the best choices for

[1] D. E. Mann, J. Chem. Phys. **22**, 70 (1954).
[2] W. E. Deeds, Ph.D. dissertation, The Ohio State University, 1952.
[3] K. Hedberg and A. J. Stosick, J. Am. Chem. Soc. **74**, 954 (1952).

atomic subgroups, but they also appear to be about the only ones. We now establish principal axes systems for each group, with the origins of these coordinate frames located at the centers-of-mass of the pertinent groups as shown in Fig. 1. Now let us concentrate the mass of each group at the center of mass of the group. The four point masses which result together with the N atom and the remaining H atom form the molecular framework which is indicated in Fig. 2. We may now proceed to the selection of the vibrational coordinates.

We are dealing with a 16-atomic molecule which, since it is quite obviously not a linear mass distribution, must possess 42 degrees of vibrational freedom. We thus desire 42 initial vibrational coordinates—it would not seem that the term "intermediate symmetry coordinates" is precisely applicable here—which satisfy the Eckart conditions. We shall first take as coordinates the normal coordinates of the internal vibrations of our four atomic subgroups. In the case of the CH_3 groups this will yield a total of twelve coordinates. In a CH_3 group we shall designate the symmetrical stretching coordinate s, the symmetrical bending coordinate u, the asymmetrical stretching coordinates v_a and v_b, and the asymmetrical bending coordinates w_a and w_b. It may be recalled that s and u go with the nondegenerate modes and v and w with the twofold degenerate vibrations. In addition those coordinates referred to frame $(x_1y_1z_1)$ will be given the subscript 1, and those coordinates referred to the frame $(x_2y_2z_2)$ will be given the subscript 2. We now consider the BH_2 groups. In the water-molecule type vibrations of these groups we shall designate the symmetrical stretching vibration as q_a, the symmetrical bending vibration as q_b, and the asymmetrical bending vibration as q_c. Those coordinates referred to frame $(x_3y_3z_3)$ will be given the subscript 3, and those coordinates referred to frame $(x_4y_4z_4)$ will be given the subscript 4. The eighteen coordinates which have so far been chosen all satisfy the Eckart conditions since none alters the position of the center-of-mass of the relevant group. In addition these are the familiar normal coordinates of the bent XY_2[4] and the pyramidal XY_3[5] molecular models.

In addition to the internal motions of these groups, infinitesimal oscillatory rotations of these groups about their principal axes will prove to be good coordinates which obviously satisfy the Eckart conditions. An infinitesimal rotation of a group about its x axis will be designated by ϑ, a rotation about a y axis by χ, and a rotation about a z axis by φ. These infinitesimal rotations yield twelve additional vibrational coordinates which means that the framework must furnish us with the remaining twelve required coordinates.

The framework may now be considered as a 6-atomic molecule, and it will certainly provide us the twelve required coordinates. These twelve coordinates are linear combinations of twelve coordinates which we shall obtain by applying the MOM to the 6-atomic framework molecule. Let us again consider Fig. 2. We select the two CH_3 groups and the N atom as one of the groups and the two BH_2 groups and the H atom as the other.[6] This has the advantage over other possible choices of yielding the force constant for the $N-CH_3$ stretching. In addition, this choice may be shown to have certain advantages which will later become apparent when molecular symmetry is considered. We now have two triatomic groups to consider. As in the case of the BH_2 groups we denote the normal vibrations of these groups by q_a, q_b, and q_c and add the subscript 5 to denote the internal vibrations of the

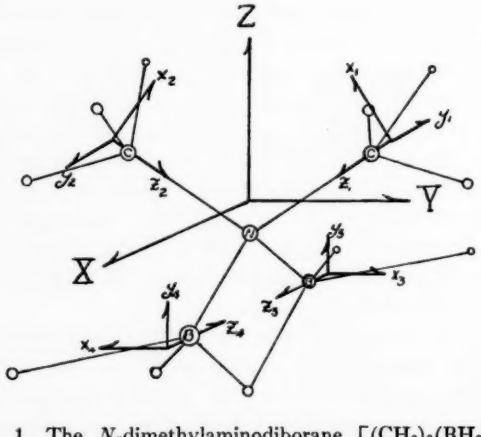

FIG. 1. The N-dimethylaminodiborane $[(CH_3)_2(BH_2)_2NH]$ molecule in which the B, C, and N atoms are labeled. The unlabeled atoms are H atoms. The principal axis system for the entire molecule together with the principal axis systems for the four molecular subgroups are indicated.

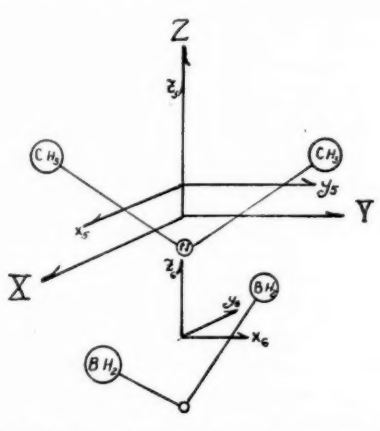

FIG. 2. The N-dimethylaminodiborane framework in which the four molecular subgroups together with the N atom are labeled. The H atom is unlabeled. The principal axis system for the entire molecule together with the principal axis systems for the two molecular sub-subgroups are indicated.

[4] W. H. Shaffer and R. R. Newton, J. Chem. Phys. **10**, 405 (1942).

[5] W. H. Shaffer, J. Chem. Phys. **9**, 607 (1941).

[6] We might instead select the two BH_2 groups as a diatomic molecule and then select the lower H, the BH_2-BH_2 sub-subgroup, and the CH_3-N-CH_3 sub-subgroup as a final framework triatomic molecule, but this would essentially yield the same results. Still other choices are, of course, possible.

upper group and the subscript 6 to denote the lower group. Next we choose certain infinitesimal oscillatory rotations of these groups about their respective x axes as good coordinates and designate them as previously by ϑ_5 and ϑ_6. Infinitesimal rotations about the y axes are next chosen and designated as χ_5 and χ_6. Let us postpone consideration of possible infinitesimal rotations of these groups about their z axes. The framework vibration of these two sub-subgroups is a simple diatomic vibration along the twofold axis of the entire molecule which we designate as q_{42}. Now let us consider the rotations about the z axes of the sub-subgroups.

If we should choose φ_5 and φ_6 as two independent coordinates, it is apparent that we would (1) have one too many vibrational coordinates and (2) allow possible violation of the Eckart conditions in that these two coordinates could combine to yield an overall molecular angular momentum. These considerations indicate that we should choose a linear combination of these two possible coordinates as a good coordinate. The choice is governed by the equation

$$I_{z5}\varphi_5+I_{z6}\varphi_6=0, \tag{1}$$

where I_{z5} is the equilibrium principal moment of the upper group about its z axis and I_{z6} is the moment of the lower groups about its z axis. The coordinate which we choose is, of course, the torsional motion of the upper group against the lower which we shall designate by φ where from (1)

$$\varphi_5=\frac{I_{z5}}{I_{z5}+I_{z6}}\varphi \quad \text{and} \quad \varphi_6=\frac{I_{z6}}{I_{z5}+I_{z6}}\varphi.$$

We have now selected 42 vibrational coordinates all of which satisfy the Eckart conditions.

III. GROUP THEORY PREDICTIONS

As we have mentioned earlier, this molecular configuration belongs to the symmetry point group C_{2v}. The symmetry species associated with the four well-known irreducible representations of this group are given in the first four rows of Table I. The fifth row of this table gives the number of nuclei which are unaffected by the various classes of covering operations, and the sixth row gives the character of the vibrational coordinates under the various covering operation classes.

An application of the familiar formula for the coefficients in the expansion of the reducible representation of the vibrational coordinates in terms of the irreducible representations tells us that we should expect 13 vibrations of species A_1, 8 of species A_2, 10 of species B_1, and 11 of species B_2. Thus, we should expect no degenerate vibrations.

In the C_{2v} group the electric dipole moment possesses the character $A_1+B_1+B_2$ and the polarizability tensor the character $3A_1+A_2+B_1+B_2$. As a result all vibrations will be Raman active, and all vibrations save the eight of species A_2 will be active in the infrared.

TABLE I. Symmetry species and character of the vibrational coordinates of *N*-dimethylaminodiborane. N_R specifies the number of atoms unaffected by the operation R and Ξ_v is the character of the vibrational coordinates.

	E	C_2	σ_x	σ_y
A_1	+1	+1	+1	+1
A_2	+1	+1	−1	−1
B_1	+1	−1	+1	−1
B_2	+1	−1	−1	+1
N_R	16	2	4	6
Ξ_v	42	0	4	6

Now let us choose the proper combinations of our 42 initial vibrational coordinates so that the covering operations merely have the effect of changing the resulting coordinates into either themselves or their negative. One example will show the simple manner in which all such coordinates may be chosen.

Let us take for our example the coordinates s_1 and s_2 which designate the symmetrical stretching vibrations of the two methyl groups, and we first consider the behavior of these two coordinates under the various covering operations. When a proper rotation through an angle of 180° about the twofold axis is carried out s_1 becomes s_2 and *vice versa*. When a reflection through the X–Z plane is accomplished s_1 becomes s_2 and *vice versa*. When a reflection through the Y–Z plane occurs s_1 and s_2 go into themselves. Thus, plus and minus combinations of these two coordinates are immediately suggested as symmetry coordinates and in particular we choose $2^{-\frac{1}{2}}(s_1+s_2)$ and $2^{-\frac{1}{2}}(s_1-s_2)$. The justification for the normalization factor lies in the kinetic energy expression, for from these two coordinates we obtain for our kinetic energy

$$2T=(1/2)(\dot{s}_1+\dot{s}_2)^2+(1/2)(\dot{s}_1-\dot{s}_2)^2=\dot{s}_1^2+\dot{s}_2^2,$$

which is surely the energy due to the internal vibrations of these two groups.

This method of approach, where necessary, yields the desired symmetry coordinates which, although a lengthy list, is best written out for clarity.

The thirteen coordinates of species A_1 are

$$q_1=1/\sqrt{2}(s_1+s_2), \quad q_{15}=1/\sqrt{2}(q_{b3}+q_{b4}), \quad q_{32}=q_{b5},$$
$$q_3=1/\sqrt{2}(u_1+u_2), \quad q_{21}=1/\sqrt{2}(\chi_1+\chi_2), \quad q_{34}=q_{a6},$$
$$q_5=1/\sqrt{2}(v_{a1}+v_{a2}), \quad q_{25}=1/\sqrt{2}(\vartheta_3+\vartheta_4), \quad q_{35}=q_{b6},$$
$$q_9=1/\sqrt{2}(w_{a1}+w_{a2}), \quad q_{31}=q_{a5}, \quad q_{42}=q_{42}.$$
$$q_{13}=1/\sqrt{2}(q_{a3}+q_{a4}),$$

The eight coordinates of species A_2 are

$$q_7=1/\sqrt{2}(v_{b1}+v_{b2}), \quad q_{23}=1/\sqrt{2}(\varphi_1+\varphi_2),$$
$$q_{11}=1/\sqrt{2}(w_{b1}+w_{b2}), \quad q_{27}=1/\sqrt{2}(\chi_3+\chi_4),$$
$$q_{17}=1/\sqrt{2}(q_{c3}+q_{c4}), \quad q_{29}=1/\sqrt{2}(\varphi_3+\varphi_4),$$
$$q_{19}=1/\sqrt{2}(\vartheta_1+\vartheta_2), \quad q_{41}=\varphi.$$

The ten coordinates of species B_1 are

$$q_8=1/\sqrt{2}(v_{b1}-v_{b2}), \quad q_{28}=1/\sqrt{2}(\chi_3-\chi_4),$$
$$q_{12}=1/\sqrt{2}(w_{b1}-w_{b2}), \quad q_{30}=1/\sqrt{2}(\varphi_3-\varphi_4),$$
$$q_{18}=1/\sqrt{2}(q_{c3}-q_{c4}), \quad q_{36}=q_{c6},$$
$$q_{20}=1/\sqrt{2}(\vartheta_1-\vartheta_2), \quad q_{38}=\chi_5,$$
$$q_{24}=1/\sqrt{2}(\varphi_1-\varphi_2), \quad q_{39}=\vartheta_6.$$

The eleven coordinates of species B_2 are

$$q_2=1/\sqrt{2}(s_1-s_2), \quad q_{14}=1/\sqrt{2}(q_{a3}-q_{a4}), \quad q_{33}=q_{c5},$$
$$q_4=1/\sqrt{2}(u_1-u_2), \quad q_{16}=1/\sqrt{2}(q_{b3}-q_{b4}), \quad q_{37}=\vartheta_5,$$
$$q_6=1/\sqrt{2}(v_{a1}-v_{a2}), \quad q_{22}=1/\sqrt{2}(\chi_1-\chi_2), \quad q_{40}=\chi_6.$$
$$q_{10}=1/\sqrt{2}(w_{a1}-w_{a2}), \quad q_{26}=1/\sqrt{2}(\vartheta_3-\vartheta_4),$$

IV. THE VIBRATIONAL SECULAR DETERMINANT

After the adoption of a few simple conventions for the moments of inertia of the various molecular subgroups the vibrational kinetic energy expression and the quadratic potential energy expression may be written down.

We designate the moment of inertia of the ith group about, say, its x axis by I_{xi}. In the case where the moment of inertia of one group is the same as that of another we use the lesser i for both, for instance, we write I_{x1} for the moment of inertia of either methyl group about its x axis. The moments of inertia are given in Table II. They have been calculated using the dimensions given by Hedberg and Stosick.[3] Before writing out the kinetic energy expression an example of the two main types of contribution to it may be in order.

In the case of a normal coordinate for an internal group vibration such as s_1 and s_2, the contribution is

$$2T=\dot{q}_1^2+\dot{q}_2^2=\dot{s}_1^2+\dot{s}_2^2.$$

In the case of an infinitesimal rotation of a group such as ϑ_1, and ϑ_2, the contribution is

$$2T=I_{x1}(\dot{q}_{19}^2+\dot{q}_{20}^2)=I_{x1}(\dot{\vartheta}_1^2+\dot{\vartheta}_2^2).$$

The torsional coordinate q_{41} represents a special case.

We may then write out the vibrational kinetic energy expression T as follows:

$$2T=\sum_{i=1}^{19}\dot{q}_i^2+\sum_{i=31}^{36}\dot{q}_i^2+I_{x1}\sum_{i=19}^{22}\dot{q}_i^2+I_{x1}\sum_{i=23}^{24}\dot{q}_i^2$$
$$+I_{x3}\sum_{i=25}^{26}\dot{q}_i^2+I_{y3}\sum_{i=27}^{28}\dot{q}_i^2+I_{z3}\sum_{i=29}^{30}\dot{q}_i^2$$
$$+I_{x5}\dot{q}_{37}^2+I_{y5}\dot{q}_{38}^2+I_{x6}\dot{q}_{39}^2+I_{y6}\dot{q}_{40}^2$$
$$+\frac{(I_{x5}^3+I_{x6}^3)}{(I_{x5}+I_{x6})^2}\dot{q}_{41}^2+\dot{q}_{42}^2. \quad (2)$$

There would not appear to be any reason for writing out the quadratic potential energy expression explicitly. We might make a few remarks about it, however.

We shall designate the quadratic force constant associated with the term q_iq_j by $k_{i,j}$. No interactions are allowed between coordinates belonging to different symmetry species. With these factors in mind we could simply write down the potential energy expression. The vibrational secular determinant could then be written out.

V. ASSIGNMENT OF THE COORDINATES

Let us now consider Table III. The frequencies are taken from Table VI of Mann's article except as indicated below. The A_2 frequencies—inactive in the infrared—were obtained by Mann from the liquid Raman spectrum of the molecule. Mann believed the asterisked frequencies to be involved in a Fermi resonance. The frequencies given in parentheses are estimated, and we shall assume them to be correct. The author is of the belief that some frequencies assigned by Mann to certain of the symmetry species are probably not correct. These frequencies are enclosed in brackets. In addition, certain frequencies have been added by the author, and these frequencies are indicated by a dagger. The coordinates which we shall associate with the various frequencies are also given in Table III.

The manner of carrying out the zeroth-order assignment for the coordinates is as follows. In associating a coordinate with a frequency (a) the frequencies of the internal vibrations of a methyl group in the methyl halide series, (b) the frequencies of internal vibration of B_2H_6,[7,8] and (c) dimethylamine frequencies assigned earlier by the author[9] will be used. In addition, the fact that a small frequency shift on deuteration would indicate that the vibration is probably primarily associated with atoms in the molecule which are unaffected by deuteration will be used as a guide in the association of these frequencies and coordinates. It should be made clear, however, that all frequencies should be shifted somewhat on isotopic modification of any portion of the molecule, since we may recall that in the A_1 block, for example, the true normal coordinates are linear combinations of all thirteen of our MOM vibrational coordinates. Thus, the substitution of an isotope for

TABLE II. Equilibrium principal moments of inertia of the various subgroups of N-dimethylaminodiborane.

	I_{xi} (g-cm²)	I_{yi} (g-cm²)	I_{zi} (g-cm²)
1	3.18×10^{-40}	3.18×10^{-40}	5.30×10^{-40}
2	3.18×10^{-40}	3.18×10^{-40}	5.30×10^{-40}
3	1.10×10^{-40}	5.07×10^{-40}	3.96×10^{-40}
4	1.10×10^{-40}	5.07×10^{-40}	3.96×10^{-40}
5	94.35×10^{-40}	12.13×10^{-40}	82.22×10^{-40}
6	1.03×10^{-40}	40.90×10^{-40}	39.87×10^{-40}

[7] R. P. Bell and H. C. Longuet-Higgins, Proc. Roy. Soc. (London) A183, 357 (1945).
[8] R. C. Lord and E. Nielsen, J. Chem. Phys. 19, 1 (1951).
[9] R. G. Breene, Jr., Ph.D. dissertation, The Ohio State University, 1953.

any atom in the molecule will have some effect on all vibrational frequencies.

Let us first discuss the zeroth-order assignment for the A_1 block. We shall go into some detail in our considerations of the A_1 block. The succeeding blocks may then be considered on the same basis but with less discussion.

In the methyl halides ν_{ij} occurs at 3050 cm^{-1} and s_i occurs at 2960 cm^{-1} (3012 cm^{-1} and 2852 cm^{-1}, respectively, in dimethylamine). Thus we assign q_5 and q_1 to 2990 and 2817 cm^{-1}, respectively. In the methyl halides u_i occurs at 1252–1475 cm^{-1} and w_{ij} occurs at 1450 cm^{-1} (1476 and 1160 cm^{-1}, respectively, in dimethylamine). On this basis we assign q_9 and q_3 to 1471 and 1393 cm^{-1}, respectively. We eliminate the possibility of assigning q_3 to 1011 cm^{-1} by other considerations which we discuss next. The framework vibrations of dimethylamine which correspond roughly to q_{31} and q_{32} occur at 933 and 390 cm^{-1}, respectively. On this basis we assign q_{31} and q_{32} to 1011 and 399 cm^{-1}, respectively. Next we assign q_{13} to 2476 cm^{-1} since a corresponding B_2H_6 stretching[10] occurs at 2523 cm^{-1}. The remaining BH_2 internal coordinate q_{15} we now assign to 1198 cm^{-1} since an analagous B_2H_6 vibration occurs at 1197 cm^{-1}. We assign q_{35} to 772 cm^{-1} with the same justification. The corresponding B_2H_6 frequency occurs at 793 cm^{-1}. A B_2H_6 vibration which corresponds roughly to the infinitesimal rotation of the BH_2 groups as given by q_{25} occurs at 1008 cm^{-1}. Thus, we assign q_{25} to 945 cm^{-1}. A remark on this appears in order.

The square root of the ratio between the appropriate moments of inertia associated with q_{25} for the normal and deuterated BH_2 group should be roughly the same as the ratio of the frequencies for these two cases. The square root of the moment ratio is 1.358. The ratio of the frequencies is 1.441 which is reasonable agreement. The same moment ratio should hold for q_{26} in the B_2 block. In this latter case the ratio is unity if we choose 950 cm^{-1} for q_{26}, not a very good agreement. Since it would certainly appear that 950 cm^{-1} is a good assignment—the corresponding frequency in B_2H_6 occurs at 981 cm^{-1}—we are forced to ignore the deuterated assignment of Mann at 950 cm^{-1}. Actually we could make other assignments, with some justification, but even more changes in Mann's deuterated assignments would be required.

We next assign q_{21} to 697 cm^{-1} on the basis of this being the single remaining frequency which is only slightly affected by deuteration. q_{34} may now be assigned to 1885 cm^{-1} with complete justification since the analagous vibration occurs at 1863 cm^{-1} in B_2H_6. We have the coordinate q_{42} and the frequency 1069 cm^{-1} remaining in the A_1 block. This coordinate and this frequency are associated.

[10] For graphic illustrations of the normal vibrations of B_2H_6, see reference 7.

TABLE III. Experimental vibrational frequencies from Mann[a] and assigned coordinates. The force constants are given with units as indicated. An asterisk indicates a Fermi resonance according to Mann. Frequencies in parenthesis were estimated by Mann. Frequencies in brackets were assigned as fundamentals by Mann but have been discarded here. Frequencies indicated by a dagger have been added here.

Vibrational coordinate q_i	Vibrational frequency $(CH_3)_2(BH_2)_2NH$	Vibrational frequency $(CH_3)_2(BD_2)_2ND$	Force constant $k_{i,i}$
		A_1 Species	
q_5	2990	2987	31.71×10^{28} sec^{-2}
q_1	2817	2818	28.16×10^{28} sec^{-2}
q_{13}	2476	1825*	21.75×10^{28} sec^{-2}
q_{34}	1885*	1416	12.61×10^{28} sec^{-2}
q_9	1471	1471	7.68×10^{28} sec^{-2}
q_3	1393	1402	6.88×10^{28} sec^{-2}
q_{15}	1198	891	5.09×10^{28} sec^{-2}
q_{42}	1069	1037	4.06×10^{28} sec^{-2}
q_{31}	1011	(1011)	3.63×10^{28} sec^{-2}
q_{25}	945	656	3.44×10^{-12} erg
q_{35}	772	721	2.11×10^{28} sec^{-2}
q_{21}	697	701	5.48×10^{-12} erg
q_{32}	399	396	0.56×10^{28} sec^{-2}
		A_2 Species	
q_7	3017	3017	32.29×10^{28} sec^{-2}
q_{17}	2475	1936	21.74×10^{28} sec^{-2}
q_{11}	1451	(1451)	7.47×10^{28} sec^{-2}
q_{19}	1046	1054	12.35×10^{-12} erg
q_{27}	896	669	14.45×10^{-12} erg
q_{29}	896	669	11.29×10^{-12} erg
...	599	396	...
q_{41}	236	(236)	8.20×10^{-12} erg
q_{23}	...	...	...
		B_1 Species	
q_8	3029	3028	32.55×10^{28} sec^{-2}
q_{18}	2547	1926	23.01×10^{28} sec^{-2}
q_{36}	1635	1244	9.48×10^{28} sec^{-2}
q_{12}	1458	1459	7.54×10^{28} sec^{-2}
q_{28}	1220	827	26.77×10^{-12} erg
q_{39}	1184	1163	5.12×10^{-12} erg
q_{20}	(1084)	1084	13.26×10^{-12} erg
q_{30}	1063	791	15.88×10^{-12} erg
q_{38}	279	(279)	3.35×10^{-12} erg
q_{24}	...	...	
		B_2 Species	
q_6	2964	2961	31.17×10^{28} sec^{-2}
q_2	2876	2876	29.35×10^{28} sec^{-2}
q_{14}	2552	1926	23.10×10^{28} sec^{-2}
q_{10}	1471	1471	7.68×10^{28} sec^{-2}
q_4	1390	1402	6.86×10^{28} sec^{-2}
q_{16}	1075	830	4.10×10^{28} sec^{-2}
q_{33}	1024	(1024)	3.72×10^{28} sec^{-2}
q_{26}	950	950	3.52×10^{-12} erg
	[770]	[566]	
q_{22}	706†	705†	5.63×10^{-12} erg
q_{37}	399	396	53.29×10^{-12} erg
q_{40}	325	214	15.13×10^{-12} erg

[a] See reference 1.

This procedure then would complete the zeroth-order approximation for the A_1 block, and the diagonal force constants are either directly given in terms of the frequencies or in terms of the frequencies and moments of inertia.

Let us consider next the B_2 block in part, since we would expect, for example, q_{21} in A_1 to occur at a frequency near q_{22} in B_2. First it would appear that 399

cm^{-1} should be assigned to q_{37} since the assignment of this coordinate to any higher-frequency results in an inordinately large value for $k_{37,37}$ (see Tables II and III). Next we assign the absorption peak at 706 cm^{-1} to B_2. Mann called this the R-branch of the band of 697 cm^{-1} which it may also be, but, since we may reasonably expect q_{22} to occur in the neighborhood of q_{21} this seems as well justified an assignment as any. Further, a band is reported by Mann in the spectra of the deuterated molecule at 705 cm^{-1} which he assigns to $\nu_{12}+\nu_i-\nu_i$ where ν_{12} is the frequency he has assigned to 697 cm^{-1} in A_1. ν_i is, of course, not given specifically. We have already discussed the proposed discard of the deuterated frequency at 950 cm^{-1}. We are also forced to discard the band at 770 cm^{-1} and the deuterated frequency at 566 cm^{-1}. The band at 770 cm^{-1} as well as the deuterated band at 566 cm^{-1} were given double duty by Mann, and we could perhaps now allow them to arise from one vibration.

Let us briefly consider a question which arises concerning the A_2 and B_1 blocks. A vibration which corresponds to q_{27} occurs at 821 cm^{-1} in B_2H_6 and, on this basis, we assign q_{27} to 896 cm^{-1}. A vibration which corresponds to q_{28} occurs at 1405 cm^{-1} in the spectrum of B_2H_6. Since q_{12} is still a more logical candidate for our frequency at 1458 cm^{-1} than q_{28}, we shall assign q_{28} to 1220 cm^{-1}. In the B_1 block we assign q_{30} to 1063 cm^{-1} on the basis of the occurrence of about the same vibration in the spectrum of B_2H_6 occurring at 1011 cm^{-1}. After the remaining assignments in the A_2 block have been made we are left with a frequency of 599 cm^{-1} and the coordinate q_{29}. The association of this coordinate and this frequency simply does not follow. In the spectrum of B_2H_6 the vibration which corresponds to this coordinate occurs at 829 cm^{-1}. Thus, we are forced to either discard 599 cm^{-1} or assign it to q_{23}. We discard it. We then assign q_{29} as well as q_{27} to 896 cm^{-1}.

This completes our coordinate assignment, and it would appear that the assignments are reasonably well justified. The approximate diagonal constants may now be obtained, and they are listed in Table III.

It would now be possible to utilize the deuterated frequencies to carry through a first-order approximate solution by evaluating some of the off-diagonal constants.

VI. VALENCE FORCE CONSTANTS FOR CH_3-N-CH_3

We may now evaluate the valence force constants for the CH_3–N–CH_3 framework. We first obtain the kinetic energy expression for the framework vibrations in terms of valence coordinates as follows:

$$2T=14.8389\times10^{-24}(r_1'^2+r_2'^2)+16.0687\times10^{-40}\beta'^2 +9.4453\times10^{-24}r_1'r_2' +12.3061\times10^{-32}(r_1'\beta'+r_2'\beta')\cdots. \quad (3)$$

In Eq. (3) r_1' and r_2' are the changes in the bond lengths, and β' is the change in the apex bond angle. Our quadratic potential energy expression may be written out as

$$2V=k_1(r_1'^2+r_2'^2)+k_2\beta'^2+2k_3r_1'r_2'. \quad (4)$$

We have here included the bond-bond interaction and neglected the bond-angle interaction, since the latter is usually the smaller of the two. Lagrange's secular determinant for the vibrational problem may now be written down in valence coordinates and when the frequencies assigned to the coordinates q_{31}, q_{32}, and q_{33} are substituted into the equations resulting from this determinant we obtain the following:

$$13.47\times10^{22}k_4+8.20\times10^{38}k_2=4.1915\times10^{28}, \quad (5)$$

$$8.38\times10^{61}k_2k_4=2.0484\times10^{56}, \quad (6)$$

$$k_5=75.2787\times10^4, \quad (7)$$

where

$$k_4=\tfrac{1}{2}(k_1+k_3), \quad k_5=2(k_1-k_3).$$

Solution of Eqs. (5), (6), and (7) yields the following values for the three force constants:

$$k_1=4.41\times10^5 \text{ dynes/cm},$$
$$k_2=0.97\times10^{-11} \text{ dyne-cm/radian},$$
$$k_3=0.64\times10^5 \text{ dynes/cm}.$$

The author[9] has previously obtained the following values for quite similar constants in the case of dimethylamine:

$$k_1=4.92\times10^5 \text{ dynes/cm},$$
$$k_2=1.09\times10^{-11} \text{ dyne-cm/radian},$$
$$k_3=0.67\times10^5 \text{ dyne/cm}.$$

Magnetic Susceptibility of Liquid Ozone-Oxygen Mixtures

CALLAWAY BROWN, CHARLES K. HERSH, AND ABRAHAM W. BERGER
Department of Chemistry and Chemical Engineering, Armour Research Foundation of Illinois Institute of Technology, Chicago, Illinois

(Received May 28, 1954)

The data needed for analysis of liquid ozone-oxygen mixtures by measurement of magnetic susceptibility are presented. Volumetric preparation of liquid ozone-oxygen mixtures in equilibrium with the vapor phase is described. A permanent magnet at the temperature of the solutions provided the key for use of the Quincke (U-tube) method for magnetic susceptibility.

Results at −195° and −183°C show a linear relation between the magnetic susceptibility of the solutions and weight percent oxygen at low oxygen content. Above about 10 percent oxygen the specific susceptibility of oxygen in solution decreases significantly. At −183°C, the ratio X_s/X_0 of specific susceptibility of oxygen in solution to that of pure liquid oxygen decreased from 1.30 at low concentrations to 1.13 at 27.6 percent oxygen, the two-liquid phase boundary. The limiting ratio at −195°C was 1.42. The discontinuity in magnetic susceptibility was used to establish the compositions at the phase boundaries; 9.2 and 91 percent by weight oxygen at −195°C, 27.6 and 70.2 percent at −183°C.

INTRODUCTION

THE initial objective of the present studies was the development of a physical method for the analysis of liquid ozone-oxygen mixtures. Since the paramagnetism of oxygen is perhaps its most distinguishing physical property and any paramagnetism of liquid ozone is less than 0.1 percent that of oxygen,[1] the magnetic susceptibility of the liquid mixtures as a function of composition is of obvious interest.

The key experimental problem was the preparation of equilibrium mixtures of liquid ozone and oxygen of known composition. The solution of this problem permitted determination of a number of other properties of the solutions. The discontinuities in the magnetic susceptibility as a function of composition provided an accurate method for establishment of the composition at the phase boundaries. The purpose of the present paper is to describe the method of preparation of the solutions and the magnetic susceptibility results. Two succeeding papers report the phase diagram of the system and density, viscosity, and surface tension results. The present work is confined to the temperature range of boiling liquid nitrogen and oxygen and the principal emphasis is on the properties at the liquid phase boundaries.

EXPERIMENTAL APPROACH

Exploratory experiments showed that an Alnico V permanent magnet could be cooled repeatedly to liquid air temperatures without serious damage. In fact a search coil revealed a slight enhancement in magnetic flux density on immersion of a magnet in liquid nitrogen. This simplified measurement of magnetic susceptibility since the simple Quincke method[2] for liquids could be used. The height of the column of liquid supported by the field is proportional to the specific susceptibility of the liquid. A very narrow pole gap ($\frac{1}{8}$ in.) is sufficient if the magnet is at the temperature of the liquid so that a magnetic flux density of around 8000 gauss may be obtained with a magnet of moderate size. This field is sufficient to support a column of liquid oxygen nearly 100 mm in height.

The basic plan for the preparation of equilibrium mixtures of liquid ozone and oxygen of known composition was to prepare the mixtures volumetrically. Recent determination of the density of liquid ozone[3] permitted accurate metering of ozone by measurement of the volume of liquid. Mixtures with oxygen of any composition could therefore be made by condensation of a measured quantity of oxygen in the ozone.

Mixing of the two liquids to insure uniform composition presented a problem. The first approach was to use a glass-enclosed iron pellet in the liquid and stir the mixture magnetically. This was awkward and occasionally terminated disastrously with a violent detonation, probably due to friction of the pellet against the walls of the container.

The successful approach evolved was to collect the liquid ozone in a U-tube of calibrated volume. Measured quantities of oxygen were then introduced from a gas burette and allowed to bubble through the liquid ozone. Arrangement was made to circulate gaseous oxygen through the liquid as long as necessary, but it was found that equilibrium was reached rapidly under these conditions. Determination of the magnetic susceptibility and other physical properties was then made in the U-tube container.

APPARATUS AND PROCEDURE

Preparation of Solutions

Concentrated liquid ozone was obtained by passage of oxygen through a laboratory ozonizer of the corona discharge type, thence through a receiver tube cooled in liquid oxygen. The receiver tube was then attached through a ground glass joint to an apparatus for puri-

[1] P. Lainé, Ann. phys. 3, 461 (1935).
[2] P. W. Selwood, *Magnetochemistry* (Interscience Publishers, Inc., New York, 1943).
[3] C. Brown and K. D. Franson, J. Chem. Phys. 21, 917 (1953).

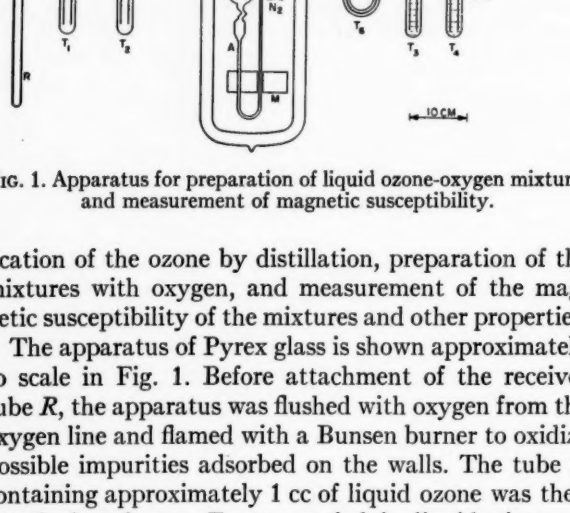

FIG. 1. Apparatus for preparation of liquid ozone-oxygen mixtures and measurement of magnetic susceptibility.

fication of the ozone by distillation, preparation of the mixtures with oxygen, and measurement of the magnetic susceptibility of the mixtures and other properties.

The apparatus of Pyrex glass is shown approximately to scale in Fig. 1. Before attachment of the receiver tube R, the apparatus was flushed with oxygen from the oxygen line and flamed with a Bunsen burner to oxidize possible impurities adsorbed on the walls. The tube R containing approximately 1 cc of liquid ozone was then attached and trap T_1 was cooled in liquid nitrogen. Traps T_3, T_5, and T_6 were cooled in liquid oxygen and trap T_4 was heated to 450°C with a tubular electric furnace. In this way vapors from the pump were trapped from the section of the apparatus receiving liquid ozone, and ozone vapor passing the cold traps was decomposed before reaching the pump. Cold trap T_3 and hot trap T_4 were packed with small sections of glass tubing to increase the area of contact with vapor without an excessive increase in the impedance to pumping to the vacuum line.

The apparatus was evacuated (rotary oil pump) with the ozone in tube R cooled in liquid oxygen. Slow distillation into T_1 began as soon as a good vacuum was attained and was accelerated by dropping the liquid oxygen level below R so that the temperature rose slowly. The ozone was distilled similarly into T_2 and finally into the analytical section of the apparatus A. When runs at −183°C were planned, liquid oxygen was used in the Dewar surrounding the analytical section. In the final distillation into A, in order to avoid excessive loss of ozone, bath temperature was lowered several degrees by bubbling a stream of helium through the bath, a useful technique for lowering the partial pressure of oxygen in equilibrium with the bath. After collection of the desired charge of ozone, bath temperature was returned to normal by substitution of oxygen for helium.

The volume of liquid ozone in the U-tube analytical section was determined by measurement with a cathetometer of the height of the liquid level above a reference mark at the bottom of the tube. This volume was obtained from a calibration curve, prepared before assembly of the apparatus by filling the tube with weighed quantities of toluene, and checked after assembly by condensation of liquid oxygen, metered from the gas burette. After collection of the ozone sample, stopcocks S_1 and S_2 were closed to minimize the volume of the vapor phase. All stopcocks in the system were lubricated with a low vapor pressure halocarbon grease chemically inert to ozone.

Oxygen was introduced from the gas burette in the oxygen line. Commercial electrolytic oxygen was liquified in a trap cooled in liquid oxygen and a substantial fraction of the liquid was pumped off to remove traces of hydrogen and nitrogen. The liquid remaining served as a reservoir of oxygen from which the gas burette was filled. The gas burette, shown in Fig. 2, was operated with concentrated sulfuric acid as the confining liquid. Initial experiments with mercury in the gas burette resulted in several explosions which may have been due to mercury sensitized detonation of liquid ozone. It is not certain that this precaution was necessary but the difficulty in adequately trapping mercury vapor in a cold trap is well-known, and after substitution of sulfuric acid in the gas burette no further unexplained explosions occurred. The volume of the gas burette at the several reference marks was determined before assembly from the weight of contained mercury. Pressure was read on the mercury manometer after equalization of the sulfuric acid levels in the two arms and adjustment of the level at one of the reference marks of the volume calibration.

After introduction of the measured volume of oxygen, an ozone-oxygen solution in equilibrium with the vapor phase was prepared in the following manner. Stopcock S_4 was closed to isolate the two arms of the U-tube

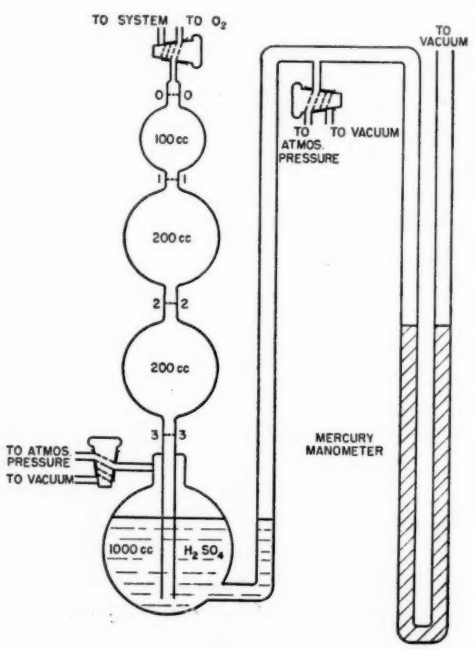

FIG. 2. Gas burette for measuring vapor pressure and volume of oxygen admitted to system.

containing liquid ozone and the level of the sulfuric acid in the gas burette was raised slowly, forcing oxygen to bubble through the liquid ozone in the U-tube. When the sulfuric acid level reached the top of the gas burette, stopcock S_4 was opened, S_7 was closed, and the sulfuric acid level in the burette was lowered. The gas burette was thereby used as a liquid piston to circulate the vapor phase through the liquid ozone in the U-tube. In practice it was found that two or three cycles was sufficient to produce an equilibrium mixture as indicated by a constant vapor pressure.

The composition of the solution was calculated from the quantity of oxygen condensed in the measured charge of ozone. This was given by the difference between the total oxygen metered in the burette and that remaining in the vapor phase at equilibrium. Since the temperature of the vapor phase was nonuniform, calibration curves giving moles of oxygen in the system *versus* pressure were determined without ozone in the system. The apparent volume of the system at room temperature as calculated from the ideal gas law (*circa* 200 cc) was independent of pressure within experimental error but was sensitive to the level of refrigerant surrounding the analytical section and the rate of evaporation of cold gas from the bath. The refrigerant liquid, nitrogen or oxygen, was stirred with a stream of nitrogen or oxygen gas, respectively, to insure uniform equilibrium temperature. It was necessary to control both the refrigerant level and the rate of bubbling of gas through the bath in order to minimize uncertainty in the quantity of gas in the vapor phase and the corollary oxygen content of the solution. The ozone content of the vapor phase was negligible at the temperatures studied since the vapor pressure of liquid ozone[4] is only 0.1 mm at −183°C.

The apparatus of Fig. 1 was enclosed in a ventilated hood with safety glass windows. The pump, the oxygen line, and stopcocks in the 2-mm capillary lines were arranged outside the hood for convenient access. The Dewar flash surrounding the analytical section (7-liter capacity) was supported on a platform attached to the shaft of a hydraulic jack. It was raised and lowered through a hole in the bottom of the hood. Strip silvering of the Dewar permitted illumination from the back and observation from the front of the position of the liquid levels inside and outside the magnet gap. At the end of a run, the flask was lowered until the bath level was just below the U-tube. Oxygen was admitted to bring the pressure in the system to one atmosphere and the tube R was removed. Oxygen was bubbled through the liquefied sample while the Dewar flask was slowly lowered until the sample evaporated. Explosions during disposal of the ozone were entirely avoided by this technique. However, liquid ozone was always treated with respect, as occasional detonations occurred during its handling. Safety glasses were worn by the experimenters at all times, supplemented by heavy face masks and gloves whenever there was direct exposure to the liquid ozone container.

[4] A. C. Jenkins and C. M. Birdsall, J. Chem. Phys. **20**, 1158 (1952).

Magnetic Measurements

The magnet used was a U-shaped Alnico V permanent magnet with soft iron pole pieces[5] adjusted to $\frac{1}{8}$ in. pole gap. The dimensions of the pole pieces were $2\times1\frac{1}{2}\times\frac{3}{4}$ in., tapered to $\frac{3}{8}$ in. depth at the pole gap. The magnet was attached to a steel rod mounted vertically and threaded at the end to fit into a gear assembly which permitted adjustment of the vertical position of the magnet from outside the hood. The solutions were prepared with the magnet moved out of influence; the magnet was lowered until liquid in the right arm of the U-tube was drawn into the field and adjusted so that the liquid-vapor boundary was centered in the field. Tests with liquid oxygen showed that the field was uniform over several mm so that centering was not critical.

The field strength (*circa* 8000 gauss) was determined roughly with a search coil flux meter but the height of the column of liquid oxygen supported by the field was used as a reference standard. Readings of the liquid levels with the magnet in and out of influence, made with a cathetometer, permitted correction for the capillary rise due to the difference in diameter in the two arms of the U-tube. Since the liquid levels were viewed through the Dewar flask and a layer of the boiling liquid bath, the usual accuracy attainable with a cathetometer was not realized but readings were reproducible to 0.1 mm.

Temperature Measurement

Temperatures were measured with a glass oxygen vapor pressure thermometer in conjunction with the oxygen vapor pressure equation of Henning and Otto.[6]

It was observed that the average temperature of the liquid nitrogen bath was −195±0.5°C (the ice point being taken as 273.2°K). This somewhat high value is attributed to oxygen contamination and hydrostatic head effects. The large average deviation is due both to barometric pressure fluctuations and varying oxygen content.

Treatment of Results

In the Quincke method for magnetic susceptibility of liquids, the height h of the column of liquid supported against gravity by a magnetic field H is given by[2]

$$h=H^2X/2g, \qquad (1)$$

where X is the specific susceptibility of the liquid and both the susceptibility of the vapor and the field strength at the external liquid-vapor boundary are

[5] The A1007 magnetizer magnet of the Indiana Steel Products Company, Valparaiso, Indiana.

[6] F. Henning and J. Otto, Z. Physik **37**, 633 (1936).

TABLE I. Magnetic susceptibility and vapor pressure of liquid ozone-oxygen solutions at −195°C.

Run No.	Composition wt % O_2	Mag. susc. ratio—h/h_0[a]	Vapor pressure ratio—p/p_0[a]
	Ozone-rich phase		
31	3.19	0.0469	0.497
	6.11	0.0861	0.765
	8.14	0.1158	0.856
32	3.47	0.0491	0.536
	5.26	0.0718	0.729
	7.61	0.1074	0.889
	8.43	0.1130	0.954
	Two-phase region		
32	9.68	0.1285[b]	0.957
1–16	9.9	0.117[b]	0.88
	12.2	0.125[b]	0.95
	14.5	0.133[b]	...
	14.9	0.140[b]	0.92
	19.2	0.131[b]	0.97
	87.9	0.925[c]	0.97
	90.0	0.935[c]	0.97
	90.1	0.930[c]	0.96
	Oxygen-rich phase		
1–16	91.3	0.935	0.95
	91.9	0.915	0.99
	92.0	0.949	0.99
	92.4	0.941	0.99
	93.6	0.946	0.99
	100	1.00	1.00

[a] h_0 (run 31–32) =9.44 cm; h_0 (run 1–16) =8.49 cm; p_0 =16 cm Hg.
[b] Ozone-rich phase in field.
[c] Oxygen-rich phase in field.

negligible. Minor correction for the susceptibility of the vapor was necessary at the higher oxygen pressures at −183°, but the simple equation suffices to illustrate the treatment of results. The field strength was determined by measurement of the height of the column of liquid oxygen, h_0, supported, so that

$$h/h_0 = X/X_0, \tag{2}$$

where X_0 is the specific susceptibility of pure liquid oxygen. Since the magnetic susceptibility of ozone is negligible, the specific susceptibility of oxygen dissolved in liquid ozone, X_s, may be defined by

$$X = X_s w, \tag{3}$$

where w is the weight fraction of oxygen in solution. Hence

$$h/h_0 = (X_s/X_0)w. \tag{4}$$

The magnet lift ratio h/h_0 is thus simply related to the weight fraction of oxygen in the solution.

RESULTS

Results at −195° and −183° are summarized in Tables I and II and are plotted in terms of the magnet lift ratio h/h_0 *versus* weight percent oxygen in Figs. 3–5. Vapor pressure data are included for reference. The vapor pressure ratio p/p_0 represents the ratio of the vapor pressure of the solution to that of pure oxygen, read on the vapor pressure thermometer, and rationalizes small variations in the temperature of the bath.

The data obtained in runs 25–32 are considered to be more accurate than those of runs 1–24, since the volume of the "dead space" was reduced from about 1200 cc (runs 1–24) to about 200 cc (runs 25–32). Since in the two-phase region the value of h/h_0 is constant, the results of the earlier work are included.

At −195°, a light blue oxygen-rich liquid phase separated in the neighborhood of 9 percent oxygen. The magnetic susceptibility of the solutions below the phase boundary (Fig. 3) is adequately represented by a

TABLE II. Magnetic susceptibility and vapor pressure of liquid ozone-oxygen solutions at −183°C.

Run No.	Composition wt % O_2	Mag. susc. ratio—h/h_0[a]	Vapor pressure ratio—p/p_0[a]	Specific susc. ratio—X_s/X_0
	Ozone-rich phase			
22	1.43	0.0170	0.331	1.19
	6.63	0.0814	0.592	1.23
23	4.15	0.0524	0.401	1.26
	15.5	0.181	0.867	1.17
24	10.54	0.125	0.741	1.19
	22.4	0.272	0.926	1.21
25	6.05	0.081	0.579	1.34
	10.7	0.140	0.792	1.31
26	5.0	0.066	0.486	1.32
	9.7	0.126	0.734	1.30
	15.3	0.190	0.858	1.24
	22.3	0.261	0.918	1.17
27	6.6	0.089	0.602	1.35
	22.2	0.256	0.919	1.15
	Two-phase region			
17	27.6	0.315[b]	0.92	
21	39.6	0.312[b]	0.92	
24	30.2[d]	0.316[b]	0.921	
26	28.0	0.310[b]	0.943	
27	26.9	0.308[b]	0.926	
	68.3	0.724[c]	0.919	
28	69.5	0.699[c]	0.929	
	71.2	0.742[c]	0.937	
29	64.0	0.715[c]	0.947	
	70.2[d]	0.746	0.954	
30	63.7	0.729[c]	0.944	
	Oxygen-rich phase			
28	77.5	0.793	0.928	1.02
29	74.2	0.765	0.943	1.03
	84.8	0.858	0.978	1.01
30	81.8	0.834	0.964	1.02
	87.6	0.891	0.975	1.02
	90.9	0.913	0.974	1.01

[a] h_0 (run 17–23) =7.95 cm; h_0 (run 24–30) =8.91 cm; p_0 =76 cm Hg.
[b] Ozone-rich phase in field.
[c] Oxygen-rich phase in field.
[d] Phase boundary not observed visually. Susceptibility ratio included in saturated phase average.

straight line of slope 1.42. The slope of the line gives the ratio X/X_0 of the specific susceptibility of oxygen in solution to that of pure liquid oxygen (Eq. (4)).

At −183° the single-phase liquid region extended to 27.6 percent oxygen. The magnetic susceptibility of the solutions, X, was still approximately proportional to the oxygen content, but above 10 percent oxygen the susceptibility of the mixtures fell significantly below the linear increase represented by the dotted line.

When two liquid phases formed, a significant result could be obtained only when homogeneous liquid was held in the magnetic field. The mixing technique described permitted the withdrawal of small amounts of the light phase liquid from the arm of the U-tube in the poles of the magnet. The constant magnetic lift of the remaining saturated heavy-phase liquid provided an excellent method for determination of the composition of the heavy phase.

The oxygen side of the phase boundary was less suitable for study by magnetic susceptibility than the ozone side since the magnetic lift ratio approaches unity. Thus, at −195° a few points in the single-phase region above the phase boundary (Table I) showed a continued increase of magnetic susceptibility with oxygen content, but the experimental scatter above 90 percent oxygen was considerable. At −183° the single-phase region was wider and the data fell closely on a straight line.

DISCUSSION OF RESULTS

Specific Susceptibility of Dissolved Oxygen

The limiting slope of the h/h_0 *versus* w curves at low oxygen concentrations gives the limiting values of X_s/X_0, the specific susceptibility of dissolved oxygen relative to pure liquid oxygen. These ratios are 1.42 and 1.30 at −195° and −183°, respectively. The specific susceptibility of oxygen in solution in ozone is significantly higher than that of pure liquid oxygen and changes more rapidly with temperature.

The slope of the curve is an accurate measure of X_s/X_0 only in the limit as w approaches zero if X_s changes significantly with oxygen concentration. However, the ratio X_s/X_0 may be calculated from Eq. (4) directly. Correction of the magnetic lift ratio for the susceptibility of the vapor phase should be made but experimental uncertainties exceed this correction so it has been omitted in order to simplify the discussion. At −195° the specific susceptibility of dissolved oxygen appears to be constant in the high ozone single-phase region within the experimental accuracy of the present work. In the high-oxygen, single-phase region, the ratio X_s/X_0 is 1.02 at the phase boundary at −195° and 1.03 at the phase boundary at −183°, so that the specific susceptibility of oxygen is changed very little by moderate additions of ozone. In the high-ozone, single-phase region, a significant variation in X_s/X_0 was detected only above about 10 percent oxygen. The limiting value of 1.30 at −183° decreased to 1.13 at the phase boundary at 27.6 percent oxygen.

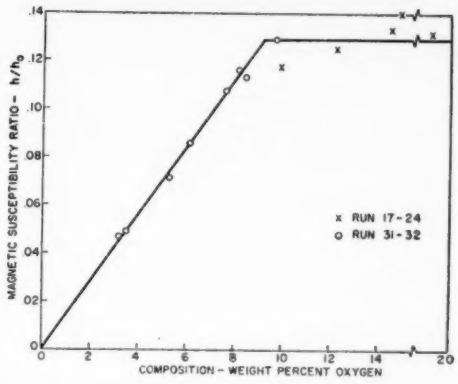

FIG. 3. Magnetic susceptibility of liquid ozone-oxygen solutions at −195°C—ozone-rich phase.

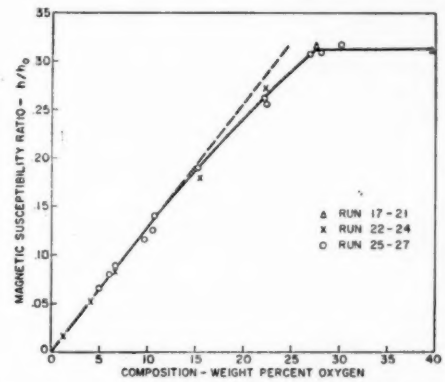

FIG. 4. Magnetic susceptibility of liquid ozone-oxygen solutions at −183°C—ozone-rich phase.

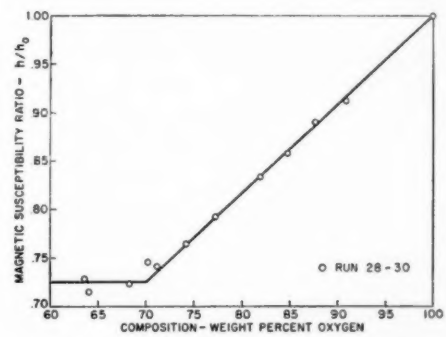

FIG. 5. Magnetic susceptibility of liquid ozone-oxygen solutions at −183°C—oxygen-rich phase.

The figures obtained in the foregoing have been procured from the smoothed curves of Figs. 3–5. The point-by-point values of the susceptibility ratio X_s/X_0, given for −183°C as an example in Table II, reflect experimental errors.

Perrier and Onnes[7] observations of the magnetic susceptibility of liquid oxygen-nitrogen solutions revealed an increase with dilution of the specific sus-

[7] A. Perrier and H. K. Onnes, Compt. rend. **158**, 941, 1074 (1914) Commun. Kamerlingh Onnes Lab. Univ. Leiden, No. 139d.

TABLE III. Magnetic susceptibility and composition at phase boundaries of liquid ozone-oxygen solutions.

	Ozone-rich phase			Oxygen-rich phase		
Temp. °C	Wt % O_2	Magnet lift ratio—h/h_0	Specific susc. ratio—X_s/X_0	Wt % O_2	Magnet lift ratio—h/h_0	Specific susc. ratio—X_s/X_0
−195°	9.2	0.129±0.006	1.42	91	0.930±0.003	1.02
−183°	27.6	0.312±0.003	1.13	70.2	0.726±0.013	1.03

ceptibility of oxygen. Lewis[8] analyzed the phenomenon in terms of a $2O_2=O_4$ equilibrium.

The specific susceptibility ratio obtained from the curves of Figs. 4 and 5 is an increasing function of ozone weight fraction up to about 90 percent ozone. At greater concentrations of ozone experimental accuracy was insufficient to distinguish between a continuing increase of the susceptibility ratio and a constant value. Within these limitations, this work confirms the reported dependence of the specific susceptibility of oxygen upon concentration.

Phase Boundaries

The discontinuity in magnetic susceptibility of the solutions at the phase boundaries provides a highly satisfactory method for establishment of the phase boundary compositions at the temperatures studied. In view of the method of preparation of the solutions, the insurance of liquid-vapor equilibrium by circulation of vapor through the liquid, and establishment of the boundaries from the discontinuity in magnetic susceptibility, it is difficult to see how the boundary composition can be in error by more than one percentage unit. The two-liquid phase region at −183° has been known for some years to lie in the region of 30–70 percent ozone,[9] which the present results confirm. The much lower mutual solubility at −195° is somewhat surprising. The only previous results at this temperature which appear in the literature are those reported by Schumacher[10] in a recent letter to the editor. The present results differ markedly but discussion of these differences will be deferred for the next paper on the phase diagram of the liquid ozone-oxygen system.

Results at the phase boundaries are summarized in Table III. It will be noted that the compositions at the phase boundaries are almost symmetrical on a weight percent basis both at −195° and at −183°. On a mole percent basis the compositions are, of course, skewed toward a lower mole percentage of ozone. In the next paper these results will be considered along with the isothermal vapor pressure data to interpret the system more completely.

Analysis of Liquid Ozone-Oxygen Mixtures

The present results clarify the problem of analysis of liquid ozone-oxygen mixtures. Since the two-phase region extends from 9 to 91 percent ozone at −195°, an equilibrium mixture at this temperature requires no analysis if the composition falls in the two-phase region; only the relative quantities of the two liquid phases is needed to establish the gross composition of the mixture. In the single-phase regions either at −183° or −195°, the simple relation between magnetic susceptibility and oxygen content shown in Figs. 3, 4, and 5 provides an excellent physical basis for analysis, especially in the ozone-rich liquid phase. These results provide the data needed for an analytical method by magnetic susceptibility.

ACKNOWLEDGMENTS

The writers are grateful to fellow workers for many helpful suggestions on the handling of concentrated liquid ozone, especially C. E. Thorp, L. C. Kinney, and R. F. Remaly. Thanks are also due G. M. Platz and K. O. Osborn for assistance on some of the experimental problems.

This work is part of a research program carried out under contract with the Air Reduction Company, New York, New York.

[8] G. N. Lewis, J. Am. Chem. Soc. **46**, 2027 (1924).
[9] F. H. Riesenfeld and G. M. Schwab, Ber. deut. chem. Ges. **55**, 2088 (1922).
[10] H. J. Schumacher, J. Chem. Phys. **21**, 1610 (1953).

C^{13} Isotope Effect in the Thermodecomposition of Ethyl Bromide

HENRY L. FRIEDMAN, RICHARD B. BERNSTEIN,* AND HARRY E. GUNNING
Department of Chemistry, Illinois Institute of Technology, Chicago, Illinois

(Received June 11, 1954)

The $C^{12}-C^{13}$ fractionation factor in the decomposition of gaseous ethyl bromide has been measured from 350–450°C, using samples of natural isotope abundance. The rate constants are defined as follows:

$$CH_3CH_2Br \rightarrow CH_2=CH_2+HBr \quad k_1,$$
$$CH_3C^*H_2Br \rightarrow CH_2=C^*H_2+HBr \quad k_2,$$
$$C^*H_3CH_2Br \rightarrow C^*H_2=CH_2+HBr \quad k_3.$$

At 400°C, the C^{12} enrichment of the first fraction of ethylene from decomposition of the ethyl bromide is

$$S_0 \equiv 1+\epsilon_0 = \frac{2k_1}{k_2+k_3} = 1.0079 \pm 0.0006,$$

with a temperature coefficient of -2.8×10^{-5}/°C.

The primary and secondary isotope effects are defined, respectively, as $\beta=k_1/k_2-1$ and $\gamma=k_1/k_3-1$; thus, to a good approximation, $\beta+\gamma=2\epsilon_0$. According to theory, $\beta>\gamma\geq0$, so that $\epsilon_0<\beta\leq2\epsilon_0$ and $\epsilon_0>\gamma\geq0$. From the data of 400°C one then obtains as an upper limit $(k_1/k_2)_{max}\leq1.0159\pm0.0012$. This is significantly lower than the value $k_1/k_2\geq1.036$ calculated for the rupture of an isolated C–Br bond. The present results, therefore, favor a mechanism involving the direct intramolecular elimination of HBr.

INTRODUCTION

THE decomposition of ethyl bromide has been the subject of a number of investigations.[1–6] The free radical mechanism proposed by Daniels and Veltman[4] involved the primary rupture of the C–Br bond, followed by H atom abstraction from the substrate by Br atoms producing $C_2H_4Br\cdot$ and HBr. The $C_2H_4Br\cdot$ was assumed to yield C_2H_4 by dissociation or reaction with $C_2H_5\cdot$ radicals. Later, Peri and Daniels[5] revised this mechanism slightly, on the basis of the results of a series of isotope exchange experiments. They stated that the primary step was wall-catalyzed, i.e., $C_2H_5Br+wall \rightleftharpoons C_2H_5\cdot\ wall+Br\cdot$, with essentially the same subsequent steps.

Blades and Murphy,[6] using the toluene carrier technique, found no evidence for dibenzyl, hydrogen, or ethane, from which they decided that the reaction was not of the free radical but rather of the intramolecular elimination type. They represented the transition state as a four-membered ring,

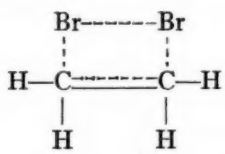

Similar results were obtained by Leigh and Szwarc.[7]

In view of the above it was thought worthwhile to make a study of the C^{13} isotope effect on the rate of decomposition of ethyl bromide, in order to obtain independent mechanistic evidence. Considering first the free radical mechanism, one would expect an appreciable difference in the rate of rupture of the $C^{12}-Br$ and $C^{13}-Br$ bonds. On the basis of current theoretical considerations[8,9] the ratio of the rate of rupture of these bonds should be at least as great as the square root of the appropriate reduced mass ratio, 1.036. This lower limit is based on Slater's[10] treatment for the rupture of an "isolated" bond. In the case of the intramolecular elimination mechanism one would expect the ratio of the rates to be much closer to unity. The lower limit in this case might be estimated to be 1.003, the Slater ratio for the $C^{12}-H$ and $C^{13}-H$ bonds.

The present study was carried out using ethyl bromide of natural isotopic composition, with the three principal isotopic (carbon) modifications: (1) $C^{12}H_3C^{12}H_2Br$, (2) $C^{12}H_3C^{13}H_2Br$, and (3) $C^{13}H_3C^{12}H_2Br$. The primary isotope effect is concerned with the relative rate of decomposition of species (1) *versus* (2). The secondary isotope effect is associated with the relative rate for (1) *versus* (3). Because the ethylene-C^{13} produced by the decomposition of (2) is indistinguishable from that of (3) it is not possible to measure separately the primary and secondary isotope effects. However, the observed $C^{12}-C^{13}$ fractionation factor (the quotient of the C^{12}/C^{13} abundance ratio for the first fraction of ethylene, divided by that of the ethylene from total decomposition) is related directly to the sum of these isotope effects. Thus it has been possible to set upper and lower limits for the individual values of the primary and secondary isotope effects. From these

* Present address: Department of Chemistry, University of Michigan, Ann Arbor, Michigan.

[1] E. T. Lessig, J. Phys. Chem. **36**, 2325 (1932).
[2] E. L. Vernon and F. Daniels, J. Am. Chem. Soc. **55**, 922 (1933).
[3] P. Fugassi and F. Daniels, J. Am. Chem. Soc. **60**, 771 (1938).
[4] F. Daniels and P. L. Veltman, J. Chem. Phys. **7**, 756 (1939).
[5] J. B. Peri and F. Daniels, J. Am. Chem. Soc. **72**, 424 (1950).
[6] A. T. Blades and G. W. Murphy, J. Am. Chem. Soc. **74**, 6219 (1952).
[7] C. H. Leigh and M. Szwarc, J. Chem. Phys. **20**, 403 (1952).
[8] J. Bigeleisen, J. Chem. Phys. **17**, 675 (1949).
[9] J. Bigeleisen, J. Phys. Chem. **56**, 823 (1952).
[10] N. B. Slater, Proc. Roy. Soc. (London) **A194**, 112 (1948).

results, it appears that the mechanism is primarily of the intramolecular elimination type.

EXPERIMENTAL

Ethyl bromide (Matheson, Practical) was purified by shaking with concentrated sulfuric acid until all color was removed. After neutralization with 10 percent sodium carbonate solution the resulting ethyl bromide was washed with water, dried over anhydrous calcium chloride, and distilled from phosphorus pentoxide in a one-meter column packed with glass helices. The purified sample boiled at 38.37°C at a pressure of 760 mm Hg, in agreement with reported values[11–15] which range from 38.34°C at 760 mm Hg to 38.5°C at 765 mm Hg. The refractive index, n_D^{25} was 1.4212. Literature values of the refractive index, [11,14,16] interpolated to 25°C gave 1.4208±0.0005. The vapor pressure at 0°C, determined with a Bodenstein quartz spiral gauge, was 163.5 mm Hg, in agreement with the literature values[17,18] which ranged between 162.5 and 165.5 mm Hg. The infrared absorption spectrum was determined on a Perkin-Elmer Model 21 double-beam recording infrared spectrophotometer (NaCl optics). The bands corresponded within experimental error to those observed by Cross and Daniels.[19]

The experiments were carried out in a high-vacuum system provided with a 254-ml fused quartz reaction chamber in an electric furnace whose temperature was controlled to ±1°C with a Taco-West Model J Thermoregulator. Measurements of the temperature profile of the reaction zone showed a maximum deviation of ±4°C from the kinetic temperature. The reaction zone was conditioned by prolonged carbonization of ethylene at 400°C.[4] Mercury vapor was excluded from the apparatus.

The degassed ethyl bromide was decomposed at initial pressures in the range 90–150 mm Hg, the decomposition being monitored with a Bodenstein gauge. When the desired extent of reaction was attained, the mixture was removed from the reaction zone by freezing with liquid nitrogen. There appeared to be no trend of isotope enrichment with the initial pressure of ethyl bromide.

Ethylene was distilled from the mixture using isopentane slush (−160°C), and oxidized by Toepler-pumping through a copper oxide converter at 720°C. Mass spectrometric analysis of products formed showed 98.7 percent conversion to CO_2 at 600°C and 100 percent conversion at 720°C. Water was removed from the oxidation products by freezing out at −78°C.

Specific reaction-rate constants based on the first-order portion of the decomposition were determined from partial decompositions whose initial pressures were greater than 130 mm Hg. The k's were considerably higher than those found by Daniels and Veltman,[4] but this is probably due to the fact that greater pains were taken to remove O_2 in the latter than in the present work. The increase in k with increase in O_2 has been observed previously.[4] An activation energy of 50 kcal/mole was approximated from the k's and this agrees with values in the literature[2,4,6] which range from 52.3 to 54.8 kcal/mole. The rate-determining step should therefore be the same in either case, and there seems to be no reason to belive that the presence of traces of O_2 should favor or retard the decomposition of any of the isotopic species.

The $C^{13}O_2/C^{12}O_2$ ratio (m/e 45/44) of the carbon dioxide was measured on a Consolidated-Nier Isotope Ratio Mass Spectrometer, Model 21–201. The value of the $C^{13}O_2/C^{12}O_2$ ratio of the original ethyl bromide was determined by total decomposition of two samples at 500°C, using the procedure outlined above. Tank CO_2 was used as the reference standard; and in the analyses each unknown sample was run between two standard analyses in the usual way. No correction for resolution or O^{17} was employed.

CALCULATIONS AND RESULTS

The over-all equations defining the rate constants are:

$$CH_3CH_2Br \rightarrow CH_2=CH_2 + HBr \quad k_1$$
$$CH_3C^*H_2Br \rightarrow CH_2=C^*H_2 + HBr \quad k_2$$
$$C^*H_3CH_2Br \rightarrow C^*H_2=CH_2 + HBr \quad k_3.$$

The following symbols are employed for concentrations:

$$a_1=[CH_3CH_2Br], \quad a_2=[CH_3C^*H_2Br],$$
$$a_3=[C^*H_3CH_2Br], \quad x_1=[CH_2=CH_2],$$
$$x_2=[CH_2=C^*H_2].$$

Superscript 0 refers to initial concentration; the asterisk denotes C^{13}.

Considering the first fraction of ethylene produced by decomposition (assuming infinitesimal extent of reaction), one obtains

$$\frac{dx_1}{dx_2}=\frac{k_1a_1^0}{k_2a_2^0+k_3a_3^0}. \tag{1}$$

For a normal isotope distribution $a_2^0=a_3^0$, so that one obtains

$$\frac{x_1^0}{x_2^0}=\frac{a_1^0}{a_2^0}\left(\frac{k_1}{k_2+k_3}\right). \tag{2}$$

We define the separation factor at zero extent of re-

[11] A. I. Vogel, J. Chem. Soc. **1943**, 636.
[12] E. L. Skau and R. McCullough, J. Am. Chem. Soc. **57**, 2439 (1935).
[13] A. Zmaczynski, J. chim. phys. **27**, 503 (1930).
[14] J. Timmermans and F. Martin, J. chim. phys. **23**, 747 (1926).
[15] D. Tyrer, J. Chem. Soc. **105**, 2534 (1914).
[16] *International Critical Tables* (McGraw-Hill Book Company, Inc., New York, 1926), Vol. VII, pp. 34, 81.
[17] D. R. Stull, Ind. Eng. Chem. **39**, 517 (1947).
[18] J. W. Smith, J. Chem. Soc. **1931**, 2573.
[19] P. C. Cross and F. Daniels, J. Chem. Phys. **1**, 48 (1933).

action, S_0,

$$S_0=\frac{x_1^0}{x_2^0}\left(\frac{a_2^0+a_3^0}{a_1^0}\right)=\frac{x_1^0}{x_2^0}\left(\frac{2a_2^0}{a_1^0}\right)=\frac{2k_1}{k_2+k_3}. \quad (3)$$

One must now relate this separation factor, S_0, with the measured one, S, based on the assay of CO_2 from the combustion of ethylene samples. This may be done using a procedure similar to that of Bigeleisen,[20] which gives the result:

$$S_0=2K\frac{\ln(1-f)}{\ln\left[1-\frac{K(1+r)}{L}\frac{f}{S}\right]}, \quad (4)$$

where $f\equiv$fraction of substrate decomposed$\cong x_1/a_1^0$,

$$S\equiv\text{measured separation factor}=\frac{x_1}{x_2}\left(\frac{a_2^0+a_3^0}{a_1^0}\right),$$

$$K=\frac{k_2^2+k_3^2}{(k_2+k_3)^2},\quad L=\frac{k_2+rk_3}{k_2+k_3},\quad \text{and}\quad r=\frac{a_3^0}{a_2^0}.$$

Since k_2 and k_3 are believed to differ by less than 2 percent, K is taken to be $\frac{1}{2}$. In addition, it is assumed that $r=1$. This assumption produces a negligible error in S_0 even if the actual r differs from unity by as much as 10 percent. A greater abnormality in the natural distribution of C^{13} in the ethyl bromide (isotopic inhomogeneity) is very unlikely.

Equation (4) is then simplified to yield the result:

$$S_0=\frac{2k_1}{k_2+k_3}=\frac{\ln(1-f)}{\ln(1-f/S)}. \quad (5)$$

Equation (5) is used to correct to zero extent of reaction.

TABLE I. Summary of experimental results.

Temp. °C (±3°)	f (±0.003)	S (±1×10⁻⁴)	$S_0=\frac{2k_1}{k_2+k_3}$ (±2×10⁻⁴)
351	0.053	1.0088_5	1.0091
355	0.050	1.0088	1.0090_5
366	0.056	1.0087_5	1.0090
366	0.057	1.0080	1.0082_5
377	0.062	1.0086	1.0088_5
379	0.057	1.0089_5	1.0092_5
387	0.050	1.0075_5	1.0077_5
389	0.059	1.0087	1.0090
402	0.061	1.0082_5	1.0085
403	0.059	1.0072	1.0074_5
410	0.056	1.0066_5	1.0068_5
410	0.057	1.0073_5	1.0076
423	0.054	1.0068	1.0070
433	0.063	1.0066	1.0068
442	0.089	1.0054	1.0056_5
442	0.078	1.0060	1.0062_5
453	0.123	1.0071_5	1.0076_5
453	0.071	1.0063_5	1.0066

[20] J. Bigeleisen, Science **110**, 14 (1949).

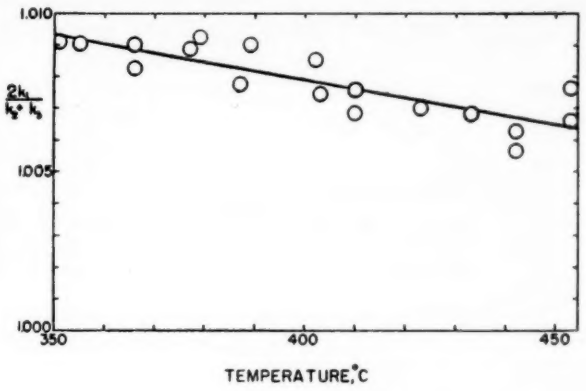

FIG. 1.

For experiments carried out to a small extent of reaction ($f<0.1$), Eq. (5) may be further simplified to give the following useful approximation formula:

$$\epsilon_0=\epsilon(1+f/2), \quad (6)$$

where $\epsilon\equiv S-1$ and $\epsilon_0\equiv S_0-1$.

An example of the original data and calculations for a typical experiment follows.

$$T=423\pm3°\text{C}.\quad f=0.054\pm0.004.$$

Mass spectrometer ratios (45/44) for CO_2 from:

(a) Product fraction C_2H_4	0.014961±0.000006
(b) Total decomposition C_2H_4	0.015059±0.000003
(c) Tank reference standard	0.014938±0.000004

$S=1.0068\pm0.0001$; $\epsilon_0=0.0070\pm0.0002$

$$\frac{2k_1}{k_2+k_3}=1.0070\pm0.0002.$$

The data for eighteen experiments are summarized in Table I. Figure 1 shows a graph of the data of Table I. The least-squares line drawn through the data passes through the point 1.0079 at 400°C, with a slope of -2.8×10^{-5}/°C. The average deviation of the points from the line is ±0.0006. The uncertainty in the slope is approximately$\pm1.0\times10^{-5}$/°C.

DISCUSSION

It is of interest to evaluate the primary and secondary isotope effects from the measured quantity

$$\epsilon_0\equiv\frac{2k_1}{k_2+k_3}-1.$$

Defining the primary isotope effect as

$$\beta\equiv\frac{k_1}{k_2}-1,$$

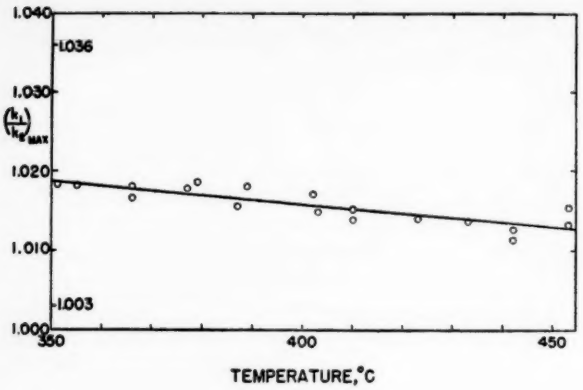

FIG. 2.

and the secondary isotope effect as

$$\gamma \equiv \frac{k_1}{k_3} - 1,$$

one obtains

$$\frac{2}{1+\epsilon_0} = \frac{1}{1+\beta} + \frac{1}{1+\gamma},$$

so that $\beta+\gamma+2\beta\gamma=\epsilon_0(2+\beta+\gamma)$. Neglecting second-order products, $\beta+\gamma=2\epsilon_0$. Thus the sum of the primary and secondary isotope effects is twice the observed overall isotope effect.

According to any reasonable theory, $\beta>\gamma\geq 0$. The upper limit for β may be found by setting $\gamma=0$; the lower limit by assuming $\gamma=\beta$. Thus $\beta_{\max}=2\epsilon_0$, and $\beta_{\min}=\epsilon_0$. Similarly γ is found to lie between the limits 0 and ϵ_0.

In summary

$$\epsilon_0<\beta\leq 2\epsilon_0,$$

$$\epsilon_0>\gamma\geq 0$$

and

$$\beta+\gamma=2\epsilon_0.$$

Figure 2 shows a graph of $(k_1/k_2)_{\max}$ *versus* T°C. From the data at 400°C, at which $\epsilon_0=0.0079$, $(k_1/k_2)_{\max}=1.0159\pm 0.0012$.

This is significantly lower than the value $k_1/k_2\geq 1.036$ calculated for the case of the rupture of an isolated C—Br bond.

The theoretical treatment of Bigeleisen[8] based on the transition-state theory is:

$$\frac{k_1}{k_2} = \left(\frac{m^*\ddagger}{m\ddagger}\right)^{\frac{1}{2}} \left[1+\sum_i G(u_i)\Delta u_i - \sum_i G(u_i\ddagger)\Delta u_i\ddagger\right],$$

where $m\ddagger$ and $m^*\ddagger$ represent the reduced masses of the normal and isotopic activated complexes along the decomposition coordinate and the other quantities have their usual significance. For the free radical C—Br rupture mechanism one would expect the reduced mass term to be 1.036. The quantity in brackets, known as the free energy term, is greater than unity, but decreases to unity as $T\rightarrow\infty$. The observed negative temperature dependence is of the proper sign, but its magnitude is in doubt by such a large amount that it offers no critical test of the theory.

For the intramolecular mechanism, the reduced mass ratio would be expected to lie somewhere between 1.003 and 1.036. No explicit theoretical formulation is available to enable a calculation of the appropriate reduced mass ratio for such a "four-center" reaction. However, Bigeleisen and Wolfsberg[21] have shown that for 3-center isotopic reactions the reduced mass ratio nearly always shows an initial decrease with an increase in the "reaction coordinate parameter" p, which is a measure of the relative amount of bond formation to bond rupture. It might be presumed that for the present case similar qualitative considerations might apply.

It is therefore believed that the results of the present investigation eliminate from consideration the simple free radical mechanism and offer support for the direct intramolecular elimination mechanism.

ACKNOWLEDGMENTS

The authors are grateful to Professor Henry Taube and Dr. Otto Forchheimer of the University of Chicago for their kind cooperation with regard to the mass spectrometer.

This research was supported by the U. S. Atomic Energy Commission.

[21] J. Bigeleisen and M. Wolfsberg, J. Chem. Phys. **21**, 1972 (1953); **22**, 1264 (1954).

Spectroscopic Studies of Rotational Isomerism in Fluorinated Ethanes. I. 1,2-Difluoro-1,1,2,2-Tetrachloroethane

R. E. KAGARISE AND L. W. DAASCH
Naval Research Laboratory, Washington 25, D. C.
(Received June 11, 1954)

The Raman spectra of solid and liquid $CFCl_2-CFCl_2$ have been investigated, and the observed frequency shifts ($\Delta\nu$ cm^{-1}), relative intensities, and depolarization factors are presented for the latter. The infrared absorption spectra of the liquid in the 2–36-μ region, and of the solid and vapor in the 2–22-μ region have also been studied.

The behavior of the infrared and Raman spectra as a function of temperature and upon solidification was anomalous in that no changes in the relative intensities of the spectral lines were observed.

Two possible explanations of the spectroscopic data are considered, neither of which is completely satisfactory. The assumption of a single molecular species, corresponding to a large energy difference, is apparently in conflict with the number of observed Raman frequencies, while the assumption of two forms of almost equal energy ($\Delta H < 300$ calories/mole) is inconsistent with the persistence of all lines upon solidification.

1. INTRODUCTION

THE phenomenon of rotational isomerism in halogenated ethanes has been the subject of a vast number of investigations during the past twenty years. However, most of this work has been concerned with chlorinated and brominated ethanes and very little is known about the phenomenon in fluorinated ethanes. Since the effect of fluorine atoms in molecules is still under discussion,[1] it is of interest to study such compounds. Furthermore, the generality and relative merits of the various potential functions that have recently been proposed[2,3] cannot be evaluated until sufficiently reliable and complete data are available for a large number of related molecules.

The Raman spectrum of $CFCl_2-CFCl_2$ in the liquid state at 40°C has been studied by Glockler and Sage.[4] They suggest that two isomeric forms of symmetry C_{2h} and C_2, respectively, are present. The spectrum was not studied at different temperatures, so that no attempt was made to identify the lines arising from the two proposed isomeric forms.

To the best of our knowledge the infrared spectrum has not been previously reported.

2. EXPERIMENTAL

The sample of $CFCl_2-CFCl_2$ used in this investigation was prepared and purified in the Jackson Laboratory of E. I. du Pont de Nemours and Company. Infrared analysis of this material showed it to contain approximately 0.8 mole percent of CCl_3-CF_2Cl which cannot be removed by fractionation. Since the infrared and Raman spectrum of this impurity are known,[5] the bands due to it were easily identified.

The infrared spectra were obtained with one of three instruments, depending upon the wavelength interval under investigation. The 2–15 micron interval was studied by means of a Perkin-Elmer Model 21 spectrophotometer employing a 60° sodium chloride prism. Spectral measurements in the 15–22-μ region were made with the large research-type instrument previously described.[6] A KBr prism (60°, 10×15-cm faces) was used as the dispersing element. Finally, the 22–36-μ region was investigated with a Perkin-Elmer Model 12-B instrument equipped with KRS-5 optics and a Hornig-type thermocouple.

At room temperature (approximately 25°C), liquids and vapors were measured using conventional absorption cells. The various sample thicknesses used are listed on the individual spectral curves. To facilitate observations of vapors at temperatures up to 180°C an absorption cell of the type described by Bernstein[7] was constructed. Basically, it consists of a standard 7-cm Pyrex cell, having AgCl windows, which is mounted within a heated container. Temperatures were measured by means of a thermocouple junction located inside the absorption cell. Spectra of solids at low temperatures were observed in the 2–22-μ region using a cell similar to the one described by Lord, McDonald, and Miller.[8]

Raman effect studies were made with an Applied Research Laboratory's spectrophotometer which records spectra either photographically or photoelectrically. The dispersive system consists of three 60-degree prisms of extra-dense flint glass having low reflection coatings. Designed especially for Raman spectroscopy, the instrument combines speed ($f/3.0$) with high dispersion (15 A/mm at 4358 A). The photographic emulsion used was Eastman Tri-X Panchromatic film, developed in Eastman Dk 60a.

To facilitate the measurement of the Raman shifts, an iron arc spectrum was photographed adjacent to each

[1] J. Leonard and L. E. Sutton, J. Am. Chem. Soc. **70**, 1564 (1948).
[2] W. D. Gwinn and K. S. Pitzer, J. Chem. Phys. **16**, 303 (1948).
[3] H. J. Bernstein, J. Chem. Phys. **17**, 262 (1949).
[4] G. Glockler and C. G. Sage, J. Chem. Phys. **8**, 291 (1940).
[5] Nielsen, Liang, Smith, and Alpert, J. Chem. Phys. **21**, 1070 (1953).
[6] Nielsen, Crawford, and Smith, J. Opt. Soc. Am. **37**, 296 (1947).
[7] H. J. Bernstein, J. Chem. Phys. **18**, 897 (1950).
[8] Lord, McDonald, and Miller, J. Opt. Soc. Am. **42**, 149 (1952).

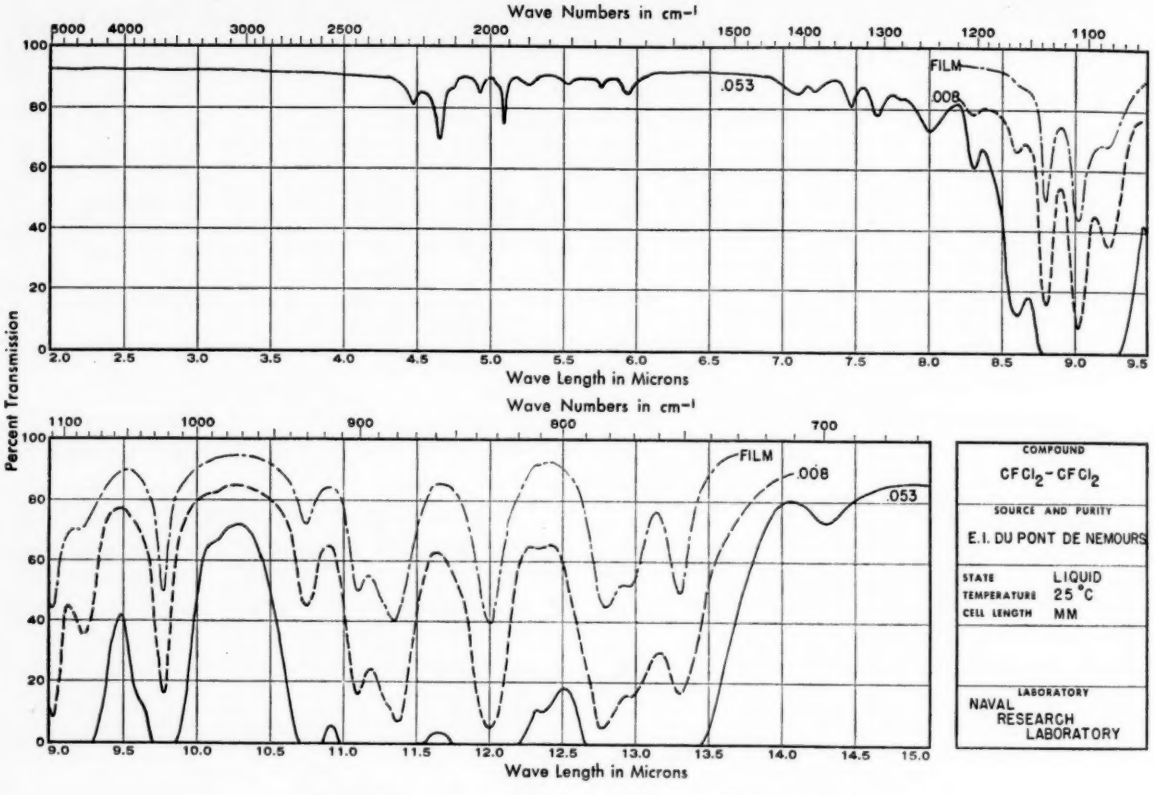

FIG. 1. Infrared spectrum of liquid $CFCl_2-CFCl_2$ (2–15 μ).

Raman spectrum. The relative positions of the Raman and iron lines were measured directly from the film using a slide comparator. Polarization measurements were obtained using the photoelectric portion of the instrument and the empirical method of correcting for convergence error described by Rank and Kagarise.[9] In the case of weaker lines qualitative values were determined photographically by means of two-exposure method of Crawford and Horowitz.[10] Relative intensities were measured with the photoelectric portion of the spectrometer.

3. RESULTS AND DISCUSSION

The observed Raman shifts ($\Delta\nu$ cm^{-1}) corrected to vacuum, semiquantitative depolarization factors, and relative intensities for the liquid are listed in Table I. In addition the results of Glockler and Sage[4] and the spectrum of CCl_3-CF_2Cl are given for comparison. An examination of Table I shows immediately that the sample used by Glockler and Sage contained a considerable quantity of CCl_3-CF_2Cl as an impurity.

Because of the weakness of the lines in the 1000–1200 cm^{-1} region of the spectrum, the depolarization factors listed are questionable. However, none of these lines are highly polarized, all of them having values greater than 0.5. Of the twenty-four observed Raman frequencies, nine are polarized, eight depolarized, and seven are too weak for satisfactory measurements.

Using the photoelectric portion of the A.R.L. instrument, no change was observed in the relative intensity of lines in the Raman spectrum of the liquid over a temperature range of 30° to 95°C. This limited range is necessitated by the physical properties of the compound, which has a melting point of 25°C and a boiling point of 93°C. In addition, the Raman spectrum of the glassy solid at −13°C showed no changes from that of the liquid. We have been unable to observe the Raman spectrum of the crystalline solid.

The infrared absorption spectrum of liquid $CFCl_2-CFCl_2$ in the region from 2 to 36 μ is shown in Figs. 1 and 2. The wavelengths and wave numbers of the observed absorption maxima are given in Table II.

The infrared spectrum of the solid at liquid nitrogen temperature was observed in the 2–22-μ region using the low temperature cell. All bands present in the spectrum of the liquid persisted in the solid and, with the exception of becoming sharper, remained unchanged. The infrared spectrum of the vapor phase was also studied in the 2–22-μ region over a temperature range from 30° to 125°C using the 7-cm cell. There were no observable changes in the relative intensities of any of the absorption bands.

In marked contrast to the behavior of the dihalo-

[9] D. H. Rank and R. E. Kagarise, J. Opt. Soc. Am. **40**, 89 (1950).

[10] B. L. Crawford and W. Horowitz, Jr., J. Chem. Phys. **15**, 268 (1947).

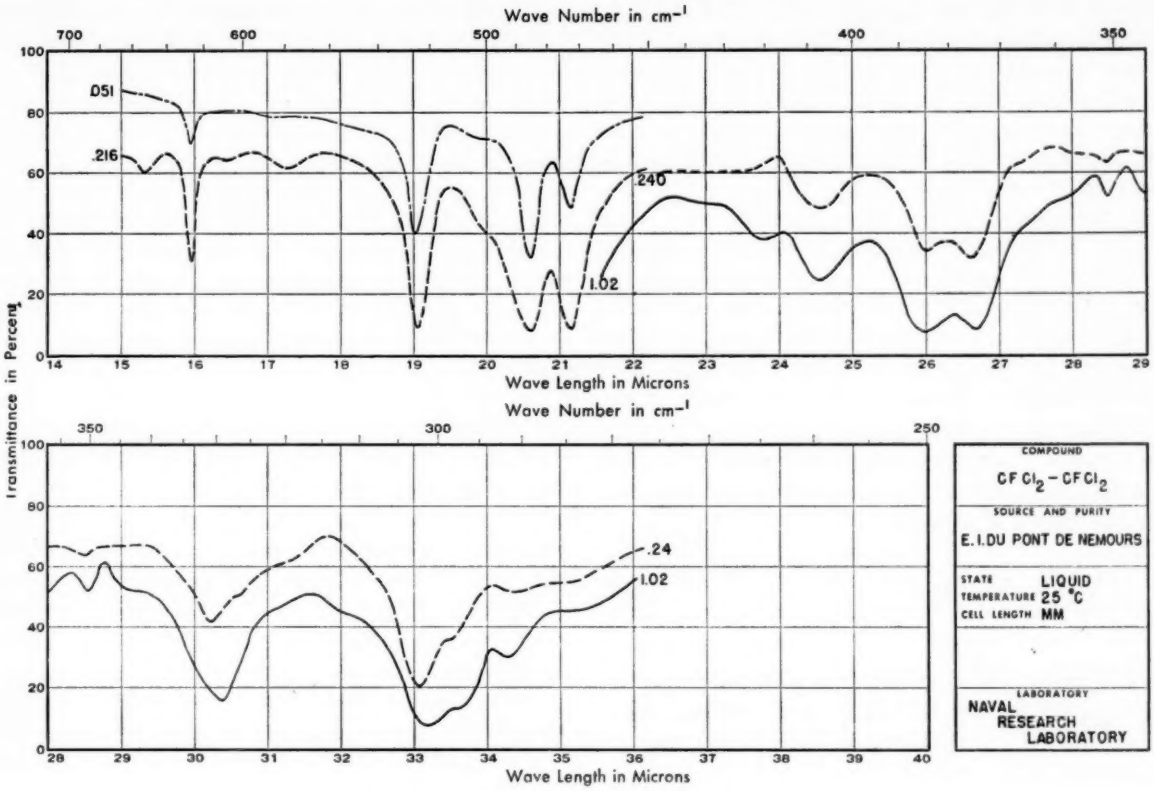

FIG. 2. Infrared spectrum of liquid $CFCl_2-CFCl_2$ (15–36 μ).

genated ethanes (1,2-dichloro and dibromo)[11–13] and tetrahalogenated ethanes (1,1,2,2-tetrachloro and tetrabromo)[14–16] there is then very little, if any, change in the Raman or infrared spectrum of sym-difluorotetrachloroethane as the temperature is varied or upon solidification. In view of existing theories on rotational isomerism, there are two possible explanations of this; either only a single molecular species is present in an appreciable concentration at temperatures up to 400°K, corresponding to a large energy difference, or a mixture of two rotational isomers of almost equal energy exists whose composition is nearly temperature independent.

(1) Assumption of a Single, Prevalent, Rotational Isomer

The fact that the spectra do not change perceptually with changes of temperature or upon solidification finds a natural explanation in terms of this assumption. From structural considerations the symmetry of this single form must be one of the following: (a) C_{2h} (*trans*-form), (b) C_{2v} (*cis*-form), or (c) C_2 (skew or *gauche*-form). A comparison of the Raman and infrared spectra listed in Table III shows that in general the very strong infrared bands have no coincident strong Raman frequencies and vice versa, indicating a molecule with a center of symmetry. Since the *trans*-form is the only one of the three species mentioned above in this category, let us further examine the spectra on the basis that the prevalent isomer is of symmetry C_{2h}. For the *trans* molecules the eighteen normal vibrations are distributed into four classes: $6A_g$, $4A_u$, $3B_g$, and $5B_u$. Classes A_g and B_g are Raman active, while A_u and B_u type modes are infrared active. Since twenty-four Raman frequencies are observed it appears certain that the *trans*-form does not exist as a single prevalent form.

Moreover, since the rule of mutual exclusion is partially satisfied it does not seem to be possible to explain the spectroscopic data on the basis of a single *cis*- or *gauche*-form. Even if this partial fulfillment is fortuitous, it is still difficult to explain the observed Raman spectrum on the basis of a single *cis*- or *gauche*-form, since at least six observed Raman lines must be explained as overtone or combination modes in either case.

(2) Assumption of Two Rotational Isomers (Small Energy Difference)

The existence of a small energy difference between the two isomeric forms of sym-difluorotetrachloroethane

[11] S. Mizushima and Y. Morino, Bull. Chem. Soc. Japan **17**, 94 (1942).
[12] H. J. Bernstein, J. Chem. Phys. **17**, 258 (1949).
[13] J. T. Neu and W. Gwinn, J. Chem. Phys. **18**, 637 (1950).
[14] Mizushima, Morino, and Kubo, Physik. Z. **38**, 459 (1937).
[15] A. Langseth and H. J. Bernstein, J. Chem. Phys. **8**, 410 (1940).
[16] R. E. Kagarise and D. H. Rank, Trans. Faraday Soc. **48**, 394 (1952).

would lead to an almost constant equilibrium composition determined mainly by the statistical weights of the components, and by the presumably small differences in their vibrational and rotational partition functions. However, the postulation of two forms of almost equal energy appears, at first sight, to conflict with certain experimental observations.

First, the energy difference is apparently very small ($\Delta H < 300$ cal/mole, as estimated from experimental error) in both the liquid and vapor phase, whereas the theory of Morino *et al.*[17] predicts that in the condensed phase the rotational isomer possessing the larger dipole moment will be stabilized due to the interaction field. Thus, for example, if the energy difference is zero in the vapor phase, the *gauche*-form should become more stable than the *trans*-form in the liquid phase (assuming staggered configurations). The magnitude of the interaction energy δE, is given by

$$\delta E = -\frac{\epsilon - 1}{2\epsilon + 1} \cdot \frac{\mu^2}{\alpha^3},$$

where μ is the dipole moment of the *gauche*-form, ϵ the dielectric constant of the medium, and α the molecular radius. Unfortunately, the values of ϵ and μ are not known for $CFCl_2-CFCl_2$. However, one can get an approximate value for δE by the following procedure. Using values of 1.92 debyes for the C—F bond moment, and 2.02 debyes for the C—Cl bond moment and assuming tetrahedral angles, the dipole moment of the gauche form is $\mu_g = 0.26$ debyes. If, in addition, the maximum value for the quantity $(\epsilon - 1)/(2\epsilon + 1)$ is used, namely 0.5, the value for δE is found to be approximately 10 calories/mole. Thus, it is quite plausible that in $CFCl_2-CFCl_2$ the energy difference between the *gauche*- and *trans*-isomers will not be changed in going from the vapor to the liquid.

Second, if there are two forms of nearly equal energy it is difficult to explain the persistence of all observable infrared bands upon solidification. Szasz and Sheppard[18] have reported similar observations in the case of 2-methyl and 2,3-dimethyl butane, which behave much differently upon solidification than do normal hydrocarbons possessing rotational isomers.

The most plausible explanation of the persistence of all infrared bands upon solidification may be based on the fact that solid, amorphous glasses have spectra similar to those of liquids. Brown and Sheppard[19] have observed this in the case of certain alkyl halides and alcohols. Thus, if the sample did not crystallize upon freezing, but became instead an amorphous glass, the persistence of all lines is readily explained.

In view of this possibility numerous methods were employed in the preparation of solid samples for the infrared studies of $CFCl_2-CFCl_2$, yet in no instance was the disappearance of bands observed. The following

TABLE I. Raman spectrum of liquid $CFCl_2-CFCl_2$ and $CF_2Cl-CCl_3$.

$CFCl_2-CFCl_2$ Present work	$CFCl_2-CFCl_2$ Glockler and Sage[a]	$CF_2Cl-CCl_3$ Nielsen *et al.*[b]
81 (20, dp)[c]	81.4 (5)	
168 (3, dp)	165.5 (3)	
177 (8, p?)	181.2 (5)	183 (25)
225 (10, dp)		
232 (25, dp)	231.0 (7)	231 (37)
255 (32, dp)	264.3 (7)	268 (38)
297 (37, 0.28)	297.2 (5)	
328 (12, 0.40)	329.1 (7)	331 (40)
400 (70, 0.72)	402.1 (3)	
411 (80, 0.52)		
422 (vw)[d]	421.2 (10)	422 (100)
442 (vw)[d]	447.7 (8)	443 (100)
	455.5 (2)	456 (21)
504 (vw)		
524 (100, 0.22)	523.8 (8)	
578 (40, 0.12)	578.2 (6)	
587 (vw)		
626 (vw)[d]	625.9 (8)	627 (73)
652 (vw)		
780 (vw)	778.9 (0)	777 (5)
812 (vw)		
851 (vw)	854.8 (4)	855 (21)
879 (vw)		
905 (40, p)	906.8 (2)	
1025 (12, dp?)	1027.2 (4)	1029 (16)
1045 (12, p)	1046.0 (0)	
1083 (7, dp?)	1086.0 (0)	
1141 (16, dp)	1143.0 (2)	
	1167.5 (3)	1165 (8)

[a] See reference 4.
[b] See reference 6.
[c] Frequency in wave numbers, relative intensity, and depolarization factor.
[d] Line due to CCl_3-CF_2Cl impurity.

TABLE II. Infrared absorption spectrum of liquid $CFCl_2-CFCl_2$.

λ (microns)	(cm^{-1})	λ (microns)	(cm^{-1})
4.47 vw	2237	11.38 vs	879
4.65 w	2151	12.00 vs	833
4.92 vw	2033	12.79 vs	782
5.09 w	1965	12.95 w[a]	774
5.27 vw	1898	13.30 s	752
5.54 vw	1805	14.30 w	699
5.74 vw	1742	15.31 w	653
5.93 w	1686	15.95 w[a]	627
7.12 w	1404	17.26 w	579.5
7.22 vw	1385	19.05 s	524.8
7.45 w	1342	20.60 s	485.4
7.63 w	1311	21.14 s	472.9
8.01 w	1248	23.76 w[a]	420.1
8.30 w	1205	24.58 m	407.0
8.60 w[a]	1163	26.00 s	384.8
8.80 s	1136	26.64 s	375
9.02 vs	1109	28.50 w	351
9.22 m	1085	30.30 m	330
9.78 vs	1022	33.16 s	302
10.76 m	929	33.6 w	297
11.11 s	900	34.30 w	292.5

[a] Bands due to $CF_2Cl-CCl_3$ as impurity.

[17] Morino, Mizushima, Kuratani, and Katayama, J. Chem. Phys. **18**, 754 (1950).

[18] G. J. Szasz and N. Sheppard, J. Chem. Phys. **17**, 93 (1949).
[19] J. K. Brown and N. Sheppard, Discussions Faraday Soc. **9**, 144 (1950).

observations tend to substantiate the view that these samples were crystalline rather than amorphous:

(a) Visual examination of samples at −180°C showed them to exhibit typical "crystalline" formations.

(b) The samples did not exhibit the high transmission properties of glasses. Indeed, upon freezing, the transmittance at 4 μ dropped from 95 percent to about 60 percent for a sample 0.02 mm thick.

(c) The spectrum of a solid film formed by allowing vapor to impinge upon a salt plate cooled to −80°C showed no marked difference from that of a liquid or solid sample formed by slow freezing.

(d) When the solid was allowed to warm up from liquid nitrogen temperatures, no visible changes occurred until the melting point was reached. Had the solid been a glass instead of crystalline, a transition to the crystalline form probably would have occurred at a temperature slightly below the melting point. Brown and Sheppard[19] have successfully used this method to crystallize certain compounds that have resisted most other techniques.

4. CONCLUSIONS

On the basis of the existing spectroscopic data, neither of two proposed explanations is completely satisfactory. On the one hand, the assumption of a single molecular form (large energy difference) is confronted with the fact that twenty-four Raman lines are observed, while at most 18 fundamentals would be Raman active if only a single form were present. Moreover, the rule of mutual exclusion is partially satisfied, which suggests the presence of the *trans*-form, for which only nine fundamentals are Raman active.

TABLE III. Comparison of infrared and Raman spectra of $CFCl_2-CFCl_2$.

Raman	Infrared	Raman	Infrared
1141 (16, dp)	1136 s	587	
	1109 vs	578 (40, 0.12)	579.5 w
1083 (7, dp?)	1085 m	524 (100, 0.22)	524.8 s
1045 (12, p)		504 vw	
1025 (12, dp?)	1022 vs		485.4 s
	929 m		472.9 s
905 (40, p)	900 s	411 (80, 0.52)	407 m
879 vw	879 vs	400 (70, 0.72)	
851 vw			384.8 s
	833 vs		375 s
812 vw			351 w
780 vw	782 vs	328 (12, 0.40)	330 m
	752 s		302 s
	699 w	297 (37, 0.28)	297 w
652 vw	653 w		292.5 w

The assumption of two forms of nearly equal energy reasonably accounts for all of the observed data, except the persistence of all infrared bands in the spectrum of the solid. There is a remote possibility, of course, that all of the solid samples investigated were amorphous rather than crystalline.

It is felt that dipole moment, electron diffraction, and thermodynamic studies, as well as additional spectroscopic work, are needed to elucidate the structure of this molecule.

ACKNOWLEDGMENT

The authors are indebted to Dr. R. C. McHarness of the Jackson Laboratory, E.I. du Pont de Nemours and Company, for supplying the sample of $CFCl_2-CFCl_2$ used in this investigation.

The Ionic Character of Diatomic Molecules*

B. P. DAILEY AND C. H. TOWNES
Columbia University, New York, New York

(Received June 11, 1954)

A relation between the electronegativity difference of two bonded atoms and the ionic character of the bond is obtained for singly bonded diatomic molecules in the gaseous state. The relation is based primarily on the wide variety of nuclear quadrupole coupling constants recently measured by microwave techniques. However, dipole moments of diatomic molecules are also used and discussed. Both quadrupole coupling constants and dipole moments indicate strongly that bonds involving electronegativity differences greater than 2 are almost completely ionic. Certain effects of hybridization, overlap, and polarization on considerations of ionicity are discussed.

NUCLEAR quadrupole coupling constants in molecules have previously been shown to be closely correlated with molecular electronic structure and in favorable cases to give fairly clear evidence about the nature of chemical bonds.[1] Quadrupole coupling constants for a number of diatomic halides and for isolated halogen atoms have now been measured so that it is possible to examine the behavior of quadrupole coupling constants and bonds for these relatively simple molecules.

Description of a chemical bond usually involves specifying the amount of ionic character, the orbital hybridization, and the degree of bond multiplicity. This threefold complexity makes the unique interpretation of a given bond structure quite difficult. Since the diatomic halides are believed to involve bonds which are essentially single, complications due to multiplicity are avoided. Hence it is possible to obtain some information about ionic character of bonds (and to a lesser extent about hybridization) from a study of these comparatively uncomplicated molecules which may be used as a guide in dealing with more complex systems.

The wave function of a bonding electron may be written in the LCAO approximation

$$\psi = a\psi_A + b\psi_B,$$

where ψ_A and ψ_B are atomic orbitals for atoms A and B. If ψ is normalized, $a^2+b^2+2abS=1$, where S is the overlap integral $\int \psi_A \psi_B d\tau$. The ionic character for such a heteropolar bond may be defined as a^2-b^2, i.e., it is the difference between the probabilities for the electron to be found on atom A or B.

DIPOLE MOMENTS

The dipole moment for a heteropolar bond is given by an expression of the following form

$$\mu = eR(b^2-a^2) + \mu_{\text{overlap}} + \mu_{\text{hybridization}} + \mu_{\text{polarization}}. \quad (1)$$

The first term is the so-called primary moment, the second term is the moment due to the overlap of orbitals from atoms of unequal size, the third term is due to the hybridization of valence shell orbitals, and the fourth term is due to the polarization of the nonbonding electrons. Unfortunately it is not possible to use an equation of this form to compare calculated and measured dipole moments because the polarization term is particularly difficult to evaluate.

In some of the earlier literature the assumption was made that only the first term in the above expression is of importance. For example, Pauling has calculated the ionic character of the bonds in HCl, HBr, and HI as μ/eR, where μ and R are the experimentally observed values of the dipole moment and internuclear distance and e is the electronic charge. From these three points Pauling[2] derived a relation between ionic character and electronegativity differences expressed by the equation

$$i = 1-\exp[\tfrac{1}{4}(X_A-X_B)^2]. \quad (2)$$

This relation is represented by one of the curves in Fig. 1. Also plotted are the points calculated in the same manner from the larger number of experimental dipole moments now available (see Hannay and Smyth)[3] which are listed in Table I.

In view of the complexity of the relation represented by Eq. (1) no close correlation of μ/eR with electronegativity differences would be expected. It is worth noting that a good rough correlation is actually observed. This would seem to be empirical evidence for considerable mutual cancellation of the overlap, hybridization, and polarization terms contributing to the dipole moment. For molecules which are completely ionic, or nearly so, the polarization and primary moments are the only important terms. As shown by Rittner,[4] polarization effects result in a marked reduction in the dipole moments of the completely ionic alkali halides. Since the polarization and primary moments are always of opposite sign, at least for large values of the ionicity, μ/eR may always be expected to be less than the ionic character a^2-b^2.

* Work supported jointly by the Signal Corps, Office of Naval Research, and Air Force.

[1] C. H. Townes and B. P. Dailey, J. Chem. Phys. **17**, 782 (1949).

[2] L. Pauling, *Nature of the Chemical Bond* (Cornell University Press, Ithaca, 1939), p. 70.

[3] N. B. Hannay and C. P. Smyth, J. Am. Chem. Soc. **68**, 171 (1946).

[4] E. S. Rittner, J. Chem. Phys. **19**, 1030 (1951).

Recent dipole moment data[5] plotted in Fig. 1 show that the curve of μ/eR *versus* electronegativity differences flattens out for values of the electronegativity difference greater than 2.0. This would seem to indicate that maximum ionicity is achieved at this point. Presumably all molecules having larger electronegativity differences than 2.0 are completely ionic and have values of μ/eR of less than 1.0 because of polarization.

The success of Honig[5] in reproducing the internuclear distances in the alkali halide molecules using crystal ionic radii and the Born-Mayer equation supports the conclusion that these molecules are largely ionic. The general agreement of Rittner's model of the alkali halides with their recently measured properties[5] lends further support.

Although the observed correlation between μ/eR and electronegativity differences indicates that dipole moments may be used as some sort of guide in evaluating ionic character, one cannot expect to deduce reliable values of the ionic character from dipole moment data alone.

NUCLEAR QUADRUPOLE COUPLING

Quadrupole hyperfine structure involves the coupling constant eqQ. Here Q is the nuclear quadrupole moment and $q \equiv \partial^2 V/\partial^2 z^2$ is the negative of the electric field at the nucleus due to all charges outside the nucleus. The z direction is along the bond axis or the internuclear axis in the case of a diatomic molecule. It has already been pointed out that q depends primarily on the electrons in p orbitals in the valence shell. For example a negative halogen ion would have an approximately spherical distribution of charge and hence a very small value of q,

TABLE I. Dipole moments of the diatomic halides.

Molecule	Internuclear distance r_e	er_e	Dipole moment in debye μ	μ/er_e	Electronegativity difference x	Reference
BrCl	2.138	10.27	0.57	0.056	0.2	a
HI	1.617	7.77	0.38	0.049	0.45	b
ICl	2.323	11.16	0.65	0.058	0.50	c
HBr	1.414	6.79	0.78	0.115	0.75	b
FCl	1.628	7.82	0.88	0.113	0.75	d
FBr	1.759	8.45	1.29	0.153	0.95	e
HCl	1.28	6.15	1.03	0.167	0.95	b
TlCl	2.541	12.20	4.444	0.364	1.25 (Haissinsky)	f
TlCl	2.541	12.20	4.444	0.364	1.75 (Gordy)	e
HF	0.92	4.42	1.91	0.432	1.7	b
LiI	2.3919	11.49	6.25	0.544	1.65	g
LiBr	2.1704	10.42	6.19	0.594	1.95	g
CsI	3.3150	15.92	12.1	0.760	1.95	g
KBr	2.8207	13.55	10.41	0.768	2.15	g
KCl	2.6666	12.81	10.48	0.818	2.35	g
CsCl	2.9062	13.96	10.40	0.745	2.45	g
CsF	2.3453	11.26	7.874	0.699	3.2	g

[a] Smith, Sidwell, and Williams, Phys. Rev. **79**, 1007 (1950).
[b] N. B. Hannay and C. P. Smyth, J. Am. Chem. Soc. **68**, 171 (1946).
[c] Townes, Merritt, and Wright, Phys. Rev. **73**, 1334 (1948).
[d] Gilbert, Roberts, and Griswold, Phys. Rev. **76**, 1723 (1949).
[e] Smith, Sidwell, and Williams, Phys. Rev. **77**, 420 (1950).
[f] Lee, Carlson, Fabricand, and Rabi, Phys. Rev. **78**, 340 (1950).
[g] See reference 5.

[5] Honig, Mandel, Stitch, and Townes, Phys. Rev. **96**, 629 (1954).

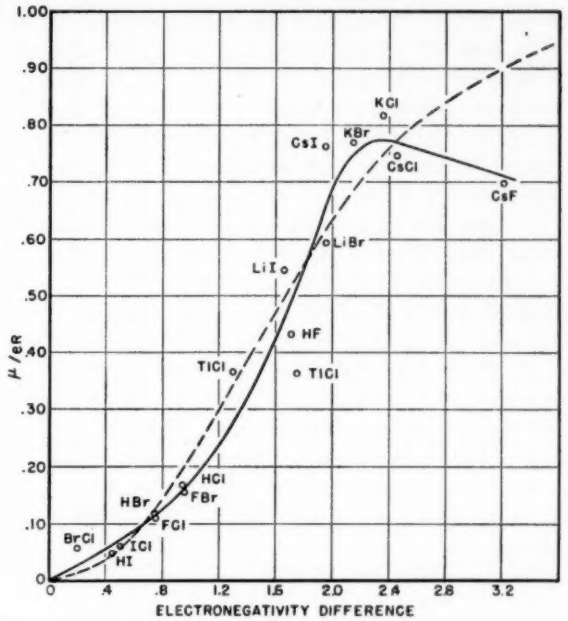

FIG. 1. Apparent ionic character μ/eR from molecular dipole moments. The dotted curve is expression (2) due to Pauling.

while a covalently bonded halogen atom, lacking one p electron in its valence shell, would have a relatively large value of q and hence of the experimentally measured coupling constant eqQ.

The quadrupole coupling constants of Cl, Br, and I (F has zero quadrupole moment) in atomic states are now known,[6] so that the contribution of an electron in an atomic p orbital to eqQ is known accurately and independently of molecular data. These values can be used in combination with measured quadrupole coupling constants in molecules to estimate the amount of ionic character in the molecular bonds. A preliminary relation between ionic character and electronegativity difference derived from quadrupole coupling constants was given some time ago.[7]

If an electron in a covalent halogen bond has a wave function about the halogen of the form

$$\psi_A = (1-s-d)^{\frac{1}{2}}\psi_p \pm (s)^{\frac{1}{2}}\psi_s \pm (d)^{\frac{1}{2}}\psi_d,$$

it may be said to have s character of an amount s and d character of amount d. Admixture of d character in the hybrid bonding orbital effectively removes part of an electron from a p orbital and hence increases the defect of p electrons. If s hybridization occurs, the two nonbonding s electrons must take on some p character and hence the defect of p electrons is decreased. Therefore the quadrupole coupling constant for an atom forming a hybrid bond with a negative ionic character i is

$$eqQ = (-1+s-d)(1-i)eqQ_{310}, \qquad (3)$$

where eqQ_{310} is obtainable from atomic data.

[6] V. Jaccarino and J. G. King, Phys. Rev. **83**, 471 (1951); J. G. King and V. Jaccarino, Phys. Rev. **91**, 209 (1953); Jaccarino, King, and Stroke (private communication).
[7] C. H. Townes and B. P. Dailey, Phys. Rev. **78**, 346 (1950).

If the bond is positively ionic, two p electrons are missing from the valence shell, but some additional considerations are involved. If there is s hybridization, one must decide whether or not the nonbonding electrons will remain in their hybrid state for both the covalent and ionic terms in the wave function. Since the promotional energy required is more than twice as great for the positive ion as for the covalent bond it will be assumed that the ionic terms involve no hybridization. The alternative, for the nonbonding electrons to be hybridized in the ionic terms, will not produce large changes in the results below. Another consideration is that the interaction between a valence p electron and the nucleus when the atom is positively ionic is somewhat larger than for the case of a neutral atom. The ratio for the two cases may be taken as $(1+\epsilon)$ where ϵ is near 0.25 for most atoms. Hence eqQ for the positive ionic state can be written as $-2(1+\epsilon)eqQ_{310}$. The coupling constant for a partially positive ionic bond is then

$$eqQ=[(-1+s-d)(1-i)-2(1+\epsilon)i]eqQ_{310}. \quad (4)$$

Although ϵ may be approximated as 0.25 for most purposes, slightly more accurate results can be obtained by using the value of ϵ tabulated for different atoms in Table II. The values are obtained by examining the experimentally measured fine structure in the spectrum of atoms and ions of most of the elements. The fine structure may be related to $(1/r^3)_{Av}$ and hence to $q=\partial^2V/\partial z^2$.

In Eqs. (3) and (4) the effects of overlap on quadrupole coupling have been neglected. A fairly complete expression which includes the effects of overlap may be found in our earlier discussion.[1] The more complete expression may be approximated by modifying (3) to $(-1-S^2+s-d)(1-i)eqQ_{310}$, where S^2 is the square of the overlap integral. Since S^2 may in some cases be as large as 0.3 or 0.4, the apparent amount of s hybridization would be very considerably increased by inclusion of this term. This point has been emphasized by Schatz.[8] There are reasons, however, for mistrusting the results which are thus obtained.

One difficulty with including the effect of overlap in some such way as indicated above is that the usual approximations to the molecular wave functions cannot be expected to give accurate values of the electron distribution near the nucleus, in the region which is most important in contributing to the hyperfine structure. Thus the atomic wave function ψ_A of atom A at nucleus B will be very much modified by the field of nucleus B. Such modifications may have little effect on the overlap integral itself, but considerable effect on the quadrupole coupling constant. In the earlier discussion,[1] contributions of the electron distribution in the overlap region to the quadrupole coupling constant were shown not to be large, but this is only provided the wave function ψ_A is not modified by the field of nucleus B. An accurate calculation of the effects of overlap on quadrupole coupling thus appears very difficult, and an approximate expression of the type given above may be in considerable error.

If effects of overlap are included in some naive way such as that indicated above, the amount of s hybridization must be supposed in some cases to be increased by as much as 30 percent, and thus becomes implausibly large. The value of $s-d$ obtained by omitting effects of overlap may properly be regarded as a lower limit, but it appears that this lower limit is close to the actual value. For example, the amounts of s character derived from (3) and (4), which neglect overlap effects, corresponds rather well with the values of 10 and 15 percent s character found[9,10] for As and S bonds in $AsCl_3$ and H_2S. For these two molecules, uncertainties due to overlap do not affect the evaluation of the s hybridization.

Since a satisfactory calculation of the effects of overlap in quadrupole coupling does not seem feasible, we shall rely on evidence which indicates that these effects are small, and shall regard them as negligible. Although experimental evidence that these effects are small seems to be fairly good, it must be kept in mind that the amount of s hybridization indicated in the following discussion may actually be somewhat too small because no allowance has been made for overlap.

It should be noted that measurement of quadrupole effects cannot independently determine the three quantities s, d, and i. If i is small, the measurements determine the quantity $s-d+i$. For an almost completely ionic bond ($i\approx 1$) however, expressions (3) and (4) give the ionic character somewhat more directly since $s-d$ may be assumed to be considerably less than one for the cases considered here.

Quadrupole coupling constants for a number of diatomic halides have been measured in the gas phase. These and the atomic coupling constants are all listed in Table III and may be compared with expressions (3) and (4). Although some additional diatomic halides have been measured in the solid state, these coupling constants cannot simply and reliably be used to indicate coupling constants for the isolated gas molecules. Since we are attempting to examine only the simplest cases with as few unknown variables as possible, coupling constants for the solid state will not be included.

TABLE II. Values of ϵ for various elements. The quadrupole coupling per electron is proportional to $(1+\epsilon)^n eqQ$, where eqQ is the coupling constant for the neutral atom and n is the degree of ionization (+1 for single positive ionic charge, −1 for single negative ionic charge).

Be	0.9	B	0.54	C	0.47	N	0.32	O	0.20	F	0.17
Mg	0.5	Al	0.27	Si	0.28	P	0.18	S	0.19	Cl	0.14
Sr	0.7	Sc	0.37	Ge	0.26	As	0.16	Se	0.20	Br	0.13
								Te	0.20	I	0.12

[8] P. N. Schatz, J. Chem. Phys. 22, 695 and 755 (1954).

[9] P. Kisliuk, J. Chem. Phys. 22, 86 (1954).

[10] G. R. Bird and C. H. Townes, J. Chem. Phys. (to be published).

If values of i can be obtained which correspond in a consistent way to the quadrupole coupling data in Table III, then the plot of these values against the appropriate electronegativity differences may be expected to give a rather generally valid relation between these variables. Values of the electronegativity which have been used are those recently presented by Huggins.[11] These are based on data for the energies of formation of molecules and as pointed out by Mulliken[12] they correspond to the element when it is forming a bond having the usual or average amount of hybridization. A change in orbital hybridization should be followed by a corresponding change in electronegativity. Such effects have been neglected, however, in this paper. Values of ϵ used in computing i were taken from Table II.

Two widely different values of the electronegativity of Tl have been given in the literature.[13,14] Points corresponding to both values are plotted in the two figures.

The simplest approximation which can be used to obtain values of i from the quadrupole data is to ignore the $s-d$ term completely. This is equivalent to assuming that in all of these diatomic halides the halogen atoms either use only pure p orbitals in bond formation or that equal amounts of s and d orbitals are used. The relation between ionic character and electronegativity differences resulting from this relatively crude assumption is shown in Fig. 2.

TABLE III. Ionic character of diatomic halides obtained from nuclear quadrupole coupling data.

Molecule	Observed eQq Mc	Ionicity assuming no hybridization	% s character assumed	Best value of ionicity	Electronegativity differences (Huggins)	Reference
Cl^{35} (atomic)	−109.74					a
BrCl	−103.6	0.056	0.0	0.056	0.20	b
ICl	−82.5	0.248	15.0	0.115	0.50	c
FCl	−146.0	0.259	0.0	0.259	0.75 1.3[e]	d
TlCl	−15.8	0.856	15.0	0.831	1.75	f
KCl	0.04	1.000	15.0	1.000	2.35	b
RbCl	+0.774	0.993	15.0	0.992	2.35	g
CsCl	3	0.973	15.0	0.968	2.45	g
Br^{79} (atomic)	769.76					a
BrCl	876.8	0.110	0.0	0.110	0.20	b
FBr	1089.0	0.329	0.0	0.329	0.95	
LiBr	37.2	0.952	15.0	0.944	1.95	g
NaBr	58	0.925	15.0	0.911	2.05	g
KBr	10.244	0.987	15.0	0.985	2.15	g
DBr	533	0.308	15.0	0.186	0.75	h
I^{127} (atomic)	−2292.84					a
DI	−1823	0.205	15.0	0.065	0.45	i
ICl	−2944	0.229[e]	0.0	0.229	0.50	e
LiI	−198.15	0.914	15.0	0.900	1.65	g
NaI	−259.87	0.887	15.0	0.867	1.75	g
KI	−60	0.974	15.0	0.970	1.85	g

[a] See reference 6.
[b] Smith, Sidwell, and Williams, Phys. Rev. **79**, 1007 (1950).
[c] Townes, Merritt, and Wright, Phys. Rev. **73**, 1334 (1948).
[d] Gilbert, Roberts, and Griswold, Phys. Rev. **76**, 1723 (1949).
[e] From Gordy (reference 13) and Haissinsky (reference 14).
[f] Lee, Carlson, Fabricand, and Rabi, Phys. Rev. **78**, 340 (1950).
[g] See reference 5.
[h] W. Gordy, and C. A. Burrus, Phys. Rev. (to be published).
[i] C. A. Burrus and W. Gordy, Phys. Rev. (to be published).

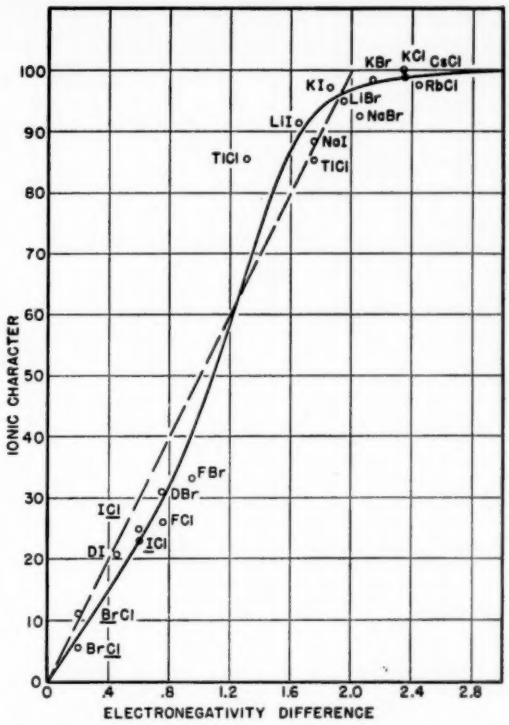

FIG. 2. Ionic character *vs* electronegativity difference calculated from quadrupole coupling and assuming no hybridization. The dashed line represents the expression $i=\frac{1}{2}|X_A-X_B|$ due to Gordy (reference 13). In cases where two different amounts of ionic character are given for the same molecule, the nucleus whose quadrupole coupling was used for each point is underlined.

The shape of Fig. 2 in the region of high ionic character is fortunately nearly independent of the validity of the above assumption as well as being quite insensitive to overlap effects. It is clear from comparing such cases as LiI and NaI, however, that one cannot obtain a unique curve of ionic character *versus* electronegativity, since the ionic character apparently depends on such additional variables as bond length.

In the region intermediate between the extremes of complete ionicity and complete covalency, the curve will be considerably more sensitive to the assumptions that are made about the hybridization or lack of it which characterizes the bonding orbitals. It is of course not possible to establish the nature of the curve in this region unambiguously on the basis of quadrupole coupling evidence alone. In particular it is quite impossible to distinguish between effects due to s hybridization from those due to d hybridization.

Our relative ignorance of these questions of detail, however, is not a sufficient excuse to ignore hybridization effects altogether. Numerous quantum-mechanical calculations of the energies of molecules containing the

[11] M. J. Huggins, J. Am. Chem. Soc. **75**, 4123 (1953).
[12] R. S. Mulliken, J. Phys. Chem. **41**, 318 (1937).
[13] W. Gordy, *Microwave Spectroscopy* (John Wiley and Sons, Inc., New York, 1953), p. 282.
[14] M. Haissinsky, J. chim. phys. **46**, 298 (1949).

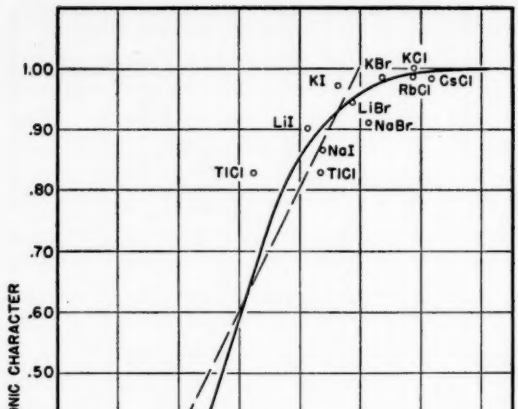

FIG. 3. Ionic character *vs* electronegativity difference calculated from quadrupole coupling and taking hybridization into account. The solid curve best represents the data. The dashed line is the expression $i=\frac{1}{2}|X_A-X_B|$ due to Gordy (reference 13). In cases where two different amounts of ionic character are shown for the same molecule, the nucleus whose quadrupole coupling was used for each point is underlined.

elements of the first two rows of the periodic table have shown the presence of $s-p$ hybridization. In an earlier paper it was shown that unless one assumed chemically unreasonably large values of the ionicity, quadrupole data showed that the bonding orbitals in chlorine compounds commonly contain approximately 18 percent s character. The use of s orbitals in the hybrid bonding orbitals of compounds of the Group V elements is indicated quite strongly by the quadrupole coupling data.[9] If small amounts of d hybridization also occur the amount of s character would have to be correspondingly larger. The evidence from quadrupole data also shows quite clearly that certain sulfur bonds are appreciably hybridized.[10]

If better values of the ionicity are desired than those obtained by neglecting hybridization completely, then certain supplementary assumptions as to the occurrence of orbital hybridization must be made. The following considerations can be used as a guide in making these assumptions.

Orbital hybridization not only increases the overlap energy but similarly increases the resonance energy between the covalent and ionic states. Therefore there should be a correlation between the ionicity and the hybridization. Such a correlation is in accord with the apparently simple relation between dipole moments and electronegativity differences. When a halogen is negatively ionic no promotional energy is required for $s-p$ hybridization in the ionic state. However, for a positive ionic state the promotional energy required is somewhat more than twice that for the covalent state, and hybridization may be expected to be somewhat suppressed. If the resonance energy between covalent and ionic states is to be a maximum it is necessary that both states possess the same hybridization, so that positive ionic character can be expected to imply less $s-p$ hybridization.

The precise amount of hybridization will of course vary from molecule to molecule in a complex way. Fortunately, however, a rather simple rule can be constructed which seems consistent with known information and which gives the quadrupole coupling constants in halogens to fairly satisfactory accuracy. The values of the ionicity given in column 5 of Table III and plotted against electronegativity differences in Fig. 3 were obtained using the following rule. Cl, Br, and I bonds are considered to have 15 percent s character whenever the halogen is bonded to an atom which is more electropositive than the halogen by as much as 0.25 unit; otherwise no hybridization is allowed.

The curve of Fig. 3 is offered then as the best relation between ionicity and electronegativity differences which can be derived from the quadrupole coupling data at this time. The scatter of the data, while not excessive, probably indicates that the bonding in these molecules in somewhat more complex than is suggested by the simple rule governing hybridization given above.

It has been suggested that d orbitals should play a role in the hybrid bonds of some of these molecules. The discussion of the quadrupole coupling data in this paper, however, seems to limit the amount of allowed d character to some 5 percent. Larger amounts of d character would call for still larger and unreasonable amounts of s character, since $s-d$ is the quantity which actually enters into the calculations.

Gordy[15] has proposed that the simple linear relation between ionic character and electronegativity given in Fig. 3 is the more accurate one. Fortunately, a considerable amount of data on diatomic molecules is now available which was not known at the time Gordy discussed ionic character. However, his principal differences with the conclusions presented here seem to come in part from his assuming no hybridization for the halogen bonds except in certain special cases, and in part from the use of a selected list of diatomic and polyatomic molecules. His arguments will be considered briefly here.

The s-shaped curve of Fig. 3 differs appreciably from the simple straight line of Fig. 3 in two regions. In the region of large ionicity recent data on the alkali halides clearly indicate a deviation from the simple linear relationship. The other large difference between the two curves occurs near $|\Delta X|=1$. If, as in this paper, the

[15] See reference 13, p. 284.

only molecules considered are diatomic then the only points available are those corresponding to FCl and FBr. Despite the uncertainty in the determination of the ionicity from the quadrupole coupling data it appears quite difficult to reconcile the FCl and FBr quadrupole coupling constants with the straight line relation shown in Fig. 3.

In his most recent discussion, Gordy does not consider FCl and FBr, because of uncertainty in the correction for positive ionic character and the possible presence of double bond character in these two molecules. It is concluded, however, that some s hybridization is present. The consideration of promotional energy in an earlier section of this paper makes it seem highly unlikely that hybridization would be absent for negatively ionic states and present for positive ionic states as Gordy assumes.

The presence of any considerable amount of double-bond character in FBr and FCl is not indicated by experimental information. Furthermore, if present, double-bond character would have little effect on the quadrupole coupling constant since the most reasonable (but still improbable) type of double bond corresponds simply to an addition of electronic charge to the d orbitals of Br or Cl, and d orbitals make only negligible contributions to the quadrupole coupling constant.

The disqualification of the FCl and FBr quadrupole data on the grounds that a small amount of double bond character may be present is difficult to justify, particularly in view of Gordy's inclusion of data for halogen derivatives of silane and germane. These compounds have been shown to have appreciable amounts of double-bond character[16,17] of a type which materially affects the quadrupole coupling constant, yet Gordy assumes them to be simple single bonds.

The use of polyatomic molecules to establish a relation between ionicity and electronegativity differences seems hazardous in any case because bond interaction effects make it difficult to assign an accurate electronegativity value to an atom forming more than one bond. It appears especially hazardous to use a particular selection of polyatomic molecules such as those picked by Gordy and to ignore others which appear equally reasonable, but which give conflicting results. Partly to avoid these types of difficulty, we have used only gaseous diatomic molecules in the above considerations, and have included all known cases of this type. However, polyatomic molecules for which quadrupole coupling constants are known appear to fit reasonably well into the scheme of ionic character *versus* electronegativity presented above, provided such complications as multiple bonding and bond interactions are allowed for.

The shape of the solid curve in Fig. 3 is significantly affected by the assumption of the presence or absence of hybridization in ICl. The bonding rules used in this paper indicate that the I—Cl bond has 15 percent s character. Gordy has argued that it is implausible to assume the I—Cl bond to be hybrid and the Br—Cl bond to have pure p character because I—Cl has the smaller bond energy. The same point could be used to argue that the I—Cl bond is no more ionic than the Br—Cl bond. The most appropriate comparison is not between the bond energies but between the extra resonance energies which are given by Pauling as 4.0 kcal/mole for ICl and only 0.7 kcal/mole for BrCl. No direct method is available to divide the extra resonance energy between effects due to hybridization and those due to ionicity.

CONCLUSION

Based on consideration of the quadrupole coupling data for the diatomic halide molecules as outlined in this paper, the s shaped curve of Fig. 3 is presented as the best relation between ionicity and electronegativity difference which can be established at present. Although uncertainties due to hybridization effects prevent detailed knowledge of the exact shape of the curve the value of the electronegativity difference at which molecules become completely ionic seems to be well established by the combination of quadrupole coupling and dipole moment data.

[16] J. Sheridan and W. Gordy, J. Chem. Phys. **19**, 965 (1951).
[17] J. M. Mays and B. P. Dailey, J. Chem. Phys. **20**, 1695 (1952).

Structure and Barrier Height of Methyl Mercaptan from Microwave Data*

N. SOLIMENE AND B. P. DAILEY
Department of Chemistry, Columbia University, New York 27, New York
(Received June 11, 1954)

The $0_{00}-1_{01}$ rotational transitions of several isotopic species of methyl mercaptan have been observed. This has permitted a complete determination of the structural parameters of this molecule. The torsional energy levels of $C^{12}H_3S^{32}H$ and $C^{12}D_3S^{32}H$ have been approximately determined by relative intensity measurements. A sinusoidal barrier height has been determined which gives torsional energy levels in agreement with the observed ones.

INTRODUCTION

INFORMATION on hindered rotation phenomena in molecules is of interest to chemists because of its importance to statistical thermodynamics. No consistent understanding of such effects has yet been achieved perhaps because of the difficulties encountered in collecting accurate and reliable values of barrier potentials. Numerous attempts have recently been made to obtain accurate values of such parameters from microwave and other spectral data. In the case of methyl alcohol the interpretation of a series of absorptions in its microwave spectrum involving both the rotational and torsional motions made possible a rather definite and precise determination of the barrier height.[1] Because of its structural similarity to methyl alcohol, methyl mercaptan was thought to be an interesting molecule for use in a microwave study of internal rotation. It is an only slightly asymmetric rotor and has a component of its dipole moment perpendicular to the axis of near symmetry which makes it possible for torsional transition frequencies to appear in the spectrum. Unlike methyl alcohol the $J=0$ to $J=1$ rotational absorption occurs in a conveniently accessible portion of the microwave region. In this investigation the study of these rotational transitions has permitted a complete structural determination and a preliminary determination of the barrier height to internal rotation from intensity measurements of rotational transitions for molecules in different states of torsional vibration.

THE SPECTRA OF SEVERAL ISOTOPIC SPECIES

The spectrometer used in this work was of the conventional Stark modulation type.[2] Square wave modulation at a frequency of 85 kc was used with lock-in phase detection. Frequency measurements were made by interpolating with a communications receiver between frequency markers generated by a crystal controlled standard[3] monitored against the 5-Mc standard frequency broadcast by station WWV.

A lecture bottle of methyl mercaptan purchased from the Matheson Company was the source of the samples used to observe the spectra of the normal species and of the naturally occurring S^{34} and S^{33} isotopically substituted species. The sample of $C^{12}H_3S^{32}D$ was prepared by equilibrating a sample of the commercial methyl mercaptan with D_2O purchased from the Stuart Oxygen Company. The $C^{13}H_3S^{32}H$ and $C^{12}D_3S^{32}H$ samples were prepared by refluxing the corresponding methyl iodides with thiourea for several hours and then hydrolysing the resulting product with sodium hydroxide. The mercaptans thus prepared were then purified by distillation in vacuum. The $C^{13}H_3I$ used in the above was an approximately fifty percent enriched sample purchased from the Eastman Kodak Company. The sample of $C^{12}D_3I$ used in the above was prepared by refluxing deuterated methyl alcohol with phosphorus and iodine. The deuterated methyl alcohol was kindly provided by Dr. J. E. Zanetti.

Methyl mercaptan, which is an almost symmetric rotor of the prolate type, has been observed to have a moderately rich spectrum in the region from 18 000 Mc to 30 000 Mc. Many of the absorptions appeared to have symmetric first order Stark effects. Some of these absorptions are undoubtedly due to simultaneous changes in both the states of the rotational and torsional motions. No attempt has been made to identify these lines. However, the $0_{00}-1_{01}$ transitions of several isotopic species of methyl mercaptan have been identified. The characteristic second order Stark effects of these transitions together with their frequencies computed from a rough model of the structure of methyl mercaptan made the identifications quite certain. The frequencies of this transition for several isotopic species in the ground vibrational state and in the lower excited torsional states are listed in Table I.

A rotational transition does not appear as a single line but rather as a group of lines each corresponding to a different vibrational state of the molecule. The rotational constants which determine the frequency of a rotational transition are functions of the internal coordinates of the molecule. As the molecule vibrates, these coordinates and hence the rotational constants change in time. Since the periods of the rotations of the molecule are much longer than the periods of almost all vibrations, the appropriate rotational constants are those

* Work supported in part by a Signal Corps contract and a grant from the Research Corporation.
[1] D. H. Burkhard and D. M. Dennison, Phys. Rev. **84**, 408 (1951); E. V. Ivash and D. M. Dennison, J. Chem. Phys. **21**, 1804 (1953).
[2] R. H. Hughes and E. B. Wilson, Jr., Phys. Rev. **71**, 562 L (1947); A. H. Sharbaugh, Rev. Sci. Instr. **21**, 120 (1950).
[3] L. C. Hedrick, Rev. Sci. Instr. **24**, 565 (1953).

arrived at by averaging over the vibrational motions.[4] As a consequence, the same molecule in different vibrational states will have slightly different rotational constants and the rotational transitions will therefore have slightly different frequencies. The preceding is summarized for nearly harmonic vibrations by the equation:

$$B_v = B_e - \sum_i \alpha_i (v_i + \tfrac{1}{2} d_i).$$

Here B_e and B_v are, respectively, the rotational constants for the equilibrium configuration and for the vibrational state v given by the quantum numbers v_i for the vibrations with degeneracies d_i. The quantities α_i are to be determined either spectroscopically or in terms of the vibrational potential constants of the molecule. Since torsional vibrations are not generally nearly harmonic, the above formula is not expected to hold. However by analogy we might expect the corrections to B_e to be proportional to the torsional energies. This will be shown to be approximately correct later.

The identification of the satellite lines listed in Table I was based on their proximity to the parent lines and on the similarity of their Stark effects with those of the parent lines. The occurrence of the same pattern for various isotopic species studied tends to confirm their assignment as vibrational satellites.

All the fundamental frequencies except that of the torsional mode are known for the normal species of methyl mercaptan from its infrared and Raman spectra.[5] The three lowest normal frequencies are 700 cm^{-1}, 800 cm^{-1}, and 1050 cm^{-1}. One may therefore expect, clustered about the ground vibrational absorption line, satellites with intensities at room temperature of 1/33, 1/55 and 1/150 of the intensity of the ground state line. Instead, the actually observed satellites are more intense by an order of magnitude. Therefore these may be attributed to the lower excited states of torsion, the frequencies of which are expected to be considerably lower than those of the normal vibrational states.

TABLE I. The $O_{00}-1_{01}$ transition for several isotopic species.

Species	Ground vibrational state	First excited torsional state	Second excited torsional state
$C^{32}H_3S^{32}H$	25 291.8±0.1 Mc 25 290.8[a]	25 219.7±0.1 Mc 25 206.8	25 155.0±0.1 Mc 25 143.6
$C^{32}H_3S^{32}H$	24 388.0 24 387.1	24 318.5 24 306.2	24 256.2 24 245.0
$C^{32}H_3S^{32}D$	24 387.5 24 385.0	24 321.6 24 301.6	
$C^{32}D_3S^{32}H$	20 732.8 20 732.0	20 678.9 20 674.8	20 627.6 20 619.0
$C^{32}H_3S^{34}H$	24 879.1[a] (24 878.9)[b] 24 879.8		
$C^{32}H_3S^{33}H$	25 079.6 25 078.7[c]		

[a] In agreement with T. M. Shaw and J. J. Windle, J. Chem. Phys. 19, 1063 (1951).
[b] G. Bird (private communication).
[c] G. Bird (private communication). Unsplit frequencies determined from quadrupole patterns.

[4] E. B. Wilson, Jr., and J. B. Howard, J. Chem. Phys. 4, 262 (1936).

[5] J. Wagner, Z. physik. Chem. B40, 36 (1938); H. W. Thompson, J. Chem. Phys. 7, 441 (1939); H. W. Thompson and N. P. Skerrett, Trans. Faraday Soc. 36, 812 (1940).

TABLE II. Structural parameters of methyl mercaptan.

	Experimental	Schomaker-Stevenson[a] rule
^dCH	1.1045±0.0020 A	1.06 A
^dSH	1.3298±0.0040 A	1.37 A
^dCS	1.8170±0.0002 A	1.81 A
∠HCH	110° 10′±5′	
∠CSH	100° 20′±10′	

[a] V. Schomaker and D. P. Stevenson, J. Am. Chem. Soc. 63, 37 (1941).

It is to be noted that the absorptions listed in TableI occur in pairs. The reasons for this are to be found by a consideration of the torsional mode of vibration. This vibration corresponds to the hindered rotation of the hydrogen bound to the sulfur about the symmetry axis of the methyl group. The potential function restricting this rotation has a threefold axis of symmetry due to the symmetry of the methyl group. As a result of the threefold symmetry of the potential, the states of torsional vibration occur in sets of three.[1,6] For symmetric rotors in rotational states for which the projection of the total angular momentum on the symmetry axis is zero, two of these three torsional states can be shown to be necessarily degenerate.[6] The twofold degenerate level is of symmetry E and the nondegenerate level is of symmetry A with respect to the coordinate describing the torsional vibration. For rotational states in which the projection of the angular momentum on the symmetry axis is $\pm\hbar K$, there are three doubly degenerate energy levels to a set. One of these levels consists of two A type states and the other two are of the E type. When the asymmetry of a molecule is taken into account the degeneracy of the two A type levels is removed and the E type levels are displaced.[1] The larger the barrier to internal rotation the more closely spaced are the energy levels within a set. The levels within a set become degenerate in the limiting case of an infinitely high barrier. Since the effective rotational constants depend on the vibrational state, the rotational transitions of a nearly symmetric rotor exhibiting restricted internal rotation will consist of doublets if the rotational states involved correspond to symmetric rotor states with $K=0$.

Since methyl mercaptan is very nearly a symmetric rotor, the projection of the angular momentum on the figure axis of the methyl group is very nearly zero for the states involved in the transition studied. Therefore the doublet nature of the observed absorptions is not unexpected and confirms their identification.

STRUCTURE DETERMINATION

The measured values of $B+C$ for the unresolved ground vibrational states of the various isotopic species were used to determine the structure of methyl mer-

[6] H. H. Nielsen, Phys. Rev. 40, 445 (1932); J. S. Koehler and D. M. Dennison, Phys. Rev. 57, 1006 (1940).

TABLE III. Rotational constants.

Species	Calculated for structure in Table II A	B	C	B+C	Observed[a] (Mc) B+C
$C^{12}H_3S^{32}H$	101 862	12 909	12 385	25 294	25 291.3
$C^{13}H_3S^{32}H$	101 861	12 436	11 949	24 385	24 387.6
$C^{12}H_3S^{32}D$	78 030	12 659	11 728	24 387	24 386.4
$C^{12}D_3S^{32}H$	61 160	10 539	10 188	20 737	20 732.3
$C^{12}H_3S^{34}H$	101 782	12 696	12 188	24 884	24 879.4
$C^{12}H_3S^{33}H$	101 822	12 799	12 284	25 083	25 079.2

[a] Unresolved ground vibrational state values.

captan. The quantity $B+C$ was expanded for each of the isotopic species to first order in the deviations from the assumed structural parameters of a rough model. The coefficients for this expansion were obtained numerically. These expressions for $B+C$ when set equal to the observed values result in a set of linear equations in terms of the deviations from the assumed model. The solution of this set of equations corrects the assumed structural parameters. The corrected parameters may then be used as the basis of a new expansion in the event that they do not yield the experimentally observed values of $B+C$. This procedure generally converges quite rapidly.

However this procedure does not lead to a unique structure for the molecule methyl mercaptan. It is possible to vary the SH distance and the CSH angle considerably without affecting the values of $B+C$ for the various isotopic species although B and C separately change. The reason for this behavior is that the hydrogen bonded to the sulfur atom is the only atom contributing to the asymmetry of the molecule.

It was therefore considered worthwhile to make the observations, which are difficult on the available apparatus, leading to the determination of B and C separately for at least one molecular species. A search for the $J=1$ to $J=2$ transition of $C^{12}H_3S^{32}H$ was made using the second harmonic of K-band klystrons. The frequency measurements were made at the fundamental. The following transitions were observed:

$$1_{10}-2_{11}=3B+C=51\ 104.8\pm0.2\ \text{Mc},$$
$$1_{11}-2_{12}=B+3C=50\ 059.0.$$

It was not possible to observe any fine structure as in the $0_{00}-1_{01}$ transitions, nor were any satellite absorptions observed. Since the sum of the $1_{10}-2_{11}$ and $1_{11}-2_{12}$ frequencies is, within experimental error, four times the $0_{00}-1_{12}$ frequency, the identification is quite certain. The qualitative Stark effects of these lines are also consistent with their identification. Using these frequencies, it is found that $B=12\ 907.1$ Mc and $C=12\ 383.1$ Mc for $C^{12}H_3S^{32}H$.

The above values of B and C make it possible to uniquely fix the position of the hydrogen bonded to the sulfur atom and thus completely determine the structure. The results are summarized in Tables II and III. The effects of zero point vibrations were completely neglected in the determination of this structure. The neglect of these effects may contribute errors as large or larger than those given in Table II.

DETERMINATION OF THE TORSIONAL ENERGY LEVELS

The ratio of the peak intensities, ρ, of the same rotational absorption of a molecular species in two vibrational states, v_1 and v_2, is given to a good approximation by[7]:

$$\rho=(g_1/g_2)e^{-(E_1-E_2)/kT},$$

where g_1 and g_2 are the statistical weights of the two vibrational states. Using this formula, it is possible to obtain the energy difference between two vibrational states by measuring ρ for at least one temperature when g_1 and g_2 are known or for two or more temperatures when g_1 and g_2 are not known.

The statistical weights of the A and E type torsional vibrational states are given in Table IV for a molecule of the symmetry of methyl mercaptan with three identical nuclei having spin I. This table was constructed using the standard group theoretical methods.[8] The statistical weights given for spin equal to $\frac{1}{2}$ apply to CH_3SH.

In this work relative intensities were measured by repeatedly recording the portion of the spectrum of interest with a recording milliammeter, maintaining constant gain, constant microwave power input, etc., and comparing the peak deflections. The intensity ratios thus measured are subject to numerous errors. Among the sources of error are the nonlinearity of the detecting, amplifying and recording apparatus and the fluctuations in the over-all gain of the apparatus due to fluctuations in the voltage supplies and in the detector efficiency. Also, because of the frequency instability of the microwave power source, it was impossible to drive the frequency tuning screw slowly enough through an absorption to permit the recording pen to attain its maximum deflection. This effect is partially compensated for by the use of ratios of peak deflections. An estimate of the magnitude of the errors contributed by the above was obtained by repeatedly recording the quadrupole hyperfine pattern of the methyl chloride transitions. The relative intensities of such transitions are theoretically known. It was found that the observed relative intensities of these transitions agreed to better than

TABLE IIIa. Moments of inertia for structure in Table II.

Species	$I_A\times10^{40}$ gcm²	$I_B\times10^{40}$ gcm²	$I_C\times10^{40}$ gcm²
$C^{12}H_3S^{32}H$	8.236	64.987	67.733
$C^{13}H_3S^{32}H$	8.236	67.461	70.207
$C^{12}H_3S^{32}D$	10.751	66.268	71.529
$C^{12}D_3S^{32}H$	13.717	79.598	82.343
$C^{12}H_3S^{34}H$	8.242	66.077	68.829
$C^{12}H_3S^{33}H$	8.239	65.544	68.293

[7] J. H. Van Vleck and V. F. Weiskopf, Revs. Modern Phys. 17, 227 (1945); Strandberg, Wentink, and Hill, Phys. Rev. 74, 827 (1949).

[8] E. B. Wilson, Jr., J. Chem. Phys. 3, 276 (1935).

twenty percent with theoretical expectations. The apparent intensity of a line will also be affected by the presence of standing waves in the absorption cell. The standing waves are caused by reflections from the Stark septum in the cell and by improper impedance matching to and from the cell. The standing wave ratio is generally a slowly varying function of frequency. When the lines whose relative intensities are being measured are not at very different frequencies, this effect will not contribute appreciably to the error. However, when the lines are not closely spaced, this effect may lead to errors as large as twenty five percent in the intensity ratio.[9]

The frequencies of the lower-lying excited torsional states relative to the ground state, determined from intensity ratio measurements at room temperature, are listed in Table V for the molecules $C^{12}H_3S^{32}H$ and $C^{12}D_3S^{32}H$. It was not possible to measure the relative intensities of the absorptions of the molecule $C^{12}H_3S^{32}D$ because of the rapid exchange of the deuterium with moisture on the cell walls which resulted in a loss of the sample during the course of observation. At the time the spectrum of $C^{13}H_3S^{32}H$ was investigated, relative intensity measurements were impossible because of instrumental difficulties. For the other isotopic species the satellite lines were not sufficiently intense to permit relative intensity data to be obtained. The uncertainty of twenty percent in the frequencies of the torsional states is almost entirely due to the uncertainty in the intensity ratio data. The calculated frequencies in the last column of Table V will be discussed in the next section.

TABLE V. Torsional energy levels for states with $K_1=0$.

Molecule	n[a]	$\lvert K-m\rvert$[b]	Sym.	Experimental (cm^{-1})	Calculated[c] (cm^{-1})
$C^{12}H_3S^{32}H$	0	0	A	0[d]	0
	0	1	E	...	1.6
	1	2	E	157±20%	175
	1	3	A	209	203
	2	3	A	319	283
	2	4	E	339	345
$C^{12}D_3S^{32}H$	0	0	A	0[d]	0
	0	1	E	...	0.80
	1	2	E	187±20%	165
	1	3	A	191	180
	2	3	A	237	269
	2	4	E	336	316

[a] n if quantum number for limiting harmonic oscillator.
[b] K_1 and m are quantum numbers for limiting prolate symmetric internal rotator.
[c] Using $V_0=371$ cm^{-1} and assuming methyl mercaptan to be a symmetric rotor.
[d] All levels measured relative to lowest.

SINUSOIDAL BARRIER HEIGHT DETERMINATION

In the preceding section the lower torsional energy levels have been approximately determined. In order to obtain a value for the height of the barrier to internal rotation from these levels it is necessary to make some assumption as to the nature of the hindering potential. It is customary and mathematically convenient to assume a potential of the form:

$$V(x)=\tfrac{1}{2}V_0(1-\cos 3x),$$

where x is the angle describing the restricted rotation and V_0 is the "barrier height." With this assumption the energy levels may be calculated as functions of V_0. These are used below to find the value of V_0 which best fits the data in Table V.

The energy levels of internal motion for molecules with one symmetric top attached to a rigid molecular frame capable of internally rotating about its axis, which is a threefold axis of symmetry for a sinusoidal hindering potential, are given in terms of the eigenvalues of

$$d^2M(x)/dx^2+(a+2\theta\cos 3x)M(x)=0,$$

where $M(x)=e^{i\sigma x}P(x)$, $P(x+2\pi)=P(x)$ and σ is determined by boundary conditions.[10]

$$\theta=(z\pi^2c/h)I_D\Omega V_0,$$
$$\Omega=1-I_D[\lambda_A{}^2/I_A+\lambda_B{}^2/I_B+\lambda_C{}^2/I_C],$$

I_A, I_B, I_C = principal moments of inertia,
$\lambda_A, \lambda_B, \lambda_C$ = direction cosines of the axis of attached symmetric top with respect to principal axes.
I_D = moment of inertia of attached symmetric top about its axis.

$$W_r=(h/8\pi^2cI_D\Omega)(a_r+2\theta).$$

The pseudo quantum number, r, may be given, for example, by K and m, the limiting free internal rotor quantum numbers and n, the limiting harmonic oscillator quantum number. The total wave function describing the molecular motion must not change for a change of 2π in x, the angle describing the internal motion. Since the variables describing the over-all rotation in this representation are not only functions of the Eulerian angles of the rigid frame of the molecule but also of x; when x changes they will also change. Therefore the factor $e^{2\pi i\sigma}$ must compensate for the changes in that part of the wave function which describes the over-all rotation produced by replacing x with $x+2\pi$ in order to satisfy the boundary condition. For a general rotor of the type described above explicit values of σ as a function of the over-all rotational state cannot be given. However, for a symmetric rotor:

$$I_D\Omega=I_D(I-I_D)/I=I_1I_2/I$$

and

$$\sigma=-KI_1/I,$$

TABLE IV. Statistical weights.

Spin	g_A	g_E
I	$\frac{1}{2}(2I+1)[(2I+1)^2+2]$	$\frac{1}{2}(2I+1)[2(2I+1)^2-2]$
0	1	0
$\frac{1}{2}$	4	4
1	11	16

[9] D. H. Baird and G. Bird, Rev. Sci. Instr. **25**, 319 (1954).

[10] K. S. Pitzer and W. D. Gwinn, J. Chem. Phys. **10**, 428 (1942).

TABLE VI.

	$C^{12}H_3S^{32}H$	$C^{12}D_3S^{32}H$
I_1	2.805×10^{-40} gcm²	2.805×10^{-40} gcm²
I_2	5.490×10^{-40} gcm²	10.971×10^{-40} gcm²
I[a]	8.293×10^{-40} gcm²	13.778×10^{-40} gcm²
I_1I_2/I	1.857×10^{-40} gcm²	2.234×10^{-40} gcm²
V_0	$60.28\,\theta$ cm^{-1}	$50.12\,\theta$ cm^{-1}
W_r	$15.07\,(\alpha_r+2\theta)$ cm^{-1}	$12.53\,(\alpha_r+2\theta)$ cm^{-1}

[a] Moment of inertia about CS bond.

where $I_D=I_2$ and $I=I_1+I_2$ is the moment of inertia about the symmetry axis and $\hbar K$ is the projection of over-all angular momentum on this axis. In the treatments of Dennison and co-workers[1,6] or Crawford,[11] the problem of determining σ for the asymmetric rotor is avoided by using representations in which the internal rotation is not formally separated from the over-all rotation and it is possible to choose $\sigma=-KI_1/I$ or $\sigma=0$ respectively and to treat the interaction terms, which appear explicitly in the Hamiltonian, by perturbation theory.

For methyl mercaptan the approximation will be made that the torsional energy levels are those of a symmetric top with internal motion. Since for the transition studied the rotational states involved correspond closely to those of a symmetric rotor with $K=0$, σ will be set equal to zero. The levels of type A for a symmetric rotor with $\sigma=0$ have been tabulated.[12] However, the levels of type E with $\sigma=0$ have not been tabulated. The lowest four eigenvalues of type E for $\sigma=0$ have been computed to four decimal places for values of θ from 0.0 to 25.0 in intervals of 0.1 by solving for the roots of continued fractions similar to those given in Koehler and Dennison.[6,13] The computation was performed by punched card methods using the facilities of the Watson Scientific Computation Laboratory. The values of $\alpha_r-\alpha_0$ are plotted *versus* $\theta\leq12$ in Fig. 1 for both the A and E levels where α_0 is the lowest eigenvalue for each value of θ. The tabulation of α_r as a function of θ for the E levels is not given here because of its bulk.

From the structural data the constants I_1I_2/I_1 have been computed for $C^{12}H_3S^{32}H$ and $C^{12}D_3S^{32}H$ where the moments of inertia are taken about the CS axis. These relate the sinusoidal barrier height, V_0, and the torsional energies to θ and the eigenvalues α_r. The numerical values, which are listed in Table VI, are used to reduce the experimentally measured energies to dimensionless units. The dimensionless energy differences are listed in Table VII in the column headed $a_{n,|m|}-a_{0,0}$. The values of θ corresponding to those eigenvalue differences were found by reference to Fig. 1 or more precisely by reference to the table from which Fig. 1 was constructed. These values of θ (and correspondingly of V_0) are also listed in Table VII. The weighted averages of the V_0's corresponding to the various measured energy differences were computed for the two isotopic species separately. Since the potential barrier is a function of the electronic distribution which to a very good approximation is independent of the isotopic species being considered, it is expected to be the same for the two isotopic species. Indeed the weighted averages for the two species agree remarkably well (see Table VII) in view of the scatter of the individual values. Therefore the combined weighted average of $(1.06\pm0.12)\times10^3$ cal/mole is considered to be the best value for the barrier height.

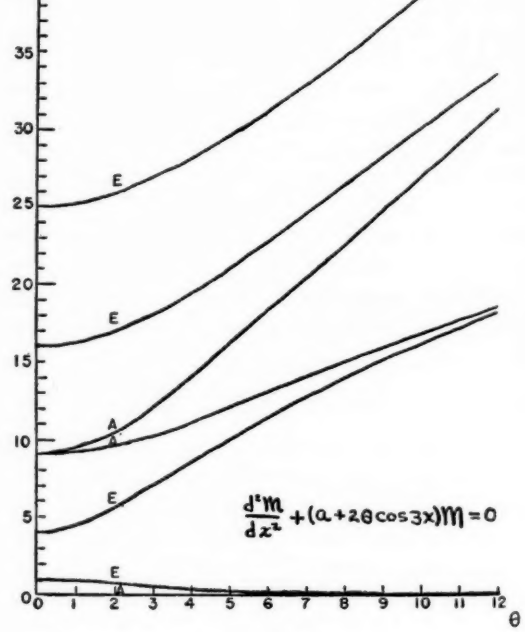

FIG. 1.

TABLE VII.

Molecule	n	$\lvert m\rvert$	$\alpha_{n,\lvert m\rvert}-\alpha_{0,0}$	Corresponding θ	V_0 cm^{-1}
$C^{12}H_3S^{32}H$	1	2	10.4±20%	5.3 (6.8−3.9)	319 (410−235)
	1	3	13.9	6.9 (9.9−4.1)	415 (597−247)
	2	3	21.2	7.3 (9.3−5.5)	440 (561−332)
	2	4	22.5	5.9 (8.3−3.0)	355 (500−181)
$C^{12}D_3S^{32}H$	1	2	14.9±20%	8.9 (11.9−6.4)	446 (596−321)
	1	3	15.2	8.3 (11.8−5.1)	416 (591−256)
	2	3	18.9	6.3 (8.1−4.5)	316 (406−226)
	2	4	26.8	8.2 (11.2−5.3)	411 (561−266)

$V_0(C^{12}H_3S^{32}H)_{\text{wtd av}}=368\pm60$ cm^{-1}.
$V_0(C^{12}D_3S^{32}H)_{\text{wtd av}}=373\pm62$ cm^{-1}.
$V_{0\text{weighted average}}=371\pm43$ cm^{-1}
$=1.06\pm0.12$ kcal/mole.

[11] B. L. Crawford, J. Chem. Phys. **8**, 273 (1940).

[12] *Tables Relating to Mathieu Functions* (Columbia University Press, New York, 1951) or see E. B. Wilson, Jr., Chem. Revs. **27**, 17 (1940).

[13] Stratton, Morse, Chu, and Hutner, *Elliptic Cylinder and Spherical Wave Functions* (John Wiley and Sons, Inc., New York, 1941).

RESULTS AND CONCLUSIONS

The structure of methyl mercaptan has been determined. The bond distances computed with the Schomaker-Stevenson rule, listed in Table II, are in rough agreement with the experimental values. The SH distance is slightly larger than that in H_2S and the CSH angle is larger than the H_2S angle.[14] However, the CSH angle is not quite as large as the SSS angle in S_8 indicating an intermediate degree of hybridization.

The sinusoidal barrier height has been determined from the torsional energy levels obtained from intensity measurements. The value determined in this work is in rough agreement with the value 1.46 ± 0.27 kcal/mole determined from entropy measurements.[15] While the data given in Table V are consistent, within experimental error, with the sinusoidal potential shape assumption, it is not sufficiently precise to rule out the possibility of other barrier shapes.

The barrier height determined in this work is surprisingly close to the more precisely known barrier for the similar molecule CH_3OH.[1] One might expect a somewhat smaller barrier for CH_3SH since the CS distance is about 0.4 A longer than the CO distance in CH_3OH. Also the bond moment of SH, 0.68 debyes, is smaller than the bond moment of OH, 1.57 debyes. In the Lassettre and Dean[16] treatment, the barrier is accounted for mainly by the interaction of the bond electric dipole and electric quadrupole moments of the mutually rotating bonds. If this theory is valid the additional interaction must be due to the greater magnitudes of the quadrupole and higher moments for the SH bond compared to the OH bond.

TABLE VIII.

	$\Delta\nu$ (Mc)	ΔE (cm^{-1})	$r=\Delta\nu/\Delta E$
$C^{12}H_3S^{32}H$	71.6	175	0.409
	84.5	203	0.416
	136.3	283	0.483
	147.7	345	0.429
$C^{12}D_3S^{32}H$	53.5	165	0.324
	57.6	180	0.320
	104.8	269	0.390
	113.4	316	0.359

$r_{Av}(C^{12}H_3S^{32}H)=0.434$.
$r_{Av}(C^{12}D_3S^{32}H)=0.348$.

As was mentioned previously the variation of the rotational constants from one torsional state to another might be expected to be roughly proportional to the torsional energy difference.[17] In Table VIII $\Delta\nu$, the frequency separations of the satellite lines from the unresolved ground state lines, are listed together with ΔE, the corresponding calculated torsional energy differences from Table V. The ratio r, listed in the last column, is constant to within ten percent for each of the two species. In view of the various assumptions and the uncertainty in the torsional energy differences, this is quite remarkable. Because of this an attempt was made to determine the barrier height on the assumption of strict proportionality. However the results were not internally consistent.

[14] C. A. Burrus, Jr., and W. Gordy, Phys. Rev. **92**, 274 (1953).
[15] Russell, Osborne, and Yost, J. Am. Chem. Soc. **64**, 165 (1942).
[16] E. N. Lassettre and L. B. Dean, Jr., J. Chem. Phys. **17**, 317 (1949).
[17] J. Sheridan and W. Gordy, J. Chem. Phys. **19**, 965 (1951).

Spectroscopic Studies of Rotational Isomerism in Fluorinated Ethanes. II. 1,2-Dibromo-1,1,2,2-Tetrafluoroethane

R. E. KAGARISE AND L. W. DAASCH
Naval Research Laboratory, Washington 25, D. C.

(Received June 14, 1954)

The Raman spectrum of liquid CF_2Br-CF_2Br has been investigated, and the observed frequency shifts ($\Delta\nu$ cm^{-1}), relative intensities and depolarization factors are presented. The infrared absorption spectrum of the liquid in the 2–34μ region, and of the solid and vapor in the 2–22μ region have also been studied.

On the basis of observations of the Raman spectrum of the liquid and the infrared spectrum of the vapor, liquid, and solid it is concluded that CF_2Br-CF_2Br exists as two isomeric species. Of these, the *trans*-form (C_{2H}) is the more stable, while the *gauche*-(C_2) is probably the higher energy form. The value of $\Delta H°$ for the reaction *trans*-(C_{2H})→*gauche*-(C_2) was found to be 925±50 calories/mole in the liquid and 945±50 calories/mole in the vapor state.

1. INTRODUCTION

ON the basis of the established general theory, one would expect the existence of rotational isomers in substituted ethanes for which the C_3 symmetry of both end groups is destroyed, as in the case of sym-dibromotetrafluoroethane. Glockler and Sage[1] have previously studied the Raman spectrum of liquid CF_2Br-CF_2Br at room temperature. Solely on the basis of the number of lines observed, they conclude that two isomers are present, namely, the *trans*-(C_{2H}) and *gauche*-(C_2) forms.

To the best of our knowledge the infrared spectrum has never been reported in the literature.

TABLE I. Raman spectrum of liquid CF_2Br-CF_2Br. (+) Indicates relative intensity increases at lower temperature. (−) Indicates relative intensity decreases at lower temperature.

Present work		Glockler and Sage[a]
$\Delta\nu$ cm^{-1}	Temperature-Intensity	$\Delta\nu$ cm^{-1}
70 (20, *dp*)		63.4 (4)
119 (5, −)[b]		
179 (100, 0.4)	(+)	179.0 (10)
263 (5, −)[b]		272.0 (1)
283 (20 *dp*?)	(−)	282.9 (4)
309 (10, *P*)		309.5 (1)
321 (100, 0.4)	(+)	320.2 (10)
334 (1, −)		334.2 (2)
343 (50, 0.1)	(−)	342.5 (6)
367 (40, 0.4)	(+)	367.3 (7)
466 (5, −)		465.3 (2)
525 (1, −)		525.0 (2)
650 (20, 0.25)	(−)	648.3 (5)
683 (50, 0.20)	(+)	679.1 (6)
690 (40, 0.20)	(+)	687.8 (4)
		733.2 (0)
872 (5, −)		871.0 (2)
922 (1, −)[c]		
967 (1, −)[b]		964.4 (0)
1004 (30, *P*)		1003.7 (3)
1024 (100, 0.50)	(+)	1021.2 (10)
1100 (5, −)		1098.5 (2)
1164 (10, −)		1162.4 (2)
1249 (5, −)		1249.4 (2)

[a] See reference 1.
[b] Excited by λ4347.
[c] Excited by λ4339.

[1] G. Glockler and C. G. Sage, J. Chem. Phys. 9, 387 (1941).

2. EXPERIMENTAL RESULTS

The spectral measurements were made with the same instruments and in the same manner as described in the first paper of this series.[2] The sample used in this work was prepared and purified by Dr. W. T. Miller of Cornell University, Ithaca, New York, and had a boiling point of 46°C at atmospheric pressure.

The observed Raman shifts ($\Delta\nu$ cm^{-1}) corrected to vacuum, depolarization factors, and relative intensities for liquid CF_2Br-CF_2Br at 30°C are listed in Table I. The results of Glockler and Sage[1] are also given for comparison.

In addition the Raman spectrum of the liquid was observed (using the photoelectric portion of the instrument) at five different temperatures ranging from −100°C to +70°C. The qualitative results of this study are listed in Table I under the Temperature-Intensity heading. Those Raman lines which increase in relative intensity as the temperature is lowered are due to the more stable isomer; those which decrease to the less stable form.

The value of $\Delta H°$, for the reaction C_{2H} dibromotetrafluoroethane→C_2 dibromotetrafluoroethane can be evaluated by means of the expression

$$K=\frac{N_{C_2}}{N_{C_{2H}}}=K_1\cdot e^{-\Delta H°/RT} \qquad (1)$$

where $\Delta H°$ is positive and measured in cal/mole, R is the gas constant, and N_{C_2} and $N_{C_{2H}}$ are the number of molecules existing in the *gauche*- and *trans*-forms, respectively. (The symmetry and relative stability of the two isomeric forms have been tentatively assumed for discussion purposes.) Since the intensity of a Raman line is proportional to the number of molecules per unit volume, Eq. (1) may be rewritten in the following form:

$$\frac{I_{C_2}}{I_{C_{2H}}}=K_2e^{-\Delta H°/RT} \qquad (2)$$

[2] R. E. Kagarise and L. W. Daasch, J. Chem. Phys. (to be published).

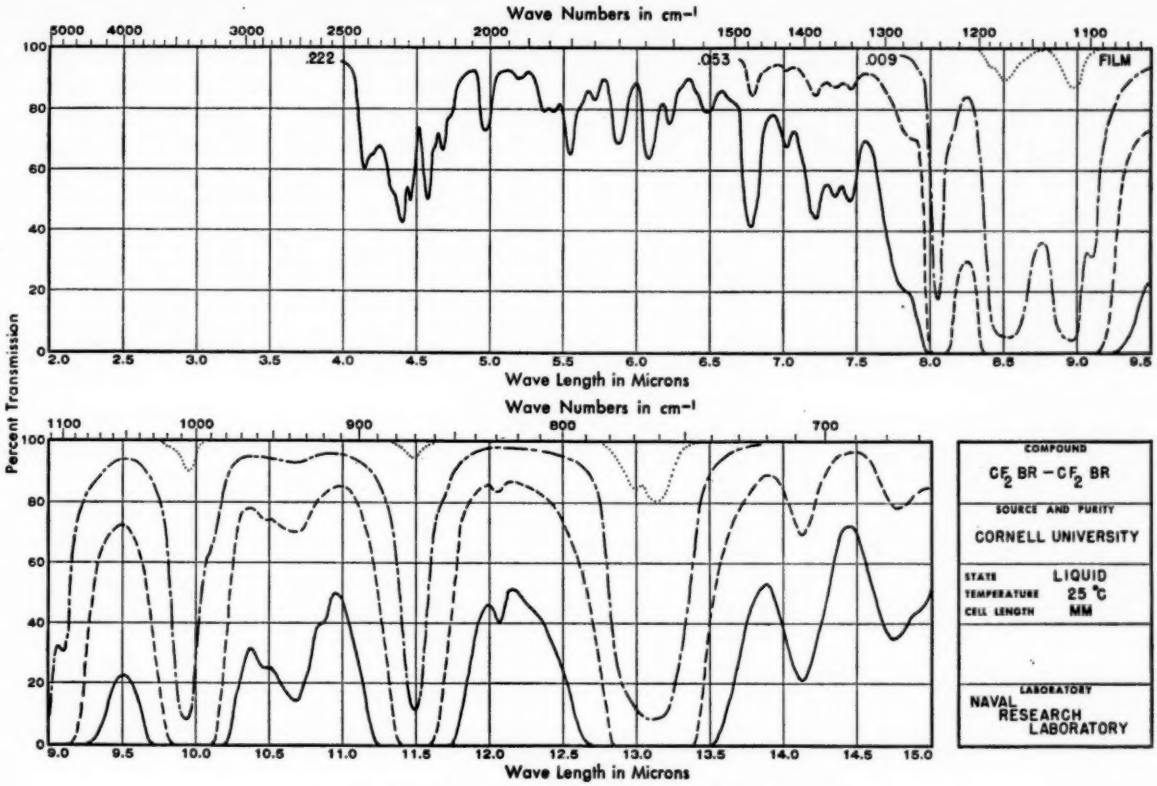

FIG. 1. Infrared spectrum of liquid CF_2Br-CF_2Br (2–15).

where I_{C_2} is the intensity of a line arising from the *gauche*-C_2 form, and $I_{C_{2H}}$ is the intensity of a line due to the *trans*-C_{2H} form. When the ratio $I_{C_{2H}}/I_{C_2}$ is known for several temperatures a least square method for $\log I_{C_{2H}}/I_{C_2}$ and $1/RT$ gives the best value of $\Delta H°$.

The ratios of the peak intensities of two line pairs (367 cm^{-1}/343 cm^{-1} and 321 cm^{-1}/343 cm^{-1}) were measured at five different temperatures and yielded l.m.s. values of $\Delta H°=900$ and 950 calories/mole, respectively.* Thus the average observed energy difference between the two isomeric forms in the liquid state is 925 ± 50 calories/mole.

The infrared absorption spectrum of liquid CF_2Br-CF_2Br is shown in Figs. 1 and 2, while the wave lengths and wave numbers of the observed absorption maxima are given in Table II.

In addition, intensity studies of the infrared spectrum of the vapor were carried out at temperatures varying from 35°C to 190°C. Strictly speaking, one should use integrated intensities rather than peak absorbance values when applying the observed data to Eq. (1). However, Bernstein[3] has pointed out that in the case of dichloroethane there is no significant difference between the results obtained with peak or integrated intensities. For the sake of simplicity, peak intensities were used in this work.

The ratios of the peak intensities of two line pairs (763 cm^{-1}/1007 cm^{-1} and 763 cm^{-1}/870 cm^{-1}) were measured at nine different temperatures and least square solutions of the data yielded values of $\Delta H°=1000$ and 890 calories/mole, respectively. Thus in the vapor phase, the average value of $\Delta H°$ for the reaction CF_2Br-CF_2Br (*trans*)$\rightarrow CF_2Br-CF_2Br$ (*gauche*) is 945 ± 50 calories/mole.

By means of a low-temperature cell similar to the one described by Lord, McDonald, and Miller,[4] the infrared spectrum of CF_2Br-CF_2Br at −180°C was observed. As expected, there was a marked simplification in the spectrum upon solidification, as is evident from an examination of Fig. 3. The strong bands at 9.93, 11.49, 15.38, 16.65, and 21.42μ in the liquid phase disappear completely upon solidification.

From the measurements of intensity variation with temperature in the vapor and liquid phases and the changes in the spectrum upon crystallization it is possible to separate the lines arising from the two isomeric species present. Thus those lines designated (+) in the tables are due to the more stable; those designated (−) to the less stable form.

* Similar measurements of the line pair at 179/343 cm^{-1} yielded a value of $\Delta H°=875$ calories/mole. However, since the intensity ratio of two Raman bands is a function of temperature irrespective of concentration and becomes appreciable for Raman bands widely different in frequency shift, this value of $\Delta H°$ is not strictly comparable with the two values listed above.

[3] H. J. Bernstein, J. Chem. Phys. **17**, 258 (1949).

[4] Lord, McDonald, and Miller, J. Opt. Soc. Am. **42**, 149 (1952).

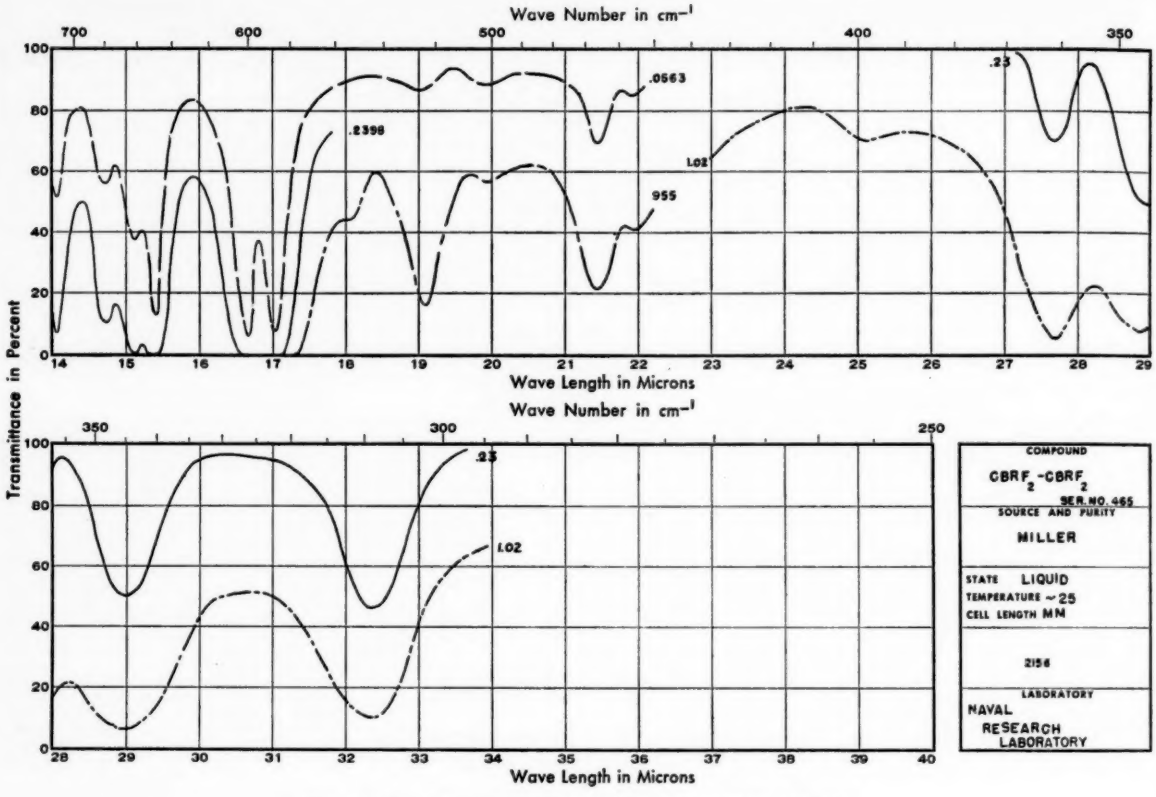

FIG. 2. Infrared spectrum of liquid CF_2Br-CF_2Br (15–34).

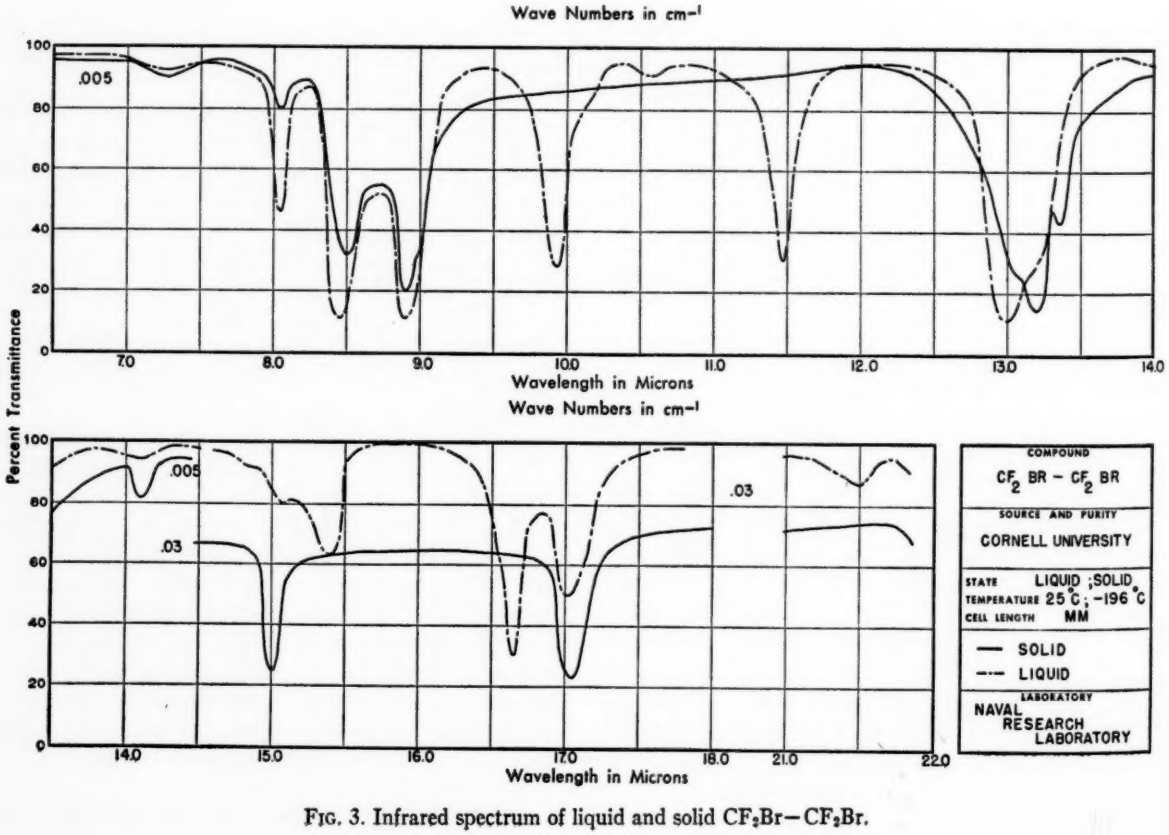

FIG. 3. Infrared spectrum of liquid and solid CF_2Br-CF_2Br.

3. DISCUSSION OF RESULTS

From the observed effects of temperature and change of state upon the relative intensities of the Raman and infrared bands, it appears certain that two stable isomeric species of CF_2Br-CF_2Br exist. Numerous studies in the past of similar molecules (e.g., CH_2Cl-CH_2Cl, CH_2Br-CH_2Br, $CHCl_2-CHCl_2$, etc.) have shown that, without exception, the stable configurations are the staggered *trans*- and *gauche*-forms. Let us, therefore, examine the vibrational spectrum of CF_2Br-CF_2Br on this premise.

Since the molecule under consideration consists of eight atoms, there are eighteen fundamental modes of vibration. For the *trans*-form, which has C_{2h} symmetry, these are divided into four species: $6A_G$, $4A_U$, $3B_G$, and $5B_U$. Species A_G and B_G are Raman active only, while A_U and B_U type modes are infrared active only. For the *gauche*- or *skew*-form, belonging to the point group C_2, the eighteen fundamental modes of vibration are divided into two species, $10A$ and $8B$, both of which are Raman and infrared active. Furthermore, vibrations in classes A_G and A should give rise to polarized Raman lines.

Of the nineteen Raman lines observed experimentally, ten were found to be polarized, two depolarized, and seven too weak for reliable measurements. Because of the limited quantity of sample available and the inherent weakness of Raman scattering in fluorinated hydrocarbons, satisfactory exposures for depolarization measurements on weak lines were prohibitively long.

An examination of Table III shows immediately that the rule of mutual exclusion is satisfied by the group of lines due to the more stable isomer, i.e., those lines designated (+). It appears certain, therefore, that the *trans*-C_{2h} form is the more stable form, since it is the only conceivable structure for CF_2Br-CF_2Br that has a center of symmetry.

Unfortunately, the spectroscopic data is not sufficiently complete to permit an assignment of the vibrational modes or to unambiguously determine the symmetry of the less stable form. All that can be said at present is that if the intramolecular forces in CF_2Br-CF_2Br are defined by a three-minima potential function, then the two equivalent *gauche*-forms (they are optical isomers) constitute the second isomer.

Comparing the values of $\Delta H°$ obtained for the liquid and vapor phases, one observes that the two values are practically equal, as predicted by the theory of Morino *et al.*[5] According to this theory, which is based primarily on the work of Onsager,[6] the energy of interaction δE is given by

$$\delta E = \Delta H°_{\text{liquid}} - \Delta H°_{\text{vapor}} = -\frac{\epsilon-1}{2\epsilon+1}\cdot\frac{\mu^2}{a^3}$$

where μ is the dipole moment of the *gauche*-form, ϵ the dielectric constant, and a the molecular radius. Assuming that the C−F and C−Br bond moments are 1.92 and 2.00D, respectively, and further that all angles

TABLE II. Infrared absorption spectrum of liquid CF_2Br-CF_2Br.

λ(μ)	ν(cm⁻¹)	λ(μ)	ν(cm⁻¹)
4.14 m	2415	8.93 vs	1120
4.18 w	2392	9.10 m	1099
4.40 m	2273	9.93 vs	1007
4.46 w	2242	10.47 m	955
4.57 m	2188	10.66 m	938
4.68 w	2137	11.49 vs	870
4.97 w	2012	12.06 m	829
5.18 vw	1930	13.04 vs	767
5.37 w	1862	13.10 vs	761
5.43 w	1842	14.12 m	708
5.54 m	1805	14.78 m	676
5.72 w	1748	15.17 m	659
5.87 m	1703	15.38 s	650
6.08 m	1645	16.65 s	600
6.21 w	1610	17.02 s	587
6.48 w	1543	18.10 w	552
6.78 m	1475	19.12 m	523
7.03 w	1422	19.93 w	502
7.22 m	1385	21.42 m	467
7.36 m	1359	21.92 w	456
7.46 m	1340	25.12 w	398
7.85 w	1274	27.68 m	361
8.05 s	1242	28.98 m	345
8.53 vs	1172	32.36 w	309

TABLE III. Comparison of Raman and infrared spectrum of liquid CF_2Br-CF_2Br.

Raman	Infrared
1249 (5)	
	(+) 1242 s
	(+) 1172 vs
1164 (1)	
	(+) 1120 vs
1100 (5)	(−) 1099 m
(+) 1024 (100, 0.5)	
1004 (30, *p*)	(−) 1007 vs
	955 m
	938 m
872 (5)	(−) 870 vs
	829 m
	(+) 767 vs
	(+) 761 vs
	(+) 708 m
(+) 690 (40, 0.2)	
(+) 683 (50, 0.2)	
	(−) 676 m
	(+) 659 m
(−) 650 (20, 0.25)	(−) 650 s
	(−) 601 s
	(+) 587 s
	552 w
525 (1)	(−) 523 m
466 (5)	(−) 467 m
	398 w
(+) 367 (40, 0.4)	361 w
(−) 343 (50, 0.1)	345 m
334 (1)	
(+) 321 (100, 0.4)	
309 (10, *P*)	309 w
(−) 283 (20, *dp*?)	
(+) 179 (100, 0.4)	
119 (5, *dp*)	
70 (20, *dp*)	

[5] Morino, Mizushima, Kuratani, and Katayama, J. Chem. Phys. **18**, 754 (1950).

[6] L. Onsager, J. Am. Chem. Soc. **58**, 1486 (1936).

are tetrahedral, one finds the moment of the *gauche*-form to be $0.25D$. Using the maximum value for $(\epsilon-1)/(2\epsilon+1)$, namely 0.5, and a value of $a^3=5\times10^{-23}$ cm^3, the magnitude of δE is 10 calories/mole, which agrees with the observed equality of $\Delta H°$ in the liquid and vapor phases.

4. CONCLUSIONS

There are two rotational isomers present in CF_2Br-CF_2Br in both the liquid and vapor phases. Of these two, the *trans*-isomer of symmetry C_{2h} is the more stable form. This conclusion follows from the fact that the Raman and infrared lines arising from the more stable form obey the rule of mutual exclusion.

The spectroscopic data are not sufficient to permit a conclusive identification of the less stable isomer. However, in view of previous results with related molecules such as 1,2-dichloro- and dibromoethane, the *gauche*-form (C_2) is probably the second form.

Neglecting differences in the rotational and vibrational partition functions and zero-point energy, the energy difference between the two forms is 945±50 calories/mole in the gas and 925±50 calories/mole in the liquid state.

THE JOURNAL OF CHEMICAL PHYSICS VOLUME 23, NUMBER 1 JANUARY, 1955

Dielectric Constants of Liquid and Solid Hydrogen Sulfide

S. HAVRILIAK, R. W. SWENSON,* AND R. H. COLE
Metcalf Chemical Laboratories, Brown University, Providence, Rhode Island

(Received June 18, 1954)

The equilibrium dielectric constants of the disordered highest temperature solid phase show a regular increase with decreasing temperature which is in moderate agreement with Onsager's equation. Larger values than would be expected on this basis are found in the intermediate solid phase, while the values in the ordered phase below 103°K are a little larger than the square of the estimated refractive index. No evidence of relaxation effects or of electrode polarization was found in the frequency range from 15 c/s to 500 kc/s studied.

I. INTRODUCTION

THE relatively large dielectric constants reported for the higher temperature solid phases of hydrogen sulfide indicate that, as in solid hydrogen bromide,[1] and chloride,[2] there is considerable freedom for reorientation of the molecules in the structures. For the hydrogen halides it has been found that the equilibrium dielectric constants have a simple temperature dependence in the face centered cubic phases stable just below the melting point, and that the values are in fair quantitative agreement with Onsager's equation[3] for polar liquids. Since hydrogen sulfide also crystallizes in cubic close packing, it is of interest to make a similar examination of the dielectric data in this case.

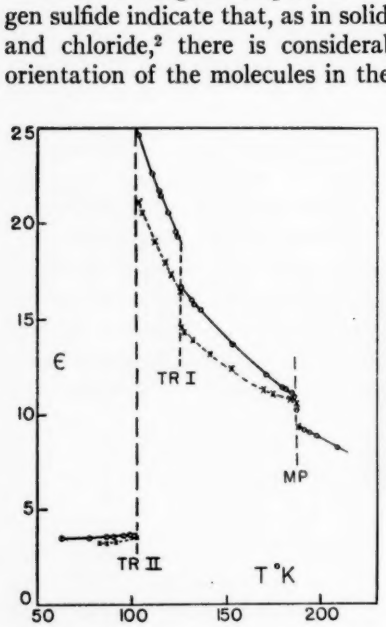

FIG. 1. Static dielectric constants of liquid and solid phases of hydrogen sulfide as a function of absolute temperature. Circles and solid curves are from data of this research; crosses and dashed curves, from data of Smyth and Hitchcock.[5]

Measurements have been reported by Kemp and Dennison[4] and by Smyth and Hitchcock.[5] The former included no tabular data, but their graph shows an erratic temperature dependence for the solid. The more complete results of Smyth and Hitchcock were more consistent, but they found somewhat irregular increases of dielectric constant in the two solid phases stable between the melting point (187.6°K) and 126.2°K, and between 126.2°K and the second solid transition at 103.5°K. Behavior of this kind in solid hydrogen halides has been found to result from sample voids and inhomogeneities unless special measures are employed in freezing and cooling of samples. The measurements reported here were undertaken using measures similar to those found effective for HCl and HBr[1,2] and were ex-

* Now with duPont Photoproducts Division, Parlin, New Jersey.

[1] N. L. Brown and R. H. Cole, J. Chem. Phys. **21**, 1920 (1953).

[2] R. W. Swenson and R. H. Cole, J. Chem. Phys. **22**, 284 (1954).

[3] L. Onsager, J. Am. Chem. Soc. **58**, 1486 (1936).

[4] J. D. Kemp and G. H. Dennison, J. Am. Chem. Soc. **55**, 251 (1933).

[5] C. P. Smyth and C. S. Hitchcock, J. Am. Chem. Soc. **56**, 1084 (1934).

tended over the frequency range 15 cps to 500 kc/s to find whether dispersion effects occurred in this range.

II. EXPERIMENT

Commercial gaseous hydrogen sulfide (Matheson) was condensed in a dry ice trap and slowly distilled into the experimental cell. The melting point (187.6°K) and specific conductance (9.2×10^{-10} mho/cm) were in good agreement with previously reported values after one distillation. The cell employed was one built by R. W. Swenson[2] for measurements of solid HCl; the conductance-capacitance bridge has been described elsewhere.[6] Measurements were made from temperatures of the liquid to 65°K, with reproducibility for different samples within 0.5 percent and precision of order 0.1 percent.

III. RESULTS

No evidence of frequency dependence of the dielectric constant or of significant dielectric loss was found either in the liquid or in the three solid phases. It is concluded therefore that the measured values are of the equilibrium dielectric constant without effects either of dispersion or of electrode polarization. Representative values from data for two samples are listed in Table I and the results are plotted against absolute temperature in Fig. 1.

IV. DISCUSSION

The behavior of hydrogen sulfide in the liquid and the two higher temperature solid phases is in fair agreement with the Onsager theory.[3] The comparison is conveniently made by using Onsager's equation to calculate the dipole moment μ from measured dielectric constant and refractive index n and comparing this value with the experimental dipole moment from gas phase measurements. Results of these calculations, given in Table I, are obtained using $n^2=2.44$ for the liquid and the liquid densities of 0.967 at 212°K and 1.004 at 190°K.[7] Values of n^2 for the solid were estimated from the Clausius-Mossotti expression by use of these liquid values together with the density of 1.17 at 103°K.[8] The variations in calculated dipole moments and differences from the gas value of 1.01 debye[9] are not much greater than the uncertainties in refractive index and density in the case of the disordered solid phases, while the values for the liquid phase are significantly smaller.

TABLE I. Dielectric constants of liquid and solid hydrogen sulfide, and dipole moments calculated from Onsager's equation.

T°K	ϵ	μ	T°K	ϵ	μ
	Liquid			Intermediate solid	
212.0	8.04	0.78	124.2	19.4	1.04
194.6	8.99	0.88	110.9	22.7	1.07
			103.4	24.7	1.08
	High-temp. solid			Low-temp. solid	
186.1	10.9	0.92	101.0	3.70	...
170.9	12.1	0.94	95.8	3.64	...
157.9	13.7	0.95	90.0	3.59	...
133.0	15.8	0.96	77.7	3.56	...
125.9	16.6	0.96	63.0	3.52	...

The values of dielectric constant in the lowest temperature phase decrease from 3.7 at 103°K to about 3.5 at 65°K. These values are thus definitely but not greatly in excess of the figure 2.4 calculated for n^2, and the difference is presumably to be attributed to molecular vibrations in the ordered structure.

The equilibrium behavior is thus quite simple and in part quite well accounted for by simple theory. The fair agreement of the results for the high temperature isotropic phase with Onsager's theory is a reasonable consequence of disordered structures without significant hydrogen bonding. The increase of the dielectric constant in the intermediate solid phase is not surprising in view of the presumably greater correlation of neighbors, but not enough is known of the structure to permit more quantitative discussion. The low value of the dielectric constant below 103.5°K indicates a high degree of order in dipole orientation.

ACKNOWLEDGMENTS

One of us (R.W.S.) is indebted to the Union Carbide and Carbon Corporation for a predoctoral fellowship in 1952–53. The work was supported in part by the Office of Naval Research.

[6] R. H. Cole and P. M. Gross, Jr., Rev. Sci. Instr. **20**, 252 (1949).
[7] Steele, McIntosh, and Archibald, Trans. Roy. Soc. **205**, 99 (1905).
[8] G. Natta, Atti. Acad. Lincei **11**, 749 (1930).
[9] H. J. von Braunmühl, Physik Z. **28**, 141 (1927).

Calculation of Energy Levels for Internal Torsion and Over-All Rotation.* I. CH_3BF_2 Type Molecules

E. Bright Wilson, Jr., Chun Chia Lin,† and David R. Lide, Jr.‡
Department of Chemistry, Harvard University, Cambridge, Massachusetts

(Received June 17, 1954)

Methods are described for calculating the energy levels for the over-all rotation and internal torsion of molecules consisting of a rigid symmetrical top attached to a rigid asymmetrical framework in such a way that the symmetry axis of the top coincides with a principal axis of the molecule. Probable examples are nitromethane and CH_3BF_2. Matrix perturbation methods are employed to obtain finite rotational secular equations valid in each of the cases: low barrier, high barrier, low asymmetry. These secular equations are modifications of the ordinary Wang equation for the rigid asymmetric rotor and can usually be solved by the continued fraction method. The symmetry groups applicable to this problem are also discussed.

MOLECULES such as CH_3BF_2 or nitromethane[1] (CH_3NO_2) may show over-all rotation, internal torsion of the methyl group relative to the NO_2 group, and vibration. For the purpose of treating the over-all rotation and internal torsion, it is convenient to think of the BF_2 or NO_2 group as a rigid framework to which is attached a symmetrical top (CH_3) which may rotate or vibrate about an axis colinear with a principal axis of inertia of the whole molecule. Furthermore, the three principal moments of inertia of the whole molecule are all different and are uninfluenced by the internal orientation of the attached top. The calculation of the rotational and internal torsional energy levels of this class of molecules is the subject of the present paper.[2]

MODEL AND COORDINATES

The model then consists of two connected rigid[3] bodies. One (the top) has two equal principal moments of inertia about axes perpendicular to a principal axis of the whole molecule. There are four degrees of freedom, three for over-all rotation and one for rotation of the top about its unique axis (see Fig. 1).

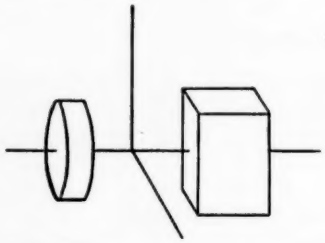

FIG. 1. A model of the CH_3BF_2 type molecule.

Let x, y, z be moving Cartesian axes rigidly attached to the framework part of the molecule and coincident with the principal axes of inertia of the whole molecule (origin is at center of mass of whole molecule). The z axis will coincide with the symmetry axis of the top. The three Eulerian angles θ, φ, and χ of x, y, z relative to space-fixed axes will describe the over-all orientation of the molecule, while the angle α will give the relative orientation of top and framework.

THE HAMILTONIAN

The kinetic energy has previously been written as[4]

$$2T=I_x\omega_x^2+I_y\omega_y^2+I_z\omega_z^2+I_\alpha\dot{\alpha}^2+2I_\alpha\dot{\alpha}\omega_z \quad (1)$$

in which I_α is the moment of inertia of the top about its symmetry axis, I_x, I_y, I_z are the principal moments of the entire molecule, and ω_x, ω_y, ω_z are components of angular velocity of the framework along x, y, z. It has been usual[5] to eliminate the cross-product terms by means of a transformation, but this will not be done in this treatment.

To obtain the Hamiltonian form, use the definitions of the momenta:

$$p=\partial T/\partial\dot{\alpha}, \quad P_x=\partial T/\partial\omega_x, \text{ etc.} \quad (2)$$

This leads in the usual way to the form

$$H=AP_x^2+BP_y^2+CP_z^2+Fp^2-2CpP_z+V(\alpha) \quad (3)$$

in which all angular momenta are in units $\hbar=h/2\pi$ and

$$A=\tfrac{1}{2}\hbar^2/I_x, \quad B=\tfrac{1}{2}\hbar^2/I_y, \quad C=\tfrac{1}{2}\hbar^2/(I_z-I_\alpha), \quad F=\tfrac{1}{2}\hbar^2I_z/[I_\alpha(I_z-I_\alpha)]. \quad (4)$$

$V(\alpha)$ is the potential energy restricting the internal rotation. In the model used here, the coefficients are all constants. Note that C involves the moment of inertia of the framework part alone while F contains the reduced moment of the two parts of the molecule.

The quantities P_x, P_y, and P_z were defined in Eq. (2) but by using the basic definition of angular momentum

* The research reported in this paper was made possible by support extended Harvard University by the Office of Naval Research under U. S. Office of Naval Research Contract N5ori 76, Task Order V.

† Socony Vacuum Predoctoral Fellow, 1953–1954.

‡ Now at National Bureau of Standards, Washington, D. C.

[1] Microwave spectra due to these motions have been recently reported for nitromethane by Tannenbaum, Johnson, Myers, and Gwinn, J. Chem. Phys. **22**, 949 (1954).

[2] The class treated here is in some ways simpler than the case of methyl alcohol which has been thoroughly studied by Dennison and co-workers [see Ivash and Dennison, J. Chem. Phys. **21**, 1804 (1954)] but the approach differs somewhat.

[3] For a discussion of vibrations in molecules of this type, see B. L. Crawford, Jr., and E. B. Wilson, Jr., J. Chem. Phys. **9**, 323 (1941).

[4] B. L. Crawford, Jr., J. Chem. Phys. **8**, 273 (1940).

[5] See K. S. Pitzer and W. D. Gwinn, J. Chem. Phys. **10**, 428 (1942).

it is easy to show that they are equal to the components of the total angular momentum of the molecule (in units $h/2\pi$), including the contributions arising from any internal rotation of the top. Similarly it can be shown that p is the total contribution of the motion of the top atoms to the z component of angular momentum, including both the internal and over-all motions.

This classical Hamiltonian becomes a quantum-mechanical operator or alternately a matrix by regarding P_x, P_y, P_z, and p as operators or matrices. The commutation rules[6] are

$$P_jP_k-P_kP_j=-iP_l, \quad (j, k, l=x, y, z \text{ in cyclic order}) \tag{5}$$

and

$$pP_j-P_jp=0, \quad j=x, y, z. \tag{6}$$

The first rule is the standard one for the components of angular momenta along molecule-fixed axes. The second follows from the fact that, as an operator,

$$p=-i(\partial/\partial\alpha)_{\theta,\varphi,\chi} \tag{7}$$

whereas the P_i's do not involve α.

By inserting in H the expressions for the P_i in terms of p_θ, p_φ, and p_χ and in turn treating these latter momenta as differential operators, the Schrödinger wave equation in the variables θ, φ, χ, α could be written down, but this is not necessary for the solution of the problem.

To simplify the later equations, let

$$\mathfrak{H}'=[H-D(P_x^2+P_y^2+P_z^2)]/(C-D) \tag{8}$$

in which

$$D=\tfrac{1}{2}(A+B). \tag{9}$$

Then

$$\mathfrak{H}'=b(P_x^2-P_y^2)+P_z^2-dpP_z+fp^2+V'(\alpha) \tag{10}$$

with

$$\begin{aligned} b&=\tfrac{1}{2}(A-B)/(C-D)\\ d&=2C/(C-D)\\ f&=F/(C-D)\\ V'&=V/(C-D). \end{aligned} \tag{11}$$

Then if Λ' is an eigenvalue of $\mathfrak{H}'$, the energy is given by

$$W=J(J+1)D+(C-D)\Lambda'. \tag{12}$$

$\mathfrak{H}'$, as well as H, is diagonal in J and M so only one JM block need be considered at a time.

TABLE I. Effect of four-group symmetry operations.

E	C_x	C_y	C_z
$P_i\to P_i$	$P_x\to P_x$ $P_{y,z}\to -P_{y,z}$	$P_y\to P_y$ $P_{x,z}\to -P_{x,z}$	$P_z\to P_z$ $P_{x,y}\to -P_{x,y}$
$p\to p$	$p\to -p$	$p\to -p$	$p\to p$
$(\alpha\to\alpha)$	$(\alpha\to -\alpha)$	$(\alpha\to -\alpha)$	$(\alpha\to\alpha)$
$(\theta\to\theta)$	$(\theta\to\pi-\theta)$	$(\theta\to\pi-\theta)$	$(\theta\to\theta)$
$(\varphi\to\varphi)$	$(\varphi\to\pi+\varphi)$	$(\varphi\to\pi+\varphi)$	$(\varphi\to\varphi)$
$(\chi\to\chi)$	$(\chi\to 2\pi-\chi)$	$(\chi\to\pi-\chi)$	$(\chi\to\pi+\chi)$

[6] O. Klein, Z. Physik **58**, 730 (1929).

TABLE II. Character table for case $s=3$.

Class	E	$2C_3$	$3C_2C_3$	C_2	$2C_2C_3$	$3C_2'C_3$
A	1	1	1	1	1	1
B_z	1	1	−1	1	1	−1
E_1	2	−1	0	2	−1	0
B_x	1	1	1	−1	−1	−1
B_y	1	1	−1	−1	−1	1
E_2	2	−1	0	−2	1	0

SYMMETRY CONSIDERATIONS

It is well known that the rigid asymmetric rotor wave equation is invariant under the group of 180° rotations about each of the principal axes. These operations variously change the signs of the P_i, which leaves the energy expression unaltered. In the present problem the cross-term in pP_z is not invariant unless p changes sign when P_z does. If the potential energy $V(\alpha)$ is an even function of α, then the four operations E, C_x, C_y, C_z whose effects are in Table I will still leave H invariant and will form a group (the "four-group") as before.

Consequently every solution of the wave equation will belong to one of the four species A, B_x, B_y, B_z of this group[7] as in the case of the asymmetric rotor, but here the part of the function involving α must be included. Further, any secular equation or energy matrix can be factored into at least four factors by using the foregoing symmetry.

Often $V(\alpha)$ will possess additional symmetry properties. For example, in nitromethane, it presumably is invariant under $\alpha\to\alpha+2\pi k/6$, where $k=0, 1, 2, 3, 4, 5$. In addition, $\alpha\to(2\pi k/6)-\alpha$ should also leave V unchanged. These operations are isomorphous with the point group C_{6v} but this group is not here used in the same way as when group theory is applied to the vibration problem.

The symmetry of $V(\alpha)$ cannot be indiscriminately applied to H because p appears in the cross term. However, the "rotations" $\alpha\to\alpha+2\pi k/s$ (here $s=6$) do leave H invariant. So do the "reflections" $\alpha\to(2\pi k/s)-\alpha$ if simultaneously $P_z\to -P_z$. The four-group operations listed earlier and the s internal rotations $\alpha\to\alpha+2\pi k/s$ generate a group of $4s$ operations. Table II shows the result when $s=3$, in which case the group is isomorphous with the group C_{6v}. The one-dimensional species are here labeled so that they correspond to the species for the subgroup V. The degenerate species E_1 would become $A+B_z$, in the subgroup while E_2 would yield B_x+B_y.

The case $s=6$ is easily constructed (see Fig. 2) from Table II because the new group is obtained by introducing the additional operation C_6^3 which causes $\alpha\to\alpha+\pi$. This commutes with all foregoing operations so the new group has twice as many classes and twice as many species as the old (see Table III).

[7] See King, Hainer, and Cross, J. Chem. Phys. **11**, 27 (1943).

TABLE III. Character table for case $s=6$.

	E	$2C_3$	$3C_xC_3$	C_z	$2C_zC_3$	$3C_yC_3$	C_6^3	$2C_3C_6^3$	$3C_xC_3C_6^3$	$C_zC_6^3$	$2C_zC_3C_6^3$	$2C_yC_3C_6^3$
A_e	1	1	1	1	1	1	1	1	1	1	1	1
B_{ze}	1	1	−1	1	1	−1	1	1	−1	1	1	−1
E_{1e}	2	−1	0	2	−1	0	2	−1	0	2	−1	0
B_{xe}	1	1	1	−1	−1	−1	1	1	1	−1	−1	−1
B_{ye}	1	1	−1	−1	−1	1	1	1	−1	−1	−1	1
E_{2e}	2	−1	0	−2	1	0	2	−1	0	−2	1	0
A_o	1	1	1	1	1	1	−1	−1	−1	−1	−1	−1
B_{zo}	1	1	−1	1	1	−1	−1	−1	+1	−1	−1	+1
E_{1o}	2	−1	0	2	−1	0	−2	1	0	−2	1	0
B_{xo}	1	1	1	−1	−1	−1	−1	−1	−1	1	1	1
B_{yo}	1	1	−1	−1	−1	1	−1	−1	1	1	1	−1
E_{2o}	2	−1	0	−2	1	0	−2	1	0	2	−1	0

These higher symmetries permit further factoring of the secular equation or energy matrix if the expansion functions are chosen to have symmetries in accord with the various species.

The dipole moment μ for this model would ordinarily be along the z axis. If this is the case, μ will have the symmetry B_z in Table II and in the case $s=6$ it will belong to B_{ze}. Consequently, for this case, the selection rules for dipole absorption will be ($s=3$): $A\leftrightarrow B_z$, $B_x\leftrightarrow B_y$, $E_1\leftrightarrow E_1$, $E_2\leftrightarrow E_2$. The rules will apply for the case $s=6$ with the additional condition that e species go only into e species, and o species into o species.

Nuclear permutation effects will be governed by the symmetry also. The subgroup which governs the exchange of the oxygen atoms in nitromethane or the fluorines in CH_3BF_2 consists of E and $C_zC_6^3$ since to exchange these atoms requires that $\alpha\leftrightarrow\alpha+\pi$, $\chi\leftrightarrow\chi+\pi$, which is $C_zC_6^3$. A_e, B_{ze}, E_{1e}, B_{xo}, B_{yo}, E_{2o} are even, the other species odd to this operation. Therefore only the first set can occur in nitromethane (with ^{16}O). In CH_3BF_2 these species will have one-third the fluorine spin weight of the others. The operations C_3, C_3^2 exchange two pairs of H atoms in the foregoing molecules. All the nondegenerate species are of species A in this subgroup, all the degenerate species will be degenerate in the subgroup. The two kinds of levels will then have equal proton spin weight.

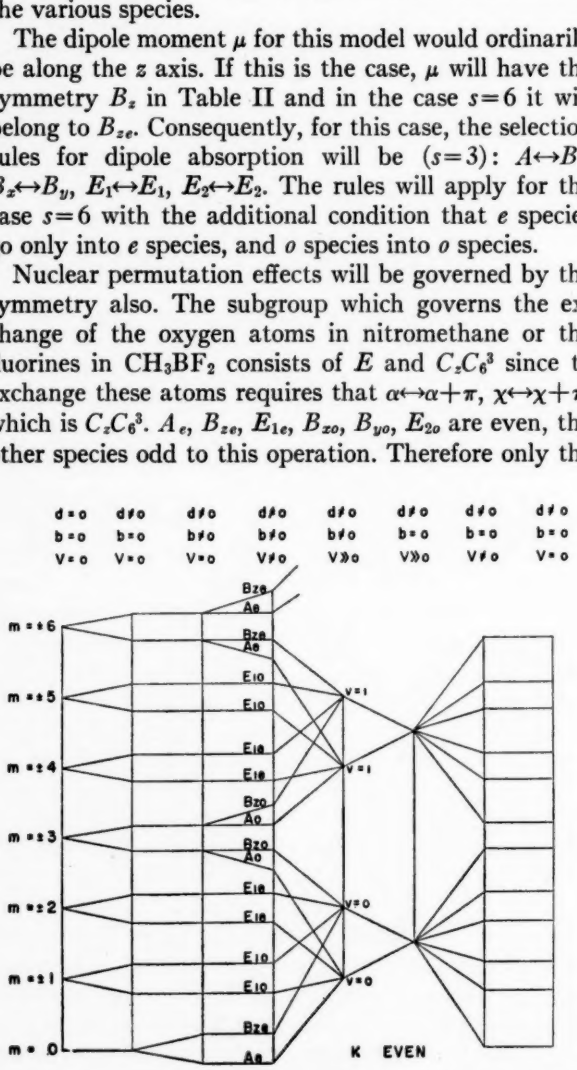

FIG. 2. Correlation of energy levels corresponding to various limiting cases as specified at the head of each column, for even values of K for the case $s=6$.

THE ENERGY MATRIX

If the asymmetry (b) were zero and there were no barrier (V'), the reduced Hamiltonian $\mathcal{H}'$ would be

$$P_z^2-dpP_z+fp^2 \tag{13}$$

which yields a diagonal matrix with the basis functions

$$S_{JKM}(\theta,\varphi)e^{iK\chi}e^{im\alpha} \tag{14}$$

in which S is the θ, φ factor of the symmetric rotor wave function and

$$K=0,\pm1,\pm2,\cdots\pm J;\quad m=0,\pm1,\pm2,\cdots\infty. \tag{15}$$

These functions may be used to set up a matrix for the general form of $\mathcal{H}'$, i.e., the true wave functions may be expanded in terms of the foregoing functions. The asymmetry term in b will give off-diagonal elements the same as those which occur with the rigid asymmetric rotor (with C calculated for framework only). The barrier potential V' is usually assumed to be of the form

$$V'=\tfrac{1}{2}V_0'(1-\cos s\alpha)=\tfrac{1}{2}V_0'-\tfrac{1}{4}V_0'(e^{is\alpha}+e^{-is\alpha}) \tag{16}$$

in which s is the number of equivalent minima and $(C-D)V_0'=V_0$ is the barrier height. The barrier will also introduce off-diagonal elements. The matrix for $\mathcal{H}'$ will then have the nonvanishing elements[8]

$$\mathcal{H}_{Km,\,Km}=\mathcal{H}'_{Km,\,Km}-\tfrac{1}{2}V_0'=K^2-dmK+fm^2$$

$$\mathcal{H}_{K,\,m;\,K\pm2,\,m}=b_{K,\,K\pm2}$$
$$=\tfrac{1}{2}b\{[J^2-(K\pm1)^2][(J+1)^2-(K\pm1)^2]\}^{\frac{1}{2}} \tag{17}$$

$$\mathcal{H}_{K,\,m;\,K,\,m\pm s}=-\tfrac{1}{4}V_0'=\zeta$$

[8] See the following for the matrix elements of P_x, P_y, and P_z.

Here the constant $\frac{1}{2}V_0'$ has been incorporated so that the eigenvalues of $\mathfrak{H}$ are related to those of $\mathfrak{H}'$ by

$$\Lambda'=\Lambda+\tfrac{1}{2}V_0'. \tag{18}$$

Unless the barrier height is zero, this form of $\mathfrak{H}$ corresponds to an infinite secular equation. Note, however, that there are no elements connecting even with odd K values so that the secular equation factors into one for even and one for odd K values. (This is part of the factoring into different symmetry species.)

CASE OF FREE INTERNAL ROTATION[8a]

When the barrier height is zero, $\zeta=-\frac{1}{4}V_0'=0$ and the energy matrix becomes diagonal in m. The secular equation therefore factors into one block for each value of m, as well as into even and odd K factors.

The secular equation for a given value of J, M, m has the elements

$$(K|K)=K^2-dmK-\lambda;$$

$$(K|K\pm2)=b_{K,K\pm2}$$

$$=\tfrac{1}{2}b\{[J^2-(K\pm1)^2][(J+1)^2-(K\pm1)^2]\}^{\frac{1}{2}}. \tag{19}$$

The energy W is then related to the roots λ by the equation (see Eq. 12).

$$W=J(J+1)D+Fm^2+(C-D)\lambda. \tag{20}$$

This secular equation is similar to the Wang[9] equation for the ordinary rigid asymmetric rotor except for the added term $-dmK$ on the diagonal. This term spoils the additional factoring possible in the rigid case.

As an example, consider the case $J=5$, K even. This factor becomes

$$\begin{vmatrix} 16+4md-\lambda & 6\sqrt{3}b & 0 & 0 & 0 \\ 6\sqrt{3}b & 4+2md-\lambda & (210)^{\frac{1}{2}}b & 0 & 0 \\ 0 & (210)^{\frac{1}{2}}b & -\lambda & (210)^{\frac{1}{2}}b & 0 \\ 0 & 0 & (210)^{\frac{1}{2}}b & 4-2md-\lambda & 6\sqrt{3}b \\ 0 & 0 & 0 & 6\sqrt{3}b & 16-4md-\lambda \end{vmatrix}=0. \tag{21}$$

For each nonvanishing value of $|m|$, there will be two identical such equations, so all levels are doubly degenerate unless $m=0$. In the latter case, the ordinary rigid rotor levels are obtained, except that the moment of inertia about the z axis is the moment of the framework group (I_z-I_a) as already seen.

The energy levels in the free rotation case must of course conform to the symmetry restrictions given for the general case. Thus, with $s=3$ or 6, if m is not a multiple of 3, the symmetry is one of the degenerate E species. If m is a multiple of 3, the levels involve A or B species which would be split into nondegenerate components if there were a sufficient barrier. If K is even, the species may be A, B_z, or E_1; if K is odd, B_x, B_y, or E_2. If $s=6$, the species further divide into even or odd (denoted by subscripts e and o) according as m is even or odd.

The selection rules for dipole radiation involve

$$\Delta J=0,\pm1 \tag{22}$$

as for the rigid asymmetric rotor. The symmetry requirements discussed earlier must also be met. If μ is along the z axis, K cannot change parity. The rule for m is

$$\Delta m=0. \tag{23}$$

This follows from the fact that the dipole moment does not depend on α whereas the wave function involves α only through the factor

$$e^{im\alpha}.$$

For small asymmetry the energy levels may be expanded in powers of b. For large values of the quantum number n, the diagonal elements of the secular equation will be large and the first terms in the expansion in powers of b may be adequate. Second-order perturbation theory then gives

$$\lambda=K^2-mdK+(b^2/8)\{[J^2-(K-1)^2]\times[(J+1)^2-(K-1)^2]/(2K-md-2)\}-(b^2/8)\{[J^2-(K+1)^2]\times[(J+1)^2-(K+1)^2]/(2K-md+2)\}+\cdots. \tag{24}$$

For very large values of m,

$$\lambda\rightarrow K^2-mdK. \tag{25}$$

For transitions with $\Delta J=1$, $\Delta K=0$, $\Delta m=0$, the transitions with large values of m would then tend to converge (from both sides) to a band head. Of course the intensities of these higher members would tend to decrease because of the unfavorable Boltzmann factors.

CASE OF LOW BARRIER

If the barrier height V_0 is small but not negligible (compared with the quantity F), a useful solution can be obtained with the Van Vleck perturbation method.[10] The reduced Hamiltonian matrix $\mathfrak{H}$ of Eq. (17) is split into an unperturbed, completely diagonal matrix $\mathfrak{H}^0$ with diagonal elements

$$\mathfrak{H}^0{}_{Km,Km}=K^2-dmK+fm^2 \tag{26}$$

[8a] This case was treated by H. B. G. Casimir, Z. Physik **59**, 623 (1930).

[9] S. C. Wang, Phys. Rev. **34**, 243 (1929).

[10] See E. C. Kemble, *The Fundamental Principles of Quantum Mechanics* (McGraw-Hill Book Company, Inc., New York, 1937), p. 394.

and a perturbation $\mathcal{H}\P$ with elements

$$\begin{aligned}\mathcal{H}\P_{K,m;K\pm2,m}&=b_{K,K\pm2}\\&=\tfrac{1}{2}b\{[J^2-(K\pm1)^2][(J+1)^2-(K\pm1)^2]\}^{\frac{1}{2}}\\\mathcal{H}\P_{K,m;K\ m\pm s}&=\zeta=-\tfrac{1}{4}V_0'=-\tfrac{1}{4}V_0/(C-D).\end{aligned}\tag{27}$$

The Van Vleck transformation reduces the elements off-diagonal in m to order ζ^2. If these are then neglected, the secular equation becomes

$$\begin{aligned}(K|K)&=K^2-dmK\\&\quad+(1/s)\zeta^2\{(1/[Kd-(2m+s)f])\\&\quad-(1/[Kd-(2m-s)f])\}-\lambda\\(K|K\pm2)&=b_{K,K\pm2}.\end{aligned}\tag{28}$$

This secular equation is similar in its properties to that for free rotation. It is not valid, however, for the case $m=\pm\frac{1}{2}s$, s even, because then a near degeneracy occurs. For this case, the unperturbed states with $m=\pm\frac{1}{2}s$ must both be taken into consideration. The equation then has the nonvanishing elements

$$\begin{aligned}\left(\tfrac{s}{2},K\middle|\tfrac{s}{2},K\right)&=K^2-\tfrac{1}{2}dsK\\&\quad+(1/s)[\zeta^2/(Kd-2sf)]-\lambda\\\left(-\tfrac{s}{2},K\middle|-\tfrac{s}{2},K\right)&=K^2+\tfrac{1}{2}dsK\\&\quad-(1/s)[\zeta^2/(Kd+2sf)]-\lambda\\\left(\tfrac{s}{2},K\middle|-\tfrac{s}{2},K\right)&=\zeta\\\left(\tfrac{s}{2},K\middle|\tfrac{s}{2},K\pm2\right)&=b_{K,K\pm2}\\\left(-\tfrac{s}{2},K\middle|-\tfrac{s}{2},K\pm2\right)&=b_{K,K\pm2}.\end{aligned}\tag{29}$$

Because of the symmetry

$$(s/2,K|\pm s/2,K')=(-s/2,-K|\mp s/2,-K')$$

this larger secular equation can be factored into two factors, similar to the way in which the Wang equation is factored. This leads to a splitting of the degeneracy.

When m is not a multiple of $\frac{1}{2}s$, the levels are inherently doubly degenerate for all barriers. For m a multiple of $\frac{1}{2}s$ the degeneracy is ultimately split at high enough barriers. With the approximation given here this splitting will not appear except for $m=\frac{1}{2}s$. The higher the multiple of $\frac{1}{2}s$ the higher the order of perturbation required to demonstrate the splitting.

The quantum number m is no longer a good quantum number when there is a barrier but if V_0 is small it can still be used to label the levels. The selection rule $\Delta m=0$ is no longer exact and must be replaced by the rigorous symmetry selection rules given earlier.

HIGH BARRIERS

If the barrier is sufficiently high so that the torsional levels of a given symmetry are widely spaced compared with the rotational levels, a different perturbation treatment is possible, in which the asymmetry and the coupling term are treated as perturbations by the Van Vleck procedure. This leads as before to a rotational secular equation. The unperturbed operator for the energy is

$$H_0=DP^2+(C-D)P_z^2+Fp^2+V(\alpha)\tag{30}$$

while the perturbation operator is

$$H_1=\tfrac{1}{2}(A-B)(P_x^2-P_y^2)-2CpP_z.\tag{31}$$

H_0 can be diagonalized with the basis functions

$$S_{JKM}(\theta,\varphi)e^{iK\chi}U_{v\kappa}(\alpha)\tag{32}$$

in which symmetric rotor functions are used as before and the U's are eigenfunctions of

$$[Fp^2+V(\alpha)]U_{v\kappa}=E_{v\kappa}U_{v\kappa}.\tag{33}$$

The torsional states are described by the quantum numbers $v\kappa$, where v is the principal quantum number of the vibrational level, and κ is a degeneracy index.

For the potential function of Eq. (16), the nondegenerate eigenvalues of the torsional Eq. (33), which is now related to the Mathieu equation, can be obtained from published[11] tabulations through the connection

$$E_v=\tfrac{1}{4}s^2Fbe_r(S)\quad\text{or}\quad\tfrac{1}{4}s^2Fbo_r(S)\tag{34}$$

in which

$$S=(4/s^2)(V_0/F)\tag{35}$$

and the eigenvalues be_r and bo_r are given in tables as functions of the parameter S. The values of the quantum number $v=0$, 1, 2, etc. are identified respectively with the eigenvalues be_0, bo_1; be_1, bo_2; be_3, etc.

The degenerate levels have not been tabulated but can be calculated to any desired degree of accuracy by expansion of the eigenfunction in a Fourier series. However, another method is easier and is reasonably accurate for high barriers. Make the substitution

$$U_{v\kappa}=e^{i\kappa\alpha}u(\alpha)\tag{37}$$

in Eq. (33), where $\kappa=-\frac{1}{2}s+1,\ -\frac{1}{2}s+2,\ \cdots,\ \frac{1}{2}s$. The equation for u is then

$$[Fp^2+2F\kappa p+F\kappa^2+V]u=E_{v\kappa}u.\tag{38}$$

If $\kappa=\pm1,\pm2,\cdots,\pm\frac{1}{2}s-1$, the degenerate levels are obtained. But the terms involving κ in Eq. (38) can be considered as perturbations on the $\kappa=0$ case, if the barrier is high enough. The term in κ^2 obviously just subtracts from $E_{v\kappa}$. To the second order the effect of

[11] *Tables Relating to Mathieu Functions* (Columbia University Press, New York, 1951).

the terms in κ and κ^2 is

$$E_{v\kappa}=E_{v0}+F\kappa^2+4F^2\kappa^2\sum_{v'}{}'\,|p_{vv'}|^2/(E_{v0}-E_{v'0}) \quad (39)$$

in which the sum is over all the nondegenerate levels and

$$p_{vv'}=-i\int_0^{2\pi}U_{v0}^*(\partial U_{v'0}/\partial\alpha)d\alpha$$

$$=\sum_{m=-\infty}^{\infty}mA_{vm}A_{v'm}\Big/\left\{\sum_{m=-\infty}^{\infty}A_{vm}{}^2\sum_{m=-\infty}^{\infty}A_{v'm}{}^2\right\}^{\frac{1}{2}}. \quad (40)$$

Here we have expanded the nondegenerate eigenfunctions as

$$U_{v0}(\alpha)=\sum_{m=-\infty}^{\infty}A_{vm}e^{im\alpha}.$$

These Fourier coefficients may be found from the tabulations of reference 11 by the identification

$$A_{v,-sk}=A_{v,sk}=(-1)^kDe_{2k}(S),\quad k\neq0$$

$$A_{v,0}=2De_0(S) \qquad \text{for even } v,$$

$$A_{v,-sk}=-A_{v,sk}=(-1)^kDo_{2k}(S) \qquad \text{for odd } v,$$

$$A_{v,-sk-\frac{1}{2}s}=A_{v,sk+\frac{1}{2}s}=(-1)^{k+1}Do_{2k+1}(S) \quad (\text{even } v),$$

$$A_{v,-sk-\frac{1}{2}s}=-A_{v,-sk-\frac{1}{2}s}=(-1)^{k+1}De_{2k+1}(S) \quad (\text{odd } v).$$

These coefficients require normalization.

The perturbation H_1 of Eq. (31) now needs to be introduced by the Van Vleck procedure. However, for the degenerate torsional states, it is convenient to combine this perturbation with that given above, yielding the secular equation

$$\begin{aligned}(K\,|\,K)&=K^2-d'\kappa K-\Lambda''\\(K\,|\,K\pm2)&=\tfrac{1}{2}b'\{[J^2-(K\pm1)^2]\\&\qquad\times[(J+1)^2-(K\pm1)^2]\}^{\frac{1}{2}}\end{aligned} \quad (41)$$

with

$$\begin{aligned}W&=J(J+1)D+E_{v0}+F'\kappa^2+\Lambda''(C'-D)\\C'&=C(1+4C\rho)\\d'&=2C(1+4F\rho)/(C'-D)\\F'&=F(1+4F\rho)\\\rho&=\sum_{v'}{}'\,|p_{vv'}|^2/(E_{v0}-E_{v'0})\\b'&=\tfrac{1}{2}(A-B)/(C'-D).\end{aligned} \quad (42)$$

VERY HIGH BARRIERS

If the barrier V is sufficiently high, the lower energy levels should approximate those of a rigid rotor with moments of inertia I_x, I_y, I_z (not I_z-I_α) and a harmonic torsional vibrator with a reduced moment of inertia

$$I_\alpha(I_z-I_\alpha)/I_z \quad (43)$$

and potential energy

$$\tfrac{1}{2}(d^2V/d\alpha^2)_0\alpha^2. \quad (44)$$

This result can be shown to follow from Eq. (41) and (42), since

$$4F\rho\longrightarrow-1 \quad (45)$$

for high barriers in which harmonic oscillator functions can be used for U_{v0} in Eq. (40).

The energy levels of rotation are then calculable by the standard methods used for the rigid asymmetric rotor. The torsional levels will be degenerate, threefold if $n=3$, sixfold if $n=6$. However, some of this degeneracy may be eliminated when permutation symmetry occurs, as in nitromethane, whose levels will be only threefold degenerate.

CASE OF SMALL ASYMMETRY

In cases for which the approximations so far described are all inadequate, another approach can be used[12] if the asymmetry of the molecule is small. Let the reduced energy matrix $\mathfrak{H}'$ of Eq. (10) be set up in terms of the basis functions

$$e^{iK\chi}S_{JKM}(\theta,\varphi)\gamma_{vK}(\alpha) \quad (46)$$

in which S is a symmetric rotor function and $\gamma_{vK}(\alpha)$ is a periodic function of α which is an eigenfunction of the equation

$$[fp^2-dKp+V'(\alpha)]\gamma_{vK}(\alpha)=W_{vK}\gamma_{vK}(\alpha) \quad (47)$$

with eigenvalue W_{vK}. K enters as a parameter. The nonvanishing matrix elements for $\mathfrak{H}'$ then become

$$\begin{aligned}\mathfrak{H}'_{vK,vK}&=K^2+W_{vK}\\\mathfrak{H}'_{v,K;v',K\pm2}&=b_{K,K\pm2}\Delta_{v,K;v',K\pm2}\end{aligned} \quad (48)$$

where

$$\Delta_{v,K;v',K\pm2}=\int_0^{2\pi}\gamma_{vK}{}^*\gamma_{v',K\pm2}d\alpha \quad (49)$$

which enters because γ's for different K's are not orthogonal.

The existence of the terms off-diagonal in v spoils the factoring into v blocks but these terms are normally small and can be reduced to lower order by a Van Vleck transformation. This yields a rotational secular equation

$$\begin{aligned}(K\,|\,K)&=K^2+W_{vK}-\Lambda'\\&\quad+|b_{K,K+2}|^2\sum_{v'}{}'\,|\Delta_{v,K;v',K+2}|^2/(W_{vK}-W_{v'K+2})\\&\quad+|b_{K,K-2}|^2\sum_{v'}{}'\,|\Delta_{v,K;v',K-2}|^2/(W_{vK}-W_{v'K-2})\\(K\,|\,K\pm2)&=b_{K,K\pm2}\Delta_{v,K;v,K\pm2}\\(K\,|\,K\pm4)&=b_{K,K\pm2}b_{K\pm2,K\pm4}\\&\quad\times\sum_{v'}{}'\frac{\Delta_{v,K;v',K\pm2}\Delta_{v',K\pm2;v,K\pm4}}{W_{vK}-W_{v'K\pm2}}.\end{aligned} \quad (50)$$

[12] This is very close to that introduced by Dennison, reference 1.

Koehler and Dennison[13] have shown that the quantities $W_{\nu K}$ can be obtained from a continued fraction of the form

$$\xi=M_0-\cfrac{1}{M_{-1}-\xi-\cfrac{1}{M_{-2}-\xi-\cfrac{1}{M_{-3}-\xi-\cdots}}}-\cfrac{1}{M_1-\xi-\cfrac{1}{M_2-\xi-\cfrac{1}{M_3-\xi-\cdots}}} \tag{51}$$

in which

$$M_l=\frac{4s^2F}{V_0}(l-g)^2, \quad l=0, \pm1, \pm2, \cdots$$

$$g=[(CK/F)-\kappa)]/s, \quad \kappa=0, 1, 2, \cdots s-1 \tag{52}$$

$$W_{nK}=\tfrac{1}{2}V_0'-[C^2K^2/F(C-D)]+\tfrac{1}{4}V_0'\xi.$$

To calculate the Δ's continued fractions may also be used. The function γ_{nK} is expanded in a Fourier series:

$$\gamma_{nK}=\sum_{m=-\infty}^{\infty} A_{nK,m}e^{im\alpha}.$$

This is substituted in the differential Eq. (47) and leads to a set of simultaneous equations for the coefficients A:

$$A_{nK,m-s}+G_mA_{nK,m}+A_{nK,m+s}=0$$

where

$$G_m=-M_l+\zeta \quad \text{where} \quad m=ls+\kappa.$$

These simultaneous equations yield the continued fraction

$$\frac{A_{nK,m}}{A_{nK,m-s}}=\cfrac{-1}{G_m-\cfrac{1}{G_{m+s}-\cfrac{1}{G_{m+2s}-\cdots}}}.$$

The normalization condition

$$2\pi\sum_{m=-\infty}^{\infty}|A_{nK,m}|^2=1$$

enables the determination of the A's to be completed.

There will of course be an infinite number of roots for each value of K and κ. These roots are most conveniently calculated if none of the denominators $M_l-\xi-\cdots$ are small. If one of these should turn out to be small, the continued fraction should be transformed so that the offending M_l appears in the leading position; i.e.,

$$\xi=M_l-\cfrac{1}{M_{l-1}-\xi-\cfrac{1}{M_{l-2}-\xi-\cdots}}-\cfrac{1}{M_{l+1}-\xi-\cfrac{1}{M_{l+2}-\xi-\cdots}} \tag{53}$$

[13] J. S. Koehler and D. M. Dennison, Phys. Rev. **57**, 1006 (1940).

For each root sought, there will be an appropriate choice of the leading term M_l which will cause the most rapid convergence.

The various values of κ yield the different component levels which in the limit of high barriers come together to form a (degenerate) harmonic oscillator level. However, Koehler and Dennison[13] showed that the roots are periodic functions of K [as may also be seen from Eq. (51)] with period Fs/C. Furthermore, if this periodic function is known for the case $\kappa=0$, it can be used to calculate the roots for the other values of κ by a "phase shift," i.e., by reading off the value of ξ for

$$K'=K-F\kappa/C$$

from the same periodic curve used for $\kappa=0$.

The dependence of ξ on K and κ vanishes for sufficiently high barriers. This suggests expanding ξ as a Fourier series (only cosine terms will appear)

$$\xi=\xi_0+\xi_1\cos2\pi g+\xi_2\cos4\pi g+\cdots.$$

For high enough barriers only a few terms are required. The coefficients ξ_0, ξ_1, ξ_2 can be found by solving the continued fraction for the necessary number of values of g, conveniently chosen to make it easy to solve for the required number of ξ's. The value of ξ_0 can also be obtained from available tables[11] by means of the relation:

$$\xi=\frac{s^2F}{V_0}be_r(S)-2$$

or

$$\frac{s^2F}{V_0}bo_r(S)-2$$

with

$$S=4V_0'/s^2f=4V_0/s^2F.$$

Then the Δ's may be written

$$\Delta_{n'K,nK}=2\pi\sum_{m=-\infty}^{\infty}A_{n'K',m}A_{nK,m}.$$

In some cases, especially when b is sufficiently low, the $(K|K\pm4)$ elements of the secular Eq. (50) can be neglected altogether. However, this procedure is not always valid. Under such circumstances the secular equation can be made easier to solve by various transformations which reduce the order of the troublesome $K,K\pm4$ elements so that they can be ignored and the remaining equation treated by the continued fraction method. These transformations are similar to Van Vleck transformations but have to be adapted to the several cases which arise because of near-degeneracies and will therefore not be detailed here.

Experimental Determination of Rotational Temperatures and Concentrations of OH in Flames from Emission Spectra*

S. S. PENNER AND E. K. BJÖRNERUD
Daniel and Florence Guggenheim Jet Propulsion Center, California Institute of Technology, Pasadena, California

(Received June 25, 1954)

In order to illustate the use of two-path experiments for correcting for self-absorption, experimental studies to determine the rotational "temperatures" and concentrations of OH in flames burning at atmospheric pressure have been carried out. For mixtures of H_2, C_2H_2, and O_2, as well as for C_2H_2-O_2 flames diluted with A, "anomalous" rotational "temperatures" were observed under conditions in which strong self-absorption was clearly indicated by the intensity ratios for the double-path to the single-path experiments. Unequivocal quantitative estimates of rotational temperatures and of OH concentrations cannot be carried out, even on the assumption that the emitting system is isothermal and in equilibrium. However, by using the results of theoretical studies on two-path experiments carried out by one of us, it is possible to obtain reasonable upper limits for the temperatures and lower limits for the OH-concentrations, based on an assumed Doppler contour for the line-shape and utilizing Oldenberg's estimates for the f values of representative spectral lines. Our experimental studies lead to reasonable rotational temperatures at the tip of luminous cones for mixtures of H_2, C_2H_2, and O_2 and for C_2H_2-O_2 flames diluted with up to 60 percent argon. These observations do not disprove the reality of rotational temperature anomalies in the inner cones of flames. Significant improvement of experimental procedure, and quantitative interpretation of results along the lines used by us, requires additional basic studies with emphasis on the measurement of spectral line-shape and absolute intensities.

I. INTRODUCTION

In recently published articles on rotational temperature measurements of OH in flames, the problem of the proper interpretation of apparent anomalous temperatures has been discussed. Two recent survey papers, in which extensive references to the published literature may be found, have been prepared by Gaydon[1] and Penner.[2] In order to illustrate the use of two-path experiments in correcting for self-absorption, we have carried out a series of single-path and two-path measurements on flames burning at atmospheric pressure. We have selected for study the $H_2-C_2H_2-O_2$ and $C_2H_2-O_2-A$ flames and restricted our attention to the tips of the luminous cones. Results obtained on the inner cones have been considered to yield true rotational temperature anomalies.[3] Our experimental data were extensively influenced by self-absorption distortions, with close correlation between apparent temperature and a parameter which measures directly the number density of OH molecules in the light path. To what extent this conclusion can be applied to the inner cones of flames can be settled only by further experimental studies. The appearance of "anomalous" temperatures in self-absorbed systems is well known and has been studied both experimentally and theoretically.

The results of our theoretical studies on two-path experiments have been used to obtain rotational temperature estimates and lower limits for the OH concentrations on the assumption that the radiating system is in equilibrium, that the spectral lines have a Doppler contour, and that Oldenberg's f values are applicable.

In Sec. II we present the results of representative theoretical calculations on two-path to single-path intensity ratios for isothermal emitters. The experimental technique used to perform two-path and single-path emission experiments is described briefly in Sec. III. The results of studies on the $H_2-C_2H_2-O_2$ system are presented in Sec. IV. Spectroscopic studies on acetylene-oxygen flames diluted with argon are described in Sec. V. A critical evaluation of results and concluding remarks are presented in Sec. VI.

II. PRELIMINARY THEORETICAL CALCULATIONS ON TWO-PATH TO SINGLE-PATH INTENSITY RATIOS

By utilizing the analytical techniques described in previous publications,[4] and the relative intensity tables of Dieke and Crosswhite,[5] it is a simple matter to calculate the ratio of the total intensity of a line observed in a double-path experiment (I_D) to the corresponding intensity for a single-path experiment (I_S). Smoothed curves drawn through the calculated intensity ratios as a function of rotational quantum number K are summarized in Figs. 1 to 3 for an isothermal, equilibrium, emitting system at 3000°K, for the P_1-branch, $^2\Sigma \rightarrow {}^2\Pi$ transitions of OH, 0,0-band. In Figs. 1 to 3 the quantity $\epsilon' = 1-\exp(-P_{\max}X)$ for the line with $K=1$ represents the usual self-absorption parameter, $P_{\max}$ equals the maximum spectral absorption coefficient for the

* Supported by the Office of Naval Research under Contract Nonr-220(03), NR 015-401.

[1] A. G. Gaydon, "Use of Spectroscopy in Elucidating Reaction Mechanism," in *Selected Combustion Problems—Fundamentals and Aeronautical Applications* (Butterworths Ltd., London, May 1954), pp. 132–143.

[2] S. S. Penner, "Spectroscopic Studies of Premixed Laminar Flames," reference 1, pp. 144–166.

[3] See, for example, H. G. Wolfhard's discussion in *Fourth (International) Symposium on Combustion* (Williams and Wilkins Company, Baltimore, 1953), pp. 230–231.

[4] S. S. Penner, J. Chem. Phys. **21**, 31 (1953); **22**, 101 (1954).

[5] G. H. Dieke and H. M. Crosswhite, "The Ultraviolet Bands of OH," Bumblebee Series Report No. 87 (The Johns Hopkins University, Baltimore, Maryland, November 1948).

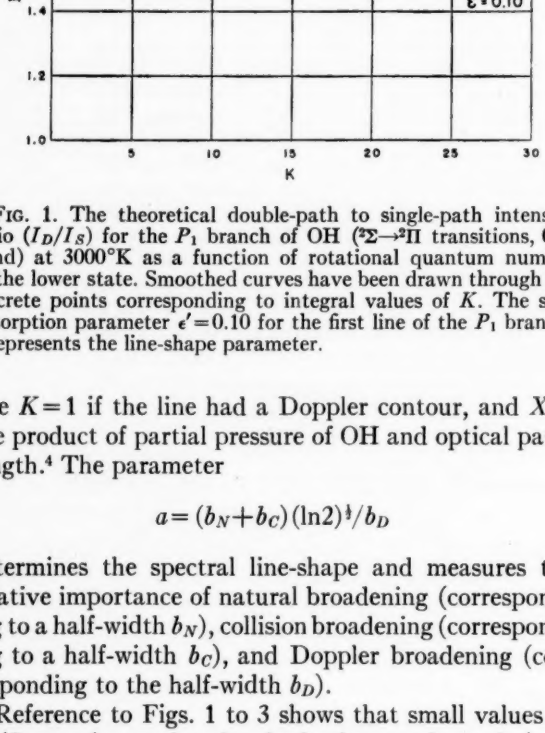

FIG. 1. The theoretical double-path to single-path intensity ratio (I_D/I_S) for the P_1 branch of OH ($^2\Sigma \rightarrow {}^2\Pi$ transitions, 0,0-band) at 3000°K as a function of rotational quantum number of the lower state. Smoothed curves have been drawn through the discrete points corresponding to integral values of K. The self-absorption parameter $\epsilon'=0.10$ for the first line of the P_1 branch; a represents the line-shape parameter.

line $K=1$ if the line had a Doppler contour, and X is the product of partial pressure of OH and optical path-length.[4] The parameter

$$a=(b_N+b_C)(\ln 2)^{\frac{1}{2}}/b_D$$

determines the spectral line-shape and measures the relative importance of natural broadening (corresponding to a half-width b_N), collision broadening (corresponding to a half-width b_C), and Doppler broadening (corresponding to the half-width b_D).

Reference to Figs. 1 to 3 shows that small values of I_D/I_S can be produced only for large values of ϵ'; in agreement with the line-shape effect noted previously,[4] strongest self-absorption, i.e., smallest values of I_D/I_S, are observed for the narrowest spectral lines ($a\sim 0$). In accord with expectations, the ratio I_D/I_S approaches two for weak spectral lines corresponding to large values of K.

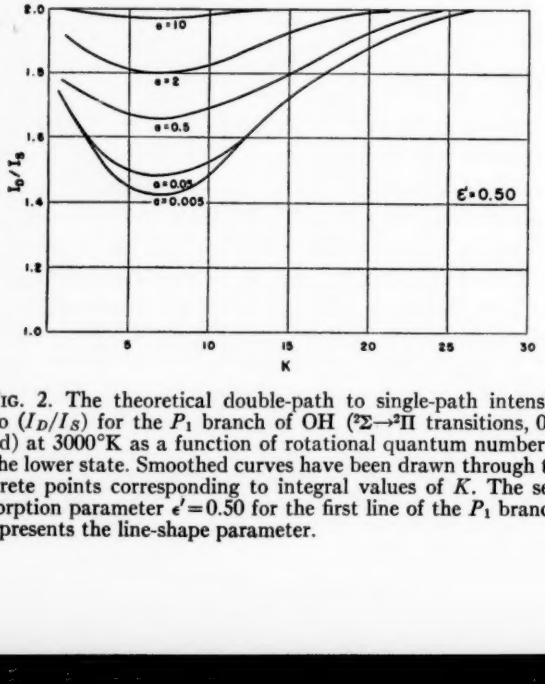

FIG. 2. The theoretical double-path to single-path intensity ratio (I_D/I_S) for the P_1 branch of OH ($^2\Sigma \rightarrow {}^2\Pi$ transitions, 0,0-band) at 3000°K as a function of rotational quantum number K of the lower state. Smoothed curves have been drawn through the discrete points corresponding to integral values of K. The self-absorption parameter $\epsilon'=0.50$ for the first line of the P_1 branch; a represents the line-shape parameter.

The theoretical results shown in Figs. 1 to 3 suggest the direct experimental determination of I_D/I_S as a sensitive method for detecting the influence of self-absorption distortions. For isothermal systems, this ratio will approach two, independently of the value of the line-shape parameter a, if ϵ' goes to zero; for all reasonable values of a (i.e., $a\leq 0.5$), I_D/I_S is small for the strongest lines for $\epsilon'\geq 0.90$, which is a rough estimate for ϵ' on the basis of equilibrium calculations[6] for representative flames utilizing the best published absolute intensity measurements for OH.[7] As long as interpretation of experimental data must be based on the assumption that the emitting system is isothermal, we propose to use the variation of the ratio I_D/I_S with K at least as a qualitative measure of the number density of OH in the light path. In more conventional terminology, an increase in the apparent rotational

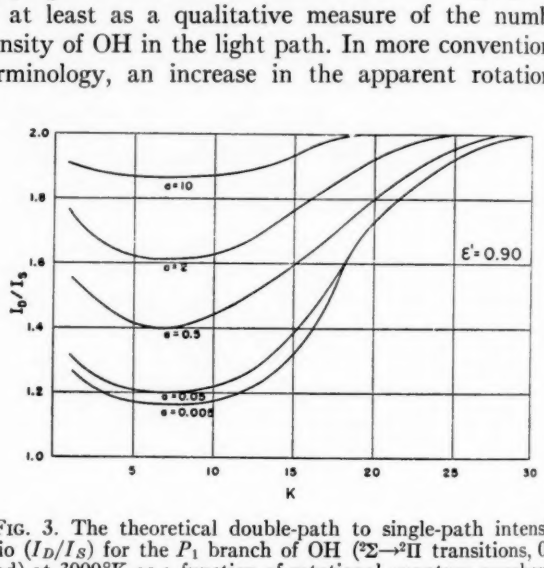

FIG. 3. The theoretical double-path to single-path intensity ratio (I_D/I_S) for the P_1 branch of OH ($^2\Sigma \rightarrow {}^2\Pi$ transitions, 0,0-band) at 3000°K as a function of rotational quantum number K of the lower state. Smoothed curves have been drawn through the discrete points corresponding to integral values of K. The self-absorption parameter $\epsilon'=0.90$ for the first line of the P_1 branch; a represents the line-shape parameter.

temperature for single-path experiments, when coupled with a decrease in the smallest observed value for I_D/I_S, is to be expected on the basis of the known distortion produced by self-absorption.[4] For minimum values of I_D/I_S below about 1.4, it has been demonstrated that rotational temperatures of 4000°K or higher are to be expected, the exact temperature depending on both the values of ϵ' and of a.

III. EXPERIMENTAL TECHNIQUE

A 1.5-m grating spectrograph with a theoretical resolving power of 48 800 was used for all of the experimental studies. The spectra were recorded photographically and densitometered according to conventional procedures. Two types of burners were employed: (a) a high quality copper oxygen-acetylene welding tip with an inside diameter of 0.071 cm; (b) a converging con-

[6] S. S. Penner, J. Chem. Phys. **20**, 507 (1952).
[7] O. Oldenberg and F. F. Rieke, J. Chem. Phys. **6**, 439 (1938); R. J. Dwyer and O. Oldenberg, *ibid.* **12**, 351 (1944).

toured nozzle with a main tube inside diameter of 0.625 cm and an exit section diameter of 0.156 cm. For some flames the converging nozzle gave a stable flame with a strongly luminous inner cone almost free of outer cone gases.

Emission spectra of the inner cone were obtained by focusing at the tip of the inner cone in such a manner that a sharp image was produced at the plane corresponding to the 20-micron wide entrance slit of the spectrograph. For each flame two sets of data were obtained: (1) an emission spectrum with a 9-in. focal length spherical mirror placed in back of the flame at a radial distance from the center of the inner cone equal to the radius of curvature of the mirror (double-path experiment)[8]; (2) an emission spectrum of the flame without the use of the spherical mirror (single-path experiment). A schematic diagram of the flame image formed at the entrance slit for single- and double-path emission spectra is shown in Fig. 4, together with a representative photograph of the two superimposed images produced in the double-path experiment. A mask was placed over the slit which admitted light from a portion of the flame 2 mm in height.

A good two-path experiment is one in which the double-path to single-path intensity ratio (I_D/I_S) approaches a value of two for the weaker spectral lines. The fact that we approached this objective satisfactorily is demonstrated by the experimental data described in Sec. IV and V and, more directly, by the plot shown in Fig. 5, where the single-path intensity for the inner cone of a stoichiometric $C_2H_2-O_2$ flame is plotted against the intensity obtained for a double-path measurement, but with a 50 percent transmission quartz filter inserted in the light path. For a perfectly reflecting mirror, the experimental data should approach the dotted curve for the weaker spectral lines, i.e., for small values of I_S. Reference to Fig. 5 shows that representative experimental data do, in fact, exhibit this behavior. The deviations from the limiting curve are the result of self-absorption, in accord with the theoretical studies presented in the previous section.

The data shown in Fig. 5, as well as the experimentally determined values of I_D/I_S discussed in the following sections, show that values of I_D/I_S surprisingly close to two were obtained, although the theoretical upper limit for a mirror with reflectivity 0.92 is $I_D/I_S=1.92$. We have studied the optical system with some care and conclude from this work that no distortions which vary with wavelength, and could conceivably influence the analysis of experimental data, were present. Among the experiments performed by us are the following:

(a) Systematic studies in which unused portions of the spherical mirror were blocked off successively showed no dependence of the I_D/I_S curves (normalized

[8] Preliminary two-path experiments were carried out in our laboratory by Mr. J. C. Stewart during the summer of 1953.

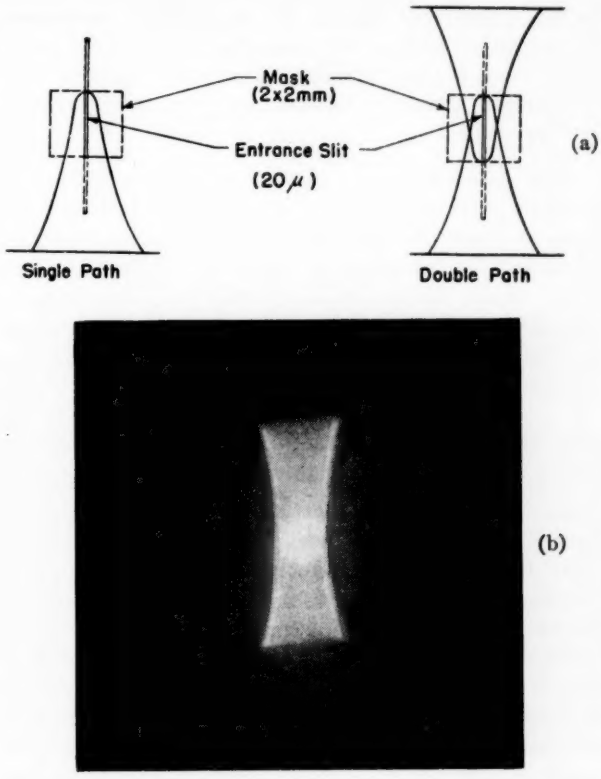

FIG. 4. (a) Schematic diagrams of single- and double-path image of the inner cone of a luminous flame at the plane of the spectrograph entrance slit. (b) Photograph of inner cone images at the plane of the spectrograph entrance slit for a double-path experiment.

to two for large values of K and low intensities) on mirror size, as long as the aperture of the spectrograph entrance slit was filled completely.

(b) Single-path "temperature" measurements with the mirror placed at 90° and 120° with respect to the flame-entrance slit axis gave the same results as flame emission studies without mirror. Fluorescence effects cannot have influenced our observed values for I_D/I_S

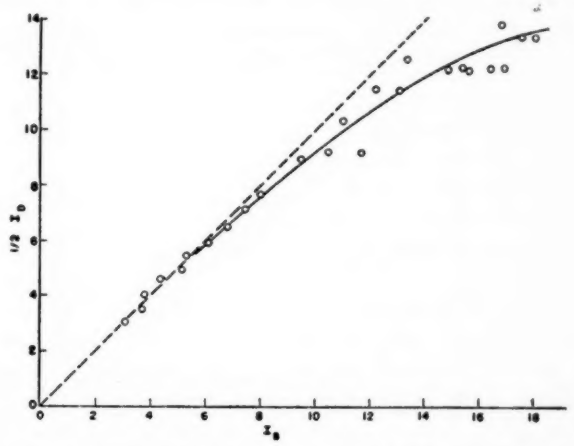

FIG. 5. Double-path intensity, reduced by 50 percent, as a function of single-path intensity for representative lines of an acetylene-oxygen flame.

to an appreciable extent. In concluding the present discussion we wish to emphasize the fact that the measured ratios I_D/I_S are most accurate for spectral lines of moderate strength and least accurate for the weakest spectral lines.

Film calibration was carried out for each film by utilizing flame spectra obtained in the outer cones of the flames studied. A calibrated two-step quartz filter was employed for this purpose. Good film calibration data could usually not be obtained from inner cone spectra because of strong temperature gradients, which affected significantly the distribution of intensities for the long spectral lines needed for calibration.

IV. EMISSION SPECTRA OF $H_2-C_2H_2-O_2$ FLAMES

Experimental measurements of emission spectra have been made for stoichiometric $H_2-C_2H_2-O_2$ mixtures in which the ratio of H_2 to C_2H_2 was varied systematically. Representative results of I_D/I_S as a function of K are summarized in Figs. 6 to 8. The experimental data shown in Figs. 6 and 7 were obtained with the contoured burner with 0.156 cm inside diameter; the data of Fig. 8 were obtained from a flame stabilized on the smaller (0.071 cm inside diameter) burner. By keeping the fuel to oxygen mixture ratio in stoichiometric proportions, the adiabatic flame temperature for the gas mixtures was also maintained at roughly the same value, thereby minimizing the effects of temperature changes on the observed results. Reference to Figs. 6 and 7, and to similar data obtained for other gas compositions, shows that the minimum value of I_D/I_S corresponds to practically the same value of K, namely $K=11$, for all gas compositions, for the P_2 branch as well as for the Q branches. Distortion of experimental data by self-absorption occurred in every experiment since I_D/I_S is always appreciably less than two for the stronger lines. The observed values of I_D/I_S are relatively largest for the H_2-O_2 system containing no acetylene (Figs. 6 and 7, and similar curves for other gas compositions), i.e., the extent of self-absorption is smallest for this gas mixture. A comparison of the data shown for stoichiometric H_2-O_2 mixtures in Figs. 6 and 8

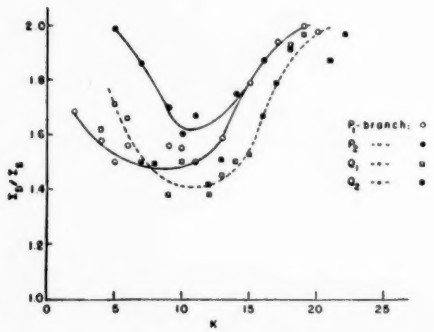

FIG. 6. Observed values of I_D/I_S as a function of K for a stoichiometric hydrogen-oxygen flame. (Inside diameter of contoured burner: 0.156 cm.)

FIG. 7. Observed values of I_D/I_S as a function of K for a mixture containing 66 percent oxygen, 25 percent acetylene, and 9 percent hydrogen. (Inside diameter of contoured burner: 0.156 cm.)

clearly shows less self-absorption of points on the P_2 branch for the smaller burner. This observation emphasizes the obvious fact that for self-absorbed emitters the apparent rotational temperature obtained from single-path experiments is a function of burner size.[9]

An interesting feature of the experimental results is the apparent splitting between the P_1 and P_2 levels for values of K less than about 9, a splitting which may indicate any one of the following: (a) relatively larger populations in the lower P_1 levels; (b) variation of the line-shape in such a way as to make the lower P_1 lines narrower; (c) an intensity ratio of P_1 to P_2 lines for small values of K which is greater than the calculated intensity ratio.[10] As is to be expected on the basis of intensity considerations based on the data given, for example, by Dieke and Crosswhite,[5] the Q-branch points lie below those of the P_2 branch in all cases.

The emission spectra obtained in single-path and in double-path experiments have been used to obtain rotational temperatures by drawing "best" curves through conventional plots of the logarithm of (observed intensity divided by the product of appropriate transition probability and fourth power of the frequency at the line center) as a function of the rotational energy of the initial (upper) state. The rotational "temperatures" obtained from the double-path experiments were invariably higher by a few hundred degrees than the corresponding "temperatures" obtained in single-path experiments. No particular significance can be attached to the absolute value of the difference between the two-path and single-path "temperatures" since a "temperature" derived by drawing a straight line, even through points following the calculated contours of self-absorbed emission curves,[4] is not defined with great accuracy. On the other hand, the fact that the two-path experiments yield the higher tempera-

[9] In order to assess the importance of self-absorption on apparent rotational temperature, studies of the type described in reference 4 should be consulted. On the basis of the experimental and theoretical data now available, it appears that reasonable "temperatures" for the inner cone are obtained for hydrogen-oxygen mixtures but not for the systems containing acetylene. See Sec. VI for further details.

[10] For further discussion of this result see Sec. VI.

tures, lends qualitative support to our contention that we are dealing with extensively self-absorbed systems.

In the absence of self-absorption, the parameter $2-(I_D/I_S)_{\min}$ would be equal to zero for all possible line profiles. Hence we may take this quantity as a qualitative measure of the extent of self-absorption in the flame. In Fig. 9 we have plotted the apparent single- and double-path emission temperatures obtained with the contoured burner (0.156 cm inside diameter), as well as the parameter $2-(I_D/I_S)_{\min}$, all obtained from the experimental data for the P_2 branch, as functions of the percentage of acetylene in the initial fuel mixture. Reference to Fig. 9 shows a remarkable parallelism between the experimentally determined self-absorption parameter $2-(I_D/I_S)_{\min}$ and apparent rotational temperatures in emission experiments. Even without further calculations, it is apparent that the "anomalous" temperatures produced by addition of C_2H_2 to H_2-O_2 mixtures simply reflect an increase in the OH concentration and in the extent of self-absorption. The temperature level for all of the inner cone emission experiments is undefined and cannot be computed, on the basis of conventional plots for the determination of rotational temperatures, from the experimental data, even assuming isothermal emitters, without quantitative knowledge of self-absorption and line-shape parameters. More detailed considerations, using our method of analysis for two-path experiments, are deferred to Sec. VI, where we attempt a quantitative interpretation of experimental data on the basis of assumed isothermal emitting systems with a line-shape parameter a which is constant and equal to zero for different values of K.

Our single-path emission experiments have yielded rotational "temperatures" (for both burner tips used by us) which are in satisfactory agreement with experimental results published by other investigators. For example, Kane and Broida[11] show a rotational "temperature" for the inner cone of stoichiometric H_2-O_2 mixtures of about 2900°K, which is seen to be in excellent agreement with our single-path temperature estimate of 3000°K (compare Fig. 9); the adiabatic flame temperature for stoichiometric H_2-O_2 mixtures is about 3100°K. For stoichiometric $C_2H_2-O_2$ mixtures, Kane and Broida report a value of about 4200°K,[11] Shuler and Broida[12] report a value of 3500°K, whereas our estimate is about 3600°K (compare Fig. 9);† the adiabatic flame temperature for the stoichiometric $C_2H_2-O_2$ flame is about 3300°K. The fact that substitution of C_2H_2 for some of the H_2 in stoichiometric fuel $-O_2$ mixtures causes an increase in the apparent rotational temperatures of OH is well known.[3]

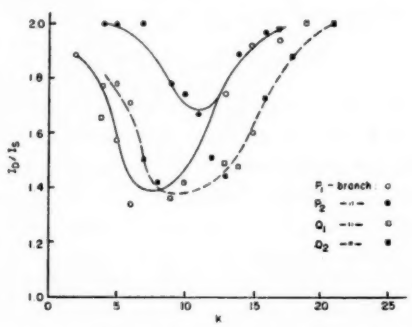

FIG. 8. Observed values of I_D/I_S as a function of K for a stoichiometric hydrogen-oxygen flame. (Inside diameter of straight burner tube: 0.071 cm.)

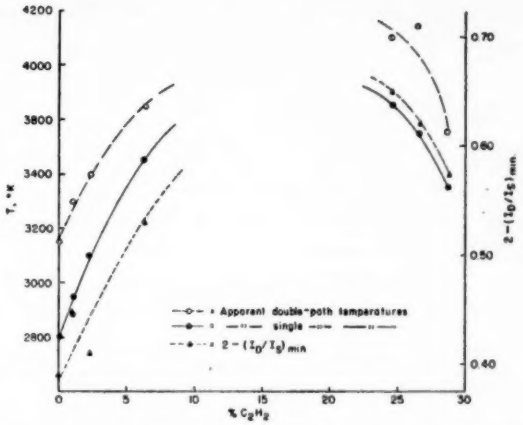

FIG. 9. Apparent rotational temperatures and the self-absorption parameter $2-(I_D/I_S)_{\min}$ as functions of percentage of acetylene for stoichiometric hydrogen-acetylene-oxygen mixtures. (Inside diameter of contoured burner: 0.156 cm; P_2 branch, $^2\Sigma \rightarrow {}^2\Pi$ transitions of OH, 0,0-band.)

V. EMISSION SPECTRA OF $C_2H_2-O_2-A$ FLAMES

Extensive single-path emission studies on the inner cones of diluted flames have been carried out by Kane and Broida.[11] We have repeated some of their studies on $C_2H_2-O_2-A$ flames using both the conventional single-path and our double-path techniques, again restricting our observations to the tips of the inner cones.

Representative results for I_D/I_S as a function of K, obtained with the contoured (0.156 cm inside diameter) burner tip, are shown in Fig. 10 for a stoichiometric acetylene-oxygen mixture containing 60 percent argon. Compared with the undiluted $O_2-C_2H_2$ data, the flames containing argon show somewhat stronger self-absorption. The reasons for this behavior are not obvious, although increased OH-number density in the light path may reflect, in part, the fact that the diluted flames show larger and less sharply bounded inner cones, which may be responsible for an increase in the optical path length.

Plots of the single-path or double-path apparent rotational temperatures and of the self-absorption parameter $2-(I_D/I_S)_{\min}$ for the P_2 or Q branches, as functions of percentage of argon, again show qualita-

[11] W. R. Kane and H. P. Broida, J. Chem. Phys. **21**, 347 (1953).

[12] K. E. Shuler and H. P. Broida, J. Chem. Phys. **20**, 1383 (1952).

† The differences in the reported rotational temperatures can be explained in terms of differences in the methods of observation.

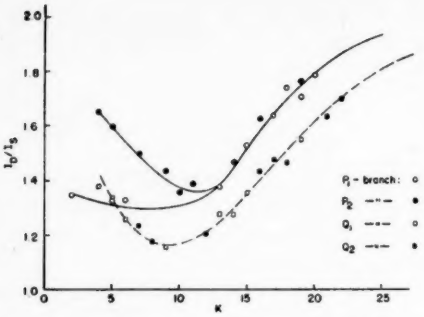

FIG. 10. Observed values of I_D/I_S as a function of K for stoichiometric acetylene-oxygen mixtures containing 60 percent argon. (Inside diameter of contoured burner: 0.156 cm.)

tive correlation, within the limits of experimental reproducibility.

The apparent rotational temperatures determined from our single-path experiments for various argon concentrations do not increase with argon concentration in the same manner as the rotational temperatures of Kane and Broida,[11] who used a straight-tip burner with about the same inside diameter as our contoured burner, and a contoured burner which was roughly eight times as large as ours.

VI. QUANTITATIVE INTERPRETATION OF EXPERIMENTAL RESULTS

Before proceeding with an attempt at quantitative interpretation of the experimental results, a remark concerning the lack of quantitative correlation between the extent of self-absorption and total emitted intensities (for the spectral lines) appears to be in order. The required exposure time to obtain the same blackening on a photographic plate is a rough measure of the total emitted radiant intensity. For cool systems, the possibility of obtaining low relative radiant intensities and, at the same time, large values for $2-(I_D/I_S)_{\min}$, cannot be ruled out.

It is the purpose of the following discussion to show that the experimental data obtained by us can be correlated satisfactorily on the assumption that we are dealing with isothermal equilibrium systems. In particular, it will be demonstrated that overall thermodynamic considerations concerning maximum possible concentrations of OH in the inner cones of flames are compatible with lower limits for OH-concentrations calculated from two-path experiments. Our method of analysis is a concession to our ignorance and represents only a first step at a true understanding of the radiation characteristics of flames. Since we must make the serious (and invalid) approximations that the emitters are isothermal and that all of the spectral lines can be characterized by a single value for the line-shape parameter a, our calculations and conclusions are not definitive. Nevertheless, it is gratifying to note that we can get a rational account for the observed results without introducing such concepts as a nonequilibrium bimodal population distribution for the excited OH radicals, which would not make proper allowance for the large extent of self-absorption observed in our flames.

The experimental determination of I_S and I_D, from which the ratios I_D/I_S are calculated, answers only the question of whether or not self-absorption distortions are present. If self-absorption does occur, then the conventional methods for the determination of rotational temperatures are inaccurate. There are three essentially undetermined parameters which can be adjusted to fit the experimental data. The unknown quantities are: (1) the spectral line-shape, which may not be uniform for a given branch and may be different from one branch to another; (2) the number density of (excited) OH radicals in the emitting light path; (3) the rotational temperature. Once the line-shape parameter a is known, we can use the analytical procedures described in previous publications[13,14] to calculate $P_{\max}X$, rotational temperature, and number density of OH-radicals in the emitting light path. In the absence of better information concerning line-shape, it will be sufficient to describe the analytical procedure for $a=0$ for several sets of experimental data. The basic theory is reviewed briefly in Sec. VIA and the results of interpretation of the experimental data are described in Sec. VIB.

VIA. Theoretical Considerations Relating to the Interpretation of Experimental Data

For isothermal systems the observable total intensity ratio for a single-path to a double-path experiment, I_S/I_D, is a function only of the parameters $P_{\max}X$, and a for the specified line, i.e.,

$$I_S/I_D=f(P_{\max}X, a). \tag{1}$$

Theoretical curves for $f(P_{\max}X, a)$ as a function of $P_{\max}X$ and a have been published previously.[13,14] Hence the experimentally determined values of I_S/I_D for the spectral lines can be used for the determination of $P_{\max}X$ (for example, with the aid of Fig. 3 of reference 14) if a is known.

The quantity $(P_{\max})_K$ is related to the integrated absorption S_K for the line identified by the rotational quantum number K through the expression

$$(P_{\max})_K=(S_K/\omega_K)(mc^2/2\pi kT)^{\frac{1}{2}}, \tag{2}$$

where ω_K is the wave number at the line center, m is the mass of the radiator, c equals the velocity of light, k is the Boltzmann constant, and T represents the absolute temperature. Suitable units for use in Eq. (2) are $P_{\max}$ in cm^{-1} atmos^{-1}, S_K in cm^{-2} atmos^{-1}, ω_K in cm^{-1}, and $mc^2/2\pi kT$ dimensionless. The quantity X is to be set equal to the product of the partial pressure (in atmos) of OH (irrespective of the energy state in which the OH occurs since X is not a function of K), and the optical path length L (in cm). The integrated intensity

[13] S. S. Penner, J. Chem. Phys. **20**, 1341 (1952).
[14] S. S. Penner, J. Chem. Phys. **21**, 686 (1953).

S_K is related to the dimensionless oscillator strength f_K associated with the Kth line through the expression[15]

$$S_K = 2.3789\times10^7(273.1/T)f_K(N_l/N_T) \times[1-\exp(-hc\omega_K/kT)] \quad (3)$$

where N_l/N_T represents the fraction of the total number of OH radicals present in the lower state for the transition or transitions giving rise to the line with quantum number K.

From Eqs. (2) and (3) it follows that

$$(P_{max})_K = \frac{2.3789\times10^7}{\omega_K}\frac{273.1}{T}f_K\frac{N_l}{N_T}\left(\frac{mc^2}{2\pi kT}\right)^{\frac{1}{2}} \quad (4)$$

since the term $\exp(-hc\omega_K/kT)$ is negligibly small in our studies. Hence the quantity $(P_{max})_K$ can be calculated if f_K and T are known.

In order to determine T, an explicit relation is needed for S_K. The basic relation[6] for S_K is

$$S_K = \frac{64\pi^4}{3}N_u(\omega_K)^4q_K^2/c\rho_K^0, \quad (5)$$

where N_u is the number of molecules per unit volume per unit pressure in the upper energy level for the transition giving rise to the line with index K, q_K^2 is the square of the matrix element for the indicated transition, and $c\rho_K^0/4$ is the intensity of radiation emitted from a blackbody at the wave number ω_K. The dimensions of S_K are cm^{-2} $atmos^{-1}$ if N_u is in cm^{-3}-$atmos^{-1}$, ω_K in cm^{-1}, q_K^2 in erg-cm^3, and $c\rho_K^0$ in ergs-cm^{-2}. At equilibrium the number of molecules in the upper energy state is given by the relation

$$N_u = N_T\frac{g_u\exp(-E_u/kT)}{Q},$$

where g_u is the statistical weight of the upper level E_u, involved in the given transition, and Q is the total partition function. Furthermore,

$$c\rho_K^0 = 8\pi hc\omega_K{}^3\frac{1}{[\exp(hc\omega_K/kT)]-1}.$$

Hence Eq. (5) becomes

$$S_K = \frac{8\pi^3N_T}{3hcQ}\omega_Kg_u(q_K)^2[\exp(-E_l/kT)] \times[1-\exp(-hc\omega_K/kT)]$$

and the following explicit relation for $(P_{max})_K$ is obtained from Eq. (2):

$$(P_{max})_K \simeq \frac{8\pi^3N_T}{3hcQ}\left(\frac{mc^2}{2\pi kT}\right)^{\frac{1}{2}}g_u(q_K)^2\exp(-E_l/kT). \quad (6)$$

On the right-hand side of Eq. (6) only the quantities $g_u(q_K)^2$ and $\exp(-E_l/kT)$ are functions of K for a given radiating system. Furthermore, X is independent of K in the present formulation. Therefore, the temperature T can be obtained from the measured values of

$$(P_{max}X)_K = (P_{max})_KX$$

from the following basic expression, which has been published previously[13]:

$$\frac{\partial ln\{(P_{max})_KX/[g_u(q_K)^2]\}}{\partial E_l} = -\frac{1}{kT}. \quad (7)$$

The form of Eq. (7) is such that it is particularly suited for the interpretation of strongly self-absorbed spectra corresponding to large values of $P_{max}X$. For values of $P_{max}X$ close to zero, for which conventional single-path techniques give useful results, the inevitable experimental scatter involved in the determination of $P_{max}X$ is often so large that the utility of Eq. (7) is greatly reduced.

The steps involved in the quantitative interpretation of flame spectra are thus seen to be the following:

(1) For an assumed, measured, or calculated line-shape parameter a, determine $(P_{max})_KX$ from the measured values of I_S/I_D from Fig. 3 of ref. 14.

(2) Determine the rotational temperature T for equilibrium according to Eq. (7).

(3) For the measured values of T calculate $(P_{max})_K$ according to Eq. (4) using the known values of f_K and ratios N_l/N_T determined from equilibrium calculations.

(4) From the measured values of $(P_{max})_KX$ and the calculated values of $(P_{max})_K$ it is now possible to estimate X, the product of partial pressure of OH, p_{OH}, and optical path length, L. If L is also known from the observed flame shape, then p_{OH} itself is determined and, since the total pressure is known, the absolute concentration of OH may be deduced.

VIB. Quantitative Interpretation of Experimental Data

We proceed with the quantitative interpretation of experimental data by making both temperature and concentration estimates.

(1) *Temperature Estimates*

Plots of $\log\{(P_{max})_KX/[g_u(q_K)^2]\}$ as a function of E_l, obtained by following the steps (1) and (2) for the interpretation of experimental data, are shown in Figs. 11 to 14.

[15] In previous publications (see references 4, 6, and 14) we have deleted the factor N_l/N_T so that the dimensions of S_K are cm^{-2} $atmos^{-1}$ evaluated for molecules in the lower state involved in the given transition. In this case it is necessary to make proper allowance for the Boltzmann factor in evaluating X, which then represents the product of the partial pressure of OH in the lower state for the given transition and the optical path length L. The factor $\exp(-hc\omega_K/kT)$ is negligibly small in most cases, and is usually omitted from Eq. (3).

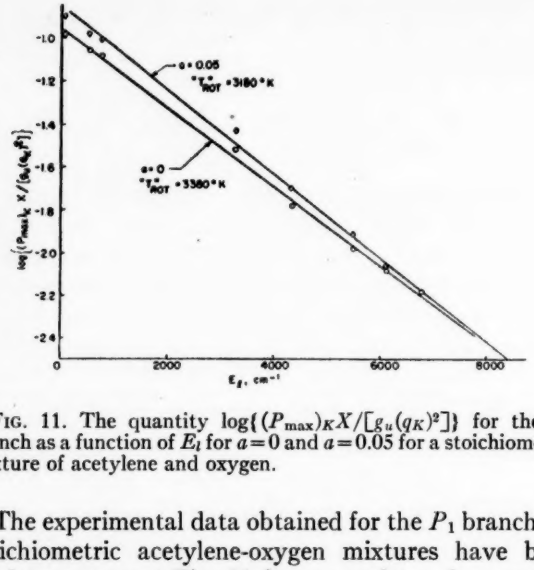

FIG. 11. The quantity $\log\{(P_{\max})_K X/[g_u(q_K)^2]\}$ for the P_1 branch as a function of E_l for $a=0$ and $a=0.05$ for a stoichiometric mixture of acetylene and oxygen.

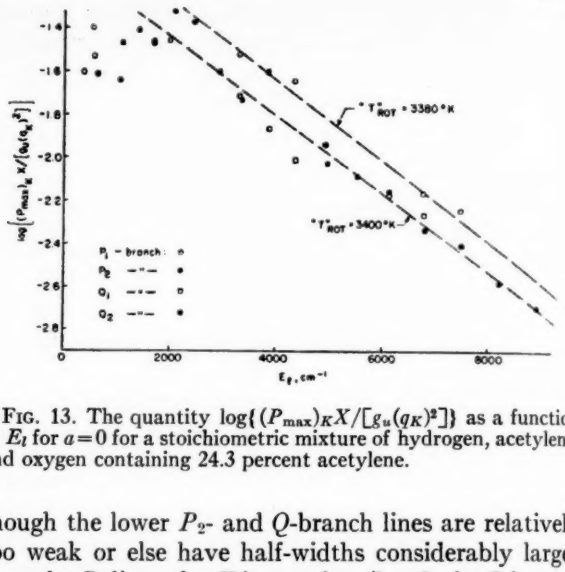

FIG. 13. The quantity $\log\{(P_{\max})_K X/[g_u(q_K)^2]\}$ as a function of E_l for $a=0$ for a stoichiometric mixture of hydrogen, acetylene, and oxygen containing 24.3 percent acetylene.

The experimental data obtained for the P_1 branch for stoichiometric acetylene-oxygen mixtures have been used to construct Fig. 11 for two values of a, namely $a=0$ (pure Doppler broadening) and $a=0.05$. Reference to Fig. 11 shows equally good fits for the experimental data for both values of a, and surprisingly good correlation of experimental data for the P_1 branch. The curves look as though the value of a is uniform for all of the P_1 lines. The apparent single-path temperature is seen to be reduced from 3600°K to about the adiabatic flame temperature (3380°K) for $a=0$ and below the adiabatic flame temperature (3180°K) for $a=0.05$. We are unable to say which temperature estimate is closer to the truth. It is easily seen that $a=0$ leads generally to upper limits for the temperature. For this reason, and for the sake of consistency, we shall use $a=0$ throughout the following discussion keeping in mind, however, that the "true" temperatures are apt to be appreciably lower than our estimates.

All the experimental data obtained for stoichiometric acetylene-oxygen flames have been used to construct Fig. 12. The lower P_2-branch points and most of the Q-branch points are seen to lie below the best curve for the P_1 branch. The data shown in Fig. 12 behave as though the lower P_2- and Q-branch lines are relatively too weak or else have half-widths considerably larger than the P_1 lines; for K larger than 7 or 8, the Q-branch points fall on a curve which is roughly parallel to, but displaced from, the best curve drawn through the P_1 points. For some value of a not much larger than 0.05 the P_2-branch and Q-branch points can be made to coincide nearly with the P_1-branch points. In the absence of estimates of the effect of vibration-rotation interactions on intensities, and without quantitative line-shape data, we are therefore unable to attach any significance to the apparent discrepancies noted in Fig. 12.[16]

A plot of $\log\{(P_{\max})_K X/[g_u(q_K)^2]\}$ as a function of E_l is shown in Fig. 13 for the stoichiometric $H_2-C_2H_2-O_2$ mixture containing 24.3 percent of C_2H_2. The "temperature" is seen to be reduced from 3850°K to below 3400°K. Splitting between the Q-branch points and the P_1-branch points is seen to occur in the same manner as for the stoichiometric $C_2H_2-O_2$ mixture.

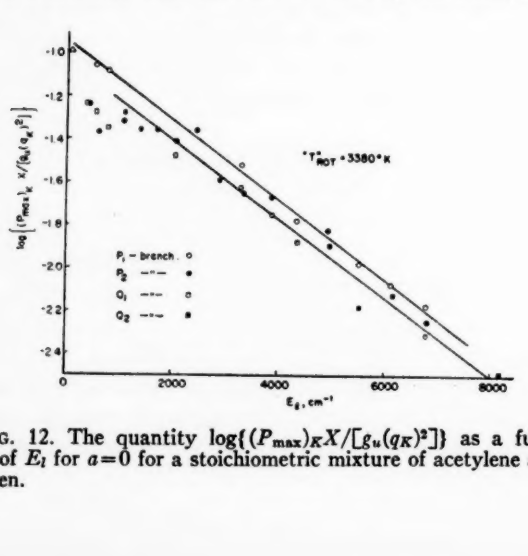

FIG. 12. The quantity $\log\{(P_{\max})_K X/[g_u(q_K)^2]\}$ as a function of E_l for $a=0$ for a stoichiometric mixture of acetylene and oxygen.

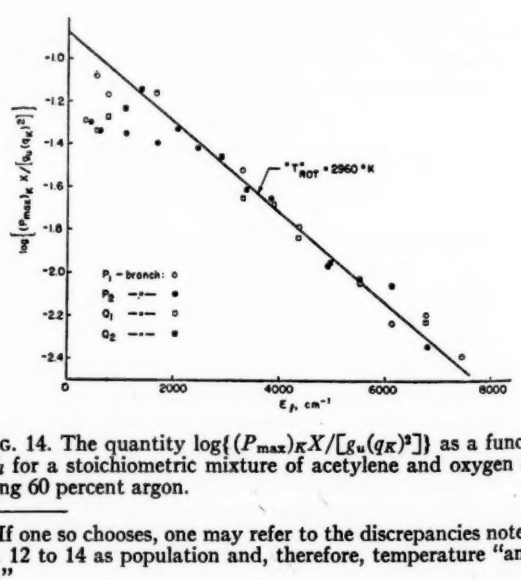

FIG. 14. The quantity $\log\{(P_{\max})_K X/[g_u(q_K)^2]\}$ as a function of E_l for a stoichiometric mixture of acetylene and oxygen containing 60 percent argon.

[16] If one so chooses, one may refer to the discrepancies noted in Figs. 12 to 14 as population and, therefore, temperature "anomalies."

Plots of $\log\{(P_{max})_K X/[g_u(q_K)^2]\}$ as a function of E_l for stoichiometric hydrogen-oxygen mixtures show large scatter of data, presumably because the values of $P_{max}X$ are relatively small, and, therefore, the demands on experimental accuracy are more stringent. Furthermore, the single-path temperature estimates remain practically unchanged.

A plot for estimating the temperature for the stoichiometric acetylene-oxygen mixture containing 60 percent argon is shown in Fig. 14. The single-path temperature estimate of over 4000°K is seen to be reduced below 3000°K by making proper allowance for self-absorption distortions; the adiabatic flame temperature for this sytem is about 3000°K. For K greater than about 7, all of the points belonging to the P and Q branches behave as though they have about the same line-shape. Correlation of experimental data is seen to be excellent.

Remarks similar to those made for the mixture containing 60 percent argon apply to the systems with 20 percent argon and 40 percent argon. In each case the lines behave as though the addition of argon tends to make all of the lines, for K greater than about 7, of the same width, the scatter being somewhat larger for the mixture containing 20 percent argon than for the mixtures containing 40 percent and 60 percent argon.

We may summarize the attempts at making quantitative temperature estimates as follows:

(1) Proper allowance for self-absorption reduces the single-path temperature estimates roughly to the adiabatic flame temperature for $a=0$ and below the adiabatic flame temperature for larger values of a.

(2) Apparent discrepancies in our plots can be "explained" by making postulates concerning either (a) the effect of vibration-rotation interactions on relative intensities of lines, or (b) the variation of equivalent line-shape parameter a from one branch to another, and from one value of K to another for a given branch.

(3) Significant improvement in the method of analysis is not possible without quantitative information concerning spectral line-shapes.

(2) *Concentration Estimates*

The product of partial pressure of OH (p_{OH}) and optical path length (L) is X, which can be determined from the available experimental data by following steps (1) to (4) for the interpretation of experimental data.

The results of representative calculations utilizing the line $K=2$ of the P_1 branch are given in Table I for the stoichiometric acetylene-oxygen flame and for the same combustible composition diluted by the addition of 60 percent argon. Reference to Table I shows that the value of X is about 13 percent larger for the diluted flame than for the undiluted flame. The optical path length L cannot be estimated with any degree of accuracy in either case. We are therefore unable to say whether or not the larger value of X for the diluted flame indicates a larger partial pressure of OH in the inner cone.[17] As was noted in Sec. V, the inner cones of diluted flames become progressively less well defined as the amount of diluent is increased. It is therefore possible that the effective value of L for the diluted flame is so much larger than for the undiluted flame that p_{OH} is actually smaller in the diluted flame. Additional quantitative work along these lines appears to be indicated. In the meantime it is of interest to note that, for reasonable estimates of L (i.e., L of the order of a few millimeters), the calculated values of p_{OH} turn out to be of the same order of magnitude as theoretical equilibrium values of p_{OH}.

In conclusion some remarks concerning the apparent absence of "anomalous" rotational temperatures above the inner cone of flames appear to be in order. It is reasonable to assume that this result indicates both the absence of "anomalous" rotational temperatures and of extensive self-absorption, or else a fortuitous compensation of errors produced by unknown temperature and concentration gradients. In view of theoretical studies showing the build-up of oxygen atom concentrations greatly exceeding the equilibrium value in ozone decomposition flames,[18] it is perhaps not unreasonable to interpret the observed extensive self-absorption at the tip of the inner cones of many flames by assuming some build-up of OH above the equilibrium concentration. An alternate "explanation" could be based on the hypothesis that the effective value of L for inner-cone

TABLE I. Concentration estimates of OH for two representative flames, based on measurements for the second line of the P_1 branch.

Flame	T(°K) for $a=0$	$P_{max}X$ for $a=0$[a]	P_{max}, (cm-atmos)$^{-1}$[b]	X (cm-atmos)
Stoichiometric acetylene-oxygen flame	3380	1.32	66	2.00×10^{-2}
Stoichiometric acetylene-oxygen flame containing 60 percent argon	3000	1.91	85	2.25×10^{-2}

[a] Determined from measured values of I_D/I_S.
[b] Calculated according to Eq. (4) from the f values reported by Oldenberg and Rieke (see reference 7). The use of absolute intensity estimates made by P. J. Dyne (Technical Report No. 12, Contract Nonr-220(03), NR 015 210, California Institute of Technology, November, 1953) would reduce P_{max} roughly by a factor of two and double the extimates for X.

[17] It is easy also to invent a change in line-shape with addition of argon which will produce lower apparent pressures of OH in the diluted flame than in the undiluted flame.

[18] Hirschfelder, Curtiss, and Bird, *Molecular Theory of Gases and Liquids* (John Wiley and Sons, Inc., New York, 1954); Theodore von Kármán and S. S. Penner, "Fundamental Approach to Laminar Flame Propagation," in *Selected Combustion Problems—Fundamentals and Aeronautical Applications* (Butterworths Ltd., London 1954).

emission studies is larger than for outer-cone experiments. It has been stressed repeatedly[4] that a relatively small increase in the value of X can be reflected by a surprisingly large apparent temperature rise in a conventional single-path emission experiment. For this reason we do not regard the absence of "anomalous" rotational temperatures for the burnt gases as a problem.

The present investigations have been confined to the tips of inner cones of flames, and suggest that rotational temperature anomalies either do not exist at this position or else are masked by self-absorption distortions. In published papers by Broida and others, emphasis is placed on the fact that the largest rotational temperature anomalies are normally observed within the inner cones of flames. The interpretation of experimental data obtained from inner cones is perhaps more complicated because of the more severe thermal gradients in the line of sight.

THE JOURNAL OF CHEMICAL PHYSICS VOLUME 23, NUMBER 1 JANUARY, 1955

LCAO MO Study of the Phenomenon of Thermochromism*

SHELDON L. MATLOW
Chemistry Department, Brookhaven National Laboratory, Upton, Long Island, New York
(Received January 28, 1954)

An LCAO MO calculation of the energies of the ground, planar triplet, and perpendicular triplet states of bianthrone and bixanthylene indicates that the thermally excited state in the phenomenon of thermochromism is the perpendicular triplet. Because of the uncertainty of the correct values of the parameters used, the best correspondence between the calculated and observed excitation energies that could be expected is that of order of magnitude. This is shown to be the case. The nature of the variation of the calculated values with the choice of parameters is indicated.

RECENTLY Nielsen and Fraenkel[1] reported that the thermally excited state of bianthrone (Fig. 1) observed in the thermochromic phenomenon is paramagnetic. If the assumption is made that no σ bonds are broken, there are two reasonable structures which can be hypothesized to explain the observed paramagnetism.† The first has essentially the same nuclear configuration as the ground state; one electron, however, has been promoted to an orbital of higher energy. This structure shall be referred to as the planar triplet. The other structure is one in which the anthracene ring systems are perpendicular to each other. This structure shall be referred to as the perpendicular triplet. The ground state and the planar triplet are strongly sterically hindered. A recent x-ray study indicates that the individual anthracene rings are not planar, but that the external benzene rings are bent away from the central ones.[2] The distortion energy of the planar configuration for the optically active biphenyls has been estimated to be of the order of magnitude of 20 kcal/mole.[3] As a first approximation, it is reasonable to assume that the steric hindrance energy of the ground state of bianthrone is of the same order of magnitude.

TABLE I. π-electronic energy levels of bianthrone.

Level	Coplanar configuration	Perpendicular configuration
I	$\alpha+1.5853\beta$	$\alpha+1.5426\beta$
II	$\alpha+1.5268\beta$	$\alpha+1.5426\beta$
III	$\alpha+1.3333\beta$	$\alpha+1.3333\beta$
IV	$\alpha+1.3333\beta$	$\alpha+1.3333\beta$
V	$\alpha+1.3286\beta$	$\alpha+1.2701\beta$
VI	$\alpha+1.2502\beta$	$\alpha+1.2701\beta$
VII	$\alpha+1.1366\beta$	$\alpha+1.0448\beta$
VIII	$\alpha+0.9722\beta$	$\alpha+1.0448\beta$
IX	$\alpha+0.8712\beta$	$\alpha+0.8693\beta$
X	$\alpha+0.8664\beta$	$\alpha+0.8693\beta$
XI	$\alpha+0.8000\beta$	$\alpha+0.8000\beta$
XII	$\alpha+0.8000\beta$	$\alpha+0.8000\beta$
XIII	$\alpha+0.8000\beta$	$\alpha+0.8000\beta$
XIV	$\alpha+0.8000\beta$	$\alpha+0.8000\beta$
XV	$\alpha+0.4699\beta$	$\alpha+0.2617\beta$
XVI	$\alpha+0.0700\beta$	$\alpha+0.2617\beta$

The excitation energies necessary to obtain the planar and perpendicular triplets from the ground state are approximated here by taking the difference of the π-electronic energies for the respective states. Because of the large steric hindrance energy in the planar configuration, this difference is corrected by 20 kcal/mole for the perpendicular triplet. Since the steric hindrance energy of the planar triplet is undoubtedly of the same order of magnitude as that for the ground state, no such correction need be applied in calculating the energy of excitation to the planar triplet. The π-electronic energies are calculated by using Wheland's method for the cal-

* Research performed under the auspices of the U. S. Atomic Energy Commission.

[1] W. G. Nielsen and G. K. Fraenkel, J. Chem. Phys. **21**, 1619 (1953).

† Since the observed thermal excitation energies are less than 10 kcal/mole and since the bond energies of the σ bonds present are all much greater than 10 kcal/mole, the assumption that no σ bond is broken seems reasonable.

[2] Harnik, Herbstein, and Schmidt, Nature **168**, 158 (1950).

[3] F. H. Westheimer and J. E. Mayer, J. Chem. Phys. **14**, 733 (1946). See also W. T. Grubb and G. B. Kistiakowsky, J. Am. Chem. Soc. **72**, 423 (1950).

culation of the energies of systems with hetero-atoms.[4] We have, however, chosen the value of δ_{oxygen} to be 1.0 instead of 0.8 as used by Wheland[4] since a carbonyl oxygen atom can presumably take on a negative charge more easily than a hydroxyl oxygen atom can and is, therefore, in this sense, more electronegative.

In Table I are listed the first sixteen energy levels for the coplanar and perpendicular configurations of bianthrone. All the levels of the perpendicular configuration are at least doubly degenerate since the ring systems are identical but do not interact.

The energy for the singlet coplanar state is obtained by placing two electrons in each of the first fifteen orbitals of the coplanar configuration. This gives an energy for the ground state of

$$E_{ground}=30\alpha+31.7476\beta, \tag{1}$$

where α is the Coulombic integral for a $2p\pi$ carbon orbital in benzene; and β is defined by

$$\beta=\gamma-S\alpha, \tag{2}$$

in which γ and S are, respectively, the exchange and overlap integrals for adjacent 2π carbon orbitals in benzene. The energy of the triplet coplanar state is obtained by placing two electrons in each of the first fourteen orbitals, one in the fifteenth and one in the sixteenth. Thus,

$$E_{\parallel}=30\alpha+31.3477\beta. \tag{3}$$

The energy of the perpendicular state is obtained by placing two electrons in each of the fourteen orbitals, one in the fifteenth and one in the sixteenth. Thus,

$$E_{\perp}=30\alpha+31.1638\beta. \tag{4}$$

Although the fifteenth and sixteenth orbitals are degenerate, both electrons are not placed in the fifteenth orbital since that electronic configuration would involve a separation of charge and would, therefore, actually be higher in energy. It is this arrangement of electrons in the fifteenth and sixteenth orbitals that results in the observed paramagnetism.

The energy differences between the ground and the coplanar and the perpendicular triplet states are obtained by subtracting (1) from (3) and (4), respectively. Thus,

$$\Delta E_{\parallel}=-0.3999\beta=15.996 \text{ kcal/mole} \tag{5}$$

and

$$\Delta E_{\perp}=-0.5838\beta=23.335 \text{ kcal/mole}. \tag{6}$$

The numerical values are obtained by using a value of -40 kcal/mole for β.[5] Since the ground state and the coplanar triplet state have about the same amount of steric hindrance, the value given in (5) is the final value. However, as stated above, the ground and perpendicular states differ by about 20 kcal steric hindrancewise; therefore, (6) should be corrected to read

$$\Delta E_{\perp}'=23.335-20.000=3.335 \text{ kcal/mole}. \tag{6'}$$

Experimentally it is observed that the thermal excitation energy is 3.4–3.5 kcal/mole.[6,7]

By the same method we shall now calculate the excitation energies for bixanthylene. In this case, however, we shall use three values for δ_{oxygen}, 0.8, 0.9, and 1.0. In Table II are listed the values for the first sixteen energy levels of the planar configuration. The ground state energy (exclusive of the steric hindrance term) is obtained by placing two electrons in each of the first fifteen levels. The planar triplet state energy is obtained by placing two electrons in each of the first fourteen levels, one in the fifteenth and one in the sixteenth. Thus,

$$\delta_{oxygen}=0.8\begin{cases}E_{ground}=30\alpha+29.1524\beta, & (7a)\\ E_{\parallel}=30\alpha+28.5155\beta, & (8a)\end{cases}$$

$$\delta_{oxygen}=0.9\begin{cases}E_{ground}=30\alpha+29.4750\beta, & (7b)\\ E_{\parallel}=30\alpha+28.8222\beta, & (8b)\end{cases}$$

$$\delta_{oxygen}=1.0\begin{cases}E_{ground}=30\alpha+29.8042\beta, & (7c)\\ E_{\parallel}=30\alpha+29.1370\beta, & (8c)\end{cases}$$

$$\Delta E_{\parallel}=-0.6369\beta=25.476 \text{ kcal}, \quad \delta_{oxygen}=0.8, \tag{9a}$$

$$\Delta E_{\parallel}=-0.6528\beta=26.112 \text{ kcal}, \quad \delta_{oxygen}=0.9, \tag{9b}$$

$$\Delta E_{\parallel}=-0.6672\beta=26.688 \text{ kcal}, \quad \delta_{oxygen}=1.0. \tag{9c}$$

In Table III are listed the values for the first sixteen levels for the perpendicular configuration. The energy of the perpendicualr triplet is obtained by placing two electrons in each of the first fourteen levels, one in the

TABLE II. π-electronic energy levels of bixanthylene, planar configuration.

Level	δ_{oxygen} 0.8	0.9	1.0
I	$\alpha+1.5827\beta$	$\alpha+1.5942\beta$	$\alpha+1.6098\beta$
II	$\alpha+1.5178\beta$	$\alpha+1.5383\beta$	$\alpha+1.5638\beta$
III	$\alpha+1.3333\beta$	$\alpha+1.3333\beta$	$\alpha+1.3333\beta$
IV	$\alpha+1.3333\beta$	$\alpha+1.3333\beta$	$\alpha+1.3333\beta$
V	$\alpha+1.2551\beta$	$\alpha+1.2850\beta$	$\alpha+1.3173\beta$
VI	$\alpha+1.1432\beta$	$\alpha+1.1703\beta$	$\alpha+1.1970\beta$
VII	$\alpha+1.1065\beta$	$\alpha+1.1141\beta$	$\alpha+1.1196\beta$
VIII	$\alpha+0.9641\beta$	$\alpha+0.9649\beta$	$\alpha+0.9656\beta$
IX	$\alpha+0.8000\beta$	$\alpha+0.8000\beta$	$\alpha+0.8000\beta$
X	$\alpha+0.8000\beta$	$\alpha+0.8000\beta$	$\alpha+0.8000\beta$
XI	$\alpha+0.8000\beta$	$\alpha+0.8000\beta$	$\alpha+0.8000\beta$
XII	$\alpha+0.8000\beta$	$\alpha+0.8000\beta$	$\alpha+0.8000\beta$
XIII	$\alpha+0.6040\beta$	$\alpha+0.6160\beta$	$\alpha+0.6273\beta$
XIV	$\alpha+0.4924\beta$	$\alpha+0.5202\beta$	$\alpha+0.5454\beta$
XV	$\alpha+0.0438\beta$	$\alpha+0.0679\beta$	$\alpha+0.0897\beta$
XVI	$\alpha-0.5931\beta$	$\alpha-0.5849\beta$	$\alpha-0.5775\beta$

[4] G. W. Wheland, J. Am. Chem. Soc. **64**, 900 (1942).
[5] G. W. Wheland, J. Am. Chem. Soc. **63**, 2025 (1941).
[6] W. T. Grubb and G. B. Kistiakowsky, J. Am. Chem. Soc. **72**, 419 (1950).
[7] Theilacker, Nortum, and Friedheim, Chem. Ber. **83**, 508 (1950).

TABLE III. π-electronic energy levels of bixanthylene, perpendicular configuration.

Level	δ_{oxygen} 0.8	0.9	1.0
I	$\alpha+1.5360\beta$	$\alpha+1.5538\beta$	$\alpha+1.5764\beta$
II	$\alpha+1.5360\beta$	$\alpha+1.5538\beta$	$\alpha+1.5764\beta$
III	$\alpha+1.3333\beta$	$\alpha+1.3333\beta$	$\alpha+1.3333\beta$
IV	$\alpha+1.3333\beta$	$\alpha+1.3333\beta$	$\alpha+1.3333\beta$
V	$\alpha+1.1615\beta$	$\alpha+1.1928\beta$	$\alpha+1.2237\beta$
VI	$\alpha+1.1615\beta$	$\alpha+1.1928\beta$	$\alpha+1.2237\beta$
VII	$\alpha+1.0448\beta$	$\alpha+1.0448\beta$	$\alpha+1.0448\beta$
VIII	$\alpha+1.0448\beta$	$\alpha+1.0448\beta$	$\alpha+1.0448\beta$
IX	$\alpha+0.8000\beta$	$\alpha+0.8000\beta$	$\alpha+0.8000\beta$
X	$\alpha+0.8000\beta$	$\alpha+0.8000\beta$	$\alpha+0.8000\beta$
XI	$\alpha+0.8000\beta$	$\alpha+0.8000\beta$	$\alpha+0.8000\beta$
XII	$\alpha+0.8000\beta$	$\alpha+0.8000\beta$	$\alpha+0.8000\beta$
XIII	$\alpha+0.5408\beta$	$\alpha+0.5618\beta$	$\alpha+0.5811\beta$
XIV	$\alpha+0.5408\beta$	$\alpha+0.5618\beta$	$\alpha+0.5811\beta$
XV	$\alpha-0.2363\beta$	$\alpha-0.2215\beta$	$\alpha-0.2080\beta$
XVI	$\alpha-0.2363\beta$	$\alpha-0.2215\beta$	$\alpha-0.2080\beta$

fifteenth and one in the sixteenth. Thus,

$$E_\perp = 30\alpha + 28.3930\beta, \quad \delta_{oxygen} = 0.8, \tag{10a}$$

$$E_\perp = 30\alpha + 28.7030\beta, \quad \delta_{oxygen} = 0.9, \tag{10b}$$

$$E_\perp = 30\alpha + 29.0212\beta, \quad \delta_{oxygen} = 1.0. \tag{10c}$$

$$\Delta E_\perp = -0.7594\beta = 30.376 \text{ kcal}, \quad \delta_{oxygen} = 0.8, \tag{11a}$$

$$\Delta E_\perp = -0.7720\beta = 30.880 \text{ kcal}, \quad \delta_{oxygen} = 0.9, \tag{11b}$$

$$\Delta E_\perp = -0.7830\beta = 31.320 \text{ kcal}, \quad \delta_{oxygen} = 1.0. \tag{11c}$$

The corrected excitation energy of the perpendicular triplet state is

$$\Delta E_\perp' = 10.376 \text{ kcal}, \quad \delta_{oxygen} = 0.8, \tag{11a'}$$

$$\Delta E_\perp' = 10.880 \text{ kcal}, \quad \delta_{oxygen} = 0.9, \tag{11b'}$$

$$\Delta E_\perp' = 11.320 \text{ kcal}, \quad \delta_{oxygen} = 1.0. \tag{11c'}$$

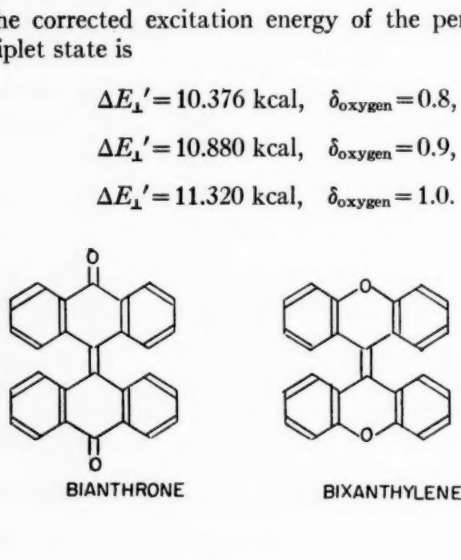

FIG. 1.

The experimentally observed value for the thermal excitation energy is 4.9 kcal/mole.[7] Thus, we see that all three cases considered for δ_{oxygen} give excitation energies which are too high. The best value is obtained for δ_{oxygen} equal to 0.8, which is the value used by Wheland for pheonolic oxygen.[4]

If we had used a value of 25.5 kcal/mole for the steric hindrance energy instead of 20 kcal/mole, the value of $\Delta E_\perp'$ for a δ_{oxygen} of 0.8 would be

$$\Delta E_\perp'' = 4.876 \text{ kcal/mole}. \tag{12}$$

There is, however, no *a priori* reason for assigning bianthrone a value of 20 kcal and bixanthylene a value of 25.5 kcal. Until a method is developed for making a better estimate of the steric hindrance energy, the best we can say is that it is of the order of magnitude of 20 kcal/mole for all cases of the type under consideration.

The values generally accepted for β are -40 kcal/mole for resonance energy calculations and -75 kcal/mole for spectral calculations. If we were to use the value of -75 kcal/mole for β, 0.8 for δ_{oxygen}, and 20 kcal/mole for the steric hindrance energy, the excitation energy for the perpendicular triplet state would be

$$\begin{aligned}\Delta E_\perp''' &= -0.7594\beta - 20 = 56.955 - 20 \\ &= 36.955 \text{ kcal/mole}.\end{aligned} \tag{13}$$

Thus, the spectral value for β is clearly not the one to be used here. The best that can be said is that the β to be used is of the order of magnitude of 40 kcal.

One could choose a set of δ_{oxygen}'s and steric hindrance energies and a β such that one would obtain the exact values for the excitation energies of bianthrone and bixanthylene. However, this would mean the setting of five parameters with two sets of experimental data, hardly a satisfactory procedure. In any case the calculations do indicate that the perpendicular triplet is much more probable than the planar triplet as the correct structure for the thermally excited state. By virtue of the uncertainty in the correct values for the parameters used, the best reproducibility that could be expected is that of the order of magnitude of the energy, which is indeed what is observed.

The author is indebted to Dr. Wallace Givens, Mr. W. Miranker, and Mr. J. H. Alexander of the U. S. Atomic Energy Commission Computing Facility at New York University for their aid in making these calculations.

Ultrasonic Dispersion in Methyl Alcohol Vapor*

CAVID ENER,† *Institute of Experimental Physics, University of Istanbul, Turkey*

AND

A. BUSALA AND J. C. HUBBARD,‡ *Catholic University of America, Washington, D. C.*

(Received July 14, 1954)

Ultrasonic velocities have been measured at temperatures of 32°C in the vapor of methyl alcohol, at pressures from 1.12 to 16 cm Hg, and at frequencies from 0.2 to 2.0 Mc sec^{-1}. A systematic variation with pressure of several percent in the measured values of velocity at the lower frequencies is attributed in large part to dimerization of the vapor. Previously determined constants in state equations for methanol have not been found adequate to reconcile the values of velocity at the higher pressures, but empirical values not far from those found by Weltner and Pitzer are satisfactory. There remains evidence of a thermal dispersion of velocity, attributed to internal rotation with a relaxation frequency of 100 Mc sec^{-1} $atmos^{-1}$, corresponding to a relaxation time of 2.27×10^{-9} sec.

INTRODUCTION

MANY investigations have been made on thermal relaxation phenomena in gases and vapors. The results until now seem to indicate that the process of energy transfer by collisions between translational and vibrational degrees of freedom occurs with a mechanism which generally involves essentially only the vibration of lowest frequency, the energy spreading from this to the other frequencies by a much faster process. The vibrational relaxation time for a given molecule is therefore determined by the lowest mode of vibration of the molecule; in simple and comparatively rigid molecules, the intermolecular collisions are rather inefficient and the vibrational relaxation phenomena occur at relatively low acoustic frequencies. In more complicated molecules, especially organic compounds with vibrations of low frequency or with internal rotation, the collisions are more efficient and one has to go to higher acoustic frequencies to find relaxation phenomena.

The present work is an investigation of the sound velocity in methyl alcohol vapor. The CH_3OH molecule has an internal rotation and is not expected to relax till at rather high frequencies. Lambert and Rowlinson[1] studied ultrasonic dispersion in several organic vapors; they measured sound velocity in methyl alcohol at 100°C up to about 13 Mc sec^{-1} $atmos^{-1}$ without finding any dispersion. In this laboratory the measurements have been made at 32°C and in the frequency/pressure range between 1 and 100 Mc sec^{-1} $atmos^{-1}$.

EXPERIMENTAL

Two ultrasonic interferometers have been used, both being of the type earlier introduced by one of the authors[2] and used since by many of his students. The instruments are used as resonators and are electrically driven by an oscillator of great amplitude and frequency stability. The construction is such as to maintain rigorous parallelism between source and reflector. This insures, when the driving frequency is kept at the frequency of the source and its associated vapor column at resonance, a simple "peak" system of the galvanometer current readings, without satellites. The instruments differ only in the mechanical means used to displace the reflector inside the vacuum tight envelope, one being similar to that used by Stewart[3] and later by Zmuda,[4] the other similar to that used by Thaler.[5] The driving voltage on the electrodes of the source was kept at values so low as to have no measurable effect on the velocity of sound in the vapor.

The methyl alcohol used was of reagent quality from Distillation Products (Eastman Organic Chemicals, No. 967), redistilled and taken at the boiling point of 64.50°C. The following routine for preparing organic vapors for acoustic measurements is usually observed: Five cc of the liquid is introduced into a small (10 cc) flask connected through a ground tapered joint and three-way stopcock to the line on one side leading through a trap to the evacuating pump, and on the other side to the interferometer system and manometers, or the liquid flask may be closed off and the interferometer system connected into the trap. Dry ice and various liquids are used for cooling the trap; at the beginning of preparation of the sample of vapor the flask is similarly cooled. The entire system is then evacuated through the trap. When the pressure is reduced below 0.1 mm Hg, the trap and pump are closed off, the cooling mixture removed from about the flask, and evaporation is allowed to take place into the interferometer system to a pressure of several cm Hg. The flask is then closed off and the interferometer system is opened into the trap for condensation of the vapor. The first time this is done with an evaporated sample there is usually a small amount of noncon-

* Supported by Office of Naval Research.

† Professor of Physics, Istanbul University, on leave at Catholic University September 1949–February 1951.

‡ Dr. Hubbard died August 2, 1954.

[1] J. D. Lambert and J. S. Rowlinson, Proc. Roy. Soc. (London) A204, 424 (1950).

[2] J. C. Hubbard, Phys. Rev. **38**, 1011 (1931); **41**, 523 (1932).

[3] J. L. Stewart, Rev. Sci. Instr. **17**, 59 (1946).

[4] A. J. Zmuda, J. Acoust. Soc. Am. **23**, 472–477 (1951).

[5] W. J. Thaler, J. Acoust. Soc. Am. **24**, 15 (1952).

densable residue. This is pumped out. In general a second evaporation yields on condensation no observable residue. The sample following the absence of residue is used for acoustic measurements. The vapor samples used for measurements are usually those coming from the middle third of the liquid.

Velocity measurements were taken at four frequencies, 0.20346, 0.4246, 1.0081, and 1.9760 Mc sec^{-1}, within the pressure range of 1.12 to 16 cm Hg. The pressures were measured by means of mercury manometers for all the runs at the three higher frequencies. For those at the lowest frequency a different method was used. A curve of the saturated vapor pressure *versus* temperature was obtained from several observations; then the pressure of the vapor for each run was obtained from the curve corresponding to the regulated temperature of the bath surrounding the liquid reservoir of the methyl alcohol.

The temperature of the interferometer system was thermoregulated at 32.2°C, and was always higher than the temperature of the bath regulating the vapor pressure.

RESULTS

Table I gives the experimental results; the measured velocities are reduced to 32°C, from them are found the "idealized" velocities as described below. For the reduction of measured velocities to 32°C, the ideal gas law is assumed, i.e., the velocity is assumed proportional to the square root of the absolute temperature. In Fig. 1 the experimental values of the velocity are plotted *versus* frequency over pressure; points corresponding to the two lower frequencies lie on two curves

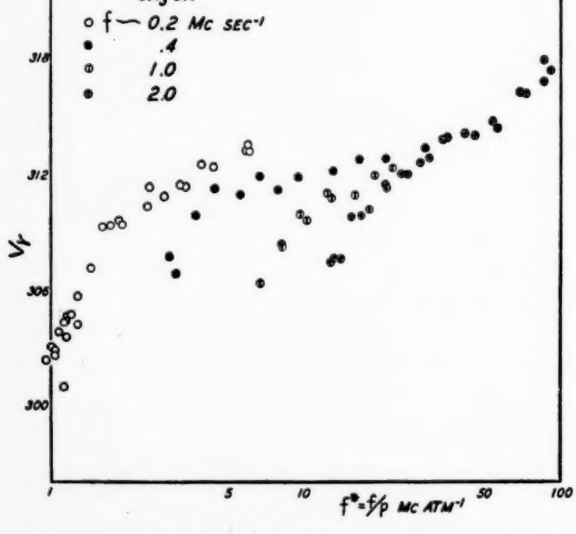

FIG. 1. Observed velocities at 32°C as function of pressure at different frequencies (Table I for precise values of f). Absence of single valued relation between V_r and f/p due to departure of vapor from ideal gas law.

TABLE I. Ultrasonic velocity as a function of frequency and pressure in methanol vapor at 32°C.

f Mc sec^{-1}	p cm Hg	f/p Mc sec^{-1} atmos^{-1}	V_r m sec^{-1}	V_i m sec^{-1}
0.20346	16.10	0.961	302.30	314.73
	15.37	1.006	303.00	313.86
	14.97	1.033	302.57	312.77
	14.90	1.038	302.83	312.91
	14.37	1.076	303.84	313.11
	13.86	1.116	300.93	309.41
	13.74	1.125	304.27	312.62
	13.56	1.141	303.49	311.59
	13.48	1.147	304.41	312.44
	13.47	1.148	304.67	312.67
	13.00	1.189	304.65	312.08
	12.34	1.253	305.62	312.30
	11.00	1.406	307.09	312.40
	9.78	1.581	309.23	313.51
	9.10	1.700	309.31	313.04
	8.43	1.835	309.46	312.68
	8.20	1.886	309.36	312.45
	6.63	2.333	310.3	312.5
	6.38	2.425	311.3	313.3
	5.63	2.747	310.8	312.5
	4.87	3.174	311.4	312.7
	4.68	3.303	311.3	312.5
	4.00	3.869	312.4	313.4
	3.62	4.274	312.3	313.2
	2.65	5.831	313.1	313.8
	2.65	5.831	313.1	313.8
	2.65	5.831	313.5	314.2
0.42460	11.2	2.89	307.64	313.15
	10.6	3.04	306.73	311.69
	8.85	3.66	309.76	313.30
	7.50	4.33	311.16	313.83
	6.00	5.44	310.9	312.7
	5.10	6.50	311.8	313.2
	4.20	7.65	311.1	312.1
	3.55	9.20	311.8	312.6
	2.55	12.50	312.1	312.6
	2.10	16.00	312.7	313.1
	1.52	20.20	312.6	312.9
	1.12	28.80	313.3	313.5
1.0081	11.80	6.491	306.20	312.29
	9.60	7.982	308.23	312.32
	8.24	9.300	309.81	312.94
1.0042	9.60	7.955	308.05	312.14
	7.78	9.816	309.55	312.36
	6.26	12.20	310.9	312.9
	6.16	12.40	310.8	312.7
	4.95	15.43	310.8	312.1
	4.12	18.54	311.9	313.0
	3.52	21.69	312.3	313.1
1.9760	12.18	12.33	307.22	313.75
	12.15	12.36	307.46	313.96
	11.19	13.42	307.56	313.07
	10.04	14.96	309.68	314.14
	9.38	16.01	309.80	313.75
	8.64	17.38	310.03	313.41
	7.44	20.18	311.26	313.90
	7.44	20.18	311.40	314.04
	6.44	23.41	312.0	314.0
	6.07	24.74	311.9	313.8
	5.39	27.86	312.3	313.8
	4.98	30.16	312.8	314.2
	4.33	34.68	313.7	314.8
	4.24	35.42	313.9	315.0
	3.61	41.60	314.0	314.9
	3.28	45.79	314.0	314.7
	2.84	52.88	314.7	315.4
	2.68	56.04	314.4	315.0
	2.19	68.57	316.1	316.6
	2.12	70.84	316.1	316.5
	1.80	83.43	316.7	317.0
	1.70	88.34	317.3	317.6

which have the same shape but are shifted parallel to the f/p axis. This shows that the gas is not ideal.

IDEALIZATION OF THE VELOCITY

Lambert, Roberts, Rowlinson, and Wilkinson[6] determined the second virial coefficients for several organic vapors and found that methyl alcohol belongs to a class of vapors for which the second virial coefficients are consistently very much higher than the values calculated by the Berthelot equation. This was interpreted in terms of dimerization. They give the second virial coefficient in the form

$$B=b-\frac{a}{T^2}-\frac{RT}{K_p},$$

where a and b are the constants calculated from the critical data with the Berthelot equation and K_p is a function of temperature determined experimentally and given in a graph for a temperature range between 40 and 130°C. This graph had to be extrapolated to the temperature of 32°C and the first and second derivatives with respect to temperature were determined graphically in order to calculate the idealization factor for the velocity of sound. The following formula was used:

$$\frac{V_r}{V_i}=1+p\left[\frac{B}{RT}+\frac{1}{C_v^0}\left(\frac{dB}{dT}+\frac{1}{2}\frac{RT}{C_p^0}\frac{d^2B}{dT^2}\right)\right], \quad (1)$$

where V_r and V_i are respectively the experimental and the ideal velocities of sound.

Weltner and Pitzer[7] made an extensive study of the thermodynamical properties of methyl alcohol; they also assumed polymerization of the vapor and gave the equation of state with second and fourth virial coefficients of the form:

$$pV=RT+Bp+Dp^3,$$

$$B=b-RTe^{-\Delta S_2/R}e^{\Delta H_2/RT},$$

$$D=-3RTe^{-\Delta S_4/R}e^{\Delta H_4/RT},$$

where

$b=80$ cc mole^{-1},

$\Delta S_2=16.5$ cal mole^{-1} deg^{-1}; $\Delta H_2=3220$ cal mole^{-1},

$\Delta S_4=81.3$ cal mole^{-1} deg^{-1}; $\Delta H_4=24\,200$ cal mole^{-1}.

These constants were determined for a temperature range between 70 and 130°C. From this equation the idealization factor for the sound velocity was calculated using the following:

$$\frac{V_r}{V_i}=1+p\left[\frac{1}{RT}\Phi+\frac{1}{C_v^0}\Psi\right], \quad (2)$$

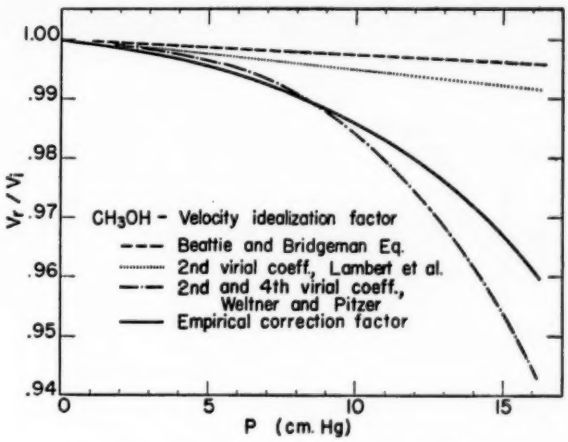

FIG. 2. Correction factor for sound velocity for nonideality of vapor.

where

$$\Phi=B+2Dp^2,$$

$$\Psi=\frac{dB}{dT}+\frac{1}{2}\frac{RT}{C_p^0}\frac{d^2B}{dT^2}+p^2\left(\frac{D}{T}+\frac{dD}{dT}+\frac{RT}{6C_p^0}\frac{d^2D}{dT^2}\right).$$

In Fig. 2 the two idealization factors calculated by Eq. (1), derived from Lambert and Rowlinson, and Eq. (2), derived from Weltner and Pitzers' results, are plotted with respect to pressure, together with a third factor derived from a Beattie and Bridgeman equation of state for methyl alcohol. These factors differ appreciably from each other and when applied to the experimental values of the velocity they did not bring all the points on to one continuous curve.

As it has been pointed out already, both the equations of state given by Lambert *et al.* and by Weltner and Pitzer are for a temperature range which does not include the temperature at which the velocity was measured and therefore in both cases an extrapolation was necessary. This could explain the different results obtained for the idealization factors; but it must be noticed also that the calculation of these factors involves second derivatives with respect to temperature, and therefore the coefficients in the equation of state have to be known very accurately as functions of temperature for these calculations.

An attempt was then made to find an empirical correction factor, function of pressure only, which, when applied to the experimental velocities, would give one continuous curve for the plot of the corrected velocities *versus* frequency over pressure, regardless of the frequency at which the measurements were taken.

For this purpose, all the experimental velocities in the range between 1 and 15 Mc sec^{-1} atmos^{-1} (where there is no evidence of thermal dispersion) were considered, and a factor calculated for each velocity which would bring its value to that of the ideal low frequency velocity. These factors were then plotted *versus* pressure

[6] Lambert, Roberts, Rowlinson, and Wilkinson, Proc. Roy. Soc. (London) **A196**, 113 (1949).

[7] W. Weltner, Jr., and K. S. Pitzer, J. Am. Chem. Soc. **73**, 2606 (1951).

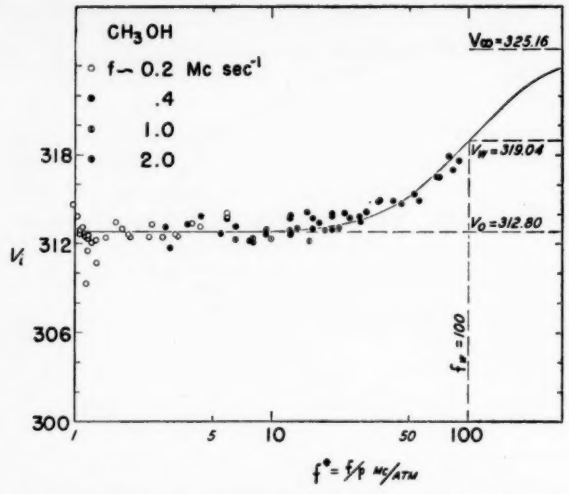

FIG. 3. Idealized sound velocities, V_i. Empirical correction gives closest approach to single valued relation between V_i and f/p. Results closely represented by normal dispersion curve shown with single relaxation f/p. Upper and lower limits independently fixed by specific heats determined from infrared and Raman spectroscopic data.

and a smooth curve drawn to best fit the points. In Fig. 2 the empirical factor so determined is shown; it is closest to the idealization factor calculated from the Weltner and Pitzer equation. The ideal low frequency velocity was calculated using the specific heat determined from spectroscopic data. Following Weltner and Pitzer, who used Halford's[8] values for the contribution to the specific heat from the internal rotation and applied Noether's[9] and Stepanov's[10] assignments for the vibration frequencies, the specific heat at 32°C was calculated with the two different assignments and an average taken. The low frequency idealized velocity at 32°C came out to be $V_0=312.80$ m sec^{-1}, corresponding to a specific heat $C_p^0=10.5$ Cal mole^{-1} deg^{-1}.

Figure 3 shows the idealized velocities *vs* f/p Mc sec^{-1} atmos^{-1}.

[8] J. O. Halford, J. Chem. Phys. **18**, 361, 1051 (1950).
[9] H. D. Noether, J. Chem. Phys. **10**, 693 (1942).
[10] B. E. Stepanov, J. Phys. Chem. (U. S. S. R.) **19**, 497 (1945).

DISCUSSION

The points in Figs. 1 and 3 have a spread somewhat greater than can be explained by experimental errors in velocity measurements. These measurements can be readily reproduced for a given sample from within 0.05 percent for the higher pressures used, to within 0.5 percent for the lowest pressures. Irregularities were also encountered when the vapor pressure was near saturation. This may be seen from the values of V_i near the left side of Fig. 3 where the vapor pressures were closest of all to saturation. Excluding, because of this effect, the first seven values of V_i given in Table I, we have, using the next 10 values, a mean for the idealized velocity before relaxation of 312.56 m sec^{-1} as compared with the theoretical value given above of 312.80 m sec^{-1}. This agreement must be considered as good in view of the fact that the criterion for idealization was taken to be that of "best fit" without regard to consideration of velocity limits.

The results of these experiments seem to leave no doubt about the existence of a dispersion of the velocity starting to be noticeable at about 30 Mc sec^{-1} atmos^{-1}. It has not been possible to reach the upper limit of the dispersion curve; but, judging from the position of the available points, it seemed reasonable to fix the limit at $V=325.16$ m sec^{-1}, which would correspond to a relaxation of all the vibrations and of the internal rotation, as was expected. Assuming a single relaxation time, it was tried to best fit the experimental velocities with a dispersion equation of the form:

$$V^2=V_0^2+(V_\infty^2-V_0^2)\omega^2\tau_c^2/(1+\omega^2\tau_c^2),$$

where V_0 and V_∞ have the values already given. The relaxation time was found to be

$$\tau=\frac{C_v^0}{C_v^\infty}\tau_c=2.27\times10^{-9}\text{ sec},$$

which corresponds to a relaxation frequency of 100 Mc sec^{-1} atmos^{-1}.

Approximate Method of Calculating Vibrational Frequencies of Polyatomic Molecules

S. BRATOŽ
Kemični Inštitut Slovenske Akademije Znanosti in Umetnosti "Boris Kidrič," Ljubljana, Yugoslavia
(Received June 7, 1954)

A new approximate method for calculating molecular vibrational frequencies is developed, based on the supposition that the molecule can be considered in zero-order approximation as a weakly coupled aggregate of partial vibrating systems, the interactions between them being taken into account by a perturbation calculation. The separation of the molecule into partial systems is discussed and a comparison is made with the results of exact calculation.

1. INTRODUCTION

THE usual theoretical procedures[1,2] of calculating the vibrational frequencies of polyatomic molecules having a large number of atoms are impracticable because of the high degree of the resultant secular equation. Therefore, some approximate methods have been developed by various authors,[3–6] especially by by Wilson,[7] and, quite recently, by Higgs.[8] They split off the high frequency vibrations from the low ones considering the mutual influences as small. This idea can be pushed further starting from the fact that in polyatomic molecules large differences in the masses as well as force constants do occur. As a consequence, the molecular vibrations can be classified into various types of hydrogen and skeletal vibrations, respectively, approximating them to normal vibrations of some smaller units. It seems therefore reasonable to consider the molecule as a weakly coupled aggregate of such units and to apply the exact procedure to these units only; the neglected interactions are taken into account afterwards by a perturbation calculation.

2. SCHRÖDINGER EQUATION

It is convenient to treat the problem in the quantum-mechanical form. If a motion with small amplitude is assumed for the nuclei, the expressions for the kinetic energy T as well as potential energy V can be written in the form

$$2T=\sum_{ik}g_{ik}\dot{r}_i\dot{r}_k \quad \text{and} \quad 2V=\sum_{ik}f_{ik}r_ir_k, \qquad (1)$$

where r_i and $\dot{r}_i$ are valence force coordinates and their respective derivatives, g_{ik} and f_{ik} are constants which depend on the molecular structure. Using the expressions (1), we obtain as the Schrödinger equation of the problem,[9] the symbols having their usual significance:

$$\sum_{ik}\left(-\frac{h^2}{8\pi^2}g^{ik}\frac{\partial^2}{\partial r_i\partial r_k}+\tfrac{1}{2}f_{ik}r_ir_k\right)\psi=E\psi. \qquad (2)$$

The coefficients g^{ik} form the well known matrix G and can be obtained very easily after the procedures published[7,10,11]; similarly, the coefficients f_{ik} form the matrix F. If the molecule has some symmetry elements, the symmetry coordinates may be introduced; G and F are to be replaced by $\mathcal{G}=UGU'$ and $\mathcal{F}=UFU'(U^{-1}=U')$.

3. ZERO APPROXIMATION

As already mentioned in the introduction, the first stage of the calculation consists in separating the molecule into several smaller units. In doing so, it is convenient to give up the geometrical representation: Eq. (2) should represent simply a coupled system of of harmonic vibrators. Each of them corresponds to one degree of freedom. Some of the vibrators are strongly coupled together, but very weakly to the rest of the molecule. It is reasonable to sort out the strongly coupled vibrators and to group them together. Such a group will be called a "partial system." In this way, the separation into partial systems is a grouping of degrees of freedom rather then a splitting of the molecule in discrete groups of bonded atoms. It will be seen later, from the results of the procedure, how a suitable separation can be achieved. For the moment, it may be assumed that a suitable separation is already performed and that the system is divided into S partial systems. In the limiting case the latter might contain one vibrator only; then, they are equal to free vibrators.

Neglecting the interactions between the partial systems, the Schrödinger equation (2) separates into S parts. Each of them has the form (2) and contains the terms describing one partial system only. Then, the zero-order solution is given by

$$\psi^{(0)}=\prod_s\psi_s^{(0)}, \quad E^{(0)}=\sum_s E_s^{(0)}, \qquad (3)$$

[1] G. Herzberg, *Molecular Spectra and Molecular Structure II. Infrared and Raman Spectra of Polyatomic Molecules* (D. Van Nostrand Company, Inc., New York, 1947).
[2] K. W. F. Kohlrausch, *Ramanspektren* (Akademische Verlagsgesellschaft Becher & Erler, Leipzig, 1943).
[3] R. Mecke, Z. Physik **104**, 291 (1937); Z. Physik **99**, 217 (1936).
[4] B. L. Crawford and J. T. Edsall, J. Chem. Phys. **7**, 223 (1939).
[5] P. Torkington, Nature **164**, 113 (1949).
[6] W. Edgell and T. R. Riethof, J. Phys. Chem. **56**, 326 (1952).
[7] E. B. Wilson, J. Chem. Phys. **7**, 1047 (1939); J. Chem. Phys. **9**, 76 (1941).
[8] P. W. Higgs, J. Chem. Phys. **21**, 1131 (1953).
[9] N. F. Mott and I. N. Sneddon, *Wave Mechanics and Its Applications* (The Clarendon Press, Oxford, England, 1948), p. 61.
[10] J. L. Decius, J. Chem. Phys. **16**, 1025 (1948).
[11] M. A. Eliaschevitch, Compt. rend. acad. sci. U.R.S.S. **28**, 605 (1940); J. Fisitscheskoi, Khimii **14**, 1381 (1940).

$\psi^{(0)}$ and $E^{(0)}$ being the total, $\psi_s^{(0)}$ and $E_s^{(0)}$ the partial wave functions and energies. $\psi_s^{(0)}$ and $E_s^{(0)}$ have the well-known form

$$\left.\begin{aligned}\psi_s^{(0)}&=\prod_e\left(\frac{\alpha_e}{\pi}\right)^{\frac{1}{4}}\cdot\frac{1}{(2^{v_e}v_e!)^{\frac{1}{2}}}e^{-\frac{1}{2}\alpha_e n_e^2}H_{v_e}((\alpha_e)^{\frac{1}{2}}n);\\ E_s^{(0)}&=\sum_e h\nu_e^{(0)}(v_e+\tfrac{1}{2})\\ \alpha_e&=\frac{2\pi}{h}(\lambda_e)^{\frac{1}{2}};\quad 4\pi^2\nu_e^{(0)2}=\lambda_e\end{aligned}\right\}. \tag{4}$$

Using the roots λ_e of the simplified secular equation, the zero-order normal coordinates

$$n_e=\sum_t B_{et}x_t \quad \text{or} \quad x_t=\sum_e a_{te}n_e \tag{5}$$

are obtained. They are orthogonal to each other and are normalized.

In this way the zero-order solution is obtained. If the choice of the partial systems has been suitably made, this approximation gives fairly good results. It can be seen, that many approximative treatments given in the literature (e.g., for long chain molecules)[12,13] are very similar to this approximation.

4. FIRST- AND SECOND-ORDER APPROXIMATION

So far, the interactions between the partial systems have been neglected. They are expressed by the first-order Hamiltonian

$$H^1=\sum_{ik}f_{ik}x_ix_k-\frac{h^2}{4\pi^2}g^{ik}\frac{\partial^2}{\partial x_i\partial x_k}. \tag{6}$$

For the perturbation calculation the usual Rayleigh-Schrödinger form is adopted, which is sufficient for this purpose. The problem can be treated nearly always as a nondegenerate one. The symmetry-caused degeneracy can be avoided by using symmetry coordinates (because of the factorization of the Schrödinger equation) and appropriate separation into partial systems. The possibility of the accidental degeneracy is, however, omitted. The perturbation calculation yields in these circumstances the well-known energy formula

$$E_v=\sum_i h\nu_i(v_i+\tfrac{1}{2}). \tag{7}$$

The parameters are

$$\nu_i=\nu_i^{(0)}+\tfrac{1}{2}\sum_k{}'\alpha_{ik}\eta_{ik}\nu_k^{(0)} \tag{7a}$$

$$\eta_{ik}=\frac{(\lambda_i\lambda_k)^{\frac{1}{4}}}{\lambda_i-\lambda_k} \tag{7b}$$

$$4\pi^2\nu_i^{(0)2}=\lambda_i \tag{7c}$$

$$\alpha_{ik}=\left(\frac{F_{ik}^2}{\lambda_i\lambda_k}+\frac{2F_{ik}G_{ik}}{\lambda_k}+G_{ik}^2\right). \tag{7d}$$

ν_i are the fundamental frequencies, whereas η_{ik} and α_{ik} are resonance and coupling factors (after Mecke).[3] In the expression for ν_i the indices k, which belong to the same partial system as i, are to be omitted. This is indicated by a prime above the summation sign in (7a). We have put the expression for ν_i in the form given by Mecke,[3] which seems to be very convenient. The coupling factors in the present work have in general a different meaning to those given in Mecke's paper. In our case, they depend on the quantities

$$F_{ik}=\sum_{st}a_{si}a_{tk}f_{st} \quad \text{and} \quad G_{ik}=\sum_{st}b_{is}b_{kt}g^{st}. \tag{7e}$$

The summation has to be extended over all pairs of indices, which do not belong to the same partial system, a_{si} and b_{is} being defined in (5). In this way, the quantities (7e) can be interpreted as to be cross-term constants effective in respective normal vibrations.

The higher approximations for the wave functions are not necessary. The symmetry, which is their most interesting feature, is correct already in zero-order approximation.

5. DISCUSSION

The quality of the approximation reached by the method outlined is strongly dependent on the choice of the partial systems. If the choice is good, small correction terms in (7a), i.e., small α_{ik} or η_{ik} will result. These quantities are small, as may be seen from (7b) and (7d), if the atomic masses or force constants implied differ sufficiently. Therefore, if the separation into partial systems is to be suitably made, the vibrators, which have similar masses and force constants, must be collected into the same partial systems. Taking into account the conditions as actually found in the spectra of polyatomic molecules, a separation is proposed in which the partial systems are formed by (1) the equivalent or nearly equivalent hydrogen valence vibrators, (2) the hydrogen deformation and skeletal valence vibrators, including multiple bond vibrators, and (3) the skeletal deformation and other low-frequency skeletal vibrators.

The above separation will probably be quite satisfactory in many cases, although some modification may be necessary from case to case, due to special conditions in individual molecules or to special purposes of the calculation. In any case, the separation proposed is a guide rather then a rule.

The coefficients α_{ik} and η_{ik} limit the usefulness of the approximate classification of the normal vibrations on various types of hydrogen and skeletal vibrations. If they are not sufficiently small, the differences between various types become uncertain and the classification becomes impracticable. The concept of the characteristic frequencies has the same limitations.

6. MATRIX FORMULATION

The results (7), (7a), (7b), (7c), (7d), and (7e) being known, the whole procedure can be greatly facilitated by

[12] J. Barriol, J. phys. et radium **10**, 215 (1939).
[13] M. Parodi, J. phys. et radium **8**, 58 (1941).

use of the Wilson's matrices F and G.[7] The above procedure appears now as an extension of Wilson's method to more complex cases. The problem can be then solved as follows.

First of all, the matrices F and G are to be constructed. An appropriate separation into partial systems might then be introduced. As a consequence, F and G split into unperturbed and perturbing parts F_0, G_0 and F_1, $G_1(F=F_0+F_1;\ G=G_0+G_1)$. Solving the unperturbed secular equation $|F_0G_0-E_\lambda|=0$ and corresponding systems of liner equations, unperturbed values for the roots λ_i as well as unperturbed normal coordinates $N=BR$ (or $R=AN$) are obtained. They are orthonormal, i.e., they have to satisfy to the matrix relation $A'G_0^{-1}A=BG_0B'=E$. The F_{ik} and G_{ik} of Eq. (7e) are the elements of the matrices $\Phi=A'F_1A$ and $\Gamma=BG_1B'$.

Putting the quantities listed into expressions (7a) etc., the corrected frequency values can be immediately obtained.

A similar procedure applies to the symmetrical case provided that symmetry coordinates have been introduced and each factor has been treated separately.

The calculations can be performed conveniently using the ordinary calculating machine.

7. EXAMPLE

As a simple example the symmetric CH_3Cl molecule has been selected because the results obtained through this method can be correlated very easily to the results of exact calculation. There are three A_1 type and three E-type vibrations for this molecule. The values for the frequencies, obtained through the exact calculation[14] and their description is given in Table I.

The numerical values of the matrices $\mathfrak{F}$ and $\mathfrak{G}$ are (the f_{ik} in 10^5 dyne/cm, the masses in $\frac{1}{16}$ oxygen mass, the lengths in A)

$$\mathfrak{F}_{A_1}=\begin{vmatrix} 3.6400 & 0.0000 & -0.4638 \\ 0.0000 & 4.7900 & 0.0000 \\ -0.4638 & 0.0000 & 0.5973 \end{vmatrix},$$

$$\mathfrak{G}_{A_1}=\begin{vmatrix} 0.1115 & -0.0481 & 0.1759 \\ -0.0481 & 1.0198 & -0.1016 \\ 0.1759 & -0.1016 & 2.0325 \end{vmatrix},$$

for the A_1 type vibrations, and

$$\mathfrak{F}_E=\begin{vmatrix} 4.7900 & 0.0000 & 0.0000 \\ 0.0000 & 0.6929 & -0.0120 \\ 0.0000 & -0.0120 & 0.5495 \end{vmatrix},$$

$$\mathfrak{G}_E=\begin{vmatrix} 1.1031 & -0.1068 & 0.1436 \\ -0.1068 & 0.9486 & 0.2770 \\ 0.1436 & 0.2770 & 2.2619 \end{vmatrix},$$

for the E-type vibrations.

[14] A. G. Meister and F. F. Cleveland, Am. J. Phys. **14**, 13 (1946).

TABLE I.

	Symmetry type	Description	Zero-order values in cm^{-1}	Corrected values in cm^{-1}	Exact calculation in cm^{-1}
ν_1	A_1	ν(CCl)	830	758	758
ν_2	A_1	δ(CH)	1435	1370	1371
ν_3	A_1	ν(CH)	2880	2885	2883
ν_4	E	δ(CH)	1023	1012	1012
ν_5	E	δ(CH)	1472	1468	1468
ν_6	E	ν(CH)	2995	3001	3001

A glance at Table I suggests the following separation into partial systems: for the A_1 type vibrations (νCH), (δCH), (νCCl); for the E-type vibrations (νCH), ($\delta CH_1\delta$CH). In this way, the zero-order solutions can be obtained. They are given in column four of Table I. Using these values, the matrices A, B, Φ, Γ are constructed. The latter are:

$$\Phi_{A_1}=\begin{vmatrix} 0.0000 & 0.0000 & -0.2209 \\ 0.0000 & 0.0000 & 0.0000 \\ -0.2209 & 0.0000 & 0.0000 \end{vmatrix},$$

$$\Gamma_{A_1}=\begin{vmatrix} 0.0000 & -0.1426 & 0.3694 \\ -0.1426 & 0.0000 & -0.0705 \\ 0.3694 & -0.0705 & 0.0000 \end{vmatrix},$$

for the A_1-type vibrations, and

$$\Phi_E=\begin{vmatrix} 0.0000 & 0.0000 & 0.0000 \\ 0.0000 & 0.0000 & 0.0000 \\ 0.0000 & 0.0000 & 0.0000 \end{vmatrix},$$

$$\Gamma_E=\begin{vmatrix} 0.0000 & 0.0698 & -0.1369 \\ 0.0698 & 0.0000 & 0.0000 \\ -0.1369 & 0.0000 & 0.0000 \end{vmatrix},$$

for the E-type vibrations.

By help of these results, the coupling and resonance factors are obtained. The corrected frequency values are given in column five Table I. The agreement between these values and the values obtained through exact calculation is excellent. The results cited show that the zero-order separation is entirely justified because of the small m_H/m_C ratio as well as of great difference between bond stretching and angle bending force constants.

ACKNOWLEDGMENT

The author wishes to express his indebtedness to Dr. D. Hadži for many stimulating disscussions and suggestions. Thanks are due also Dr. F. F. Cleveland, Dr. J. Duchesne, and Dr. N. Sheppard for a critical reading of the manuscript.

Irradiation of Ferrous Ammonium Sulfate Solutions: Energy Absorption and Ionization Calculations for Cobalt-60 and Betatron Radiation

D. V. CORMACK,* R. W. HUMMEL,† H. E. JOHNS,‡ AND J. W. T. SPINKS†
Departments of Chemistry and Physics, University of Saskatchewan, Saskatoon, Saskatchewan, Canada
(Received June 18, 1954)

G values for the irradiation of ferrous ammonium sulfate by cobalt-60 and betatron radiation have been recalculated taking into account wall effects which were neglected in the original paper.

IN a recent paper[1] published in the *Journal of Chemical Physics* we have developed an expression relating the energy ϵ absorbed per cm³ at a point in a solution to the ionization J produced per cm³ of air in a minute cavity at the same point, when the solution is exposed to radiation. Values of this ratio were calculated for Co^{60} gamma rays and for a betatron operating at 23 Mev and were used to determine the energy absorbed in $0.8N$ H_2SO_4 solutions from the readings obtained with a Victoreen chamber. These values are shown in column A of Table I. It has been pointed out to us[2,3] that values of the absorbed energy obtained in this way are considerably different from values which would be obtained by considering the Victoreen reading as giving the dose in roentgens and then calculating the energy absorbed using the appropriate real absorption coefficients. In view of this discrepancy, the problem has been reassessed according to the following considerations.

In Eq. (2) of the paper,

$$\epsilon=\int S_z^{\text{coll}}(E)\cdot N(E)\cdot dE,$$

it is seen that the value of the energy absorbed ϵ at any point in the solution is a function of $N(E)$, the energy distribution of electrons at the point. This distribution will be due to electrons which originate in a region surrounding the point. The limiting dimensions of this region are determined by the ranges of electrons set in motion by the radiation. If the dimensions of the solution to be irradiated are comparable to the average electron range, the distribution $N(E)$ will be partly due to electrons coming from the solution and partly to the electrons from the surrounding wall material. If then the wall material has a stopping power appreciably different from that of the solution, the value of $N(E)$ will not be uniform throughout the solution. If the solution is small compared with the electron ranges, the values of $N(E)$ will be essentially constant throughout the volume and will be characteristic of the surrounding walls. If the dimensions of the solution are large compared with the ranges, the distribution will also be uniform through the volume but will be characteristic of the solution itself.

The expression for the ionization J given by Eq. (3) as

$$J=\int \frac{S_a^{\text{coll}}(E)N(E)dE}{W}$$

involves the distribution function $N(E)$ also. The size of the air cavity may generally be considered small compared to the range of electrons in air, and thus the distribution $N(E)$ to be used in Eq. (3) will be that for the surrounding wall material. The use of Eq. (4),

$$\frac{\epsilon}{J}=W\frac{\int S_z^{\text{coll}}(E)N(E)dE}{\int S_a^{\text{coll}}(E)N(E)dE},$$

for determining the relation between energy absorption in the solution and the ionization produced in an air cavity in the same position is valid only if the electron distribution $N(E)$ is the same in both cases. This can occur only if the dimensions of the solution are small compared with the electron ranges or if the stopping power of the solution (per electron) is essentially the same as that of the material surrounding both the solution and the air cavity.

In the experimental arrangement used for obtaining the data reported in our paper, the irradiated solutions had a cylindrical volume about 1 cm in diameter. For

TABLE I. Summary of values of ϵ/J and G.[a]

		A[b]	B[c]	C[d]	D[e]
Co^{60}	ϵ/J	6.50	5.87	5.82	5.77
	G	15.8	17.5	17.7	17.8
Betatron	ϵ/J	6.38	6.30	5.82	5.93
	G	15.5	15.7	17.0	16.7

[a] Value of ϵ/J in ev $\times 10^{13}$/cm³ of solution per measured roentgen. Values of G in molecules oxidized per 100 ev.
[b] A. Values in original paper.
[c] B. Corrected values considering various wall effects and attenuations of radiation in the solution. Original values of I.
[d] C. Same as B using revised values of I and Steinheimer's values for the density effect.
[e] D. Determined from the expression $J=1/W\cdot n_s/n_a\times$attenuation correction factor.

* British Empire Cancer Campaign Exchange Fellow, 1953–1954.
† Department of Chemistry, University of Saskatchewan, Saskatoon, Canada.
‡ Department of Physics, University of Saskatchewan, Saskatoon, Canada.

[1] Cormack, Hummel, Johns, and Spinks, J. Chem. Phys. **22**, 6 (1954).
[2] Howard-Flanders, Gray, and Miller (private communication).
[3] Weiss, Bernstein, and Kuper, J. Chem. Phys. (to be published) and private communication.

Co^{60} radiation, the electrons have ranges of a few millimeters which certainly cannot be considered large compared with the solution dimensions. The conditions for validity of Eq. (4) are therefore not met and our use of it in determining the energy absorbed from the Victoreen readings is not justified. Neither does it appear entirely valid to regard the dimensions as large compared to electron ranges. It is therefore necessary to determine the distribution $N(E)$ at various points in the volume of the solution and find the energy absorbed at each point. The total energy absorbed in the volume of solution can then be found by integration. The electrons set in motion by betatron radiation have ranges of the order of a few centimeters. For this radiation also, the electron distribution will vary from point to point in the sample of solution. The energy absorbed must therefore be determined at several points and integrated over the total volume. If $N(E)$ is known for some point in the solution, the energy absorbed per cm^3 at that point can be found by the use of Eq. (2). Similarly, the ionization produced per cm^3 of air in the cavity may be found using Eq. (3) provided the value of $N(E)$ for the electron distribution at the position of the cavity is used.

The values of ϵ/J, the ratio of the energy absorbed per cm^3 of solution to the reading of the Victoreen chamber (esu/cm^3 if we assume the chamber has an "air-wall") were redetermined for our experimental arrangement according to the consideration described above. The values of E for various points in the volume of solution were found as follows. For each point the fraction of the absorbed energy due to electrons originating in each of the various surrounding materials was estimated from the "build-up" curves of the variation of ionization with wall thickness.[4] "Build-up" curves for water, Lucite and "air-wall" material were determined by interpolation from the curves for carbon and aluminum. The distribution $N(E)$ was calculated for each of those materials using Eq. (6). It may be shown, for radiations and materials where only Compton absorption need be considered, that $N(E)$ is inversely proportional to the total stopping power per electron, $(S)_Z$ total. To find the distribution at a point surrounded by layers of various materials, the distribution for each material was multiplied by the fractional contribution of that material to the absorbed energy. It was assumed that the electrons set in motion by the radiation travel mainly in the original direction of the radiation beam. For Co^{60} the average energy absorbed per cm^3 in the solution was calculated to be 1.004 times the energy which would have been absorbed if the surrounding walls had also consisted of solution. The corresponding factor for betatron radiation is 1.016.

The values for $N(E)$ and ϵ also vary from point to point in the solution because of the attenuation of the radiation in passing through the material. The attenuation correction was determined for Co^{60} radiation from the published depth dose curves.[5] The cross sectional area was estimated to be 4 cm^2, so the depth dose curve for a field of this area was found by interpolation. The attenuation correction for Co^{60} was determined to be about 3 percent for the size of solutions used. The experiments with betatron radiation were carried out with the sample in a position corresponding to the broad maximum of the "build-up" curve and the radiation intensity was essentially constant throughout the sample of solution.

The value of J, the ionization produced in the chamber, was determined in a similar way, the $N(E)$ distribution being due partly to the "air-wall" of the chamber (73 percent for Co^{60} and 10 percent for betatron radiations) and partly due to the additional Lucite. The value of J in the composite wall chamber was calculated to be 1.078 times the ionization in a water-wall chamber for Co^{60} radiation and 1.029 for 23-Mev betatron radiation.

The recalculated values for ϵ/J, the ratio of the energy absorbed per cm^3 of solution to the reading on the Victoreen meter, are given in column B of the table. For Co^{60} radiation, $\epsilon/J = 5.87\times10^{13}$ ev/cm^3 of $0.8N$ H_2SO_4 solution per roentgen as indicated on the Victoreen; for 23-Mev betatron radiation $\epsilon/J = 6.30\times10^{13}$ ev/cm^3 per r. The corresponding values of G are then: Co^{60} -17.5 molecules oxidized per 100 ev; betatron -15.7 molecules per 100 ev. In calculating these values the collisional stopping power has been calculated from the Bloch formula, as quoted by Heitler[6] and polarization effects have been neglected. The values used for the various constants are those used in the original paper, namely: $I(\text{air}) = 96$ ev, $I(0.8N\ H_2SO_4) = 45$ ev, $W(\text{air}) = 32.5$ ev. The average ionization energy for Lucite, I(Lucite) was determined to be 60 ev from values of I for hydrogen, carbon and oxygen in compounds given by Thompson.[7] This value agrees well with the value of 61 ev for polystyrene used by Weiss *et al.*[3] in their calculation, and which they have checked experimentally by comparison with Al for which I is reasonably well known.

The value of 96 ev for I(air) is considerably different from the value of 83.2 ev adopted by Weiss *et al.* in their calculations. The latter value is probably somewhat more reliable. The value of 45 ev for the average ionization energy of $0.8N$ H_2SO_4 is probably too small and a better value would be 62 ev calculated from Thompson's data. It was therefore thought advisable to recalculate ϵ/J using these revised values of I. The adoption of these values changes the average ratio of the stopping powers of water and air for Co^{60} radiation from 1.09 to 1.04. This tends to decrease the effect of heterogeneity of the walls.

[4] D. V. Cormack, thesis, University of Saskatchewan, 1953.

[5] Johns, Epp, Cormack, and Fedoruk, Brit. J. Radiol. **25**, 302 (1952).

[6] W. Heitler, *The Quantum Theory of Radiation* (Oxford University Press, New York, 1944).

[7] T. J. Thompson, University of California Radiation Laboratory—1910 (1952).

In calculating the second revision the values of ϵ/J using the more reliable values of I(air) and $I(H_2O)$ the stopping powers were also corrected to allow for the density effect due to polarization of the medium. The reduction in the energy loss in $0.8N$ H_2SO_4 due to polarization effects was taken from Steinheimer's data for water.[8] The density effect in air is negligible for the electron energies used. It will be noted that Weiss *et al.* have used a formula due to Bethe for the calculation of collisional stopping powers whereas we have used a formula derived by Bloch. A comparison of these formulas shows that the values obtained by the two formulas for 0.2-Mev electrons (about the average for Co^{60} radiation) differ by only about 4 percent and that the ratio of the stopping powers of air and water differ by only 0.2 percent. Thus, it appears that for these calculations either formula may be used.

The values of ϵ/J obtained using the revised values of I are given in column C of the table together with the corresponding values of G. *These values are believed to be the most reliable values of G for this experiment.*

For comparison, values of ϵ/J have been calculated from the simple expression $J=1/W\cdot n_z/n_a\times$attenuation correction factor. This expression assumes that the energy gained by electrons per cm^3 of solution from the radiation (i.e., the energy "truly absorbed" from the radiation as calculated from the real absorption coefficients) is equal to the energy dissipated by these electrons per cm^3 of solution. It also assumes that the Compton absorption, which is proportional to the electron density, is the predominant mechanism by which energy is absorbed from the radiation beam. The values of ϵ/J obtained in this way are given in column D of the table. It will be noted that this value for Co^{60} is almost identical with the value in column C obtained by a detailed consideration of the electron distribution in the air cavity and at various points in the sample of solution. This is to be expected, since for Co^{60} (1) absorption of radiation is almost entirely by the Compton effect, (2) the electron distribution is essentially in equilibrium with the radiation in nearly all the volume of solution, and (3) loss of energy by electrons through bremsstrahlung is almost negligible. None of these conditions applies to betatron radiation and therefore one would not in this case expect agreement between the values of columns C and D. Actually, however, the effects tend to cancel each other out and the actual difference between the values in columns C and D is less than 2 percent.

[8] R. M. Sternheimer, Phys. Rev. **88**, 851 (1952).

THE JOURNAL OF CHEMICAL PHYSICS VOLUME 23, NUMBER 1 JANUARY, 1955

Shape of the Coexistence Curve near the Critical Temperature*

O. K. Rice
University of North Carolina, Chapel Hill, North Carolina

(Received June 22, 1954)

It is shown that diffusion in the gravitational field in binary liquid systems is so slow that the effect of gravity may be completely neglected in studies of the coexistence curve. The data arising from the direct measurement of the coexistence curve of the cyclohexane-aniline system have been correlated with those from measurements of the densities of coexisting phases. A graph has been constructed which confirms the earlier conclusion that the coexistence curve is flatter at the top than can be accounted for by a cubic relation between temperature and density. Finally, a discussion is given of the liquid-vapor equilibrium in a one-component system. It is pointed out that the range of densities over which the meniscus has been reported to disappear within the tube in earlier work is so small that measurements of the coexistence curve need to be made with a temperature control of the order of 0.0001°. Only the recent work of Lorentzen on carbon dioxide meets this requirement. His data appear to be favorable to the idea that there is a short flat portion on the top of the coexistence curve, but are still not quite adequate to settle the question.

1. INTRODUCTION

RECENTLY there has been considerable discussion of the shape of the coexistence curve in the neighboring of a critical point. According to the classical van der Waals theory T_c-T should be proportional to $(\rho_l-\rho_v)^2$ near the critical point, ρ_l and ρ_v being densities of liquid and vapor, respectively, T being the temperature, and T_c being the critical temperature. Guggenheim,[1] however, has collected data on a number of liquid-vapor equilibria, and has found that T_c-T is more nearly proportional to $(\rho_l-\rho_v)^3$. A similar relation seems to hold in binary liquid systems. Thus Zimm[2] has found that $(x''-x')^3$ is proportional to T_c-T in the perfluoromethylcyclohexane-carbon tetrachloride system. Here x'' is the mole fraction of one of the components in one of the existing phases and x' that of the same component in the other phases. Atack and Rice[3] have found that a similar relation exists for the densities in the cyclohexane-aniline system, $(\rho''-\rho')^3$

* Work supported by the Office of Naval Research.

[1] E. A. Guggenheim, J. Chem. Phys. **13**, 253 (1945).

[2] B. H. Zimm, J. Phys. & Colloid Chem. **54**, 1306 (1950).

[3] D. Atack and O. K. Rice, Discussions Faraday Soc. **15**, 210 (1953).

being almost proportional to T_c-T up to very small values of T_c-T. In either case, $x''-x'$ or $\rho''-\rho'$ is a measure of the "difference" between the two phases, and the analogy of the van der Waals theory would suggest that the square rather than the cube should be proportional to T_c-T.

There are some theoretical reasons for expecting the coexistence curve to deviate from the cubic law at very small values of T_c-T; it has been suggested on various grounds[4] that there should be a flat horizontal portion of the coexistence curve at its top; i.e., that there should be a range of critical concentrations at T_c. There have been a number of attempts to decide this question experimentally, and these have received various interpretations. It is the purpose of the present article to consider these experiments critically, to see what conclusions can be drawn from them, and to make some suggestions regarding the possible course of future experiments.

It will be helpful to start this discussion by considering what one may hope to determine experimentally. It will be clear that no direct measurements of the coexistence curve can ever decide whether the top of this curve is a geometrically straight line, for no matter how accurate the work may be there will always be some remaining error. Only if a qualitative criterion can be found, such as Mason, Naldrett, and Maass[5] at one time believed they had found, will it be possible to say whether the top is geometrically straight, and even in such a case difficulties in interpretation will be likely to remain, as we shall see. On the other hand, if the measurements are carried out accurately enough it should be possible to define limits of accuracy of the Guggenheim cubic relationship, and find out whether the top of the coexistence curve is appreciably flatter than would be expected from the cubic relationship, though exceedingly accurate experiments will be required.

In what follows we shall wish to consider both the liquid-vapor equilibrium, and the binary liquid systems. Theoretically these are essentially similar, but from the experimental point of view there is a fundamental difference with respect to the effect of gravity. In the liquid-vapor equilibrium gravity is extremely important. Because of the compression of the gas by itself at a temperature just above the critical temperature where the substance is highly compressible, gradients of density will develop so that there will be, at some particular height, a density equal to the critical density, even though the average or over-all density differs somewhat from the critical density. On cooling such a system to the critical temperature a meniscus will be expected to appear at the position where the density is equal to the critical density. Since in most experiments only the average density is measured, there will be an apparent range of critical densities, and there will be an apparent flat top to the coexistence curve, which must be distinguished from any residual true flat top, which would in general extend over a much smaller range of densities. It has been shown experimentally that equilibrium with respect to the density gradients in a gravitational field is reached in the course of some hours or at most a day or two.[6]

In a binary liquid system there will also be a tendency for concentration gradients to develop just above the critical temperature, because of the different effective densities of the different constituents. It can be shown in this case, however, that the time required for the development of such concentration gradients is so great that if a solution above its critical temperature is once brought to equilibrium and thoroughly stirred no separation will take place until the temperature is lowered below the critical temperature and two distinct phases of different density separate out. In the case of an ideal solution the concentration gradient which will be established in the gravitational field at equilibrium is given by[7]

$$dx_1/dh=(M\bar{V}_1/V-M_1)x_1g/RT.$$

Here x_1 is the mole fraction of constituent 1, M_1 its molecular weight, $\bar{V}_1$ its partial molal volume, M the average molecular weight of the solution, V the volume of one mole of solution, and h the height. We may write, to order of magnitude,

$$(dx_1/dh)/x_1\sim Mg/RT.$$

With $M=100$ and $T=300°\text{K}$

$$(dx_1/dh)/x_1\sim 0.4\times 10^{-5}\ \text{cm}^{-1}.$$

Now with diffusion constants of the order of magnitude of those found in liquids the "half-life" of a concentration gradient in an ideal solution is of the order of one day. We see then that the force of gravity in a solution is about large enough to establish a gradient of 10^{-6} to 10^{-5} mole fraction per cm per day. This is clearly far too small to have any effect on an ordinary experiment.

2. BINARY LIQUID SYSTEMS

Since no difficulty will arise from gravity in the case of binary liquid systems, we shall consider them first. Actually only two binary systems have been studied carefully enough to warrant consideration. These are the perfluoromethylcyclohexane-carbon tetrachloride system, studied by Zimm,[2] and the cyclohexane-aniline system studied by Rowden and Rice[8] and by Atack and Rice.[3,9]

[4] J. E. Mayer and S. F. Harrison, J. Chem. Phys. **6**, 87, 101 (1938); O. K. Rice, J. Chem. Phys. **15**, 314 (1947).

[5] Mason, Naldrett, and Maass, Can. J. Research **B18**, 103 (1940).

[6] M. A. Weinberger and W. G. Schneider, Can. J. Chem. **30**, 847 (1952).

[7] G. N. Lewis and M. Randall, *Thermodynamics* (McGraw-Hill Book Company, Inc., New York, 1923), p. 244.

[8] R. W. Rowden and O. K. Rice, J. Chem. Phys. **19**, 1423 (1951); *Changements de Phases* (2e Réunion Soc. Chim. Phys., Paris, 1952), p.78.

[9] D. Atack and O. K. Rice, J. Chem. Phys. **22**, 382 (1954).

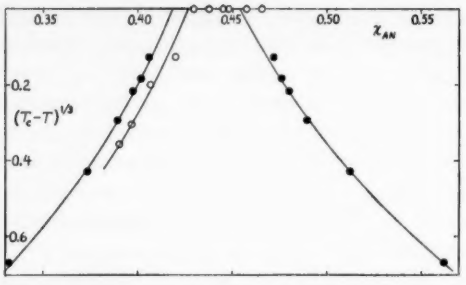

FIG. 1. Coexistence curve for cyclohexane-aniline system, mole fraction of aniline against $(T_c-T)^{\frac{1}{3}}$. Open circles, direct measurement of compositions; black circles, compositions obtained from density measurements.

The measurements of Zimm indicate that the coexistence curve in the perfluoromethylcyclohexane-carbon tetrachloride system does not have a flat top, but is rounded and follows a cubic curve clear to the top. However, Zimm's investigation did not include compositions as close to the critical composition as might be desired. Furthermore, his materials were not protected from air and atmospheric moisture. It therefore seems to me that his results cannot be considered as entirely conclusive.

In the case of the cyclohexane-aniline system Rowden and Rice found that for a range of aniline mole fractions from 0.42 to 0.46 the transition for a one-phase to a two-phase system occurred at the same temperature. Zimm,[10] however, showed that within the stated limit of error, 0.003°, the data could be fitted by a cubic curve. In their later paper, Rowden and Rice indicated that the *difference* in the transition temperatures for the various solutions in the range of concentrations noted was probably considerably less than 0.003°, and Atack and Rice[8] have found the transition to be the same within 0.001° for six solutions in the range 0.43 to 0.465 mole fraction aniline. Their measurements of the densities of the coexisting phases[3,9] also lend support to the idea that the coexistence curve is flat on top.

It seems desirable to replot and compare more carefully the results obtained by Atack and Rice by using separate solutions of known composition and those obtained from the density measurements. Densities of the coexisting phases in the immediate neighborhood of the critical point can be converted into mole fractions from a curve obtained from values of the densities of pure cyclohexane (0.7702 g/cc) and pure aniline (1.0135 g/cc) at temperature T_c and the density of a solution of 0.4451 mole fraction aniline just above the critical point (0.8636 g/cc)[11] obtained in the work of Atack and Rice. In using these data it is necessary to bear in mind that the temperature listed as T_c in reference 3 is about 0.005° too high; if a corrected or "true" value of T_c is used, then it is actually found that $(\rho''-\rho')^3$ is more closely proportional to $T_c-T+0.005°$ than to T_c-T.

Unfortunately Atack and I, in our work on the direct observation of the transition temperature in mixtures of varying composition, did not obtain any points on the aniline-rich side of the critical region. However, it is not necessary to have values of $x''-x'$; instead we may plot the mole fractions x'' and x' separately, so far as available, against $(T_c-T)^{\frac{1}{3}}$. This has been done in Fig. 1, using "true" values of T_c, with x_{AN} the mole fraction of aniline, obtained both directly and from density measurements; in the latter case the points for which T_c-T was appreciably greater than 0.3° were not used. In Fig. 2 we have plotted x_{AN} against $(T_c-T+0.005°)^{\frac{1}{3}}$.

We note first that a curve drawn through the points obtained from the density measurements parallels a curve through the points for which the mole fraction was obtained directly, but that they are displaced with respect to each other. This presumably arises from some difficulty with our density measurement of the homogeneous solution just above the critical point. We observed the same shift in reference 9 when comparing the range of critical concentrations obtained directly and from the density measurements, and attributed it to error in this particular density measurement. However, it is hard to see why the density should be more difficult to measure accurately above the critical point than below. Further investigation of the possibility of an anomalous density behavior just above T_c would be desirable. Our results, if taken literally, would indicate a negative coefficient of expansion just above T_c, as may be seen from Fig. 1 of reference 9.

We see that the points fall more nearly on straight lines in Fig. 2 than in Fig. 1. When T_c-T is very small (i.e., 0.000° to 0.002°), an error of 0.001° can make a considerable difference in the position of a point in Fig. 1 because of the sensitiveness of the $(T_c-T)^{\frac{1}{3}}$ function (i.e., just because the coexistence curve is very flat). Nevertheless, unless there are appreciable systematic errors, it must be concluded from either figure that the top of the coexistence curve is flatter than the cubic curve. It would be desirable to improve the temperature control to about ±0.0002° and to obtain a number of

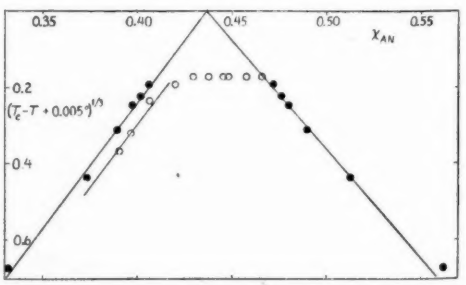

FIG. 2. Coexistence curve for cyclohexane-aniline system, mole fraction of aniline against $(T_c-T+0.005°)^{\frac{1}{3}}$. Open circles, direct measurement of compositions; black circles, compositions obtained from density measurements.

[10] B. H. Zimm, J. Chem. Phys. **20**, 538 (1952).

[11] The range of temperatures involved is small enough so that it should not be necessary to consider temperature coefficients of the densities.

points in the region $T_c - T < 0.001°$; however, this would certainly entail great experimental difficulties.

3. LIQUID-VAPOR EQUILIBRIUM

In the case of the liquid-vapor equilibrium the effect of gravity will be of paramount importance. Density gradients have been demonstrated by some of the Canadian workers,[6,12] and Weinberger and Schneider[13] have found that the apparent flat top of the coexistence curve becomes much less marked in a tube which is short vertically than in one which has a long vertical extension. They have concluded that the flat top would disappear altogether if a tube of zero height could be used. Whiteway and Mason[14] have investigated the effect of stirring and they found that a strongly stirred tube, if observed shortly after stirring so that the density gradients have not had time to form, also shows a less marked flat top. They conclude that the effect of gravity is eliminated almost entirely by stirring and that the flat top disappears as nearly as can be observed.

However, in their earlier experiment, Mason, Naldrett, and Maass[5] studied ethane in a strongly shaken tube, and found that over a range of concentrations the meniscus disappeared within the confines of the tube rather than going out either at the top or the bottom. From this they concluded that the coexistence curve had a mathematically flat top over a range of concentrations. Entirely similar results were obtained by Naldrett and Maass[15] for ethylene. Two questions may arise as to the validity of these results. In the first place, did they entirely eliminate the effect of gravity? In the tubes with critical fillings the details of the phenomena could hardly be observed without at least momentarily stopping the shaking; however in a noncritical filling the last drop of liquid or bubble of vapor, as the case might be, could be observed while the shaking was still going on. The other question which arises has to do with the necessary difference in density between two phases in order to be able to observe a meniscus. If a definite nonzero density difference is required, the meniscus could not be seen just at the top of the coexistence curve, and a temperature very slightly less than the critical temperature would be required. Thus, one would come to believe that the coexistence curve had a flat top, the width of which was equal to the density difference necessary to make possible the observation of a meniscus.

But, however doubtful these earlier observations may have been, it is important to note that the density range of the flat top was only 1 to 2 percent of the density. In the later experiments accurate measurements have not been made this close to the critical density, and without such measurements the shape of the coexistence curve is not sufficiently well defined to eliminate the possibility of a flat top over the range in which Mason, Naldrett, and Maass,[5] and Naldrett and Maass[15] believed they had observed one. While it was necessary to have accurate measurements within a few thousandths of a degree of the critical temperature in order to find the flat top in the binary liquid system, it is to be anticipated that it will be necessary to measure within an even smaller temperature range in the liquid-vapor case, since the relative critical range of concentrations is smaller in the latter case.

The data which come nearest to penetrating the critical region are those recently published by Lorentzen,[16] who has achieved temperature control within about 0.0001°, and who has made measurements within about 0.001° of the critical temperature in the case of carbon dioxide. Lorentzen attempted to attain equilibrium in the gravitational field, and he has measured the density at different heights in the tube by an optical method. Since change in height is correlated with a density gradient, he has been able to determine isotherms, and he has also determined densities of coexisting phases below the critical temperature. He has concluded that there is no evidence for a flat top on the coexistence curve. However, I feel that this conclusion is open to question; indeed, the opposite conclusion appears more probable from his results.

There are two methods one can use to check on the shape of the coexistence curve. (A third possibility is discussed in the following paper.)[17] One is to plot a figure like Fig. 1 or Fig. 2. This Lorentzen has done, except that he used as his ordinate $T^{0.357}$ instead of $T^{\frac{1}{3}}$ (we feel, however, that this can be considered to be essentially a cubic coexistence curve). He has drawn two practically straight lines through the vapor and liquid branches, which meet at a point designated as the critical point. It is not quite clear, however, how the critical temperature was determined in this case, and from his later remarks it appears that there may be some difficulty in attempting to determine the critical temperature exactly by observation of the meniscus. The nearest points on the lines approaching the critical point are 0.0014° below the apex of this curve. This is certainly very close to the critical temperature by any standards, but still not close enough, for the density difference between the phases is still above 5 percent. It is quite possible that the curve is flattened at a higher temperature.

The second method for investigating the coexistence curve is to plot the minimum slope of the isotherms above T_c against the temperature, and by extrapolation to find the temperature at which the slope vanishes. This can then be compared with the temperature which one obtains by extrapolating the densities of coexisting liquid and vapor below the critical temperature to the

[12] F. E. Murray and S. G. Mason, Can. J. Chem. **30**, 550 (1952).
[13] M. A. Weinberger and W. G. Schneider, Can. J. Chem. **30**, 422 (1952).
[14] S. G. Whiteway and S. G. Mason, Can. J. Chem. **31**, 569 (1953).
[15] S. N. Naldrett and O. Maass, Can. J. Research **B18**, 118 (1940).
[16] H. L. Lorentzen, Acta Chem. Scand. **7**, 1335 (1953).
[17] O. K. Rice, following paper, J. Chem. Phys. **22**, 169 (1954).

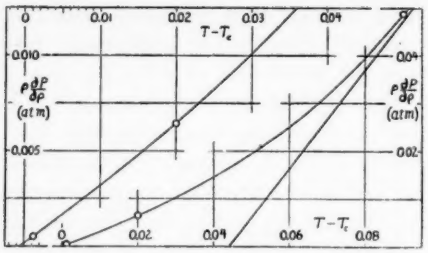

FIG. 3. Slope of isotherms at the inflection point against $T-T_c$ for carbon dioxide.

point where they coincide. If the temperature obtained from the isotherms is less than the temperature estimated from the coexisting phases, it indicates a flattening of the coexistence curve. By careful measurement of Lorentzen's Figs. 4, 5, and 6, I have estimated the slopes of his isotherms at the inflection points at $T-T_c = 0.0012°$, $0.020°$ and $0.090°$. (The slope for $0.020°$ was taken from his Fig. 5; if taken from his Fig. 6 it would be slightly less at the inflection point, though the isotherm as a whole appears steeper.) These have been plotted against his estimates of $T-T_c$ in Fig. 3, and a curve drawn through the points. Two different scales have been used. It appears from the plot with the larger scale that the point of zero slope comes about $0.0006°$ below the temperature considered as critical by Lorentzen. The straight line indicates the slope of the $\rho\partial P/\partial\rho$ *vs* $T-T_c$ curve as calculated from the data of Michels, Blaisse, and Michels.[18] If these data and Lorentzen's are both correct, the $\partial P/\partial\rho$ *vs* $T-T_c$ curve must tend to flatten out as the critical point is approached, as it does in the case of xenon, whose isotherms have recently been studied by Habgood and Schneider (for a more detailed comparison see reference 17). Lorentzen stated that his values of $\partial P/\partial\rho$ agreed with those calculated from Michels, Blaisse, and Michels for the values of $T-T_c$ given by Lorentzen, but this appears to be in error.

Returning now to Lorentzen's Fig. 4, we note that the isotherm at $T-T_c=0.0012°$ (his scale) appears to have a linear section extending over a range of densities equal to about 0.019 g/cc. As the temperature is lowered this apparently linear section should rotate until it becomes horizontal, and its length will be the difference in density of the solid and liquid phases at the critical temperature; we assume that this density difference remains constant at 0.019 g/cc. As indicated in the following paper, it is difficult to decide from the experimental data whether the apparent linear section actually is a straight line; however, if we assume that it is, we can make an estimate of the true critical temperature which we can compare with the estimate made in the preceding paragraph. For if this analysis is correct, it means that the triangular figure of the type shown in our Fig. 2 or Lorentzen's Fig. 2 will be truncated where the triangle has this width of 0.019 g/cc, and this will give the critical temperature. Now it can be seen from Lorentzen's Fig. 2 that a length of 0.024 g/cc corresponds very closely to a temperature $0.0014°$ below the apex of the triangle. The approximate length of the straight part of the isotherm marked $-0.0014°$ in Lorentzen's Fig. 4, is 0.026; hence, most probably, the temperature scale in this figure may be taken as referring to the apex of the triangle. We estimate, therefore, that the true critical temperature will be about

$$0.0014\times(0.019/0.026)^{1/0.357}=0.0006°$$

below the apex of the triangle, i.e., $0.0006°$ below the temperature Lorentzen considered to be the critical temperature. This agrees with our estimate from Fig. 3. We conclude, therefore, that we get a consistent picture if we suppose that the critical temperature is slightly lower than that estimated by Lorentzen, and that the coexistence curve has a flat horizontal top with a length in density units of approximately 0.02 g/cc.

It must be stated that this conclusion can be only tentative. For one thing, it is not absolutely certain that Lorentzen's mass distributions represent true equilibrium. Nor does it seem clear that the same results would be obtained from the data of Lorentzen's Fig. 3, which seem, however, to be less accurate. Nevertheless, the conclusion that the coexistence curve has a flat top does seem very resonable, and it is now clear how the matter can be settled definitely. What is needed are measurements very close to the critical point, so that the temperature at which the minimum slope of the isotherms extrapolates to zero, and the temperature at which the difference in density of coexisting phases below the critical point extrapolates to zero, can be determined simultaneously and accurately. If the former temperature lies below the latter, the coexistence curve must have a flat top, or at least a flatter one than a cubic coexistence curve; if they coincide, the coexistence curve is rounded.

[18] Michels, Blaisse, and Michels, Proc. Roy. Soc. (London) **A160**, 358 (1937).

Relation between Isotherms and Coexistence Curve in the Critical Region*

O. K. Rice
University of North Carolina, Chapel Hill, North Carolina
(Received June 22, 1954)

A general relation has been given relating the slope of the isotherms along the liquid-vapor coexistence curve to the shape of the latter, and has been applied to the case where the coexistence curve is rounded on the top and to the case where it has a flat horizontal portion. If the coexistence curve has the form $T-T_c=-a|\rho_c-\rho|^n$ (where T=temperature, ρ=density, subscript c indicates a value at the critical point, and a and n are constants) it can be shown that the critical isotherm is given by

$$P-P_c=a(\partial^2P/\partial T\partial\rho)_c(\rho-\rho_c)|\rho-\rho_c|^n,$$

provided $(\partial^2P/\partial T\partial\rho)_c$ is finite. This equation should hold over the region where $\partial^2P/\partial T\partial\rho$ is approximately constant. If there is a flat, horizontal portion at the top of the isotherm a similar equation will be approximately true under the same conditions beyond the flat portion. The actual shape of experimental isotherms in the critical region is considered. $\partial^2P/\partial T\partial\rho$ is approximately constant only over a limited range of densities, and beyond this range the slopes of the isotherms become greater than indicated by the equation; however, general orders of magnitude are as expected. It is not possible to decide definitely from the data considered whether the critical isotherm has a horizontal region over a finite range of densities. Finally, a discussion is given of the discontinuities of thermodynamic quantities, particularly C_v, as one passes from the one-phase to the two-phase region. It is shown that C_v must be much larger in the two-phase than in the one-phase region.

THE shape of the liquid-vapor coexistence curve in the immediate neighborhood of the critical temperature is closely related to the shape of the isotherms. In the classical van der Waals theory the first and second derivatives of pressure with respect to molal volume $(\partial P/\partial V)_T$ and $(\partial^2P/\partial V^2)_T$ vanish at the critical point, while $(\partial^3P/\partial V^3)_T$ has a nonzero value. The coexistence curve has a parabolic shape, so that along the curve† $T-T_c$ is proportional to $(V-V_c)^2$, where the subscript c indicates values at the critical point. It can be shown[1] that the following relation holds:

$$\left(\frac{d^2T}{dV^2}\right)_c=-\frac{(\partial^3P/\partial V^3)_{T,c}}{3(\partial^2P/\partial T\partial V)_c}. \tag{1}$$

Here the total derivative is used to indicate a change along the coexistence curve.

It is now well known, however that the actually observed coexistence curves do not follow the van der Waals form. To a much better approximation $T-T_c$ is proportional to $(V-V_c)$,[3] as has been shown by Guggenheim,[2] and there is some evidence[3] that the coexistence curve may have a flat horizontal stretch at the top or, at least, is flatter very close to the critical point than the cubic curve proposed by Guggenheim. Since the derivation of Eq. (1), as given by Fowler and Guggenheim,[1] depends rather explicitly on the van der Waals theory and the particular form of S-shaped isotherm peculiar thereto, a more general theory will be required to give a generalization of Eq. (1).

It is clear that certain complications will arise in attempting to work out such a theory. If $T-T_c$ is proportional to $(V-V_c)^3$, then it is seen that the sign of the proportionality constant must change at the critical point, and the latter must be a point of discontinuity. However, if it is possible to expand the entropy S and the pressure P as separate Taylor series in $V-V_c$ on the two sides of the critical point, we may show that if $d^n(T-T_c)/d(V-V_c)^n$ (differentiation along coexistence curve) vanishes at $V=V_c$, then $(\partial^{n+1}P/\partial V^{n+1})_T$ also vanishes at the same point, and *vice versa*.[4] This means that if the coexistence curve has the form $T-T_c=\text{const}\times(V-V_c)^n$, where n is an integer, the critical isotherm has the form $P-P_c=\text{const}\times(V-V_c)^{n+1}$. However, we are not even sure n is an integer. If it is not, it will not be possible to expand $P-P_c$ in a Taylor series, because of the difficulties with the higher derivatives. Another method of attack, therefore, seems desirable, and we shall attempt to supply this in the following section.

1. COEXISTENCE CURVE WITH ROUNDED TOP

As implied in the preceding paragraph, we shall first suppose that the coexistence curve does not actually have a flat top, and that in the immediate neighborhood of the critical point we may represent $T-T_c$ along the coexistence curve as a simple power of $(V-V_c)$. The experimental data are usually given in terms of the density ρ, so that we write

$$T-T_c=-a|\rho-\rho_c|^n, \tag{2}$$

* Work supported by the Office of Naval Research.

† Proportionalities of this type hold, of course, only near the critical point, and can be considered as the first part of a series expansion of $T-T_c$ in terms of $V-V_c$.

[1] See R. H. Fowler and E. A. Guggenheim, *Statistical Thermodynamics* (Macmillan Company, New York, 1939), p. 317.

[2] E. A. Guggenheim, J. Chem. Phys. **13**, 253 (1945).

[3] See the preceding paper, O. K. Rice, J. Chem. Phys. **22**, 164 (1954).

[4] O. K. Rice, Sec. E of *Thermodynamics and Physics of Matter* (F. D. Rossini, Editor, to be published by Princeton University Press, Princeton).

which is equivalent to a first approximation to Guggenheim's equation (leaving out terms in higher powers of $\rho-\rho_c$, which are important in producing the asymmetry of the coexistence curve far from the critical point, but are negligible near the critical point), provided n is equal to or very close to 3 and a is equal to 0.1865 $T_c\rho_c^{-3}$. The curve of Eq. (2) actually has, of course, two distinct branches depending upon whether $\rho>\rho_c$ or $\rho<\rho_c$. Although these can be handled together, it must not be forgotten that they are two different analytic functions unless n should be an even integer.

Since it is more convenient thermodynamically to work with V, we shall do this, later converting to equations using ρ.

We shall make one fundamental assumption, regarding isotherms in the one-phase region, namely that $\partial^2P/\partial V\partial T$ is finite, nonvanishing, and continuous. That this must be true is fairly obvious from the fact that the isotherms in the one-phase region near the critical point are smooth curves, which are, indeed, almost straight lines which apparently do not cross in the neighborhood of the critical point; it implies, of course, that $(\partial P/\partial V)_T$ and $(\partial P/\partial T)_V$ are continuous. This assumption, together with the character of the isotherms just noted, upon which it is based, has a further consequence which is of importance. We may write

$$\partial^2P/\partial T\partial V=-(\partial^2P/\partial T^2)_V(\partial T/\partial V)_{(\partial P/\partial T)_V} \quad (3)$$

considering $(\partial P/\partial T)_V$, T, and V as the three related variables to which we apply the standard formula of partial differentiation. Since $\partial^2P/\partial T\partial V$ is finite we see from Eq. (3) that $(\partial^2P/\partial T^2)_V$ can be infinite only where the lines in the $T-V$ plane along which $(\partial P/\partial T)_V$ is constant, become parallel to the V-axis. (Equation (3) will not, of course, be valid at a point of discontinuity but may be used approaching such a point.) Since the isotherms are nearly straight lines of gradually increasing (negative) slope as T increases above T_c it is seen that $(\partial P/\partial T)_V$ is a decreasing function of volume everywhere in the neighborhood, and the lines of constant $(\partial P/\partial T)_V$ will never lie parallel to the V-axis. Therefore, though $(\partial^2P/\partial T^2)_V$ is known to become large in the neighborhood of the critical point, it cannot approach infinitely large values.

We may now proceed to consider changes along the coexistence curve in the neighborhood of the critical point, for which we may write

$$dV/dT=(\partial V/\partial T)_P+(\partial V/\partial P)_T dP/dT. \quad (4)$$

Also we have

$$(\partial V/\partial T)_P=-(\partial V/\partial P)_T(\partial P/\partial T)_V$$
$$=-(\partial V/\partial P)_T(\partial S/\partial V)_T,$$

and, by the Clapeyron equation, $dP/dT=\Delta S/\Delta V$, where Δ indicates the isothermal change on evaporation. Therefore Eq. (4) may be written in the form

$$\frac{dT}{dV}=\left(\frac{\partial P}{\partial V}\right)_T\left[\frac{\Delta S}{\Delta V}-\left(\frac{\partial S}{\partial V}\right)_T\right]^{-1}. \quad (5)$$

Equation (5) may be applied either to the liquid side of the coexistence curve (subscript l) or to the vapor side (subscript v). To evaluate $(\partial S/\partial V)_T$ we note that if we are close to the critical point we may write

$$(\partial S/\partial V)_{T,v}=(\partial S/\partial V)_{T,c}+(\partial^2S/\partial V^2)_{T,c}(V_v-V_c) \quad (6)$$

and

$$(\partial S/\partial V)_{T,l}=(\partial S/\partial V)_{T,c}+(\partial^2S/\partial V^2)_{T,c}(V_l-V_c). \quad (7)$$

We have omitted a term $(\partial^2S/\partial V\partial T)(dT/dV)(V_v-V_c)$ in Eq. (6) [and a similar term in Eq. (7)] because the coefficient of (V_v-V_c) in such a term will approach zero [since $\partial^2S/\partial V\partial T=(\partial^2P/\partial T^2)_V$ is always finite and dT/dV approaches zero] when $V_v\to V_c$. Equations (6) and (7) will hold in the limit of small $V-V_c$ regardless of the behavior of higher derivatives, provided only the derivatives written down are defined and finite. $(\partial^2S/\partial V^2)_{T,c}$ is equal to $\partial^2P/\partial T\partial V$, and hence is finite according to our fundamental assumption.

For the entropy itself along the coexistence curve we write

$$S_v=S_c+\left(\frac{\partial S}{\partial V}\right)_{T,c}(V_v-V_c)+\frac{1}{2}\left(\frac{d^2S}{dV^2}\right)_{c,v}(V_v-V_c)^2 \quad (8)$$

and

$$S_l=S_c+\left(\frac{\partial S}{\partial V}\right)_{T,c}(V_l-V_c)+\frac{1}{2}\left(\frac{d^2S}{dV^2}\right)_{c,l}(V_l-V_c)^2. \quad (9)$$

In these equations we have also omitted a term in V_v-V_c or V_l-V_c with a factor of dT/dV, and in the quadratic term have retained a total derivative. We can also claim that these equations will hold sufficiently close to the critical point, regardless of higher derivatives, if d^2S/dV^2 has the proper behavior. Omitting terms like $(\partial^2S/\partial V\partial T)_c(dT/dV)_{c,v}$, and $(\partial^2S/\partial T^2)_{V,c}\times(dT/dV)_{c,v}^2$, we have

$$(d^2S/dV^2)_{c,v}=(\partial^2S/\partial V^2)_{T,c}$$
$$+(\partial S/\partial T)_{v,c}(d^2T/dV^2)_{c,v} \quad (10)$$

and

$$(d^2S/dV^2)_{c,l}=(\partial^2S/\partial V^2)_{T,c}$$
$$+(\partial S/\partial T)_{v,c}(d^2T/dV^2)_{c,l}. \quad (11)$$

Since $\partial^2S/\partial T\partial V$ is not infinite, $(\partial S/\partial T)_{v,c}$ is not, and if $n>2$, then d^2T/dV^2 is zero at the critical point. Thus we may omit the last terms in Eqs. (10) and (11). Using Eqs. (8) and (9), then, and substituting into Eq. (5), noting $\Delta S/\Delta V=(S_v-S_l)/(V_v-V_l)$, we obtain

$$\left(\frac{\partial P}{\partial V}\right)_T=-\frac{dT}{dV}\left(\frac{\partial^2S}{\partial V^2}\right)_{T,c}$$
$$\times\left[(V-V_c)-\frac{(V_v-V_c)^2-(V_l-V_c)^2}{2(V_v-V_l)}\right]. \quad (12)$$

This equation holds if V refers to either vapor or liquid. If n is the same for the vapor and liquid sides, as is to be expected, V_v-V_c and V_l-V_c will be proportional to each other, and $(\partial P/\partial V)_T$ will be proportional to $(dT/dV)(V-V_c)$. Indeed, the last term in Eq. (12) will generally be relatively small; substituting $(\partial^2 S/\partial V^2)_{T,c}=(\partial^2 P/\partial T\partial V)_c$ we may write as a good approximation

$$(\partial P/\partial V)_T=-(dT/dV)(\partial^2 P/\partial T\partial V)_c(V-V_c). \quad (13)$$

We are now ready to convert this equation to the variable $\rho=V^{-1}$:

$$(\partial P/\partial \rho)_T=(dT/d\rho)(\rho_c/\rho)(\partial^2 P/\partial T\partial \rho)_c(\rho_c-\rho). \quad (14)$$

To a sufficiently good approximation ρ_c/ρ can be set equal to 1. By Eq. (2), then, this becomes

$$(\partial P/\partial \rho)_T=n(T_c-T)(\partial^2 P/\partial T\partial \rho)_c. \quad (15)$$

Since $(\partial P/\partial \rho)_T$ is to be evaluated on the coexistence curve we may write (using subscript T_c to denote a value at temperature T_c but at the same density as the quantity with subscript T)

$$\begin{aligned}(\partial P/\partial \rho)_T&=(\partial P/\partial \rho)_{T_c}+(\partial^2 P/\partial T\partial \rho)(T-T_c)\\ &\cong(\partial P/\partial \rho)_{T_c}+(\partial^2 P/\partial T\partial \rho)_c(T-T_c), \quad (16)\end{aligned}$$

so that Eq. (14) becomes, with ρ_c/ρ set equal to 1,

$$(\partial P/\partial \rho)_{T_c}=(\partial^2 P/\partial T\partial \rho)_c[(\rho_c-\rho)dT/d\rho+T_c-T]. \quad (17)$$

Using Eq. (2) in Eq. (17) we find

$$(\partial P/\partial \rho)_{T_c}=(\partial^2 P/\partial T\partial \rho)_c(n+1)a|\rho-\rho_c|^n. \quad (18)$$

Integrating this equation, with proper regard to signs, we obtain

$$P-P_c=a(\partial^2 P/\partial T\partial \rho)_c(\rho-\rho_c)|\rho-\rho_c|^n. \quad (19)$$

We thus see that regardless of the value of n, and depending only upon $\partial^2 P/\partial T\partial V$ being finite, the same relation holds between the coexistence curve and the critical isotherms as was described in the introductory paragraphs. Just as in the case of Eq. (2) we must remember that this curve has two distinct branches, depending upon whether $\rho>\rho_c$ or $\rho<\rho_c$, unless n is an even integer.

2. COEXISTENCE CURVE WITH FLAT TOP

If the coexistence curve has a flat horizontal top, the critical isotherm coincides with the coexistence curve along the flat top. We shall attempt to apply Eq. (5) at, or very slightly beyond, the edge of the flat top. In this case we shall define V_c as the volume at the middle of the flat top. By the principle of continuity, $\Delta S/\Delta V$ will approach a value at the critical temperature equal to the average value of $(\partial S/\partial V)_T$ taken along a line just above the flat top of the coexistence curve. With very good approximation we may say that $\Delta S/\Delta V$ will be equal to the value of $(\partial S/\partial V)_T$ at V_c, and at the edge of the flat top (either the liquid or vapor edge), we may write in good approximation,

$$\begin{aligned}(\partial S/\partial V)_T&=\Delta S/\Delta V+(\partial^2 S/\partial V^2)_{T,c}(V-V_c)\\ &=\Delta S/\Delta V+(\partial^2 P/\partial V\partial T)_c(V-V_c). \quad (20)\end{aligned}$$

From Eq. (5), then, Eq. (13) and hence Eq. (14) will hold in exactly the same form as before.

If the coexistence curve meets the flat part with a rounded corner, so that $dT/dV=0$, it will also be true that $(\partial P/\partial V)_T=0$ there, so that the isotherm would connect with the flat part at the top of the coexistence curve with zero slope, but not necessarily with zero curvature, if $(\partial^2 P/\partial V\partial T)_c$ and d^2T/dV^2 are not zero. This is the situation that I have considered in a number of previous papers.[3]

In the theory of Mayer and Harrison[5] there was a series of isotherms with regions of zero slope above the temperature at which two distinct phases could be seen, which is the temperature taken here as the critical temperature. This would cause $(\partial^2 P/\partial V\partial T)_c$ to be zero (in fact $\partial^2 P/\partial V\partial T$ vanishes all along the flat top) and so $(\partial P/\partial V)_T$ would vanish even if dT/dV did not become zero as the flat part of the coexistence curve was approached from outside, in contrast to the situation noted in the preceding paragraph. Equation (13) holds exactly in this case just at the edge of the flat part, but beyond this point becomes less exact; the fact that it appears to make the slope of the isotherm vanish all along the coexistence curve is, thus, not to be taken seriously. We shall not consider Mayer and Harrison's case further.

If the coexistence curve does have a flat top, it will probably be a reasonably good approximation, in order to get a rough idea of the shape of the isotherms, to suppose it to be sharply truncated, as shown in Fig. 1, and to suppose that along the coexistence curve

$$T-T_c'=-a|\rho-\rho_c|^n, \quad (21)$$

where T_c' is the temperature at the top of the rounded extension of the coexistence curve, as indicated in Fig. 1. Using this expression in Eq. (14), again setting $\rho_c/\rho=1$, we get instead of Eq. (15)

$$(\partial P/\partial \rho)_T=n(T_c'-T)(\partial^2 P/\partial T\partial \rho)_c, \quad (22)$$

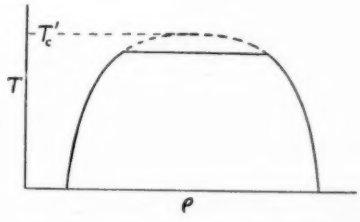

FIG. 1. Truncated coexistence curve.

[5] J. E. Mayer and S. F. Harrison, J. Chem. Phys. 6, 87, 101 (1938). In the case of carbon dioxide, discussed in Sec. 3, there seems to be good evidence that there are no regions of zero slope above the temperature of disappearance of the meniscus.

and for the behavior along the critical isotherm we get from Eq. (16), instead of Eq. (18),

$$(\partial P/\partial\rho)_{T_c}=(\partial^2 P/\partial T\partial\rho)_c \times[(n+1)a|\rho-\rho_c|^n+T_c-T_c']. \quad (23)$$

Integrating this with due regard to sign, we find

$$P-P_c=(\partial^2 P/\partial T\partial\rho)_c \times[a(\rho-\rho_c)|\rho-\rho_c|^n+(T_c-T_c')(\rho-\rho_c)]. \quad (24)$$

Equations (23) and (24) hold, of course, only beyond the edge of the flat horizontal part of the coexistence curve. The value of ρ at the edge of the flat top is given by substituting T_c for T in Eq. (21), and we thus see that at the edge $P-P_c$ becomes zero, as it should, indicating that we have chosen the right constant of integration in Eq. (24). Beyond the edge of the flat top $|P-P_c|$ starts to increase rapidly, mainly due to the first term in the bracket of Eq. (24). The first term is, however, identical with the right-hand side of Eq. (19). We may therefore conclude that Eq. (19) will give a reasonable approximation to the critical isotherm beyond the flat top. In fact, since Eq. (19) itself indicates a very slow change in $P-P_c$, over the range of the flat top, and a rapid change only beyond that range, it may be used as a first approximation even over the entire range of $\rho-\rho_c$.

3. THE EXPERIMENTAL ISOTHERMS

The equations for the isotherms should hold well over the range of variables for which $\partial^2 P/\partial T\partial V$ or $\partial^2 P/\partial T\partial\rho$ is essentially constant. This can be tested either by comparing the critical isotherm with Eq. (19), or by testing Eq. (15) along the coexistence curve. Habgood and Schneider[6] have made a rather detailed study of the isotherms of xenon, from which we may see what can be expected. These authors[7] plotted $(\partial^2 P/\partial T^2)_\rho$ as a function of ρ, with results such as are indicated in Fig. 2. From this figure we may infer that $\partial^3 P/\partial T^2\partial\rho$ is a function of T but independent of ρ from ρ/ρ_c equal to 0.95 or 0.96 to $\rho/\rho_c=1.04$ or 1.05. Also it appears, for $T=T'$, where T' is sufficiently greater than T_c, that $\partial^2 P/\partial T\partial\rho$ does not vary strongly with ρ. We may find $\partial^2 P/\partial T\partial\rho$ at T_c by subtracting

$$\int_{T_c}^{T'}(\partial^3 P/\partial T^2\partial\rho)dT$$

from the more or less constant value at T'. Since $\partial^3 P/\partial T^2\partial\rho$ is independent of ρ and positive from $\rho/\rho_c\sim 0.95$ to $\rho/\rho_c\sim 1.05$ we expect $\partial^2 P/\partial T\partial\rho$ to be smaller at T_c than at T' and fairly constant between these limits of ρ. From the behavior of the slope, $(\partial P/\partial\rho)_T$, of the isotherms at the inflection point (see Fig. 4 of ref. 6) this behavior of $\partial^2 P/\partial T\partial\rho$ would be inferred. Outside these limits of ρ/ρ_c the value of $\partial^3 P/\partial T^2\partial\rho$ rapidly changes sign; therefore at T_c the value of $\partial^2 P/\partial T\partial\rho$ must rapidly increase beyond these limits of ρ/ρ_c. This means that for $\rho/\rho_c<0.95$ and $\rho/\rho_c>1.05$ the isotherms become steeper than is indicated by Eqs. (15) or (19). This is illustrated by Fig. 3, in which $(\partial^2 P/\partial\rho^2)_{T_c}$ is plotted against ρ. The points are taken from Fig. 6 of reference 6; the curve is from Eq. (19) twice differentiated, with $n=3$; $(\partial^2 P/\partial T\partial\rho)_c$ is taken to be 0.37 atmos deg.$^{-1}$ g^{-1} cc from Fig. 4 of reference 6 [since the isotherms are so nearly linear it seems safe to take the limiting value of the slope of the curve for $(\partial P/\partial\rho)_T$ at the *inflection point* of the isotherm *vs* T as giving $(\partial^2 P/\partial T\partial\rho)_c$], and a is given Guggenheim's value. In drawing this curve we have taken into account the fact that there are two distinct branches of Eq. (19). Habgood and Schneider supposed that the shape of this curve indicated that $(\partial^4 P/\partial\rho^4)_T$ would vanish as well as $(\partial^3 P/\partial\rho^3)_T$, at the critical point. By Eq. (19) with $n=3$, the third derivative vanishes but the fourth does not. It is, of course, extremely difficult to decide experimentally whether the apparent point of inflection really means that there is a discontinuity in $(\partial^4 P/\partial\rho^4)_T$ or that this quantity actually vanishes. The latter alternative does not seem at all necessary, and the analysis we have given seems to give a reasonable correlation of the experimental data.

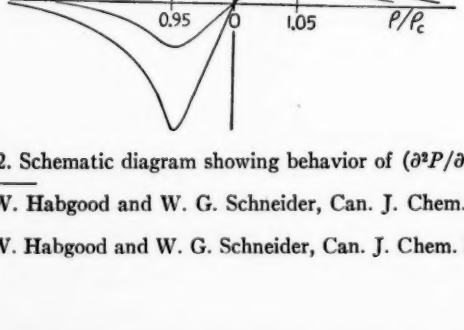

FIG. 2. Schematic diagram showing behavior of $(\partial^2 P/\partial T^2)_\rho$.

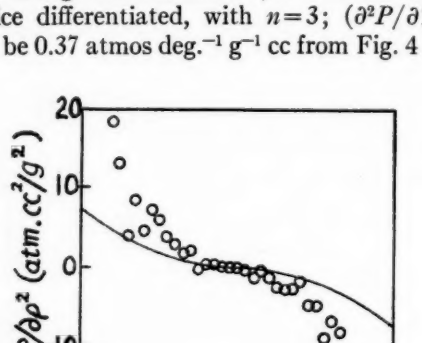

FIG. 3. Diagram based on critical isotherm for xenon.

In Fig. 4 we have given a similar analysis of the isotherms of carbon dioxide given by Lorentzen[8] in his

[6] H. W. Habgood and W. G. Schneider, Can. J. Chem. **32**, 98 (1954).
[7] H. W. Habgood and W. G. Schneider, Can. J. Chem. **32**, 164 (1954).
[8] H. L. Lorentzen, Acta Chem. Scand. **7**, 1335 (1953).

Fig. 4. We have plotted P_c-P where P_c is the pressure at the critical density (regardless of the temperature) against ρ. Pressures are given in mm of CO_2 at the critical point (density=0.463 g/cc). Three isotherms are represented for $T-T_c=0.0012°$, $-0.0014°$, and $-0.0090°$, respectively, according to Lorentzen's estimate. We have compared the isotherm at 0.0012° to that of Eq. (19) to which an increment linear in $\rho-\rho_c$ has been added. We again used $n=3$, and the value of $a=500$ (c.g.s.—centigrade units) was obtained from Lorentzen's Fig. 2; $(\partial^2P/\partial T\partial\rho)_c=0.635$ atmos deg^{-1} g^{-1} cc was obtained from Fig. 3 of the preceding paper, in essentially the same way it was obtained for xenon. In the case of the other isotherms we give a short segment of a straight line having the slope calculated from Eq. (15).

An interesting question arises, as to whether the section of the 0.0012° isotherm near ρ_c is straighter than one would predict from Eq. (19), modified in the way we have indicated. There is a slight suggestion that this is true, as would of course be anticipated if the top of the coexistence curve is flat. However, the calculated isotherm is itself so flat in this region that no certain conclusion can be drawn.

It is seen that the isotherms of xenon and carbon dioxide behave in very similar fashion. However, there are some differences which should be noted. For xenon Guggenheim's value of a is 40, experimental[8a] 48; carbon dioxide Guggenheim's value of a is 571 as compared to 500 from Lorentzen's data. The value of $\partial^2P/\partial T\partial\rho$ at the critical point for carbon dioxide shows a much more marked discrepancy; it is about half what one would expect from that of xenon by the law of corresponding states. And $\partial^2P/\partial T\partial\rho$ seems to increase above the critical temperature much more rapidly in the case of carbon dioxide than in the case of xenon. It is possible that the experimental results are not yet conclusive. However, it is interesting to speculate on the possibility that a system in the critical region is so sensitive to what would otherwise be minor influences, that inordinately large deviations from the law of corresponding states occur.

4. DISCONTINUITIES ACROSS THE COEXISTENCE CURVE

It is interesting to consider the transition from the one-phase to the two-phase condition. This is really a second-order transition,[9] and Eq. (5) may be considered to be a type of Ehrenfest relationship. If we use the symbol δ to indicate the value of a quantity in the two-phase region minus the value of the same quantity

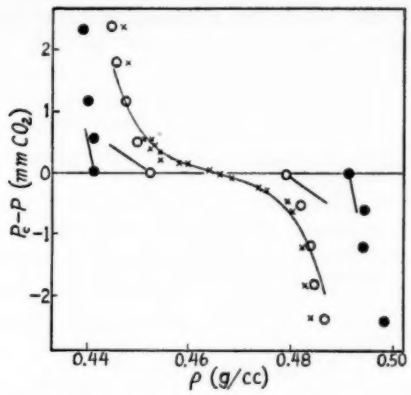

FIG. 4. Isotherms for carbon dioxide. Crosses, $T-T_c=0.0012°$; open circles, $T-T_c=-0.0014°$; black circles, $T-T_c=-0.0090°$.

just over the coexistence curve in the one-phase region, we see that Eq. (5) can be written in the form

$$dT/dV=-\delta(\partial P/\partial V)_T/\delta(\partial P/\partial T)_V, \tag{25}$$

since $(\partial P/\partial V)_T$ vanishes in the two-phase region, and since $\Delta S/\Delta V=(\partial P/\partial T)_V$ for the two-phase region and $(\partial S/\partial V)_T=(\partial P/\partial T)_V$ for the one-phase region. We can also write[9] a relation involving the heat capacity at constant volume,

$$dT/dV=-T\delta(\partial P/\partial T)_V/\delta C_v. \tag{26}$$

From Eqs. (25) and (26), then

$$\delta C_v/T=\delta(\partial P/\partial V)_T/(dT/dV)^2. \tag{27}$$

Using Eq. (13), recalling again that $(\partial P/\partial V)_T$ vanishes in the two-phase region, and that Eq. (13) refers to the one-phase region, and setting $\rho_c/\rho=1$,

$$\delta C_v/T=(\partial^2P/\partial T\partial V)_c(V-V_c)/(dT/dV)$$
$$=(\rho_c-\rho)(\partial^2P/\partial T\partial\rho)_c/\rho^2(dT/d\rho). \tag{28}$$

If Eq. (2) holds,

$$\delta C_v/T=(\partial^2P/\partial T\partial\rho)_c/an\rho^2|\rho_c-\rho|^{n-2}. \tag{29}$$

It is thus seen that if Eq. (2) holds C_v in the two-phase region becomes positively infinite compared to C_v in the one-phase region, as the critical point is approached. This would not be true if the coexistence curve had a flat top, but in any event C_v in the two-phase region should become much larger than that in the one-phase region, even though the latter is quite large in the critical region. In the two-phase region C_v of course, includes heat of evaporation or condensation. Data of Michels and Strijland[10] show that C_v is always large, though it is hard to make any estimate of δC_v.

I am greatly indebted to Dr. Benjamin Widom for many discussions of this subject.

[8a] M. A. Weinberger and W. G. Schneider, Can. J. Chem. **30**, 436 (1952).

[9] L. Goldstein, J. Washington Acad. Sci. **40**, 97 (1950); O. K. Rice, Phys. Rev. **93**, 1161 (1954).

[10] A. Michels and J. Strijland, Physica **18**, 613 (1952).

Overlaps of Trial Functions for the Hydrogen Molecule. I. Ground-State Character of the *1s* A.O. Approximations*

JERRY BRAUNSTEIN†‡ AND WILLIAM T. SIMPSON
Department of Chemistry, University of Washington, Seattle 5, Washington
(Received December 8, 1952)

The contributions of the ground state wave function in some of the trial functions for the hydrogen molecule have been evaluated as the overlap integrals of the trial functions with the thirteen term function of James and Coolidge. The rms errors and mean excited state energies are presented and the results of a binding energy calculation reported.

INTRODUCTION

THE usual criterion in the comparison of molecular electronic approximate wave functions is the accuracy of the calculated average energy, although it has been recognized that this is not always the most useful criterion.[1] Accurate wave functions are not available for most molecules, and one is generally more interested in the energies than in the wave functions themselves. Considering the thirteen-term function of James and Coolidge to be an accurate analytical wave function for the ground state of the hydrogen molecule,[2] it is possible to compute the coefficient a_1 of the ground state function ψ_1 in the expansion,

$$\psi\ (\text{trial}) = a_1\psi_1 + a_2\psi_2 + \cdots$$

of a $^1\Sigma_g$ trial function in terms of the correct $^1\Sigma_g$ wave functions. We have computed this coefficient, which is the overlap integral of the James and Coolidge function (to be referred to as ψ_1) with a trial function for some of the approximate wave functions for the hydrogen molecule.

The trial functions considered are those constructed from 1*s* atomic orbitals: the molecular orbital (LCAO–MO), the Wang, the Weinbaum (Wang plus ionic terms), and the ionic terms.[3] The notation used is illustrated by the expressions for the Wang and the ionic terms functions; the letters represent atomic orbitals, the numbers electrons, and N is a normalization factor.

$$\psi\ (\text{Wang}) = N(a_1b_2 + b_1a_2).$$

$$\psi\ (\text{ionic terms}) = N(a_1a_2 + b_1b_2).$$

The leading term of the James and Coolidge function was also considered; this may be written as a product of atomic orbitals, and is an MO type function (PMO),

$$\psi\ (\text{PMO}) = N(a_1b_1a_2b_2)^{\frac{1}{2}}.$$

The overlap integrals were evaluated at $zR = 1.5$, z being the scale factor and R the internuclear distance, which is equivalent to taking $R = 1.4$ atomic units (0.74 A) and $z = 1.5/1.4$. These values of z and R are close to the values which minimize the energy of all of the functions considered and eliminate the need for interpolation in tables of molecular integrals. Also, a constant R is required since the expansion theorem is used. The overlap of (PMO) with ψ_1 was obtained from tables of matrix elements lent to us by James and Coolidge. The other integrals were computed using the tables of $A_n(\alpha)$, $B_n(\alpha)$, $G_\tau{}^\nu(n,\alpha)$, and $W_\tau{}^\nu(m,n,\alpha)$ of Kotani *et al.*[4]

OVERLAPS, RMS ERRORS, AND ENERGY ERRORS

The values of the overlap integrals of ψ_1 with the trial functions are listed in column 1 of Table I. The height of the energy of the foregoing trial functions the ground-state energy ($\epsilon = E - E_1$) is listed in column 2, and the root-mean-square error $\{\int[\psi\ (\text{trial}) - \psi_1]^2 d\tau\}^{\frac{1}{2}} = (2 - 2a_1)^{\frac{1}{2}} = q$ in column 3. Column 4 lists the energy of the composite excited state function,

$$\psi_x = (1 - a_1^2)^{-\frac{1}{2}}(\psi\ (\text{trial}) - a_1\psi_1),$$

above the ground state ($\epsilon_x = E_x - E_1$). The notation used is that of James and Coolidge.[1]

It is seen that the overlap integrals, the squares of which are the weights of the ground state function ψ_1 in the trial functions, are greater than 0.95, even for functions which are considered to be quite poor. It should be remembered, however, that the binding energy of the hydrogen molecule is only fifteen percent of the total energy, and the coefficients a_1 are the overlaps of the total wave functions rather than of the parts which refer to binding.

TABLE I.

	1 a_1	2 ϵ ev	3 q	4 ϵ_x ev
ψ (ionic terms)	0.9556	3.8	0.298	44
ψ (PMO)	0.9792	2.16	0.204	51
ψ (LCAO)	0.9826	1.25	0.187	36
ψ (Wang)	0.9852	0.96	0.172	32
ψ (Weinbaum)	0.9871	0.72	0.161	28

* This work was supported in part under contract with the Air Research and Development Command, Contract No. R. 351.20.2.
† Agnes Anderson Research Fellow, 1950–1951.
‡ Present address: Department of Chemistry, University of Maine, Orono, Maine.
[1] H. M. James and A. S. Coolidge, Phys. Rev. **51**, 860 (1937).
[2] H. M. James and A. S. Coolidge, J. Chem. Phys. **1**, 825 (1933).
[3] L. Pauling and E. B. Wilson, *Introduction to Quantum Mechanics* (McGraw-Hill Book Company, Inc., New York, 1935), p. 349.
[4] Kotani, Amemiya, and Simose, Proc. Phys. Soc. Japan, **20** extra No. 1 (1938); **22** extra No. (1940).

The rms error, q, is seen to decrease more slowly than the energy error ϵ. The fact that the order of the rms errors of the trial function is the same as the order of the energy errors is not required by the expansion theorem. However, the ratio of the coefficients of ψ (ionic terms) and ψ (Wang) in the linear combination of these functions having the maximum overlap with ψ_1 (minimum rms error)[5] is 0.250, which is very nearly equal to the value 0.254 for this ratio in the Weinbaum function (minimum energy) at $zR=1.5$.

One may conclude from the decrease of ϵ_x with decreasing q that the errors in these functions are of the long-range type, resulting from the poor starting functions (unmodified atomic orbitals). With more accurate functions (e.g., superposition of configurations, or the inclusion of the coordinate r_{12}), the short-range errors become increasingly important and the values of ϵ_x should increase. The values of ϵ_x in column 4 may be compared with the estimated value of 14.1 ev for (E_2-E_1) at $R=1.4$.[6] The anomalous value of ϵ_x for ψ (PMO) may be attributed to the fact that this function is the leading (and most important) term of the James and Coolidge function which has been taken to represent the true ground state function.

[5] If φ is a linear combination of normalized functions φ_i,

$$\varphi=\sum_i d_i\varphi_i,$$

and c is the overlap integral of φ with a function ψ,

$$c=\int\varphi\psi d\tau=\sum_i d_i\gamma_i,$$

where

$$\gamma_i=\int\varphi_i\psi d\tau.$$

The condition that c be an extremum while φ remains normalized leads to the set of inhomogeneous equations

$$\sum_i d_i\Delta_{ik}=\gamma_k/\langle c\rangle,$$

where $\langle c\rangle$ is the extreme value for c, and

$$\Delta_{ik}=\int\varphi_i\varphi_k d\tau.$$

Solution of these equations, together with the normalization condition gives the coefficients d_i (which maximize the overlap integral) and the value of $\langle c\rangle$.

[6] O. W. Richardson, *Molecular Hydrogen and its Spectrum* (Yale University Press, New Haven, 1934), pp. 262, 324. The difference in equilibrium values for the ground state and the so-called X state, uncorrected for change in ν_0, is 12.5 ev. It was assumed that the compression energy could be taken from the potential curve for the first $^1\Sigma_u$ state since this has about the same internuclear distance as the X state, and presumably a similar compressional restoring force. The compression energy was therefore taken as 1.6 ev giving 14.1 ev for E_2-E_1.

BINDING ENERGY CALCULATION

Since ψ (PMO) is not linearly dependent on ψ (Wang) and ψ (ionic terms), a variation calculation with a linear combination of these three functions must give a lower energy than ψ (Weinbaum). The secular determinant was solved for $z=1$ at $R=1.5$ and 2.0 atomic units and the energy was found to be negligibly lower (0.001 and 0.017 ev) than the energy of ψ (Weinbaum) for these values of z and R. If the minimization with respect to z and R were carried out, it is likely that the energy improvement over ψ (Weinbaum) still would be less than 0.1 ev. (The energy improvement due to the inclusion of polarization terms in ψ (Weinbaum) is 0.1 ev.) Applying the criterion of maximum overlap, one obtains the function

$$\varphi=N[\psi\text{ (Wang)}+0.14\psi\text{ (ionic terms)}+0.30\psi\text{ (PMO)}]$$

with $a_1=0.9873$ ($q=0.159$). Thus inclusion of ψ (PMO) in ψ (Weinbaum) results in essentially no decrease of either the rms error or the energy error, and in spite of the difference of its apparent analytical form, ψ (PMO) is not significantly different from the classical trial functions.

We are indebted to Drs. H. M. James and A. S. Coolidge for the use of their tables of matrix elements.

Overlaps of Trial Functions for the Hydrogen Molecule. II. Covalent and Ionic Character of H_2†

JERRY BRAUNSTEIN*‡ AND WILLIAM T. SIMPSON
Department of Chemistry, University of Washington, Seattle 5, Washington
(Received December 8, 1952)

The mutual overlaps of some of the trial functions for the hydrogen molecule are presented and their relation to the covalent and ionic character of the bond are discussed. Difficulties involved in the definition of covalent and ionic as orthogonal components of wave functions are pointed out and contour maps indicating the shapes of some of the functions discussed are given.

INTRODUCTION

IN this paper, the mutual overlaps (or scalar products)[1] of some of the trial functions for the hydrogen molecule are presented and their relation to ideas on the covalent and ionic character of the bond in hydrogen is discussed. The notation used is that of the preceding paper and the overlaps, listed in Table I, are for $zR=1.5$.[2]

NONORTHOGONALITY OF COVALENT AND IONIC

The magnitude of the overlap of the ionic terms and the Wang functions, regarded as the wave functions for extreme ionic and extreme covalent bonds respectively, is at first surprising since the terms ionic and covalent are mutually exclusive; that is, the ionic character of bonds is considered to range from a few percent in essentially covalent bonds to almost one hundred percent in essentially ionic bonds.[3] Because of this nonorthogonality, it is not possible to interpret the squares of the coefficients in the trial functions as the contributions of ionic and covalent structures.[4] Thus the Weinbaum function,

$$\psi\ (\text{Weinbaum})=N(\psi\ (\text{Wang})+0.25\psi\ (\text{ionic terms})),$$

may not be called 66 percent covalent and 4 percent ionic on the basis of the squares of the coefficients being $N^2=0.66$ and $(0.25N)^2=0.041$.

Also, because of the nonorthogonality of the functions it is not possible to interpret the overlaps of the Wang and ionic terms functions with the James and Coolidge function as the covalent and ionic characters of the ground state of hydrogen. Since the James and Coolidge function may be written

$$\psi_1=\left(\int\psi_1\psi\ (\text{Wang})d\tau\right)\psi\ (\text{Wang})$$
$$+\text{other terms orthogonal to }\psi\ (\text{Wang}),$$

the ground state of hydrogen may be considered 97.06 percent covalent in the sense of ψ (Wang). However, the remaining 2.94 percent is not ionic in the sense of ψ (ionic terms); 0.38 percent of the electron distribution is accounted for by the *non-Wang part* of ψ (ionic terms), $N(\psi\ (\text{ionic terms})-0.9505\ \psi\ (\text{Wang}))$; the remaining 2.56 percent is described by a composite function orthogonal to both ψ (Wang) and ψ (ionic terms) which accounts for the deformation of the atomic orbitals, polarization and electron repulsion.

TABLE I.

	ψ (Wang)	ψ (Ionic terms)
ψ (Ionic terms)	0.9505	1.0000
ψ (PMO)	0.9817	0.9817
ψ (LCAO–MO)	0.9875	0.9875
ψ (Wang)	1.000	0.9505
ψ (Weinbaum)	0.9980	0.9681
ψ (James and Coolidge)	0.9852	0.9556

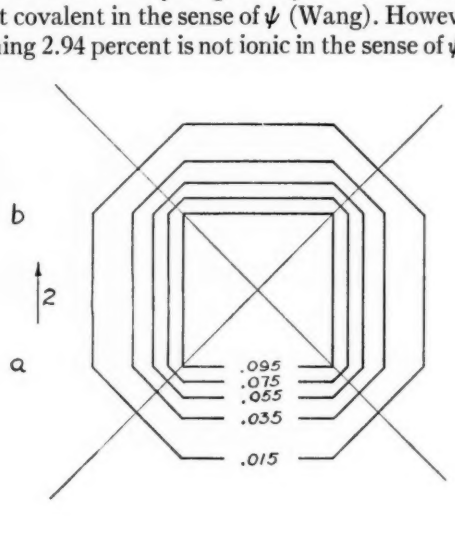

FIG. 1. The PMO function squared: $N^2a_1b_1a_2b_2$.

Despite the foregoing considerations, the names covalent and ionic for the Wang, and ionic terms functions are not anomalous, since the electron distributions associated with these functions fit the ideas of covalent and ionic qualitatively. In the prevailing definitions of

* Agnes Anderson Research Fellow, 1950–1951.

† This work was supported in part under contract with the Air Research and Development Command, Contract No. R. 351.20.2.

‡ Present address: Department of Chemistry, University of Maine, Orono, Maine.

[1] J. C. Slater, J. Chem. Phys. **19**, 220 (1951).

[2] J. Braunstein and W. T. Simpson, preceding article.

[3] See, for example, L. Pauling, *Nature of the Chemical Bond* (Cornell University Press, Ithaca, 1945), Secs. 7–8.

[4] Reference 3, page 35.

the covalent bond (sometimes called atomic) the electron distribution of the individual atoms is regarded as deformed by the sharing or exchange of electrons with a consequent increase of the electron density in the region between the nuclei. [The partial ionic character of the bond between two identical atoms (increased probability for both electrons together near one or the other of the nuclei) is not here included in the term covalent.][5] Only the parts of the covalent and ionic functions which refer to the covalent and ionic modification of the atomic electron distribution may be regarded as mutually exclusive, and since bond formation results in only a small decrease in the total energy of the system (e.g., the binding energy of hydrogen is less than 15

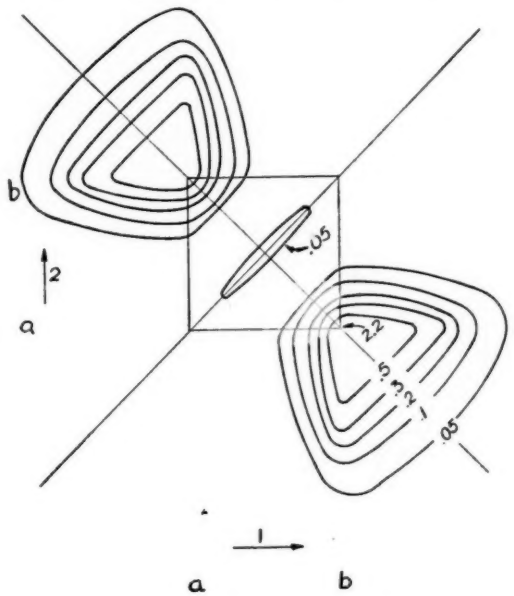

FIG. 2. The covalent function squared: $N^2[\psi\ (\text{Wang}) - 0.9817\psi\ (\text{atomic})]^2$.

percent of the total energy) the high overlap of the functions is not inappropriate.

ORTHOGONAL FUNCTIONS

The quantitative application of the ideas of covalent and ionic binding to arbitrary wave functions would be possible if the bond types were represented by orthogonal functions. These functions should be simple (e.g., constructed from atomic orbitals) in order that the classical trial functions be easily expressed in terms of the new ones, and that computation be feasible. The shapes of the functions should resemble the physical concepts which they are supposed to represent. The atomic wave function should have zero binding energy, should overlap the James and Coolidge function by about 0.90, and have a high probability only for one electron near each nucleus. The covalent function should have a high electron density in the region between the nuclei, and

[5] K. S. Pitzer, *Quantum Chemistry* (Prentice-Hall, Inc., New York, 1953), p. 143.

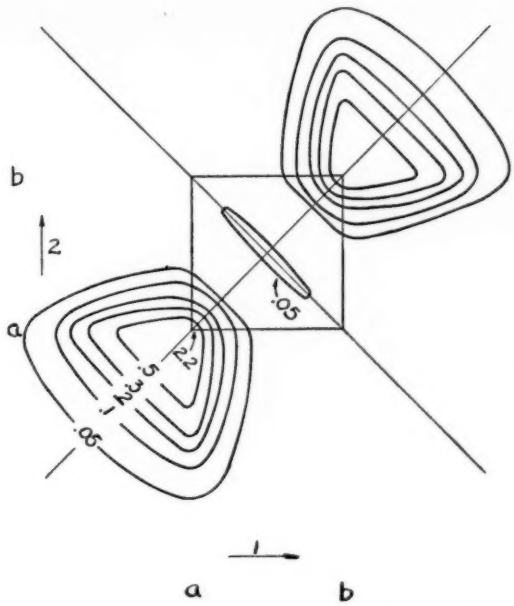

FIG. 3. The ionic function squared: $N^2[\psi\ (\text{ionic terms}) - 0.9817\psi\ (\text{atomic})]^2$.

the ionic function should have a high probability for both electrons together near one or the other of the nuclei. The scheme outlined below illustrates some of the difficulties involved in defining a set of orthogonal valence functions. The PMO function, which overlaps the Wang and ionic terms functions by 0.9817, was defined to be ψ (atomic). [This satisfies only the first requirement since the binding energy is too high (2.56 ev) and the electron density in the region between the nuclei is too high.] Two functions orthogonal to ψ (PMO) were then constructed.

$$\psi\ (\text{covalent}) = N(\psi\ (\text{Wang}) - 0.9817\psi\ (\text{atomic}));$$
$$\psi\ (\text{ionic}) = N[\psi\ (\text{ionic terms}) - 0.9817\psi\ (\text{atomic})].$$

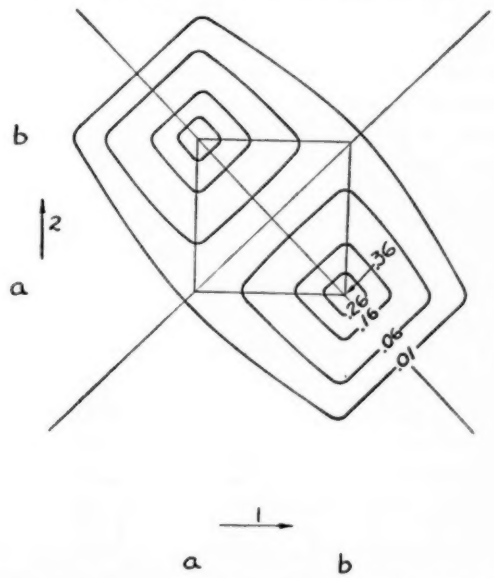

FIG. 4. The Wang function squared: $N^2[a_1b_2 + b_1a_2]^2$.

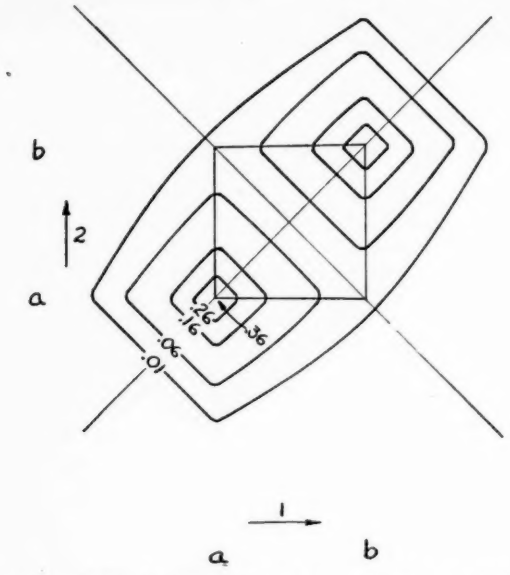

FIG. 5. The ionic terms function squared: $N^2[a_1a_2+b_1b_2]^2$.

These covalent and ionic functions are still not orthogonal, their overlap being -0.3663, and a new ionic function orthogonal to both ψ (covalent) and ψ (atomic) was defined:

$$\psi \text{ (ionic}')=N[\psi \text{ (ionic)}+0.3663\psi \text{ (covalent)}].$$

GRAPHIC REPRESENTATION

In order to judge the suitability of the names for the functions, their shapes should be examined. These are difficult to visualize, but some ideas as to their nature may be obtained from contour maps showing the correlated probability of the two electrons as a function of their positions along the internuclear axis. Figures 1–6 are contour maps of the squares of the PMO, Wang, ionic terms, LCAO–MO, covalent, and ionic functions in the z_1z_2 plane. (The center of the Cartesian coordinate systems for electrons one and two is the midpoint of the internuclear axis and the z axes coincide with the internuclear axis.) The shape of ψ (PMO) (Fig. 1) is seen not to fit the name atomic because of the large value of the function in the region between the nuclei. The covalent function looks more atomic than ψ (Wang) and is therefore inadequate. The ionic function, however, appears more ionic than ψ (ionic terms), the function being quite small for the electrons on different atoms or in the region between the nuclei.

TABLE II.

	c_a	c_c	c_i'
ψ (Ionic terms)	0.9817	−0.0697	0.1772
ψ (PMO)	1.0000	0	0
ψ (LCAO–MO)	0.9941	0.0611	0.0897
ψ (Wang)	0.9817	0.1904	0
ψ (Weinbaum)	0.9896	0.1394	0.0357
ψ (James and Coolidge)	0.979	0.125	0.015

The coefficients of the orthogonal functions in the expansion of the classical trial functions,

$$\psi \text{ (trial)}=c_a\psi \text{ (atomic)}+c_c\psi \text{ (covalent)}+c_i'\psi \text{ (ionic}'),$$

are given in Table II.

DISCUSSION

Although the covalent and ionic characters (squares of the coefficients in Table II) are largely in the expected order, the magnitudes are too low. Also, small changes in the definitions of the covalent and ionic functions lead to inconsistencies. For example, if ψ (covalent) and ψ (ionic) are symmetrically orthogonalized [so that the ionic″ character of ψ (covalent) is equal to the covalent′ character of ψ (ionic)], the Weinbaum function turns out to have essentially no ionic″ character. A number of rotations of ψ (atomic) and ψ (covalent) about the ionic′ axis (here orthonormal functions are considered as orthogonal unit vectors) also were studied to see whether

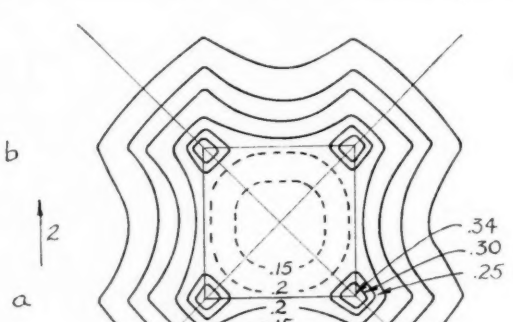

FIG. 6. The molecular orbital function squared: $N^2[(a_1+b_1)(a_2+b_2)]^2$.

more reasonable coefficients could be obtained. These always led to inconsistencies in the order of the magnitudes of the coefficients, which is to be expected in view of the inappropriateness of the basic definition [of ψ (atomic)].

A workable scheme might be obtained by paying closer attention to the shape and energy of the atomic function, but in the absence of physical guides to the manner in which the functions should be orthogonalized, the scheme would have to be empirical. Since the calculated energy is not very sensitive to small changes in the electron distribution, the definitions of covalent and ionic would vary considerably with small changes in the definition of the atomic function.

Vibrational Intensities. IV. Bond Moments in C_2F_6†

DALE G. WILLIAMS,* WILLIS B. PERSON,‡ AND BRYCE CRAWFORD, JR.
School of Chemistry, University of Minnesota, Minneapolis, Minnesota

(Received April 16, 1954)

The intensities of four of the infrared-active fundamentals of C_2F_6 have been determined and interpreted in terms of the bond-moment hypothesis. The bond-moment parameters are overdetermined so that an internal check is provided. This check, supplemented by comparison with data on related molecules, shows that the bond-moment picture is a useful approximation but that it is not quantitatively reliable.

POSTWAR improvements in the reliability of infrared spectrometers, together with important advances in the design[1] and technique[2] of spectrophotometric experiments, have made it possible to study the the intensities of infrared absorption by simple molecules, and a number of laboratories have engaged in such studies. The data so obtained give information concerning the change of dipole moment of the molecule with vibrational motion and may be interpreted to shed useful light on molecular structure without making further approximations.[3] However, the chemist would be false to his native instincts and his traditions if he did not seek to interpret all molecular behavior in terms of bond properties; hence infrared intensities have been widely interpreted in terms of hypothetical independent "bond moments" associated with each (hetero-atomic) bond in the molecule. This concept has not yet been fully tested, but the data available indicate that the values of bond moments, μ, and bond effective charges, $\epsilon(=d\mu/dr)$, vary considerably, not only from molecule to molecule, but also within a given molecule.[4]

To examine the limitations of this bond-moment approximation one needs reliable experimental intensities on a number of molecules which contain a given bond, say C−H or C−F, in a variety of locations, preferably free from polarization, conjugation, or other complicating effects. We report here such data on the C−F bond.

Hexafluoroethane has four easily measured fundamentals. The intensities of these lead to two independent sets of values of μ and ϵ. These two values of μ should agree, and the two values of ϵ should agree, if the bond-moment hypothesis is valid. A further, though more demanding, test of the bond-moment hypothesis is that our C−F bond moments for C_2F_6 should agree with those reported for CH_3F[5] and CF_4.[6]

EXPERIMENTAL

For the hypothetical case of absorption of a monochromatic beam of light, the following equation[1] holds:

$$A=\int_{\text{band}}\alpha_\nu d\nu=1/nl\int_{\text{band}}\ln(I_0/I)d\nu. \qquad (1)$$

Here A is the integrated molar absorption coefficient, and is the total intensity associated with the transition from the ground state to the first excited vibrational state, α_ν is the molar absorption coefficient at the frequency ν, n is the molar concentration, l is the length of the absorption path, and I_0 and I are the intensities of the incident and transmitted light of frequency ν, respectively. For a real spectrometer, the measured intensity T is not that of a monochromatic beam, but is an average weighted according to the slit function. Hence we define the experimental quantity B, the apparent integrated molar absorption coefficient.

$$B=1/nl\int_{\text{band}}\ln(T_0/T)d\nu. \qquad (2)$$

According to Wilson and Wells,[1] B approaches A when there is sufficient pressure broadening to make α_ν slowly varying over the slit width. If, at these high pressures, the envelope of the absorption band still varies over the slit width enough to make B different from A, then extrapolation to zero pressure of the absorbing gas causes B to become equal to A. Penner and Weber[2] have pointed out the importance of having the pressure sufficiently high so that B does not differ significantly from A over a wide range of nl.

The sample of C_2F_6 was obtained from the National Bureau of Standards through the courtesy of Dr. D. E. Mann. It was reported to be better than 99 percent pure. Some air was removed from the sample by fractional distillation from a liquid nitrogen trap. The in-

† Based on a thesis presented by Dale G. Williams in partial fulfillment for the degree of Master of Science, University of Minnesota, March, 1954.

* Present address: Department of Chemistry, University of Iowa, Iowa City, Iowa.

‡ Du Pont Instructor in Chemistry, 1952–1953.

[1] E. B. Wilson, Jr., and A. J. Wells, J. Chem. Phys. **14**, 578 (1946).

[2] S. S. Penner and D. Weber, J. Chem. Phys. **19**, 807 (1951).

[3] B. L. Crawford, Jr., and H. L. Dinsmore, J. Chem. Phys. **18**, 983 (1950); D. F. Eggers, Jr., and B. L. Crawford, Jr., *ibid.* **19**, 1554 (1951).

[4] See, for example, the data on the C−H bond moments and effective charges presented in (a) Thorndike, Wells, and Wilson, J. Chem. Phys. **15**, 157 (1947), and (b) A. Thorndike, J. Chem. Phys. **15**, 868 (1947).

[5] G. Barrow and D. McKean, Proc. Roy. Soc. (London) **A213**, 27 (1952).

[6] P. Schatz and D. Hornig, J. Chem. Phys. **21**, 1516 (1953).

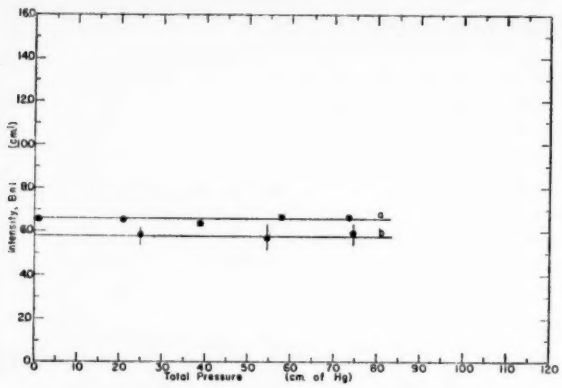

FIG. 1. Intensities of two bands of C_2F_6 as a function of total pressure. (a) A parallel band (714 cm^{-1}); the partial pressure of C_2F_6 is 9.21-mm Hg. (b) A perpendicular band (1250 cm^{-1}); the partial pressure of C_2F_6 is 0.274 mm Hg.

frared spectrum appeared to be identical with that reported by Nielsen, Richards, and McMurry.[7]

Pressures of the C_2F_6 were measured with a closed, wide-bore, U-tube mercury manometer, equipped with a traveling microscope capable of reading pressures up to 100 mm of Hg within 0.02 mm. Pressures of C_2F_6 used varied from 0.1 to 80 mm of Hg. Pressures below 1 mm of Hg were measured by expansion from a known volume in the line to the known volume of the cell. The expansion ratio was about 10 to 1.

The cell was a 10.0-cm glass cell with KBr windows attached with beeswax and rosin. A dummy cell consisting of two KBr windows on a wire frame was used to obtain backgrounds. A teflon leaf was placed in the cell to aid in mixing. The cell volume was measured by expansion from the known volume of the vacuum line using helium, nitrogen, and C_2F_6. Each gas gave the same volume for the cell, thus indicating that no significant absorption of C_2F_6 was taking place in the stopcock grease, or on the surfaces inside the cell.

A given partial pressure of C_2F_6 was measured into the cell, using the traveling microscope. Then, about one atmosphere of pressurizing gas (Matheson "prepurified" nitrogen) was added. In order to establish that one atmosphere of pressurizing gas was sufficient, the absorption of one parallel band (714 cm^{-1}) and one perpendicular band (1250 cm^{-1}) were each measured as as a function of total pressure of N_2 up to one atmosphere. The results in Fig. 1 show that, within the experimental scatter, there is no dependence on total pressure.

The spectrometer used throughout this work was a Perkin-Elmer Model 12C, with a double-pass monochromator. The double-pass feature reduces the stray light to a negligible amount. It does, however, cause a slight zero shift due to the fact that reradiation from the hot slit is not constant over the frequency range of a band. This hot-slit effect is not serious in these regions, and the error introduced in neglecting it is less than one percent. A sodium chloride prism was used for the 714, 1116, and 1250 cm^{-1} bands, and a potassium bromide prism was used for the 522 cm^{-1} band. Spectral slit widths varied from 1.5 to 3.0 cm^{-1}.

Some fluctuations due to variation in the source intensity occurred despite attempts to regulate the Globar power. Also, variations in room temperature, in the thermocouple vacuum, etc., caused some fluctuations in sensitivity in the thermocouple. In order to minimize these instrumental errors, three traces were taken for each intensity measurement; these three were replotted on the same graph; and the best smooth curve was drawn through them. The difference between the area under this best average curve and that under the most extended curve through the data is the indicated

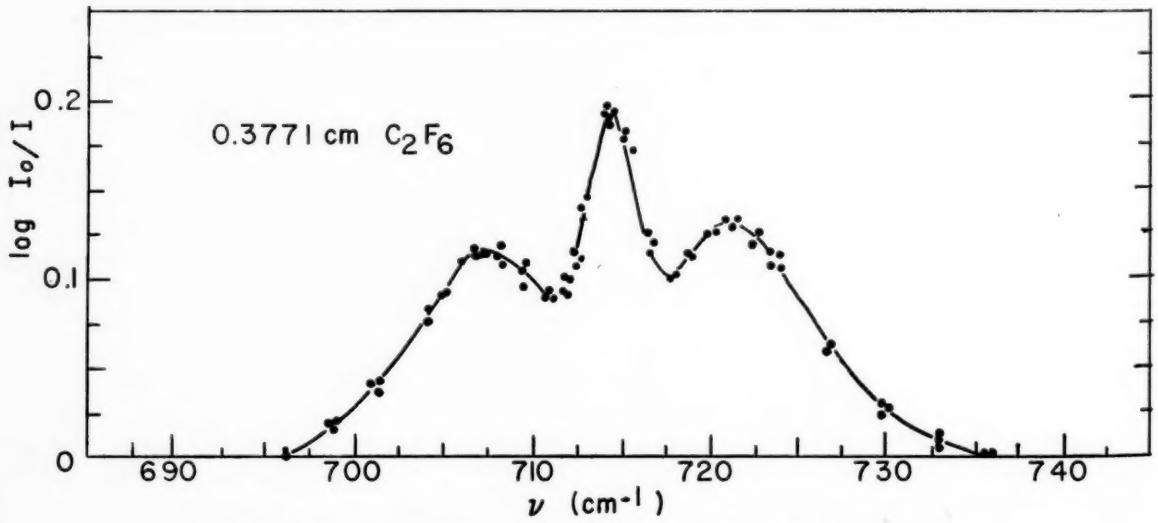

FIG. 2. Typical plot of transmittance *vs* frequency showing how the data were averaged. The points shown come from three separate measurements.

[7] Nielsen, Richards, and McMurry, J. Chem. Phys. **16**, 67 (1948).

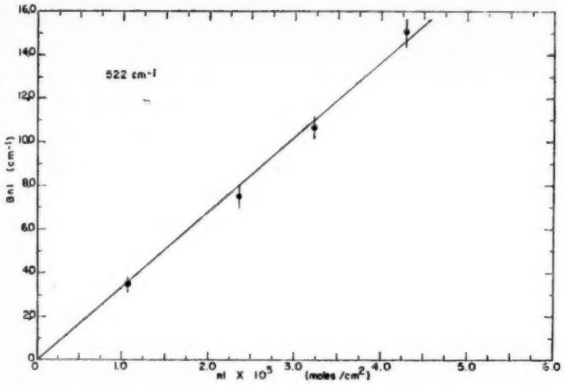

FIG. 3. Beer's law plot for the 522 cm^{-1} band (E_u) of C_2F_6.

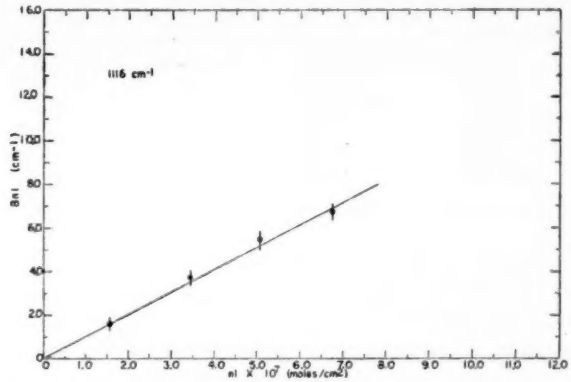

FIG. 5. Beer's law plot for the 1116 cm^{-1} band (A_{2u}) of C_2F_6.

error in the plots of absorption, *Bnl*, against *nl*. A sample plot is shown in Fig. 2. The areas were measured with a planimeter.

Figures 3 through 6 show the plots of *Bnl versus nl* for the 522, 714, 1116, and 1250 cm^{-1} bands, respectively. These plots are linear, within the experimental scatter. This may be taken as a further indication that the fine structure of the bands has been sufficiently pressure-broadened. Furthermore, it indicates that the envelope effect[1] is not important at these slit widths for these bands. The deviation of all the experimental points from the straight line is within the scatter due to the aforementioned instrumental instability.

The values of A (i.e., the slopes of the straight lines) are listed in Table I. The units are cm^{-1}/millimoles/cm^2—a unit which we have come to call the "dark."[8]

INTERPRETATION OF DATA

The integrated molar absorption coefficient for the ith fundamental A_i is given by

$$A_i=\frac{\pi N_0 g_i}{3000c^2}\left|\frac{\partial \mathbf{p}}{\partial Q_i}\right|^2. \tag{3}$$

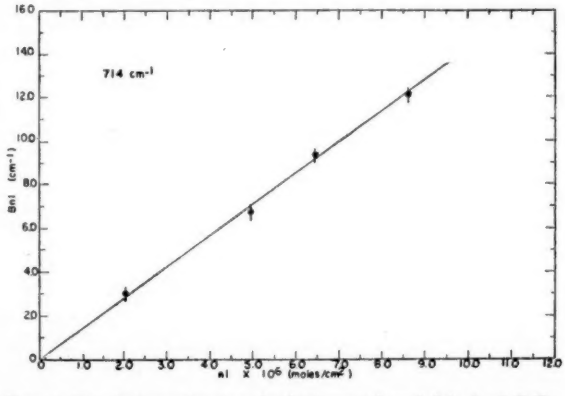

FIG. 4. Beer's law plot for the 714 cm^{-1} band (A_{2u}) of C_2F_6.

[8] This unit is, save for a power of ten, the same as the "intensity unit" used by Norman Jones *et al.*, J. Am. Chem. Soc. **74**, 80 (1952). We prefer the smaller size of the dark because it produces convenient numbers for relatively weak bands as well as for intense fundamentals.

Here N_0 is Avogadro's number, g_i is the degeneracy of the excited vibrational state, c is the velocity of light, $\mathbf{p}$ is the dipole-moment vector of the entire molecule, and Q_i is the normal coordinate of the ith mode of vibration. If A_i is measured in darks, $\mathbf{p}$ in esu, and Q_i in cgs units, then,

$$|\partial \mathbf{p}/\partial Q_i| = \pm 1.1936(A_i/g_i)^{\frac{1}{2}}. \tag{4}$$

The values of $|\partial \mathbf{p}/\partial Q_i|$ so calculated are given in Table I.

By the methods of Wilson,[9] the normal coordinates Q may be related to the symmetry coordinates S by the L matrix defined by the equation

$$S=LQ.$$

The symmetry coordinates are in turn related to the bond coordinates R by the U matrix defined by

$$S=UR, \quad \text{or} \quad R=U^{-1}S.$$

In relating the $|\partial \mathbf{p}/\partial Q_i|$ to the symmetry coordinates, one must remember the vectorial nature of these quantities. The *vector* equation always holds, that

$$(\partial \mathbf{p}/\partial Q_i)=\sum_k L_{ik}(\partial \mathbf{p}/\partial S_k), \tag{5}$$

where the sum runs over the symmetry species containing Q_i. In cases of favorable symmetry where that

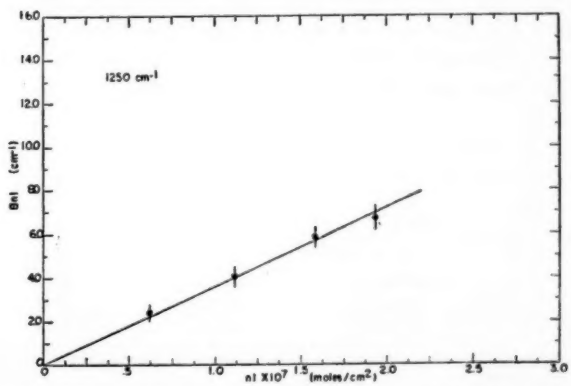

FIG. 6. Beer's law plot for the 1250 cm^{-1} band (E_u) of C_2F_6.

[9] E. B. Wilson, Jr., J. Chem. Phys. **7**, 1047 (1939); **9**, 76 (1941).

TABLE I. Experimental intensity data for C_2F_6.

ν_i(cm^{-1})	Intensity, A_i(darks)	Degeneracy, g_i	$\lvert\partial\mathbf{p}/\partial Q_i\rvert$ (cgs units)
$\nu_5=1116$	10300	1	121
$\nu_6=714$	1420	1	44.9
$\nu_7=1250$	35600	2	160
$\nu_8=522$	343	2	15.6

symmetry species contains only one vector component, say p_x, we may replace $\mathbf{p}$ by p_x and reduce (5) to an algebraic equation; moreover, then $\partial p_x/\partial Q_i=\lvert\partial\mathbf{p}/\partial Q_i\rvert$, which we know from experiment. Then the $\partial p_x/\partial S_k$ may be related to the bond coordinates R by

$$(\partial p_x/\partial S_k)=\sum_j(U^{-1})_{kj}(\partial p_x/\partial R_j). \tag{6}$$

Here the sum is carried out over all the bond coordinates.

Under the bond-moment hypothesis, the dipole-moment vector $\mathbf{p}$ is said to be made up of the vector sum of individual bond moments μ_j which are directed along the bonds. In C_2F_6, the vector change $(\partial\mathbf{p}/\partial Q_i)$ is directed parallel to the z(C−C) axis for the A_{2u} vibrations of C_2F_6 and perpendicular to that axis for the E_u vibrations. A little consideration shows that, for either the p_z or the p_x component, we can write relations of the form

$$\partial p_z/\partial R_j=b_{zj}\mu_{CF}, \tag{7}$$

if R_j is a bending coordinate, and

$$\partial p_z/\partial R_j=c_{zj}\epsilon_{CF}, \tag{8}$$

if R_j is a stretching coordinate; here μ_{CF} is the C−F bond moment, $\epsilon_{CF}=\partial\mu_{CF}/\partial r_{CF}$ is its "effective charge," and b_{zj} and c_{zj} are geometrical constants.

Through this chain of relations, our intensity data may be interpreted in terms of bond moments and effective charges. In order to find the L transformation, one must have the force-constant matrix F. For C_2F_6, the F matrix has been determined by Pace,[10] by Shimanouchi,[11] and by Berryman;[12] the calculated frequencies of Pace do not agree with the observed as well as the other sets. We determined the L transformation using both Berryman's and Shimanouchi's F, and got essentially the same transformation from both, despite their noticeable difference. The details of all transformations used are given in the Appendix.

TABLE II. Bond-moment parameters for C_2F_6.

	Signs of $\partial p/\partial Q_i$	ϵ (Debyes/A)	μ (Debyes)
A_{2u}	the same	±7.02	±0.0796
(∥)	different	±2.25	±1.494
E_u	the same	±2.40	±1.073
(⊥)	different	±3.10	±0.030

[10] E. L. Pace, J. Chem. Phys. **16**, 74 (1948).
[11] T. Simanouti, J. Chem. Phys. **17**, 848 (1949).
[12] L. H. Berryman, Ph. D. thesis, University of Oklahoma, 1950.

Using these transformations in the relations (5) through (8), we got two independent sets of equations, one set using the A_{2u} data and the other the E_u data; each set consisted of two simultaneous linear equations in μ and ϵ. Because of the ambiguity of sign indicated in Eq. (4), four possible solutions must be considered for each set. All possibilities are presented in Table II, where the top signs in each line are for $\partial p_z/Q_5$ or $\partial p_x/\partial Q_{7a}$ taken positive.

DISCUSSION

The first thing we notice in Table II is that, as it happens, all solutions lead to the conclusion that μ and ϵ have the same sign. Hence, unambiguously, the magnitude of the C−F bond moment increases when the bond length increases.

Next, we may consider the magnitudes of the possible values in Table II in terms of their "reasonableness." From either the electronegativity considerations of Pauling[13] or the experimental dipole moment of CF_3H,[14] one would expect the C−F moment to be about 1.5 Debyes. Hence, we may discard with confidence the choices of sign which lead to the extremely low values of μ (less than 0.1 Debye). Thus we are lead unambiguously to one value of μ and one value of ϵ from the parallel vibrations, and one of each from the perpendicular vibrations.

TABLE III. Comparison with C−F bond moments from other molecules.

Molecule		ϵ	μ
CH_3F[a]		4.70 or 4.50	1.9 to 3.1
CF_4[b]		4.88 or 3.35	1.12 or 2.36
C_2F_6[c]	∥	2.25	1.49
	⊥	2.40	1.07

[a] See reference 5.
[b] See reference 6.
[c] This research.

In Table III we present a comparison with other data on C−F bond moments. It would appear that transfer of bond moments from one molecule to another would be very risky. Furthermore, although the values of ϵ obtained in C_2F_6 agree with each other very well, there is a very large discrepancy between these C_2F_6 values and those obtained in other molecules, which are also reasonably consistent with each other. There does not seem to be any such grouping in the values of μ.

There are three possible explanations for the discrepancies noted in Tables II and III. First, the experimental data may be inaccurate; second, the normal-coordinate analysis, and hence the L transformation, may be in error; third, the bond-moment hypothesis may actually be this poor an approximation.

[13] L. Pauling, *The Nature of the Chemical Bond* (Cornell University Press, Ithaca, 1940), pp. 64 ff.
[14] A. A. Maryott and F. Buckley, *Table of Dipole Moments* (National Bureau of Standards, Washington, D. C., 1953), circular 537.

With regard to experimental error, the scatter of our own intensity data is less than 5 percent. Making a conservative estimate of systematic errors, we feel that our A values given in Table I are certainly good to within 20 percent; because of the favorable square-root (see Eq. 4) the uncertainty in the $|\partial \mathbf{p}/\partial Q|$ values is then less than 10 percent. While we should not care to estimate precisely the error in the data from other laboratories, we feel that the *experimental* error in the numbers summarized in Table III should be less than 20 percent.

The problem of the L transformation arises from the inherent ambiguity in the potential function for polyatomic molecules. This has been nicely discussed by Schatz and Hornig,[6] and we can only concur that "no bond moment or derivative calculated from the infrared intensities of a polyatomic molecule can be regarded as reliable unless the general potential function has been determined accurately or the sensitivity of the results to reasonable variations in the potential function has been calculated." The general potential function is perhaps best determined by the study of isotopic molecules, a method which is not readily applicable to C_2F_6. Failing this, one may have recourse to study of homologous molecules, assuming a particular type of potential function with "bond force constants" that can be transferred from one molecule to another; the Urey-Bradley field has been especially successful, and Shimanouchi's F matrix for C_2F_6 is based on such studies. Hence we may say that our L transformation, though not unique, is as good as one is likely to get.

The question arises whether one can, by careful adjustment of the L transformations for CF_4 and C_2F_6, obtain consistency both in the bond force constants and in the bond moments. Using a method under development in this laboratory, which we hope to report in detail later, we have attempted such an adjustment, and have found that if we are to bring the bond-moment parameters from our A_{2u} data into agreement with those from CF_4, we must use force constants which are absurd when interpreted as a Urey-Bradley field, and which moreover do not satisfactorily reproduce the E_u frequencies of C_2F_6.

We therefore conclude that the bond-moment picture is useful only as a first order-of-magnitude approximation; bond-moment parameters may be expected to be "reasonable" in magnitude, but cannot be transferred from molecule to molecule in any quantitative sense.

ACKNOWLEDGMENTS

We wish to thank Dr. D. E. Mann for the loan of the C_2F_6. We gratefully acknowledge financial support from the Office of Naval Research.

APPENDIX

The symmetry coordinates for C_2F_6 are chosen as follows:

A_{2u} Class (parallel vibrations)

$$S_5=(1/\sqrt{6})(r_1+r_2+r_3-r_4-r_5-r_6);$$

$$S_6=(d/\sqrt{12})[\beta_1+\beta_2+\beta_3-\beta_4-\beta_5-\beta_6-(\alpha_{12}+\alpha_{13}+\alpha_{23}-\alpha_{45}-\alpha_{46}-\alpha_{56})].$$

E_u Class (perpendicular vibrations)

$$S_{7a}=(1/\sqrt{3})[r_1-r_4-\tfrac{1}{2}(r_2+r_3-r_5-r_6)];$$

$$S_{7b}=\tfrac{1}{2}(r_2-r_3+r_5-r_6);$$

$$S_{8a}=(d/\sqrt{3})[\beta_1-\beta_4-\tfrac{1}{2}(\beta_2+\beta_3-\beta_5-\beta_6)];$$

$$S_{8b}=(d/2)(\beta_2-\beta_3+\beta_5-\beta_6);$$

$$S_{9a}=(d/\sqrt{3})[\alpha_{23}-\alpha_{56}-\tfrac{1}{2}(\alpha_{13}+\alpha_{12}-\alpha_{46}-\alpha_{45})];$$

$$S_{9b}=(d/2)(\alpha_{13}-\alpha_{12}+\alpha_{46}-\alpha_{45}).$$

Here d is the equilibrium C−F distance, taken to be 1.36 A. Fluorine atoms 1,2, and 3 are on one carbon atom, and fluorine atoms 4, 5, and 6 are on the other. We have considered the staggered form (D_{3d}) in the normal coordinate analysis. Fluorine atom 1 is pointing in the positive x direction, and atom 4 is pointing in the negative x direction. Atoms 2 and 5 are on the same side of the C−C axis. In the symmetry coordinates given above, r_i is the change in length of the C−F$_i$ bond, β_i is the change in the C−C−F$_i$ angle, and α_{ij} is the change in the F$_i$−C−F$_j$ angle.

The relations above determine the U matrix, and from this, U^{-1} may easily be obtained. From Eqs. 6–8 we then obtain relations between $\partial p_x/\partial S_k$ and μ and ϵ, with only the geometrical constants b and c to be determined. There are then two ways in which to proceed. The most common path is to make the necessary geometrical considerations in order to find these constants. However, these are not always obvious, particularly for the perpendicular vibrations of C_2F_6, and so a method worked out by Crawford and Barrow[15] is more generally useful. Under their formalized procedure, a minimum reliance is placed on geometrical intuition. The method of Crawford and Barrow was used to obtain the geometrical constants of Eqs. 7 and 8 for the perpendicular vibrations, and the geometrical reasoning was used for the easier case of the parallel vibrations. The resulting relations between $\partial p/\partial S_k$ and μ and ϵ are given as follows.

Parallel vibrations:

$$(\partial p_z/\partial S_5)=(2/3)^{\frac{1}{2}}\epsilon;$$

$$(\partial p_z/\partial S_6)=2(2/3)^{\frac{1}{2}}\mu/d;$$

Perpendicular vibrations:

$$(\partial p_x/\partial S_{7a})=(\partial p_y/\partial S_{7b})=(\sqrt{3}\sin\beta)\epsilon;$$

$$(\partial p_x/\partial S_{8a})=(\partial p_y/\partial S_{8b})=-[(3/2)^{\frac{1}{2}}\sin\beta]\mu/d=-(\partial p_x/\partial S_{9a})=-(\partial p_y/\partial S_{9b}).$$

The L matrices obtained from the normal coordinate analyses of either Shimanouchi or Berryman are given below.

[15] B. Crawford, Jr., and G. Barrow (to be published).

For the parallel vibrations:

$$L_{55}=0.262\sqrt{N}; \qquad L_{56}=-0.108\sqrt{N};$$
$$L_{65}=0.602\sqrt{N}; \qquad L_{66}=0.433\sqrt{N}.$$

For the perpendicular vibrations (using Shimanouchi's constants):

$$L_{77}=0.402\sqrt{N}; \quad L_{78}=-0.0417\sqrt{N}; \quad L_{79}=-0.0175\sqrt{N};$$
$$L_{87}=-0.0863\sqrt{N}; \quad L_{88}=0.00623\sqrt{N}; \quad L_{89}=0.242\sqrt{N};$$
$$L_{97}=0.433\sqrt{N}; \quad L_{98}=0.406\sqrt{N}; \quad L_{99}=0.0236\sqrt{N}.$$

Here N is Avogadro's number, and the L's have units of $g^{-\frac{1}{2}}$.

THE JOURNAL OF CHEMICAL PHYSICS VOLUME 23, NUMBER 1 JANUARY, 1955

The Microwave Spectrum of Ethyl Fluoride*

J. KRAITCHMAN† AND B. P. DAILEY
Department of Chemistry, Columbia University, New York 27, New York

(Received January 4, 1954)

The microwave spectrum of ethyl fluoride has been investigated in the region from 17 to 38 kMc. The values of the rotational constants of the molecule obtained from the analysis of the spectrum are: $A=36070.30\pm0.10$ Mc, $B=9364.54\pm0.10$ Mc, and $C=8199.74\pm0.10$ Mc. The following structural parameters have been fitted to these rotational constants: $r_{CH}=1.091A$, $r_{CC}=1.540A$, $r_{CF}=1.375A$, and tetrahedral bond angles. The dipole moment components along the principle axes of the molecule are $\mu_A=1.69D$ and $\mu_B=1.00D$; the total dipole moment, $\mu=1.96\pm0.03D$, is oriented at an angle of 64° with respect to the C−C bond axis, or approximately 7° from the C−F bond axis. The barrier height for internal rotation is 1490 ± 50 cm^{-1} (4260 cal/mole).

INTRODUCTION

THE microwave spectrum of ethyl fluoride has been investigated because of its relevance to a number of problems of general interest. Because of the possibility of hindered rotation or torsional oscillation about the C−C bond axis, analysis of the spectrum of ethyl fluoride will provide information bearing on the magnitude of the potential barrier to such internal rotation.

Ethyl fluoride has several special advantages which make it a suitable molecule for a study of hindered rotation phenomena. It is an asymmetric rotor, and therefore representative of the most numerous class of molecules. However, its asymmetry is slight ($\kappa\approx-0.92$) and the resulting spectral complexity should not be too great. Unlike other halogen derivatives, there is no nucleus possessing a quadrupole moment in ethyl fluoride, and therefore no complication of the spectrum due to quadrupole hyperfine structure.

The task of identifying the vibrational satellite lines in the microwave rotational spectrum of ethyl fluoride has been greatly simplified by the assignment of the fundamental vibrational frequencies resulting from the recent study of the infrared and Raman spectra of the molecule.[1]

Since a low-lying frequency observed in the Raman spectrum has been tentatively identified as the torsional frequency, the hindering barrier height in the molecule can be accurately evaluated if this frequency assignment is confirmed and if an accurate set of structural parameters for the molecule can be obtained. The magnitude of the observed torsional frequency indicates that the barrier has a rather high value. It will be shown that in this case the rotational spectrum of the molecule in the ground vibrational state can be interpreted satisfactorily even if the internal rotational motion is neglected.

It has been found possible to determine the dipole moment of ethyl fluoride, as well as its orientation in the molecule, from a study of the Stark effect in the rotational spectrum. This information has an important bearing on the interpretation of the hindered rotation in terms of a bond moment expansion of the charge distribution in the molecule.[2]

The determination of the barrier height to internal rotation for ethyl fluoride also serves to complete the

* Work assisted in part by a contract with the Signal Corps and a grant from the Research Corporation.

† Present address: Westinghouse Research Laboratories, East Pittsburgh, Pennsylvania.

[1] Smith, Saunders, Nielsen, and Ferguson, J. Chem. Phys. **20**, 847 (1952).

[2] E. E. Lassettre and L. B. Dean, Jr., J. Chem. Phys. **17**, 317 (1949).

data necessary for a comparison in the interesting series: CH_3CH_3, CH_3CH_2F, CH_3CHF_2, and CH_3CF_3. Regularities observed in such a series, or the lack of them, should provide a test for any general theory on the nature of hindered rotation.

THE SPECTRUM

The microwave spectrum of ethyl fluoride[3] was investigated in the region from 17 to 38 kMc using a Stark modulation spectrometer.[4] Frequency measurements of the observed transitions were made in the conventional manner using a crystal-controlled frequency standard[5] monitored against WWV.

While no previous structural information on CH_3CH_2F has been reported, a reasonably probable structure can be assigned on the basis of information available from related molecules. Assuming the following parameters: $r_{CH}=1.10A$, $r_{CC}=1.54A$, $r_{CF}=1.38A$, and tetrahedral bond angles, the rotational constants of the molecule are: $A=36$ kMc, $B=9.3$ kMc, and $C=8.2$ kMc. The molecule is a slightly asymmetric prolate rotor with an asymmetry parameter $b=(C-B)/(2A-B-C)$ of approximately $-0.021(\kappa\approx-0.92)$. Since the rotational constant A is rather sensitive to variations in the structural parameters, the approximate value given above was not considered very reliable.

Calculations were then made using these approximate rotational constants in order to determine what transitions might be expected to be observed in the spectral region investigated. The energy levels of the states involved in these expected transitions were calculated using a power series expansion of the rigid rotor eigenvalues.[6] Initially it was only necessary to carry out the expansion to the first power of the asymmetry parameter. As the analysis of the spectrum progressed, these calculations were refined by including additional higher order terms in the expansion.

Using the approximate transition frequencies obtained from these calculations, and on the basis of the qualitative Stark effects[7] and the relative intensities[8] of the observed transitions, it was possible to analyze the spectrum. The frequencies of three of the four lines observed in the $J=0\rightarrow1$ and $J=1\rightarrow2$ transitions depend only on B and C. From these frequencies accurate values of B and C were obtained. The frequency of the fourth line, the $1_{01}\rightarrow2_{02}$ transition, depends on B and C and very slightly on A. However, it was possible to obtain a more accurate value of A from this line than the value obtained from the approximate structural parameters. A still more accurate value of A was then obtained from the $1_{01}\rightarrow1_{10}$ and $2_{02}\rightarrow2_{11}$ transitions. This procedure gave the following values: $A=36\,070.30\pm0.10$ Mc, $B=9364.54\pm0.10$ Mc, $C=8199.74\pm0.10$ Mc, and $b=-0.02134261$ $(\kappa=-0.9164135)$.

TABLE I. Rotational transitions of CH_3CH_2F.

Transition $J_{K_{-1},K_{+1}}\rightarrow J'_{K_{-1}',K_{+1}'}$		Frequency (Mc) Observed[a]	Calculated
5_{15}	5_{14}	17 449.16	17 451.16
0_{00}	1_{01}	17 564.27	17 564.28
6_{24}	7_{17}	21 523.28	21 530.32
6_{16}	6_{15}	24 393.70	24 398.37
3_{12}	2_{21}	25 698.47	25 700.89
2_{12}	3_{03}	26 964.70	26 965.77
1_{01}	1_{10}	27 870.51	27 870.56
6_{24}	5_{33}	28 990.42	28 995.52
2_{02}	2_{11}	29 072.68	29 072.64
3_{03}	3_{12}	30 945.15	30 945.01
6_{25}	5_{32}	31 564.84	31 571.15
7_{17}	7_{16}	32 449.89	32 458.79
2_{20}	3_{13}	32 723.83	32 726.23
4_{04}	4_{13}	33 568.38	33 568.26
1_{10}	2_{11}	33 963.77	33 963.77
1_{01}	2_{02}	35 091.16	35 091.29
5_{24}	6_{15}	35 263.45	35 272.38
1_{11}	2_{12}	36 293.37	36 293.37
5_{05}	5_{14}	37 042.99	37 043.44

[a] All frequencies accurate to ±0.10 Mc.

The lines which have been identified are listed in Table I. In addition to the power series expansion form mentioned above, the continued fraction form of the eigenvalues[6] was also used to check the values listed in the column of calculated frequencies. Except for a few levels of high J and low K, calculations using the power series expansion form carried out to the fifth power of the asymmetry parameter were found to be sufficiently accurate. The agreement between the observed and calculated frequencies becomes somewhat poorer for transitions involving higher values of J and K. Since no correction was made for centrifugal distortion, this behavior is not unexpected.

In addition to the lines listed in Table I, the majority of which exhibit a second order Stark effect, many lines exhibiting a first order Stark effect were observed. Lines of this type were so numerous that no attempt was made to measure and identify them. Presumably the unidentified lines arise from transitions involving high values of J and K.

THE MOLECULAR STRUCTURE

A complete structural determination is not possible, since at least seven bond distances and bond angles must be determined and only the three rotational constants of the $C^{12}H_3C^{12}H_2F$ species are known. Even assuming that the C−H distances and the H−C−H bond angles are the same for the hydrogens on the CH_3 and CH_2F groups, the number of required parameters is only reduced to five. However, since the approximate rotational constants which were calculated initially to aid in the interpretation of the spectrum are not very different from the values finally obtained, it is reason-

[3] A sample was kindly supplied by Dr. R. C. McHarness, Jackson Laboratory, E. I. Du Pont de Nemours and Company.
[4] R. H. Hughes and E. B. Wilson, Jr., Phys. Rev. **71**, 562(L) (1947); A. H. Sharbaugh, Rev. Sci. Instr. **21**, 120 (1950).
[5] L. C. Hedrick, Rev. Sci. Instr. **24**, 565 (1953).
[6] King, Hainer, and Cross, J. Chem. Phys. **11**, 27 (1943).
[7] S. Golden and E. B. Wilson, Jr., J. Chem. Phys. **16**, 669 (1948).
[8] Cross, Hainer, and King, J. Chem. Phys. **12**, 210 (1944).

able to assume that the "true" parameters are close to the ones used to obtain the approximate rotational constants. An attempt to improve the fit was made by allowing only small variations in these parameters. The final values obtained are given in Table II. The values of the principal moments of inertia obtained from the structural parameters and those calculated from the spectroscopically determined rotational constants agree within the accuracy to which the structural parameters are given. More accurate calculation of the structural parameters is not warranted because of the limited data available. Furthermore, even if data on other isotopic species of ethyl fluoride were available, zero point vibrational effects would probably make it difficult to obtain the structural parameters more accurately.[9]

Table II also lists some additional data needed in the evaluation of the barrier height to the internal rotational motion. Two different coordinate systems have been used: an x, y, z system and an X, Y, Z system. In the former, the x and y axes are in the plane determined by the carbon and fluorine atoms, with the x axis directed along the C−C bond. The axes X, Y, Z are the principal axes of the molecule; the principal moments of inertia of the molecule, i.e., $I_A = I_X$, etc., lie along these axes. The orientation of the two systems with respect to one another is determined by the angle θ between the x and X axes (see Fig. 1); the $\lambda_{2i}^2 (i = X, Y, Z)$ are the squares of the direction cosines between the x axis and the i axes.

THE DIPOLE MOMENT

Quantitative Stark effect measurements were made on the $0_{00} \rightarrow 1_{01}$ and $1_{01} \rightarrow 2_{02}$ transitions in order to determine the dipole moment of the molecule. To calculate the Stark effect energies for an asymmetric rotor such as ethyl fluoride, it is necessary to evaluate the direction cosine matrices[8] in the representation in which the rigid rotor Hamiltonian is diagonal.[7] For the J values involved in the above transitions, it is possible to calculate the direction cosine matrices explicitly as a function of the asymmetry parameter (for higher values of J this is, in general, not possible, and they must be obtained numerically). From the symmetry of the molecule it was assumed that there was no component of the dipole moment along the Z axis.

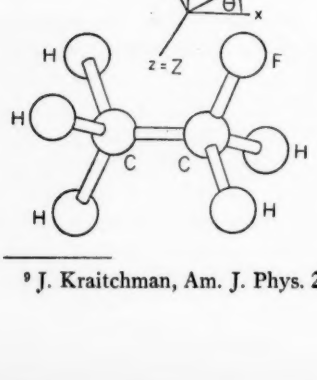

FIG. 1. The structure of ethyl fluoride.

[9] J. Kraitchman, Am. J. Phys. **21**, 17 (1953).

TABLE II. Structural parameters of CH_3CH_2F.[a]

r_{CH}	1.091
r_{CC}	1.540
r_{CF}	1.375
$\angle FCC = \angle HCH$	109°28′
I_{xx}	42.62
I_{yy}	70.25
I_{xy}	−30.18
$(I_x)_{CH_3} = I_2$	5.310
$I_A = I_X$	23.25 = 23.26[b]
$I_B = I_Y$	89.63 = 89.58
$I_C = I_Z$	102.3 = 102.3
θ	32°42′ (see Fig. 1)
$(\lambda_{2X})^2$	0.7081
$(\lambda_{2Y})^2$	0.2919

[a] The values $m_H = 1.0081$, $m_C = 12.0038$, $m_F = 19.0045$, $h = 6.62377 \times 10^{-27}$ erg sec, $c = 2.99790 \times 10^{10}$ cm/sec, and $N = 6.02544 \times 10^{23}$ molecules/mole were used in the calculations. All bond distances are in angstroms; all moments of inertia in 10^{-40} g cm^2.

[b] The first value is that obtained from the structural parameters, the second from the rotational constants used in analyzing the spectrum.

Since none of the states involved in the $0_{00} \rightarrow 1_{01}$ and $1_{01} \rightarrow 2_{02}$ transitions are degenerate or nearly degenerate with any other state with which they are connected by a nonzero dipole matrix element, the Stark effect energies can be calculated using nondegenerate second order perturbation theory.[7] This calculation gives the following results:

$$0_{00} \rightarrow 1_{01}\,(M=0): \Delta\nu/\mathcal{E}^2 = (0.7687\mu_A^2 + 1.0720\mu_B^2) \times 10^{-6}$$

$$1_{01} \rightarrow 2_{02}\,(M=0): \Delta\nu/\mathcal{E}^2 = (-2.1954\mu_A^2 + 2.4048\mu_B^2) \times 10^{-6}$$

$$1_{01} \rightarrow 2_{02}\,(M=1): \Delta\nu/\mathcal{E}^2 = (0.1786\mu_A^2 + 3.2854\mu_B^2) \times 10^{-6}$$

where $\Delta\nu$ is the difference in Mc between the undisplaced line at zero field and the Stark component at a field $\mathcal{E}$ in volts/cm; μ_A and μ_B are the components of the dipole moment in Debye units along the X and Y axes.

Measurements on ethyl fluoride were made at a number of different voltages. In agreement with theory, the Stark effect was found to be second order even at the largest fields used (over 2000 volts/cm). Average values of the quantity $\Delta\nu/\mathcal{E}^2$ are listed in Table III. A least squares analysis of the data gives: $\mu_A = 1.69D$, $\mu_B = 1.00D$, $\mu = 1.96 \pm 0.03D$. A value of $\mu = 1.92D$ has previously been obtained from measurement of the dielectric constant of ethyl fluoride in the vapor state.[10]

The total dipole moment μ makes an angle of approximately 31° with the X axis, or an angle of 64° with the C−C axis. Since the C−F bond axis makes an angle of 71° with the C−C axis, the total dipole moment is directed approximately 7° from the C−F bond axis. It is of interest to compare these results with the prediction obtained from the bond moment picture, in which the dipole moment is calculated from the vector sum of moments ascribed to the various bonds in the molecule.[11] Using a bond moment of $0.4D$ for the C−H bond and $1.5D$ for the C−F bond, a total moment of $1.9D$ directed along the C−F bond axis is obtained. While this

[10] C. P. Smyth and K. B. McAlpine, J. Chem. Phys. **2**, 499 (1934).

[11] L. Pauling, *The Nature of the Chemical Bond* (Cornell University Press, Ithaca, N. Y., 1939), pp. 67 *ff*.

very simple model fails to predict the observed 7° difference in the orientations of the total dipole moment and the C—F bond axis, this failure is not surprising. It should be recalled that this model does not take into account any of the changes in the charge distribution which effects such as polarization would produce in a complicated molecule like ethyl fluoride. In fact, in view of the simplicity of this model, its predictions are in surprisingly good agreement with the experimental results.

INTERNAL ROTATION

The treatment of the internal rotation problem in methyl alcohol by Koehler and Dennison,[12] as modified by Burkhard and Dennison,[13] is general enough to be applied to any molecule consisting of a rigid frame with an attached symmetric top, e.g., ethyl fluoride. Koehler and Dennison treat the case in which the entire molecule is a symmetric rotor and the hindering potential is a simple sinusoidal n-fold potential of the form

$$V=(V_0/2)(1-\cos nx). \tag{1}$$

They apply a transformation to the complete rotational Hamiltonian of the molecule which allows separation of the Hamiltonian into the usual rigid rotational part plus an internal rotational part.

The eigenvalues E^{Ktv} of the internal rotational part of the Hamiltonian are obtained from the eigenvalues R^{Ktv} of Mathieu's equation (subject to the proper boundary conditions):

$$\partial^2\mathfrak{M}(x)/\partial x^2+(R^{Ktv}+2\alpha\cos nx)\mathfrak{M}(x)=0, \tag{2}$$

where

$$R^{Ktv}=(2I_r/\hbar^2)(E^{Ktv}-V_0/2), \tag{3}$$

and

$$2\alpha=(2I_r/\hbar^2)(V_0/2). \tag{4}$$

V_0 is the barrier height, and I_r the reduced moment of inertia.

The wave functions which are solutions of Mathieu's equation can be written in the form

$$\mathfrak{M}(x)=e^{i\sigma x}P(x)=e^{i\sigma x}\sum_{m=-\infty}^{\infty}a_m e^{imx}. \tag{5}$$

The quantity σ is determined by the boundary conditions imposed on the solutions of Mathieu's equation.

TABLE III. Stark effect measurements.

Transition	$(\Delta\nu/\mathcal{E}^2)$ [Mc/(volts/cm)^2] Observed	Calculated
$0_{00}\rightarrow 1_{01}$ $(M=0)$	23.196×10^{-6}	22.905×10^{-6}
$1_{01}\rightarrow 2_{02}$ $(M=0)$	-3.849×10^{-6}	-3.860×10^{-6}
$1_{01}\rightarrow 2_{02}$ $(M=1)$	8.326×10^{-6}	8.374×10^{-6}

[12] J. S. Koehler and D. M. Dennison, Phys. Rev. **57**, 1006 (1940).

[13] D. G. Burkhard and D. M. Dennison, Phys. Rev. **84**, 408 (1951).

TABLE IV. Eigenvalues of Mathieu's equation for $\sigma=0$.

$R^{Ktv}\backslash\alpha$	49.50	54.00	57.36	57.98
R^{010} (A_1)	−78.47198712	−86.53268963	−92.57667709	−93.69412478
R^{020} (E)	−78.47198416	−86.53268825	−92.57667630	−93.69412407
R^{021} (E)	−38.6492934	−44.8258090	−49.5141014	−50.3858077
R^{011} (A_2)	−38.64910223	−44.82571561	−49.51404581	−50.38575712

By substituting these wave functions into Mathieu's equation, a secular equation is obtained, the roots being the eigenvalues R^{Ktv}. For the particular case $n=3$, the secular determinant can be factored into three subdeterminants with values of $m=\pm 3s$, $1\pm 3s$, or $2\pm 3s$, where $s=0, 1, 2, \cdots$. The eigenvalues of the first subdeterminant $(m=\pm 3s)$ are labeled $t=1$, the second $t=3$, and the third $t=2$. The eigenvalues are most commonly obtained by use of continued fractions (see Appendix).

The eigenvalues R^{Ktv} as a function of α are listed for a few selected values of α in Table IV, for $\sigma=0$ and $n=3$.[14] The symmetry of the internal rotational wave functions which characterizes these states is also given. (The eigenvalues R^{03v} are the same as the R^{02v}.)

When the entire molecule is a symmetric rotor the overall rotational energy of a particular state is simply the sum of the rigid rotational eigenvalue and the internal rotational eigenvalue. The selection rules in this case are: $J\rightarrow J$, $J\rightarrow J\pm 1$; $K\rightarrow K$ with $t\rightarrow t$; and $K\rightarrow K\pm 1$ with $t\rightarrow t\mp 1$ (t being cyclic). These selection rules are somewhat modified for the asymmetric rotor. However, the symmetric rotor selection rules will generally correspond to the transitions which are most intense for the asymmetric rotor. This is particularly true if the molecule is only slightly asymmetric, e.g., ethyl fluoride.

Not only are the selection rules modified when the entire molecule is an asymmetric rotor, but the transformation employed by Koehler and Dennison no longer allows a complete separation of the rigid and internal rotations.[13] This makes the application of this method extremely difficult. Another treatment of the problem has been given by Pitzer and Gwinn.[15] While for the general case their method is probably even more difficult to apply, it appears to offer certain simplifications for molecules with sufficiently high barriers.

Pitzer and Gwinn apply a transformation to the complete rotational Hamiltonian which allows separation into a rigid rotational part and an internal rotational part, even if the entire molecule is an asymmetric rotor. However, this advantage is in large measure offset by the difficulty in determining the boundary conditions on the solutions of the internal rotational part. Aside from the difference in the boundary conditions, the wave equation Pitzer and Gwinn obtain, for internal rotation

[14] The eigenvalues of the A levels can be obtained to ten figures from *Tables Relating to Mathieu Functions* (Columbia University Press, New York, 1951), for values of $\alpha\leqslant 56.25$. An extensive bibliography relating to Mathieu's equation is given by W. G. Bickley, Mathematical Tables and Other Aids to Computation **1**, 409 (1945); **2**, 1 (1946).

[15] K. S. Pitzer and W. D. Gwinn, J. Chem. Phys. **10**, 428 (1942).

is identical with that given in Eq. (2). Their reduced moment of inertia is defined as

$$I_r = I_2(1 - I_2 \sum \lambda_{2i}^2/I_i), \quad i = X, Y, Z, \qquad (6)$$

where the λ_{2i} are the direction cosines between the unique axis of the attached symmetric top and the principal moments of inertia I_i; I_2 is the moment of inertia of the attached symmetric top about its unique axis. (If the entire molecule is a symmetric rotor this expression should and does reduce to the form used by Koehler and Dennison.)

While the determination of the boundary conditions is a very complex problem when the treatment of Pitzer and Gwinn is used, for the state $J=0$, $K=0$ this difficulty does not arise. For this state, the solution with $\sigma=0$ is the proper one, and the internal rotational energy is just the E^{0tv} obtained from the eigenvalue R^{0tv} of Mathieu's equation. Furthermore, when the barrier is quite high, E^{0tv} will also be a very good approximation to the internal rotational energy when J and K are not zero. In fact, in this case the energies of the internal rotational levels will be practically independent of t, so that it becomes proper to speak of a torsional frequency. When the barrier is high, but not high enough to use the parabolic approximation to the sinusoidal barrier, the torsional frequency is defined by

$$\nu_T = (E^{Ktv+1} - E^{Ktv})/h. \qquad (7)$$

While the torsional frequency is not observable in the microwave region, its magnitude can be determined from intensity measurements. In general, not only will a rotational transition be observed for molecules which are in the ground vibrational state, but the same rotational transition will be observed for molecules which are in an excited vibrational state. The relative intensity of the transitions depends upon the difference in the energies of the vibrational states; these vibrational energy differences can in turn be used to compute vibrational frequencies.

Intensity measurements were made on two satellite lines of the $0_{00} \rightarrow 1_{01}$ and $1_{01} \rightarrow 2_{02}$ transitions at room temperature (Table V). The spacing of the lines in the $1_{01} \rightarrow 2_{02}$ transition is approximately twice that in the $0_{00} \rightarrow 1_{01}$ transition. This behavior is to be expected if the satellite lines are the corresponding rotational transitions in excited vibrational states. Furthermore, the Stark effect of the satellite lines is qualitatively similar to that of the ground state line. These data permit unambiguous identification of the satellite lines as rotational transitions in excited vibrational states of ethyl fluoride, since any other chemical species present as a sample impurity would not give rise to lines with this behavior. From the intensity ratio of satellite I and the ground state line, a vibrational frequency of 440 ± 80 cm^{-1} is obtained; the intensity ratio of satellite II and the ground state line gives 300 ± 40 cm^{-1}. The former is in satisfactory agreement with the reported infrared frequency of the A' fundamental at 415 cm^{-1}; the latter with a frequency of 278 cm^{-1} obtained from the Raman spectrum.[1] This Raman frequency was tentatively assigned to the torsional fundamental, but its assignment was contingent upon sample purity since the presence of this band in the Raman spectrum could be due to impurities in the sample. If satellite I is assigned to the rotational transition in the first excited vibrational state of the A' fundamental at 415 cm^{-1}, and the torsional frequency is evaluated from the most accurately known intensity ratio, i.e., the ratio of the intensities of satellites I and II, a frequency of 270 cm^{-1} is obtained. This value is not contingent upon sample purity and is in excellent agreement with the more accurate Raman value.

TABLE V. Intensity measurements.

Transition	Frequency (Mc)	Intensity[a]
$0_{00} \rightarrow 1_{01}$, ground state	17 564	1.0
satellite I	17 549	0.1
satellite II	17 530	0.2
$1_{01} \rightarrow 2_{02}$, ground state	35 091	1.00
satellite I	35 060	0.12
satellite II	35 024	0.24

[a] Relative intensity measurements with respect to ground state.

TABLE VI. Barrier height as a function of the torsional frequency.

α	ν_T (cm^{-1})	ν' (Mc)	ν'' (Mc)	V_0 (cm^{-1})
49.50	256	0.57	36.80	1271
54.00	268	0.27	17.55	1387
57.36	276	0.15	10.78	1473
57.98	278	0.14	9.74	1489

From the data given in Table II, the reduced moment of inertia calculated using Eq. (6) is 4.359×10^{-40} g cm^2. Using this value, the barrier height has been evaluated for a number of different torsional frequencies. The results are listed in Table VI. (The eigenvalues of Mathieu's equation required for these calculations were taken from the data given in Table IV.) In Table VI, ν' is the frequency difference between the two t states for $K=0$ and $v=0$; ν'' is the same for $v=1$.

For a torsional frequency of 278 cm^{-1}, the barrier height is 1490 ± 50 cm^{-1} (4260 ± 150 cal/mole). At this barrier height the splitting of the t levels for a given K (as estimated from ν') is of the order of 0.1 Mc in the ground state. This splitting manifests itself in the appearance of the $K \rightarrow K \pm 1$ rotational transitions, since in these transitions a change in t of $t \rightarrow t \mp 1$ occurs. Transitions of this type, which would appear as a single line in the absence of internal rotation (infinitely high barrier), are split into a number of closely spaced lines. While accurate computation of the separation of these closely spaced lines is rather difficult, a good estimate of

the overall spacing of the lines can be obtained from the splitting of the t levels.

In the ground vibrational state no splitting of the $K \rightarrow K \pm 1$ transitions was observed. This is not surprising since the expected splitting of about 0.1 Mc is less than the observed line widths of these transitions. In fact, this provides confirmatory evidence that the barrier height calculated for ethyl fluoride is of the correct order of magnitude.

Not only is this splitting too small to be observed, but its magnitude is of the same order as the experimental error in the frequency measurements. Consequently, within the precision of measurement, the observed rotational spectrum in the ground vibrational state approximates the spectrum that would be expected if the barrier to internal rotation were infinitely high. These arguments are not restricted to ethyl fluoride, but would apply to other asymmetric rotors with sufficiently high barriers to internal rotation. In general, when no splitting of the $K \rightarrow K \pm 1$ transitions is observed in the ground vibrational state, it should be possible to analyze the rotational spectrum in the ground state by the procedure used here of completely disregarding the internal rotation.

On the other hand, the splitting of the t levels for a given K (as estimated from ν'') is of the order of 10 Mc in the first excited torsional state. Consequently, it would be expected that the rotational transitions $K \rightarrow K \pm 1$ in this excited state should appear as a number of closely spaced lines with an over-all separation of approximately 10 Mc. Closely spaced lines with approximately this separation have been observed as satellites of a number of the stronger ground state $K \rightarrow K \pm 1$ transitions and presumably can be attributed to $K \rightarrow K \pm 1$ transitions occuring for molecules which are in the first excited torsional state.

It is of interest to compare the barrier of 1490 cm^{-1} obtained for CH_3CH_2F with the barriers of the related molecules CH_3CH_3, CH_3CHF_2, and CH_3CF_3. In addition to the spectroscopic determination of the torsional frequencies, the barriers of some of these molecules have been estimated from thermodynamic data.

In comparing these barrier heights, the actual method of evaluation of the barrier height must be considered. Some investigators have evaluated their data using the parabolic approximation to a sinusoidal barrier. Even for the high barriers predicted for the fluorosubstituted ethanes, this method gives barriers more than 100 cm^{-1} lower than those obtained using the exact solution of Mathieu's equation.

Another important consideration is the actual shape of the barrier. If detailed experimental information on the energies of a large number of the excited torsional states were available, it would probably be possible to compute the actual shape of the barrier to internal rotation. Since such information is not available, barrier heights have generally been calculated assuming a simple sinusoidal shape. However, as Blade and Kimball[16] have pointed out, the value of the barrier height calculated from the experimental data is very sensitive to the shape of the barrier assumed. Since the limited experimental data available allow considerable freedom in the choice of the barrier shape, a rather large range of barrier heights consistent with this data can be obtained.

TABLE VII. Barrier heights in fluorosubstituted ethanes.

Molecule	V_0 (cm^{-1})	V_0 (cal/mole)	Reference
CH_3CH_3	1100±150	3100±450	a
CH_3CH_2F	1490± 50	4260±150	b
CH_3CHF_2	1300±200	3700±600	c
CH_3CF_3	1300±150	3700±450	d

[a] D. C. Smith, J. Chem. Phys. **17**, 139 (1949).
[b] This paper; Smith, Saunders, Nielsen, and Ferguson, J. Chem. Phys. **20**, 847 (1952).
[c] N. Solimene, Columbia University (private communication). Calculated using the value $\nu_T = 235 \pm 40$ cm^{-1} obtained from microwave intensity data.
[d] Nielsen, Classen, and Smith, J. Chem. Phys. **18**, 1471 (1950); H. T. Minden and B. P. Dailey, Phys. Rev. **82**, 338(A) (1951).

Values of the barrier heights for the fluorosubstituted ethanes, calculated assuming a sinusoidal barrier shape, are given in Table VII along with what appear to be reasonable estimates of their precision. The barrier for CH_3CH_2F is considered the most precise chiefly because its torsional frequency has been observed directly in the Raman spectrum and confirmed by this microwave study. Aside from the lower value obtained for ethane, the other values are not significantly different within the precision to which they are known, nor does the trend indicate any particular regularity. However, it is important to remember that the barrier shape has been assumed to be identical in all of these molecules. Hence, while it is quite reasonable to conclude that the barrier heights are all of the same order of magnitude, any small variation might easily be masked by this assumption of identical barrier shape.

In conclusion, it can be said that while the experimental data available at present permit a reasonable estimate of barrier heights, they do not provide sufficient information to determine the small differences between these molecules. On the other hand, there can be no question that the difference between the high barrier heights for these molecules and the low barrier height for a molecule such as methyl alcohol[13] ($V_0 = 380$ cm^{-1}) is real.

APPENDIX. NUMERICAL EVALUATION OF THE EIGENVALUES OF MATHIEU'S EQUATION

The eigenvalues of Mathieu's equation are most conveniently evaluated by use of continued fractions. One such form has been given by Koehler and Dennison.[12] However, their form is best for the lowest eigenvalue, and is not applicable to the A_2 levels with $\sigma = 0$. A more general form (the labeling Ktv of the eigenvalue

[16] E. Blade and G. E. Kimball, J. Chem. Phys. **18**, 630 (1950).

R^{Ktv} is omitted for brevity) is

$$R-(\sigma+m)^2-\cfrac{\alpha^2}{R-(\sigma+m-3)^2-\cfrac{\alpha^2}{R-(\sigma+m-6)^2-\cdots}}-\cfrac{\alpha^2}{R-(\sigma+m+3)^2-\cfrac{\alpha^2}{R-(\sigma+m+6)^2-\cdots}}=0. \quad (8)$$

For $\sigma=0$ this form is not correct for the A_2 levels since the coefficient a_0 in the solution of Mathieu's equation becomes zero. Instead

$$R-m^2-\cfrac{\alpha^2}{R-(m-3)^2-\cfrac{\alpha^2}{R-(m-6)^2\cdots-\cfrac{\alpha^2}{R-6^2-\cfrac{\alpha^2}{R-3^2}}}}-\cfrac{\alpha^2}{R-(m+3)^2-\cfrac{\alpha^2}{R-(m+6)^2-\cdots}}=0. \quad (9)$$

Since $a_0=0$, m must not be set equal to zero in Eq. (9). For $m=3$, the first continued fraction in Eq. (9) vanishes; for $m=6$, the first continued fraction reduces to $-\alpha^2/[R-3^2]$, etc.

The general form of Eq. (8) can be simplified somewhat for the A_1 levels with $\sigma=0$. For $m=0$, Eq. (8) becomes

$$R-\cfrac{2\alpha^2}{R-3^2-\cfrac{\alpha^2}{R-6^2-\cdots}}=0, \quad (10)$$

and for $m=3$,

$$R-3^2-\cfrac{2\alpha^2}{R}-\cfrac{\alpha^2}{R-6^2-\cfrac{\alpha^2}{R-9^2-\cdots}}=0. \quad (11)$$

For higher values of m, the eigenvalues can be evaluated from the expression

$$R-m^2-\cfrac{\alpha^2}{R-(m-3)^2-\cfrac{\alpha^2}{R-(m-6)^2\cdots-\cfrac{\alpha^2}{R-3^2-\cfrac{2\alpha^2}{R}}}}-\cfrac{\alpha^2}{R-(m+3)^2-\cfrac{\alpha^2}{R-(m+6)^2-\cdots}}=0. \quad (12)$$

Usually the best convergence is obtained if m is chosen so that $(\sigma+m)^2$ is as nearly equal to R as possible.

The coefficients a_m of the wave functions $\mathfrak{M}(x)$ can also be evaluated using continued fractions:

$$a_m=-\cfrac{\alpha}{R-(\sigma+m)^2-\cfrac{\alpha^2}{R-(\sigma+m+3)^2-\cdots}}a_{m-3} \quad (13)$$

and

$$a_m=-\cfrac{\alpha}{R-(\sigma+m)^2-\cfrac{\alpha^2}{R-(\sigma+m-3)^2-\cdots}}a_{m+3}. \quad (14)$$

For $\sigma=0$, the coefficients $a_{3m}=a_{-3m}$ for all the A levels, and a_0 is zero for the A_2 levels.

Sedimentation Velocity and Diffusion of a Solvated Substance*

PING-YAO CHENG†
Department of Biochemistry and The Virus Laboratory, University of California, Berkeley, California
(Received January 12, 1954)

Based on the contention that the driving force for the motion of a species relative to the mass flow in a particular direction is the negative gradient of total potential of that species in that direction, equations for both the sedimentation velocity and the diffusion of a solvated substance are derived. They are reduced to the usual expressions for a nonsolvated substance. The partial specific volume term in the equations of sedimentation velocity is shown to have theoretical justification. The advantages of expressing the sedimentation velocity in terms of solvated species are discussed. It is also shown that for the diffusion of a solvated species the "thermodynamic factor" calculated in the usual way is always greater than the gradient of chemical potential of the solvated species, except at zero concentration, by a previously neglected term arising from solvation. The effect of solvation on diffusion coefficient and on the relation between the frictional coefficients in the sedimentation and diffusion are also discussed in the light of this theory.

IN dealing with sedimentation velocity and diffusion in liquid solution the apparent motion of a species can be, as in the treatment of gaseous mutual diffusion, regarded as a resultant of two components: mass-flow of the whole solution and the motion of the species relative to the mass-flow. The mass-flow is due to the fact that the net transport of the volumes associated with the relative motion of all species in the solution is, in general, not zero. The net volume transport and the mass-flow are equal and opposite. In case the solution is contained in a cylinder of uniform cross section and the motion is in the direction of axis of the cylinder, x, this concept can be formulated as follows:

$$\left(\frac{dx}{dt}\right)_i^* = \left(\frac{dx}{dt}\right)_i - \sum_{i=1}^{n} \left(\frac{dx}{dt}\right)_i c_i G_i,$$

where $(dx/dt)_i^*$, $(dx/dt)_i$, c_i, and G_i are the apparent velocity, relative velocity, concentration (number of moles per unit volume of solution), and hydrodynamic volume (volume per mole) of species i at the same position, and n is the number of species present. To deal with the effect of solvation the present treatment will be confined to the relative motion. The problem of mass-flow will be considered in a later communication.

The driving force for the relative motion of a species in a particular direction is the negative gradient of total potential of that species in that direction. Thus

$$-\frac{dV}{dx} = -\frac{d(\mu + M\phi_c + e\phi_e)}{dx} = f\frac{dx}{dt}, \tag{1}$$

in which d/dx is the gradient in the x direction, V, μ, M, e, f, and dx/dt are the total potential, chemical potential, molecular weight, electrical charge, frictional coefficient, and relative velocity of the species, respectively, and ϕ_c and ϕ_e are the centrifugal and electrical potentials. All quantities, except M and e, are functions of the position x, and strictly speaking must be referred to a same plane $x=x$ in the ultracentrifuge or diffusion cell in applying the equation. In case the gradient of gravitational potential ϕ_g is not negligible a corresponding term $M\phi_g$ has to be added to the expression for V. As a matter of fact, the gradient of electrical potential is either zero or is sufficiently suppressed by the addition of salt in every experiment of sedimentation or diffusion, except diffusion of simple electrolytes which has been elegantly treated by Onsager and Fuoss.[1] Hence the electrical force will not concern us here. It should also be noted that μ is at present interpreted in terms of species rather than substance as is usually the case in the treatment of diffusion problem. And when the substance is solvated, μ as well as other quantities in Eq. (1) refers to the solvated species. Furthermore, Eq. (1) applies to each form of the substance when it exists in more than one form.

SEDIMENTATION VELOCITY OF A SOLVATED SPECIES

Accordingly, the motion of a solvated species m relative to the mass-flow in an ultracentrifuge cell can be described as follows:

$$\frac{d\mu_m}{dx} + M_m\frac{d\phi_c}{dx} = -f_{m,s}\left(\frac{dx}{dt}\right)_m, \tag{2}$$

where subscripts m and s refer to species m and sedimentation, respectively. To describe the motion of the species being subjected to centrifugal force alone, it is simpler and sufficient to consider the species in the solution where the concentration gradient of any component is zero (plateau region). Besides, the temperature is uniform throughout the cell. Hence, Eq. (2) becomes

$$\left(\frac{\delta\mu_m}{\delta P}\right)_{T,c}\frac{dP}{dx} + M_m\frac{d\phi_c}{dx} = -f_{m,s}\left(\frac{dx}{dt}\right)_m, \tag{3}$$

* The investigation was supported by the Corn Industries Research Foundation.
† Present address: Kerckhoff Laboratories of Biology, California Institute of Technology, Pasadena, California.

[1] L. Onsager and R. M. Fuoss, J. Phys. Chem. **36**, 2689 (1932).

in which P is the pressure, T the temperature, and c the concentration of any component. Now,

$$\begin{aligned}(\partial\mu_m/\partial P)_{T,c}&=M_m\bar{v}_m,\\ dP/dx&=\omega^2x\rho,\\ d\phi_c/dx&=-\omega^2x,\end{aligned}\tag{4}$$

where $\bar{v}$ is the partial specific volume, ω the angular velocity of the rotor, x the distance from the axis of rotation, and ρ the solution density at x. Coupled with Eqs. (4), Eq. (3) leads to the following relation

$$M_m(1-\bar{v}_m\rho)=f_{m,s}s_m,\tag{5}$$

where s_m is the sedimentation coefficient $(dx/dt)_m/x\omega^2$. Equation (5) is true regardless of the number of components of the system and of the solvation state of m. M_m and $\bar{v}_m$ are simply related to the molecular weights and partial specific volumes of the component substances. For example, if the solvent is of q components and r_i moles of solvent component B^i are bound to each mole of macromolecule A, we may write

$$M_m=M_A+\sum_{i=1}^{q}r_iM_i$$

and (6)

$$(M_A+\sum_{i=1}^{q}r_iM_i)\bar{v}_m=M_A\bar{v}_A+\sum_{i=1}^{q}r_iM_i\bar{v}_i.$$

The solvent components of the system usually have negligible sedimentation velocities in comparison with the macromolecule. Hence, at infinite dilution in the macromolecules, mass-flow practically vanishes, and the difference between the s_m and the apparent sedimentation coefficient, $s_m{}^*$, disappears. Equation (5) is then identical to that of Wales and Williams for the sedimentation coefficient at infinite dilution of a binary system,[2] and is comparable with that of Schachman and Lauffer,[3] although the latter two equations were derived in two radically different ways from the present treatment.

For nonsolvated species, Eq. (5) becomes the Svedberg equation[4]

$$M_A(1-\bar{v}_A\rho)=f_{A,s}s.\tag{7}$$

However, the present derivation is free from the substitution of reciprocal density of the macromolecule for $\bar{v}_A$, and hence, seems subject to less theoretical objection.

Recently Goldberg[5] formulated s relative to the velocity of the local center of mass of the solution, v_0, and stated: "Any interactions which may occur as a result of intermolecular forces can be absorbed by the friction coefficient in a manner analogous to that in which the excess chemical potential absorbs nonideal effects. We have considerable freedom, therefore, in choosing our components and may choose them irrespective of solvation . . . ." Since v_0 will remain the same no matter how we define our components, Goldberg's statement implies that the equation

$$s_m=\frac{1}{f'}M_A(1-\bar{v}_A\rho)\tag{8}$$

and Eq. (5) are equivalent for solvated species m, and

$$f'=f_{m,s}\frac{M_A(1-\bar{v}_A\rho)}{M_m(1-\bar{v}_m\rho)}.$$

However, it will become apparent soon that it is advantageous to use Eq. (5) except for binary system at infinite dilution. From Eq. (6) we have

$$M_m(1-\bar{v}_m\rho)=M_A(1-\bar{v}_A\rho)+\sum_{i=1}^{q}r_iM_i(1-\bar{v}_i\rho).$$

It is seen that at, and only at, the infinite dilution of a macromolecule substance in a single solvent we may expect

$$M_A(1-\bar{v}_A\rho)\cong M_m(1-\bar{v}_m\rho),$$

and hence (9)

$$f'\cong f_{m,s}.$$

In a mixed solvent system Eqs. (9) are, in general, not true even at infinite dilution.[6] Equation (8) is then not useful and can be misleading. $f_{m,s}$ at infinite dilution is related to the dimensions of the sedimenting molecule (rigorously speaking, dimensions of its equivalent hydrodynamic model), and, as a matter of fact, being able to give information concerning the dimensions of the molecule constitutes an advantage of all the dynamic methods over most equilibrium methods. The fact that f' fails to reduce to $f_{m,s}$ or $f_{A,s}$ should be considered as a drawback of using Eq. (8). Besides, Eq. (5) does suggest that zero sedimentation can be, in principle, an experimental approach to evaluate $\bar{v}_m$ and the approach has already been widely adopted.[7–14] On the other hand, the use of Eq. (8) might give the wrong impression that the sedimenting force is $M_A(1-\bar{v}_A\rho)x\omega^2$.

[2] M. Wales and J. W. Williams, J. Polymer Sci. **8**, 449 (1952).
[3] H. K. Schachman and M. A. Lauffer, J. Am. Chem. Soc. **72**, 4266 (1950).
[4] T. Svedberg and K. O. Pedersen, *The Ultracentrifuge* (The Clarendon Press, Oxford, 1940), p. 5.
[5] R. J. Goldberg, J. Phys. Chem. **57**, 194 (1953).
[6] See W. D. Lansing and E. O. Kraemer, J. Am. Chem. Soc. **58**, 1471 (1938); see also reference 3.
[7] J. W. McBain, J. Am. Chem. Soc. **58**, 315 (1936).
[8] Smadel, Pickels, and Shedlovsky, J. Exptl. Med. **68**, 607 (1938).
[9] Sharp, Beard, and Beard, J. Biol. Chem. **182**, 279 (1950).
[10] D. G. Sharp and J. W. Beard, J. Biol. Chem. **185**, 247 (1950).
[11] H. K. Schachman and M. A. Lauffer, J. Am. Chem. Soc. **71**, 536 (1949).
[12] Lauffer, Taylor, and Wunder, Arch. Biochem. Biophys. **40**, 453 (1952).
[13] M. A. Lauffer and N. W. Taylor, Arch. Biochem. Biophys. **42**, 102 (1953).
[14] P. Y. Cheng, Ph.D. thesis, University of California, 1952, p. 36.

DIFFUSION OF A SOLVATED SUBSTANCE

Consider a solution consisting of substances A and B, and A exists in solution as species AB_r (drop the superscript 1 and subscript 1 for B and r, respectively, for simplicity) where $r=0, 1, \cdots, n$. The following equilibria exist:

$$AB_{r-1}+B \rightleftarrows AB_r; \quad r=1, \cdots, n. \tag{10}$$

The diffusion of substance A is the sum of diffusion of all the A-containing species, $A\cdots AB_n$. The number of moles of *substance* A passing per unit time across a plane of unit area moving with the mass-flow is

$$\frac{dn_A}{dt}=\sum_{r=0}^{n} c_r\frac{dx_r}{dt}=-\sum_{r=0}^{n}\frac{c_r}{f_{r,D}}\frac{d\mu_r}{dx}, \tag{11}$$

where Eq. (1) has been applied. In Eq. (11) c is the concentration expressed in terms of number of moles of A contained in unit volume of solution, subscripts r and D denote species AB_r and diffusion, respectively. On account of the existing equilibria (10), we have

$$c_r=F_r(c_A),$$

where c_A is the concentration of *substance* A. Equation (11) can, therefore, be further transformed into the following equation:

$$\frac{dn_A}{dt}=-\frac{dc_A}{dx}\sum_{r=0}^{n}\frac{c_r}{f_{r,D}}\frac{d\mu_r}{dc_A}.$$

Hence, the true diffusion coefficient, D, of a solvated substance which may exist in more than one form can be given by the general equation

$$D=\sum_{r=0}^{n}\frac{c_r}{f_{r,D}}\frac{d\mu_r}{dc_A}, \tag{12}$$

where D is defined as follows:

$$dn_A/dt=-D(dc_A/dx).$$

No restriction concerning the nature, relative molecular size and concentration has been imposed on A and B in the foregoing derivation. Since, in most cases, solvation results in an increase in the molecular size and, hence, in the frictional coefficient, Eq. (12), therefore, implies that the observed diffusion coefficient of a solvated substance is, in general, smaller than that which would be expected assuming that all of the substance exists only in an anhydrous form. This solvation effect will be greatly magnified in the case that B has a much larger molecular size than A. An example is diffusion in a colloidal medium which has been considered by Reiner.[15] It should be pointed out in passing that Eq. (12) without modification can be also applied to the diffusion of an associated substance.[16] This can be easily seen by merely replacing B with A and AB_{r-1} with A_r in the preceding paragraph.

Consider now a system of A and B, in which substance A has concentration c_A and substance B concentration c_B. Suppose substance A in solution exists only in the form AB_h and thus equilibrium between A and AB_h does not exist. The concentrations of species AB_h and B are then c_A and (c_B-hc_A), respectively, remembering that the concentrations are expressed in number of moles per volume of solution. Equation (12) now becomes

$$D=\frac{1}{f_{h,D}}\frac{d\mu_h}{d\ln c_A}. \tag{13}$$

The question hereby arises as to how the quantity $d\mu_h/d\ln c_A$ is related to the "thermodynamic factor" $d\mu_A/d\ln c_A$ which is usually calculated from the corresponding quantity of the solvent $d\mu_B/d\ln c_A$ through the Gibbs-Duhem equation. $d\mu_B/d\ln c_A$ is determined by measuring a colligative property of the system as a function of concentration. Let $\gamma_B{}^*$ denote the deviation of the behavior of *species* B from ideality, then the chemical potential of the solvent can be described

$$\mu_B=\mu_B{}^0+RT\ln(c_B-hc_A)\gamma_B{}^*,$$

where $\mu_B{}^0$ is the chemical potential of B at standard state, R the gas constant, and T the absolute temperature. However, the solvation number, h, is, in general, thermodynamically indeterminate, and, in practice, the knowledge of the solvation is avoided through the conventional activity coefficient, γ_B,[17]

$$\mu_B=\mu_B{}^0+RT\ln c_B\gamma_B.$$

μ_B is related to μ_A by the Gibbs-Duhem equation

$$c_A d\mu_A+c_B d\mu_B=0. \tag{14}$$

Now, if the Gibbs-Duhem equation is applied in terms of species, we have

$$c_A d\mu_h+(c_B-hc_A)d\mu_B=0. \tag{15}$$

Eliminating $d\mu_B$ from Eqs. (14) and (15), the equation

$$d\mu_h=\left(1-h\frac{c_A}{c_B}\right)d\mu_A \tag{16}$$

is obtained. Therefore, the thermodynamic factor so calculated is not equal to, but is always greater than $d\mu_h/d\ln c_A$ except at zero concentration, and it is the latter quantity which has to be used in the expression for diffusion coefficient, according to the present treatment.

Substituting the value $d\mu_h$ in Eq. (16) into Eq. (13), we have finally

$$D=\frac{1}{f_{h,D}}\frac{d\mu_A}{d\ln c_A}\left(1-h\frac{c_A}{c_B}\right). \tag{17}$$

[15] J. M. Reiner, Bull. Meth. Biophys. **1**, 143 (1939).
[16] See O. Lamm, J. Phys. Chem. **51**, 1063 (1947).
[17] G. N. Lewis and M. Randall, *Thermodynamics* (McGraw-Hill Book Company, Inc., New York), 1923.

Hence, it is concluded that if the expression

$$D=\frac{1}{f_D}\frac{d\mu_A}{d\ \ln c_A}$$

similar to that for nonsolvated substance is used, f_D here does not imply the commonly adopted meaning of $f_{h,D}$, i.e., the force required to produce unit relative velocity of species AB_h. However, the difference between f_D and $f_{h,D}$ vanishes at infinite dilution. The present conclusion does not, therefore, affect the validity of those procedures which are based on the diffusion coefficient at infinite dilution, e.g., the evaluation of dimensions of solvated macromolecules.

When $h=0$, Eq. (17) is reduced to the equation for the nonsolvated substance

$$D=\frac{1}{f_{A,D}}\frac{d\mu_A}{d\ \ln c_A}$$

as it should.

An interesting feature of Eq. (17) is that when the composition of the system is such that the ratio of c_B to c_A equals the solvation number, h, then $D=0$. This would mean that the system becomes a one-component system of AB_h, and hence no relative motion between components can occur. The apparent diffusion coefficient, D^*, will then also be expected to be zero. This conclusion may have practical significance for the evaluation of solvation. However, one is aware that h may vary with the concentration in certain cases and that the situation might even be further complicated through the existence of the substance in more than one form.

When h is a constant, $(1-hc_A/c_B)$ is a decreasing function of c_A and constitutes an additional factor responsible for the decrease of $D/d\mu_A/d\ \ln c_A$, and hence, $D^*/d\mu_A/d\ \ln c_A$ with increasing c_A. As the tendency for solvation increases with increasing polarity, it seems suggestive to test Eq. (17) with experimental results of diffusion of polar systems. Unfortunately this cannot be done in the absence of a complete theory for diffusion of a polar substance. According to Eyring's kinetic theory of liquid, $D^*\eta/d\mu_A/d\ \ln c_A$ is a linear function of concentration, provided that the activation energy for the diffusion is the same as that for viscous flow where η is the solution viscosity.[18,19] Although the linear relationship holds for the nonpolar liquids tested,[19,20] it fails in all the polar systems which have so far been properly investigated up to high concentration.[20,21] Indeed, little beyond the thermodynamic term is known about the diffusion of a polar system. Nevertheless, it seems certain that $[1-h(c_A/c_B)]$ cannot be regarded as a part of the viscosity term. The factor is important in the diffusion of a polar substance at high concentration, and it can be detected experimentally down to probably fairly low concentration owing to the great improvement in the accuracy of diffusion measurements recently achieved.

The preceding conclusion has a corollary with regard to the problem of the concentration dependence of sedimentation coefficient. In the past much attention has been directed to the identity between the frictional coefficients in sedimentation and in diffusion. It is seen from above that $f_{m,s}$, unlike f_D, does have the exact meaning of the force required to produce unit relative velocity of the solvated species. If the force required in sedimentation is equal to that in the diffusion in the same medium at the same temperature, i.e., $f_{m,s}=f_{h,D}$, then upon using the definition for μ_A, Eqs. (5) and (17) lead to that

$$f_{m,s}/f_D'=(1+d\ \ln\gamma_A/d\ \ln c_A)(1-hc_A/c_B) \quad (18)$$

and

$$s=M_m(1-\bar{v}_m\rho)D/RT\left(1+\frac{d\ \ln\gamma_A}{d\ \ln c_A}\right)\left(1-h\frac{c_A}{c_B}\right), \quad (19)$$

where, for the convenience of further discussion, f_D', which is defined according to the following equation

$$D=RT/f_D',$$

has been introduced. When the substance is nonsolvated and if D, s, $f_{m,s}$, and f_D' are set to their corresponding apparent quantities, D^*, s^*, f_s^*, and f_D^*, Eqs. (18) and (19) are identical with the equations of Beckmann and Rosenberg.[22]

[18] H. Eyring, J. Chem. Phys. 4, 283 (1936).
[19] Powell, Roseveare, and Eyring, Ind. Eng. Chem. 33, 430 (1941).
[20] Kincaid, Eyring, and Stearn, Chem. Rev. 28, 301 (1941).
[21] A. C. English and M. Dole, J. Am. Chem. Soc. 72, 3261 (1950).
[22] C. O. Beckmann and J. L. Rosenberg, Ann. N. Y. Acad. Sci. 46, 329 (1945).

Hydrogen Overvoltage and Electrode Material. A Theoretical Analysis

PAUL RÜETSCHI* AND PAUL DELAHAY
Department of Chemistry, Louisiana State University, Baton Rouge 3, Louisiana
(Received June 28, 1954)

It is shown on a theoretical basis that the overvoltage for hydrogen evolution on various metals and for otherwise identical conditions of electrolysis is essentially a linear function of the heat of adsorption of atomic hydrogen on the electrode. This relationship is deduced on the assumptions that the effect of the backward electrode reaction—the oxidation of hydrogen—can be neglected, and that the current is controlled by the discharge of hydrogen ions. This is the case for overvoltages larger than 0.1–0.15 volt. The relationship between overvoltage and heat of adsorption is tested for metals for which reliable overvoltage data are available, that is for Ag, Be, Cd, Cr, Cu, Fe, Ga, Hg, In, Ni, Pb, Tl. The argument is based on a kinetic equation for hydrogen overvoltage and on the use of potential energy curves for the initial and final states. These curves are determined from spectroscopic data. Heats of adsorption of atomic hydrogen are calculated by assuming the additivity of the M—M and H—H bond energies. Calculated heats of adsorption are listed for 25 metals. It is also shown that there is no correlation between hydrogen overvoltage for various metals and the electronic work function of these metals.

ALTHOUGH the quantitative interpretation of hydrogen overvoltage is rather well advanced,[1] the dependence of overvoltage on the characteristics of the electrode material has not yet been accounted for on a theoretical basis. Bonhoeffer[2] pointed out many years ago that the hydrogen overvoltage for given conditions of electrolysis decreases as the catalytic action of the metal on the recombination of hydrogen atoms increases. More recently, Bockris[3] and Potter[4] attempted to correlate overvoltage values to the sequence of electronic work functions of various metals, and Fischer[5] pointed out qualitatively that there is a relationship between hydrogen overvoltage and the surface energy of the metal. Kortüm and Bockris in their text of electrochemistry, while they retain the views of Bockris and Potter, also indicate that "the dependence of overpotential at a given current density upon the electrode material should vary in a way parallel to the heat of adsorption of hydrogen upon the metal" (reference 1, p. 431). This qualitative observation is expressed in quantitative terms in this paper. It is also shown that there is essentially no correlation between the sequence of overvoltages for various metals and the corresponding work functions.

KINETIC EQUATION FOR THE OVERVOLTAGE

The following treatment holds for hydrogen overvoltage values larger than approximately 0.1–0.15 volt; the kinetics of the electrode process is then essentially controlled by the rate of discharge of hydrogen ions. The overvoltage for hydrogen evolution can be written in the form (reference 2, Eq. (80), p. 430; note that the authors unwittingly dropped the term e_0 in this equation)

$$\eta=\frac{RT}{\alpha F}\ln P-\frac{\Delta G^{\ddagger}}{\alpha F}+\left(1-\frac{1}{\alpha}\right)\psi_0-e_0 \qquad (1)$$

where α is the transfer coefficient for the hydrogen ion discharge; $\Delta G^{\ddagger}$ is the free energy of activation for the discharge process;[6] ψ_0 is the difference of potential across the diffuse part of the Stern double layer at unit hydrogen ion activity; e_0 is the difference of potential from electrode to the Helmholtz outer plane for the reversible normal hydrogen electrode; and P represents a group of terms whose form is not needed here. The quantity P can be regarded as independent of the electrode material.

The factors in Eq. (1) which might depend on the electrode material are α and $\Delta G^{\ddagger}$; the difference of potential e_0 certainly depends on the electrode material, since it includes the electronic work function for the electrode. The difference of potential ψ_0 can be regarded as independent of the electrode material, since ψ_0 is determined by the properties of the diffuse double layer. The study of the dependence of $\Delta G^{\ddagger}$ on electrode material is simplified if one assumes that the entropy of activation $\Delta S^{\ddagger}$ is independent of the electrode material. $\Delta S^{\ddagger}$ corresponds to a loss of three degrees of translation freedom, and in principle $\Delta S^{\ddagger}$ can be calculated from the proper partition functions.[7,8] The as-

* Postdoctoral fellow 1953–1954.

[1] For a summary, see G. Kortüm and J. O'M. Bockris, *Textbook of Electrochemistry* (Elsevier Publishing Company, Inc., New York, Houston, 1951), Vol. II, pp. 420–437. Reference should also be made to the work of Horiuti and Polanyi, Acta Physicochim. **2**, 505 (1935). We are indebted to Dr. Bockris for calling this reference to our attention.

[2] K. Bonhoeffer, Z. physik. Chem. **A113**, 199 (1924).

[3] J. O'M. Bockris, Chem. Revs. **43**, 561 (1948).

[4] J. O'M. Bockris and E. C. Potter, J. Electrochem. Soc. **99**, 169 (1952). However, see N. K. Adams, *The Physics and Chemistry of Surfaces* (Oxford University Press, London, 1941), p. 320.

[5] H. Fischer, Z. Elektrochem. **52**, 111 (1948).

[6] The following discussion is based on the use of $\Delta G^{\ddagger}$ and electrode potentials, but the argument can also be presented in terms of electrochemical potentials. Such potentials were used by Van Rysselberghe in a treatment of hydrogen overvoltage; see P. Van Rysselberghe, J. Chem. Phys. **17**, 1226 (1949); **20**, 1522 (1952); J. chim. phys. **49**, C 47 (1952).

[7] For an evaluation of $\Delta S^{\ddagger}$, see Eyring, Glasstone, and Laidler, J. Chem. Phys. **7**, 1053 (1939).

[8] R. Parsons and J. O'M. Bockris, Trans. Faraday Soc. **47**, 914 (1951).

sumption that $\Delta S^{\ddagger}$ is independent of the electrode material is substantiated, without recourse to any theoretical considerations, by the validity of the conclusions derived from this hypothesis. If $\Delta S^{\ddagger}$ is constant, the overvoltage for given hydrogen ion activity and current density can be written in the abridged form

$$\eta=\frac{RT}{\alpha F}\ln\xi-\frac{\Delta H^{\ddagger}}{\alpha F}+\left(1-\frac{1}{\alpha}\right)\psi_0-e_0 \qquad (2)$$

where ξ can be regarded as independent of electrode material.

POTENTIAL ENERGY CURVES

The dependence of $\Delta H^{\ddagger}$ and α on the electrode material can be studied from potential energy curves. The application of such curves to electrode processes was first made by Butler,[9] and, at a later date, Gurney and Fowler[10] used these curves in a quantitative fashion. Several authors have since used such curves in discussing electrode processes. The following determination of potential energy curves follows very closely the treatment of Parson and Bockris.[8]

The initial state corresponds to one equivalent of hydrogen ions in solution and one equivalent of electrons in the metal. The final state corresponds to one equivalent of adsorbed hydrogen atoms on the metal. The corresponding heat contents (with respect to H_2) are calculated from the following reactions:

Initial states: 1/2 H_2 (1 atmos)$\rightarrow$H (1 atmos); H (1 atmos)$\rightarrow H^+$ (gas)$+e$; H^+ (gas)$\rightarrow H^+$ (aq.); H^+ (aq.)$\rightarrow H^+$ (double layer); M$+e\rightarrow$M (e).

Final state: 1/2 H_2 (1 atmos)$\rightarrow$H (1 atmos); H (1 atmos)$+$M$\rightarrow$MH; HM$+H_2O\rightarrow H_2O-$HM.

The corresponding heat contents (in kcal) are

$$H_i=101.7-\phi_w \qquad (3)$$

for the initial state and

$$H_f=51.7-A+R \qquad (4)$$

for the final state, the notations being as follows: ϕ_w electronic work function of the metal, A heat of adsorption of atomic hydrogen on the metal, and R the energy of interaction between a molecule of water and hydrogen adsorbed on the metal.

The term 101.7 kcal in Eq. (3) is the algebraic sum of the energy of the dissociation of one-half mole of hydrogen (51.7 kcal), the ionization energy of hydrogen (313 kcal), the energy of hydration of the proton (-263 kcal), and the energy of adsorption in the double layer. The latter term is negligible.[8] The hydration energy of hydrogen ion used here (-263 kcal) is the average of the value -250 kcal obtained by Latimer *et al.*[11] and the value -276 kcal calculated by Bernal and Fowler.[12] It is to be noted that the value of the term 101.7 kcal in Eq. (3) is independent of the electrode material, and consequently errors affecting this datum are unimportant in the comparison of overvoltage values for different metals.

The term 51.7 kcal in Eq. (4) is the energy of dissociation of one-half mole of hydrogen at one atmosphere. Quite obviously this datum does not depend on the electrode material.

It should be noted that the surface potential of Lange[13] is neglected in the writing of Eq. (3). The objection to the treatment of Latimer, Pitzer, and Slanski,[11] which was raised by several authors[14–16] and was recently emphasized by Van Rysselberghe,[17] could be made here. However, the sequence of overvoltage values for different metals will not be affected by the neglecting of the surface potential, if this surface potential is essentially independent of the electrode material. It will be assumed that this is the case.

Variations in heat content of the initial state from the equilibrium position are given by the Morse curve for the hydration of proton. Conversely, variations in heat content of the final state are given by the sum of the Morse curves for the adsorption of hydrogen on the metal (energy A) and the interaction of water and MH (energy R).[8] These curves are represented in Fig. 1 for mercury, silver, and nickel.

The Morse curve for the hydration of the proton was calculated from the equation[18]

$$D-V=D\{2\exp[-2\beta(r-r_e)/r_e]-\exp[-4\beta(r-r_e)/r_e]\} \qquad (5)$$

where D is the dissociation energy referred to the

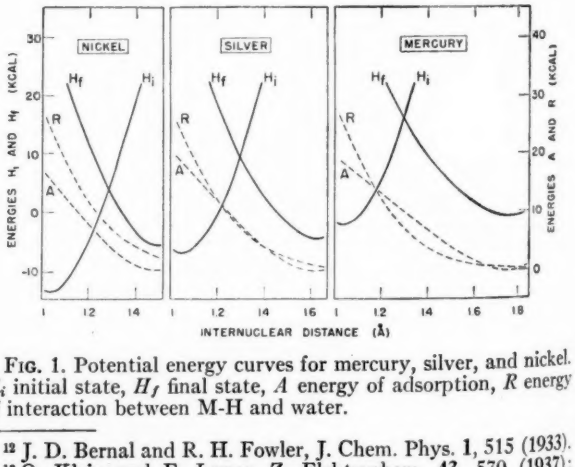

FIG. 1. Potential energy curves for mercury, silver, and nickel. H_i initial state, H_f final state, A energy of adsorption, R energy of interaction between M-H and water.

[9] J. A. V. Butler, Trans. Faraday Soc. **19**, 729 (1924).
[10] R. W. Gurney and R. H. Fowler, Proc. Roy. Soc. (London) **A136**, 378 (1932).
[11] Latimer, Pitzer, and Slansky, J. Chem. Phys. **7**, 108 (1939).
[12] J. D. Bernal and R. H. Fowler, J. Chem. Phys. **1**, 515 (1933).
[13] O. Klein and E. Lange, Z. Elektrochem. **43**, 570 (1937); E. Lange, *ibid.* **55**, 76 (1951).
[14] W. G. Burgers, Chem. Weekblad **39**, 1 (1942).
[15] R. Piontelli, Internation. Committee Electrochem. Therm. Kinet., Proc. 2nd Meeting, Tamburini, Milan, 1951, pp. 344–369.
[16] H. Strehlov, Z. Elektrochem. **56**, 119 (1952).
[17] P. Van Rysselberghe, J. Chem. Phys. **21**, 1550 (1953).
[18] G. Herzberg, *Molecular Spectra and Molecular Structure* (D. Van Nostrand Company, Inc., New York, 1950), second edition, p. 101.

minimum of the potential energy curve, V the potential energy at a position different from equilibrium, r_e the equilibrium internuclear distance. The constant β is defined by

$$\beta=\omega_e/4(B_eD)^{\frac{1}{2}} \tag{6}$$

where ω_e is the vibrational constant and B_e the rotational constant for the equilibrium position. The following values for the OH bond were used[19]: $r_e=1.0289$ A, $\omega_e=2955$ cm^{-1}, and $B_e=16.793$ cm^{-1}; D was 263 kcal (see above, energy of hydration of the proton). Morse curves for the adsorption of hydrogen were computed in the same fashion, the energy of adsorption at the equilibrium position being calculated as indicated in the following section. Data were as follows: for mercury[20] $D=52.9$ kcal, $r_e=1.7404$ A, $\omega_e=1387.09$ cm^{-1}, and $B_e=5.549$ cm^{-1}; for silver[21] $D=57.5$ kcal, $r_e=1.6174$ A, $\omega_e=1760.0$ cm^{-1}, and $B_e=6.453$ cm^{-1}; for nickel[22] $D=60.2$ kcal, $r_e=1.4746$ A, $\omega_e=1926.6$ cm^{-1}, and $B_e=7.823$ cm^{-1}.

The potential energy curve for the interaction between MH and water was calculated according to an equation established by Amdur[23] and quoted by Parson and Bockris.[8] For details, see reference 8.

The energy of activation for the discharge of hydrogen ion is given by the difference in energy between the equilibrium position for the initial state and the intersection of the H_i and H_f curves (neglecting the resonance effect). When a difference of potential $|\Delta\phi|$ exists at the electrode-solution interface the potential energy curve for the initial state is raised by $F\Delta\phi$ calories, and the energy barrier is decreased by $|\alpha F\Delta\phi|$ by definition of the transfer coefficient α. Values of α can thus be determined graphically from potential energy curves such as those of Fig. 1. It can be seen from this diagram that α varies slightly with $\Delta\phi$ because of the shape of the energy curves. However, the curvature of these curves in the region of intersection is rather small, and variations of α with potential are rather minor. Since the potential energy curves vary with the electrode material, α depends also on the nature of the electrode, but α is generally in the vicinity of 0.5.[24]

The electronic work function ϕ_w and the energy of adsorption A vary as the electrode material is changed. Furthermore, the adsorption energy curve becomes flatter as the energy of adsorption of hydrogen decreases (Fig. 1), and the internuclear distance between the two equilibrium positions varies from one metal to another. The effect of these different factors on the overvoltage for hydrogen ion discharge can be determined as follows.

[19] See reference 18, p. 561.
[20] See reference 18, p. 538.
[21] See reference 18, p. 502.
[22] See reference 18, p. 557.
[23] J. Amdur, J. Chem. Phys. **17**, 844 (1949).
[24] See experimental data in an article by J. O'M. Bockris in *Electrochemical Constants*, Natl. Bur. Standards, (U. S.) Circ. 524, 1953, pp. 243–262.

Compare two metals 1 and 2 for which the overvoltages under identical conditions of electrolysis are η_1 and η_2, respectively. If one assumes that α is the same for these two metals (see above), one has, in view of Eq. (2),

$$\eta_1-\eta_2=-(\Delta H_1^{\ddagger}-\Delta H_2^{\ddagger})/\alpha F \quad -[(e_0)_1-(e_0)_2]. \tag{7}$$

The difference between the e_0's is equal to the difference between the work functions for the two metals. From Eq. (3) and the definition of α one deduces that the difference between the $\Delta H^{\ddagger}$'s includes the product of α by the difference of the work functions of the two metals. Hence, this difference between the two work functions cancels in the expression of $\eta_1-\eta_2$ of Eq. (7). The foregoing considerations show that *there is no correlation between experimental overvoltage values for a series of metals and the corresponding electronic work functions*. This was already pointed out by Adam (see reference 4).

One can assume that the interaction energy R in Eq. (4) is independent of the nature of the electrode, and one then deduces from this equation that the only other factors to be considered in comparing overvoltage values for different metals are variations in the energy of adsorption and the effect of the internuclear distance between the equilibrium positions. The effect of these factors could be deduced by analytical geometry considerations but the writing would be rather heavy. It can be seen from Fig. 1 that one has

$$\Delta H_1^{\ddagger}-\Delta H_2^{\ddagger}\approx-(A_1-A_2) \tag{8}$$

for the difference in the $\Delta H^{\ddagger}$'s for two metals. For example (Fig. 1) the difference between the $\Delta H^{\ddagger}$'s for mercury and silver is 4.5 kcal while the corresponding difference in the A's is -4.5 kcal. Likewise the difference in the $\Delta H^{\ddagger}$'s for mercury and nickel is 7.5 kcal while the difference for the A's is -7 kcal. Relationship (8) can be explained qualitatively as follows. As the energy of adsorption A varies by ΔA the minimum of the energy curves for the final state is shifted by $-\Delta A$. The energy of activation would be changed by $-(1-\alpha)\Delta A$ if the shape of the energy curve remained identical. However, the curve A becomes steeper as the heat of adsorption increases, and the internuclear distance between the equilibrium positions varies from one metal to another. The combination of these two effects results in (8). Of course relationship (8) is only approximate, but it holds remarkably well for many metals as will be shown below.

OVERVOLTAGE *VERSUS* ENERGY OF ADSORPTION OF ATOMIC HYDROGEN

One deduces from the foregoing considerations that differences in overvoltage from one metal to another result primarily from variations in the energy of adsorption of hydrogen on the metal. Reliable overvoltage data are available to test this conclusion, but heats of adsorption of hydrogen are very scanty. How-

ever, such adsorption energies can be calculated, as was pointed out by Eley,[25] by the simple Pauling equation[26]

$$D(\mathrm{M-H})=\tfrac{1}{2}\{D(\mathrm{M-M})+D(\mathrm{H-H})\}+23.06(x_{\mathrm{M}}-x_{\mathrm{H}})^2 \quad (9)$$

where the D's are the bond energies and the x's are the electronegativities. Eley points out that the small moment of M−H bonds is an indication of small differences in electronegativity. Hence, the electronegativity correction will be neglected in the following calculations. In applying Eq. (9) one assumes that there is only one atom of hydrogen bound to each atom of the metal. It was shown by Roberts[27] that this is indeed the case even when the metal is saturated.

The value of $D(\mathrm{H-H})$ is 102.4 kcal per mole,[28] and $D(\mathrm{M-M})$ can be deduced from the surface energy of the metal. It was pointed out by Volmer[29] that the difference between the potential energy ϵ_0 of a free metal atom removed from its lattice and the potential energy ϵ_w of the metal in a half-crystal position at the absolute zero is

$$\epsilon_0-\epsilon_w=L+kT/2 \quad (10)$$

where L is the heat of vaporization of the metal at T degrees.

The number of neighboring atoms to be considered in calculating the bond energy $D(\mathrm{M-M})$ depends on the lattice type of the metal. Forces involved are of short range, since Stransky[30] has shown that forces between metal atoms decrease with the 8th to 13th power of the distance between atoms. Only the bonds to the nearest atoms must be considered, except in the case of the cubic body-centered lattice for which the next nearest neighbors have some influence. Our calculations were made according to Fricke[31,32] who considers that the energy to remove a next nearest neighbor for the cubic body-centered lattice is one-half to the energy for removing a nearest neighbor. The numbers of neighbors to be considered are as follows: simple cubic lattice, 3; cubic face-centered, 6; cubic body-centered, 4 plus 3 next nearest neighbors. Metals having the diamond, bismuth, and selenium types of lattice probably do not evaporate in the monoatomic form, and consequently the calculation of the bond energy $D(\mathrm{M-M})$ from heats of vaporization is uncertain. Such elements (Sn, Si, Ge, Sb, As, Bi, Se, Te) were not considered here.

Bond energies as calculated from Eq. (9) and pertaining data are listed in Table I. The heats of volatilization are those critically compiled by Baughan[33] except for gallium.[34] The heats of adsorption of Table I are for a fraction, θ, of covered surface equal to zero. Actually, heats of adsorption decrease either linearly with increasing values of θ according to Fowler and Guggenheim[35] or with increasing values of $\log\theta$ according to Halsey and Taylor.[36] The value $\theta=0$ was adopted here for the sake of simplicity.

The heats of adsorption listed in Table I are approximate, but the agreement with the few available experimental values[37] is rather good as can be seen from Table II. It should be noted that it is not an easy task to obtain precise experimental heats of adsorption.

TABLE I. Heats of adsorption, overvoltages, and pertaining data.

Metal	Heat of volatilization at 0°K kcal/g atom	$D(\mathrm{M-M})$ for ½ crystal kcal/g atom	Heat of adsorbtion kcal/g atom	Overvoltage (*) volts	Ref.
Ag	69	11.5	57.5	0.59	c
Al	76	12.6	58.0		
Au	91	15.2	59.3	0.12	c
Be	78	13.0	58.2	0.63	d
Cd	26.8	4.5	53.9	0.99	e
Cr	93	16.9	60.1	0.42	e
Cu	82	13.6	58.5	0.46–0.57	f, d
Fe	97	17.6	60.5	0.40	e
Ga	66	11.0	56.5	0.68	g
Hg	14.5	2.4	52.9	1.04–1.03	e, h
In	57	9.5	56.5	0.80	d
Mg	35.4	5.9	54.7	···	
Mn	69	11.5	57.5	···	
Mo	155	28.2	65.8	0.13–0.30	c, d
Nb	176 [a]	32.0	67.7	···	
Ni	102	17.0	60.2	0.32–0.33	d, e
Pb	46.5	7.7	55.6	0.85	d
Pd	93 [b]	15.5	59.5	0.09–0.01	i, c
Pt	134	22.4	62.9	0.27–0.01	c
Ta	186	33.8	68.6	0.2	c
Ti	112	18.7	61.0	···	
Tl	43	7.2	55.3	0.61–1.05	c, d
V	120	20.0	61.7	···	
W	202	33.7	68.6	0.11	c
Zn	31.2	5.2	54.3	···	

[a] At 10^{-3} amp cm^{-2} in 1 N HCl and at 25°C. All overvoltage values are negative.
[b] Uncertain datum.
[c] J. O'M. Bockris and R. Parsons, Trans. Faraday Soc. **44**, 860 (1948).
[d] J. O'M. Bockris, Trans. Faraday Soc. **43**, 417 (1947).
[e] A. Hickling and F. W. Salt, Trans. Faraday Soc. **36**, 1226 (1940).
[f] J. O'M. Bockris and S. Ignatowicz, Trans. Faraday Soc. **44**, 520 (1948).
[g] F. B. Bowden, Proc. Roy. Soc. (London) **A128**, 317 (1930).
[h] B. Kabanov and S. Jofa, Acta Physicochim., U.R.S.S. **10**, 617 (1939).
[i] J. O'M. Bockris and A. M. Azzam, Trans. Faraday Soc. **48**, 145 (1952).

[25] D. D. Eley, J. Phys. Colloid Chem. **55**, 1016 (1951).
[26] L. Pauling, *The Nature of the Chemical Bond* (Cornell University Press, Ithaca, 1939), p. 60.
[27] K. Roberts, Proc. Roy. Soc. (London) **A152**, 445 (1935).
[28] See reference 26, p. 23.
[29] M. Volmer, *Kinetik der Phasenbildung* (Steinkopff, Dresden and Leipzig, 1939), p. 36.
[30] I. N. Stransky, Ber. deut. chem. Ges. **A72**, 141 (1939); Ann. Physik (6) **1**, 153 (1947).
[31] R. Fricke, Naturwiss. **29**, 365 (1941); Z. Elektrochem. **52**, 72 (1948).
[32] R. Fricke and C. Wagner, Z. physik. Chem. **B52**, 284 (1942).
[33] E. C. Baughan, Trans. Faraday Soc. **50**, 322 (1954). We had made a rather thorough survey of literature before the publication of this paper, and our values were in good agreement with those listed by Baughan.
[34] *Selected Values of Thermodynamic Properties*, Series 1, Table 28-1, National Bureau of Standards, 1949.
[35] R. H. Fowler and E. A. Guggenheim, *Statistical Thermodynamics* (Cambridge University Press, Cambridge, 1939), p. 421.
[36] G. Halsey and H. S. Taylor, J. Chem. Phys. **15**, 624 (1947).
[37] Mainly from the work of Beeck and co-workers: O. Beeck and A. Wheeler, J. Chem. Phys. **7**, 631 (1939); Beeck, Smith, and Wheeler, Proc. Roy. Soc. (London) **A177**, 62 (1940); O. Beeck, Revs. Modern Phys. **17**, 61 (1945); Beeck, Wheeler, and Cole, Discussions Faraday Soc. **8**, 118, 159, 314 (1950); Beeck, Ritchie, and Wheeler, J. Colloid Sci. **3**, 505 (1948). See also references 8 and 25.

A plot of hydrogen overvoltage against heat of adsorption of hydrogen is shown in Fig. 2. This plot yields essentially a straight line as is to be expected from considerations developed in the previous section. The slope of this line should be $1/\alpha F$ according to (7) and (8). This is indeed the case, and the value of α deduced from Fig. 2 is 0.45 in good agreement with experimental data.[24]

The majority of the overvoltage values used in the construction of Fig. 2 were determined by Bockris and co-workers. These data can be regarded as reliable, because of the great care taken in experimental work. Whenever two apparently reliable values were available, the average value was utilized in the construction of Fig. 2. A critical survey of overvoltage data has been prepared by Bockris.[24]

TABLE II. Experimental and calculated heats of adsorption.

Metal	Experimental heat of adsorption of H_2 [a] kcal/mole	Experimental heat of adsorption of H [b] kcal/g atom	Calculated heat of adsorption of H kcal/g atom
W	46	74	68.6
Ta	39–46	71–74	68.6
Cr	44	73	60.1
Fe	32	67	60.5
Ni	30	66	60.2
Pd	27	65	59.5
Cu	9	56	58.5
Hg	0	51	52.9

[a] Fraction of covered surface equal to zero.
[b] Equal to one-half the experimental heat of adsorption of H_2 plus one-half the heat of dissociation of H_2 (51 kcal).

It should be emphasized that the foregoing considerations hold only when the overvoltage exceeds 0.1 to 0.15 volt, i.e., when the effect of the backward electrode reaction (oxidation or hydrogen) can be neglected. Thus data for gold, palladium, platinum, molybdenum, tungsten, and tantalum should not be considered.[38]

CONCLUSION

Differences in hydrogen overvoltage from one metal to another and under given conditions of electrolysis are essentially determined by variations in the heat of adsorption of atomic hydrogen on the metal. There is practically a linear relationship between this heat of adsorption and overvoltage. Differences in overvoltage for different metals virtually do not depend on the electronic work functions of these metals.

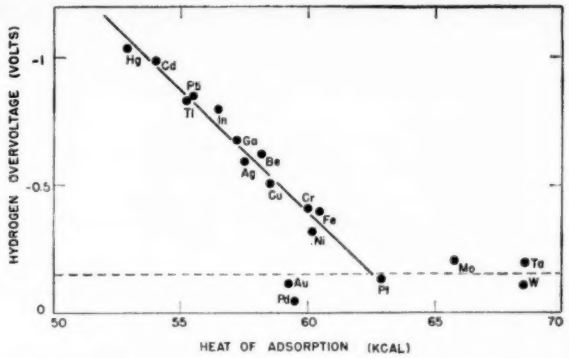

FIG. 2. Hydrogen overvoltage *versus* heat of adsorption of atomic hydrogen on the metal. Overvoltage data for 1 *N* hydrochloric acid and 10^{-3} amp cm^{-2} at 25°. No correlation is established for overvoltage values below dashed line.

This study shows how the influence of the electrode material, which is very important in many irreversible electrode processes, can be interpreted on a rational theoretical basis. Further work in this direction for other electrode processes is now in progress. *Carefully controlled* experimental studies of the effect of the electrode material should be very interesting and particularly valuable in organic electrochemistry,[39] as was pointed out, for example, by Rüetschi and Trümpler in their study of the electrolytic reduction of diazo compounds.[40]

ACKNOWLEDGMENT

We are indebted to the Office of Naval Research for the support of this investigation. Dr. P. Van Ryssel-berghe of the University of Oregon made valuable comments on the electrochemistry of hydrogen ion discharge, and Dr. B. S. Rabinovitch of the University of Washington called our attention to the effect of electrode coverage on the heat of adsorption of hydrogen.

[38] Reliable overvoltage data for Mo, W, Ta are very difficult to obtain.

[39] A wealth of practical information can be found in F. Fichter's *Organische Elektrochemie* (Steinkopff, Dresden and Leipzig, 1942).

[40] P. Rüetschi and G. Trümpler, Helv. Chim. Acta **36**, 1655 (1953).

Some Complexities in the Reaction System: $H_2+I_2=2HI$†

SIDNEY W. BENSON,* AND R. SRINIVASAN‡
Department of Chemistry, University of Southern California, Los Angeles 7, California
(Received June 11, 1954)

Existing thermal and kinetic data are sufficient to show that in the reaction $H_2+I_2=2HI$, free radical processes may contribute significantly to the overall rate at temperatures above 600 K. This provides a reasonable explanation for some of the anomalies observed in this system and indicates that further kinetic study of the system is desirable.

THE reaction system

$$H_2+I_2=2HI \tag{1}$$

was first studied by M. Bodenstein,[1] who found that over the temperature range 556° to 781°K, both forward and reverse reactions are bimolecular, and can be represented kinetically by Eq. (1). Kassel[2] has shown that the empirical equation, which fits Bodenstein's data for the bimolecular rate constants of the combination reaction, leads to an abnormally high value for the temperature coefficient of the activation energy. Further, it has been pointed out[3,4] that Bodenstein's values for the equilibrium constants do not fall on a straight line when plotted against temperature in the usual way, i.e., log K *vs* $1/T$. However, later workers[4] were able to obtain a linear plot, though over a shorter range of temperature. Since the equilibrium constant is equal to the ratio of the rates of the forward and reverse reactions, and since the forward reaction shows a high temperature coefficient for the activation energy, the reverse reaction should also show a similar effect. The observed change in activation energy with temperature[2] is about 21 cal/mole degree, which is far beyond what can be accounted for in terms of any reasonable model for a simple bimolecular reaction. These considerations suggest that the reaction may be actually more complex than indicated by Eq. (1).

A simple chain mechanism can be written as follows[5,6]:

$$I_2+M \underset{k_3}{\overset{k_2}{\rightleftharpoons}} 2I+M-35.6 \text{ kcal}, \tag{2,3}$$

$$I+H_2 \underset{k_5}{\overset{k_4}{\rightleftharpoons}} HI+H-32.8 \text{ kcal}, \tag{4,5}$$

$$H+I_2 \underset{k_7}{\overset{k_6}{\rightleftharpoons}} HI+I+35.5 \text{ kcal}. \tag{6,7}$$

Using stationary state kinetics we find for the initial rate of the reaction (neglecting the slower back reaction in this region):

$$\frac{d(HI)}{dt}=\frac{2k_4(H_2)(I_2)^{\frac{1}{2}}(k_2/k_3)^{\frac{1}{2}}}{1+k_5(HI)/k_6(I_2)}. \tag{8}$$

Since E_6 is probably less than or equal to E_5, it is very likely that $k_5<k_6$. In any case for the initial stages of the reaction when $(HI)<(I_2)$ this expression reduces to:

$$\frac{d(HI)}{dt}\approx 2k_4(H_2)(I_2)^{\frac{1}{2}}K_{23}^{\frac{1}{2}}, \tag{9}$$

where $K_{23}=k_2/k_3$, the equilibrium constant for the dissociation of I_2. If we write for the rate of the concurrent bimolecular step:

$$\frac{d(HI)}{dt}\approx k_b(H_2)(I_2), \tag{10}$$

then the over-all initial rate is given by the sum of these two expressions, or,

$$\frac{d(HI)}{dt}=k_b(H_2)(I_2)[1+R], \tag{11}$$

where R is the ratio of the two rate processes

$$R=2k_4K_{23}^{\frac{1}{2}}/k_b(I_2)^{\frac{1}{2}}. \tag{12}$$

Since K_{23} is known quite accurately from spectroscopic data, only k_4 need be calculated to evaluate R. This would assume the value of k_b given by the experimental data. An alternative method, which promised greater internal consistancy and which gave quite reasonable results, was to calculate the ratio k_4/k_b using the transition state theory. In terms of the latter,

$$\frac{k_4}{k_b}=\frac{\kappa_4 Q(I_2)Q(H_2I)^{\ddagger}}{\kappa_b Q(I)Q(H_2I_2)^{\ddagger}}\exp[(E_b^0-E_4^0)/RT], \tag{13}$$

† Presented at the Southwest Regional Meeting of the American Chemical Society in Los Angeles, May 1954.

* Professor of Chemistry.

‡ Graduate Research Fellow.

[1] M. Bodenstein, Z. physik. Chem. **13**, 56 (1894); **22**, 1 (1897); **29**, 295 (1899).

[2] L. Kassel, Proc. Natl. Acad. Sci. U. S. **16**, 358 (1930). For the reverse reaction, Kassel has calculated from Bodenstein's original data an even greater change of activation energy with temperature, namely 35 cal/°C.

[3] N. F. H. Bright and R. P. Hagerty, Trans. Faraday Soc. **43**, 697 (1947).

[4] A. H. Taylor and R. H. Crist, J. Am. Chem. Soc. **63**, 1377 (1941).

[5] The thermal data given here were taken from "Selected Values of Chemical Thermodynamic Properties," Natl. Bur. Standards, (U. S.), Circ. No. 500 (1952).

[6] Equations (2), (3), and (4) were suggested as possible steps in this reaction by Lewis and Rideal as early as 1926. [J. Am. Chem. Soc. **48**, 2553 (1926).]

in which κ_4/κ_b = the ratio of the transmission coefficients for the two transition state complexes ($H_2I^\ddagger$ and $H_2I_2^\ddagger$), the Q's are the appropriate partition functions for the species indicated, and $(E_b^0-E_4^0)$ = the difference in activation energies at 0°K.

The transition state complex $H_2I^\ddagger$ was assumed to be a linear molecule while a symmetrical, planar structure was assumed for $H_2I_2^\ddagger$. For the dimensions of the latter the data of Eyring *et al.*[7] was used. For $(H-H-I)^\ddagger$ the H−H distance was assumed to be 0.97A, while the H−I distance was assumed to be 1.75A. No attempt was made to evaluate the vibrational partition functions for the complexes, nor was any attempt made to evaluate their zero point energies. Instead it was assumed that $E_b^0-E_4^0$ could be taken as the difference in activation energies of the two reactions involved, namely, E_b-E_4.

With these assumptions we found that:

$$k_4/k_b=6[Q_{el}(H_2I)^\ddagger/2]K_{vib}e^{(E_b-E_4)/RT} \qquad (14)$$

which for the purposes of our present calculation we set equal to[8]:

$$k_4/k_b=e^{(E_b-E_4)/RT}. \qquad (15)$$

This value seems to be a lower limit for the ratio of the steric factors for the reactions involved[9] since the approximations made have been such as to deliberately favor the value of k_b.[8]

The experimental values of E_b fall in the range 39–41 kcal/mole or higher if calculated from the reverse reaction and the spectroscopically calculated K_{eq}. There are no experimental values of E_4, but from the estimated values of the reverse reaction and the known heat of reaction it may be estimated that E_4 will range from 32.8 to 35 kcal/mole.[9a] Thus E_b-E_4 has a minimum value near 4.0 kcal/mole and probably does not exceed 8.2 kcal/mole.

In Table I are presented the pressures of iodine (in mm of Mercury) at which the ratio R has the values 100, 1, 0.1, and 0.01. The two values at each temperature correspond to the maximum and minimum values for E_b-E_4. The importance of the chain reaction is seen to diminish with increasing iodine pressure, at constant temperature. At temperatures above 600°K, and pressures below 400 mm, the chain reaction is a tenth or more of the total reaction, but even at 800°K, it does not replace the bimolecular reaction completely.

TABLE I. Pressure of iodine in mm of mercury, when the ratio R has specific values.

Temperature 600°K			$K_{23}=1.17\times10^{-8}$		
$R\rightarrow$	100	1	0.1	0.01	E_b-E_4
Pressure	3.39×10^{-3}	33.96	3.39×10^{3}	3.39×10^{5}	8.2
(I_2) mm Hg	2.99×10^{-6}	2.99×10^{-2}	2.99	2.99×10^{2}	4.0
Temperature 700°K			$K_{23}=9.55\times10^{-7}$		
$R\rightarrow$	100	1	0.1	0.01	E_b-E_4
Pressure	4.00×10^{-2}	400	4.00×10^{4}	4.00×10^{6}	8.2
(I_2) mm Hg	9.30×10^{-5}	0.93	93.0	9.30×10^{2}	4.0
Temperature 800°K			$K_{23}=2.50\times10^{-5}$		
$R\rightarrow$	100	1	0.1	0.01	E_b-E_4
Pressure	2.37×10^{-1}	2.37×10^{3}	2.37×10^{5}	2.37×10^{7}	8.2
(I_2) mm Hg	1.18×10^{-3}	11.8	1.18×10^{3}	1.18×10^{5}	4.0
Temperature 900°K			$K_{23}=9.77\times10^{-4}$		
$R\rightarrow$	100	1	0.1	0.01	E_b-E_4
Pressure	2.94	2.94×10^{4}	2.94×10^{6}	2.94×10^{8}	8.2
(I_2) mm Hg	2.64×10^{-2}	2.64×10^{2}	2.64×10^{4}	2.64×10^{6}	4.0

If we set $r=R(I_2)^{\frac{1}{2}}$, the rate of disappearance of iodine is given by [Eq. (11)]:

$$-d(I_2)/dt=k_b(H_2)(I_2)[1+r/(I_2)^{\frac{1}{2}}]. \qquad (16)$$

If under specific conditions R has the value 0.5,[10] and during the course of the reaction the relative concentration of iodine changes from 1 to 0.7, the apparent change in the experimental bimolecular rate constant would be only 7 percent. The uncertainty in the rate constants from Bodenstein's data appears to exceed this figure, and hence it is not possible, from his data, to note the effect of the chain reaction on the rate constants. Even for $R=1$ and $\Delta(I_2)/(I_2)_0=0.5$ the change is only 20 percent in k_b(exp) which is still unfortunately within the limits of error of Bodenstein's measurements.

The effect of the nature of the reaction vessel on this system has been pointed out by Taylor and Crist[4] and Kistiakowsky[11] who disagree on its explanation. This wall sensitivity cannot be explained by either a purely homogeneous, bimolecular reaction or the atomic mechanism discussed here. It seems to indicate still a third heterogeneous component to the reaction. It is of course possible that the anomalies of this system are due to a partly heterogeneous reaction. In this case the real value of E_b would be even higher than those quoted here and the chain mechanism would be even more important than indicated by the values in Table I.

We can make a final check on the self-consistancy of these thermal and kinetic data by computing the expected variation of the experimentally observed activation energy with temperature. If we ignore the slight difference in mechanism, then we can write for the ex-

[7] Glasstone, Laidler, and Eyring, *The Theory of Rate Processes* (McGraw-Hill Book Company, Inc., New York, 1941), p. 235. The authors have erroneously given the symmetry No. of $H_2I_2^\ddagger$ as 4 rather than 2. It is this latter which is used above. The ratio of the transmission coefficients κ_4/κ_b is assumed to be unity.

[8] $Q_{el}(H_2I^\ddagger)\geq 2$ since it is an odd electron molecule. For the contribution of the vibrations it is to be noted that the total number of vibrations of $I_2+H_2I^\ddagger$ is 5 while for $H_2I_2^\ddagger$ it is 6. If we assume that the individual vibration frequencies are comparable, then K_{vib}, which is the ratio of the vibrational partition functions, reduces to that for a single unmatched frequency for $H_2I_2^\ddagger$. If this frequency is about 70 cm^{-1} or less, which seems unlikely, then $K_{vib}=\frac{1}{6}$ and we arrive at the result shown in Eq. (15).

[9] In general it is to be expected that steric factors for atom-molecule reactions will be close to unity and greater than steric factors for molecule-molecule reactions.

[9a] Schwarz, Williams, and Hamill, J. Am. Chem. Soc. **74**, 6007 (1952), from studies of hot radical effects, suggest a value as high as 37.3 kcal for E_4.

[10] This would signify contributions of chain and bimolecular mechanism to the overall rate in the ratio of 1:2.

[11] G. B. Kistiakowsky, J. Am. Chem. Soc. **50**, 2315 (1928).

perimentally observed rate constant k_a, the sum of the rate constants for the bimolecular step k_b, and the over-all chain $k_c=2k_4K_{23}^{\frac{1}{2}}$ (Eq. (9)):

$$k_0=k_b+k_c, \tag{17}$$

or expressed in Arrhenius form:

$$k_0=A_0e^{-E_0/RT}=A_be^{-E_b/RT}+A_ce^{-E_c/RT}. \tag{18}$$

Then,

$$k_0\left(\frac{\partial \ln k_0}{\partial T}\right)=k_b\left(\frac{\partial \ln k_b}{\partial T}\right)+k_c\left(\frac{\partial \ln k_c}{\partial T}\right), \tag{19}$$

or since $E=RT^2(\partial \ln k/\partial T)$, assuming the A's constant,

$$E_0=\frac{k_b}{k_0}E_b+\frac{k_c}{k_0}E_c \tag{20}$$

$$=E_b+\frac{k_c}{k_0}(E_c-E_b)=E_b+\frac{k_c}{k_0}\Delta E. \tag{21}$$

For the temperature coefficient,[12]

$$\frac{\partial E_0}{\partial T}=\Delta E\left(\frac{k_c}{k_0}\right)\left(\frac{E_c-E_0}{RT^2}\right), \tag{22}$$

which on substituting for E_0 from Eq. 20 becomes

$$\frac{\partial E_0}{\partial T}=R\left(\frac{\Delta E}{RT}\right)^2\left(\frac{k_c}{k_0}\right)\left(1-\frac{k_c}{k_0}\right) \tag{23}$$

$$=R\left(\frac{\Delta E}{RT}\right)^2[x(1-x)], \tag{24}$$

where the symmetric product $x(1-x)$ has a maximum value of $\frac{1}{4}$ when $x=k_c/k_0=\frac{1}{2}$; i.e., when the chain reaction amounts to half the over-all rate.

Since

$$\Delta E=E_c-E_b=[E_4+(E_{23}/2)]-E_b=E_{23}/2-(E_b-E_4),$$

and $E_{23}/2=18$ kcal, then ΔE will lie between 10 and 14 kcal. Choosing a mean temperature for the experimental range of 680°K we then find $(\Delta E/RT)^2$ is in the range 54 to 106 so that $(\partial E_0/\partial T)$ has a maximum value in the range 27 cal/°C to 53 cal/°C (i.e., when $x=\frac{1}{2}$). For $x=0.1$ or 0.9 we find $(\partial E_0/\partial T)$ in the range 10 to 20 cal/mole°C. These numbers are in the proper range for the observed value of 21 cal/°C and while not very discriminating would suggest that the true value of E_b-E_4 (See Table I) is probably nearer 8 kcal than the lower limit of 4 kcal. That is, for $E_b-E_4=4$ kcal, the mean value of $(\partial E_0/\partial T)$ over the range $x=0.1$ to 0.9 is about 40 cal/°C while for $E_b-E_4=8$ kcal the mean value in the same range is about 19 cal/°C, in good agreement with the observed value.

A corresponding treatment can be made for the reverse reaction, the decomposition of HI which seems to show an even larger temperature coefficient for the activation energy. It turns out in this case that the ratio of the atomic to molecular mechanisms (R_b) is given by the same expression already considered for the forward reaction:

$$R_b=\frac{(2k_4k_6/k_b)(k_2/k_3)^{\frac{1}{2}}(\mathrm{I}_2)^{\frac{1}{2}}}{k_5(\mathrm{HI})+k_6(\mathrm{I}_2)}. \tag{25}$$

This has a maximum value when the mole ratio $(\mathrm{I}_2)/(\mathrm{HI})=k_5/k_6$. The work of Schwarz, Williams, and Hamill[9a] suggests that k_5/k_6 may be of the order of about $\frac{1}{4}$ at temperatures above 600°K, which would place this maximum close to the composition of the equilibrium system and indicate that the atomic mechanism may have relatively the same importance in both systems (i.e., $\mathrm{H}_2+\mathrm{I}_2$ or decomposing HI). Lower values of k_5/k_6 would of course shift the relative importance of the atomic mechanism towards the HI system and *vice versa*.

In the case of HI, the back reaction cannot be neglected and the resultant kinetic equation becomes algebraically very awkward to handle. Thus a study of the $\mathrm{H}_2+\mathrm{I}_2$ system might be easier to interpret. It seems clear that this supposedly "classical, bimolecular reaction" is in need of further investigation.

One of the authors (S.W.B.) would like to express his appreciation to the Office of Ordnance Research for a grant in support of the present work.

[12] Note that (k_c/k_0) has the form $(A_c/A_0)e^{-(E_c-E_0)/RT}$ which itself has an exponential temperature dependence. We see from Eq. (21) that E_0 will change in a nonlinear fashion with temperature from the value E_b to E_c.

Letters to the Editor

THIS section will accept reports of new work, provided these are terse and contain few figures, and especially few half-tone cuts. The Editorial Board will not hold itself responsible for opinions expressed by the correspondents. Contributions to this section should not exceed 600 words in length and must reach the office of the Editor not later than the 15th of the second month preceding that of the issue in which the Letter is to appear. No proof will be sent to the authors. A publication charge of $15.00 per Letter is made which, when honored, will entitle the Institution to 100 free reprints.

Heat of Chemisorption of Hydrogen in Metals

D. P. STEVENSON
Shell Development Company, Emeryville, California
(Received November 12, 1954)

ELEY[1] has proposed that heats of chemisorption of gases on metals may be computed by means of Pauling's[2] formulation of bond energies. Thus for the chemisorption of hydrogen,

$$H_2+2M\rightarrow 2\overset{|}{M}\!\!-\!\!\overset{|}{H}$$

the heat of sorption, ΔH_a, becomes,

$$\Delta H_{ads}=-E(M-M)-46.12(X_M-X_H)^2 \text{ (kcal/mol)}, \quad (1)$$

where $E(M-M)$ is the metal atom-metal atom bond energy and X_M and X_H are the electronegativities of metal atom and hydrogen atom respectively. Eley[1] proposes that $E(M-M)$ is a fraction of the heat of atomization of the metal ($\frac{1}{6}$ in the case of metals with "closest packed" lattices) and that the electronegativity difference, $|X_M-X_H|$, may be computed from the contact potential associated with a monolayer of the adsorbed gas (hydrogen) on the metal.

It is the purpose of this communication to point out that if the electronegativities of the metals are computed from their work function, Φm, (ev/atom) by the formula,

$$X_M=0.355\Phi m \quad (2)$$

and Pauling's[2] assignment of electronegativities ($X_H=2.10$, $X_C=2.50$, $X_N=3.00$, etc.) are taken for adsorbate atoms, there obtains much better agreement between calculated and observed heats of adsorption than for Eley's original method of calculation. This new method of evaluating the electronegativity difference term in Eq. (1) has the added advantage of not depending on a measurement of considerable difficulty, the contact potential.

The formula (2), is based on Mulliken's[3] association of the electronegativity of an atom with the average of the first ionization potential and the electron affinity of the atom. By definition, the work function of a metal is its surface ionization potential, and to the extent that there are unfilled electron energy levels at the Fermi level of the metal, the electron affinity should also be equal to the work function. Thus one has,

$$X_M=0.177_5(I^z+E_a)=0.177_5(2\Phi m),$$

where $0.177_5=23.06/130$, is an empirical scale factor.[4]

Table I shows the heats of chemisorption [Eq. (1)] of hydrogen on a variety of metals as calculated by Eley,[1] by the new formulation and the observed values. Similar calculations have been made for nitrogen, oxygen, carbon monoxide, acetylene, and ethylene with similar improvement in agreement between calculated and observed values. These calculations are described and their significance discussed in a paper that will be submitted for publication in the near future.

TABLE I. Heats of chemisorption of hydrogen on metals.

Metal	Eley[a]	Heat of adsorption; this paper[b]	kcal/mole Observed
Chromium	−16.	−24.0	−45[c]
Iron	−17.	−31.6	−32.6;[c] −32±4[d]
Cobalt	...	−31.0	−24±4[d]
Nickel	−17.	−28.9	−29.6;[c] −24±1[d]
Copper		−25.6	−28±4[d]
Molybdenum	...	−42.9	(∼−40)[e]
Ruthenium	...	−38.1	−26±2[d]
Rhodium	−24.	−32.3	−26.2;[c] −25±2[d]
Palladium		−22.5	−26[c]
Tantalum	−32.	−49.6	−45[c]
Tungsten	−44.	−45.6	−45.5[c]
Iridium	...	−38.1	−26±2[d]
Platinum	...	−22.6	−27±1[d]

[a] Reference 1.
[b] Heats of atomization from N.B.S. Circular No. 500 Work functions; Cr, Fe, Co, and Ni; Jain and Krishnan, Proc. Roy. Soc. (London) **215A**, 436 (1952); other metals, Michaelson, J. Appl. Phys. **21**, 536 (1950).
[c] Beeck and co-workers, this laboratory, Trans. Faraday Soc. **8**, 127 (1950).
[d] Schuit and co-workers, B.P.M. Laboratory, Amsterdam (private communication).
[e] Ritchie, this laboratory (private communication).

[1] Eley, Trans. Faraday Soc. **8**, 34 (1950).
[2] Pauling, *Nature of the Chemical Bond* (Cornell University Press, Ithaca, New York, 1940), p. 50 ff.
[3] Mulliken, J. Chem. Phys. **2**, 782 (1934); **3**, 573 (1935).
[4] See reference 2, page 66.

Water Dimer and Its Relation to Mass Spectrometric Measurement of C_3^+ in Carbon Vapor

W. A. CHUPKA AND M. G. INGHRAM
Argonne National Laboratory, Lemont, Illinois, and University of Chicago, Chicago, Illinois
(Received November 15, 1954)

DWIGHT A. Hutchison, in a recent publication in this journal,[1] has suggested that "In light of the present work [Hutchison's work] one can state that some fraction, or possibly all, of the measured C_3^+ can be interpreted as $(H_2O)_2^+$." This C_3^+ measurement refers to the experiments of Chupka and Inghram[2] and Honig[3] on the composition of carbon vapor over graphite as related to the heat of vaporization of carbon. As far as the measurements of Chupka and Inghram are concerned, this statement of Hutchison's is completely incorrect. We can state, in the light of the work we have done, that none of the mass 36 ion intensity ascribed by us to C_3^+ could conceivably be $(H_2O)_2^+$. The reasons behind this conclusion are as follows.

In our earlier experiments[2] in which the carbon vapor evaporating from filaments was studied, we used the criterion that only that part of the mass 36 peak which followed rapid changes in filament temperature would be ascribed to C_3^+. It was found experimentally that peaks resulting from residual gases such as H_2O, CO, CO_2, HCl, etc., varied much more slowly with filament temperature. Upon suddenly dropping the filament temperature, there would occur a sharp drop in the intensity of the mass 36 peak, followed by a very much slower decrease in intensity. The intensity of the sharply temperature-sensitive part of the mass 36 peak was found to be dependent only on the carbon filament temperature and was completely independent of the degree of outgassing and the concentration of residual gases such as H_2O which varied by about two orders of magnitude during these experiments. The slowly changing part of the ion intensity did depend on residual gas pressure and was always subtracted as background. It is possible that a fraction of this background could be due to $(H_2O)_2^+$, but it in no way affects our conclusions concerning C_3.

Hutchison has inferred, from a conversation with one of us (MGI), that the conditions in our filament experiments were such that the formation of dimer ions of water was highly probable. We do not agree with this inference, but in any case it could only

affect the analysis of the background ions which was of little interest to us at the time.

In Knudsen cell effusion experiments[4] we have used a shutter before the effusion hole in the cell to distinguish between gases effusing from the cell and background gases. The 36 intensity ascribed to C_3^+ was taken as proportional to the difference between the 36 peak height with the shutter closed as compared with shutter open, minor corrections being made for photoelectric effect. A similar study of the mass 18 peak, H_2O^+, showed no detectable change on operating the shutter. Thus the H_2O pressure in the source remained constant when the shutter was operated while the mass 36 peak which we ascribed to C_3^+ changes at 2400°K by two orders of magnitude. Therefore the dimer ion of water cannot be responsible for the peak height at mass 36 which we ascribe to C_3^+. The possibility of a dimer of water itself effusing from the Knudsen cell at 2400°K is untenable thermodynamically.

Hutchison's investigation of the water dimer ion is of considerable interest but we reject his suggestion that our C_3^+ is actually $(H_2O)_2^+$.

[1] D. A. Hutchison, J. Chem. Phys. **22**, 1789 (1954).
[2] W. A. Chupka and M. G. Inghram, J. Chem. Phys. **21**, 1313 (1953).
[3] R. E. Honig, J. Chem. Phys. **22**, 126 (1954).
[4] W. A. Chupka and M. G. Inghram (to be published).

Reduction of Alkaline Earth Oxides by Methane

J. C. S. WAGENER
Kemet Company, Division of Union Carbide and Carbon Corporation, Cleveland, Ohio
(Received November 5, 1954)

IN a recent paper by Moore, Allison, and Wolfstein[1] some convincing experiments were described showing that alkaline earth oxides, such as used in oxide cathodes, can be reduced by application of methane. Considerable quantities of the respective alkaline earth metal can be produced in this way. When discussing their results, Moore, Allison, and Wolfstein pointed to the contradiction between their results and previous attempts to activate oxide cathodes by means of methane which gave an electron emission, low compared with the emission produced by other activation methods. In the opinion of the author this contradiction can be clarified by some results recently obtained.

When measuring pulsed emission currents from oxide cathodes at a temperature of 1075°K it was found that a high electron emission could be obtained by the application of methane as long as the methane pressure was kept lower than 5×10^{-5} mm Hg. When exceeding this pressure, however, the action of the methane, instead of being activating, became more and more poisoning (reducing the emission). Details of these experiments were published elsewhere.[2] The explanation given for them was as follows.

Owing to dissociation of the methane, carbon is deposited on the cathode surface. This carbon if not removed, will poison the oxide cathode. Removal of the carbon only is possible if the pressure of the carbon monoxide, resulting from reaction between the carbon and the alkaline earth oxide, is lower than the equilibrium value. These equilibrium values which are very nearly the same for barium and strontium oxide were calculated from the free energy values computed by White.[3] They are:

Temperature:	875°K	1075°K	1275°K	1475°K
Equilibrium Pressure of Carbon Monoxide: (mm Hg)	3×10^{-9}	9×10^{-6}	2×10^{-3}	8×10^{-2}

At 1075°K the equilibrium pressure is 9×10^{-6} mm which, because of the inaccuracy of the free energy values, is not very different from the observed critical pressure of 5×10^{-5} mm, limiting the two ranges in which methane acts either activating or poisoning.

It is believed that the low emission values, obtained in previous attempts to activate by means of methane, were due to the high methane pressure employed. (Hannay, MacNair, and White,[4] for instance, used pressures $\geq10^{-2}$ mm at a temperature of 1300°K.) In these attempts excess barium was produced in the oxide coating but the effect of this barium on the emission was more than compensated by carbon which could not be removed owing to the high pressure. A residual atmosphere of carbon monoxide above the cathode would also prevent the removal of the carbon during further operation of the cathode and would therefore explain why the low emission, once obtained, persisted indefinitely.

If methane is used for increasing the quantity of free barium in oxide cathodes, the methane pressure should be kept considerably lower than the values given in the table above. Therefore, even at 1475°K, the maximum applicable pressure would be about 10^{-2} mm. At this pressure a volume of 10 cm³ methane would only produce about 1 μg free barium. Therefore, in order to get barium quantities of the same order of magnitude as obtained by Moore, Allison, and Wolfstein, either a continuous flow of methane has to be used or the tube containing the oxide cathode has to be filled, evacuated, and refilled with methane a great many times.

[1] Moore, Allison, and Wolfstein, J. Chem. Phys. **22**, 726 (1954).
[2] S. Wagener, Proc. Phys. Soc. (London) **B67**, 369 (1954).
[3] A. H. White, J. Appl. Phys. **20**, 856 (1949).
[4] Hannay, MacNair, and White, J. Appl. Phys. **20**, 669 (1949).

Singlet-Triplet Excitation Energy of Aromatic Compounds and Their Reactivities

M. SZWARC
Chemistry Department, State University of New York, College of Forestry, Syracuse 10, New York
(Received November 3, 1954)

IT has been shown[1] that radicals may add to aromatic compounds, such a reaction being represented by the equation

$$R+A \rightarrow R\cdot A,$$

where R denotes a radical, while A denotes an aromatic molecule. It seems that the course of this reaction may be represented by the heavy line shown in the energy diagram, Fig. 1. The energy of the system radical-aromatic molecule in its ground state (singlet state) is represented by the rising curve (for the decreasing r_{AR}). The increase in energy is due to the repulsive force resulting from the interaction between a radical and an aromatic molecule in its singlet state. On the other hand, the interaction between an excited triplet molecule and a radical results in an attractive force leading to the formation of a chemical bond. Consequently, the energy of a system radical-triplet state aromatic molecule decreases with decreasing distance between the components, and the

TABLE I.

Compound	Methyl affinity	E_{S-T} cm^{-1}	Reference
Benzene	1	29,400	b, c
Diphenyl ether	2.5	28,200	c
Pyridine	3	26,050	c
Diphenyl	5	22,800	c
Benzophenone	11	24,100	b
Naphthalene	22	21,300	b, c
Phenanthrene	27[a]	21,600	b
Quinoline	29	21,700	b
Stilbene	183 (*trans*)	21,700 (*cis*)	c
Chrysene	57.5	19,800	b
Pyrene	125	16,800	b
Benzanthracene	468	16,500	b
Anthracene	820	14,700	b

[a] This number was given incorrectly in J. Chem. Phys. **22**, 1621 (1954). The error resulted from the presence of small amounts of anthracene in the phenanthrene.
[b] D. S. McClure, J. Chem. Phys. **17**, 905 (1949).
[c] R. V. Nauman, thesis, Berkley, 1944 (unpublished).

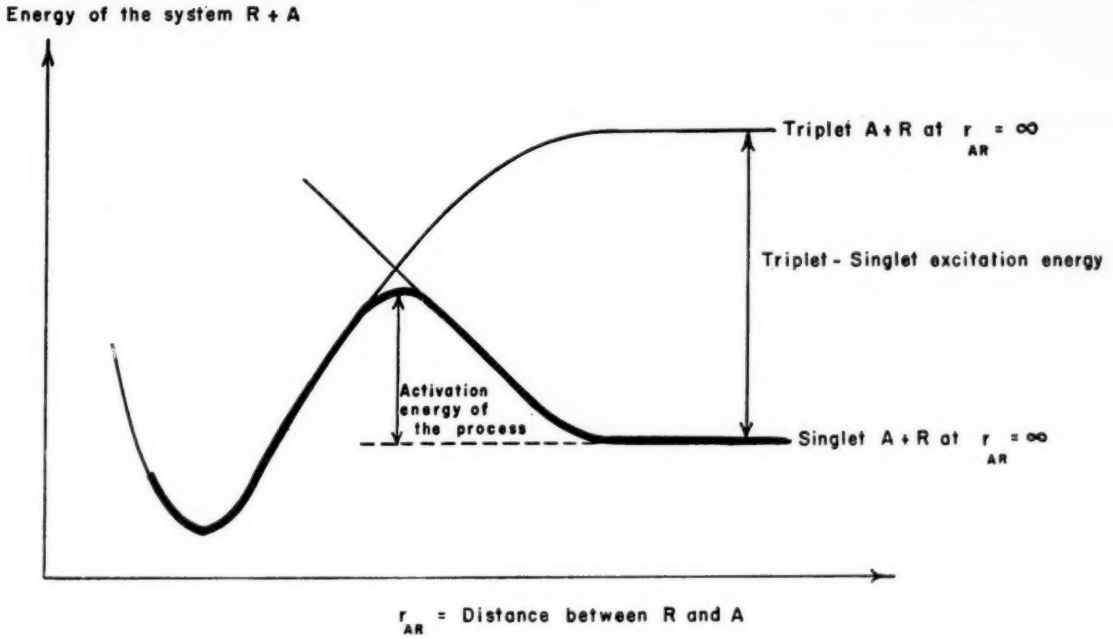
Energy of the system R + A
Triplet A + R at $r_{AR} = \infty$
Triplet - Singlet excitation energy
Activation energy of the process
Singlet A + R at $r_{AR} = \infty$
r_{AR} = Distance between R and A

FIG. 1.

curve has the shape of the familiar Morse curve. The actual path of the process results from the crossing from the first repulsion curve to the second attraction curve, the hump corresponding to the transition state.

If we deal with a series of reactions of the above type in which the same radical R interacts with various aromatic molecules A_1, A_2, $\cdots$ we deduce, applying the well known approach of Polanyi,[2] that the differences in the activation energies ΔE_a are proportional to the differences in the respective singlet-triplet excitation energies ΔE_{S-P}, i.e.,

$$E_a = \alpha \cdot E_{S-P}.$$

This relation is approximate. In its derivation it is assumed that the slopes of the crossing lines remain constant for the series of reactions, and it does not account for the rounding at the intersection point which is caused by resonance between the two levels.

The relative rate constants* for the reactions

$$CH_3 + A \rightarrow A \cdot CH_3$$

involving various aromatic compounds A_1, A_2, $\cdots$ have been determined recently.[3] Assuming that the variations in these rate constants result essentially from differences in the respective activation energies, we conclude that a linear relation should exist between log of methyl affinities and the respective singlet-triplet excitation energy. Such a relation is shown by Fig. 2, the relevant data being given in Table I.

It is striking to notice that the points represented in Fig. 2 refer to molecules belonging to various classes of compounds, such as hydrocarbons, heterocyclic nitrogen bases, ketones, and ethers. There are only two points which seem to be displaced: the one corresponds to diphenyl and the other to stilbene. However, the reactivity of the latter refers to the *trans*-isomer while the phosphorescence was measured for the *cis*-isomer. Consequently, the

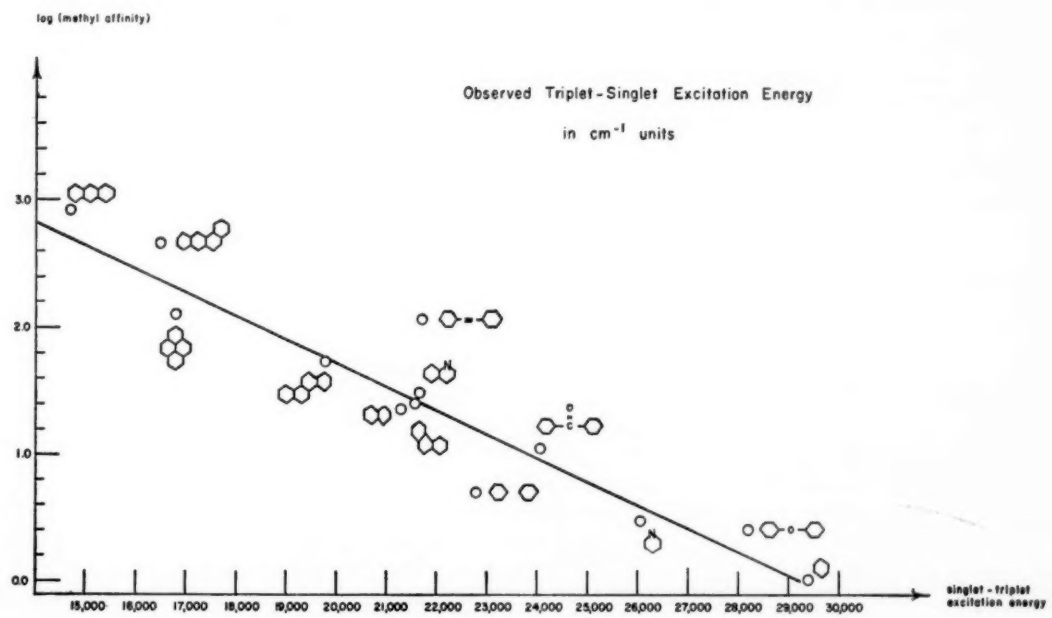
log (methyl affinity)
Observed Triplet - Singlet Excitation Energy
in cm^{-1} units
3.0
2.0
1.0
0.0
15,000 16,000 17,000 18,000 19,000 20,000 21,000 22,000 23,000 24,000 25,000 26,000 27,000 28,000 29,000 30,000
singlet - triplet excitation energy

FIG. 2.

discrepancy may result from the difference in the properties of the isomers. All these results show definitely that the suggested model for the reaction is plausible, and the assumptions introduced are justified at least in the first approximation. The above discussed correlation implies that one might predict the reactivity of an aromatic molecule towards radicals from the observed singlet-triplet excitation energy, or vice versa.

* We refer to these rate constants as methyl affinities.

[1] M. Magat and R. Boneme, Compt. rend. **232**, 1657 (1951); W. H. Stockmayer and L. H. Peebles, J. Am. Chem. Soc. **75**, 2279 (1953); E. C. Kooyman and E. Farenhorst, Trans. Faraday Soc. **49**, 58 (1953); Levy, Steinberg, and Szwarc, J. Am. Chem. Soc. **76**, 3439 (1954).
[2] R. Ogg and M. Polanyi, Trans. Faraday Soc. **31**, 604 (1935); M. A. Evans and M. Polanyi, Trans. Faraday Soc. **34**, 11 (1938).
[3] M. Levy and M. Szwarc, J. Chem. Phys. **22**, 1621 (1954); J. Am. Chem. Soc. (to be published).

Contraction of Germanium on Melting

R. C. Sangster and J. N. Carman, Jr.
Research and Development Department, Semiconductor Division, Hughes Aircraft Company, Culver City, California
(Received August 19, 1954)

SOLID germanium possesses the diamond crystal lattice, an open, non-close-packed structure. When germanium melts, the lattice collapses in part so that the liquid is more dense than the solid. Klemm *et al.*[1] have studied the change of volume of germanium on melting by several independent methods. The values obtained for the contraction on melting ranged from 4.3 percent to 6.4 percent; 5.5±0.5 percent was selected as the probable mean value. The volume expansion coefficient of the liquid was reported as 100×10^{-6}/°C (960–1100°C); direct computation from the density data presented gives 85×10^{-6}/°C.

Similar experiments were being conducted in this laboratory while the paper of Klemm *et al.* was in press. Due to several experimental difficulties, the work was abandoned after preliminary values had been obtained. However, the authors feel that their data (see Table I) are worth publishing, since they afford significant additional support for the results of Klemm and his coworkers.

The volume change of germanium on melting or freezing and the volume expansion coefficient of the liquid were determined using essentially the apparatus of Fig. 1. In runs 1–3, the graphite pycnometers consisted of two parts threaded together below the narrow neck; for runs 4 and 5, the pychometer shown in Fig. 1 was used. The furnace coils were so spaced that the vertical temperature gradient could be controlled and the germanium frozen from the bottom up or melted from the top down. An electrical probe, whose position could be read to ±0.001 in., was used to measure the height of the germanium in the neck of the pycnometer. The coil and crucible temperatures were measured with a Leeds and Northrup optical pyrometer which has been calibrated to ±3°C by comparison with a National Bureau of Standards calibrated instrument. At the end of a run, the germanium ingot proper was removed and weighed, and the amount of material in the narrow neck computed from dimensional measurements. The density of liquid germanium[1] was taken as 5.575 g/cm³. The expansion and contraction of the apparatus was neglected in computing the volume expansion coefficients.

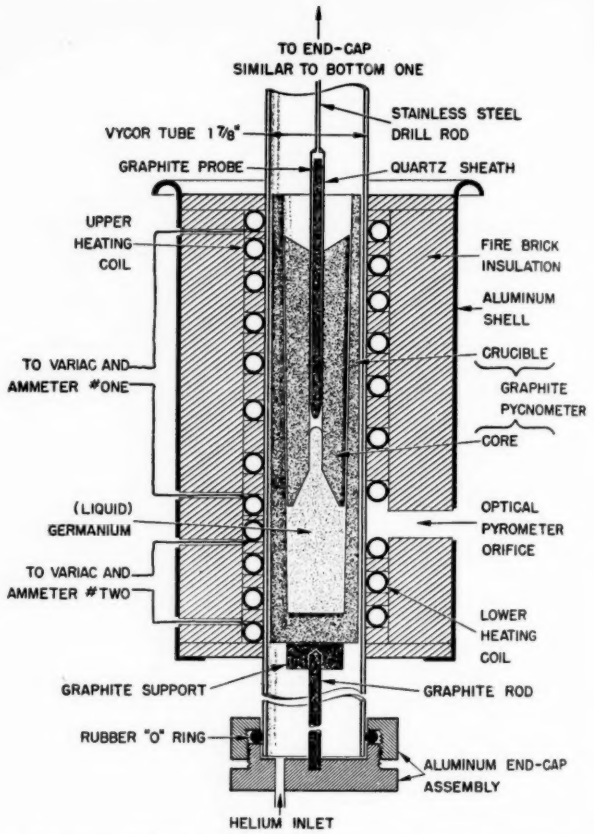

FIG. 1. Cross-sectional diagram of the apparatus used to determine the change in volume of germanium on melting or freezing and the volume expansion coefficient of the liquid. The rod supporting the graphite probe is clamped to a vernier depth gauge which is rigidly mounted with respect to the pycnometer. An ohmmeter connected to the bottom end cap and to the probe indicates when contact is made with the liquid in the neck of the pycnometer.

TABLE I. Data for experimental runs.

Run number	Mass	Change of volume on melting or freezing $(V_{s0}-V_{l0})/V_{s0}$*	Elapsed time for melting or freezing	Volume expansion coefficient of the liquid $\frac{1}{V_{l0}}\frac{\partial V_l}{\partial T}$	Temperature range ΔT
[1		4% (estimated)]			
3	198 g	4.5% (freezing)		79×10^{-6}/°C	950–1150°C
4	184±1 g	5.0% (freezing)	30 min	76×10^{-6}/°C	950–1150°C
5	181 g	5.6% (melting)	45 min		
		6.3% (freezing)	80 min	79×10^{-6}/°C	940–1020°C
Average		5.4±0.4%		78±1 $\times10^{-6}$/°C	950–1150°C

* V_s = volume of solid, V_l = volume of liquid; subscript 0 denotes value at melting point (934.5°C). [D. M. Van Winkle, this laboratory, private communication.]

Insofar as possible, the same germanium was used in all runs. It was *n* type, 20 ohm cm or better at the beginning, and *p* type, 1–2 ohm cm at the end. The resistivity decreased toward the top of the final ingot, indicating that freezing had indeed occurred from the bottom up.

There have been several indications that liquid germanium may show anomalous behavior near the melting point similar to that observed for water. Some of these appear to be valid, although such factors as gas bubbles, variations of temperature within the melt, floating contaminants on the surface of the germanium, and the absorption or leakage of germanium by or through the graphite crucibles undoubtedly have caused some of the experimental difficulties and irregularities observed. Leakage through the crucible during freezing of as much as 0.8 percent of the germanium has been detected. However, for run 5, regardless of how the data have been analyzed, there still remains an apparent 0.75 percent variation in the density of liquid germanium at its melting point. In run 5, the germanium was melted under good control starting from a known absolute reference level. For the next 2–3 hours, difficulties probably due to several different causes were experienced in making valid position readings. After the probe was removed and cleaned, the trouble cleared up, and a normal freezing run was made. With the initial level of the solid at 0, the level of the liquid in the 0.25 in. diameter neck, immediately after melting, corrected to the melting point, was −2.40 in. The level

of the liquid just before freezing was −2.81 in., and that of the solid after freezing −0.10 in. All levels have been corrected for the rounding of the liquid meniscus. The uninterrupted trend toward greater values of $\Delta V/V$ the more the germanium was used suggests that impurities leached from the graphite may have affected the structure and density of the liquid. Unfortunately time has not yet permitted the additional study necessary to resolve this problem.

[1] Klemm, Spitzer, Lingenberg, and Junker, Monatsh. Chem. 83, 629 (1952).

On the Structure of Sym-Tetrabromoethane

R. E. KAGARISE
Naval Research Laboratory, Washington, D. C.
(Received November 15, 1954)

THE existence of rotational isomers in certain halogenated ethanes is perhaps most strikingly demonstrated by the marked simplification which occurs in their vibrational spectra upon solidification. This simplification occurs because only one isomeric species exists in the crystalline solid, whereas all of the various isomers contribute to the spectrum in the liquid or vapor state. In liquid 1,2-dibromoethane the *trans*-form (C_{2h} symmetry) and the skew or *gauche*-form (C_2 symmetry) are generally accepted as being the low and high energy form, respectively.[1] When this compound is solidified, all of the molecules assume the *trans*-configuration and those lines in the spectrum of the liquid due to the *gauche*-form are absent in the spectrum of the solid. Thus, by comparing these two spectra one can readily separate the bands due to the different isomers.

In 1,1,2,2-tetrabromoethane, however, the relative stability of the two isomeric species is reversed and the *gauche* is now the more stable or low energy form, while the *trans* is the high energy form. The energy difference between these two isomers in the liquid state is about 950 calories/mole.

We have recently studied the infrared absorption spectrum of liquid and crystalline $CHBr_2$-$CHBr_2$ in the region from 2–15 μ using a Perkin-Elmer Model 21 Spectrometer. The spectra thus obtained are shown in Fig. 1. The wavelengths and frequencies of the absorption maxima are listed in Table I. As expected, many of the bands present in the spectrum of the liquid disappear with solidification. Outstanding examples are the strong bands at 1244, 1196, 1134, 1009, 829, and 706 cm^{-1}. It has been shown in an earlier investigation,[2] that these bands are the result of the more stable isomer, i.e., the *gauche*-form. One must conclude, therefore, that in crystalline sym-tetrabromoethane all of the molecules

TABLE I. Infrared absorption spectrum of liquid and crystalline sym-tetrabromoethane.

Liquid λ (microns)	Liquid (cm^{-1})	Crystalline solid λ (microns)	Crystalline solid (cm^{-1})
2.400 *w*	4167	2.400 *w*	4167
3.335 *s*	2998	3.335 *s*	2998
4.120 *w*	2427	4.130 *w*	2421
4.415 *w*	2265	4.415 *w*	2265
7.210 *w*	1387	...	
7.375 *vw*	1356	...	
7.655 *vw*	1306	7.630 *vw*	1311
7.820 *vw*	1279	7.830 *vw*	1277
8.040 *s*	1244	...	
8.360 *m*	1196	...	
8.725 *s*	1146	8.740 *s*	1144
8.815 *vs*	1134	...	
8.950 *m*	1117	8.960 *m*	1116.0
9.905 *s*	1009	...	
10.820 *vw*	924	...	
11.150 *vw*	897	...	
11.660 *vw*	858	11.680 *m*	856
12.055 *m*	829	...	
12.700 *vw*	787	...	
13.160 *w*	760	12.990 *m*	770
14.170 *vs*	706	...	

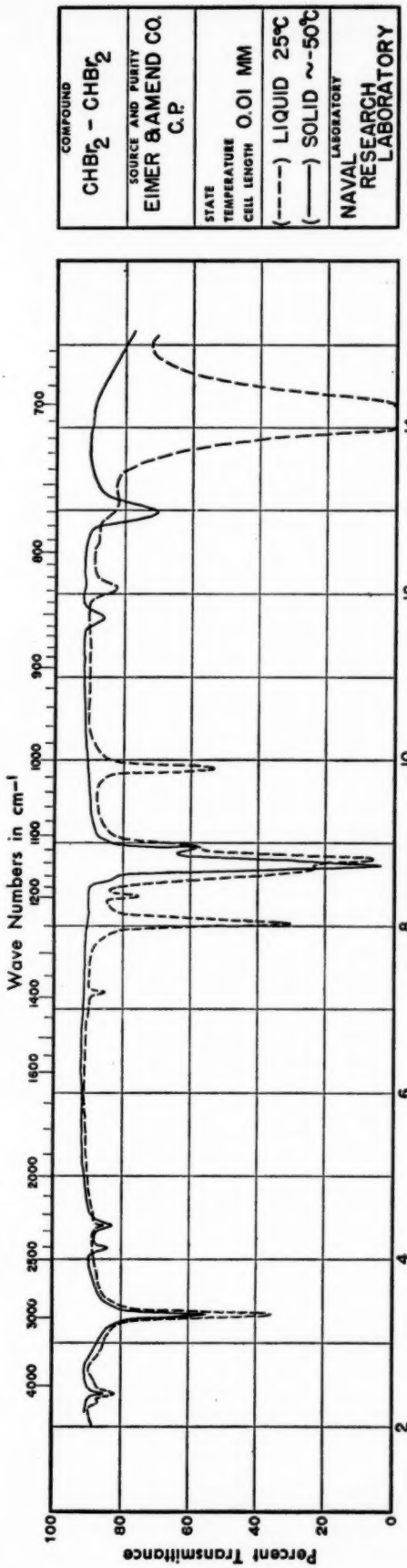

FIG. 1.

assume *trans*-configurations, in spite of the fact that in the liquid state the *trans* isomer is the high energy form. This situation may be responsible for the marked tendency of the compound under consideration to form a glass (supercooled liquid) rather than a crystal. When the temperature is lowered, the concentration of *trans*-molecules is reduced as required by the thermal equilibrium conditions. Accordingly, the probability of finding a sufficient number of *trans*-molecules in proximity to initiate crystalline growth is reduced.

Moreover, energy must be added to a molecule in order to convert it from the *gauche*- to *trans*-form, so that one might expect sym-tetrabromoethane to exhibit an abnormally low heat of fusion.

A similar situation with respect to the relative stability of the rotational isomers exists in the case of liquid 1,1,2,2-tetrachloroethane. However, all attempts to crystallize thin films of this compound have been unsuccessful to date.

[1] J. T. Neu and W. D. Gwinn, J. Chem. Phys. **18**, 1642 (1950).
[2] R. E. Kagarise and D. H. Rank, Trans. Faraday Soc. **48**, 394 (1952).

Decomposition of Methyl Alcohol by Co^{60} Gamma Radiation

WILLIAM R. MCDONELL* AND SHEFFIELD GORDON
Chemistry Division, Argonne National Laboratory, Lemont, Illinois
(Received August 19, 1954)

THE yields of decomposition products resulting from Co^{60} gamma irradiation of methyl alcohol have been determined. Acetone-free reagent grade methyl alcohol (Baker and Adamson) was deaerated by evacuation through a liquid nitrogen trap with a mechanical pump and irradiated at room temperature in 12-ml Pyrex cells. The dosage rate corresponded to 3.0×10^{20} ev/liter-min energy absorption in 0.8 *N* sulfuric acid, as determined using the aqueous ferrous sulfate dosimeter, with a specific yield of 15.6 ferric ions per 100 ev.[1] Calculation from absorption coefficients[2] indicated a 79 percent absorption efficiency of methyl alcohol compared to 0.8 *N* sulfuric acid, giving a dose rate of 2.4×10^{20} ev/liter-min for the alcohol irradiations.

Gaseous decomposition products were measured on samples irradiated from 15 to 60 minutes at room temperature. The gases were extracted from the alcohol into vacuum by complete distillation of the irradiated sample through a liquid nitrogen trap. Analyses for hydrogen, carbon monoxide, and methane were carried out by the Saunders-Taylor manometric technique.[3] Gaseous products volatile between dry ice and liquid nitrogen temperatures were negligible (<0.5 percent) in these samples.

Oxidation products, formaldehyde, and ethylene glycol, were determined in the liquid phase on samples irradiated from one to five days at room temperature. Formaldehyde was precipitated directly by dimedone (5,5-dimethylcyclohexanedione-1,3) from dilute aqueous solution of the irradiated alcohol buffered at *p*H 4.6,[4] as was ethylene glycol after oxidative splitting to formaldehyde by periodic acid, using a technique previously described.[5]

The decomposition products determined were all formed linearly with irradiation dosage, and yields were derived from the slopes of the irradiation curves. A summary of the specific yields is given in Table I. For comparison, the corresponding yields for products formed in the bombardment of methyl alcohol with 28-Mev cyclotron-accelerated helium ions are also given.[5]

TABLE I. Products of the decomposition of methyl alcohol by Co^{60} gamma radiation and by 28-Mev He ions.

Product	*G* (molecules/100 ev) Co^{60} gamma rays	*G* (molecules/100 ev) 28-Mev He ions[a]
H_2	4.0 ±0.3	3.46±0.05
CO	0.16±0.02	0.23±0.01
CH_4	0.24±0.06	0.36±0.01
Formaldehyde	1.3 ±0.1	1.67±0.05
Ethylene glycol	3.0 ±0.2	1.74±0.04

[a] See reference 5.

Especially notable is the difference in the ratio of ethylene glycol to formaldehyde in the two types of irradiations. Phibbs and Darwent[6] have shown in the photolysis of methanol vapor that formaldehyde formation is a high activation energy process, competing substantially with glycol formation only at temperatures above 400°C. This suggests that formaldehyde formation may involve reactions taking place only in the small, highly energized regions of the initial energy absorption, and that it is the chemically active species which escape these regions which are responsible for glycol formation.

Phibbs and Darwent proposed that the formation of formaldehyde occurs through reactions (1) and (2):

$$CH_3OH \rightarrow CH_2OH+H \quad (1)$$

$$CH_2OH \rightarrow H_2CO+H. \quad (2)$$

The glycol formation is necessarily bimolecular and to account for its increased yield in alcohol irradiated with the less densely activating gamma radiation, the following mechanism is proposed:

$$H+CH_3OH \rightarrow CH_2OH+H_2. \quad (3)$$

$$2CH_2OH \rightarrow CH_2(OH)CH_2(OH) \quad (4)$$

$$2H \rightarrow H_2 \quad (5)$$

$$H+CH_2OH \rightarrow CH_3OH. \quad (6)$$

Promotion of reactions (5) and (6) by a high concentration of radical species in the heavy particle reaction spurs would reduce the yield of hydrogen atoms available for reaction with alcohol molecules in reaction (3), and thus decrease the net yield of glycol resulting from heavy-particle radiation as compared with that from the less densely activating gamma radiation.

A single gamma-ray irradiation conducted at 0°C resulted in a yield of formaldehyde equal to that obtained at room temperature, while ethylene glycol was produced with a yield of 2.4±0.2 molecules/100 ev, appreciably lower than the room temperature yield. This result needs to be verified, but such a dependence upon temperature would indicate that the formation of ethylene glycol involves a reaction occurring to some extent in homogeneous solution, where such bulk temperature effects apply.

The authors are indebted to Dr. E. J. Hart and Dr. O. C. Simpson for many helpful discussions.

* Employee of E. I. Du Pont de Nemours on loan to Argonne National Laboratory. Present address: Savannah River Laboratory, Augusta, Georgia.
[1] C. J. Hochandel and J. A. Ghormley, J. Chem. Phys. **21**, 880 (1953).
[2] C. M. Davisson and R. D. Evans, Revs. Modern Phys. **24**, 79 (1952).
[3] W. K. Saunders and H. A. Taylor, J. Chem. Phys. **9**, 616 (1941).
[4] J. H. Yoe and L. C. Reid, Ind. Eng. Chem. Anal Ed. **13**, 238 (1951).
[5] A. S. Newton and W. R. McDonell (to be published); W. R. McDonell, University of California Radiation Laboratory Publication, UCRL-1378 (July 6, 1941).
[6] M. K. Phibbs and B. de D. Darwent, J. Chem. Phys. **18**, 495 (1950).

Decomposition of Methyl Alcohol—Water Solutions by Co^{60} Gamma Radiation

WILLIAM R. MCDONELL*
Chemistry Division, Argonne National Laboratory, Lemont, Illinois
(Received August 19, 1954)

THE yields of formaldehyde and ethylene glycol resulting from Co^{60} gamma irradiation of methyl alcohol—water solutions have been determined over the composition range 100 to 1 volume percent methyl alcohol. The solutions were prepared from acetone-free reagent grade methyl alcohol (Baker and Adamson), which was added without further purification to triply-distilled water. The solutions were deaerated and irradiated as described in the previous communication.[1] Dosage rates were calculated from atomic densities and absorption coefficients[2] of the solutions,

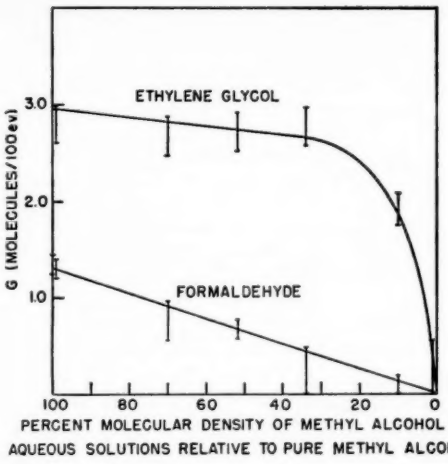

FIG. 1. Yield of formaldehyde and ethylene glycol in methyl alcohol—water solutions irradiated with Co^{60} gamma rays.

referred to a standard absorption in 0.8 N sulfuric acid of 3.00 $\times 10^{20}$ ev/liter min. This calibration was obtained by use of the aqueous ferrous sulfate dosimeter, with a specific yield of 15.6 ferric ions per 100 ev.[3]

Formaldehyde and ethylene glycol were determined by the dimedone method[4] on samples irradiated for one to five days. The product concentrations ranged from 0.001 to 0.100 M and in general were proportional to the length of time of irradiation. Possible exception to this occurred in formaldehyde formation at the low alcohol concentrations (<50 percent), where a tendency toward saturation to steady-state concentrations of less than 0.010 M was noted. Specific yield values were taken from the slopes of curves representing the build-up of product as the irradiations proceeded; the values obtained for formaldehyde may fail to represent precisely initial yields at low alcohol concentrations.

The results are shown in Fig. 1, where specific yields are plotted against the partial density of methyl alcohol molecules, expressed as a percentage of that in pure methyl alcohol. Formaldehyde falls off linearly with decreasing methyl alcohol, while ethylene glycol remains at a high value down to rather low alcohol concentrations.

These data suggest that formaldehyde is a characteristic product of the radiolytically-excited methyl alcohol molecule, formed in a yield proportional to the number of alcohol molecules exposed to the radiation. On the other hand, excess ethylene glycol is formed as a result of attack by the radical species of the water decomposition, which may be represented as follows:

$$H_2O \rightarrow H+OH$$
$$H+CH_3OH \rightarrow H_2+CH_2OH$$
$$OH+CH_3OH \rightarrow H_2O+CH_2OH$$
$$2CH_2OH \rightarrow CH_2(OH)CH_2(OH).$$

These results are in accord with the hypothesis of the preceding communication,[1] i.e., that formaldehyde formation is a rapid high activation energy process, occurring by decomposition of the methanol molecule essentially within a "track" or reaction spur, while glycols are formed characteristically in relatively homogeneous solution by reaction of CH_2OH radicals, produced either through radiation activation or by free radical attack.

The author is indebted to Dr. E. J. Hart and Dr. O. C. Simpson for enlightening discussion of this research.

Depolarization Ratios of the Raman Bands of Thionyl Chloride

G. ALLEN* AND C. A. MCDOWELL†
Division of Pure Chemistry, National Research Council, Ottawa, Canada
(Received October 11, 1954)

ALL previous depolarization data[1-4] on the Raman bands of thionyl chloride agree in that the bands at 1230, 490, and 344 cm^{-1} are polarized and in that the bands at 445 and 284 cm^{-1} are depolarized. The classification of the remaining fundamental at 194 cm^{-1} as a polarized band is doubtful because of the experimental method used to obtain these data. The data were obtained by the photographic method where the accurate estimation of a depolarization ratio is a difficult procedure. Furthermore, the spectra were excited by high-pressure arcs and the high background obtained in the region of the exciting line when this type of arc is used makes the estimation of a depolarization ratio exceedingly difficult. Hence, although the Raman band at 194 cm^{-1} in thionyl chloride has been reported as a polarized band ($\rho = 0.6$)[1,3,4] it is possible that it could be a depolarized band ($\rho = 6/7$) as reported by Venkateswarlu.[2] The unequivocal classification of this Raman band as polarized or depolarized is necessary to determine the geometry of thionyl chloride since a recent infrared investigation[5] has not given conclusive evidence that the molecule is nonplanar.

We have, therefore, reinvestigated the Raman spectrum of thionyl chloride using a photoelectrically recording spectrometer equipped with a low-pressure water-cooled mercury arc which greatly reduces the background in the region of the exciting line. The spectra were excited by the 4358A Hg line. Depolarization measurements were made by the method of Edsall and Wilson[6] and the observed depolarization ratios were corrected for convergence by the method of Rank and Kagarise.[7] A direct reproduction of the traces obtained is shown in Fig. 1. Examination of the figure shows that the background is flat thus allowing accurate measurements of the depolarization ratios of all six bands to be made. In Table I the observed and corrected depolarization ratios are presented; the experimental error for ρ_{obs} is ± 0.02, and for ρ_{true} the error is ± 0.05.

These results leave little room to doubt that the Raman band in thionyl chloride at 194 cm^{-1} is polarized. The reversal in the intensities of the perpendicular and parallel components of the 194 cm^{-1} and 284 cm^{-1} bands also shows clearly that the former is a polarized band. We conclude, therefore, that there are 4 polarized and 2 depolarized fundamentals in the Raman spectrum of thionyl chloride and that the molecule is nonplanar and belongs to the point group C_s. If the molecule were planar and so belonged to the point group C_{2v}, three of the fundamental Raman bands would be polarized and three depolarized. Our data are in agreement with electron diffraction data[8] and with the more recent

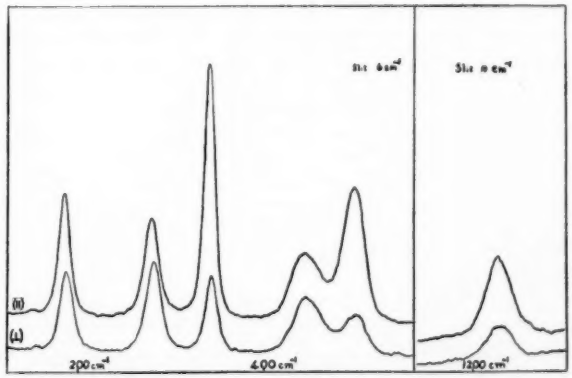

FIG. 1. Photoelectric record of Raman spectrum of $SOCl_2$. The upper record (‖) was made with parallel polarized exciting light, the lower record (⊥) with perpendicularly polarized exciting light.

*Employee of E. I. Du Pont de Nemours on loan to Argonne National Laboratory. Present address: Savannah River Laboratory, Augusta, Georgia.

[1] W. R. McDonell and Sheffield Gordon, J. Chem. Phys. **23**, 208 (1955).
[2] C. M. Davisson and R. D. Evans, Revs. Modern Phys. **24**, 79 (1952).
[3] C. J. Hochanadel and J. A. Ghormley, J. Chem. Phys. **21**, 880 (1953).
[4] J. H. Yoe and L. C. Reid, Ind. Eng. Chem. Anal. Ed. **13**, 238 (1941); W. R. McDonell, University of California Radiation Laboratory Publication, UCRL-1378 (July 6, 1951); see also Reference 1.

TABLE I.

$\Delta\nu$ cm^{-1}	ρ_{obs}	ρ_{true}[a]
1230	0.38	0.25
490	0.29	0.15
445	0.95	6/7
344	0.31	0.18
284	0.98	6/7
194	0.67	0.53

[a] ρ_{true} is the observed depolarization ratio (ρ_{obs}) corrected for convergence.

investigations of the Raman spectrum[3,4] by the photographic method. The assignment of the observed infrared spectrum given by Martz and Lageman in Table I of their recent paper is consistent with these results.

We wish to thank Dr. H. J. Bernstein for facilities in his laboratory and for helpful advice.

* National Research Laboratories Postdoctorate Fellow, 1952–54.
† Guest worker, National Research Laboratories, summer, 1954. Present address: Department of Chemistry, University of Liverpool, Liverpool, England.

[1] J. Cabbannes and A. Rousset, Ann. phys. **19**, 259 (1933).
[2] K. Venkateswarlu, Proc. Indian Acad. Sci. **10A**, 156 (1939).
[3] Gerding, Smit, and Westrik, Rec. trav. chim. **60**, 513 (1941).
[4] C. A. McDowell, Trans. Faraday Soc. **49**, 371 (1953).
[5] D. E. Martz and R. T. Lageman, J. Chem. Phys. **22**, 1193 (1954).
[6] J. T. Edsall and E. B. Wilson, J. Chem. Phys. **6**, 124 (1938).
[7] D. H. Rank and R. E. Kagarise, J. Opt. Soc. Am. **40**, 89 (1950).
[8] K. J. Palmer, J. Am. Chem. Soc. **60**, 2360 (1938).

Structure and Barrier to Internal Rotation of Formic Acid from Microwave Data

R. G. LERNER, J. P. FRIEND, AND B. P. DAILEY
Department of Chemistry, Columbia University, New York 27, New York
(Received October 20, 1954)

THE determination of the precise molecular structure of the monomer of formic acid is a difficult problem to which a considerable number of workers[1–4] in infrared and microwave spectroscopy and electron and x-ray diffraction have contributed somewhat conflicting results. The microwave spectra of five isotopically substituted species of formic acid have been studied in this laboratory and a number of rotational transitions have been identified and measured. The observed frequencies are given in Table I. The spectral identifications were confirmed by observation of the Stark effect for each line. If small centrifugal distortion effects are neglected, the frequency of the $0_{00}\rightarrow 1_{01}$ line is equal to $B+C$, $1_{11}\rightarrow 2_{12}$ equals $B+3C$, and $1_{10}\rightarrow 2_{11}$ equals $3B+C$, where B and C are the two smaller, nearly degenerate rotational constants of the prolate rotor. The measurement of any two of these lines for an isotopic species of formic acid determines the values of the two rotational constants; derived values of the rotational constants are given in Table II. The results for formic acid are in partial disagreement with the data of Rogers and Williams[2] in that a different line has been identified as the $5_{14}\rightarrow 5_{15}$ transition. The results presented here for HCOOH and HCOOD are in good general agreement with those given in a recent paper by Trambarulo and Moser,[4] although certain of the frequency differences are greater than the sum of the two quoted probable errors.

TABLE I. Observed frequencies.

(3)	$0_{00}\rightarrow 1_{01}$ Mc	$1_{10}\rightarrow 2_{11}$ Mc	$1_{01}\rightarrow 2_{02}$ Mc	$1_{11}\rightarrow 2_{12}$ Mc
$HC^{12}OOH$	22 471.0±0.3	46 581.4±0.6	44 911.4±0.6	43 303.3±0.6
$HC^{13}OOD$	21 732.6±0.3	45 257.8±0.6	43 420.2±0.6	41 673.0±0.6
$DC^{13}OOH$	22 011.3±0.3	46 122.6±0.6		41 923.0±0.6
$DC^{12}OOD$	21 293.9±0.3	44 813.4±0.6		
$HC^{13}OOH$	22 432.6±0.3			43 190.4±0.6

	$4_{13}\rightarrow 4_{14}$ Mc	$5_{14}\rightarrow 5_{15}$ Mc
$HC^{13}OOH$		24 569.1±0.3
$HC^{13}OOD$		26 865.5±0.3
$DC^{12}OOH$	20 989.6±0.3	
$DC^{12}OOD$	22 237.5±0.3	

The most reasonable set of structural parameters which has been found to give a fairly good fit to the observed rotational constants is presented in Table III. In deriving this model, the molecule was assumed to have a planar structure. The neglect of centrifugal distortion and zero-point vibrational effects is sufficient to prevent an exact fit of the calculated to the observed rotational constants.

If the molecule is planar, it would be expected to undergo a torsional vibration of the O−H group about the C−O bond. A weak line at 22 432.7 Mc has been identified as the torsional satellite of the $0_{00}\rightarrow 1_{01}$ line for HCOOH. Rough measurements of the intensity ratio of the ground state and excited state transitions using the oscilloscope gave a value of approximately 25; this corresponds to a torsional frequency of 667 cm^{-1}, which is in good agreement with the value of 658 cm^{-1} obtained by Bonner and Hofstadter[5] from infrared data. The large hindering potential for torsion and the short bond between C and O−H both seem to indicate that this bond has an unusually large amount of double-bond character.

TABLE II. Rotational constants.

	Observed		Calculated	
	B	C	B	C
$HC^{12}OOH$	12 055.1 Mc	10 416.0 Mc	12 055.3 Mc	10 416.1 Mc
$HC^{12}OOD$	11 762.5	9 970.1	11 764.6	9 977.2
$DC^{12}OOH$	12 055.6	9 955.8	12 051.4	9 955.1
$DC^{12}OOD$	11 759.8	9 534.1	11 754.2	9 539.6
$HC^{13}OOH$	12 053.7	10 378.9	12 054.1	10 377.7

TABLE III. Suggested structure for formic acid.

C−H	1.085 A
C=O	1.245 A
C−O	1.312 A
O−H	0.95 A
∠OCO	124° 18′
∠COH	107° 48′
∠HCO	117° 51′
O−O	2.261 A

[1] V. Z. Williams, J. Chem. Phys. **15**, 232 (1947).
[2] J. D. Rogers and D. Williams, Phys. Rev. **83**, 210 (1951).
[3] I. L. Karle and J. Karle, J. Chem. Phys. **22**, 43 (1954).
[4] R. Trambarulo and P. M. Moser, J. Chem. Phys. **22**, 1622 (1954).
[5] L. Bonner and R. Hofstadter, J. Chem. Phys. **6**, 531 (1938).

Fine Structure of Olefine Deuteration

TOMINAGA KEII
Research Institute for Catalysis, Hokkaido University, Sapporo, Japan
(Received October 7, 1954)

WAGNER *et al.*[1] proposed a new mechanism for the olefine hydrogenation in order to explain their findings that a random distribution law holds among the observed relative amounts of deutero-butanes from the *cis*-2-butene deuteration. Their mechanism has been supported by Laidler *et al.*[2] who found the same distribution in the data reported by Turkevich *et al.*[3] On the other hand, the writer[4] explained the experiment of the latter authors by the "associative mechanism."[5,6]

According to the associative mechanism, the scheme of pro-

pylene hydrogenation may be written as,

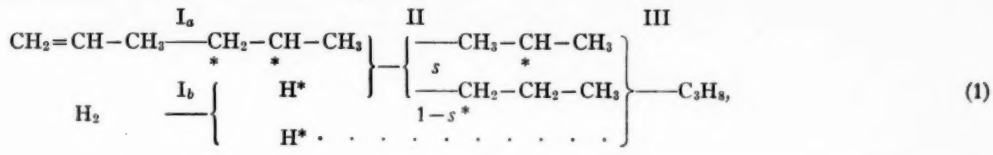

(1)

where asterisk indicates a chemisorption bond, and s the probability that a chemisorbed propylene becomes an iso-propyl radical. Applying the writer's theory[4] to (1) with the assumption that the rates of I_a are faster than the others, we obtain the expressions for the relative amounts of the initial products:

Hydrogen $$H_2:HD=1:2\Omega, \quad (2)$$

Propane $$d_0:d_1:d_2\sim 1:2\Omega+O(R):\Omega^2+O(R)(2\Omega+O(R)),$$
$$d_n/d_2\sim O^{n-2}(R), \quad (2\leq n\leq 8). \quad (3)$$

Propylene $$d_n/d_0\sim O^n(R), \quad (0\leq n\leq 6) \quad (4)$$

with

$$\Omega=y/(1-y)=(12/3+2s)(v_R(I_b)/v_L(II))>R$$
$$=y(v_L(II)/v_L(I_a))<1, \quad (5)$$

where y represents the ratio of D* to (D*+H*), and $v_R(I_a)$, $v_L(I_a)$ etc. the forward and the backward rates of I_a etc.

Applying the theory to some appropriate schemes of 2-butene hydrogenation, we have similar expressions as above.

From these we conclude that the relative amounts of alkenes and of alkanes ($n\geq 2$) always decrease with increase of n, while those of alkanes ($n\leq 2$) and of hydrogens increase or decrease when $\Omega\gg 1$ or $\Omega\ll 1$.

According to the random distribution theory,[1,2] the relative amounts of alkanes may be given by

$$d_n/d_0=(N!/(N-n)!n!)Q^n, \quad (0\leq n\leq N) \quad (6)$$

where Q represents the ratio of D to H on the surface (in any form), and that of hydrogen by

$$H_2:HD=1:2Q. \quad (7)$$

The comparison of our theory with the ethylene deuteration[3] was described in the previous paper,[4] where it was predicted that the predominant formation of H_2 must be found at the temperatures below *ca* 130°C. This is in agreement with the observation of Twigg and Rideal[7] that the hydrogen returned was mainly H_2 at temperatures up to *ca* 150°C. The distribution of deutero-butanes[1] can be explained also by our theory (3) with $\Omega\sim 1.2$ and $O(R)\sim 0.6$. Most of the data of deutero-propanes[8] are those of the final products. There are, however, the two data of the initial ones: that $d_0:d_1:d_2:d_3:d_4:d_5:--=1.00:2.21:1.91:0.94:0.45:0.24:--$, obtained from the reaction of 102 mm propylene and 91 mm deuterium, and that $d_1=50$ percent and $d_2=30$ percent from 100 mm propylene and 307 mm deuterium. The former can be explained by (6) with $Q\sim 0.27$ as well as by (3) with $\Omega\sim 0.9$ and $O(R)\sim 0.5$. These two data clearly show that the maximum of distribution lies at $n=1$, from which the random distribution theory (7) predicts $H_2>HD$ while our theory (2) $H_2<HD$. The latter prediction is in agreement with the observation[8] of $H_2<HD$ from 98 mm propylene and 140 mm deuterium, the condition of which lies between the above two. Moreover the random distribution theory (6) has no agreement with the data of the final products from the reactions of the larger excesses of deuterium, as shown in Table I. It is surprising that our theory (3), which is valid for the initial ones, has apparently good agreements with the data.

It seems to the writer that all phenomena of this type can be explained satisfactorily by the "associative mechanism"[6] without introducing any new mechanism.

TABLE I. Comparisons of the observed distributions to the theoretical ones.[a] ($P_{prop}=13$ mm Hg, 18°C $d_0=1$).

P_{deut} mm		d_1	d_2	d_3	d_4	d_5	d_6	d_7	d_8	Max
16.5	obs	1.98	1.79	1.10	0.88	0.64	0.42	0.27	0.05	d_1
	(6), $Q=0.25$	1.98	1.68	0.88	0.25	0.05	0.00	0.00	0.00	d_1
	(3), $\Omega=0.61$ $O(R)=0.61$	1.98	1.88	1.10	0.67	0.41	0.25	0.15	0.09	d_1
109.	obs	10.4	17.9	8.95	4.19	2.14	1.29	1.05	0.67	d_2
	(6), $Q=1.30$	10.4	47.4	123.	200.	271.	135.	50.2	8.03	d_5
	(3), $\Omega=4.94$ $O(R)=0.52$	10.4	29.8	8.95	4.65	2.42	1.26	0.66	0.34	d_2
521.	obs	14.0	32.1	13.2	5.36	2.64	1.29	1.07	0.72	d_2
	(6), $Q=1.75$	14.0	85.5	299.	650.	1910.	806.	403.	88.2	d_5
	(3), $\Omega=6.80$ $O(R)=0.41$	14.0	52.0	13.2	5.41	2.22	0.91	0.37	0.15	d_2

[a] Values of Q, Ω and $O(R)$ were obtained from $d_1/d_0=8Q$, $d_3/d_2=O(R)$, and $d_1/d_0=2\Omega+O(R)$.

[1] Wagner, Wilson, Otvos, and Stevenson, J. Chem. Phys. **20**, 338, 1331 (1952).
[2] Markham, Wall, and Laidler, J. Chem. Phys. **20**, 1331 (1952).
[3] Turkevich, Schissler, and Irsa, J. Phys. & Colloid Chem. **55**, 1078 (1951).
[4] T. Keii, J. Chem. Phys. **22**, 144 (1954); J. Research Inst. Catalysis, Hokkaido Univ. **3**, 36 (1953).
[5] Horiuti and Polanyi, Trans. Faraday Soc. **30**, 1164 (1934).
[6] Horiuti, Catalyst **2**, 1 (1948).
[7] Twigg and Rideal, Proc. Roy. Soc. (London) **A171**, 55 (1939).
[8] Bond and Turkevich, Trans. Faraday Soc. **49**, 281 (1953).

Barrier Hindering Internal Rotation in Methylamine*

J. G. ASTON AND FRANK L. GITTLER†
College of Chemistry and Physics, The Pennsylvania State University, State College, Pennsylvania

(Received November 15, 1954)

VALUES of the barrier hindering internal rotation in methylamine of 1800 cal mole^{-1} [1] and 1940 cal mole^{-1} [2] have recently been estimated from the microwave spectrum.

We have recently determined values of the entropy of methylamine by measuring the equilibrium constant and hence the free energy change in the reaction

$$CH_3NH_2Cl(s)=CH_3NH_2(g)+HCl(g) \quad (A)$$

at 298.16°K from cell measurements in absolute ethyl alcohol. In these measurements the hydrogen chloride partial pressure in equilibrium with the solid salt at certain amine partial pressures was determined by measuring the electromotive force of the cell

$$H_2, HCl(g), AgCl(s)Ag(s)$$

with very pure ethyl alcohol as solvent.[3] Measurements were made at several temperatures thus allowing the entropy of methylamine to be obtained from the temperature coefficients since the entropies of methylammonium chloride[4] and hydrogen chloride[5] were known. Indeed it was to determine the barrier that the measurements were made since there was some doubt about the calorimetric (third law) value[6] of the entropy in view of its lack of agreement with the value calculated on the bases of a barrier of 1520 cal mole^{-1} determined from an infrared line.[7a,b] Table I summarizes the values of the entropy (column 2) obtained from the equilibrium data along with the values calculated (column 3) on the basis of a barrier of 1900 cal mole^{-1}, and the spectroscopic data previously used by Aston and Doty,[7b] except using moments calculated from bond distances. The agreement is well within experimental error. In the last column of the table

TABLE I. The spectroscopic entropies of methylamine based on a barrier of 1900 cal mole^{-1}.

T °K	$S^0_{CH_3NH_2}$ exp. (slope) eu ±0.13	$S^0_{CH_3NH_2}$ (spect.) eu	ΔH_0^0 cal mole^{-1}
276.16	57.13	57.23	43 515
282.16	57.39	57.50	43 515
295.16	57.97	58.03	43 506
298.16	58.10	58.15	43 516
301.16	58.24	58.28	43 509
308.16	58.53	58.55	43 494
313.16	58.74	58.76	43 481
			Av 43 505
		From $\Delta H^0_{298.16}$	43 469 ±54[a]

[a] This error is based on the experimental error in $\Delta H^0_{298.16}$ and in ΔS from the equilibrium data.

are given the values of ΔH_0^0 at (0°K) for reaction A computed from the free energies of reaction A deduced from the equilibrium measurements. For this purpose the $(F^0-E_0^0)$ values for methylamine were computed from the spectroscopic data[7] using a barrier of 1900 cal mole^{-1}. The $(F^0-E_0^0)$ values for methylammonium chloride were calculated from the calorimetric data,[3] while the spectroscopic values were used for hydrogen chloride.[4]

It is also possible to calculate a value of ΔH_0^0 (at 0°K) for this reaction using the value of $\Delta H^0_{298.16°K}$[4] determined calorimetrically. This value is shown at the foot of column 4 of Table I.

The agreement of this value is well within experimental error. The value of the entropy from the calorimetric (third law) data at the normal boiling point (266.84°K) is 56.42±0.3 eu, while the entropy calculated from the spectroscopic data, using bond distances, with a barrier of 1900 cal mole^{-1} is 56.83 eu or 56.74 with spectroscopic moments. The assigned error of ±0.3 eu in the calorimetric value is due to observed hysteresis in the solid heat capacities of methylamine. In view of this the agreement is satisfactory. It now seems certain that the barrier of 1520 cal mole^{-1} assumed by Aston and Doty[7b] in calculating an entropy from the data of Owens and Barker[7a] was incorrect and that the interpretation of the microwave data is essentially correct. The values of the spectroscopic entropy in Table I and at the normal boiling point are thus the correct ones and the barrier is near 1900 cal mole^{-1}.

* This research was carried out under Contract N6 ONR-269 T. O. III of the Office of Naval Research.
† Present address, Sylvania Electric Products Inc., Montoursville, Pennsylvania.

[1] Shimoda, Nishikawa, and Itoh, J. Chem. Phys. **22**, 1456 (1954).
[2] David R. Lude, J. Chem. Phys. **22**, 1613 (1954).
[3] Aston, Hu, and Gittler, J. Am. Chem. Soc. **76**, 4492 (1954).
[4] J. G. Aston and C. Ziemer, J. Am. Chem. Soc. **68**, 1405 (1946).
[5] W. F. Giauque and R. Overstreet, J. Am. Chem. Soc. **54**, 1736 (1932).
[6] Aston, Siller, and Messerly, J. Am. Chem. Soc. **59**, 1744 (1937).
[7] (a) R. G. Owens and E. F. Barker, J. Chem. Phys. **8**, 229 (1940). (b) J. G. Aston and Paul M. Doty, J. Chem. Phys. **8**, 743 (L) (1940).

On Photovariation of Conductivity in Non-Self-Maintained Region of a Low-Frequency Electric Discharge

N. A. RAMAIAH, B. D. KHOSLA, AND H. C. GAUR
Department of Chemistry, University of Delhi, Delhi, India
(Received November 10, 1954)

IN a narrow potential region below the threshold potential V_m of a self-maintained discharge, the current i in a system is given by

$$i=i_0 \exp\alpha d, \qquad (1)$$

where α is the Townsend first coefficient of ionization; d, the electrode separation; and $i_0=n_0\cdot e$; here, n_0 is the number of electrons of charge e produced by external radiation. With increase of intensity, or the number of photons, of the light, i increases exponentially [Eq. (1)]. Figure 1 gives data indicating, contrary to the expectations from (1), a decrease in i with moderate increase in

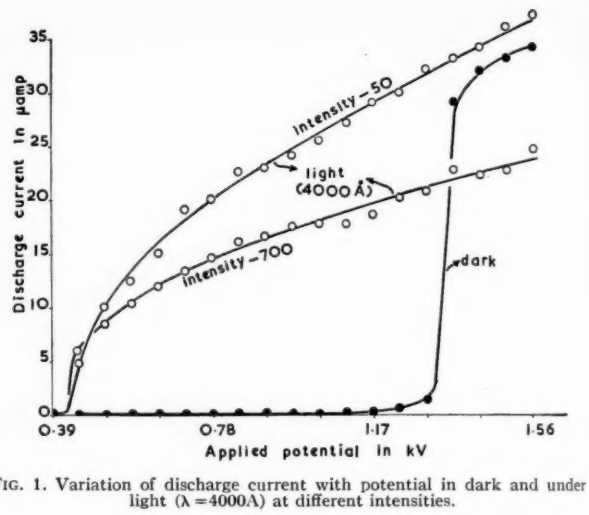

FIG. 1. Variation of discharge current with potential in dark and under light (λ = 4000A) at different intensities.

intensity of the radiation (λ=4000A) used for irradiating the discharge tube. The latter consisted of a cylindrical glass vessel containing iodine vapor (0.45 mm Hg); and was excited by external sleeve electrodes with 50-cycle potentials. At a potential below (V_m=) 1.30 kv, the conductivity in dark was negligible (Fig. 1); the current trace on an oscillograph was sinusoidal without superimposition of any pulses. Exposure of the system to even visible light increased i markedly; certain pulses appeared on the current trace.[1] These persisted so long as the radiation was on. When the external light was cut off, the initial value of i was restored and the current pulses disappeared. This increase of i under light is referred to as positive Joshi effect, $+\Delta i$.[1] From Fig. 1, it could be seen that the magnitude of $+\Delta i$ decreased with an increase of light intensity from 50 to 700 (relative units). Essentially similar data were reported by Arnikar[2] and others.[3] It may be added that this decrease in i with increase of light intensity, distinct from the familiar negative photoelectric effect,[4] could not be observed in systems of which the preadsorbed water vapor layers on glass surface were removed before introducing iodine vapor therein. In what follows, an attempt is made to elucidate the decrease of i with increase of light intensity.

Let Θ be the number of photons entering the system due to external radiation; and ψ, their coefficient of absorption in the gas phase. If we assume the existence of pre-excited gas particles below V_m, the number of photoelectrons produced by the radiation is given by $\psi\Theta Z$, where Z is the coefficient of photoionization. Under fields, these photoelectrons generate avalanches in which the number of electrons or positive ions produced is roughly

$$N=\psi\Theta Z\cdot\exp\alpha d.$$

The electrons go to the anode, while positive ions move slowly towards the cathode. As a result, a varied field gradient (F) is developed near the cathode (see Fig. 2). Further,

$$F=f(N).$$

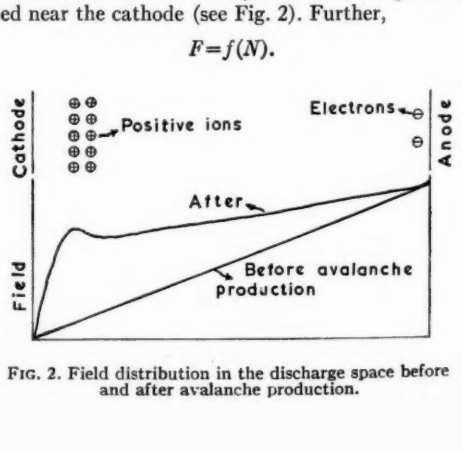

FIG. 2. Field distribution in the discharge space before and after avalanche production.

F controls the velocity of the positive ion falling on to the cathode, rather bombarding the molecules of H_2O adsorbed thereon; in other words, the energy E imparted to the adsorbed molecule by positive ion depends on F. When this energy E combined with the quantum energy of the radiation is enough to dissociate a surface molecule, the latter dissociates to give atoms or/and radicals. This process occurs at large F which, at a fixed applied potential and electrode separation, increases primarily with Θ or intensity of light; the factors ψ and Z are assumed to be roughly constant under the experimental conditions. As van der Waal's adsorption involves evaporation and condensation, the atoms or/and radicals produced on account of dissociation of adsorbed molecules *evaporate* and travel into the gas space where, due to their large electron affinity, these capture the photoelectrons to form negative ions. These last, because of their low mobility, are ineffective in avalanche production; and their formation leads, therefore, to a reduction in the conductivity at large intensity of light, as actually observed.

[1] Ramaiah, Bhatawdekar, and Subrahmanyam, J. Chem. Phys. **21**, 1160 (1953).
[2] H. J. Arnikar, J. Opt. Soc. Am. **43**, 804 (1953).
[3] Ramaiah, J. Sci. Research Benares Hindu Univ. **2**, 1 (1951–52).
[4] Hughes and DuBridge, *Photoelectric Phenomena* (McGraw-Hill Book Company, Inc., New York, 1932).

The Heat of Evaporation of Helium

JOHAN VAN DRANEN*
Laboratory for Analytical Chemistry, University of Amsterdam, Amsterdam, Netherlands
(Received October 11, 1954)

IN a series of Letters to the Editor the consequences of a hypothesis concerning the critical state have been discussed.[1] This hypothesis is as follows. The critical state is the result of the fact that at the critical point the average kinetic energy (K_c) is equal to the average (negative) potential energy (U_c), or $K_c+U_c=0$.

It has been proved that in the case of those substances for which experimental data are available (Ar, CH_4, N_2, CO_2, and H_2O) K_c is equal to U_c within the limits of error (a few percent).

An accurate determination of U_c is not possible, because there are great difficulties in obtaining the exact isotherms in the neighborhood of this point. Moreover, the values for the thermodynamic properties, deduced from the PVT-measurements, are in general even ten times more inaccurate. The uncertainty in this region is consequently much greater than elsewhere.

Habgood and Schneider obtained 1116 cal/mole for the internal energy of gas imperfection of xenon at the critical point.[2] This value, according to the hypothesis, should be equal to $-(3/2RT_c+P_cV_c)=-1032$ cal/mole. The experimental value is too high; this follows from the dependence of U', at the critical density, on the temperature. We obtain nearly the hypothetical value for U_c' if we extrapolate from $T_c+50°=340°$K.

In a recent article Palmer[3] concludes from his observations on the behavior of a fluid in the neighborhood of the critical point that these observations are consistent with the concept that within the fluid the energies of motion and of attraction are nearly equal.

We can obtain further support for the view that our hypothesis indicates the physical cause for the critical point if we can show that K_c is also equal to $-U_c'$ for those substances showing an anomalous behavior.

On the basis of the hypothesis we have calculated the zero-point energy of He(4) and He(3) at the critical point (Z_c), and we have found a good agreement with the interpolation formula of London, which gives Z as a function of the volume.[4]

Prigogine[5] has recently given the following formula for Z

$$Z=3Nh^2/8my(a-d)^2. \quad (1)$$

TABLE I. The heat of evaporation of helium (4).[a]

T	H (exp)[b]	H (theor.)[c]	H (theor.)[d]
4.23	21.2	23	19
4.59	17.2	19	16
4.71	15.2	17	14

[a] Units: °K and cal/mole.
[b] J. Kistenmaker, Ph.D. thesis (Leiden, 1945).
[c] Z_1 calculated with $y=4.5$.
[d] Z_1 calculated with $y=4.0$.

Here a is the mean distance between first neighbors, assuming a face-centered cubic lattice and d is the diameter of the particle. Furthermore y must be equal to or greater than 4; the best value, according to Prigogine, is 4.5. For Z_c Eq. (1) gives practically the same results as the formula of London (nearly 12 cal/mole instead of 11 cal/mole; the values according to the hypothesis are 10 and 11 cal/mole for He^4 and He^3 respectively).[6]

We have calculated the heats of evaporation (H) of He(4) at various temperatures, in order to have a further check of the values given in reference 4, Table I. For H we have the expression

$$H=U_g'-U_1'-Z_1(1)+\Delta K(\text{B.E.})+P(V_g-V_1),$$

where ΔK(B.E.) is the correction for the Bose-Einstein degeneration of liquid He(4). In order to obtain values for U' at different volumes, we have started from the accepted value for U_c', namely -27 cal/mole, and have assumed a linear dependency of U' on the density, which is always a very reasonable approximation.

The results, given in Table I, show a satisfactory agreement. Although this agreement is in no respect a definite proof for the accepted value for U_c', which we estimated as carefully as possible at the time, it follows from the "self-consistency" of the expressions for U' and Z, that the exact value for U_c' cannot differ much from the accepted one. For that reason we believe that helium does not violate the hypothesis, but actually gives it some support.

We have had much benefit from a discussion with Dr. R. J. Lunbeck on the accuracy of the calculation of thermodynamic functions from the PVT-measurements.

* Present address: Koninklijke/Shell-Laboratory, Amsterdam, Netherlands.
[1] J. van Dranen, J. Chem. Phys. **20**, 1175 (1952); J. Chem. Phys. **21**, 567, 1404, 2095 (1953).
[2] H. W. Habgood and W. G. Schneider, Can. J. Chem. **32**, 164 (1954).
[3] H. B. Palmer, J. Chem. Phys. **22**, 633 (1954).
[4] J. van Dranen, J. Chem. Phys. **21**, 2095 (1953).
[5] I. Prigogine, Advances in Phys. **3**, 131 (1954).
[6] It is certain that the value given by Eq. (1) for Z, at the large critical volume, is somewhat too high.

Intrinsic Viscosity of Flexible Macromolecules: Corrected Tables

JOHN G. KIRKWOOD, ROBERT W. ZWANZIG, AND RICHARD J. PLOCK
Sterling Chemistry Laboratory, Yale University, New Haven, Connecticut
(Received October 15, 1954)

IN a recent note,[1] attention was called to an error in the solution of the integral equation

$$\varphi(x)=f(x)-\lambda\int_{-1}^{+1}\frac{\varphi(t)}{(|x-t|)^{\frac{1}{3}}}dt; \quad -1\leq x\leq+1 \quad (1)$$

entering into the theory of viscosity of solutions of flexible macromolecules developed by Kirkwood and Riseman.[2] It is the purpose of this note to complete the solution and to correct Table I of the article of Kirkwood and Riseman for $F(x)$, the function which determines the intrinsic viscosity,

$$[\eta]=\left(\frac{N\zeta b^2}{3600\eta_0 M_0}\right)zF(\lambda_0 z). \quad \text{(KR 22)}$$

TABLE I.

x	$F(x)$	$xF(x)$
0.0	1.00	0.00
0.1	0.92	0.09
0.2	0.85	0.17
0.3	0.79	0.24
0.4	0.74	0.30
0.5	0.69	0.35
0.6	0.66	0.39
0.7	0.62	0.43
0.8	0.59	0.47
0.9	0.56	0.51
1.0	0.54	0.54
1.5	0.44	0.66
2.0	0.38	0.75
2.5	0.33	0.82
3.0	0.29	0.88
3.5	0.26	0.92
4.0	0.24	0.96
4.5	0.22	0.99
5.0	0.20	1.02
10.0	0.12	1.17
20.0	0.07	1.31
∞		1.48

The corrected Table I is presented above. The revised values of $xF(x)$ differ by less than seven percent from the old values, the maximum difference being in $\lim_{x\to\infty} xF(x)$, which is changed from 1.59 to 1.48. This requires a change in the numerical constant of Eq. (KR 24) from 2267 to 2435. The corrections are therefore of no practical significance in the use of the theory in interpreting structure, since they are within the limits of error of certain approximations underlying the formulation of the theory.

A brief description of the method of numerical solution of Eq. (1) will be presented, since it might prove useful to others encountering a similar problem. If the function $\varphi(x)$ is expanded in the Fourier series,

$$\varphi(x)=\sum_{k=-\infty}^{+\infty}\varphi_k e^{i\pi kx},\qquad f(x)=\sum_{k=-\infty}^{+\infty}f_k e^{i\pi kx}. \tag{2}$$

Equation (1) yields the following infinite set of linear equations for the coefficients

$$\varphi_k+\lambda\sum_{j=-\infty}^{+\infty}\alpha_{kj}\varphi_j=f_k, \tag{3}$$

where the f_k are the Fourier coefficients of $f(x)$, and the matrix α_{kj} is given by the expressions

$$\alpha_{00}=8\sqrt{2}/3;\quad \alpha_{k0}=(-1)^{k+1}4(\pi)^{\frac{1}{2}}\frac{S(2\pi|k|)}{(2\pi|k|)^{\frac{1}{2}}},$$
$$\alpha_{kk}=4(\pi)^{\frac{1}{2}}\left(\frac{C(2\pi|k|)}{(2\pi|k|)^{\frac{1}{2}}}+\frac{1}{2}\frac{S(2\pi|k|)}{(2\pi|k|)^{\frac{1}{2}}}\right), \tag{4}$$
$$\alpha_{kj}=\frac{2(-1)^{j-k}}{(\pi)^{\frac{1}{2}}(j-k)}\left(\frac{k}{|k|}\frac{S(2\pi|k|)}{(2\pi|k|)^{\frac{1}{2}}}-\frac{j}{|j|}\frac{S(2\pi|j|)}{(2\pi|j|)^{\frac{1}{2}}}\right),$$

where $C(x)$ and $S(x)$ are the Fresnel integrals,

$$C(x)=\int_0^x\frac{\cos t}{(2\pi t)^{\frac{1}{2}}}dt,\qquad S(x)=\int_0^x\frac{\sin t}{(2\pi t)^{\frac{1}{2}}}dt.$$

The Kirkwood-Riseman solution is obtained, if the matrix elements α_{kj} are approximated by their asymptotic values $(2/|k|)^{\frac{1}{2}}S_{kj}$, valid for either large $|k|$ or $|j|$.

Equations (3) were solved numerically by inversion of the matrix $\delta_{kj}+\lambda\alpha_{kj}$ by a method of successive approximation which involved the neglect of all off-diagonal elements for which $|k|$ and $|j|$ were greater than an assigned integer n, a process which was found to converge with adequate rapidity for all values of λ of interest, with increasing n.

The same method may be used for correcting the corresponding function determining the intrinsic viscosity of rod-like macromolecules.[3] However, since this function as given by Kirkwood, Riseman, and Auer is asymptotically correct for large ratios of length to radius, the most important practical case, and since no numerical values were tabulated for intermediate ratios of length to radius in the previous articles, it has not been thought worth while to present numerical tables for the corrected function for the intermediate ratios here. As in the case of flexible molecules, the corrections to the solutions presented in the previous articles will be too small to be of practical significance in the use of the theory for structural interpretations.

[1] John G. Kirkwood, J. Chem. Phys. **22**, 1626 (1954).
[2] J. G. Kirkwood and J. Riseman, J. Chem. Phys. **16**, 565 (1948).
[3] J. Riseman and J. G. Kirkwood, J. Chem. Phys. **18**, 512 (1950); J. G. Kirkwood and P. L. Auer, *ibid.* **19**, 281 (1951).

Evidence for the Interconversion of Monochloroacetic Acid by Its Pure Quadrupole Spectrum

HISAO NEGITA
Department of Chemistry, Hiroshima University, Hiroshima, Japan
(Received October 22, 1954)

SOLID monochloroacetic acid was subjected to various heat treatments and its pure quadrupole spectrum due to Cl^{35} was observed at room temperature. To determine the resonance frequencies, a frequency-modulated super-regenerative spectrometer[1] and a heterodyne frequency meter were used. First, the ordinary acid was melted at above its melting point and cooled rapidly to room temperature. For convenience, the initial acid and the final acid were assigned to the solid (1,2) and the solid (1′) respectively, the meanings of which would be evident later. Next, the solid (1,2) was distilled slowly and left to be cooled. It was assigned to the solid (2′).

The resonance frequencies of these three samples were observed at room temperature and the results obtained are listed in Table I. The experimental error in the frequency was about several kc/s.

As seen from Table I, only one resonance frequency was observed in each of the solids (1′) and (2′). Their intensities were very strong compared to those of the solid (1,2). If other frequencies existed, they might be too weak to be detected. It is very interesting to see that the frequency of the solid (1′) is near the lower frequency of the solid (1,2) and that of the solid (2′) is very close to the higher one of the solid (1,2).

Furthermore, the following facts were found from the spectrum of the acid. (a) The solid (1′) was easily converted to the solid (2′) by a slight shock and this process was exothermic. (b) Both the solids (1′) and (2′) were reversed to their initial state, that is, the solid (1,2), by melting again and cooling gradually. (c) The solid (1,2) remained in its initial state by melting and cooling gradually. Thus the solids (1,2), (1′), and (2′) should be referred to the α-, γ-, and β-modifications of the acid which are so far known.[2]

According to H. C. Allen,[3] the two frequencies of the acid are contributed to the acid dimer which presumably exists in the solid state. If this were the case, they may not be caused only by one form of the dimer, but two forms of the dimer corresponding to the solids (1′) and (2′), which are supposed to be at equilibrium in the ordinary solid state. The small differences in

TABLE I. Cl^{35} resonance frequencies of monochloroacetic acid at 292°K.

	Solid (1,2), α acid	Solid (1′), γ acid	Solid (2′), β acid
Resonance Frequency (Mc/sec)	34.973 35.524	35.108 ...	... 35.539

resonance frequencies between the solids (1,2) and (1′), or between the solids (1,2) and (2′) seem to be caused by the other form of the dimer.

If two forms of the dimer are assumed as above, they will be probably the *gauche*- and *trans*-forms analogous to 1,2-dichloroethane,[4] and the solid (1′) or γ-modification may be regarded as to be the *gauche*-form and the solid (2′) or β-modification as to be the *trans*. The former is less stable than the latter. Above all, the extraordinary behavior of the acid appears to be attributed to its weak hydrogen bonds[5] which associate the acid molecules to the dimer. The study of the other effects on the resonance frequency is now in progress.

The author wishes to express his sincere thanks to Dr. T. Ichikawa, Dr. H. Yamamura, Dr. M. Miura, and T. Kushida for their useful discussions about this research and to T. Kawano for the use of the frequency meter.

[1] H. G. Dehmelt and H. Krüger, Z. Physik **129**, 401 (1951).
[2] *Beilsteins Handbuch der Organischen Chemie* (Julius Springer, Berlin), fourth edition, **H2**, 194 (1920); **EI2**, 87 (1929); **EII2**, 187 (1942).
[3] H. C. Allen, Phys. Rev. **87**, 227 (1952); J. Am. Chem. Soc. **74**, 6074 (1952); J. Phys. Chem. **57**, 501 (1953).
[4] L. N. Ferguson, *Electron Structures of Organic Molecules* (Prentice-Hall, Inc., New York, 1952), p. 94.
[5] Pohl, Hobbs, and Gross, J. Chem. Phys. **9**, 408 (1941).

Paramagnetic Resonance from Broken Carbon Bonds

J. E. Bennett, D. J. E. Ingram, and J. G. Tapley
University of Southampton, Southampton, England
(Received November 15, 1954)

SINCE the first report of paramagnetic resonance absorption in charcoals, and other low-temperature carbons, by Ingram and Bennett,[1] it has also been observed by others,[2,3] and studied more thoroughly in coals and coal derivatives.[3,4] It may not be generally realized, however, that exactly the same resonance absorption can be obtained by simply charring any natural or artificial carbohydrate, under the right conditions. This fact has been briefly mentioned before,[1,5] but the results are reported here in more detail, and they throw considerable light on the nature of the "free radical" responsible for this absorption.

The experimental observations have been made at frequencies of 36 000 Mc/sec, 25 000 Mc/sec, 9000 Mc/sec, 40 Mc/sec, and in some cases over a temperature range from 20°K to 290°K. The absorption line obtained from the charred carbohydrates is exactly the same as that obtained from coal, having a width at half-power of 8 ± 2 gauss and a spectroscopic splitting factor of 2.0030 ± 0.0003, at all the frequencies and temperatures employed.

A list of the different charred organic compounds, from which this resonance has been obtained, is given in Table I. It may also be produced by charring any diamagnetic organic salt, such as an acetate, lactate, etc. In this case however, there is a small variation in line width and g value, which has been shown to be due to the presence of the diamagnetic metal atoms.[5]

It would in fact appear that any organic material will show this absorption, if charred slowly, and below 600°C. Detailed quantitative measurements[4] on various coals have shown that the free radical concentration rises to a maximum at a charring temperature of 550°C, and then falls sharply to zero. This seems to be true of all the other charred compounds. The signal intensity is quite strong in comparison with hydrazyl which gives an approximate value of 10^{19} free-radicals per gm (or one per 2000 carbon atoms).

TABLE I. Substances showing sharp absorption line.

a	Charred glucose and other sugars.
b	Deposits from luminous flames.
c	Charred natural or artificial cellulose.
d	Charred anthracene and glycerine.
e	Charred vegetable root and other complex natural organic material.
f	Charcoals formed below 600°C.
g	Coals and coal derivatives formed below 600°C.

These results, together with the fact that the intensity of the signal increases linearly with the percentage of aromatic carbon present,[4,6] seem to confirm the previous suggestion[4,5] that the free radical is in fact associated with a broken bond in the condensed carbon rings. The sharp fall of absorption to zero at 600°C can be explained on the supposition that all the volatile matter has then been removed, and the carbon rings are sufficiently mobile to join up their broken bonds and begin forming graphitic planes. This is confirmed by the fact that the electrical conductivity starts to rise markedly at this same temperature.

The variation of signal intensity with carbonizing temperature, and also the fact that the line width is the same at radio-frequencies, as at microwave frequencies, shows that this is quite a different absorption mechanism to that observed by Castle[7] and Henning[8] *et al.* for the conduction electrons in carbons and graphites formed above 1400°C.

[1] D. J. E. Ingram and J. E. Bennett, Phil. Mag. **45**, 545 (1954).
[2] Commoner, Townsend, and Pake, Nature **174**, 689 (1954).
[3] Uebersfeld, Etienne, and Combrisson, Nature **174**, 614 (1954).
[4] Ingram, Tapley, Jackson, Bond, and Murnaghan, Nature **174**, 740 (1954).
[5] Bennett, Ingram, and Tapley, London Physical Society Report of Bristol Conference on "Defects in Solid State," July, 1954.
[6] D. W. Van Krevelen and H. A. G. Chermin, Fuel **33**, 79 (1954).
[7] J. G. Castle, Phys. Rev. **92**, 1062 (1953); **94**, 1410 (1954); **95**, 846 (1954).
[8] Henning, Smaller, and Yasaitis, Phys. Rev. **95**, 1088 (1954).

The Vibration-Rotation Spectrum of Silyl Iodide

R. N. Dixon and N. Sheppard
Department of Colloid Science, Cambridge University, England
(Received November 7, 1954)

THE infrared spectrum of gaseous silyl iodide has been recorded in the region 2 μ to 20 μ with a Perkin-Elmer spectrometer and with a prism-grating spectrometer. Silyl iodide hydrolyzes very readily, and great care had to be taken in order to eliminate strong bands of silyl ether at 9 μ, 10.5 μ, and 13.2 μ.

The parallel bands show P and R branches, the Q branches being very weak as the moment of inertia about the top axis (I_A) is much smaller than I_B. The perpendicular bands are well resolved and show the intensity alternation "strong, weak, weak, strong . . ." of the Q branches as expected for a molecule with a threefold axis. All the fundamentals have been measured except $\nu_3(a_1)$, which lies beyond the region investigated. A vibrational assignment has been made for all the observed overtone and combination bands in terms of the fundamentals given in Table I.

The region of Si—H stretching vibrations contains two strong bands; a parallel band (ν_1) with a weak Q branch at 2191.8$_0$ cm^{-1}, and a perpendicular band (ν_4) with band origin at 2205.6$_5$ cm^{-1}. The $^RQ_0$ line is determined by comparing the intensity of ^PQ and ^RQ lines of high K value, where the absorption of the parallel band is negligible. In the region of SiH_3 deformation vibrations there is a very strong parallel band (ν_2) with its center at 903 cm^{-1}, and a strong perpendicular band (ν_5) with Q lines from 820 to 1060 cm^{-1}. The ^RQ lines of ν_5 are very strongly perturbed near $K=4$ due to Fermi resonance with the combination band $\nu_3+\nu_6$. In this region there is a mixing of the vibrational eigenfunctions[1] giving two lines for each K value. An examination of the separation of these pairs of lines gives the constants of the perturbation, after the subtraction of which the Q lines obey the usual formula. The $^RQ_0$ line is determined as for ν_4, and the unperturbed band centers of ν_5 and $\nu_3+\nu_6$ are calculated as 941.$_0$ and 947.$_5$ cm^{-1}, respectively. The perpendicular SiH_3 rocking vibration (ν_6) has its band center at 592.4$_0$ cm^{-1}.

From the mean separation of the P and R maxima in three parallel bands the rotational constant $B=0.107\pm0.009$ cm^{-1}.

TABLE I. The fundamentals of SiH_3I.

Description	Designation	vac. cm^{-1}	$2(A''-A'\zeta-B'')$	ζ
Symmetric Si−H stretching	$\nu_1(a_1)$	2191.8_0	...	...
Symmetric SiH_3 deformation	$\nu_2(a_1)$	903	...	...
Degenerate Si−H stretching	$\nu_4(e)$	2205.6_5	5.39_5	0.01_5
Degenerate SiH_3 deformation	$\nu_5(e)$	$941._0$	6.59_0	-0.19_5
Degenerate SiH_3 rocking	$\nu_6(e)$	592.4_0	4.344	0.199
Estimated from $(\nu_3+\nu_6)-(\nu_6)$ Si−I stretching	$\nu_3(a_1)$	355	...	...

Combining this with the data from the perpendicular fundamentals, $A''=2.848\pm0.014$ cm^{-1}, and the zeta values are as shown in Table I. Polo and Wilson[2] have recently measured by infrared spectroscopy the Si−H internuclear distance in SiH_3D and reviewed the earlier infrared and microwave work on molecules of the type SiH_3X (X=H, F, Cl, Br). They conclude that the most probable value of this distance is 1.48 ± 0.01 A. If this is assumed to be correct for silyl iodide, the values of the other structural parameters based on our infrared measurements are: HSiH angle=109° 54′±25′, and Si−I distance 2.45 ± 0.09 A. The latter is in satisfactory agreement with the value of 2.43 ±0.02 A determined by electron diffraction for the Si−I distance in SiI_4.[3]

The Perkin-Elmer spectrum shows a mean spacing of 7.7_3 cm^{-1} for the Q lines in the perpendicular component of $2\nu_6$ in excellent agreement with that expected from the zeta sum rules, 7.74 cm^{-1}.[4]

We are indebted to Dr. Maddock of the Cambridge University chemical laboratory for the specimen of silyl iodide, and for his advice in the identification and elimination of the silyl ether impurity.

[1] G. Herzberg, *Infrared and Raman Spectra of Polyatomic Molecules* (D. Van Nostrand Company, Inc., New York, 1945), p. 215.
[2] S. R. Polo and M. K. Wilson, J. Chem. Phys. **22**, 1559 (1954).
[3] Allen and Sutton, Acta Cryst. **3**, 46 (1950).
[4] Johnston and Dennison, Phys. Rev. **48**, 868 (1935).

Mass Spectrometric Study of Gaseous Species in the Si-SiO_2 System*

RICHARD F. PORTER, WILLIAM A. CHUPKA, AND MARK G. INGHRAM
Department of Physics, University of Chicago, Chicago, Illinois, and Argonne National Laboratory, Lemont, Illinois
(Received October 18, 1954)

IN a recent study and review of the silicon-oxygen system Brewer and Edwards[1] interpreted thermochemical and spectroscopic data as showing that solid SiO_2 in the presence of silicon vaporizes to SiO gas and that SiO_2 under neutral oxidizing conditions vaporizes by decomposition to gaseous SiO and oxygen. The thermochemical data are calculated from measurements of total vapor pressure; and although the data are accurate enough to show that SiO is the principal vaporizing species in these cases, other molecular species may constitute a small percentage of the total vapor. To obtain further knowledge of the vapor composition a mass spectrometric search has been made for other gaseous molecules vaporizing from Si-SiO_2 mixtures and from SiO_2 under neutral oxidizing conditions.

The Knudsen effusion assembly for the mass spectrometer has been described earlier.[2] Vapor in equilibrium with solid effuses out of the crucible and enters directly into the ion source of the mass spectrometer. The ions, then formed, are accelerated and directed into the magnetic field for the purpose of mass resolution. A shutter arrangement allows one to distinguish between ions formed from gases coming out of the crucible and background currents. Knudsen cells were constructed of high purity alumina crucibles and covers. The temperature range investigated was between 1200°K and 1950°K.

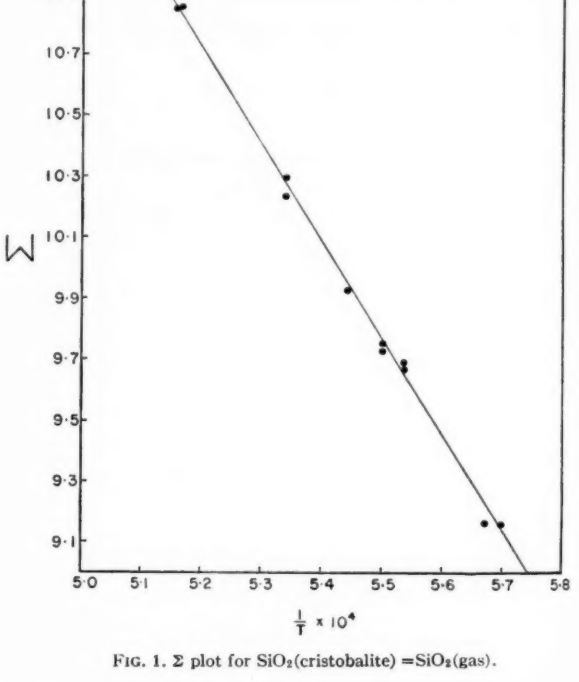

FIG. 1. Σ plot for SiO_2(cristobalite) $=SiO_2$(gas).

TABLE I. Results of pressure calibration.

Equilibrium vapor conditions	Gaseous species, X	X^+ ion current (arbitrary units)	Temperature °K	Pressure (in atmos)	Remarks
Over Si-SiO_2 (tridymite) mixtures	Ag^{107}	3.0×10^5	1245	(1.0×10^{-6})	See reference 3
	SiO	1.0×10^6	1345	5.0×10^{-6}	
	SiO	2.3×10^7	1463	1.1×10^{-4}	
	Si_2O_2	1.8×10^4	1463	4.5×10^{-8}	
Over SiO_2 (cristobalite), near neutral oxidizing conditions	Au	4.0×10^6	1750	(2.0×10^{-5})	See reference 3
	SiO	9.0×10^5	1800	6.8×10^{-6}	
	SiO_2	3.2×10^3	1800	1.6×10^{-8}	
	O_2	7.0×10^3	1800	5.2×10^{-8}	
	SiO	4.5×10^6	1900	3.4×10^{-5}	
	SiO_2	2.0×10^4	1900	1.0×10^{-7}	
	O_2	1.1×10^4	1900	8.2×10^{-8}	
	O	1.5×10^4	1900	2.2×10^{-7}	

At low temperatures, on Si-SiO_2 runs, ion currents of SiO^+ and $Si_2O_2^+$ were observed while at higher temperatures; on runs with SiO_2 under neutral oxidizing conditions, ion currents of SiO_2^+, O_2^+, and O^+ were also observed. Appearance potentials for SiO^+, SiO_2^+, and $Si_2O_2^+$ are 10.8 ± 0.5 ev, 11.7 ± 0.5 ev, and 10 ± 1 ev, respectively. Temperature dependence measurements show that SiO_2^+ and $Si_2O_2^+$ are formed from direct ionization of effusing SiO_2 and Si_2O_2 gases, respectively, and can not be formed in a second-order mechanism involving SiO^+.

It was possible to obtain the equilibrium partial pressures of the gaseous species inside the Knudsen cell by calibrating the system against a reference pressure. At the beginning of each run a small weighed amount of silver or gold was vaporized out of the crucible. The observed ion current of Ag^+ or Au^+ combined with the known pressure of $Ag(g)$ or $Au(g)$ inside the Knudsen cell gives a direct measure of the ion current per atmosphere. The following estimated relative ionization cross sections were used: $Ag^+:Au^+:SiO^+:SiO_2^+:Si_2O_2^+:O_2^+:O^+=1.5:1.5:1:1.5:2:1:0.5$. For each species the ionizing voltage was 5 ev above the

appearance potential. A summary of the calibration[3] is given in Table I. The calibration was checked by comparing the time required for all of the silver or gold sample to vaporize with the ion current of Ag^+ or Au^+, integrated over the same time interval. The estimated uncertainty in the calibrated pressures is within a factor of two or three.

The heat of sublimation of SiO_2 was obtained by measuring the variation in SiO_2^+ ion current with temperature. Using an estimated heat capacity of 13 cal/deg for SiO_2 gas and an average heat capacity of 16.5 cal/deg for SiO_2 (cristobalite) between 298°K and 2000°K, calculated from Kelley's table,[4] we obtain for SiO_2 (cristobalite$=SiO_2$ (gas), $\Delta H^0=\Delta H^0_{298}-3.5(T-298)$. Substituting this expression for ΔH into the van't Hoff equation, integrating, setting the ion current of SiO_2^+ proportional to the partial pressure of SiO_2 gas inside the Knudsen cell,[5] and defining the quantity Σ, we obtain

$$\Sigma=\log I_{SiO_2^+}+2.7\log T=-\frac{(\Delta H^0_{298}+1050)}{4.575T}+\text{const.}$$

A typical Σ plot is shown in Fig. 1. Intensity measurements were made with 20 and 40 volt ionizing electrons. From slopes of five sets of data we obtain for SiO_2 (cristobalite)$=SiO_2$ (gas), $\Delta H^0_{298}=136\pm8$ kcal.

The authors would like to thank Mr. Paul Schissel for assisting with these measurements.

* This work was supported in part by a grant from the National Science Foundation.

[1] L. Brewer and R. K. Edwards, J. Phys. Chem. **58**, 351 (1954).
[2] Porter, Schissel, and Inghram, J. Chem. Phys. (to be published).
[3] L. Brewer, Paper 3, National Nuclear Energy Series, Vol. 19B, edited by L. L. Quill (McGraw-Hill Book Company, Inc., New York, 1950).
[4] K. K. Kelley, U. S. Bur. Mines Bull. No. 476 (1949).
[5] The relationship between the pressure of gaseous species, x, inside the Knudsen cell and the observed ion current of x^+ is given by $P_x=kI_{x^+}T$, where T is the temperature of the Knudsen cell and k is the proportionality constant. See W. A. Chupka and M. G. Inghram, J. Chem. Phys. **21**, 371 (1953).

Divalent Hydrogen in the FHF^- Ion

R. T. Sanderson
Department of Chemistry, State University of Iowa, Iowa City, Iowa
(Received October 15, 1954)

THE results of recent nuclear magnetic resonance studies[1] agree with conclusions reached earlier[2] from thermodynamic and other evidence. These results show that the anion of KFHF is linear and that the proton is equidistant from the two fluorine nuclei. Equivalence of bonding is thus indicated.

The charge distribution in this FHF^- ion is of especial interest. This is true in view of the apparently unambiguous and symmetrical divalency of the hydrogen and the stability of the bonds —four times that of an average "hydrogen bond."[2] This distribution can be estimated by methods recently described,[3] basing the calculations on an assumed ionicity in NaF of 75 percent.[4] First, there seems to be little doubt of the completely ionic nature of the salt. The electronegativity of the FHF^- ion is 3.38 whereas that of the K^+ ion is only 2.12. Thus this indicates that the FHF group is more than capable of removing an electron completely from an atom of potassium. An electronegativity of 3.38 would correspond to partial charges of -0.044 on hydrogen and -0.478 on each fluorine. Certainly the charge on hydrogen seems reasonable and not in violation of the Pauli principle, even though the hydrogen orbital appears to be involved simultaneously with orbitals of each of the two fluorine atoms.

The reaction of a molecule of HF with a F^- ion is of interest. The polarity of the bond in HF is estimated as 24.7 percent, not 43 percent as usually accepted from the dipole moment[5] and bond length. (Recent estimates[6] of "lone pair" contributions to the total dipole have strongly suggested that the actual HF bond is much less polar than previously supposed, in qualitative support of the above estimate.) Even with a charge of 0.247, however, there can be a strong electrostatic attraction between the hydrogen and a fluorine atom of charge -0.247, as shown by the proton bridges existing in hydrogen fluoride. It is not surprising that attraction between the hydrogen and a fluorine atom of charge of -1.000 is even greater—sufficient for orbital interaction resulting, through electronegativity adjustments, in the FHF^- ion. The stabilization and equalization of the hydrogen divalence may be attributed to the extra electron available on the anion.

The essential chemical reasonableness of FHF^- ion may be shown by various hypothetical syntheses. For example, it might be synthesized from two fluoride ions and a proton. The calculated electronegativities of F^- ion and H^+ ion are 0.76 and 7.47. With this high electronegativity, a hydrogen ion is capable of removing 0.753 electron from one fluoride ion, forming HF. This could combine with the second fluoride ion as described above. Another possibility would be the synthesis from two fluorine atoms and a hydride ion. The first step might be the combination of one fluorine atom with the hydride ion to form an ion, HF^-. In this, the charges would be -0.313 on H and -0.687 on F. A second fluorine atom would find this hydrogen still very susceptible to oxidation, and the FHF^- would result. A third possibility would be formation by the convergence of two fluorine atoms, each bearing a partial charge of -0.500, upon a neutral hydrogen atom. Neutral hydrogen is more electronegative (3.55) than a fluorine atom of -0.500 charge (3.26) and therefore is capable of withdrawing charge from such fluorine atoms to itself until electronegativities are equalized. The formation of an FHF^- ion by whatever means thus seems quite within ordinary chemical expectations.

Presumably as a result of the extra electron which makes all electrons more available for bond formation, the hydrogen divalence of the FHF^- ion seems clearly unlike the more common proton and hydride bridges between neutral molecules.

[1] Waugh, Humphrey, and Yost, J. Phys. Chem. **57**, 486 (1953).
[2] E. F. Westrum, Jr., and K. S. Pitzer, J. Chem. Phys. **15**, 526 (1947); J. Am. Chem. Soc. **71**, 1940 (1949).
[3] R. T. Sanderson, J. Chem. Educ. **31**, 2 (1954).
[4] R. T. Sanderson, J. Chem. Educ. **31**, 238 (1954).
[5] N. B. Hannay and C. P. Smyth, J. Am. Chem. Soc. **68**, 171 (1946).
[6] A. B. F. Duncan and J. A. Pople, Trans. Faraday Soc. **39**, 217 (1953).

The Pure Rotational Spectra of DBr, HI, and DI in the Spectral Region between 45 and 170 Microns

E. D. Palik
Department of Physics, The Ohio State University, Columbus, Ohio
(Received November 7, 1954)

THE pure rotational spectra of the hydrogen halides were first measured by Czerny.[1] Recently, additional measurements have been made of the rotational spectra of HCl by McCubbin and Sinton[2] and McCubbin[3] and of HCl, DCl, and HBr by Hansler and Oetjen.[4] One rotational line of DI has been observed in the microwave region by Burrus and Gordy.[5]

The spectra of DBr, HI, and DI were obtained with the far infrared spectrograph in this laboratory.[6] The gas DBr was prepared according to the chemical equation $PBr_3+3D_2O\rightarrow 3DBr+P(OD)_3$. Furthermore, HI and DI were prepared by similar reactions of PI_3 with H_2O and D_2O, respectively. The gases were dried by passing them through a drying tube containing phosphorus pentoxide. The path lengths of the cells used were 5 and 7.5 in. Each cell was provided with two polyethylene windows 0.010 in. thick. Gas pressures were varied from 20 to 50 cm Hg.

In the records of DBr and DI, lines of HBr and HI, respectively, appeared. This indicated the presence of hydrogen, probably in the form of H_2O absorbed on the walls of the gas generating system, even though some effort was made to remove such contaminations. In most cases, however, the lines of the hydrogen halide did not interfere with accurate determination of the positions of the deuterium halide lines.

TABLE I. Pure rotational lines of DBr, HI, and DI.

J'	DBr Frequency Observed	DBr Frequency Calculated	HI Frequency Observed	HI Frequency Calculated	DI Frequency Observed	DI Frequency Calculated
5			64.19K	64.17K		
6			76.98	76.96		
7	59.32K	59.33K	89.66	89.70		
8	67.83	67.77	102.37	102.42		
9	76.19	76.18	115.10	115.09	58.45K	58.41K
10	84.62	84.58	127.76	127.73	64.89	64.86
11	92.93	92.96	140.32	140.31	71.33	71.29
12	101.29	101.31	152.90	152.85	77.70	77.72
13	109.64	109.64	165.32	165.31	84.17	84.13
14	117.91	117.94	177.65	177.72	90.53	90.51
15	126.21	126.21	189.99	190.06	96.85	96.89
16	134.40	134.45	202.52[b]	202.33	103.24	103.25
17	142.63	142.66	214.49	214.51	109.60	109.57
18	150.84	150.83	226.59	226.61	115.92	115.89
19	158.98	158.96			122.18	122.18
20	166.93[a]	167.05			128.42	128.45
21	175.05	174.98			134.62	134.61

[a] Falls beside HBr line corresponding to $J'=8$.
[b] Distorted by strong H_2O line.

The frequencies of the pure rotational lines of a diatomic molecule are given by the formula $\nu=2B_0J'-4D_0J'^3$ where ν is the frequency of the line in kaysers, B_0 is the rotational constant

TABLE II. Rotational constants and centrifugal stretching constants of DBr, HI, and DI.

Molecule	Rotational constant B_0	Centrifugal stretching constant D_0
DBr	4.246$_7$	0.000088
HI	6.427$_5$	0.000205
DI	3.2535	0.000053

or the reciprocal of inertia of the molecule in the ground state, D_0 is the centrifugal stretching constant for the ground state, and J' is the usual rotational quantum number associated with the upper energy level of the transition. Values of B_0 and D_0 have been chosen to fit the observed lines for each molecule. In the case of DI, the value of B_0 obtained by Burrus and Gordy[5] is used. There is fair agreement between the values obtained here and those obtained from other available near and far infrared data. Table I lists the data obtained. The observed and calculated line positions are denoted by their upper state J values. Table II lists the molecular constants B_0 and D_0.

[1] M. Czerny, Z. Physik **34**, 227 (1925); **44**, 235 (1927).
[2] T. K. McCubbin and W. W. Sinton, J. Opt. Soc. Am. **40**, 537 (1950).
[3] T. K. McCubbin, J. Chem. Phys. **20**, 668 (1952).
[4] R. L. Hansler and R. A. Oetjen, J. Chem. Phys. **21**, 1340 (1953).
[5] C. A. Burrus and Walter Gordy, Phys. Rev. **92**, 1437 (1953).
[6] The spectrograph was available for this investigation through the courtesy of Wright Air Development Center, who through a contract with the Ohio State University Research Foundation, provide partial support for its construction and maintenance.

The Properties of Substances at the Critical Point

JOHAN VAN DRANEN*
Laboratory for Analytical Chemistry, University of Amsterdam, Amsterdam, Netherlands
(Received October 11, 1954)

WITH the aid of our hypothesis concerning the critical state, we have calculated a value for the kinetic energy of the disturbed rotation of CO_2 at the critical point.[1] We found that, at any instant, only a part of the molecules rotate freely; the energy associated with the freely rotating molecules is equal to 40 percent of the normal value. Using the thermodynamic values obtained by Michels and co-workers[2] we find, in the same way, that this value is 73 percent for ethene and 69 percent for propene. During a collision the energy of rotation of freely rotating molecules, which as an intramolecular energy has no significance in our hypothesis, is transformed partly in positive (repulsive) potential energy. The latter cannot, of course, be distinguished from the repulsive potential energy into which the ordinary kinetic energy of translation partly transforms itself upon a collision. By compressing a gas, more and more of the original rotational energy is transformed into repulsive potential energy; the duration of a collision becomes an appreciable part of the time between two collisions. A part of the intramolecular energy occurring in the diluted gas state is therefore transformed into interaction energy between the molecules.

Let b be the short distance between the surfaces of two colliding molecules, b being small as compared with their diameter. For the mean duration of a collision t we have $t=b(\pi M/RT)^{\frac{1}{2}}$. Here M is the molecular weight.

The length of the CO_2 molecule is 5.1A and the "thickness" is 2.8A; it therefore seems reasonable to assume that b must be at least equal to 1.0A in order to make a free rotation possible. Although it is impossible to use an unambiguous value for the diameter d and the formulas of the kinetic gas theory are crude approximations at the critical point, the duration of a collision, defined in the above manner, is always greater for all reasonable values for b and d than the time between two collisions. For example, when $b=1.0$A and $d=3.0$A, the average time between two collisions is equal to 10^{-12} sec and the average duration of a collision 0.7×10^{-12} sec. The shape of the ethene and propene molecule is somewhat more suited to free rotation at the critical point.

Two independent methods, the rotation-Raman effect[1] and this gaskinetical method, give support to the value for the "free" rotational energy calculated with the aid of the hypothesis.

The following attempt to correlate the phenomenological description with the molecular aspect may be of interest. It does not however constitute a proof.

Since "an equal number of links must be broken," a complete equivalent to the hypothesis is obtained by stating that the average attractive potential energy of this molecule with respect to that part of the system lying below the plane through the molecule, perpendicular to its velocity vector. Under these conditions the molecules are therefore not bound together, but are able to move through the whole container. Thus $(\partial V/\partial T)_P$ becomes infinite at this point. The mathematical equivalent is $(\partial P/\partial V)_T=0$.

The term P_cV_c in the expression for the total energy denotes the energy gained from the environment of the system when the molecules are brought to infinity.

* Present address: Koninklijke/Shell-Laboratory, Amsterdam, Netherlands.
[1] J. van Dranen, J. Chem. Phys. **21**, 1404, 2095 (1953); J. Chem. Phys. **22**, 1265 (1954).
[2] Michels, Geldermans, and De Groot, Physica **12**, 105 (1946).

Dislocation Model of Liquids

JEROME ROTHSTEIN
Signal Corps Engineering Laboratories, Fort Monmouth, New Jersey
(Received October 15, 1954)

A LIQUID model is suggested which appears to combine the advantages of hole[1] and crystallite[2] theories of liquids and of cooperative theories of melting.[3] It also explains some properties of crystals grown from the melt or from solution in addition to those of liquids.

Consider a crystal approaching the melting point from below. Schottky defects diffuse in from the surface. With increase in their concentration they can condense into dislocations,[4] and, from a law of mass action consideration, are expected to do so. Vacancies and dislocations near the surface permit the formation of new free volume in their vicinity, i.e., formation of an adjacent associated vacancy, at a smaller cost in broken bonds than forming the same increment in free volume as an isolated vacancy would entail. Similarly, a sheet of vacancies, i.e., a dislocation, requires far

fewer broken bonds for its formation than a similar number of separated vacancies. This stabilizes the dislocations against dissociation to a large extent, if E_b is the energy to break a bond and each molecule has z neighbors. Thus zE_b is the energy occurring in the Boltzmann factor giving the concentration of vacancies for Schottky defects. The cooperative effect in grouping vacancies contiguously gives far fewer broken bonds than z for each unit of free volume (taking the isolated vacancy as the unit of free volume), leading to an avalanche effect in increase of free volume with rising temperature far more precipitous than the Boltzmann factor temperature variation for increase in number of broken bonds. This sudden increase in free volume is the same as a sudden increase in the density of dislocations. This in turn is tantamount to a loss of resistance to shear (though not to compression or dilatation). This is perhaps the most obvious difference between liquids and solids. From the dislocation model of grain boundaries in solids,[5] it follows that loss of resistance to shear is equivalent to the breaking up of the crystal into crystallites with fluctuating boundaries. There should be a moderate drop in density because of the free volume increase, an increased resistivity for a normal metal because of additional scattering of electron waves by dislocations, and a vanishing of long-range order, but a retention of short-range order, as observed by x-ray diffraction. The heat of fusion should be perhaps two orders of magnitude less than the heat of vaporization, for the bulk of the molecules are within crystallites rather than at the dislocations.

A simple explanation also emerges of why real crystals have a mosaic structure, or what is equivalent, contain many dislocations. For crystal growth from the melt could often be by deposition of whole crystallites, rather than by deposition of single molecules only, with misalignments taking place when two of them grow to meet each other. Steps of hundreds or thousands of lattice distances observed in growth spirals when crystals are grown from solution seem more reasonable when big aggregates can deposit than if only single molecules can. Furthermore, when the melting point is approached from below, an anomalous increase in C_p should be observed, as befits a cooperative phenomenon, with a similar anomaly in expansion coefficient, and abnormally large internal friction, creep, and slip. Many of these phenomena have been observed for a variety of substances.[6]

Some work in progress indicates a number of reasons for believing that interstitials, rather than vacancies, may dominate the process of fusion in germanium. It is unclear at the moment whether to expect the fluidity of molten Ge to be associated with vacancy-born dislocations or those of opposite sign due to cooperative groupings of interstitials. Either is consistent with the foregoing and with the observed contraction of Ge on melting, and increase of coordination number to eight found in the liquid phase. Orientation disorder can also form dislocations in the same way.[7]

The foregoing has developed out of a series of studies of a unified kinetic approach to defects, disorder, and phase change, of which preliminary notes have appeared,[8] and is the analogue of a treatment of the order-disorder transformation in preparation.

[1] H. Eyring, J. Chem. Phys. **4**, 283 (1936); Hirschfelder, Stevenson, and Eyring, *ibid.* **5**, 896 (1937); W. Altar, *ibid.* **5**, 577 (1937); R. W. Gurney and N. F. Mott, Trans. Faraday Soc. **35**, 364 (1939); S. Bresler, Acta Physicochim. URSS **10**, 491 (1939).
[2] P. Debye and H. Menke, Physik. Z. **31**, 797 (1930); A. Ookawa, J. Phys. Soc. Japan **2**, 108 (1947); J. K. Mackenzie and N. F. Mott, Proc. Phys. Soc. (London) **A63**, 411 (L) (1950).
[3] J. E. Lennard-Jones and A. F. Devonshire, Proc. Roy. Soc. **A169**, 317 (1939); F. C. Frank, *ibid.* **170**, 182 (1939); J. W. H. Oldham and A. R. Ubbelohde, *ibid.* **176**, 50 (1940); G. H. Wannier, J. Chem. Phys. **7**, 810 (1939); J. G. Kirkwood and E. Monroe, *ibid.* **8**, 845 (1940); S. Bresler, J. Exptl. Theoret. Phys. USSR **9**, 711 (1939).
[4] F. Seitz, Phys. Rev. **79**, 890 (L) (1950).
[5] W. T. Read and W. Shockley, Phys. Rev. **78**, 275 (1950); J. H. v. d. Merwe, Proc. Phys. Soc. (London) **A63**, 616 (1950).
[6] E. Brody, Physik. Z. **23**, 197 (1922); W. F. Hachkowsky and P. G. Strelkow, Nature **139**, 715, 803 (1937); A. R. Ubbelohde, Trans. Faraday Soc. **34**, 292 (1938); J. Frenkel, J. Chem. Phys. **7**, 538 (1939).
[7] For the anomalous contraction of Bi below the melting point see J. K. Roberts, Proc. Roy. Soc. (London) **A106**, 385 (1925).
[8] J. Rothstein, Phys. Rev. **89**, 901 (A) (1953); Proceedings of the 14th Annual Conference on Physical Electronics, M. I. T., 1954; Phys. Rev. **94**, 1429 (A) (1954).

Activations by Anions in the Oxy-Acid Phosphors

YOSHIHIDE KOTERA
Government Chemical Industrial Research Institute, Tokyo Hatagaya, Tokyo, Japan
(Received October 22, 1954)

IN the case of sulfide phosphors, it is said that anions, for example, chlorine or oxygen ion, act as activators,[1] but it is not yet reported that such is the case in oxy-acid phosphors. We thought that the anions might be able to activate the oxy-acid phosphors, when they have a smaller electron affinity than that of the host crystal.

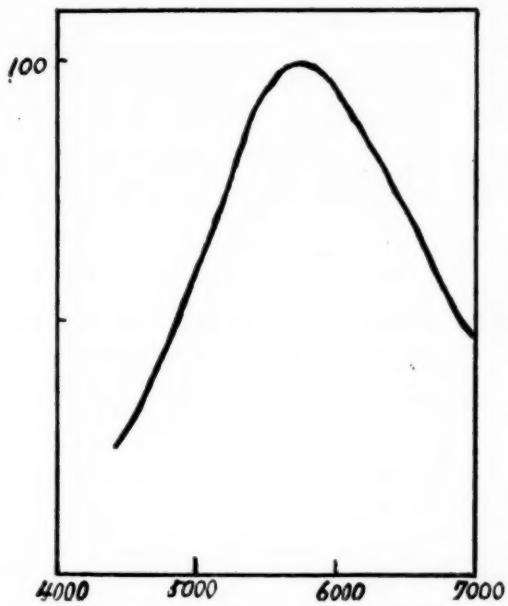

FIG. 1. Emission of $MgSiO_3$ activated by pyrovanadate ion.

The phosphors prepared are shown in Table I and emit light of various colors. Though their luminescence was weak, it was confirmed that in the oxy-acid phosphors anionic centers are present.

TABLE I. The color of luminescence of oxy-acid phosphor activated by anions under the ultraviolet excitation.[a]

	WO_4''	MoO_4''	V_2O_7''''	PO_4'''	AsO_4'''	Sb_2O_4''''
$CaSO_4$	blue s[b]	yellowish green s[b]	none	blue m	yellow m	red m
$BaSO_4$	none	none	none	yellow m[b]	blue f	blue f
	GeO_4''''	SiO_4''''	CO_3''	BO_3'''	AlO_2'''	S''
$CaSO_4$	green m	yellowish green s	blue f	yellow f[b]	blue f	bluish green s
$BaSO_4$	red s	blue m	none	white m	white m[b]	orange s
	V_2O_7''''	PO_4'''	AsO_4'''	Sb_2O_7''''	GeO_4''''	BO_3'''
$CaSiO_3$	yellow ff	none	none	none	none	yellow ff[b]
Ca_2SiO_4	none	red m	red m[b]	red ff[b]	red m[b]	red m
$BaSi_2O_5$	yellow f	yellow f[b]	yellow f	bluish white f	yellow f[b]	bluish white f[b]
$Ba_2Si_3O_8$	yellow m	yellow f[b]	yellow f	yellow f[b]	yellow f	yellow f[b]
$MgSiO_3$	yellow s	yellow ff	red m	yellow ff[c]	yellow ff	none
Zn_2SiO_4	yellow m	yellow m	yellow m	yellow m	yellowish white f	yellow m[c]

s: strong, m: medium, f: faint, ff: very faint

[a] The concentrations of activators are: 0.01–0.1 mole for 1 mole sulfate, 0.001–0.05 mole for 1 mole silicate.
[b] They have the luminescence only under 2537-A excitation.
[c] They have the luminescence only under 3650-A excitation.

From Table I we can see that the anionic activations are generally more difficult than cationic ones. This idea may be supported by the fact that the emission spectra are weak and broad, although the amount of anions used for activation is larger than in the cationic ones.

Magnesium silicate activated by vanadate ion showed the luminescence given in Fig. 1, which is almost the same as that of magnesium pyrovanadate phosphor reported by us,[2] and calcium sulfate activated by tungstate or molybdate ion showed a similar result. We suggest that anionic activations are divided into two groups: one in which the luminescence originates from the electronic transition in the anion as in pyrovanadate, tungstate, or molybdate, while the others are activated by the anions because of their smaller electron affinity compared with the host crystal.

The author wishes to express his thanks to Dr. Shoji Makishima for his suggestions and to Miss Michiko Yonemura for her cooperation.

A detailed account of this work will be published elsewhere.

[1] F. A. Kroeger and J. E. Hellingman, Trans. Electrochem. Soc. **93**, 156 (1948); A. H. McKeag and P. W. Ranby, *ibid.* **96**, 85 (1949); J. S. Prener, *ibid.* **98**, 406 (1951); R. H. Bube, J. Chem. Phys. **19**, 985 (1951).
[2] Y. Kotera and T. Sekine, Bull. Chem. Soc. Japan **27**, 13 (1954).

Photoconductance in Tetracene-Type Crystals: Theory of the Spectral Dependence

L. E. Lyons
Department of Physical Chemistry, University of Sydney, Sydney, N.S.W., Australia
(Received October 15, 1954)

RECENT work[1,2] in these laboratories has shown that the curve of the spectral distribution of the photoconductance in an anthracene or tetracene single crystal shows a very close resemblance to the ordinary absorption spectrum of the crystal. Such a resemblance is preserved even when the thickness of the crystal used in photoconductance is increased to such an extent that at all wavelengths of interest over 99 percent of the incident light is absorbed. Therefore if the photocurrent were determined solely by the number of quanta absorbed, the spectral distribution would be very nearly a straight line. The actual distribution therefore needs explanation, and a theory to account for the observed results may be based on the following considerations:

I. Photoconductance is a surface phenomenon.[1,3,4]

II. The primary process is absorption of light in the crystal to produce a stable excited state. This follows from the close resemblances between the gas and the crystal spectra: in particular, the structure observable in the crystal spectrum does not indicate that internal ionization is the immediate result of light absorption.

III. When light is absorbed by such crystals energy migrates as "excitons." The theoretical discussion of this has been given fully by Davydov,[5] and has been used recently.[6] Experimental confirmation is to be found in the crystal spectra and in the fluorescence of mixed crystals.[7]

IV. If the "origin" of the exciton denotes the site at which a quantum is absorbed, then the distance of the origin from the surface will vary with the optical density. For any wavelength there will be an exponential distribution of the origins over the successive molecular layers beneath the surface. For a given wavelength the average distance of an origin from the surface will be great if the optical density is small, and vice versa.

V. Since the current is associated with the surface layer, only those excitons which are absorbed by or which migrate to the surface layer will be active in producing a current.

VI. The further from the surface an exciton originates, the less chance it will have of reaching the surface, because of the possibilities of fluorescence and conversion of the absorbed energy into heat. The probability of reaching the surface may be discussed in various ways, of which the simplest is to associate with the exciton a probability q of crossing a molecular layer. When this is done,

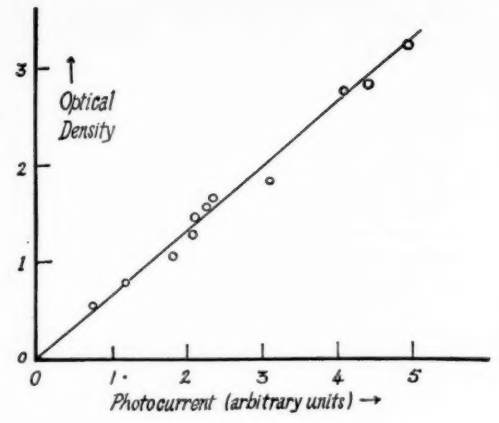

FIG. 1.

calculations may be made and the result for the photocurrent i is

$$i=kI_0[E/(1-q)-E^2q/2!\{2/(1-q)^2+1/(1-q)\}+E^3\{\cdots\}-\cdots],$$

where E is the optical density of a single molecular layer, I_0 the incident light intensity, and k a constant which depends on the efficiency of surface excitons in giving rise to electrons in the outer circuit.

In many cases E is small enough for E^2 and higher powers to be neglected. The probability, q, of an exciton crossing a molecular layer will be constant for a given direction in a crystal and so the current should be proportional both to I_0 and to E. It is already known[1] that $i\approx10^{-4}I_0$, and the plot in Fig. 1 for tetracene crystals shows that $i\propto E$. The points on the diagram were plotted from experimental results[8] at wavelengths between 460 and 520 $m\mu$. It is seen that the line, as predicted for a low value of E, passes through the origin. Thus the theory is supported.

If the constant k could be evaluated then a determination of q becomes possible. When $q=0$ only the surface layer is concerned and the expression takes a simple form.

The Commonwealth Research Fund has given welcome assistance in this project.

[1] D. Carswell, Ph.D. thesis, Sydney, 1954. J. Chem. Phys. **21**, 1890 (1953).
[2] A. Bree and L. E. Lyons, J. Chem. Phys. **22**, 000 (1954).
[3] A. T. Vartanyan, Doklady Akad. Nauk, S.S.S.R. **71**, 642 (1950).
[4] A. G. Chynoweth, J. Chem. Phys. **22**, 1029 (1954).
[5] A. S. Davydov, Izvestia Akad. Nauk S.S.S.R., Ser Fiz. **15**, 605 (1951). Akad. Nauk S.S.S.R., Pamyati S. I. Vavilov, 210 (1952).
[6] D. P. Craig and P. C. Hobbins, J. Chem. Soc. (to be published).
[7] F. R. Lipsett and A. J. Dekker, Can. J. Phys. **30**, 165 (1952).
[8] A. Bree and L. E. Lyons (to be published).

Cl^{35} Pure Quadrupole Resonances in Substituted Chlorobenzene*

P. J. Bray
Department of Physics, Rensselaer Polytechnic Institute, Troy, New York
(Received November 1, 1954)

THE investigation of Cl^{35} pure quadrupole resonances in substituted chlorobenzene compounds has been continued.[1-3] It is hoped that sufficient correlation between resonance frequencies and the substituent parameter sigma[1,4] will be established to allow accurate prediction of unknown or poorly determined substituent effects from resonance data. The present letter presents new data obtained with a self-quenching superregenerative oscillator and oscilloscope presentation of the resonance. Analysis of these and several dozen other compounds for substitution effects will be contained in a later communication.

Several compounds in Table I deserve comment. The frequencies for 1,2,4,5-tetrachlorobenzene have also been determined at room temperature. Within the resolving power of the apparatus,

TABLE I. Cl^{35} resonance frequencies at liquid nitrogen temperature.

Compound	Frequency	Signal-to-noise ratio
1,2,4,5-tetrachlorobenzene[a]	36.708 ±0.002[b]	4–5
	36.898 ±0.002[b]	2⁻
$C_6H_2Cl_4$		
2,4,6-trichloroaniline[a]	34.925 ±0.002	2
	34.976 ±0.002	2–3
$Cl_3C_6H_2NH_2$	35.177 ±0.002	2
	35.591 ±0.002	3+
	35.780 ±0.002	2
	35.885 ±0.002	1½
2,4,6-trichlorophenylhydrazine	35.569 ±0.002	3
	35.810 ±0.002	2
$Cl_3C_6NHNH_2$	36.235 ±0.002	3
0-chlorobenzonitrile[a]	35.410 ±0.002[c,d]	3
	35.453 ±0.002[c,d]	4
ClC_6H_4CN	35.500 ±0.002[c,d]	4
	35.541 ±0.002[c,d]	3
0-chloroacetanilide[a]	35.150 ±0.002	10
$ClC_6H_4NHCOCH_3$		
0-chloroacetoacetanilide[a]	35.049 ±0.004	2–3
$ClC_6H_4NHCOCH_2COCH_3$		
4-chloro-3,5-xyleneol[a]	34.348 ±0.002[e]	8
	34.416 ±0.002[e]	8
$ClC_6H_2(CH_3)_2OH$		
2-chloro-5-nitrobenzenesulfonic acid sodium salt	36.627 ±0.004	2⁻
$ClC_6H_3NO_2SO_3Na$		
4-chloro-3-nitrobenzenesulfonic acid potassium salt	37.957 ±0.004	2–3
$ClC_6H_3NO_2SO_3K$		

[a] Compound melted into vial.
[b] It is possible, according to the observed oscilloscope pattern, that there is another weak resonance between these two. Comparison should be made with the close-spaced doublet of equal amplitudes observed in 1,2,4,5-tetrabromobenzene.
[c] Apparently more than one resonance here. Values given are all possibilities, though there are probably no more than three resonances present.
[d] Resonance should be investigated with a lock-in amplifier and recorder system employing a regenerative oscillator.
[e] If there is any difference in size in these two resonances, the higher frequency resonance is weaker.

two lines appear with frequencies of 36.358 and 36.286 Mcps at 25°C. The resonances both exhibit signal-to-noise ratios of about 5 at this temperature. A plot of frequency separation of the two lines as a function of temperature predicts (on the basis of a linear temperature dependence) a coalescence of the two lines at 155–160°C, a value not too far from the melting point (140°C) of the compound.

If the two frequencies are averaged at each temperature the average frequency satisfies the equation $f_{\text{Mcps}} = -2.18\times10^{-3}T + 36.972$ where T is in degrees Kelvin. At 173°K the value would be 36.595 Mcps with a corresponding coupling constant of 73.13 Mcps. Duchesne and Monfils[5,6] have plotted the Cl^{35} average quadrupole coupling constant at 173°K against the number of Cl atoms in the substituted chlorobenzenes. A quadrupole coupling constant of approximately 73.6 Mcps is predicted for 1,2,4,5-tetrachlorobenzene which is in substantial agreement with the observed value of 73.1 Mcps. The out-of-plane bending of the CCl bond in this compound is found to be approximately 20° from the method of Duchesne and Monfils.[5] This is the same value observed for 1,2,4-trichlorobenzene.[6]

The six resonances in 2,4,6-trichloroaniline are grouped in a manner suggesting a tripling of each of the two resonances expected on the basis of the two nonequivalent sites for Cl atoms in the molecular structure. However, the analogous bromine compound shows three distinct resonances of equal amplitude.[7]

The three resonances in 2,4,6-trichlorophenylhydrazine presumably arise from nonequivalence of all three chlorine positions in the molecule. There are apparently two nonequivalent orientations of the 4-chloro-3,5-xyleneol molecule in the crystalline unit cell.

* Research supported by a grant from the National Science Foundation and by the Rensselaer Polytechnic Institute Research Grants Committee.
[1] H. C. Meal, J. Am. Chem. Soc. 74, 6121 (1952).
[2] P. J. Bray and P. J. Ring, J. Chem. Phys. 21, 2226 (1953).
[3] P. J. Bray and D. Esteva, J. Chem. Phys. 22, 570 (1954).
[4] P. J. Bray and R. G. Barnes, J. Chem. Phys. (to be published).
[5] J. Duchesne and A. Monfils, J. Chem. Phys. 22, 562 (1954).
[6] A. Monfils and J. Duchesne, J. Chem. Phys. 22, 1275 (1954).
[7] P. J. Bray, J. Chem. Phys. 22, 950 (1954).

Erratum: Application of the Hertz Theory of Impact to Explosion Phenomena

[J. Chem. Phys. 22, 1687 (1954)]

M. P. MURGAI
Defence Science Laboratory, N.P.L. Buildings, Pusa, New Delhi-12, India

TABLE I should be replaced by the following table:

TABLE I.

Explosive	Weight of the ball g	Height of fall for 50 percent efficiency cm	Time of impact calc. μ sec	Impact explosive delay obs. μ sec	Pressure of impact calculated atmos	Rise in temperature of an air bubble °C: Calculated	Rise in temperature of an air bubble °C: Observed (by compression of air, and not impact)
	1860	16.0	···	···	208	919	460–500
		40	···	···	361	1155	
PETN (5,6)	1860	60	204	131			
	530	155	122	65			
	250	180	94	103			
Nitroglycerine (5)	112	12[a]	···	···	137	655	450–480
Mercury Fulminate	225	100	···	···	531	1343	630–690

[a] This result has been calculated from a graph of efficiency *versus* height.

Taking the pressure p as calculated in Table I to be that in the pressure pulse is perhaps a poor approximation. An improvement of this will be a subject of another communication. In fact, the calculated pressures should be comparable to the experimental pressures, rather than to the temperature rise of an air bubble as a consequence of these pressures, or to the minimum temperature for explosion found experimentally by compression of air over the explosive layer.

Anomalous Infrared Intensity in Ethylene

D. F. EGGERS, JR.
Department of Chemistry, University of Washington, Seattle, Washington
(Received September 30, 1954)

THE infrared spectrum of ethylene, C_2H_4, contains three bands which are essentially bending motions. These include ν_7, ν_{10}, and ν_{12} at 949, 810, and 1444 cm^{-1}.[1] The intensities of these three bands are not at all comparable.[2] The bond moments calculated from them in the standard fashion are about 0.8 and 0.4 Debye for ν_7 and ν_{12}. The revised assignment for ν_{10}[1] means that the bond moment from this vibration is uncertain. However, upon examination of the spectrum one estimates that the bond moment is surely less than half the value for ν_{12}.

Wheatley and Linnett have proposed,[3] on the basis of the low value for the force constant[4] and some simplified energy calculations, that the p orbitals forming the π bond in ethylene remain

perpendicular to, or "follow," the CH_2 planes during vibration. This will give a dipole moment perpendicular to the molecular plane in addition to that produced by the CH bonds. We may calculate the additional dipole as follows. Let the angle displacement between the CH_2 plane and the CC axis be α. Then each rotated orbital, $2p\pi'$, can be expressed in terms of undisplaced $2p\pi$ and $2p\sigma$ orbitals as

$$2p\pi' = 2p\pi \cos\alpha + 2p\sigma \sin\alpha. \quad (1)$$

The molecular orbital then becomes, denoting the carbon atoms a and b,

$$\psi' = (2+2S')^{-\frac{1}{2}}(2p\pi_a' + 2p\pi_b'), \quad (2)$$

where S' is the overlap integral. Finally, we calculate the average distance of the electrons from the plane of the molecule, x.

$$\bar{x} = \int \psi'^* x \psi' d\tau = 2\cos\alpha \sin\alpha (1+S')^{-1} \int 2p\pi_a x 2p\sigma_b d\tau. \quad (3)$$

As Mulliken[5] has shown, the transition-moment integral in Eq. (3) can be written in terms of overlap integrals; therefore,

$$\bar{x} = \cos\alpha \sin\alpha (1+S')^{-1} R \int 2p\pi_a 2p\pi_b d\tau, \quad (4)$$

where R is the internuclear distance. Using the tables of Mulliken, Rieke, Orloff, and Orloff[6] we find, at $R=1.35$ A, $S=0.265$. With two electrons in this molecular orbital we find the dipole moment of the displaced orbital, μ, becomes

$$\mu = 2e\bar{x} = 2.72\alpha \text{ Debye} \quad (5)$$

if α is small. To compare with experiment, we express this moment in terms of components along the four CH bonds, and find 1.36 Debye at each bond.

To make a valid comparison with experiment, this calculated discrepancy should be compared with that between two vibrations in which the motions of orbitals other than $2p\pi$ are most similar. Since our model assumes complete "following" of the hydrogen atoms, the CCσ bond is also bending. We must then compare ν_7 with ν_{10}, rather than with ν_{12}. The observed discrepancy is about half that calculated. Since the correlation of the two electrons is completely neglected as well as polarization, the calculated value should be greater than the observed.

Similar calculations could be carried out for many molecules; however, experimental data are lacking in most cases. Treatment of the out-of-plane CH bending in benzene by this method gives 0.63 Debye projected onto each CH bond. The experimental value of μ(CH) for benzene in this bending mode, measured in solution,[7,8] is about 0.6 Debye. Calculations carried out on formaldehyde, rotating only the carbon orbitals, give an additional μ(CH) of 1.23 Debye. While the experimental measurements may be forced into qualitative agreement with this calculation, they can also be interpreted reasonably without serious anomaly.[9]

The exact numerical values calculated here should not, of course, be regarded as precise. We may conclude that this model predicts a greater effect in ethylene than in benzene, which seems to be experimentally verified. However, the prediction in formaldehyde may be at variance with experiment. Further checks of the model with experiment are needed before it may be used with confidence.

[1] R. L. Arnett and B. L. Crawford, Jr., J. Chem. Phys. **18**, 118 (1950).
[2] Thorndike, Wells, and Wilson, J. Chem. Phys. **15**, 157 (1947).
[3] P. J. Wheatley and J. W. Linnett, Trans. Faraday Soc. **45**, 897 (1949).
[4] Linnett, Heath, and Wheatley, Trans. Faraday Soc. **45**, 832 (1942).
[5] R. S. Mulliken, J. Chem. Phys. **8**, 234 (1940).
[6] Mulliken, Rieke, Orloff, and Orloff, J. Chem. Phys. **17**, 1248 (1949).
[7] A. R. H. Cole and H. W. Thompson, Trans. Faraday Soc. **46**, 103 (1950).
[8] Bell, Thompson, and Vago, Proc. Roy. Soc. (London) **A192**, 498 (1948).
[9] I. C. Hisatsune and D. F. Eggers, Jr. (to be published).